



PACIFIC EARTHQUAKE ENGINEERING RESEARCH CENTER

Performance of Lifelines Subjected to Lateral Spreading

Scott A. Ashford

and

Teerawut Juirnarongrit

Stanford University

Technical Report Documentation Page

1. Report No. SSRP-04/18	2. Government Accession No.	3. Recipient's Catalog No.	
4. Title and Subtitle Performance of Lifelines Subjected To Lateral Spreading		5. Report Date December 2004	
		6. Performing Organization Code	
7. Author(s) Scott A. Ashford and Teerawut Juirnarongrit		8. Performing Organization Report No.	
9. Performing Organization Name and Address Department of Structural Engineering School of Engineering University of California, San Diego La Jolla, California 92093-0085		10. Work Unit No. (TRAIS)	
		11. Contracts or Grant No. 65A0058 and EEC-9701568	
12. Sponsoring Agency Name and Address California Department of Transportation Engineering Service Center 1801 30 th St., West Building MS-9 Sacramento, California 95807		13. Type of Report and Period Covered Final Technical Report through 2006	
		14. Sponsoring Agency Code 06681	
15. Supplementary Notes Prepared in cooperation with PEER Lifelines Program with support from the California Department of Transportation (Caltrans), the Pacific Gas & Electric Company, and the California Energy Commission.			
16. Abstract This report presents the results of full-scale lateral spreading tests in the port of Tokachi on Hokkaido Island, Japan, to assess the behavior of piles and pipelines subjected to lateral spreading. This research project was the joint collaboration between the University of California, San Diego, (UCSD) and several Japanese organizations. Controlled blasting was used to liquefy the soil and subsequently induce lateral spreading in the 4–6% surface slope test beds. Several instrumentations including pore-pressure transducers, global positioning system (GPS) units, inclinometers, etc. were installed to measure pore-pressure buildup and movements of the soils, piles, and pipelines during lateral spreading. The test piles and pipelines were extensively instrumented with strain gages to measure the distribution of bending moment during lateral spreading; this allowed the back-calculation of the loading conditions, as well as the assessment of damage and the performance of the structures. This report presents the back-calculated soil pressure exerted on the piles during lateral spreading. In addition, the potential of using the <i>p-y</i> analysis method for single piles and pile groups subjected to lateral spreading was evaluated. Finally, the design implications are given for piles subjected to lateral spreading.			
17. Key Words Pile, Pipelines, Lateral Spreading, p-y		18. Distribution Statement Unlimited	
19. Security Classification (of this report) Unclassified	20. Security Classification (of this page) Unclassified	21. No. of Pages 326	22. Price

Performance of Lifelines Subjected to Lateral Spreading

Scott A. Ashford

Professor of Geotechnical Engineering

and

Teerawut Juirnarongrit

Postdoctoral Researcher

Department of Structural Engineering
University of California, San Diego

PEER Report 2006/03
Pacific Earthquake Engineering Research Center
College of Engineering
University of California, Berkeley

July 2006

ABSTRACT

This report presents the results of full-scale lateral spreading tests in the port of Tokachi on Hokkaido Island, Japan, to assess the behavior of piles and pipelines subjected to lateral spreading. This research project was the joint collaboration between the University of California, San Diego (UCSD), and several Japanese organizations. Controlled blasting was used to liquefy the soil and subsequently induce lateral spreading in the 4–6% surface slope test beds. Several instrumentations including pore-pressure transducers, global positioning (GPS) units, and inclinometers, were installed to measure pore-pressure buildup and movements of the soils, piles, and pipelines during lateral spreading. The test piles and pipelines were extensively instrumented with strain gages to measure the distribution of bending moment during lateral spreading; this allowed the back-calculation of the loading conditions, as well as the assessment of damage and the performance of the structures. This report presents the back-calculated soil pressure exerted on the piles during lateral spreading. In addition, the potential of using the p - y analysis method for single piles and pile groups subjected to lateral spreading was evaluated. Finally, the design implications are given for piles subjected to lateral spreading.

ACKNOWLEDGMENTS

This project was sponsored by the Pacific Earthquake Engineering Research Center's Program of Applied Earthquake Engineering Research of Lifelines Systems supported by the California Energy Commission, the California Department of Transportation, and the Pacific Gas and Electric Company.

This work made use of the Earthquake Engineering Research Centers Shared Facilities supported by the National Science Foundation under award number EEC-9701568 through the Pacific Earthquake Engineering Research (PEER) Center. Any opinions, findings, and conclusions or recommendations expressed in this material are those of the author(s) and do not necessarily reflect those of the National Science Foundation.

This report was prepared as a result of work sponsored by the California Department of Transportation.

EXECUTIVE SUMMARY

Two full-scale experiments using controlled blasting were conducted in the port of Tokachi on Hokkaido Island, Japan, to assess the behavior of piles and pipelines subjected to lateral spreading. The test piles and pipelines were extensively instrumented with strain gages to measure the distribution of bending moment during lateral spreading which allowed the back-calculation of the loading conditions, as well as the assessment of damage and performance of the structures. Based on the test results, it was concluded that using controlled blasting successfully liquefied the soil and subsequently induced lateral spreading in the 4–6% surface slope test beds. The free-field soil displacements at the location of the test piles were over 40 cm for both tests. When compared with the results from the single pile case, the effect of pile-head restraint from the pile cap improved overall pile performance by decreasing the displacement of the pile groups and by lowering the maximum moments in individual piles within each group. Finally, back-calculated soil reactions indicated that the liquefied soil layer imparted insignificant force to the piles.

The potential of using the p - y analysis method for single piles and pile groups subjected to lateral spreading was evaluated. The computed responses were compared with the results from the full-scale lateral spreading tests. The responses of the single piles subjected to lateral spreading were determined by imposing the known free-field soil movement profile to the Winkler spring model. The soil springs of nonliquefied soils used in this study were based upon standard p - y springs, while zero spring stiffness was used for liquefied soils. For the case of pile groups, they were modeled as an equivalent single pile with a rotational spring at the pile head to simulate the effect of pile-head restraint. A decrease of soil spring stiffnesses using the p -multiplier approach was used to account for pile group effects. Based on the results of analyses, the computed responses of all sets of the test piles using a single set of baseline soil properties were in good agreement with the measured responses. These results suggest that the p - y analysis method may be used to estimate the behavior of piles subjected to lateral spreading.

CONTENTS

ABSTRACT	iii
ACKNOWLEDGMENTS	iv
EXECUTIVE SUMMARY	v
TABLE OF CONTENTS	vii
LIST OF FIGURES	xi
LIST OF TABLES	xvii
1 BACKGROUND	1
1.1 Introduction	1
1.2 Objectives.....	5
2 SOIL CHARACTERIZATION	7
2.1 Subsurface Investigation	7
2.2 Liquefaction Susceptibility Evaluation	11
3 PILOT TESTS	13
3.1 First Pilot Test.....	14
3.1.1 Single Borehole Tests	15
3.1.2 Embankment Test (ET).....	19
3.2 Second Pilot Test	21
3.2.1 Test Setup.....	22
3.2.2 Blasting Sequence	23
3.2.3 Test Results	24
4 FIRST FULL-SCALE LATERAL SPREADING TEST	29
4.1 Site Layout	29
4.2 Pile Description	32
4.3 Pipeline Description	39
4.4 Instrumentation	47
4.5 Blasting Sequence	52
4.6 Data-Acquisition System	53
4.7 Test Results	53

4.7.1	Excess Pore Pressure.....	53
4.7.2	Displacements of Soil and Test Lifelines.....	56
4.7.3	Pile and Pipeline Responses.....	63
4.7.4	Results from Other Instrumentation.....	72
5	SECOND FULL-SCALE LATERAL SPREADING TEST	81
5.1	Site Layout.....	81
5.2	Instrumentation	84
5.3	Blasting Sequence.....	84
5.4	Test Results.....	86
5.4.1	Excess Pore Pressure.....	86
5.4.2	Displacements of Soil and Test Lifelines.....	88
5.4.3	Pile and Pipeline Responses.....	93
5.4.4	Results from Other Instrumentation.....	101
5.5	Pile-Cap Condition after Test.....	108
6	ANALYSES OF PILE RESPONSES.....	111
6.1	Back-Calculation of Pile Responses	111
6.1.1	Single Pile	112
6.1.2	Pile Groups.....	114
6.2	Push-Over Analysis Using <i>p-y</i> Method.....	115
6.2.1	Concept of <i>p-y</i> Method	115
6.2.2	Analyses of Single Piles.....	117
6.2.3	Analyses of Pile Groups.....	120
6.2.4	Results of Analyses.....	126
6.2.5	Design Implications	132
7	SUMMARY AND CONCLUSIONS.....	135
	REFERENCES.....	137
	APPENDIX A SUMMARY OF SOIL PROPERTIES AND BORING LOGS	143
	APPENDIX B SWEDISH WEIGHT SOUNDING TEST RESULTS	159
	APPENDIX C SIEVE ANALYSIS RESULTS.....	173
	APPENDIX D EXCESS PORE-WATER PRESSURE DATA (FIRST TEST).....	179

APPENDIX E GPS DATA (FIRST TEST)	189
APPENDIX F INCLINOMETER DATA (FIRST TEST).....	207
APPENDIX G STRAIN GAGE DATA (FIRST TEST)	219
APPENDIX H EXCESS PORE-WATER PRESSURE DATA (SECOND TEST)	247
APPENDIX I GPS DATA (SECOND TEST)	255
APPENDIX J INCLINOMETER DATA (SECOND TEST).....	267
APPENDIX K STRAIN GAGE DATA (SECOND TEST)	279

LIST OF FIGURES

Fig. 1.1	Location map of Tokachi port, Hokkaido Island, Japan.....	2
Fig. 1.2	Aerial view of Tokachi port.....	2
Fig. 1.3	Layout of overall test site.....	4
Fig. 2.1	Location plan of four blast experiments at port of Tokachi, Japan	8
Fig. 2.2	Location plan of in-situ testing and soil boreholes	8
Fig. 2.3	Typical soil profile and soil strength characteristics at test site (a) soil profile, (b) standard penetration tests, (c) cone penetration tests, (d) Swedish weight sounding tests, (e) shear wave velocity tests, (f) soil relative density profile, (g) friction angle profile, (h) undrained shear strength profile	10
Fig. 2.4	Typical grain-size distribution of soil at test site	11
Fig. 3.1	ULTEX explosive	13
Fig. 3.2	Layout of first pilot test.....	14
Fig. 3.3	Layout of single borehole tests	15
Fig. 3.4	Photograph showing borehole locations for single borehole tests.....	16
Fig. 3.5	Blasting sequence for single borehole tests	17
Fig. 3.6	Relationship between excess pore-pressure ratio and scale distance (after Nagao et al. 2003)	18
Fig. 3.7	Contour of settlement in mm 11 days after single borehole tests (after Nagao et al. 2003)	18
Fig. 3.8	Layout of embankment test.....	19
Fig. 3.9	Photograph of embankment test.....	20
Fig. 3.10	Sequence of blasting for embankment test (ET).....	20
Fig. 3.11	Horizontal displacement vectors and contour of settlements (after Nagao et al. 2003)	21
Fig. 3.12	Layout of second pilot test.....	22
Fig. 3.13	Photograph showing front view of second pilot test.....	23
Fig. 3.14	Photograph showing side view of second pilot test	23
Fig. 3.15	Blasting sequence of second pilot test	24
Fig. 3.16	Excess pore-pressure responses during second pilot test.....	25
Fig. 3.17	Sand boils observed following second pilot test.....	26

Fig. 3.18	Horizontal displacement vectors and settlement contour (second pilot test).....	26
Fig. 3.19	Lateral movement of sheet pile wall after the test	27
Fig. 4.1	Layout of first full-scale lateral spreading experiment	30
Fig. 4.2	3D view of first full-scale lateral spreading experiment (PARI 2002).....	31
Fig. 4.3	Aerial photo of first full-scale lateral spreading experiment (PARI 2002)	31
Fig. 4.4	Layout of test piles.....	32
Fig. 4.5	Pile cross section.....	33
Fig. 4.6	Moment-curvature relationship of test pile.....	33
Fig. 4.7	Instrumentation of steel pipe piles	34
Fig. 4.8	Pile driving using diesel hammer.....	35
Fig. 4.9	Pile length left over after pile installation: (a) 4-pile group (left), (b) 9-pile group (right)	35
Fig. 4.10	Pile-cap details of 4-pile group.....	36
Fig. 4.11	Pile-cap details of 9-pile group.....	37
Fig. 4.12	Pile-cap construction for 9-pile group	38
Fig. 4.13	Instrumentation plan for (a) transverse gas-pipeline (b) transverse electrical conduit, and (c) longitudinal gas-pipeline	40
Fig. 4.14	Construction procedure of transverse pipelines.....	41
Fig. 4.15	Cross sections of multiple compacted layers for (a) pipelines A and B and (b) pipeline C	43
Fig. 4.16	Construction procedure of longitudinal pipeline	44
Fig. 4.17	Instrumentation layout for first full-scale lateral spreading test	48
Fig. 4.18	Layout of instrumentation in the area of test piles (area A)	49
Fig. 4.19	Layout of instrumentation in the area of test pipelines (area B).....	50
Fig. 4.20	Locations of soil pressure cells on pile caps.....	51
Fig. 4.21	Blasting sequence for first full-scale lateral spreading test	52
Fig. 4.22	Sand boils observed at the ground surface: (a) near test pile area, (b) near embankment area	54
Fig. 4.23	Excess pore-pressure time histories nearby 9-pile group	55
Fig. 4.24	Excess pore-water pressure ratio time history near 9-pile group.....	56
Fig. 4.25	Example of GPS data of unit GPS-1C (after Turner 2002)	57
Fig. 4.26	Horizontal displacement vectors after the test.....	60

Fig. 4.27	Soil displacement profiles (a) S5 (level ground) and (b) S10 (embankment)	62
Fig. 4.28	Comparison of surface displacements from inclinometer and GPS unit	63
Fig. 4.29	Strain and moment profiles of single pile (No.9) after the test.....	64
Fig. 4.30	Strain and moment profiles of pile No. 7 (4-pile group) after the test.....	65
Fig. 4.31	Strain and moment profiles of pile No. 8 (4-pile group) after the test.....	65
Fig. 4.32	Strain and moment profiles of pile No. 1 (9-pile group) after the test.....	66
Fig. 4.33	Strain and moment profiles of pile No. 2 (9-pile group) after the test.....	67
Fig. 4.34	Strain and moment profiles of pile No. 3 (9-pile group) after the test.....	67
Fig. 4.35	Strain and moment profiles of pile No. 4 (9-pile group) after the test.....	68
Fig. 4.36	Strain and moment profiles of pile No. 5 (9-pile group) after the test.....	68
Fig. 4.37	Strain and moment profiles of pile No. 6 (9-pile group) after the test.....	69
Fig. 4.38	Strain distribution along transverse pipelines: (a) side gages and (b) top gages	70
Fig. 4.39	Strain distribution along longitudinal pipeline: (a) side gages and (b) top and bottom gages	71
Fig. 4.40	Soil pressure time histories on pile caps	73
Fig. 4.41	Pile-head accelerations for (a) single pile, (b) 4-pile group, (c) 9-pile group	74
Fig. 4.42	Pile-head rotations for (a) single pile, (b) 4-pile group, (c) 9-pile group	75
Fig. 4.43	Relative displacement between (a) S1 and 9-pile group, (b) S2 and 9-pile group, and (c) S7 and single pile.....	78
Fig. 4.44	Relative displacement between (a) S8 and 4-pile group, (b) S11 and W1 pile, and (c) S11 and W2 pile	79
Fig. 4.45	Relative displacement between (a) pile W1 and pile W3, (b) 4-pile group and anchor pile, and (c) anchor pile and quay wall	80
Fig. 5.1	Layout of second full-scale lateral spreading test.....	82
Fig. 5.2	Site condition of second full-scale lateral spreading test (front)	83
Fig. 5.3	Site condition of second full-scale lateral spreading test (side).....	83
Fig. 5.4	Bad weather during the second test	84
Fig. 5.5	Layout of instrumentation for second full-scale lateral spreading test.....	85
Fig. 5.6	Blasting sequence for second full-scale lateral spreading test.....	86
Fig. 5.7	Excess pore-pressure time history nearby 9-pile group.....	87
Fig. 5.8	Observed settlement near 9-pile group (one day after the first experiment)	88
Fig. 5.9	Horizontal displacement vectors after second test.....	91

Fig. 5.10	Displacement time histories of GPS unit 2E.....	91
Fig. 5.11	Soil displacement profiles obtained from slope inclinometer (S8).....	93
Fig. 5.12	Strain and moment profiles of single pile after second full-scale lateral spreading test.....	94
Fig. 5.13	Strain and moment profiles of pile No. 7 of 4-pile group after second full-scale lateral spreading test	95
Fig. 5.14	Strain and moment profiles of pile No. 8 of 4-pile group after second full-scale lateral spreading test	95
Fig. 5.15	Strain and moment profiles of pile No. 1 of 9-pile group after second full-scale lateral spreading test	96
Fig. 5.16	Strain and moment profiles of pile No. 2 of 9-pile group after second full-scale lateral spreading test	97
Fig. 5.17	Strain and moment profiles of pile No. 3 of 9-pile group after second full-scale lateral spreading test	97
Fig. 5.18	Strain and moment profiles of pile No. 4 of 9-pile group after second full-scale lateral spreading test	98
Fig. 5.19	Strain and moment profiles of pile No. 5 of 9-pile group after second full-scale lateral spreading test	98
Fig. 5.20	Strain and moment profiles of pile No. 6 of 9-pile group after second full-scale lateral spreading test	99
Fig. 5.21	Profiles of additional strain along pipeline A in second test: (a) side gages and (b) top gages.....	100
Fig. 5.22	Profiles of additional strain along pipeline B in second test: (a) side gages and (b) top gages.....	101
Fig. 5.23	Pile-head acceleration time histories in second test: (a) single pile, (b) 4-pile group, (c) 9-pile group	102
Fig. 5.24	Pile-head rotations for (a) single pile, (b) 4-pile group, (c) 9-pile group	103
Fig. 5.25	Relative displacement between (a) S1 and 9-pile group, (b) S2 and 9-pile group, and (c) S7 and single pile, second blast test.....	105
Fig. 5.26	Relative displacement between (a) S8 and 4-pile group, (b) S11 and W1 pile, and (c) S11 and W2 pile, second blast test	106

Fig. 5.27	Relative displacement between (a) pile w1 and pile w3, (b) 4-pile group and reference post, and (c) 9-pile group and reference post.....	107
Fig. 5.28	Relative displacement between single pile and reference post.....	108
Fig. 5.29	Concrete spalling underneath pile cap of 4-pile group (pile N3).....	109
Fig. 5.30	Concrete spalling underneath pile cap of 9-pile group (pile No. 8).....	109
Fig. 6.1	Back-calculated pile responses (a) single pile, (b) 4-pile group, (c) 9-pile group.....	113
Fig. 6.2	Moment distribution of each pile from first full-scale test: (a) 4-pile group and (b) 9-pile group	114
Fig. 6.3	Concept of p - y curves to account for movement of soil mass (after Reese et al. 2000)	116
Fig. 6.4	p - y analysis model for single pile subjected to lateral spreading.....	117
Fig. 6.5	p - y analysis model for single pile	118
Fig. 6.6	p - y analysis model for pile group (after Mokwa 1999)	121
Fig. 6.7	Relationships between p -multiplier and pile spacing for each row in the group (after Mokwa 1999)	122
Fig. 6.8	Conceptual model for estimating pile group rotational restraint: (a) pile-cap rotational restraint model, (b) assumed linear relationship between M and θ (c) schematic diagrams for estimating ultimate pile-cap rotation (after Mokwa and Duncan 2003).....	124
Fig. 6.9	Comparison between measured and computed pile responses for UCSD single pile (flexible pile) for first and second tests.....	126
Fig. 6.10	Pile-head displacement and maximum moment vs. ground surface displacement for UCSD single pile: (a) assume linear pile and (b) nonlinear pile.....	128
Fig. 6.11	Comparison between measured and computed pile responses for WU single piles (rigid piles) for first test	128
Fig. 6.12	Comparison between measured and computed pile responses for 4-pile group for first test.....	130
Fig. 6.13	Comparison between measured and computed pile responses for 9-pile group for first test.....	130
Fig. 6.14	Pile-head displacement and maximum moment vs. ground surface displacement: (a) 4-pile group and (b) 9-pile group	131

LIST OF TABLES

Table 1.1	Participants in the Japan lateral spreading test	4
Table 3.1	Summary of ULTEX characteristics (after Nagao et al. 2003)	13
Table 3.2	Specification of explosives used for single borehole tests	16
Table 4.1	Summary of final pile length	34
Table 4.2	Summary of concrete strength of pile caps.....	37
Table 4.3	Summary of field density test results for transverse pipelines	45
Table 4.4	Summary of field density test results for longitudinal pipeline.....	46
Table 4.5	Summary of Caltrans' GPS data, approximately 1 minute following blasting	58
Table 4.6	Summary of Caltrans' GPS data, approximately 22 hours following blasting.....	59
Table 4.7	Summary of WU's GPS data, approximately 30 minutes following blasting.....	59
Table 4.8	Summary of measured soil displacements at ground surface from inclinometers	62
Table 4.9	Summary of relative displacements obtained from linear potentiometers	77
Table 4.10	Verification of GPS measurements with data from potentiometers	77
Table 5.1	Summary of GPS data for second Japan blast test, approximately 1.3 minutes following blasting (data from Caltrans).....	89
Table 5.2	Summary of GPS data for second Japan blast test, approximately 20 hours following blasting (data from Caltrans).....	89
Table 5.3	Summary of displacement at ground surface from slope inclinometer data, second blast test	92
Table 5.4	Summary of relative displacements after second full-scale lateral spreading test ...	104
Table 5.5	Verification of GPS measurements with data from potentiometers	104
Table 6.1	Summary of soil properties used in analyses of piles subjected to lateral spreading.....	119
Table 6.2	Summary of soil parameters and estimated ultimate pile skin resistance	125

1 Background

1.1 INTRODUCTION

In past earthquakes, liquefaction-induced lateral spreading has caused considerable damage to deep foundations, which in turn has resulted in damage to the superstructures, including port facilities, buildings, and bridges. Examples of damage to deep foundations due to lateral spreading include the foundation piles of the Yachiyo and Showa bridges and the NFCH building during the 1964 Niigata, Japan, earthquake (Hamada 1992); the railway bridge foundations during the 1991 Limon, Peru, earthquake (Youd et al. 1992); and the batter piles supporting the 7th Street Terminal Wharf in the 1989 Loma Prieta, California, earthquake (Benuzka 1990). In addition to pile foundations, lateral spreading has also caused damage to numerous gas pipelines resulting in a large destructive fire in the 1906 San Francisco earthquake; and significant damage in that area in the Loma Prieta earthquake. Based on these past examples, it is essential to gain better understanding of the behavior of piles and pipelines during lateral spreading in order to improve current design methods for these structures and prevent catastrophic failure during future earthquakes. Most liquefaction and lateral spreading research to date for deep foundations has focused on small-scale centrifuge studies (e.g., Abdoun et al. 1996; Ramos et al. 2000; Wilson et al. 2000; Dobry and Abdoun 2001), limited area 1g shake table tests (e.g., Tokida et al. 1993; Hamada 2000; Meneses et al. 2002), or case histories (e.g., Hamada and O'Rourke 1992; O'Rourke 1996). Alternatively, some full-scale testing has been carried out to study behavior of deep foundations in sand liquefied by controlled blasting (e.g., Ashford et al. 2000; Ashford and Rollins 2002), but these tests were conducted on level ground and did not account for kinematic loading from laterally spreading soil.

In light of this, several full-scale instrumented piles and pipelines were subjected to blast-induced lateral spreading in experiments carried out in November and December 2001 in the port of Tokachi on Hokkaido Island, Japan, as shown in Figures 1.1–1.2. The objectives of the study were

to conduct damage and performance assessments of the piles and pipelines, as well as to evaluate loading conditions on the structures due to the kinematic loading from laterally spreading soils. The test results will be a valuable source of data for further development of the state of practice of seismic design of deep foundations, as well as pipelines against liquefaction-induced lateral spreading.

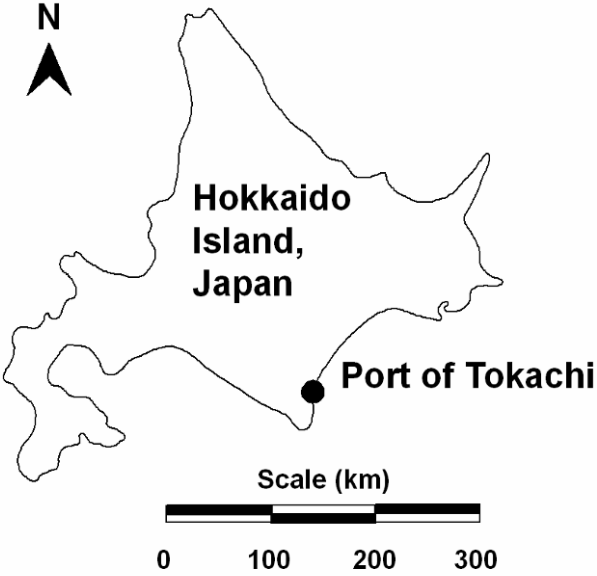


Fig. 1.1 Location map of Tokachi port, Hokkaido Island, Japan



Fig. 1.2 Aerial view of Tokachi port

This research project was the joint collaboration between the University of California, San Diego, (UCSD) and several Japanese organizations as summarized in Table 1.1. The overall research effort was lead by the Port and Airport Research Institute (PARI), with a primary objective of assessing the performance of two different quay walls subjected to lateral spreading as shown in Figure 1.3. One quay wall was of traditional design, and new seismic design criteria were applied to the other. Since the test area was so large, it enabled researchers to include additional experiments in the zone of liquefaction and lateral spreading without interfering with the primary objective of the quay wall test. Through the PEER Lifelines Program, with support from the California Department of Transportation (Caltrans), Pacific Gas & Electric, and the California Energy Commission, UCSD and Waseda University (WU) collaborated with other Japanese researchers to install test piles and pipelines in the zone of the traditional design quay wall where lateral spreading was expected. Examples of key experiments conducted by other researchers are an experiment by WU on the behavior of rigid piles; study by the National Institute for Land Infrastructure Management of impervious sheet behaviors during lateral spreading; a study by the University of California, Berkeley (UCB), of the influence of improvement depth on the degree of settlement induced by liquefaction; and an uplift experiment by the Japanese Geotechnical Society on structures buried due to soil liquefaction.

In summary, UCSD installed three instrumented pile foundation systems and three instrumented pipelines as shown in Figure 1.3. The pile foundation consisted of a single pile, a 4-pile group, and a 9-pile group. The pipelines consisted of two natural gas pipelines and one electrical conduit. One of the natural gas pipelines and electrical conduit were installed perpendicular to the direction of flow. The other gas pipeline was installed parallel to the direction of flow. Prior to the full-scale lateral spreading tests, two pilot tests were conducted in order to determine the specifications of the explosives such as blast hole configuration, charge size, charge depths, and time delay in blasting, etc. The details of each experiment are described in the subsequent chapters.

Table 1.1 Participants in the Japan lateral spreading test

Universities /Institutes	Industrial Participants
Port and Airport Research Institute (PARI) Civil Engineering Research Institute Waseda University University of Tokyo University of California, Berkeley University of California, San Diego PEER Japanese Geotechnical Society (JGS) Chuo University National Institute for Land and Infrastructure Management National Institute of Advanced Industrial Science and Technology	Japan Reclamation & Dredging Association Japan Association for Steel Piles Japan Association for Marine Structures Japan Gas Association Tokyo Electric Power Company Kanden Kogyo Sato Kogyo Caltrans Pacific Gas & Electric California Energy Commission Cement Deep Mixing Association Permeable Grouting Method Association

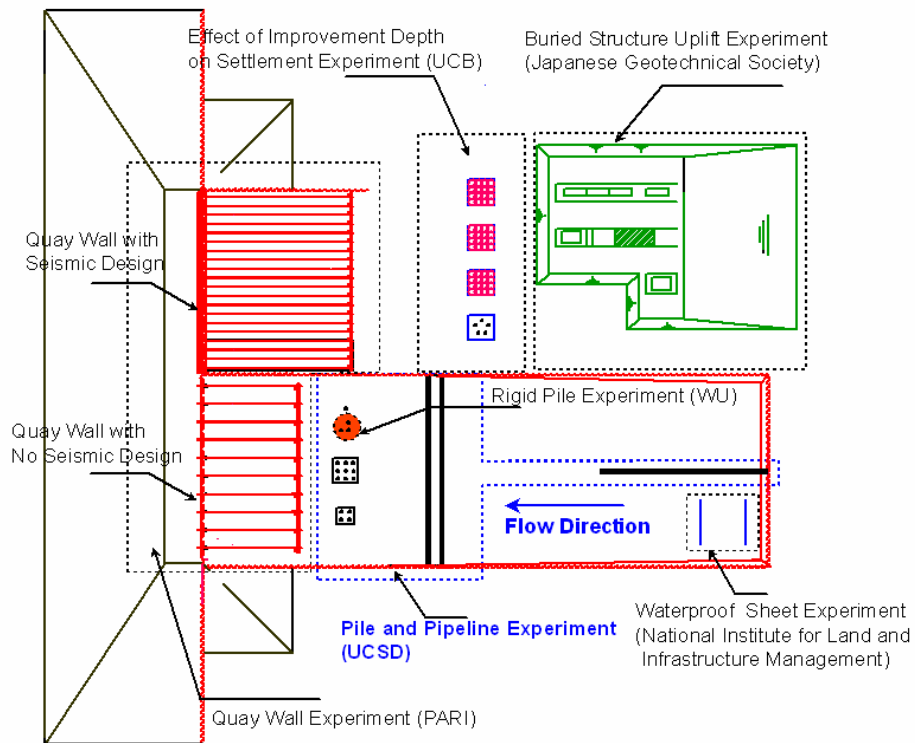


Fig. 1.3 Layout of overall test site

1.2 OBJECTIVES

Specifically, the objectives of this research study can be summarized as follows:

- Conduct damage and performance assessments of a single pile, a 4-pile group, and a 9-pile group subjected to lateral spreading.
- Conduct damage and performance assessments of natural gas pipelines as well as an electrical conduit subjected to lateral spreading.
- From instrumentation in the piles and pipelines, evaluate loading conditions on the structures during lateral spreading.
- Utilize simple numerical models (i.e., push-over analysis using the p - y method) to analyze the behavior of single piles and pile groups subjected to lateral spreading.
- Utilize developing numeral platforms within PEER (OpenSees) to gain better understanding on the behavior of piles and pipelines subjected to lateral spreading (ongoing research).

2 Soil Characterization

The test site is composed of man-made fill, placed approximately two years before conducting the experiments. It was built as a part of an expansion of the Tokachi port capacity by hydraulically placing fill without any ground improvement; as a result, the soil was very loose and highly susceptible to liquefaction. The details of soil conditions and the results from several in-situ tests are described in this chapter.

2.1 SUBSURFACE INVESTIGATION

A total of four tests were conducted at the test site, including two pilot tests and two full-scale lateral spreading tests, as shown in Figure 2.1. During the planning stage, three boreholes (i.e., No. 1, No. 2, and No. 3) were drilled to initially characterize the soil condition and decide whether or not the site was appropriate for lateral spreading experiments. A summary of soil properties of individual boreholes is presented in Appendix A. In addition to the soil boring investigation, a large number of Swedish weight sounding tests were carried out in several areas throughout the site. Locations of Swedish weight sounding tests are shown in Figure 2.2. The results of individual Swedish weight sounding tests are given in Appendix B.

Based on the preliminary boring logs and results from Swedish weight sounding tests, it was found that the first 6–7 m was hydraulic fill consisting of very loose silty sand with the SPT N-values of less than 10. In addition, a Japanese criterion for liquefaction evaluation based on grain-size distribution (PHRI 1997) indicated that most of the soil was susceptible to liquefaction. As a result, the site was chosen for full-scale lateral spreading experiments.

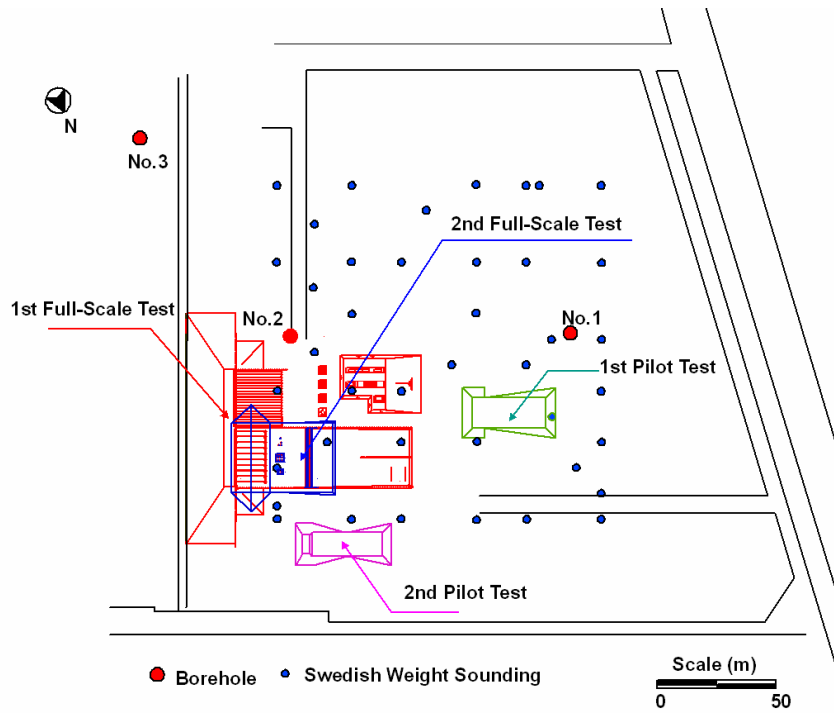


Fig. 2.1 Location plan of four blast experiments at port of Tokachi, Japan

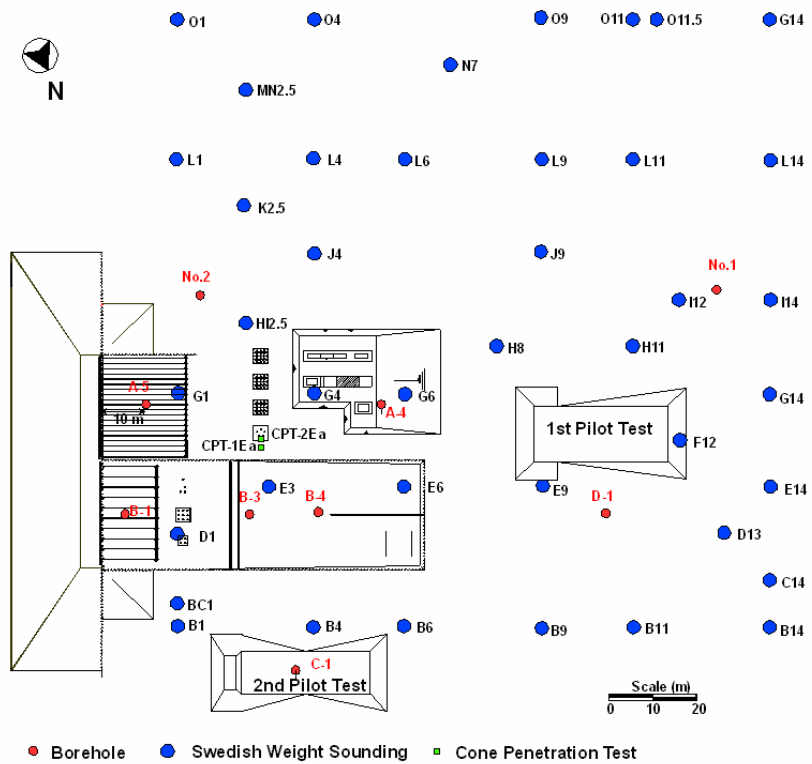


Fig. 2.2 Location plan of in-situ testing and soil boreholes

After the preliminary soil investigation, an additional subsurface soil exploration program was carried out in several areas throughout the site to obtain soil information in more details. Seven additional soil boreholes were drilled as shown in Figure 2.2. Individual boring logs and a summary of soil properties are given in Appendix A. Other field in-situ testing included cone penetration tests and down-hole shear wave velocity tests.

Figure 2.3 shows a typical soil profile in the vicinity of the UCSD test area, together with in-situ test results. Generally, the soil profile consisted of 7.5 m of hydraulic fill, underlain by 1-m of medium dense sand overlying a very dense gravel layer. The groundwater table was approximately 1 m below the ground surface. The hydraulic fill consisted of a 4-m layer of very loose to loose silty sand (SM) underlain by a 3.5-m layer of very soft lean to fat clay with sand (CL to CH). The SPT N-values (Fig. 2.3b) for cohesionless soils presented herein were corrected for field procedures and overburden pressure using the method proposed by Seed and Harder (1990). Only field procedures were used to correct the SPT N-values for the clay layer. Shear wave velocities of less than 100 m/s (Fig. 2.3e) indicate that the soil strength of the hydraulic fill layer was very low.

The SPT, CPT, and SWS results were used to estimate soil properties. The SWS results for the cohesionless soils were converted to SPT N-values using a correlation proposed by JIS A 1221-199 (Japanese Geotechnical Society 1995). The relative density of cohesionless soils (Fig. 2.3f) was estimated using correlations proposed by Peck et al. (1974) for the SPT N-values, and Kulhawy and Mayne (1990) for the CPT results. The soil friction angle (Fig. 2.3g) was then estimated from the relative density using the Peck et al. (1974) correlation. The undrained shear strength of the clay layer (Fig. 2.3h) was estimated using correlations proposed by Lunne and Kleven (1982) for the CPT results, NAVFAC (1982) for the SPT N-values, and Bergdahl et al. (1988) for the SWS results. The undrained shear strength of the clay layer based on unconfined compression tests was also plotted in Figure 2.3h for comparison. A review of Figure 2.3 shows that the friction angles obtained from different in-situ tests were in reasonable agreement. The undrained shear strength of the clay layer averaged 15 kN/m².

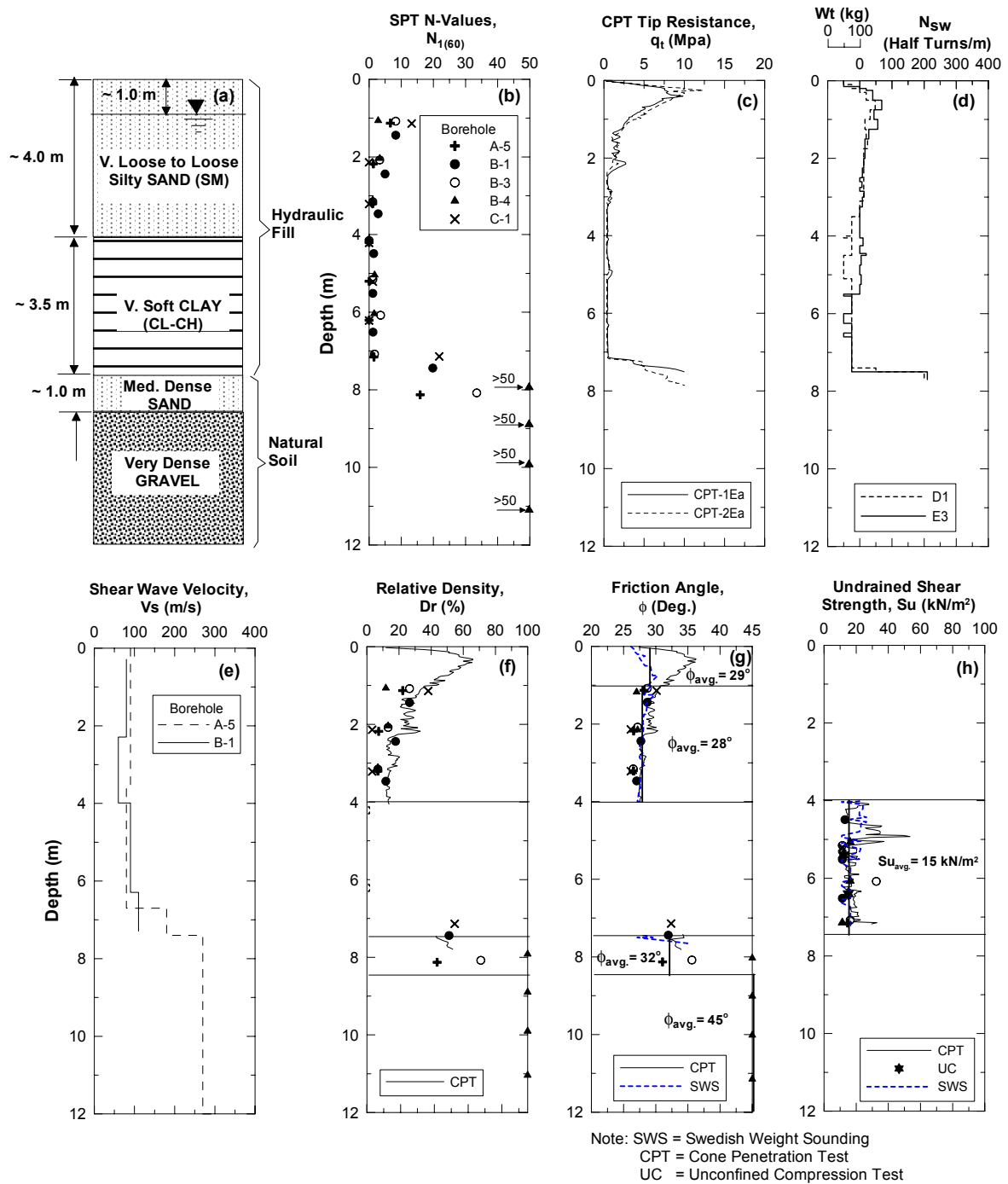


Fig. 2.3 Typical soil profile and soil strength characteristics at test site: (a) soil profile, (b) standard penetration tests, (c) cone penetration tests, (d) Swedish weight sounding tests, (e) shear wave velocity tests, (f) soil relative density profile, (g) friction angle profile, (h) undrained shear strength profile

2.2 LIQUEFACTION SUSCEPTIBILITY EVALUATION

Two different criteria, a U.S. criterion (Seed and Idriss 1971) and a Japanese criterion (PHRI 1997), were used to evaluate the liquefaction susceptibility of the soils at the test site. Using the U.S. criterion, the first and second sand layers below the groundwater table (Fig. 2.3) are susceptible to liquefaction, while the middle clay layer (i.e., fines content greater than 50%) is not liquefiable. Typical grain-size distribution curves of the soils plotted with the Japanese standard curves for liquefaction potential evaluation are shown in Figure 2.4. Grain-size distribution curves of other boreholes are summarized in Appendix C. Generally, the fines content gradually increases with depth. The results indicate that the soils in the first and second sand layers are highly susceptible to liquefaction. Most parts of the grain-size distribution curves of the clay layer, between 4m and 7m deep, are within the “susceptible to liquefaction” zone. As a result, this layer may be liquefiable according to the Japanese criterion. However, the results of pile bending moments in Chapter 4 indicate that the clay layer was not liquefiable. Only the sand layer experienced strength loss due to soil liquefaction, while the clay layer imparted driving force to the piles. As a result, in this study the U.S. criterion appears to be more appropriate for liquefaction susceptibility evaluation.

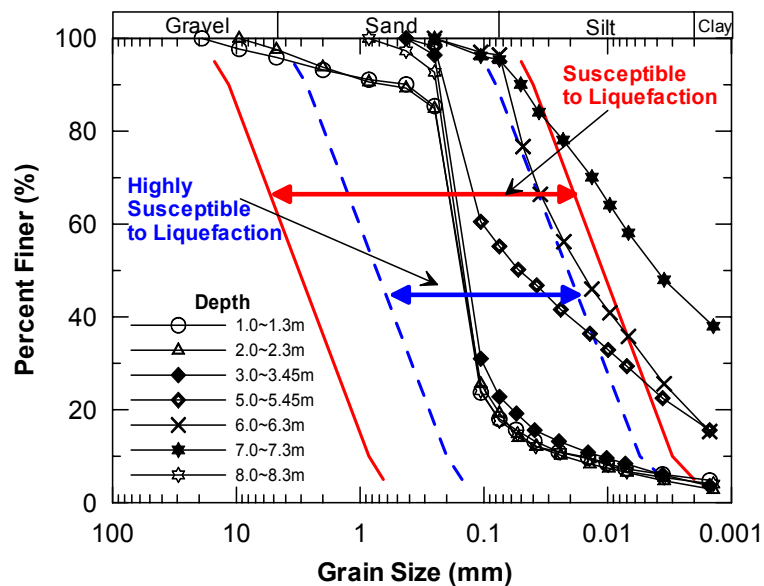


Fig. 2.4 Typical grain-size distribution of soil at test site

3 Pilot Tests

Controlled blasting has been a successful method of inducing liquefaction as reported by several researchers (e.g., Ashford et al. 2000; Charlie et al. 1992; Gohl et al. 2001; Narin van Court and Mitchell 1994; Rollins et al. 2004). This technique was used to liquefy the soil for the experiments, and thus induce lateral spreading. Before performing the full-scale lateral spreading experiments, two pilot tests were carried out to determine blasting specifications to be used in the actual full-scale tests, including optimum charge weights, locations of charges, and time delay in blasting. This was to ensure that the soil can be successfully liquefied and the amount of global translation of the soil satisfied the requirement. The locations of each pilot test are presented in Figure 2.1. The explosives used in the tests were ULTEX (Fig. 3.1), a water gel-type emulsion explosive (Nagao et al. 2003). The characteristics of ULTEX are summarized in Table 3.1. The detonator used in this study was a low-energy nonelectric signal conductor. More detail regarding the explosives can be obtained elsewhere in Nagao et al. 2003.



Fig. 3.1 ULTEX explosive

Table 3.1 Summary of ULTEX characteristics (after Nagao *et al.* 2003)

Unit Weight (gram/cc)	Detonation Velocity (m/sec)	Ballistic Pendulum (mm)	Water Resistance
1.15~1.23	5,800~6,000	78~84	Very good

3.1 FIRST PILOT TEST

The layout of the first pilot test is presented in Figure 3.2. The first pilot test was carried out in June 2001, which consisted of two different kinds of experiments; the first one, as shown on the left, was single borehole tests (SBT) and the other one, as shown on the right, was an embankment test (ET). The SBT was aimed at deciding blasting sequence, optimum explosive weight, and depth of explosive. The ET was to determine the amount of lateral spreading caused by blast-induced liquefaction.

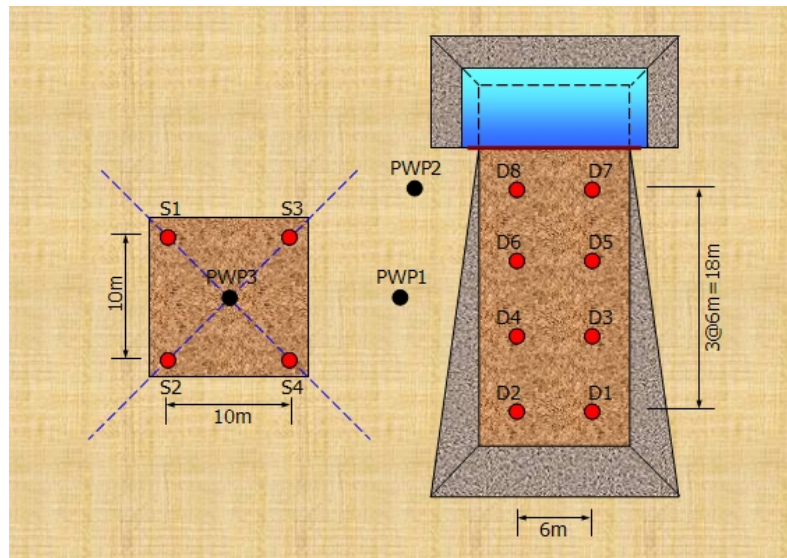


Fig. 3.2 Layout of first pilot test

3.1.1 Single Borehole Tests

3.1.1.1 Test Setup

For the SBT, boreholes were spaced at 10 m intervals as shown in Figure 3.3. A photograph of the SBT site is shown in Figure 3.4. The effects of explosive weight, depth of explosive, and order of blasting on excess pore-water pressure response were studied in order to assist the researchers in deciding the blasting specification in the full-scale lateral spreading tests. For S1 and S2, the explosives were installed at 5 m depth, while for S3 and S4 they were installed at depths of 5 m and 10 m below the ground surface. The weight of explosives for each borehole was 2–3 kgf as summarized in Table 3.2.

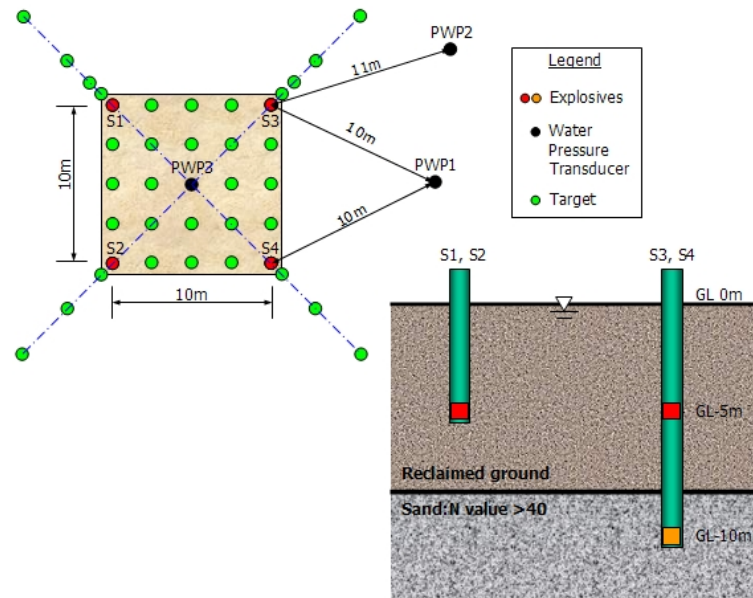


Fig. 3.3 Layout of single borehole tests



Fig. 3.4 Photograph showing borehole locations for single borehole tests

Table 3.2 Specification of explosives used for single borehole tests

Borehole	Depth below Ground Surface (m)	Charge Weight (kgf)
S1	5	2
S2	5	3
S3, S4	5	3
	10	3

3.1.1.2 Blasting Sequence

The sequence of the tests was S1, S2, S3, and S4, respectively; i.e., the following single borehole test was carried out after the excess pore-water pressure induced by the previous test adequately dissipated. For the S3 test, the sequence of blasting began from the lower depth to the upper depth, while for the S4 test the blasting sequence began from the upper depth to the lower depth as shown in Figure 3.5. The time interval between the blasts of the upper and lower explosives was 0.3 sec.

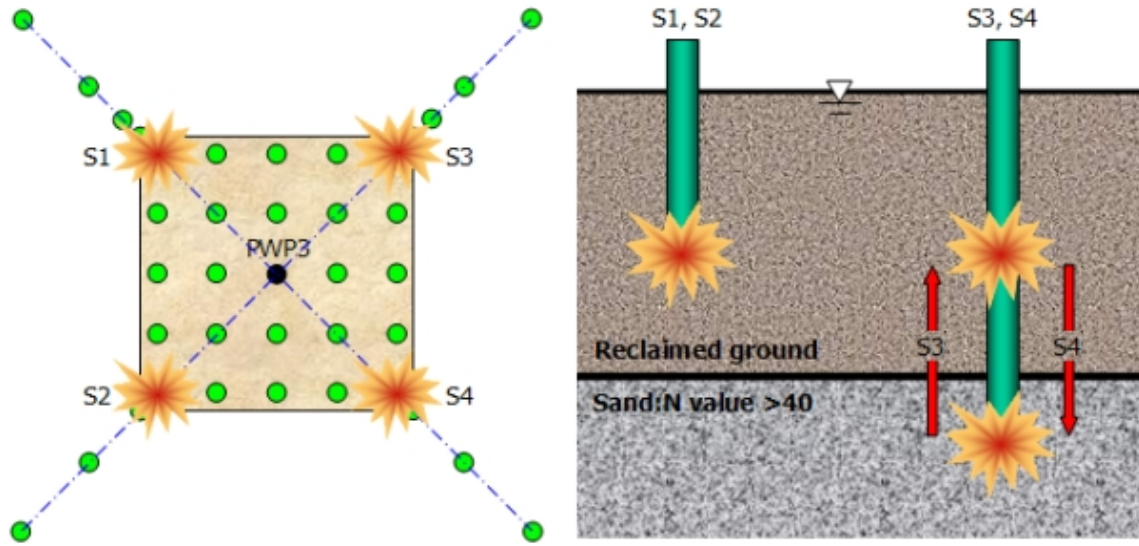


Fig. 3.5 Blasting sequence for single borehole tests

3.1.1.3 Test Results

A comparison of results from S1 and S2 tests shows that increasing the explosive weight resulted in higher excess pore-water pressure ratio, R_u . In addition, the excess pore-water pressure decreased with increasing the distance from the blast hole. The R_u depended not only on explosive weight and distance from explosive but also sequence of blasting. Nagao et al. (2003) found that blasting from the bottom to the top was more effective than from the top to the bottom.

Based on the excess pore-pressure data from a series of single borehole tests, a relationship between excess pore-pressure ratio and scale distance was developed as shown in Figure 3.6. Scale distance, R_w , is defined as $R_w = R / W^{(1/3)}$, where R is a distance from boreholes in meter and W is amount of explosive in kgf. Scale distance represents the average energy per unit area. It was found that the relationship can be defined as

$$R_u = 8.284R_w^{-2.107} \quad (3.1)$$

Nagao et al. (2003) used the relationship shown in Equation (3.1) to determine the amount of explosive charge and the pattern to be used in future full-scale testing. It was found that using 3 kg explosives at 2 depths with 6 m blast hole spacing, corresponding to R_w of 1.47 ($R = 4.24$ m, $W = 3$ kgf * 2 depths * 4 boreholes = 24 kgf), would yield the excess pore-water pressure of greater than 1.0 at the center of the blasting area, indicating sufficient blasting energy to liquefy the soil. Figure

3.7 shows settlement contours due to the dissipation of excess pore pressure 11 days after the blasting.

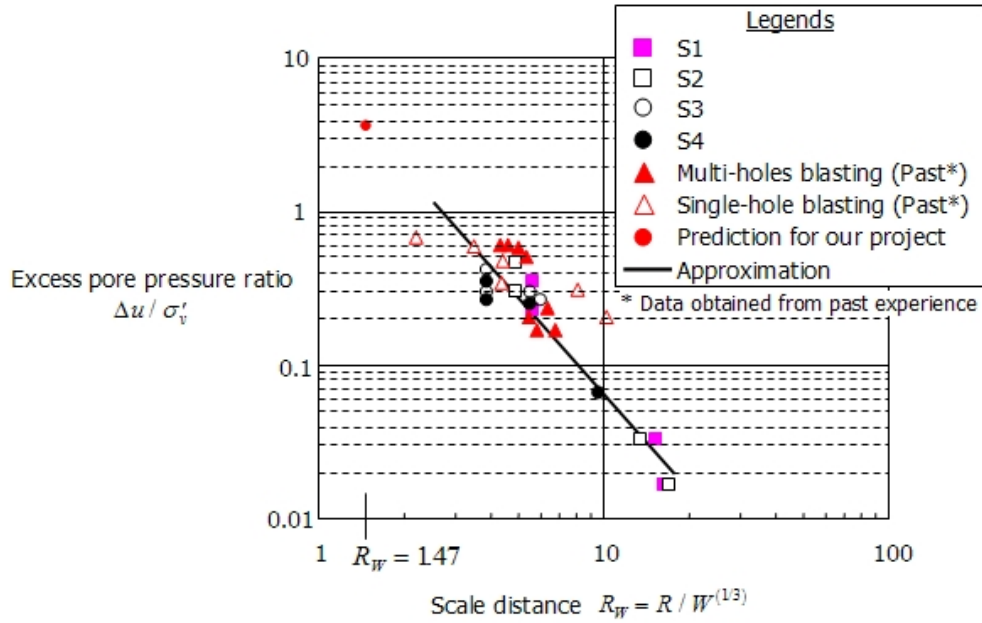


Fig. 3.6 Relationship between excess pore-pressure ratio and scale distance (after Nagao et al. 2003)

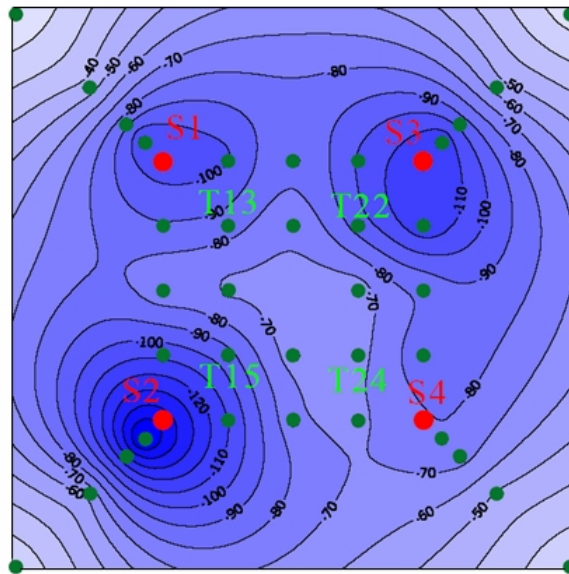


Figure 3.7 Contour of settlement in mm 11 days after single borehole tests (after Nagao et al. 2003)



Fig. 3.9 Photograph of embankment test

3.1.2.2 Blasting Sequence

The sequence of blasting is illustrated in Figure 3.10. The blasting first began at the lower layer from borehole D1 and continued subsequently to borehole D7. After that, the upper layer with the same order as the lower layer was detonated.

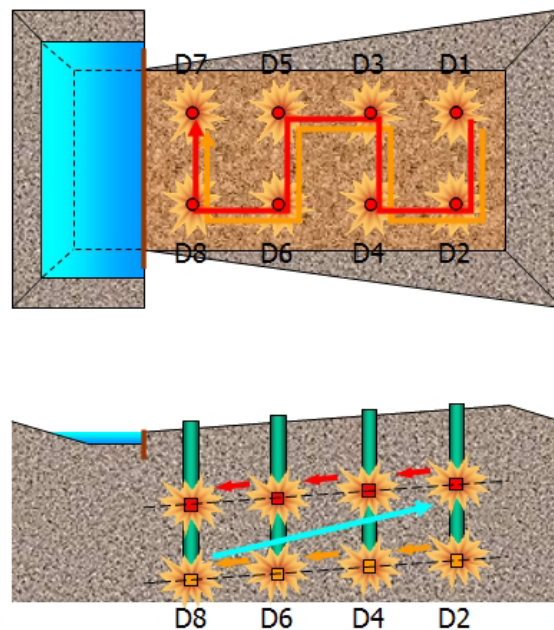


Fig. 3.10 Sequence of blasting for embankment test (ET)

3.1.2.3 Test Results

Horizontal ground displacement vectors, together with settlement contour at 10 days after blasting are shown in Figure 3.11. The maximum settlement reached 18 cm at the center of the embankment, and the maximum horizontal displacement was 16 cm at the quay wall. These horizontal displacements appeared to be not adequate for the purpose of future full-scale lateral spreading tests. As a result, the second pilot test was carried out in an attempt to increase the amount of lateral spreading. Details of the second pilot test are described in the following section.

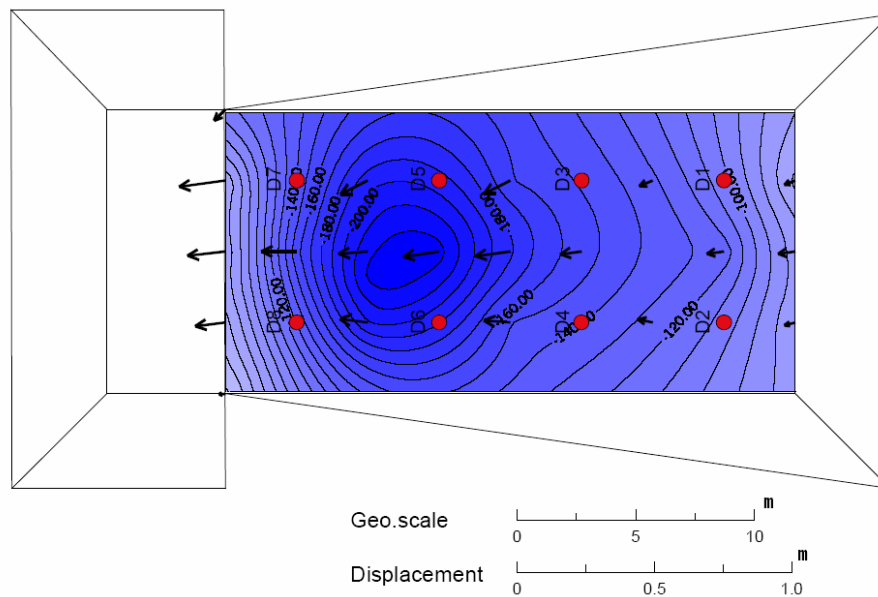


Fig. 3.11 Horizontal displacement vectors and contour of settlements (after Nagao et al. 2003)

3.2 SECOND PILOT TEST

The second pilot test was carried out on September 14, 2002. The main objective of this test was to ensure that adequate lateral spreading caused by blast-induced liquefaction could be obtained. This was done by increasing the length of the embankment, making the slope of embankment steeper, and modifying the blasting sequence.

3.2.1 Test Setup

Layout of the second pilot test is presented in Figure 3.12. Photographs of the test site are shown in Figures 3.13–3.14. The length of the embankment was increased from 24 m in the first pilot test to 30 m in the second pilot test. The embankment in the second test was steeper, with 7% slope. Blast holes were spaced at 6.0 m on center in the regular grid pattern as similar to the first pilot test. However, the number of blast holes was increased from 8 holes to 10 holes as denoted by M1 to M10. Explosives were installed in each borehole at depths of 3m and 6m below the ground surface. The amount of charge was 3 kg at each depth. Several pore-pressure transducers were installed in various locations as denoted by PWP1 to PWP6 to measure an increase in pore-water pressure during the test.

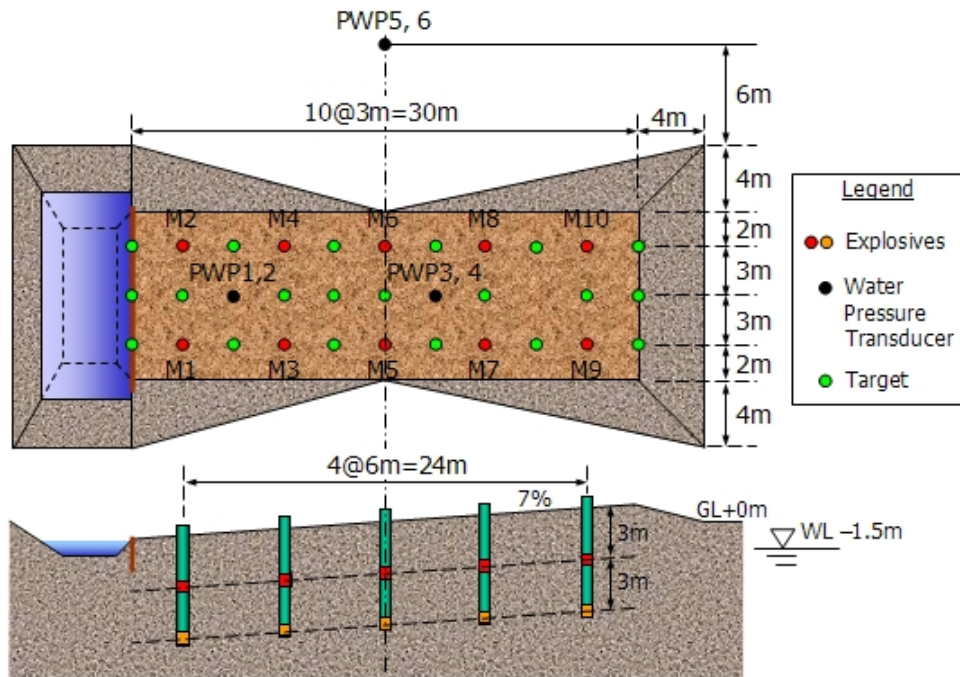


Fig. 3.12 Layout of second pilot test



Fig. 3.13 Photograph showing front view of second pilot test



Fig. 3.14 Photograph showing side view of second pilot test

3.2.2 Blasting Sequence

The sequence of the blasting in the second pilot test was different from that of the first pilot test; i.e., for ET, all of the lower explosives were detonated first, followed by the upper explosives, while for the second pilot test the upper explosive of the same borehole was detonated just after the lower explosive as shown in Figure 3.15. The explosive at the back corner of the embankment (M9) was initially detonated and continued one after the other toward the waterway (M2).

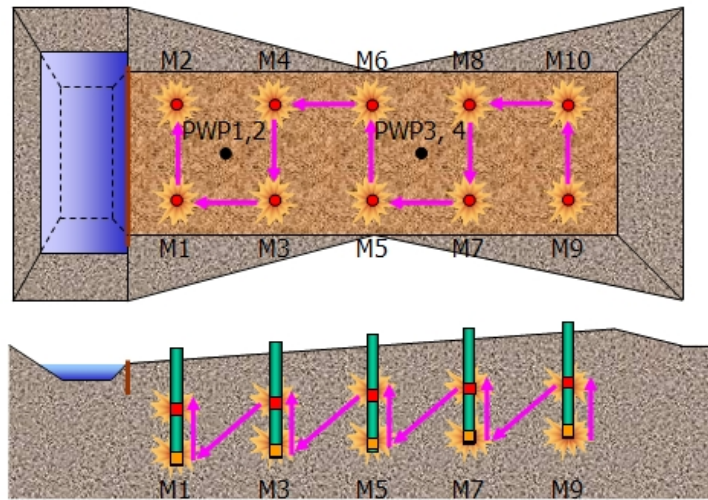


Fig. 3.15 Blasting sequence of second pilot test

3.2.3 Test Results

Figure 3.16 shows excess pore-pressure responses at multiple depths measured during the test, together with their effective vertical stresses. The excess pore-pressure ratios after the blast were generally over 60% in several locations. Two of them were close to 100%. Sand boils as shown in Figure 3.17 were observed in several places, which confirmed that the soil was successfully liquefied.

Figure 3.18 shows the vector displacements and contour of settlement after the completion of the test. The results indicate that the maximum surface soil movement was about 70 cm at the sheet pile wall. Figure 3.19 shows a photograph of the movement of sheet pile after the test. The magnitude of these horizontal movements, as well as direct evidence of liquefaction in the second pilot test indicate that the blasting specification used in the second pilot test met the researcher's requirement, and therefore was appropriate to use in the future full-scale lateral spreading experiments to cause sufficient liquefaction and lateral spreading. The success of the second pilot test led the research teams to advance to the full-scale lateral spreading experiments as described in the following chapters.

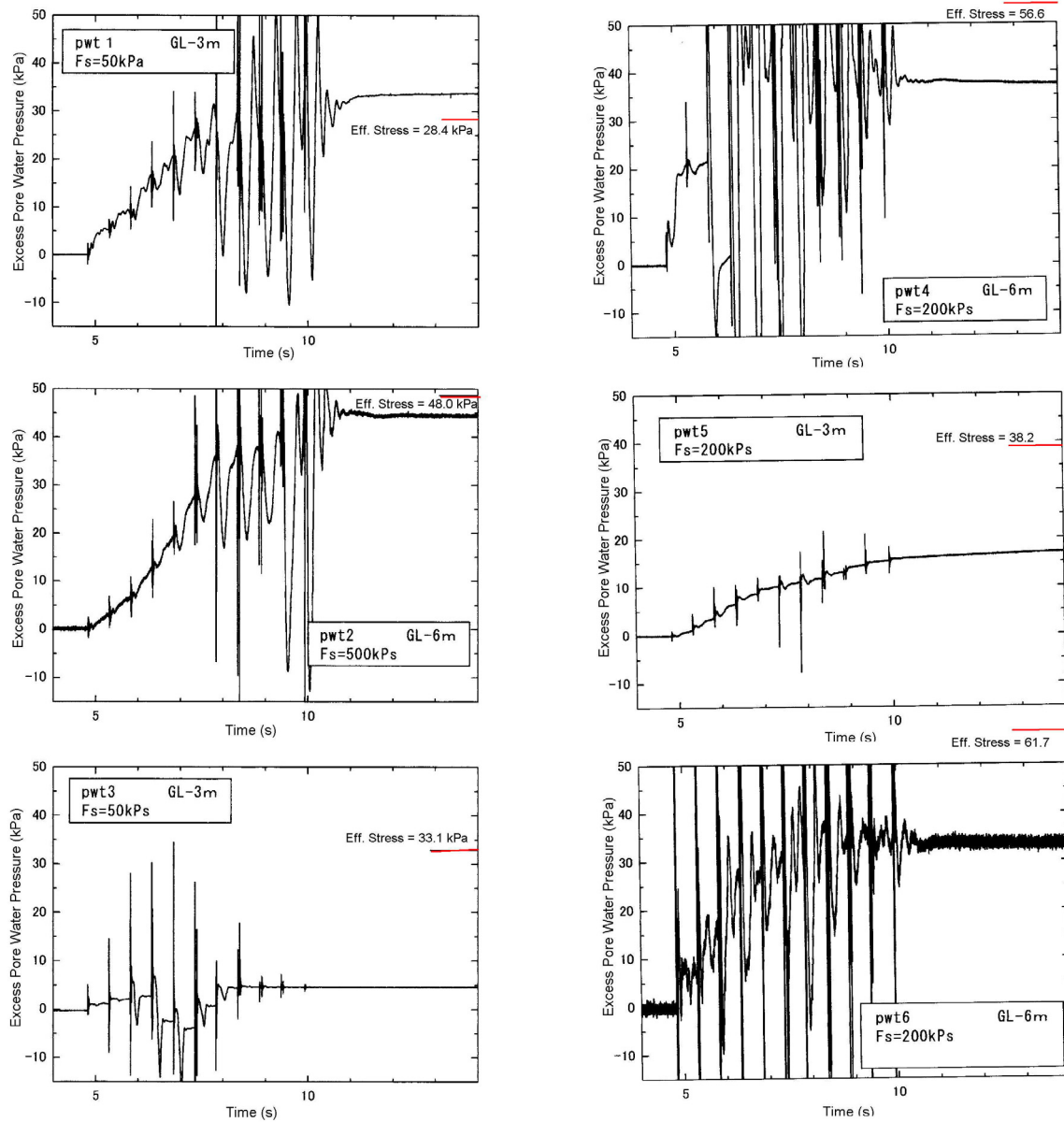


Fig. 3.16 Excess pore-pressure responses during second pilot test



Fig. 3.17 Sand boils observed following second pilot test

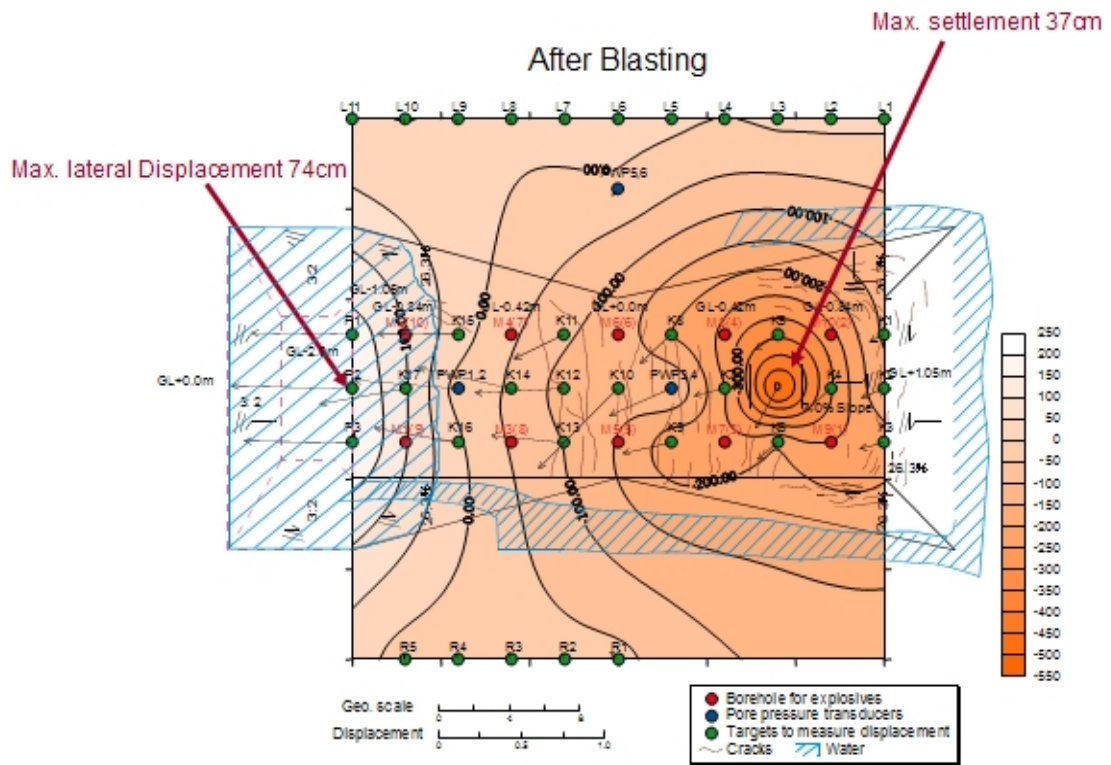


Fig. 3.18 Horizontal displacement vectors and settlement contour (second pilot test)



Fig. 3.19 Lateral movement of sheet pile wall after the test

4 First Full-Scale Lateral Spreading Test

With the success in the second pilot lateral spreading test, the construction of the actual test site for the first full-scale lateral spreading experiment was then launched in late August 2001 and completed early November 2001. Details of the test site and description of test piles and pipelines are provided in this chapter. This is followed by the detailed instrumentation and installation procedure. The locations of blast holes, the amount of charges, and the sequence of blasting are also described. Finally, the test results are presented and discussed.

4.1 SITE LAYOUT

A layout of the first full-scale lateral spreading experiment is shown in Figure 4.1. As mentioned earlier in Chapter 1, the UCSD experiment was located in the area of a traditional design quay wall where large lateral ground movement was expected. The UCSD test site was surrounded by sheet piles. The water elevation in front of the sheet pile quay wall was approximately +2.00 m, the same elevation as the groundwater table. The quay wall was anchored by a series of tie rods which were fixed to H-piles to reduce movement of the quay wall. The ground surface was at elevation +3.00 m at the quay wall and began to slope upward at 4%, 25.2 m away from the quay wall. Figure 4.2 shows a 3D view of the test site. An aerial photograph of the test site is shown in Figure 4.3.

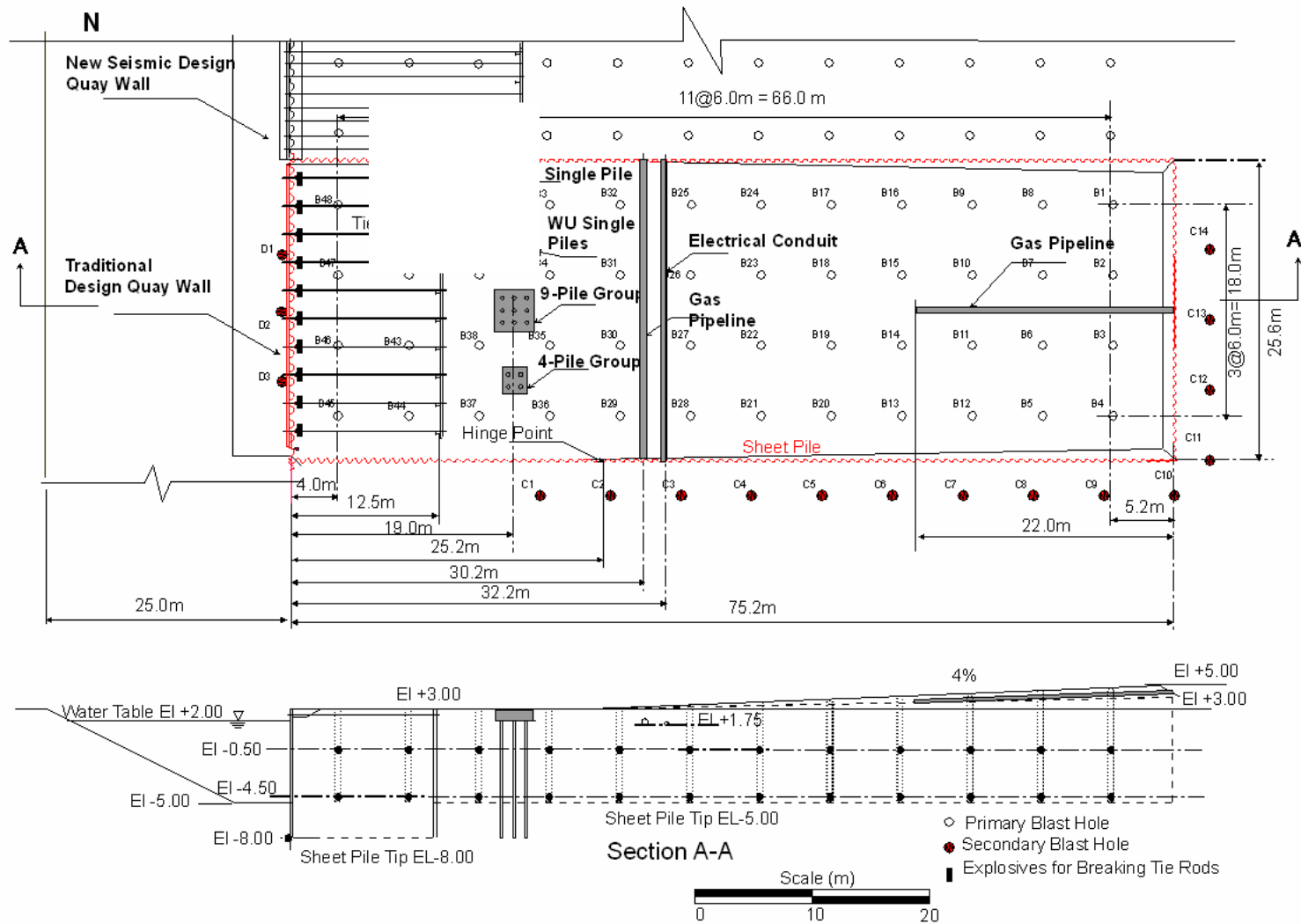


Fig. 4.1 Layout of first full-scale lateral spreading experiment

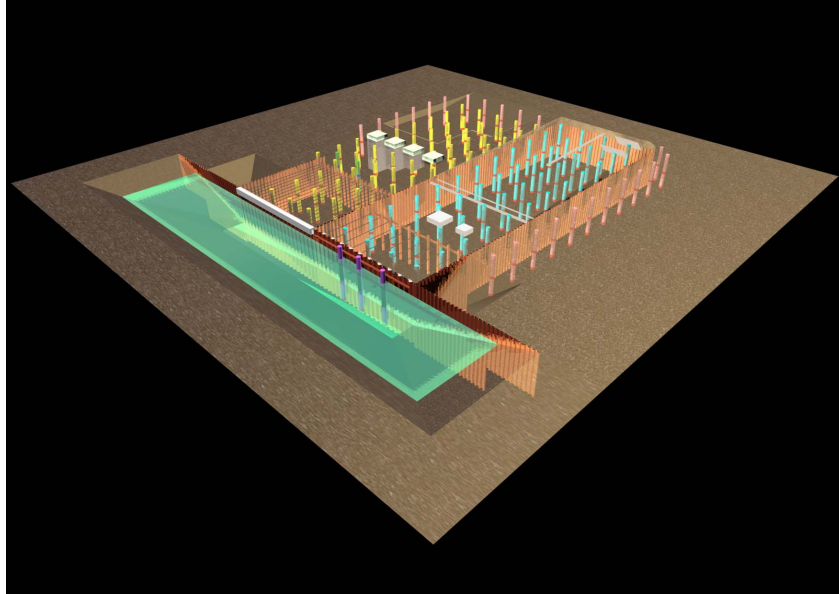


Fig. 4.2 3D View of first full-scale lateral spreading experiment (PARI 2002)



Fig. 4.3 Aerial photo of first full-scale lateral spreading experiment (PARI 2002)

4.2 PILE DESCRIPTION

The UCSD test piles consisted of a single pile, a 4-pile group, and a 9-pile group as shown in Figure 4.4. The pile outside diameters were 318 mm with a wall thickness of 10.5 mm, a nominal length of 11.5 m, and a yield strength of 400 MPa. Steel channels (C 75 mm x 6.92 kg/m) with a yield strength of 400 MPa were welded to the steel pipe piles to protect the strain gages from damage during pile driving. Figures 4.5–4.6 show the pile cross section and its moment-curvature relationship, respectively. Three similar free-head single piles were also installed in the area by Waseda University (WU) as shown in Figure 4.4. The cross sections and properties of the WU piles were the same as those of the UCSD piles, but the pile lengths were shorter.

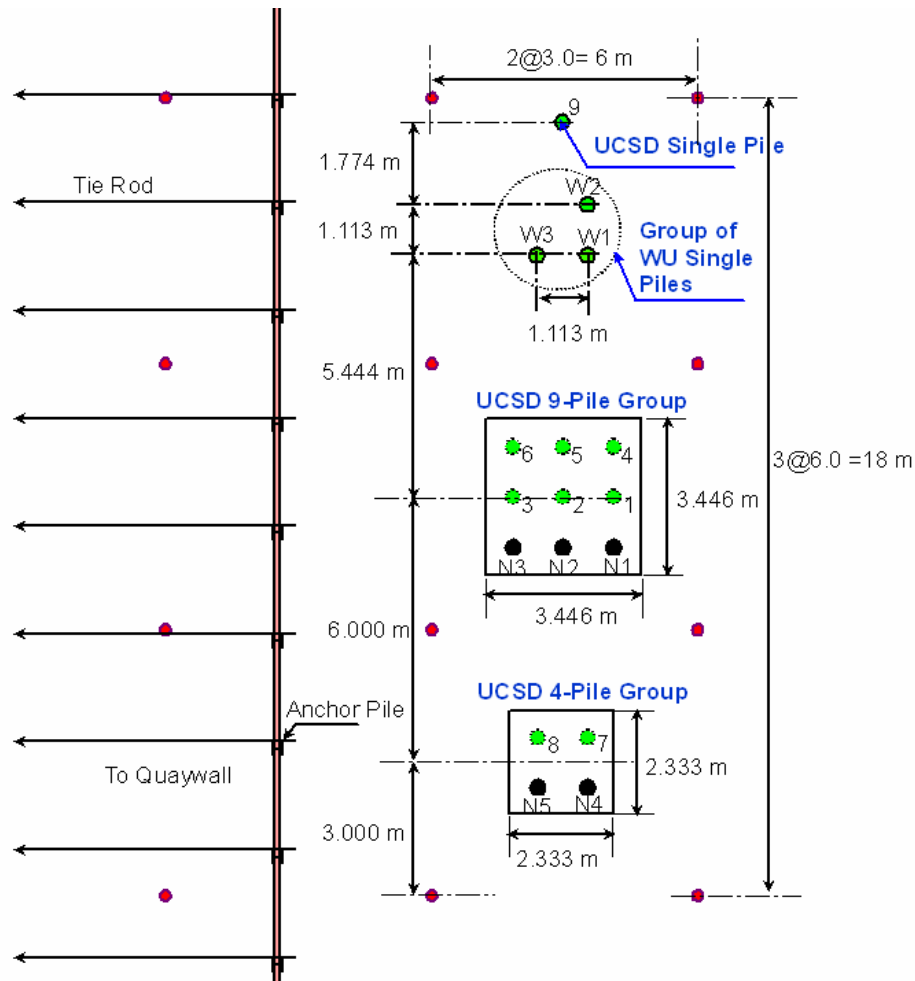


Fig. 4.4 Layout of test piles

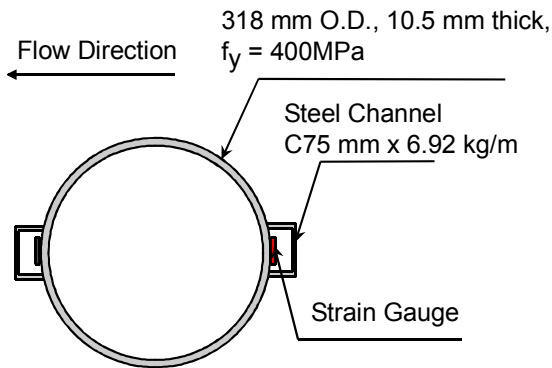


Fig. 4.5 Pile cross section

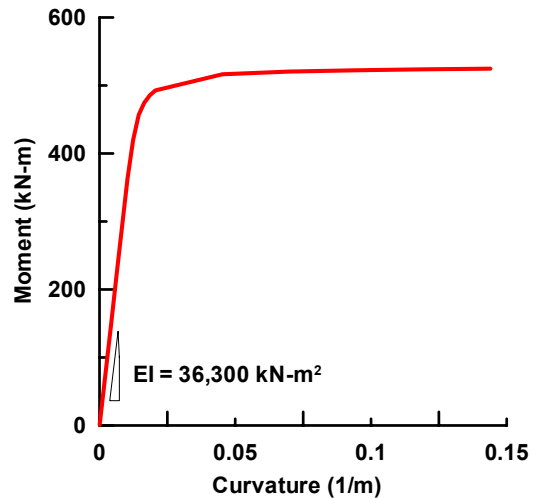


Fig. 4.6 Moment-curvature relationship of test pile

A total of 9 UCSD test piles were extensively instrumented with electrical strain gages (Fig. 4.4): the single pile, two of the 4-pile group, and six of the 9-pile group. The gages were located at 0.6 m intervals on both upstream (front) and downstream (back) sides of the piles (Fig. 4.7) to obtain the strains from which the bending moments along the lengths of the piles could be computed. In addition, two rosette strain gages were attached to each pile to measure the shear force developed in each pile in the pile group during lateral spreading. One was attached at a depth of 1.9 m below the original pile head and the other one was attached just below the pile cap. A series of tiltmeters at various depths were also installed on one of the piles of each foundation system to use as back-up data for strain gages.

A diesel hammer with a mass of 4,000 kg (Fig. 4.8) was used to install the piles. The piles were pushed into the ground for the first 7.5 m by the self weight of the hammer, indicating the low soil strength. The driving started below this layer with drop heights varying between 20 cm and 60 cm. The UCSD piles were planned to be driven full length into the ground, corresponding to about 3.0–3.5-m penetration into the dense soils to obtain a degree of fixity at the pile tips. Unfortunately, some of the piles could not be driven to the desired depth due to the presence of the cobbles at the final depth (Fig. 4.9). As a result, the pile lengths in the group varied between 10.2–11.5 m. A summary of pile lengths in the groups is given in Table 4.1.

Table 4.1 Summary of final pile length

Pile No.	1	2	3	4	5	6	7	8	9	W1	W2	W3	N1-N6
Final Pile Length (m)	11.1	10.4	11.1	10.2	11.2	11.1	11.1	11.1	11.2	8.6	8.7	8.6	11.5

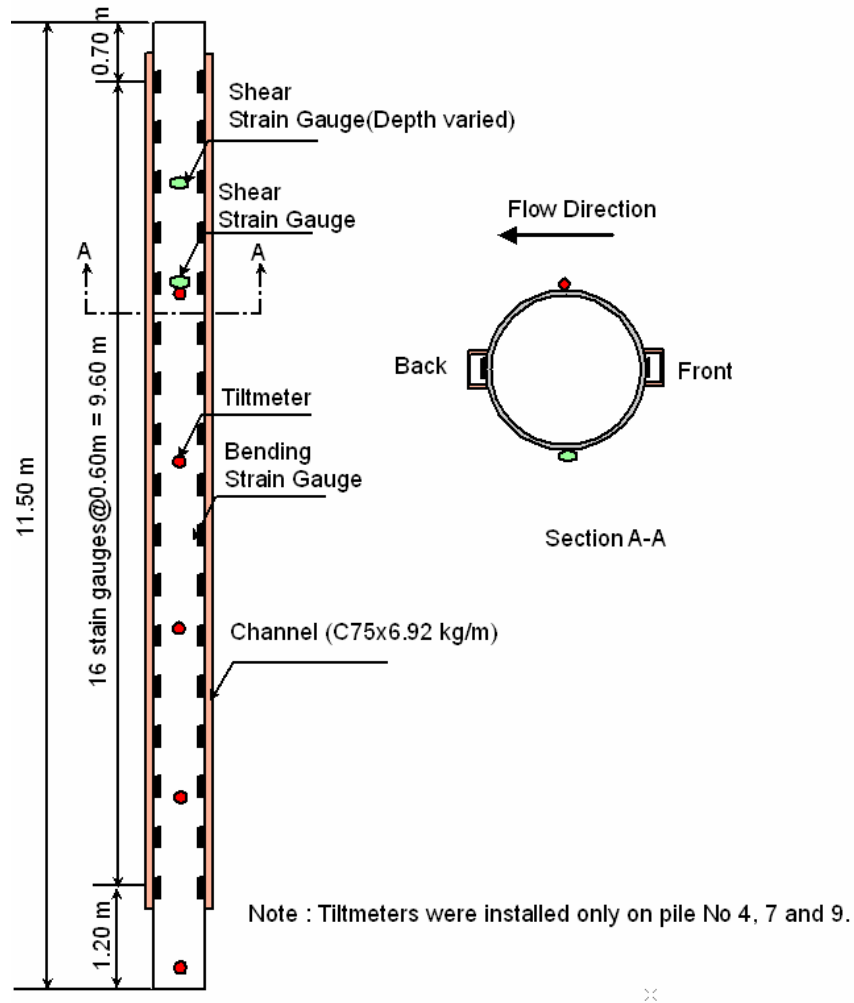


Fig. 4.7 Instrumentation of steel pipe piles



Fig. 4.8 Pile driving using diesel hammer



Fig. 4.9 Pile length left over after pile installation: (a) 4-pile group (left), (b) 9-pile group (right)

In the pile groups, the piles were spaced at 3.5 pile diameters, center-to-center, corresponding to 1.11 m. The pile heads were fixed against rotation by reinforced concrete pile caps based on typical Caltrans design practice. Steel V-shape anchor bars were used to connect the pile heads to the concrete pile cap. Figures 4.10–4.11 show pile-cap details of the 4-pile group and the 9-pile group, respectively. Figure 4.12 shows the construction sequence for the pile cap of the 9-pile group. A summary of concrete strength for the pile caps at 7 and 28 days, respectively, is given in Table 4.2.

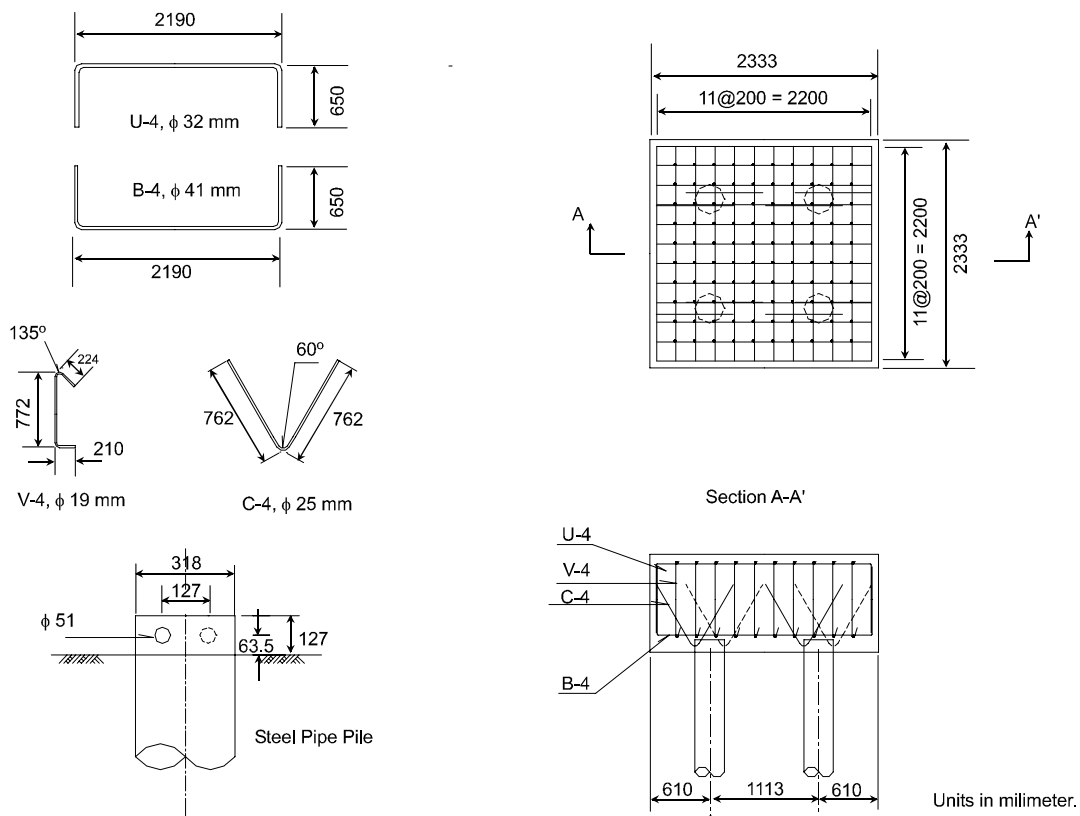


Fig. 4.10 Pile-cap details of 4-pile group

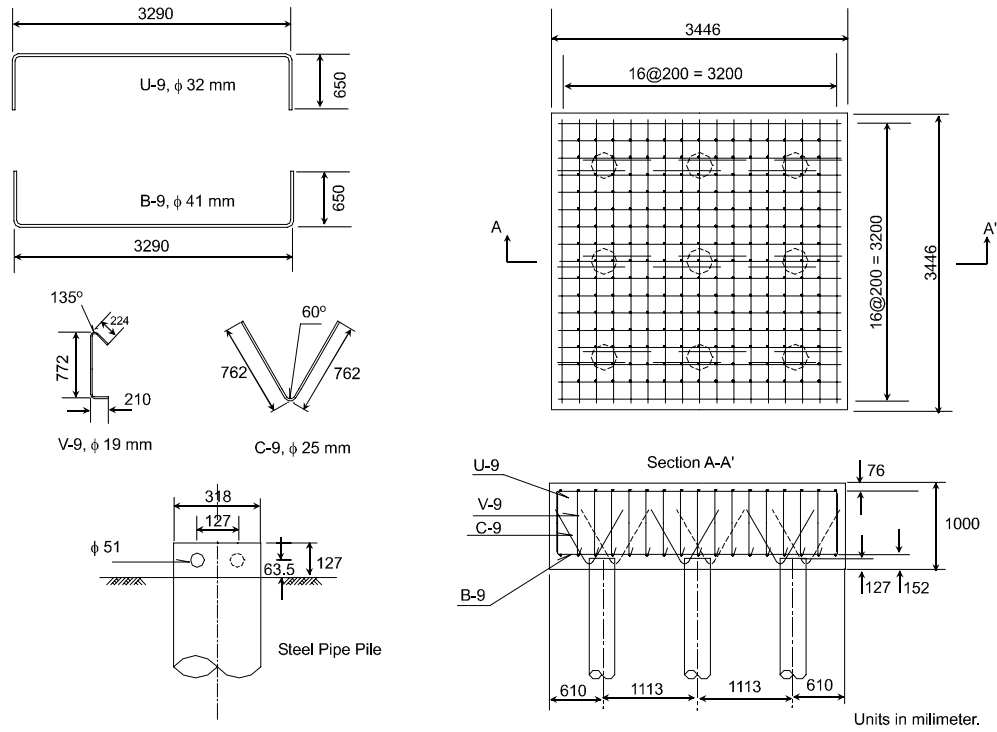


Fig. 4.11 Pile-cap details of 9-pile group

Table 4.2 Summary of concrete strength of pile caps

Date of Casting	Date of Test	Concrete Age (Days)	Truck No.	Slump (cm)	Air (%)	Sample No.	f'_c (MPa)	$f'_{c,ave}$ (MPa)
10/15/02	10/22/02	7	1	7.0	4.3	1	29.3	29.5
						2	29.4	
						3	29.8	
			2	8.0	4.6	1	29.5	29.5
						2	29.7	
						3	29.7	
			3	7.0	4.4	1	28.6	29.0
						2	28.9	
						3	29.4	
10/15/02	11/12/02	28	1	7.0	4.3	1	36.7	36.7
						2	36.8	
						3	36.6	
			2	8.0	4.6	1	35.9	35.9
						2	35.5	
						3	36.2	
			3	7.0	4.4	1	36.1	36.2
						2	36.7	
						3	35.7	



1. Cutting piles to design elevation



2. Cutting holes for v-shape anchors



3. Placement of 10 cm gravel



4. Placement of 10 cm lean concrete



5. Installation of v-shape anchors



6. Construction of reinforcement



7. Construction of formworks



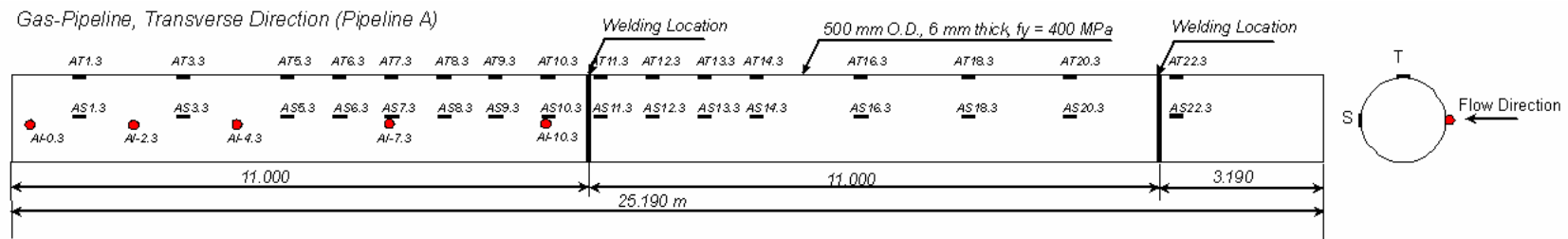
8. Pile cap after concrete work

Fig. 4.12 Pile-cap construction for 9-pile group

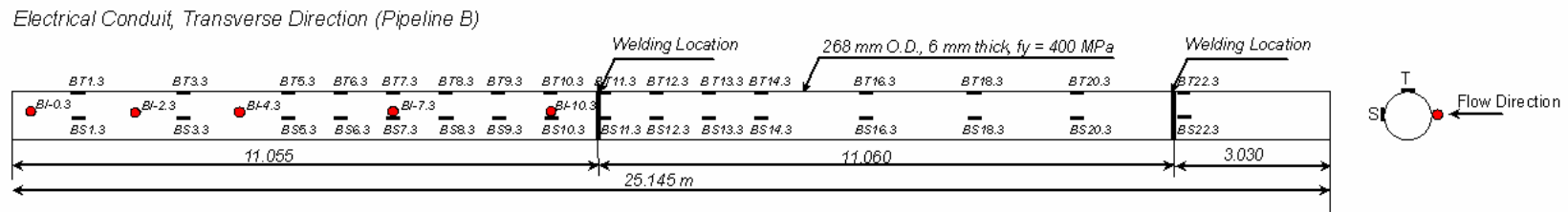
4.3 PIPELINE DESCRIPTION

In addition to the test piles, two transverse pipelines (i.e., natural gas pipeline (pipeline type A) and electrical conduit (pipeline type B)) and one longitudinal natural gas pipeline (pipeline type C) were installed as shown in Figure 4.1. The objective of the test for transverse pipelines was to assess the pipeline performance subjected to bending moment from global translation of the soil, while the test for the longitudinal pipeline was to evaluate the pipeline performance subjected to axial frictional forces imposed by the soil moving relative to the pipeline. The gas pipeline consisted of a 500-mm diameter pipe with a wall thickness of 6 mm and a yield strength of 400 MPa. The electrical conduit consisted of a 268 mm diameter with a wall thickness of 6 mm, and a yield strength of 400 MPa. The transverse gas pipeline and electrical conduit were both approximately 25 m long and located at 30 m and 32.2 m away from the quay wall, respectively. The bottoms of both pipelines were installed at an elevation of +1.75 m. The longitudinal gas pipeline was 22 m long and installed 1m below the ground surface, parallel to the direction of the flow. All of them were instrumented with electrical strain gages and tiltmeters along the lengths, as shown in Figure 4.13.

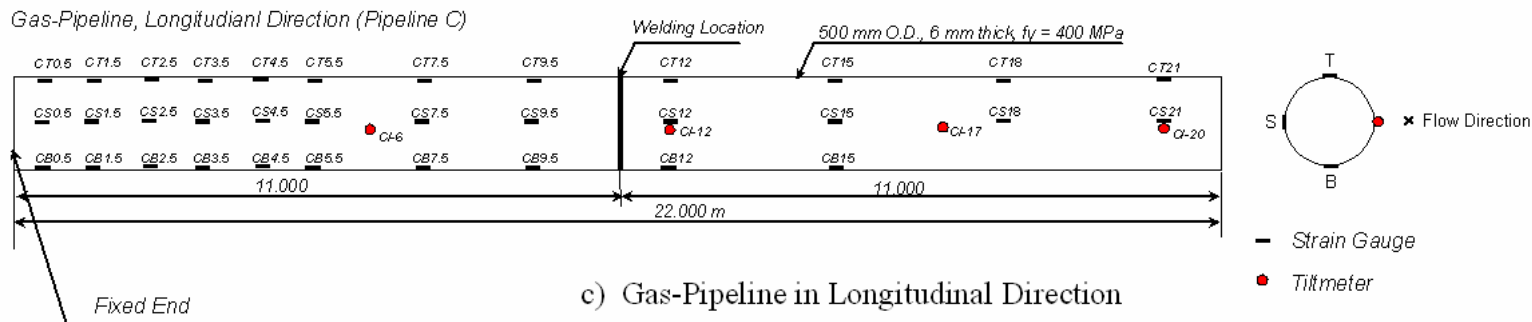
The construction sequence of the transverse pipelines is shown in Figure 4.14. The pipeline segments were first welded together at the test site. The transverse pipelines were installed by excavating the ground and setting them on a compacted sand layer with a thickness of 20 cm. Then, both ends were anchored to the sheet pile wall using high-strength bolts. This type of connection allowed some rotation at each end. Subsequently, the sand was backfilled in multiple compacted layers (Fig. 4.15) in accordance with Japanese Gas Association specifications. The specification requires that a compacted dry unit weight shall be 90% of the maximum dry unit weight obtained from the standard Proctor test ASTM D-698 (ASTM 1998).



a) Gas-Pipeline in Transverse Direction



b) Electrical Conduit in Transverse Direction



c) Gas-Pipeline in Longitudinal Direction

Fig. 4.13 Instrumentation plan for (a) transverse gas pipeline, (b) transverse electrical conduit, and (c) longitudinal gas pipeline



1. Welding of pipeline segments together



2. Welding of connection plate



3. Excavation for pipeline AB installation



4. Measurement of cross section



5. Compaction of base layer



6. Installation of pipeline A



7. Installation of pipeline B



8. Pipeline A and B in place

Fig. 4.14 Construction procedure of transverse pipelines



9. Connection of pipeline to sheet pile wall



10. Compaction of first layer



11. Compaction of second layer



12. Field density test of second layer



13. Compaction of third layer



14. Field density test of fourth layer

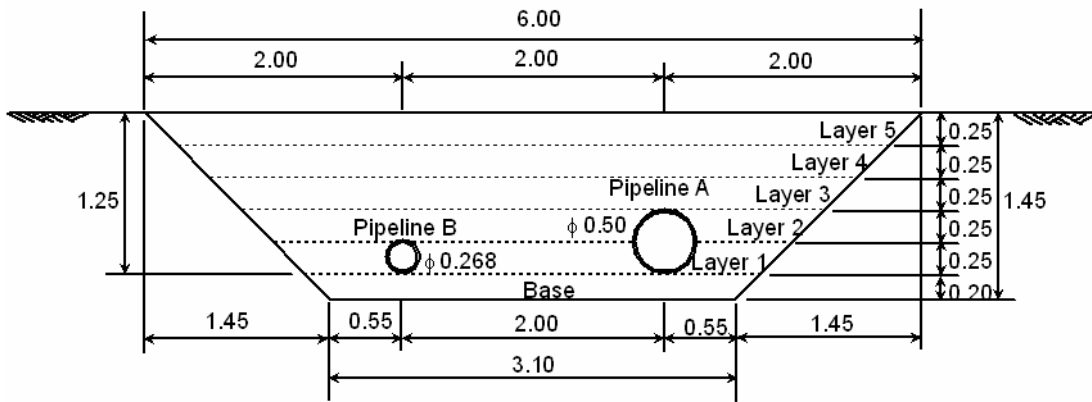


15. Sand placement for fifth layer

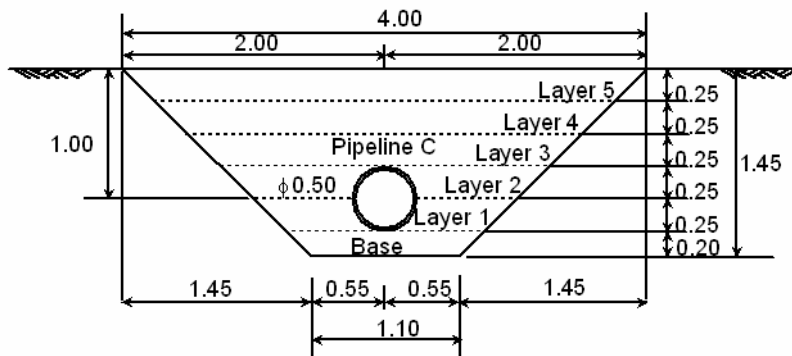


6. Completion of pipeline installation

Fig. 4.14 (continued) Construction procedure of transverse pipelines



(a) Pipelines A and B



(b) Pipelines C

Note: Units are in meter.

Fig. 4.15 Cross sections of multiple compacted layers for (a) pipelines A and B and (b) pipeline C

The longitudinal gas pipeline was installed in the same way as the transverse pipelines, but only one end was connected to the sheet pile wall. Figure 4.16 shows the construction sequence of the longitudinal pipeline. The field density test results of each layer, as presented in Tables 4.3–4.4, indicate that the density of compacted soil for both transverse and longitudinal pipeline areas met the specification with the relative compaction (R) of more than 90%.



1. Soil excavation for installation of pipeline C



2. Measurement of cross section



3. Compaction of base layer



4. Field density test for base layer



5. Installation of pipeline Type C



6. Connection of pipeline to sheet pile wall



7. Compaction of first layer



8. Completion of pipeline installation

Fig. 4.16 Construction procedure of longitudinal pipeline

Table 4.3 Summary of field density test results for transverse pipelines

Location	Layer No.	Sample No.	Total Density (kN/m ³)	Water Content (%)	Dry Density (kN/m ³)	Relative Compaction, R (%)	Average Relative Compaction (%)
Pipeline A and B	Base	1	17.27	25.0	13.81	94.0	96.1
		2	17.75	24.9	14.21	96.7	
		3	17.74	23.8	14.33	97.5	
	1	1	16.87	17.8	14.31	97.4	96.3
		2	16.22	15.5	14.05	95.6	
		3	16.72	18.7	14.08	95.8	
	2	1	16.35	17.6	13.90	94.6	96.1
		2	17.37	19.4	14.55	99.0	
		3	15.89	14.2	13.91	94.6	
	3	1	15.92	15.6	13.77	93.7	94.1
		2	15.56	12.5	13.84	94.2	
		3	15.82	13.9	13.89	94.6	
	4	1	16.12	13.3	14.23	96.8	95.2
		2	15.43	13.3	13.62	92.7	
		3	16.13	14.3	14.11	96.0	
	5	1	15.82	15.0	13.76	93.7	95.6
		2	16.62	16.0	14.33	97.5	
		3	15.98	13.8	14.05	95.6	

Note: $R(\%) = \frac{\gamma_{d(field)}}{\gamma_{d(max-lab)}} \times 100\%$

$\gamma_{d(field)}$ = Field dry density

$\gamma_{d(max-lab)}$ = Maximum dry density measured in laboratory by standard Proctor test

Table 4.4 Summary of field density test results for longitudinal pipeline

Location	Layer No.	Sample No.	Total Density (kN/m ³)	Water Content (%)	Dry Density (kN/m ³)	Relative Compaction, R (%)	Average Relative Compaction (%)
Pipeline C	Base	1	16.01	14.7	13.96	95.0	96.1
		2	16.57	16.0	14.28	97.2	
		3	16.17	14.7	14.10	96.0	
	1	1	16.34	14.4	14.28	97.2	97.2
		2	16.86	14.6	14.72	100.0	
		3	16.28	17.4	13.86	94.3	
	2	1	16.27	13.8	14.30	97.3	97.2
		2	15.90	14.7	13.86	94.3	
		3	16.76	14.1	14.69	100.0	
	3	1	16.33	14.4	14.28	97.2	95.9
		2	15.80	12.6	14.03	95.5	
		3	15.83	13.2	13.98	95.1	
	4	1	15.55	12.7	13.80	93.9	92.2
		2	15.09	12.9	13.36	90.9	
		3	15.35	14.0	13.47	91.7	
5	1	16.00	14.4	13.99	95.2	95.8	
	2	16.00	14.8	13.94	94.9		
	3	16.14	12.8	14.30	97.3		

Note: $R(\%) = \frac{\gamma_{d(field)}}{\gamma_{d(max-lab)}} \times 100\%$

$\gamma_{d(field)}$ = Field dry density

$\gamma_{d(max-lab)}$ = Maximum dry density measured in laboratory by standard Proctor test

4.4 INSTRUMENTATION

In addition to strain gages, other instrumentation was also installed to capture the behavior of soil and test lifelines. These included pore-pressure transducers, string-activated linear potentiometers, accelerometers, soil pressure cells, tiltmeters, slope inclinometer casings, and Global Positioning System (GPS) units. A layout of the instrumentation for the first full-scale test is shown in Figure 4.17. Figures 4.18–4.19 show a zoomed-in version of Figure 4.17 in the areas of test piles and pipelines, respectively.

A total of 24 pore-pressure transducers were installed at several locations throughout the test site to measure the excess pore-water pressure buildup and to evaluate the degree of soil liquefaction. The transducers were installed near the test piles, the pipelines, and in the embankment area, as shown in Figure 4.17. Three accelerometers were installed on the top of the pile caps and single pile to measure horizontal acceleration responses during the test. The direction of accelerometers was parallel to the flow direction. Tiltmeters were also installed adjacent to those accelerometer locations to measure pile-head rotations at the end of the test. Furthermore, inclinometer casings were installed to measure soil displacement profiles. The measurements were made by lowering an inclinometer probe into the casing to measure the rotations along the casing before and after the test. Assuming that the rotation and displacement at the tips were zero, the soil displacement profile can then be determined. GPS units were installed in several locations to measure the movements in both horizontal and vertical directions during the test. The string-activated linear potentiometers were installed to measure the relative displacement between two points of interest and were also used for verification of the displacements obtained by GPS units.

For the 4-pile group and the 9-pile group, soil pressure cells were installed at the front and back sides of the pile-cap surfaces to measure the pressure distribution of the soil acting on both upstream and downstream sides. A total of 8 cells were used for this test. It was anticipated that the magnitude of resultant forces acting on both pile caps can be evaluated based on the data from the soil pressure cells. The locations of soil pressure cells are presented in Figure 4.20.

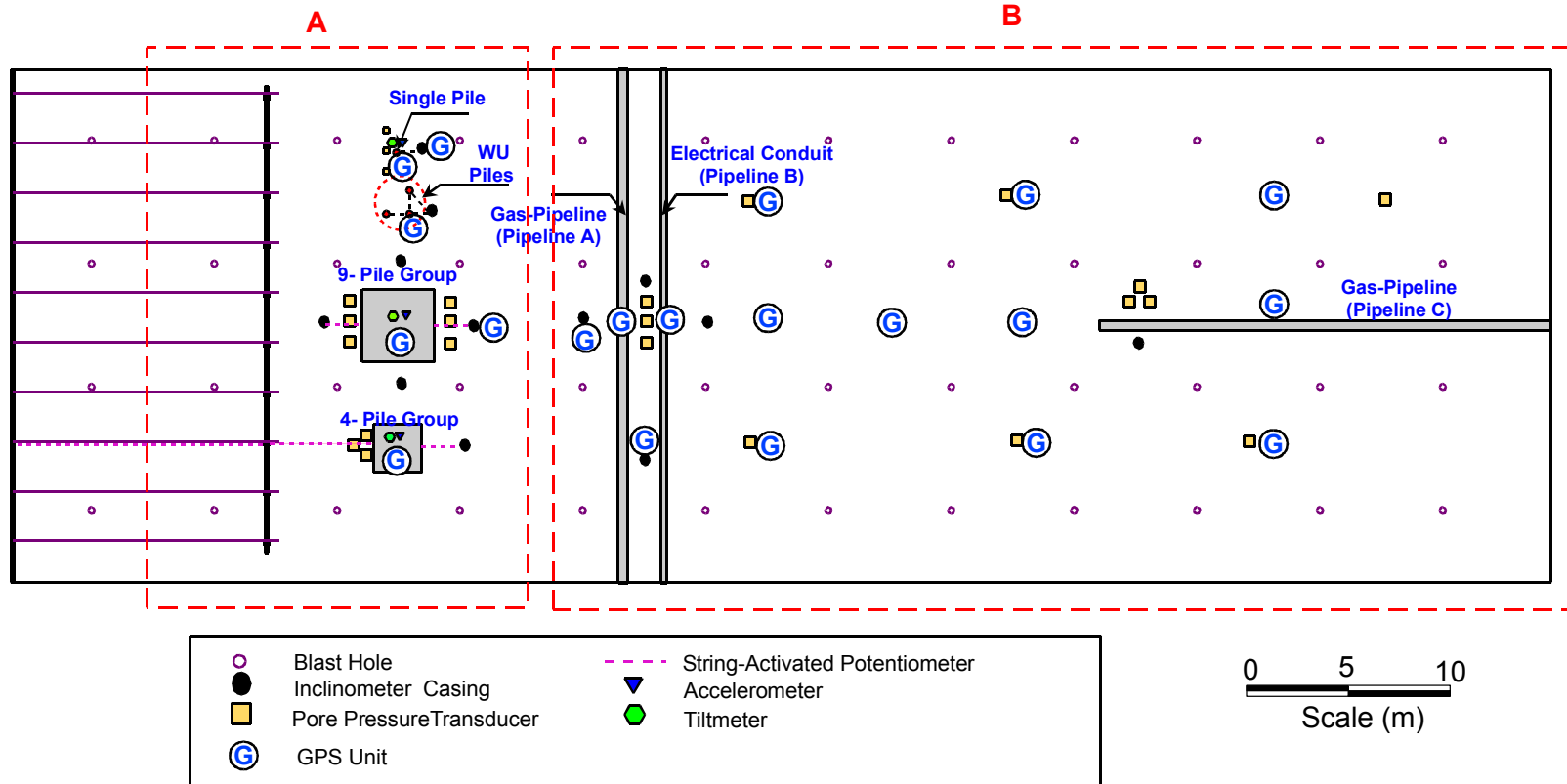


Fig. 4.17 Instrumentation layout for first full-scale lateral spreading test

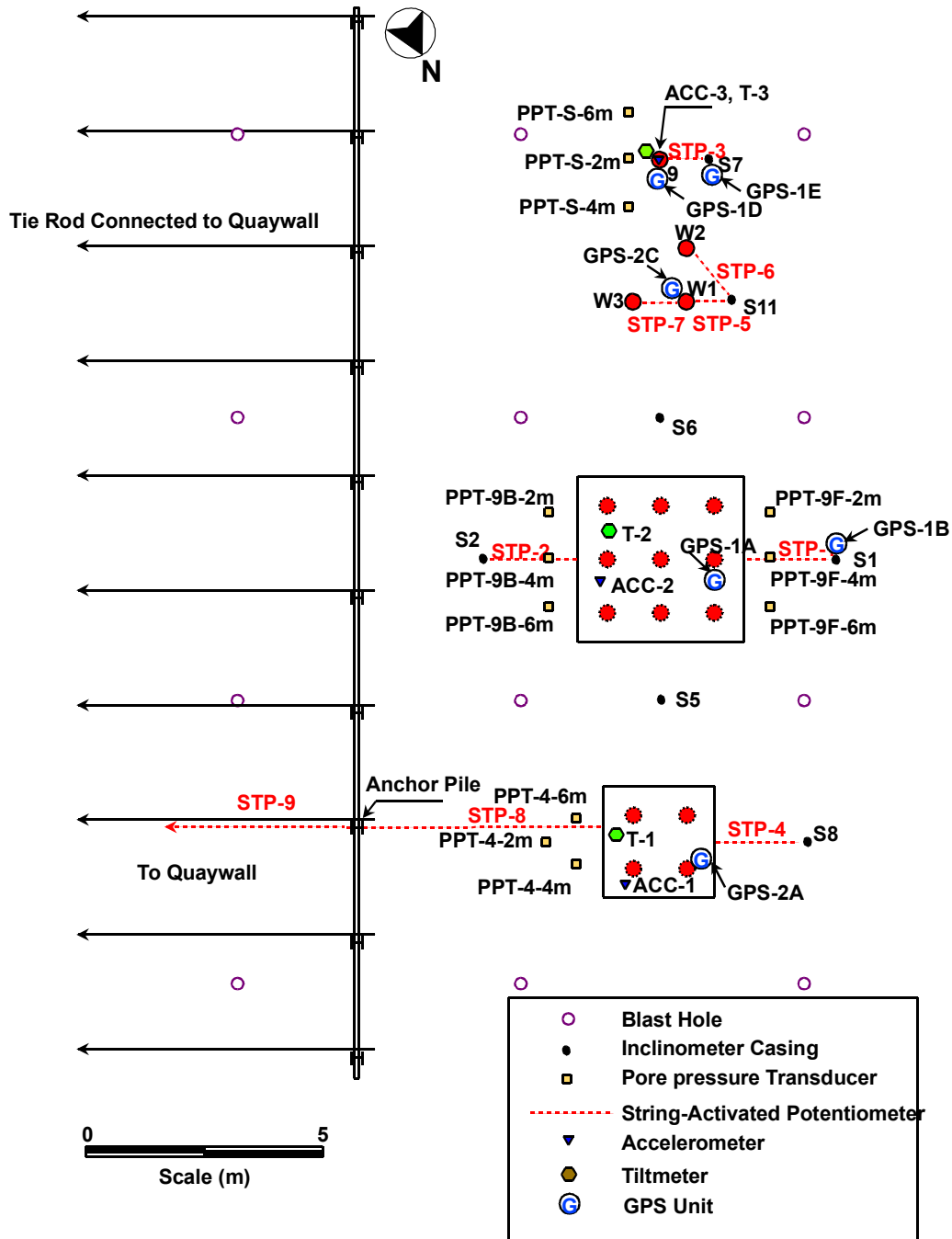


Fig. 4.18 Layout of instrumentation in the area of test piles (area A)

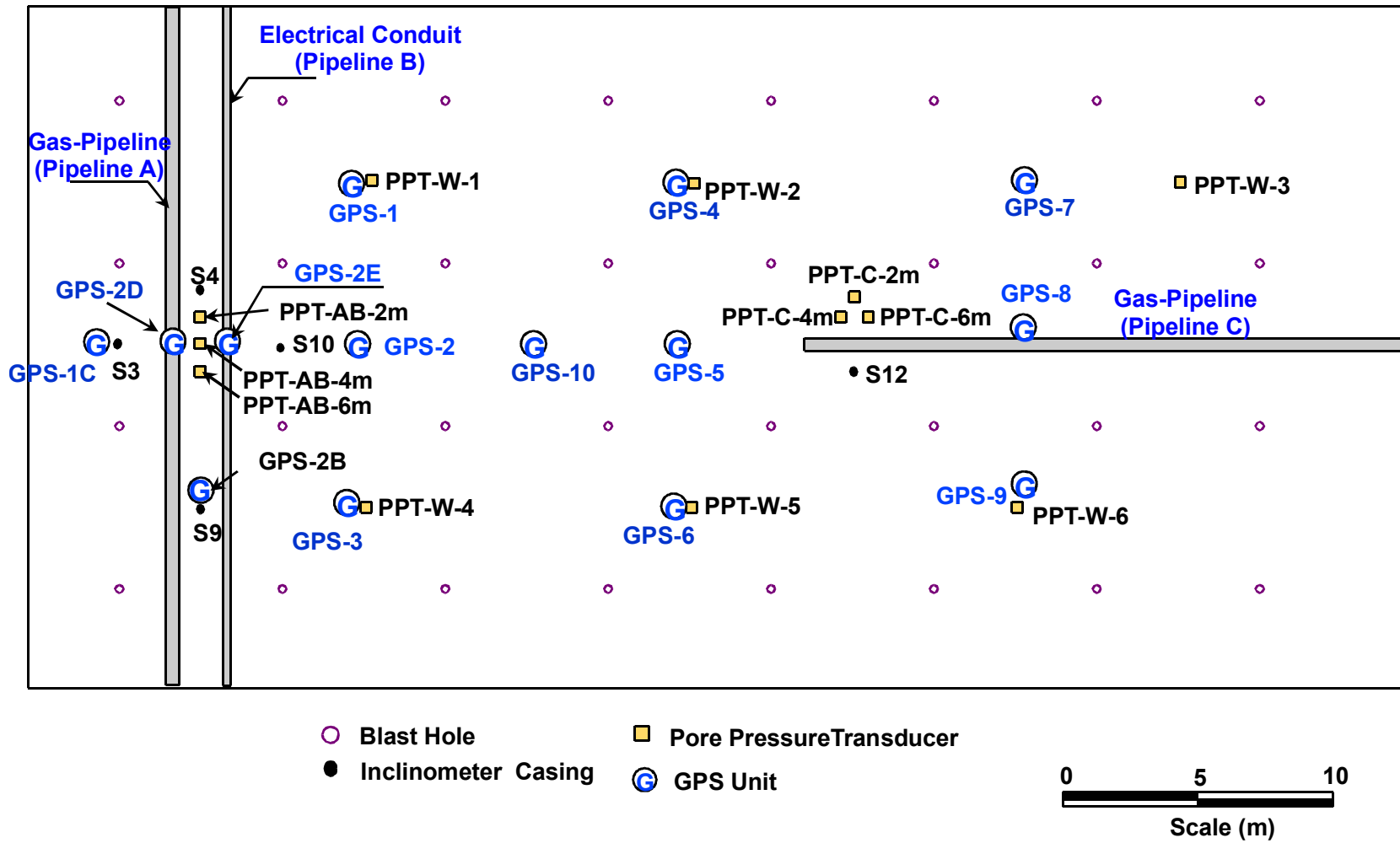
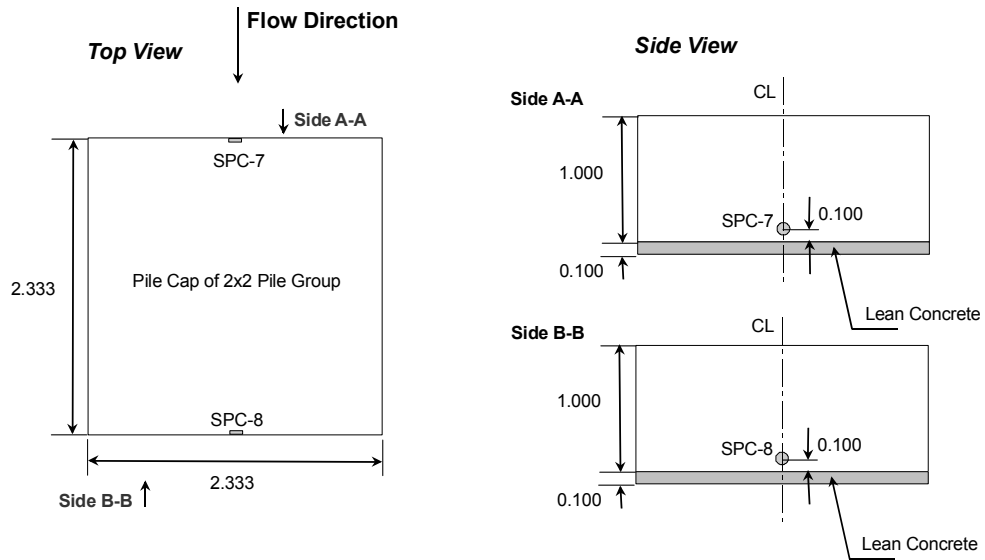
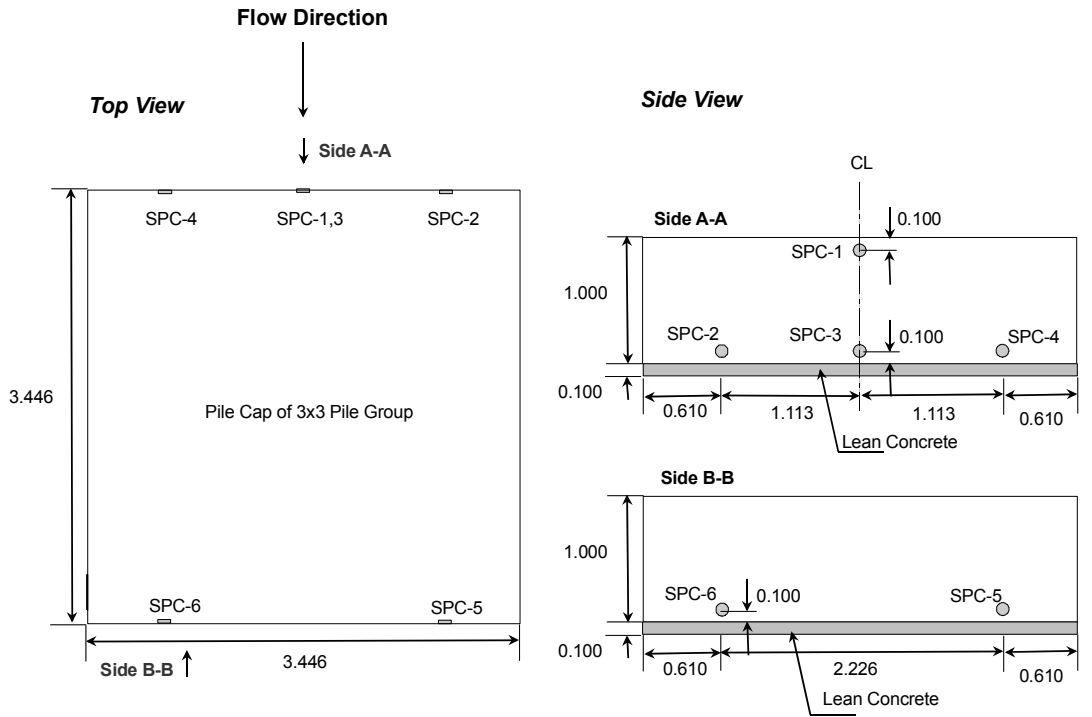


Fig. 4.19 Layout of instrumentation in the area of test pipelines (area B)



All units in meter

Fig. 4.20 Locations of soil pressure cells on pile caps

4.5 BLASTING SEQUENCE

The explosive charges used in the test were the same as those used in the pilot tests. Blast holes were spaced at 6.0 m on center in the regular grid pattern, similar to the second pilot test, as shown in Figure 4.1. Charges were installed at depths of 3.5 m and 7.5 m below the design ground surface (El. +3.00). The mass of charges varied from 2 kg near the test piles to 3–5 kg at other areas. The charge was reduced near the test piles in order to prevent damage to the large number of instruments installed in the vicinity.

The sequence of the primary blasting, as shown in Figure 4.21, started from the southwest corner of the embankment (B1) and proceeded to the next hole of the same row (B1–B4), and continued successively to the next rows toward the quay wall. The blasting interval between two adjacent blast holes was approximately 0.75 seconds, with the elapsed time of approximately 35 seconds. It should be noted that the blasting of primary sequences for the traditional quay wall and the new seismic design quay wall tests were essentially the same, and occurred nearly simultaneously. However, the elapsed time of the new seismic design quay wall test was about 5 seconds longer because it had more blast holes.

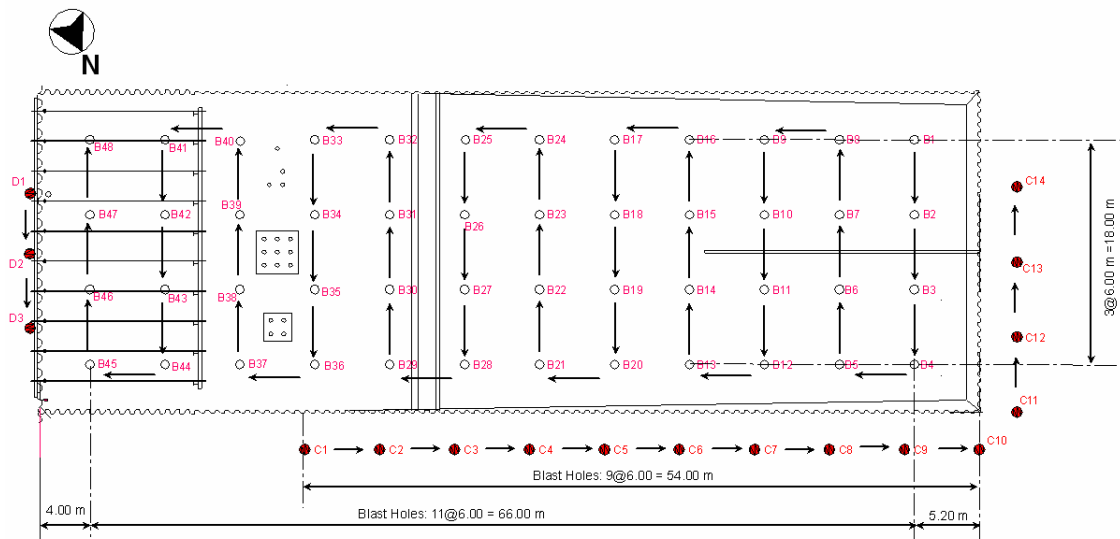


Fig. 4.21 Blasting sequence for first full-scale lateral spreading test

Immediately following the primary blasting, the secondary blast holes located around the perimeter of the test site (from C1 to C14) were detonated with the time interval between each blast hole of 1 second. The purpose of these explosives was to liquefy the soil in the vicinity of

the sheet pile to minimize boundary effects. Approximately 20 seconds after the completion of the secondary blasting, additional explosives were detonated to break the tie rods of the quay wall, which allowed additional movement of the soil within the test area. From first to last detonation, the elapsed time was 86 seconds.

4.6 DATA-ACQUISITION SYSTEM

A total of over 400 channels were connected to high-speed data-acquisition systems to collect and process the data during the test. The number of channels required for this test was more than the capacity of the UCSD data-acquisition system, therefore an additional data-acquisition system was rented from Tokyo Soil Research Company to satisfy the requirement. The UCSD system was the SCXI system manufactured by National Instruments. It consisted of SCXI-1001 chassis, SCXI-1120, SCXI-1520, and SCXI-1121 modules, together with SCXI-1320, SCXI-1321, and SCXI-1314 front-mounting terminal blocks. The UCSD system had the capacity to support up to 320 channels comprising 280 channels of strain gages and 40 channels of other instruments (i.e., accelerometers, linear potentiometers, and tiltmeters). The Japanese system was manufactured by Kyowa and consisted of 150 strain gage channels. Both systems started recording the data at the same time, approximately three minutes before the blasting. The data were synchronized with other test participants using the five-volt signal. The data were acquired at a sampling rate of 100 Hz for about 3 minutes following the blasting to capture all the important information during the test. The scan rate was then changed to 10 Hz for the next 2 hours, and 0.1 Hz for the next 24 hours to measure a decrease in excess pore-water pressure over a long period of time.

4.7 TEST RESULTS

4.7.1 Excess Pore Pressure

Sand boils forming at the ground surface as shown in Figure 4.22 provided direct evidence that the ground had indeed liquefied as a result of the blasting. However, the array of pore-pressure transducers was used to provide the quantitative record of the blast effect on the pore-water.



(a) near test pile area



(b) near embankment area

Fig. 4.22 Sand boils observed at the ground surface: (a) near test pile area and (b) near embankment area

A typical example of the observed excess pore-pressure time histories at various depths with their initial effective stresses is presented in Figure 4.23. These transducers were located upslope of the 9-pile group at depths of 2 m, 4 m, and 6 m (Fig. 4.18). The excess pore-water pressures began to build up immediately after the initiation of blasting. The increase in pore-water pressures became more rapid as the detonations approached the transducers. Fluctuation of pore pressures was observed when charges were detonated in the vicinity of the transducers. Excess pore-water pressures at all depths reached a liquefaction plateau at about 25 seconds (i.e., excess pore-pressure ratio, R_u , reached 100%). The increases in excess pore-water pressure at about 40 seconds and 86 seconds were due to the effect of secondary blasting and blasting of tie rods, respectively. Figure 4.24 presents the long-term excess pore-water pressure ratio time history of transducer PPT-9F-2m, which indicated that the R_u continued to dissipate with time to approximately 30% about 16 hours after the test.

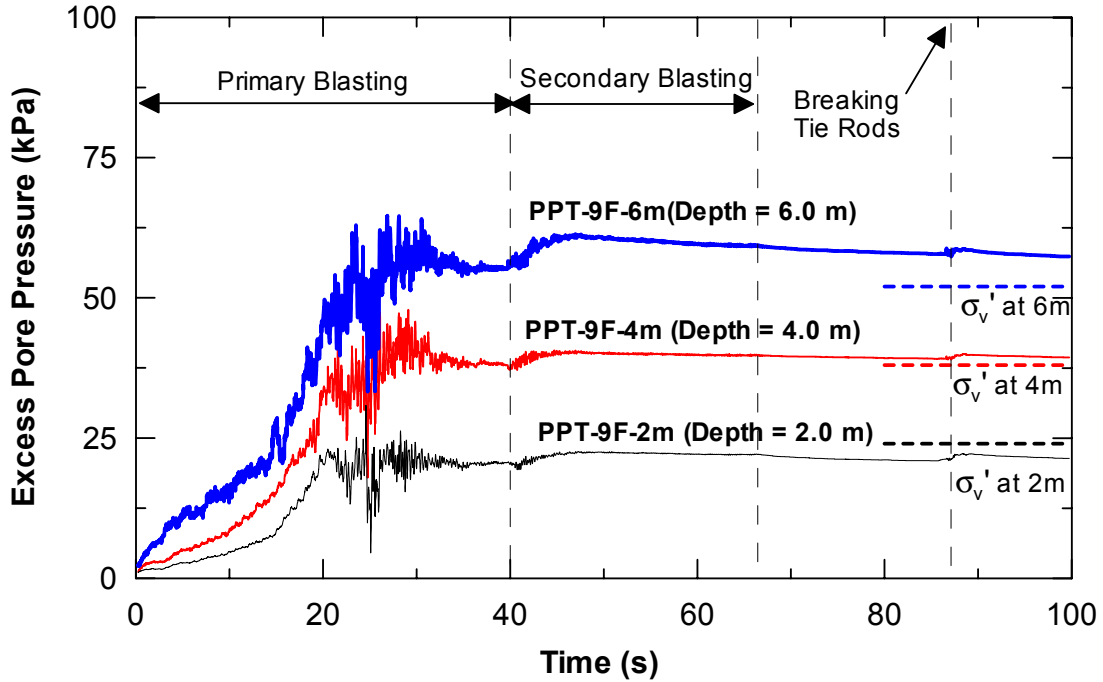


Fig. 4.23 Excess pore-pressure time histories nearby 9-pile group

The characteristics of R_u time histories at other locations, as shown in Appendix D, were similar to those presented herein. In summary, the R_u of the site at the end of the primary blasting ranged from 57% to slightly over 100%, and averaging 82%. The R_u ranged from 22% to 58%, averaging 37%, at about 16 hours after the test. The reasons that R_u was slightly above 100% at some locations include (1) error in estimating the soil unit weight and depth of the water table and (2) the possibility that some of the transducers might have moved downward during and after the blasting, resulting in an increase of excess pore-water pressure.

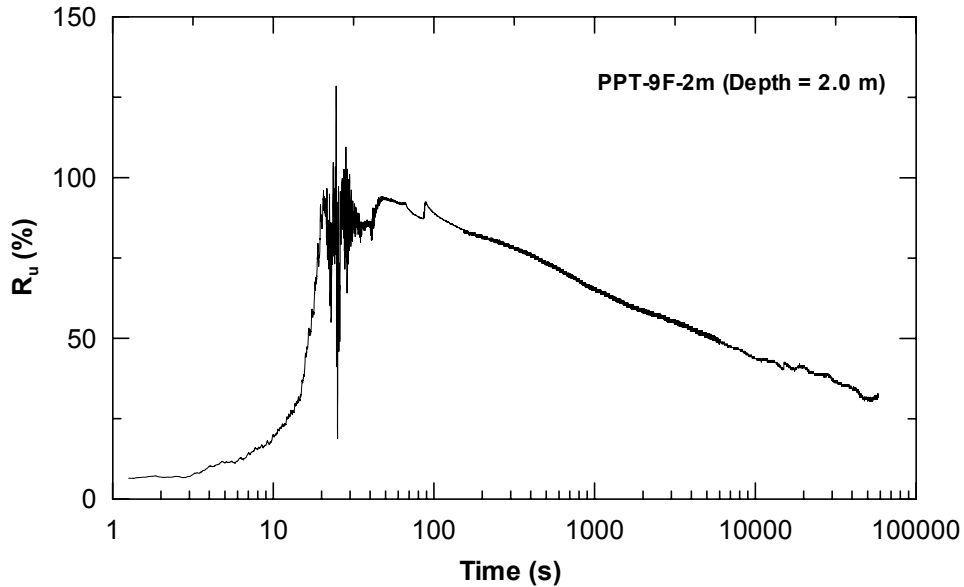


Fig. 4.24 Excess pore-water pressure ratio time history near 9-pile group

4.7.2 Displacements of Soil and Test Lifelines

4.7.2.1 Surface Displacement

GPS units were used to monitor the surface movements of both the soil and test lifelines (i.e., piles and pipelines) during lateral spreading. The measurements in the vicinity of test piles and transverse pipelines were conducted by a research team from Caltrans (Turner 2002), while those in the embankment area were carried out by WU (Takahashi 2002). An example time history of soil movements on the upslope side of the 9-pile group (unit 1C) in the longitudinal, transverse, and vertical directions is presented in Figure 4.25a, together with R_u near the GPS unit (PPT-AB-4m). It was found that once R_u reached about 50% (about 10 seconds), the soil strength apparently dropped below the driving shearing stress of the soil mass. As a result, a translation of the soil mass began to occur. As the blasting approached the GPS unit, more movements in all directions were observed (i.e., spikes in the displacement time histories). The rate of longitudinal movement between 10 seconds and 27 seconds (i.e., time at the blasting past the location of GPS unit) was fairly constant, about 1 cm/s. Beyond 27 seconds, the effect of dynamic force from the blasting was not important as indicated by the insignificant movements in the transverse and vertical directions. However, the rate of lateral spreading of 1 cm/second still continued for another 5 seconds, likely due to the inertial effect of the soil mass. After 32 seconds, the lateral

movement began to die out. Increase in the soil movements at 40 seconds was due to the effect of secondary blasting around the sheet pile wall. Figure 4.25b presents the displacement path of the GPS unit in the horizontal plane, showing that the horizontal movement mainly occurred in the longitudinal direction toward the quay wall.

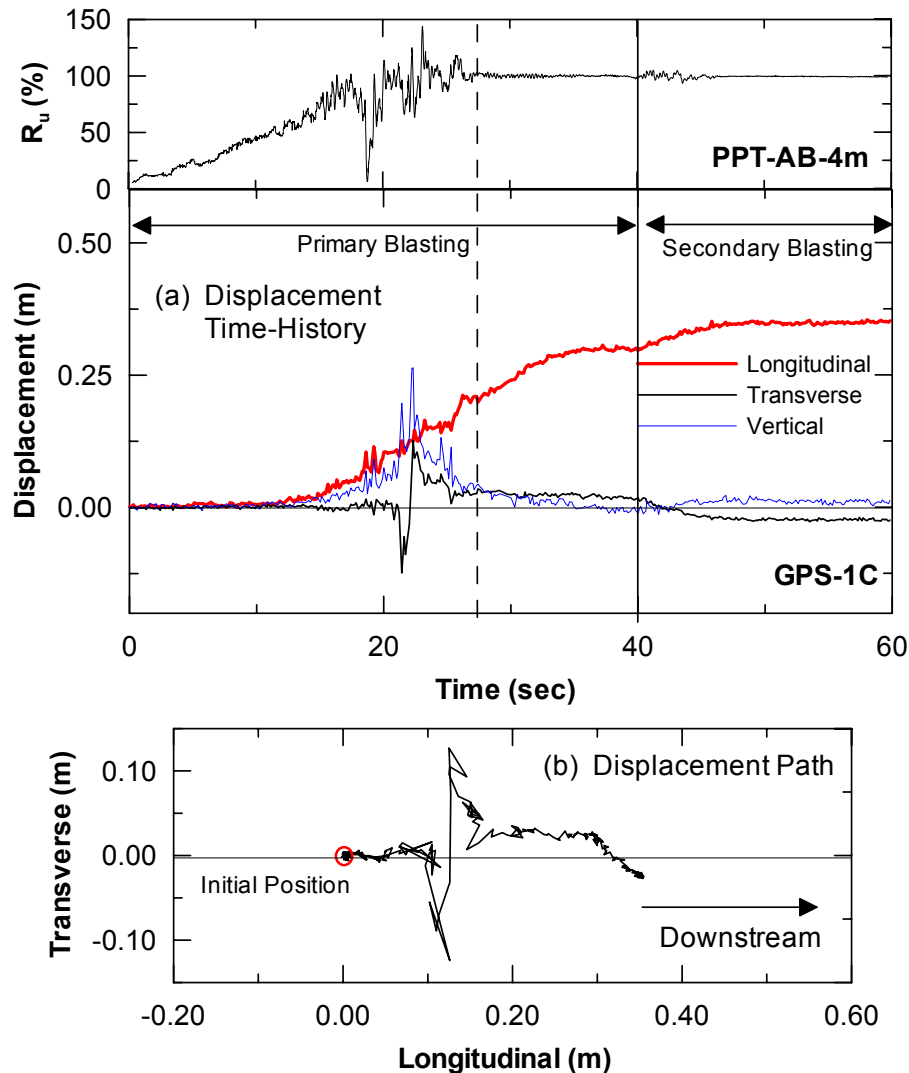


Fig. 4.25 Example of GPS data of unit GPS-1C (after Turner 2002)

The results of GPS units from other locations are presented in Appendix E. It should be noted that data obtained from four of the Caltrans' GPS units were lost during the critical blasting period, probably due to intermittent GPS antenna interference and wireless communications loss (Turner 2002). One of Waseda GPS units (GPS-5) was not working during the test. Tables 4.5–4.6 summarize the displacements in the longitudinal, transverse, and vertical

directions obtained from Caltrans' GPS units at 22 hours and one minute after the blasting. A summary of the movements of the embankment soil at 30 minutes after the blasting is given in Table 4.7.

Based on the GPS data, it was found that no horizontal creep was observed over a period of 22 hours after the blasting. Most of the horizontal displacements associated with lateral spreading took place within tens of seconds following the blasting. However, the data revealed that the maximum settlement of 10 cm was observed over an extended period of time as the pore-water pressures dissipated.

Table 4.5 Summary of Caltrans' GPS data, approximately 1 minute following blasting

Location	Displacement (m)			Horizontal Displacement (m) (x-y plane)	Angle to Flow Direction (Degree)
	Longitudinal (x)	Transverse (y)	Vertical (z)		
1A					
1B					
1C	0.341	-0.023	-0.001	0.341	3.88
1D	0.364	0.005	0.006	0.364	-0.78
1E					
2A	0.214	-0.037	0.014	0.217	9.79
2B					
2C	0.552	-0.016	0.010	0.552	1.68
2D	0.367	-0.080	-0.011	0.376	12.36
2E	0.368	-0.093	-0.043	0.380	14.24

Table 4.6 Summary of Caltrans' GPS data, approximately 22 hours following blasting

Location	Displacement (m)			Horizontal Displacement (m) (x-y plane)	Angle to Flow Direction (Degree)
	Longitudinal (x)	Transverse (y)	Vertical (z)		
1A	0.176	-0.042	0.014	0.181	13.39
1B	0.282	-0.025	0.032	0.283	5.11
1C	0.331	-0.018	-0.090	0.332	3.08
1D	0.350	0.005	0.008	0.350	-0.86
1E	0.338	-0.003	0.026	0.338	0.51
2A	0.209	-0.035	0.005	0.212	9.42
2B	0.343	-0.088	-0.091	0.354	14.45
2C	0.547	-0.012	0.012	0.547	1.28
2D	0.362	-0.078	-0.111	0.371	12.18
2E	0.372	-0.096	-0.128	0.384	14.49

Table 4.7 Summary of WU's GPS data, approximately 30 minutes following blasting

Location	Displacement (m)			Horizontal Displacement (m) (x-y plane)	Angle to Flow Direction (Degree)
	Longitudinal (x)	Transverse (y)	Vertical (z)		
1	0.332	-0.175	-0.072	0.375	27.79
2	0.389	-0.100	-0.045	0.402	14.41
3	0.347	-0.032	-0.005	0.348	5.27
4	0.314	-0.406	-0.246	0.513	52.28
5	--	--	--	--	--
6	0.337	-0.021	-0.171	0.338	3.56
7	-0.002	-0.590	-0.507	0.590	89.81
8	0	-0.302	-0.490	0.302	90.00
9	0.126	-0.001	-0.333	0.126	0.46
10	0.385	-0.169	-0.117	0.420	23.70

At the end of the test, two survey teams, from Sato Kogyo Company and Tobishima Company, measured soil surface displacements and movements of piles and pipelines due to blast-induced lateral spreading. Based on the GPS data (Turner 2002; Takahashi 2002) and survey data (Sato Kogyo 2002), the displacement vectors in the horizontal plane after the first test are presented in Figure 4.26.

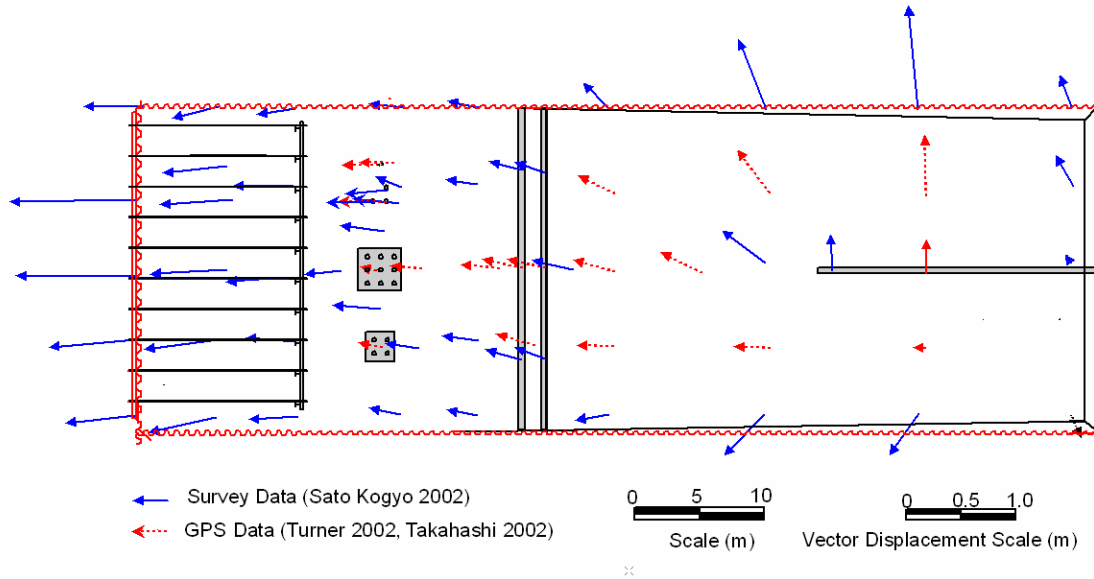


Fig. 4.26 Horizontal displacement vectors after the test

Soil surface movement generally increased with decreasing distance from the quay wall. The soil in the vicinity of the embankment, however, moved considerably in the transverse direction as opposed to the expected flow direction. This is because in the embankment area the lateral confinement in the transverse direction was lower than that in the longitudinal direction. For the level ground area, the displacements of the soil were mainly in the longitudinal direction with the soil movement being quite uniform. The average displacement of the soil on the upslope side of the pile groups was approximately 30 cm. The movement of this upslope soil was somewhat impeded by the pile foundations. Without this influence, as for the case of the soil between the groups, the soil movement was approximately 30% greater than that of the upslope soil movement with a magnitude varying between 40 and 43 cm. The soil movement between the pile foundations likely represented a true “free-field” soil displacement for the location of test piles (i.e., no influence from pile foundations). Beyond the range of test piles, the soil displacement continued to increase toward the quay wall where the maximum movement over 1 m had occurred.

The pile-head displacement of the single pile (free-head pile) was 32 cm, while the 4-pile group and the 9-pile group (fixed-head pile), moved about 21 cm and 18 cm, respectively. The movements of both pile groups were approximately 50% of the free-field soil movement at the location of the test piles. The movements of the pile foundations appeared to be dependent on the pile-head condition. The pile groups with a fixed-head condition moved less than the free-head pile due to the effect of pile-head restraint in the groups contributing to resist the moment induced by the lateral soil pressure. This phenomenon was also recently observed in centrifuge testing conducted at Rensselaer Polytechnic Institute (Abdoun 1997). The longitudinal pipeline moved transversely 33 cm at the free end of the pipeline. The movements of both transverse pipelines were similar to the surrounding soil with the maximum movements of 35 cm occurred at the middle of both pipelines.

4.7.2.2 Soil Displacement Profile

Profiles of soil displacement obtained from the inclinometer readings after the completion of the blast test are presented in Appendix F. A summary of lateral soil movement at the ground surface at each location is given in Table 4.8. Typical soil displacement profiles are presented in Figure 4.27. The results indicate that the maximum movement of the soil occurred at the ground surface as expected. The soil movement profiles in the vicinity of the test piles where the ground was level were quite linear, indicating a uniform shear strain over a thickness of 8 m. However, those located in the embankment area where the top layer was nonliquefiable showed a sign of zero shear strain of the nonliquefiable layer and higher shear strain below that layer. It should be noted that the displacements obtained from inclinometer data were slightly less than the actual soil displacement (i.e., compared with GPS data) because an absolutely fixed boundary condition at the tip of an inclinometer casing was assumed in computing the soil displacement profile (Fig. 4.28).

Table 4.8 Summary of measured soil displacements at ground surface from inclinometers

Name	Displacement in A-Axis (m)	Displacement In B-Axis (m)	Total Vector (m)	Remarks
S1	-	-	-	Casing damaged
S2	0.310	-0.059	0.315	
S3	0.233	-0.049	0.238	
S4	0.179	-0.031	0.182	
S5	0.413	-0.050	0.416	
S6	0.348	0.078	0.356	
S7	0.309	-0.057	0.314	
S8	0.242	-0.059	0.249	
S9	0.315	0.096	0.330	
S10	0.323	-0.021	0.324	
S11	0.307	0.025	0.308	
S12	0.236	0.165	0.288	

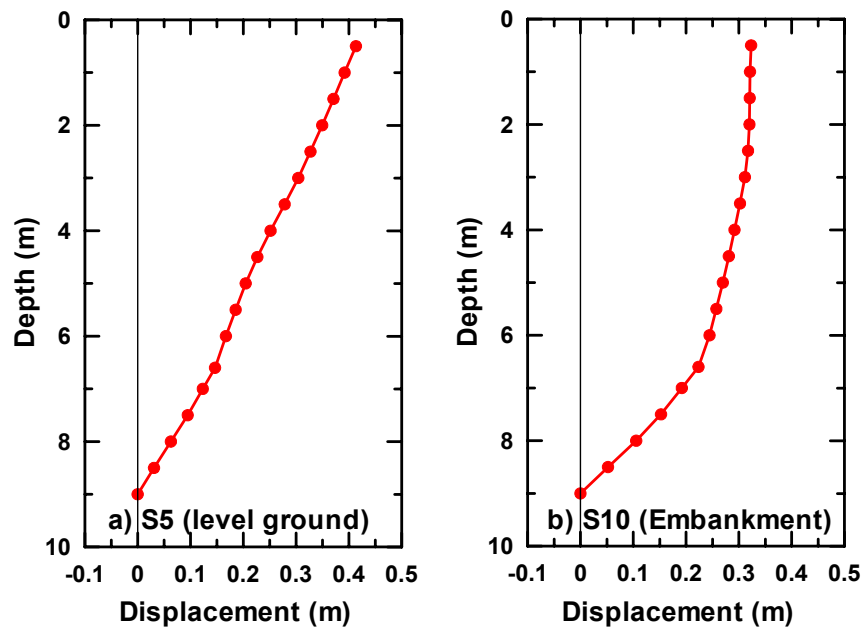


Fig. 4.27 Soil displacement profiles (a) S5 (level ground) and (b) S10 (embankment)

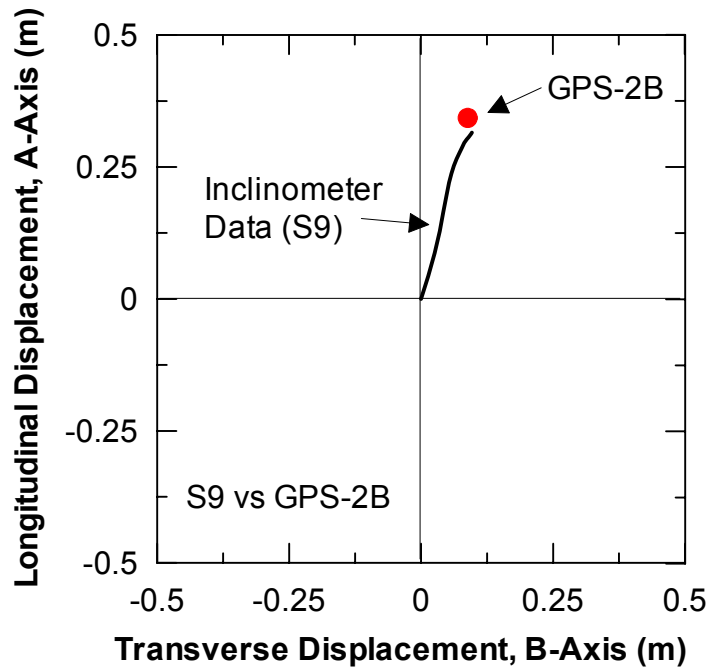


Fig. 4.28 Comparison of surface displacements from inclinometer and GPS unit

4.7.3 Pile and Pipeline Responses

4.7.3.1 Single Pile

Strain time histories along both sides of the single pile at various depths are shown in Appendix G. Figure 4.29 presents the strain profiles at the end of the test corresponding to maximum free-field soil displacement. It is noted that most strain gages on the back side of the single pile, as well as a series of tiltmeters, were damaged during pile installation.

As expected, because this was a free-head pile, the moments at the head were zero. The maximum moment occurred in the dense soil layer at a depth of about 9 m. Based on the strain data, the single pile remained elastic throughout the test. Interestingly, the moment was insignificant through the first 4 m of the very loose liquefied sand layer indicating that the resultant force on the pile produced by the liquefied soil was negligible. Below the liquefied soil layer, the moment increased with depth for the next 3.5 m, through a very soft clay layer.

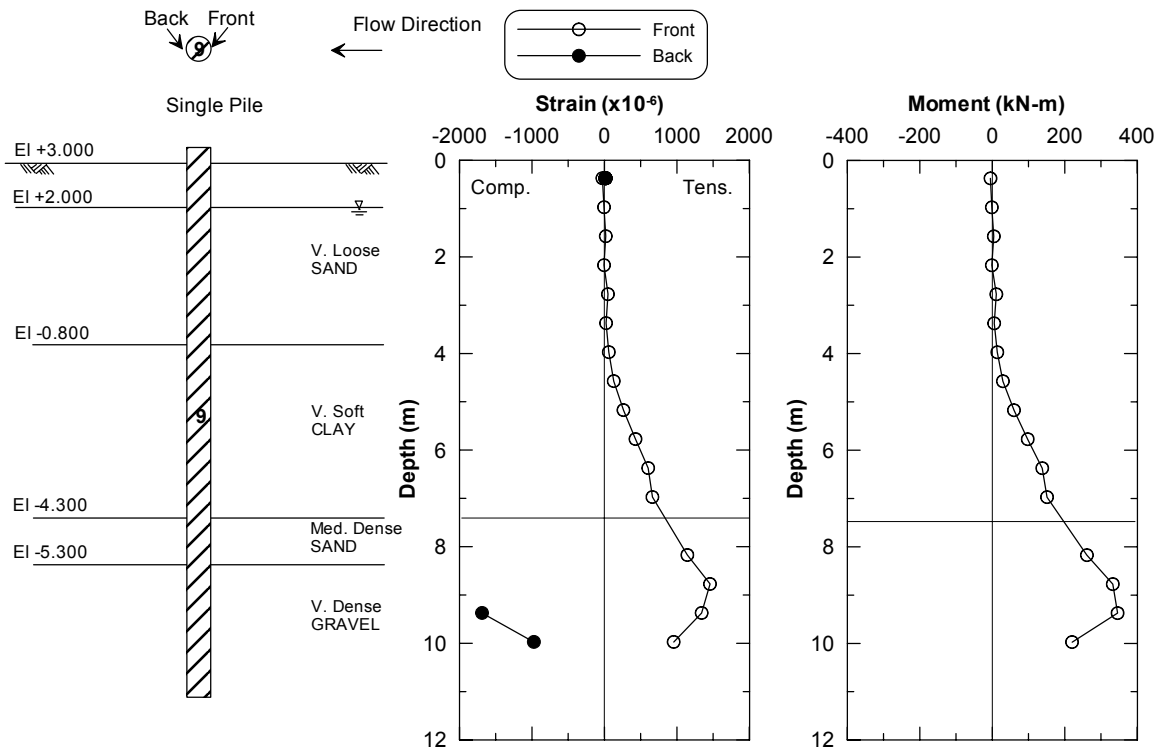


Fig. 4.29 Strain and moment profiles of single pile (No. 9) after the test

4.7.3.2 4-Pile Group

Two piles of the 4-pile group, denoted as No. 7 and No. 8, respectively, were instrumented with strain gages. Time histories of strain along the piles are presented in Appendix G. The strain profiles of pile No. 7 and No. 8 are presented in Figures 4.30 and 4.31, respectively. For pile No. 8, the strains on both sides along the pile were reasonably symmetric, indicating the consistency of strain gage data. The moment distribution of each pile was estimated as presented in Figures 4.30–4.31. The shape of the moment profiles agreed well with the expected behavior of a pile with a fixed-head condition, where a negative moment occurred at the pile head due to the effect of pile-head restraint. The maximum moment occurred at a depth of 9 m below the ground surface as in the case of the single pile. However, the magnitude of the maximum moment was significantly less than that of the single pile because rotational restraint at the pile cap led to a stiffer response under loading applied by the mobile layer. Based on the moment data, all piles in the groups remained elastic.

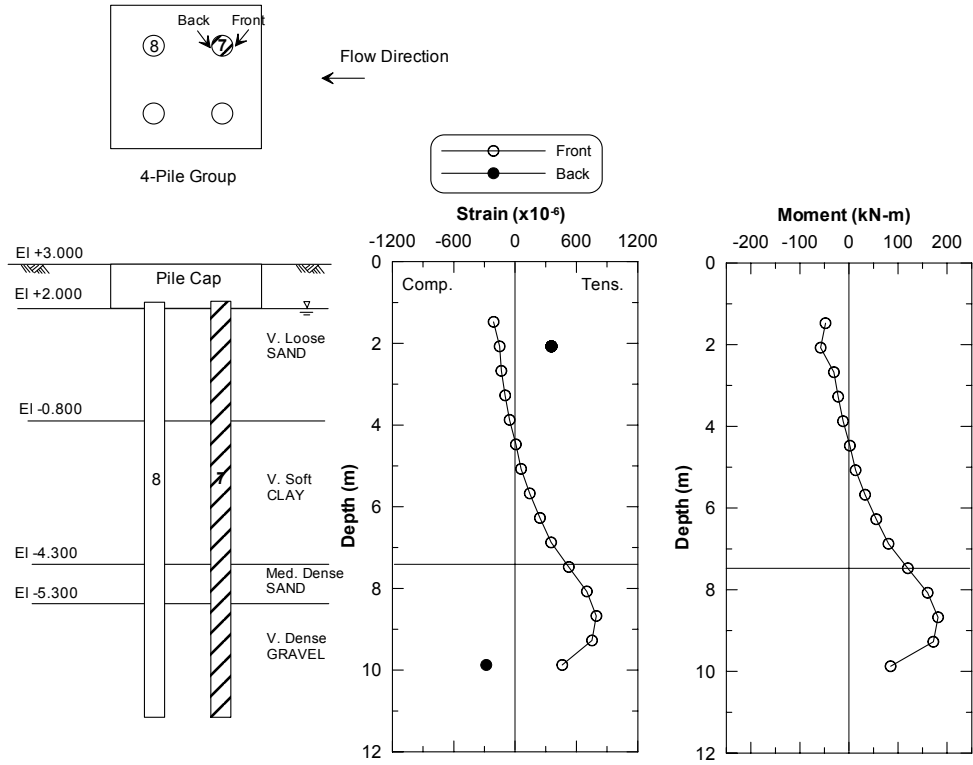


Fig. 4.30 Strain and moment profiles of pile No. 7 (4-pile group) after the test

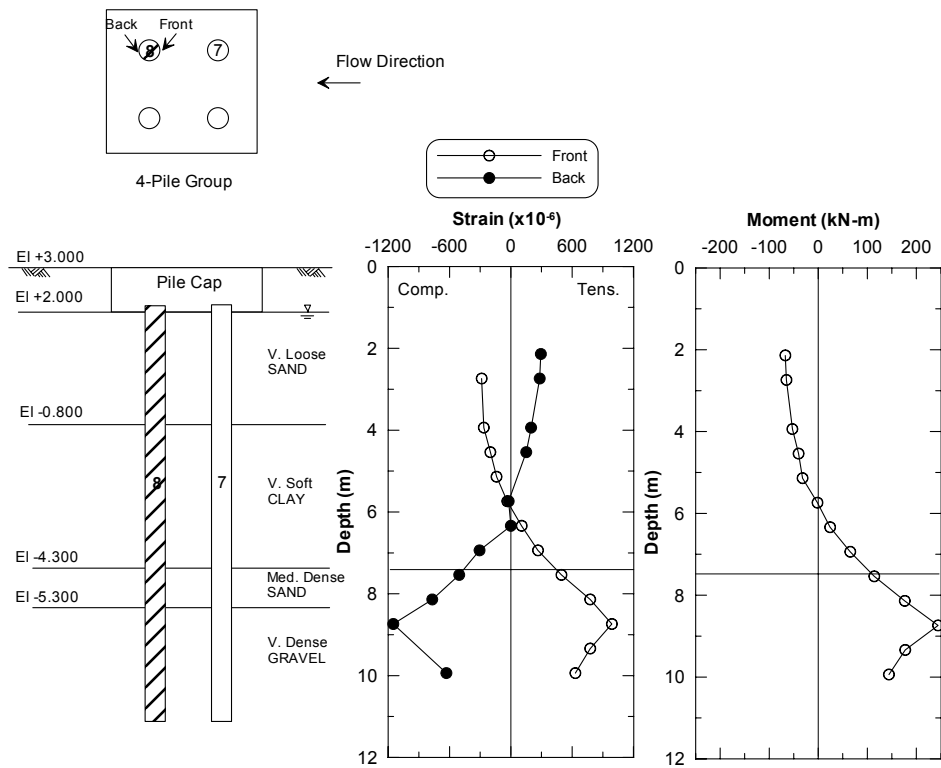


Fig. 4.31 Strain and moment profiles of pile No. 8 (4-pile group) after the test

4.7.3.3 9-Pile Group

Six piles of the 9-pile group, denoted as No. 1, No. 2, No. 3, No. 4, No. 5, and No. 6, respectively, were instrumented with strain gages as presented in Figure 4.4. Time histories of strain along the piles are presented in Appendix G. The strain and moment profiles of each pile are presented in Figures 4.32–4.37. Similar to the results of the 4-pile group, the strain profiles of both sides were reasonably symmetric, showing the consistency of strain data. In addition, the shape of the moment profiles agreed well with the expected behavior of a pile with a fixed-head condition. The moment of each pile in the group was quite similar. However, the moments of piles No. 2 and No. 4 were smaller than the others in the group because both piles were shorter in length, as mentioned earlier, and therefore had a smaller degree of fixity into the dense soil layer. Based on the moment data, all piles in the group remained elastic.

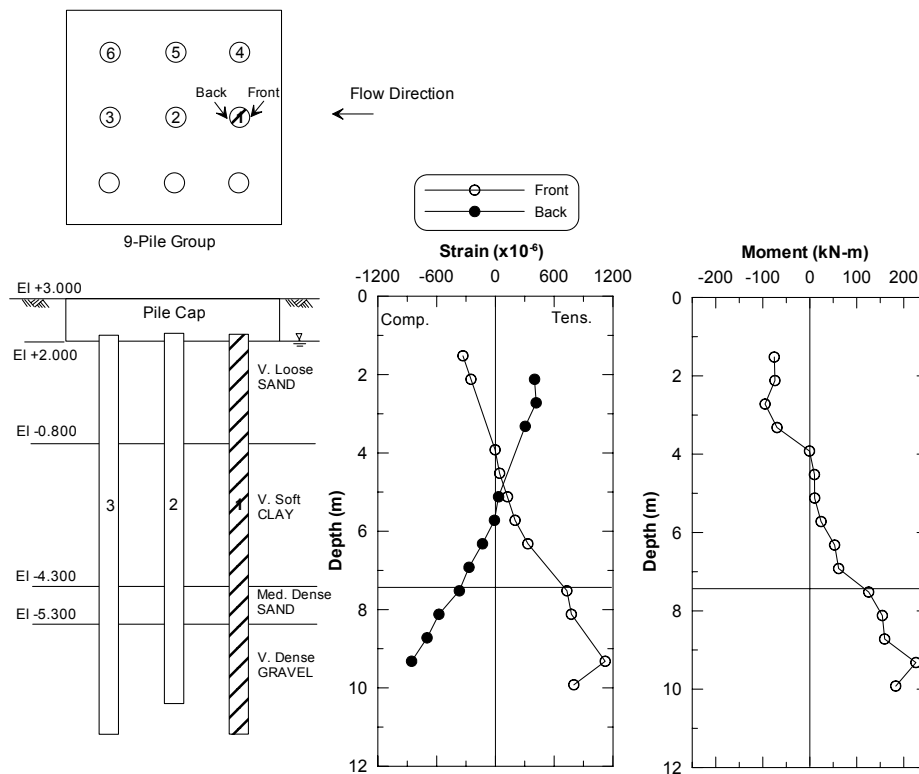


Fig. 4.32 Strain and moment profiles of pile No. 1 (9-pile group) after the test

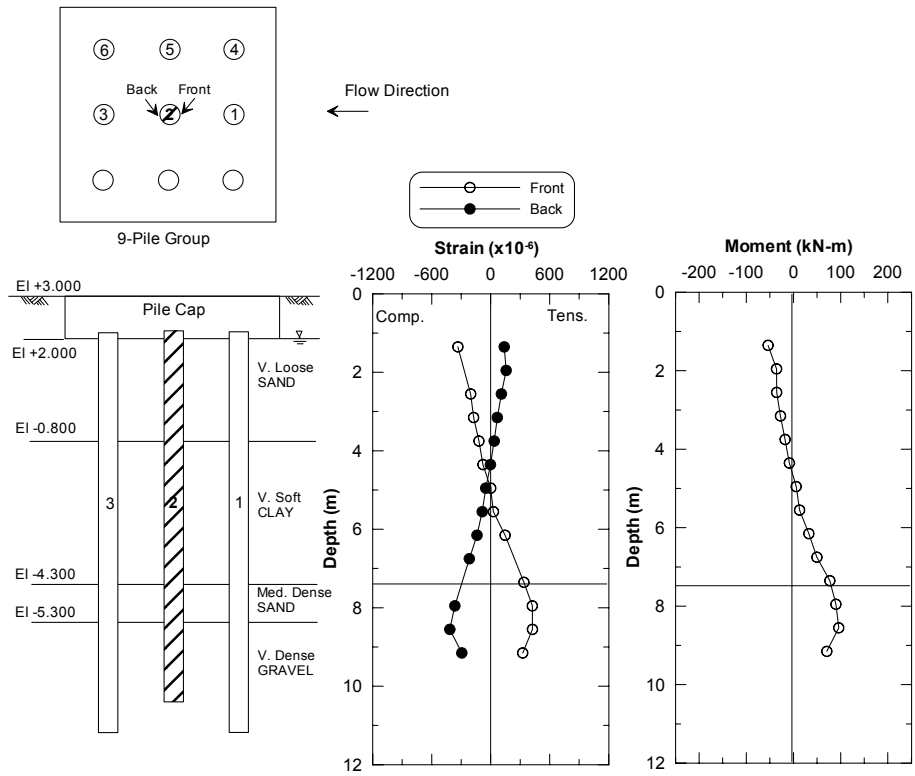


Fig. 4.33 Strain and moment profiles of pile No. 2 (9-pile group) after the test

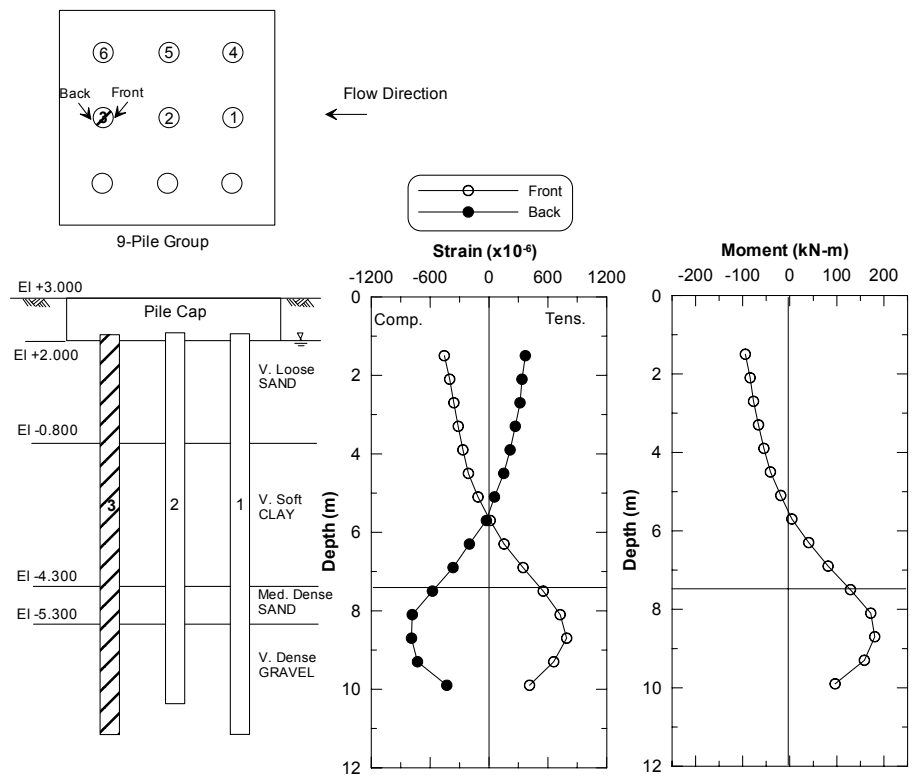


Fig. 4.34 Strain and moment profiles of pile No. 3 (9-pile group) after the test

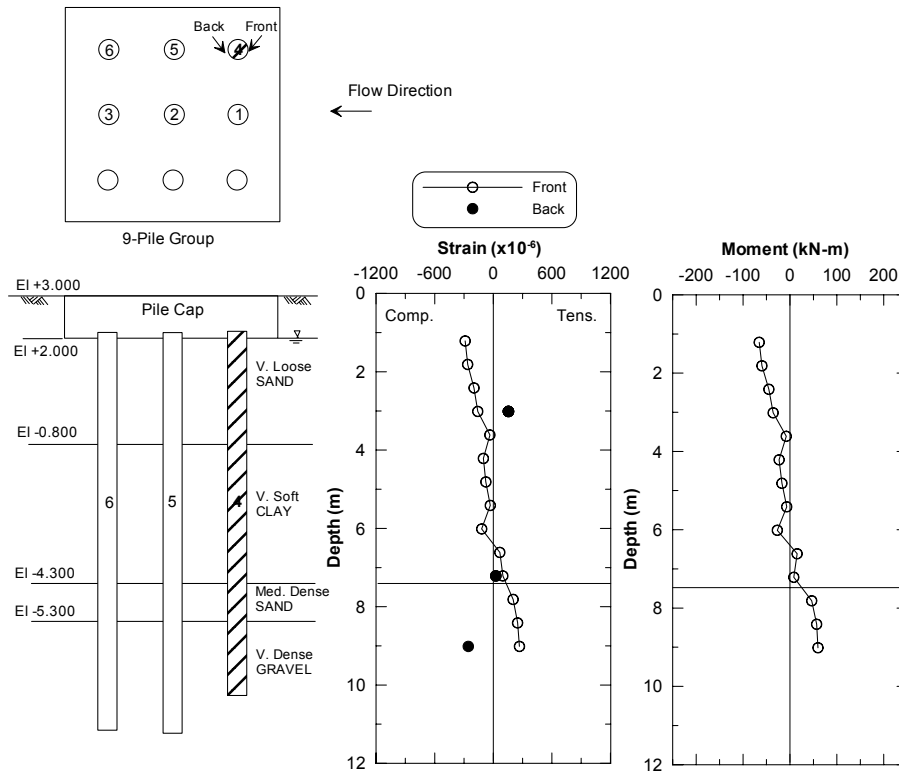


Fig. 4.35 Strain and moment profiles of pile No. 4 (9-pile group) after the test

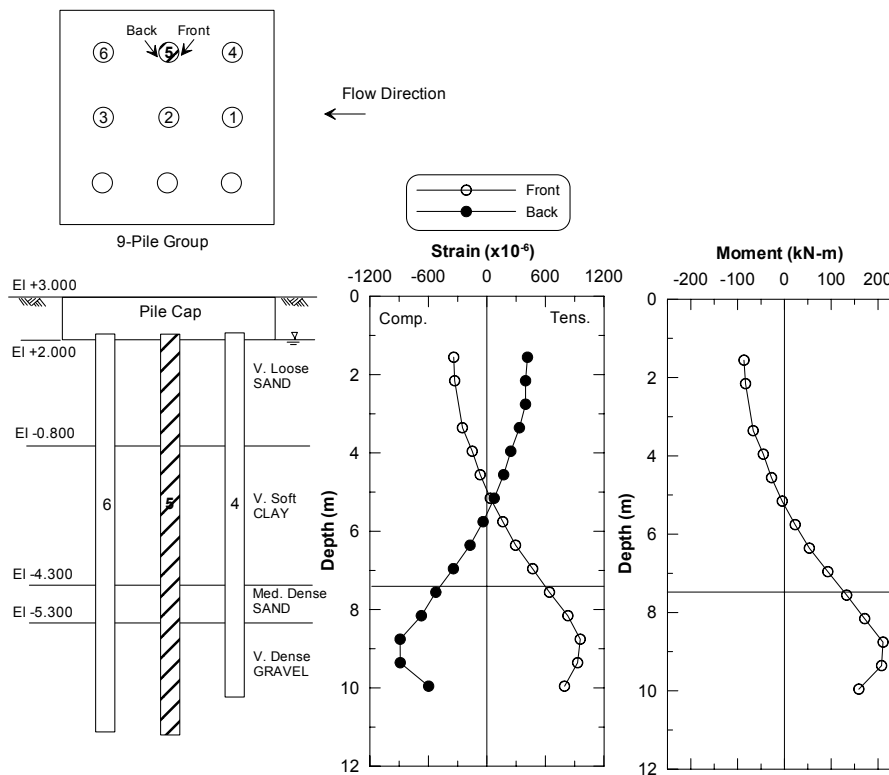


Fig. 4.36 Strain and moment profiles of pile No. 5 (9-pile group) after the test

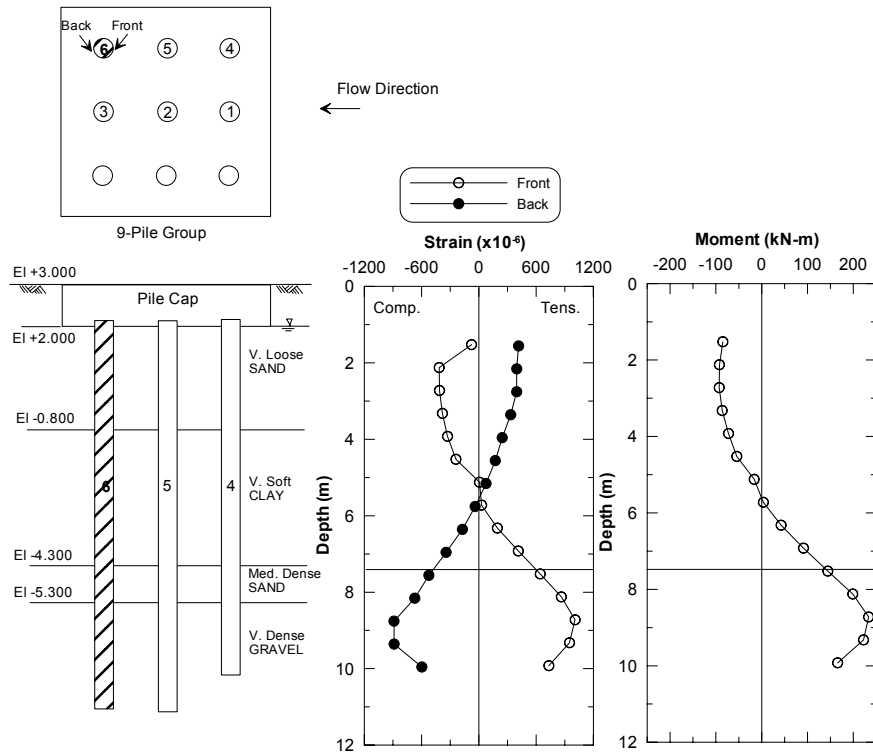


Fig. 4.37 Strain and moment profiles of pile No. 6 (9-pile group) after the test

4.7.3.4 Pipelines

Strain time histories of both transverse and longitudinal pipelines are summarized in Appendix G. The strain distributions along the transverse pipelines are presented in Figure 4.38. The strain data of pipelines were somewhat irregular because the pipelines were subjected to nonuniform soil pressure along their entire lengths, produced by compression waves from the blasting. The strain distribution along the side of the electrical conduit was smaller than the gas pipeline. The reason is that for the same pipeline curvature distribution (i.e., both pipelines experienced the same movement, as shown in Figure 4.26), the larger diameter pipeline produces larger strain. Strain data also show that both pipelines performed relatively well without yielding.

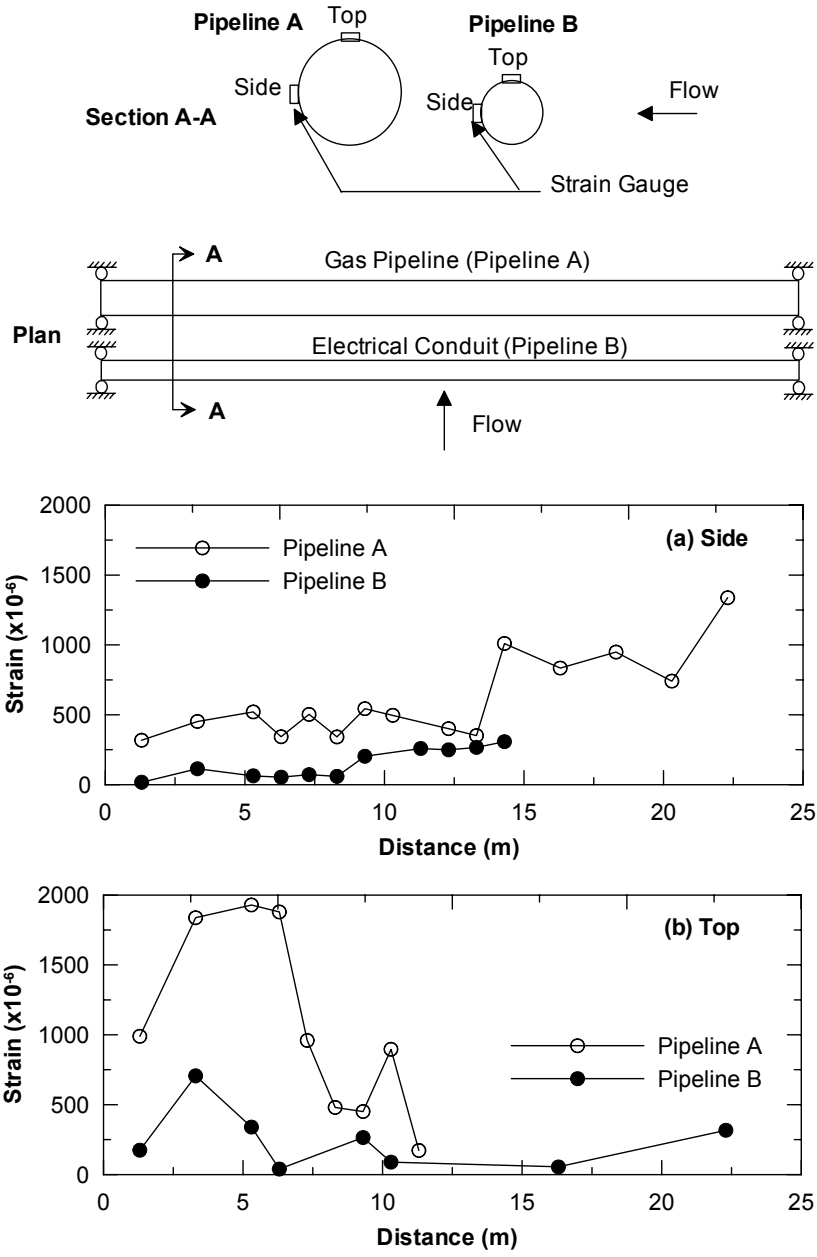


Fig. 4.38 Strain distribution along transverse pipelines: (a) side gages and (b) top gages

The strain distribution along the side of the longitudinal gas pipeline is shown in Figure 4.39a. Initially, it was aimed at measuring the axial strain along the pipeline due to the axial frictional forces imposed by the soil movement relative to the pipeline. Theoretically, if the soil moves parallel to the direction of the pipeline, the maximum strain should occur at the support and gradually decrease to zero at the end of the pipeline. However, the measured strain distribution shows that the maximum moment occurred at the middle of the pipelines because the

soil movement produced by the blasting caused the pipeline to move significantly in the transverse direction compared to the longitudinal direction, as shown by the survey data in Figure 4.26. Small strain observed in the vicinity close to the support indicates that the frictional forces imposed by the soil movement in this case was negligible and would not cause damage to the pipeline. However, the amount of strain along the top and bottom of the pipeline due to settlement was noticeable, as shown in Figure 4.39b. The symmetry of strain gage data along the top and bottom indicated the consistency of data. This bending strain, due to the soil settlement, appeared to be more important than that due to the frictional forces, and therefore should be considered in the design.

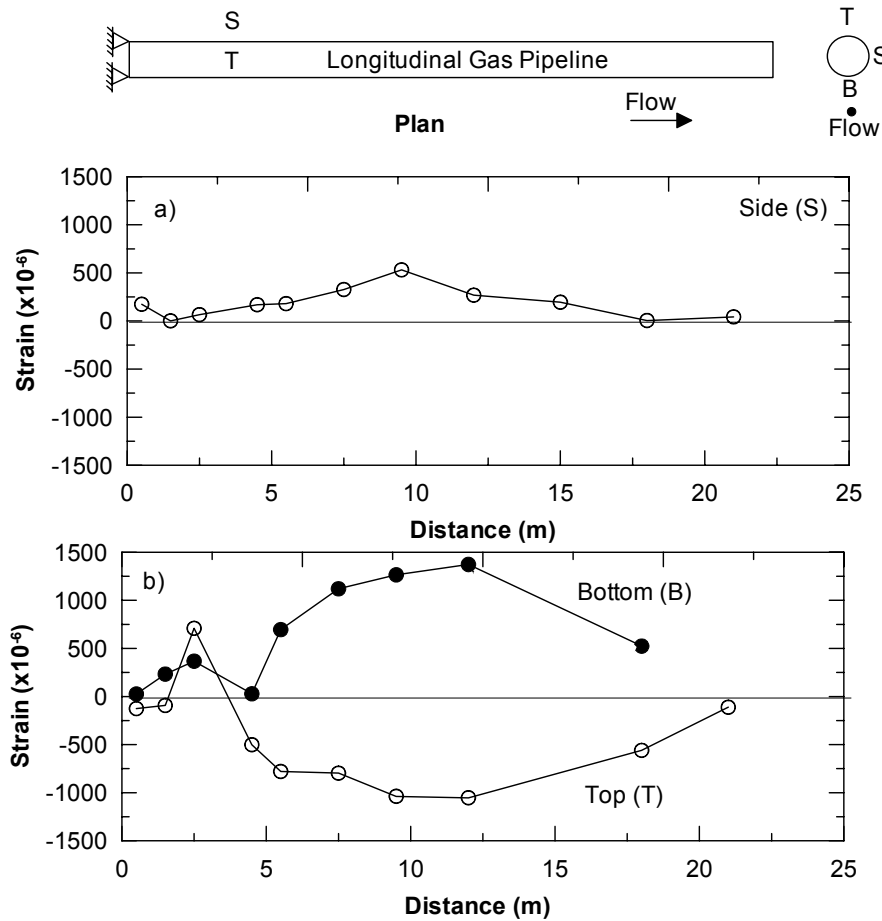


Fig. 4.39 Strain distribution along longitudinal pipeline: (a) side gages and (b) top and bottom gages

4.7.4 Results from Other Instrumentation

4.7.4.1 Soil Pressure Cells

The data of soil pressure cells on the caps of the 4-pile and 9-pile groups are presented in Figure 4.40. The data of several soil pressure cells seem to be inconsistent. However, a few soil pressure cells (i.e., SPC-3, SPC-5, and SPC-7) appeared to work properly (i.e., small noise in the time-history plot). By considering only the good ones, the results show that the soil pressures on both sides of the pile cap were fluctuating during the test due to the effect of the blasting. Once the blasting stopped, the soil pressure cells on the upstream side of the pile caps (i.e., SPC-3 and SPC-7) show an increase of the pressure, indicating that the soil pushed the caps and provided passive pressure to the caps. Soil pressure cell SPC-5 located on the downstream side of the cap, on the other hand, shows a decrease of the soil pressure, implying that the soil moved away from the cap and provided active pressure to the cap. However, the change in soil pressures acting on the pile caps appeared to be relatively small, less than 3 kN/m^2 .

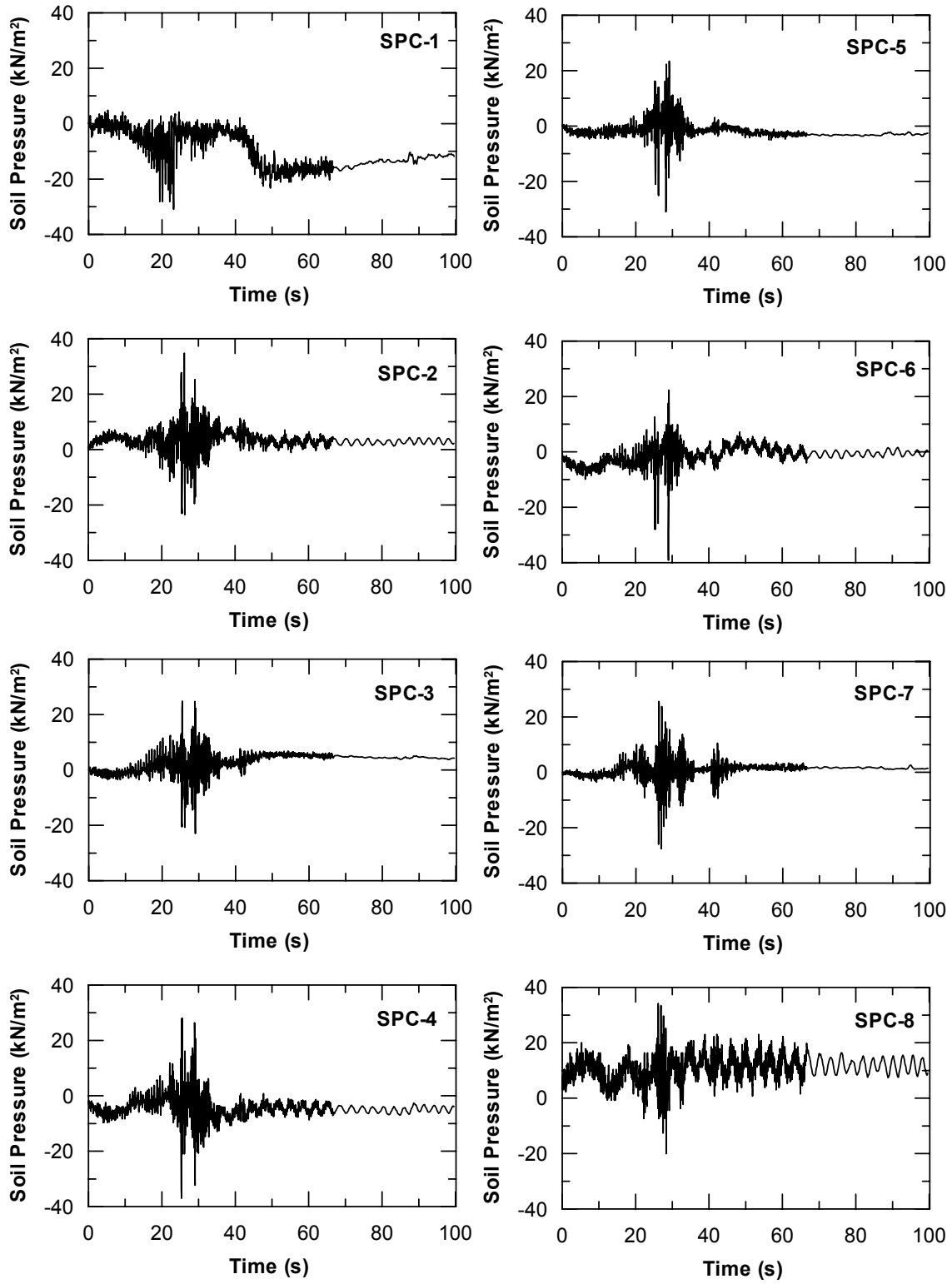


Fig. 4.40 Soil pressure time histories on pile caps

4.7.4.2 Accelerometers

An accelerometer was installed at the pile head of each test pile foundation system. Acceleration time histories at the pile heads are presented in Figure 4.41. The test results show that the peak acceleration was dependent on the lateral stiffness of pile foundation system. The peak acceleration of the 9-pile group was lowest, while that of the single pile was largest.

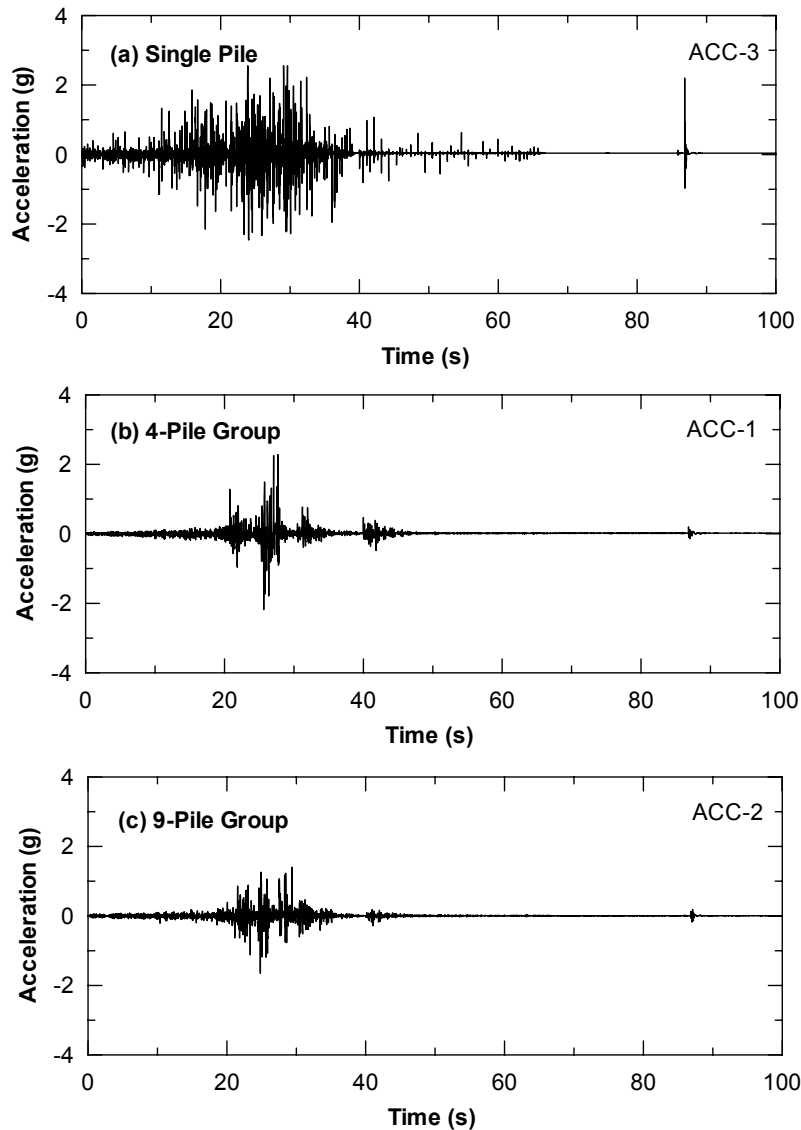


Fig. 4.41 Pile-head accelerations for (a) single pile, (b) 4-pile group, and (c) 9-pile group

4.7.4.3 Tiltmeters

Several tiltmeters were installed along the piles but most of them were damaged during pile driving. Only two tiltmeters installed at the pile tops were available: the single pile and 9-pile group. The data in Figure 4.42 show that the pile-head rotation of the single pile (free-head condition) was approximately 2 degrees at the end of the test, while the rotation of the 9-pile group (fixed-head condition) was insignificant, about 0.2 degrees.

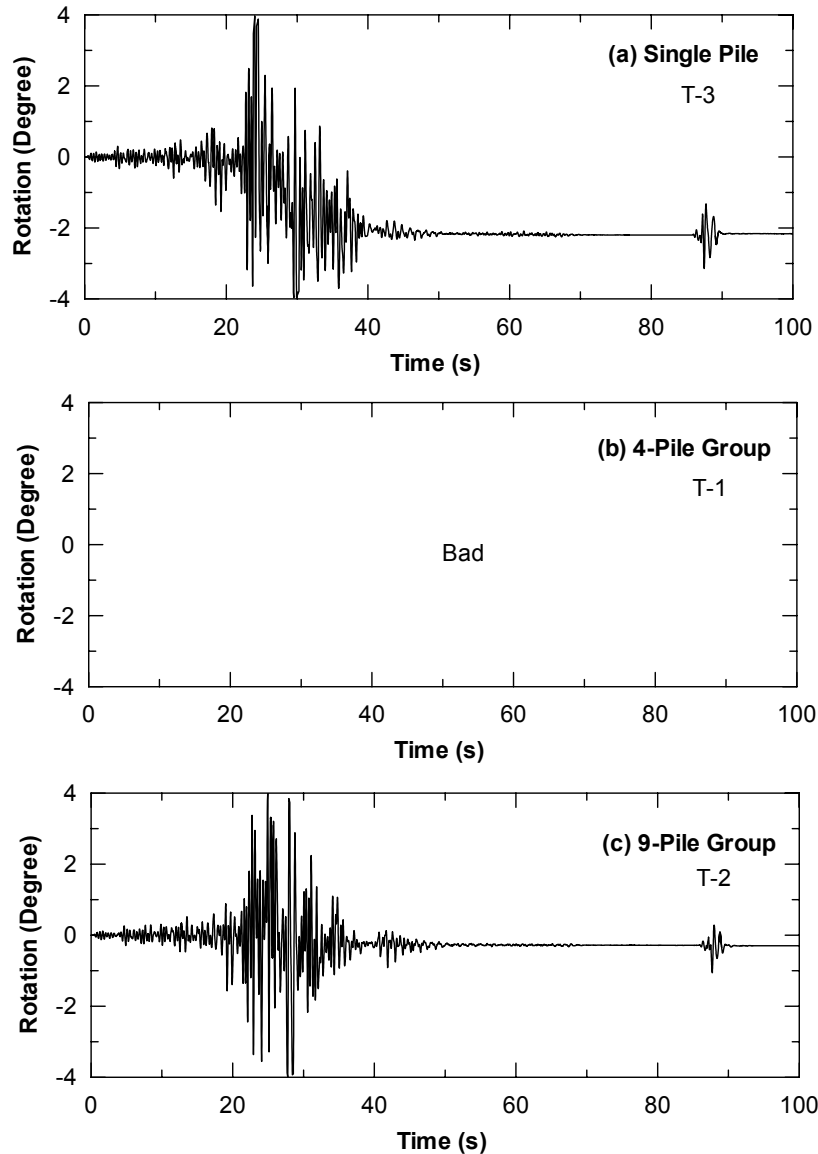


Fig. 4.42 Pile-head rotations for (a) single pile, (b) 4-pile group, and (c) 9-pile group

4.7.4.4 Linear Potentiometers

The measurements obtained from string activated linear potentiometers are presented in Figures 4.43–4.45. A summary of relative movement between two points of interest after the blast is given in Table 4.9. According to the measurements, it can be observed that the movements of the single pile (No. 9) and the soil in front of the pile were approximately the same, while the movements of the Waseda single piles were greater than the soil. This might be due to the fact that the pile tips of Waseda piles were located just above the dense layer; while the UCSD pile was penetrated 3 m into the dense layer. The Waseda piles were therefore likely to behave like rigid piles in which the rotation and movement at the pile tip were expected. In contrast, the UCSD pile behaved more like a flexible pile where the rotation and the movement at the pile tip was insignificant. Therefore, the displacement at the pile head of the UCSD single pile was less than those of the Waseda piles. As expected, the soil in front of and behind the pile groups moved approximately 8–15 cm more than the pile groups. It is noted that some error on the measurements was expected due to the uplift of slope inclinometer casing, as noted in Table 4.9.

The relative displacements obtained from linear potentiometers were also used to verify the accuracy of the measurements from GPS units. Two locations were evaluated in this study. One of them was the relative displacement between the single pile (GPS-1D) and slope inclinometer casing S7 (GPS-1E). The other was the relative displacement between the 9-pile group and slope inclinometer casing S1.

Table 4.10 presents comparisons of relative displacements obtained from GPS units and linear potentiometers. Excellent agreement between both measurements was observed. The difference between both measurements was within the accuracy of real time kinematics GPS methods, 1 cm. This confirmed the accuracy of the measurements obtained from the GPS units.

Table 4.9 Summary of relative displacements obtained from linear potentiometers

Name	Location	Relative movement (m)	Interpretation	Remarks
STP-1	9-pile group and Inc. S1 (upstream)	-0.096	The soil moved 96 mm more than the pile group.	
STP-2	9-pile group and Inc. S2 (downstream)	+0.144	The soil moved 144 mm more than the pile group.	
STP-3	Single pile and Inc. S7 (upstream)	+0.002	The soil and the single pile moved together.	
STP-4	4-pile group and Inc. S8 (upstream)	-0.080	The soil moved 80 mm more than the 4-pile group.	S8 moved 0.3 m upward.
STP-5	Single pile (W1) and Inc. S11 (upstream)	+0.158	The pile moved 158 mm more than the soil.	S11 moved 0.2 m upward.
STP-6	Single pile (W2) and Inc. S11 (upstream)	+0.074	The pile moved 74 mm more than the soil.	S11 moved 0.2 m upward.
STP-7	Single pile (W1) and Single pile (W3)	+0.008	Both piles had the same movement.	
STP-8	4-pile group and anchor pile	+0.170	The anchor pile moved more than the 4-pile group.	
STP-9	Anchor pile and quay wall	+0.347	The quay wall moved more than the anchor pile.	

Table 4.10 Verification of GPS measurements with data from potentiometers

GPS Location	Potentiometer Location	GPS Measurement (m)	Potentiometer Measurement (m)
GPS 1A - 1B	STP-1	0.106	0.096
GPS 1E -1D	STP-3	0.012	0.002

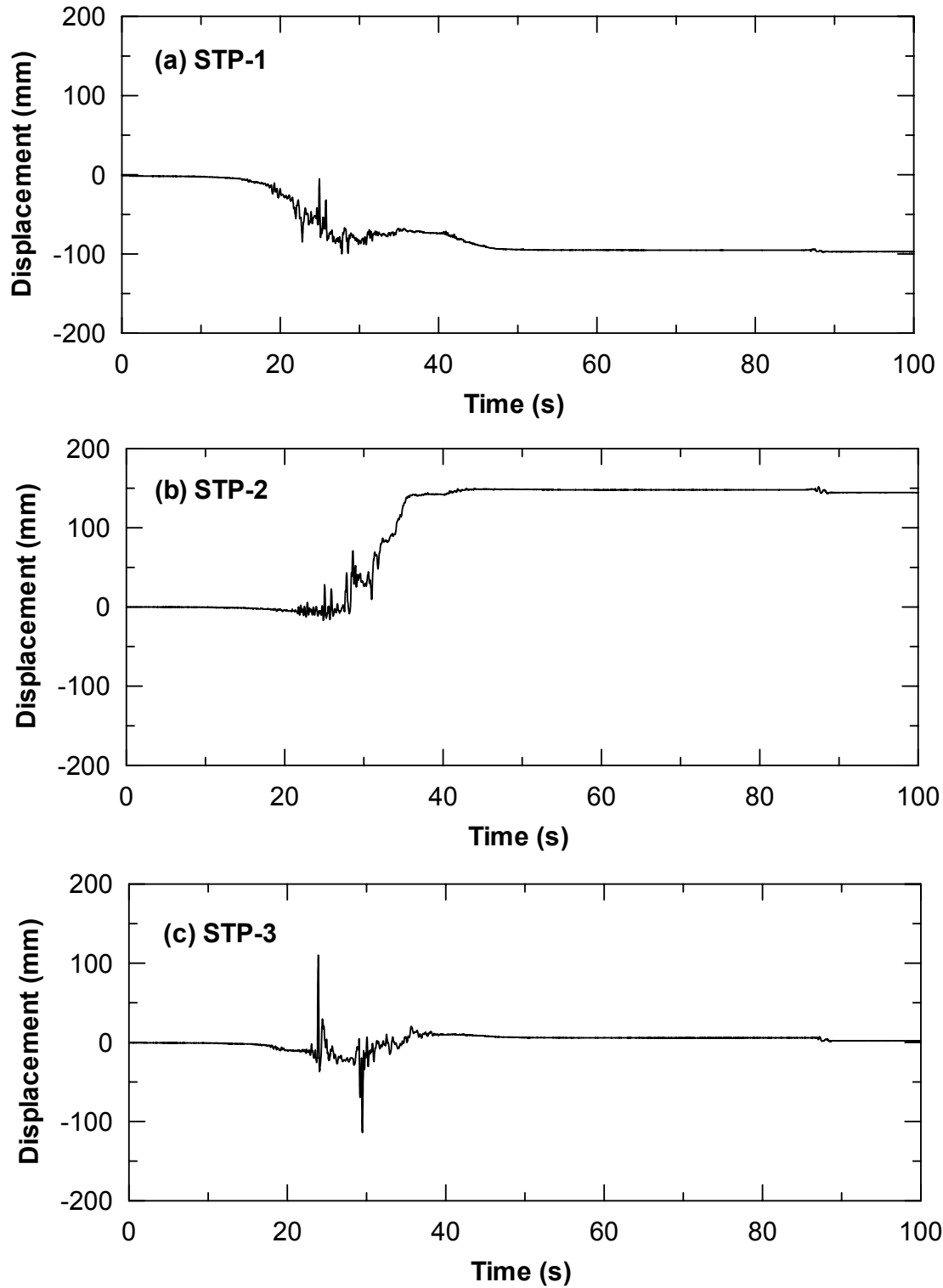


Fig. 4.43 Relative displacement between (a) S1 and 9-pile group, (b) S2 and 9-pile group, and (c) S7 and single pile

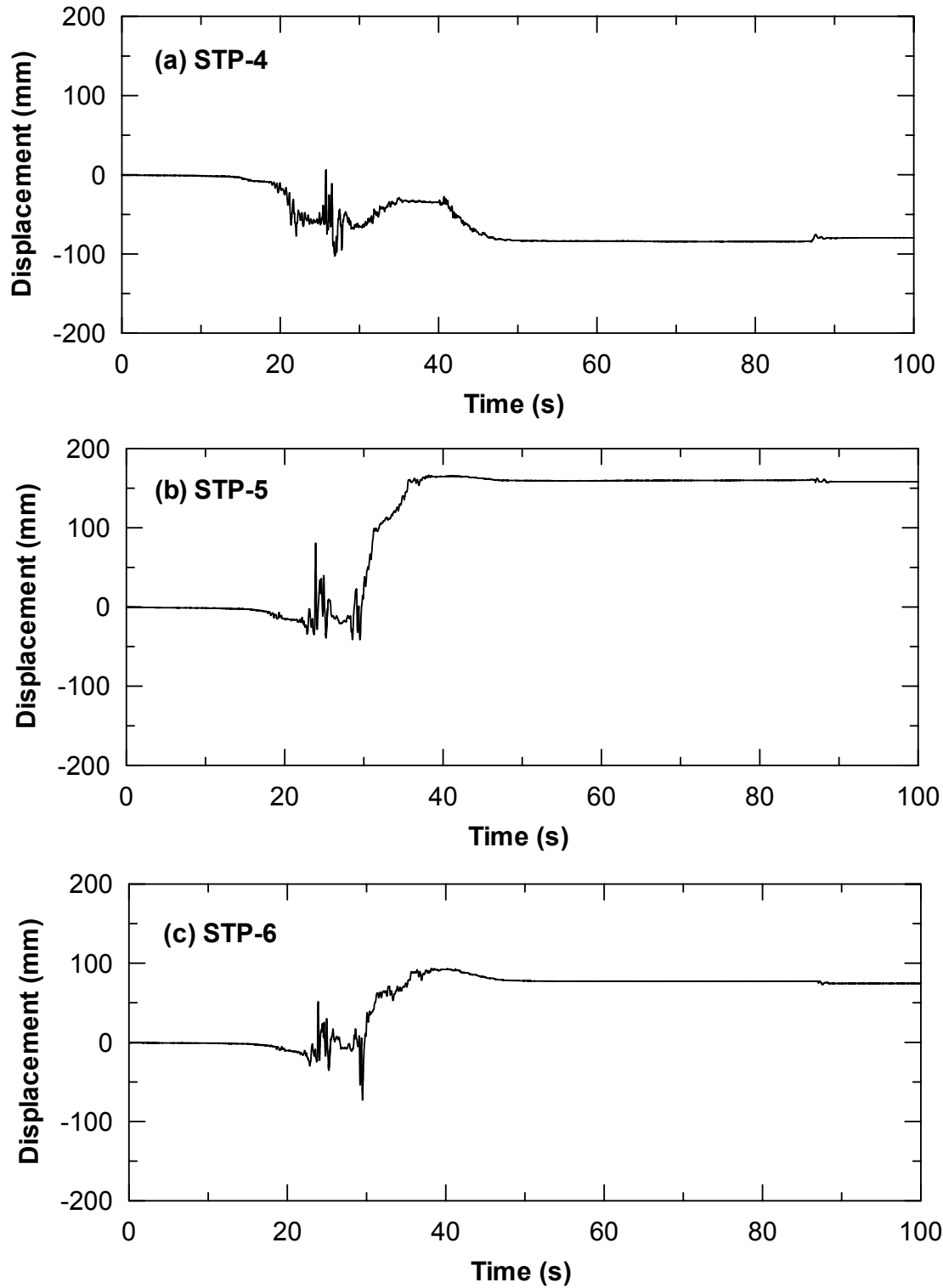


Fig. 4.44 Relative displacement between (a) S8 and 4-pile group, (b) S11 and W1 pile, and (c) S11 and W2 pile

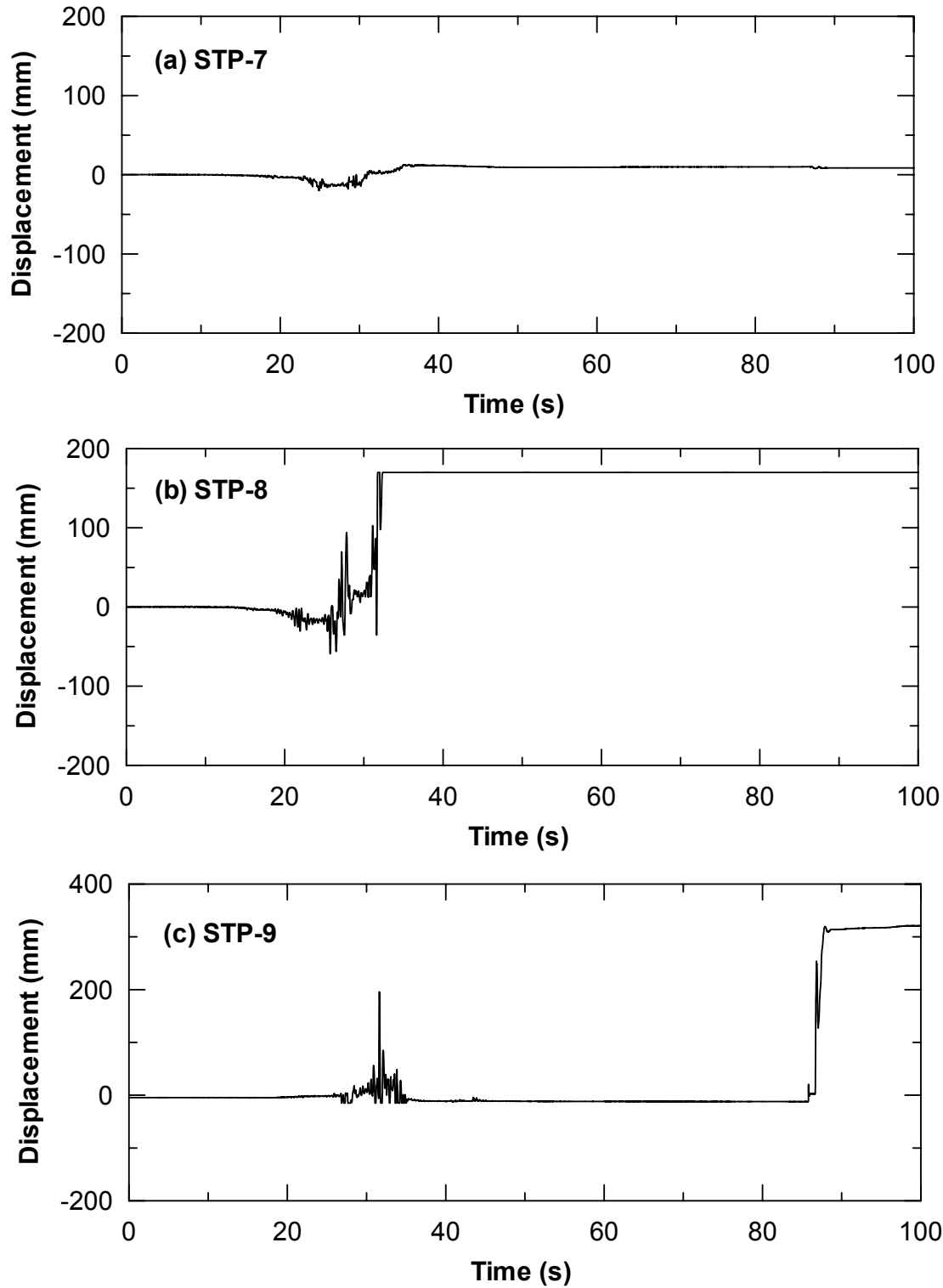


Fig. 4.45 Relative displacement between (a) pile W1 and pile W3, (b) 4-pile group and anchor pile, and (c) anchor pile and quay wall

5 Second Full-Scale Lateral Spreading Test

The second lateral spreading test was carried out about one month after the first test with the same test piles and instrumentation from the first experiment still in place. The test was performed in an attempt to induce additional ground deformations and further evaluate the performance of the piles subjected to a higher level of soil deformation.

5.1 SITE LAYOUT

The test site for the second lateral spreading test was modified from the first as shown in Figure 5.1. Photographs of the site are shown in Figures 5.2–5.3. The quay wall and sheet piles surrounding the test site were removed. The waterway was excavated on one end of the test site to an elevation of -1.00 m with a slope of 2:1. Water was then filled to an elevation of +2.00 m. However, the actual groundwater table observed from the soil excavation adjacent to the test area was approximately 1 m lower, likely due to lack of rain for about one month. The ground surface was level for a distance of 7.5 m away from the edge of the waterway, and then started sloping upward at 6%.

The weather during the second lateral spreading experiment was quite poor as shown in Figure 5.4, with a heavy snowfall of about 0.50 m and wind speeds of 100 kph on the test day. The ground was frozen to a depth of approximately 0.20 m below the ground surface. The frozen ground would likely impede lateral spreading. In an attempt to mitigate this problem, jackhammers were used to break up the frozen ground into small blocks in the vicinity of the test piles.

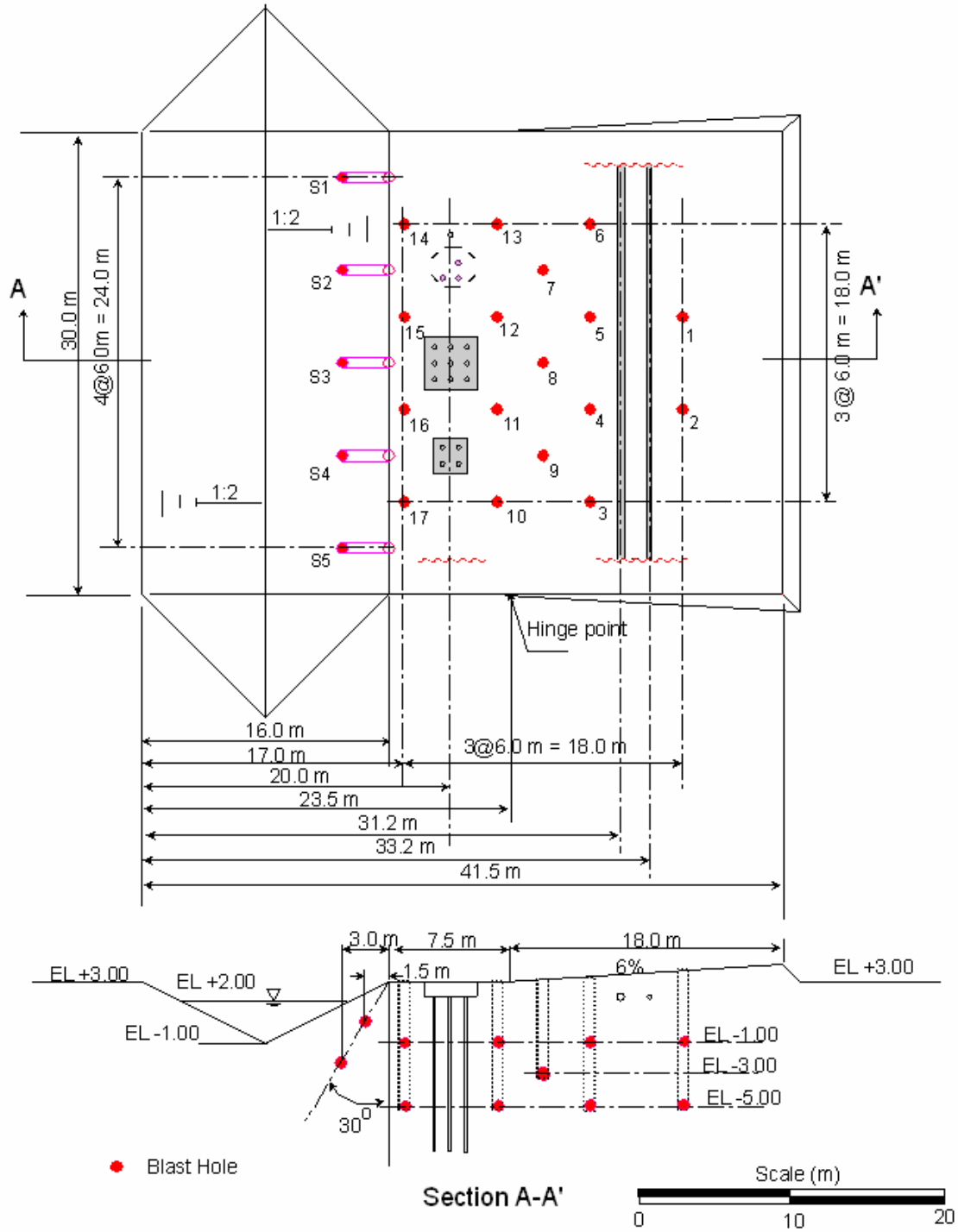


Fig. 5.1 Layout of second full-scale lateral spreading test



Fig. 5.2 Site condition of second full-scale lateral spreading test (front)



Fig. 5.3 Site condition of second full-scale lateral spreading test (side)



Fig. 5.4 Bad weather during the second test

5.2 INSTRUMENTATION

Since the same test piles and instrumentation from the first experiment still in place, the instrumentation in the second test was essentially the same as the first experiment. Only locations of GPS units and linear potentiometers were changed from the first test. A layout of instrumentation for the second full-scale test is presented in Figure 5.5.

5.3 BLASTING SEQUENCE

The blast holes were spaced at 6.0 m on center in a regular grid pattern as shown in Figure 5.6. The charges were installed at depths of 4.0 m and 8.0 m below the design ground surface (El +3.00 m). The amount of charges varied from 2–4 kg with the charges being smaller in the vicinity of test piles to prevent damages to the large number of instruments installed in the vicinity. Two additional rows of blast holes were drilled. One was located on the steep slope adjacent to the waterway, with the amount of explosives ranging from 1–3 kg. The purpose of these explosives was to create movement at the slope toe prior to the primary blasting sequence such that the embankment soil behind it had a high potential to move freely with larger deformation once the primary blasting initiated. The other additional blast holes were located

between the pipelines and pile as denoted as blast holes No. 7–No.9. Three kilograms of explosives were installed at El. –3.00 m.

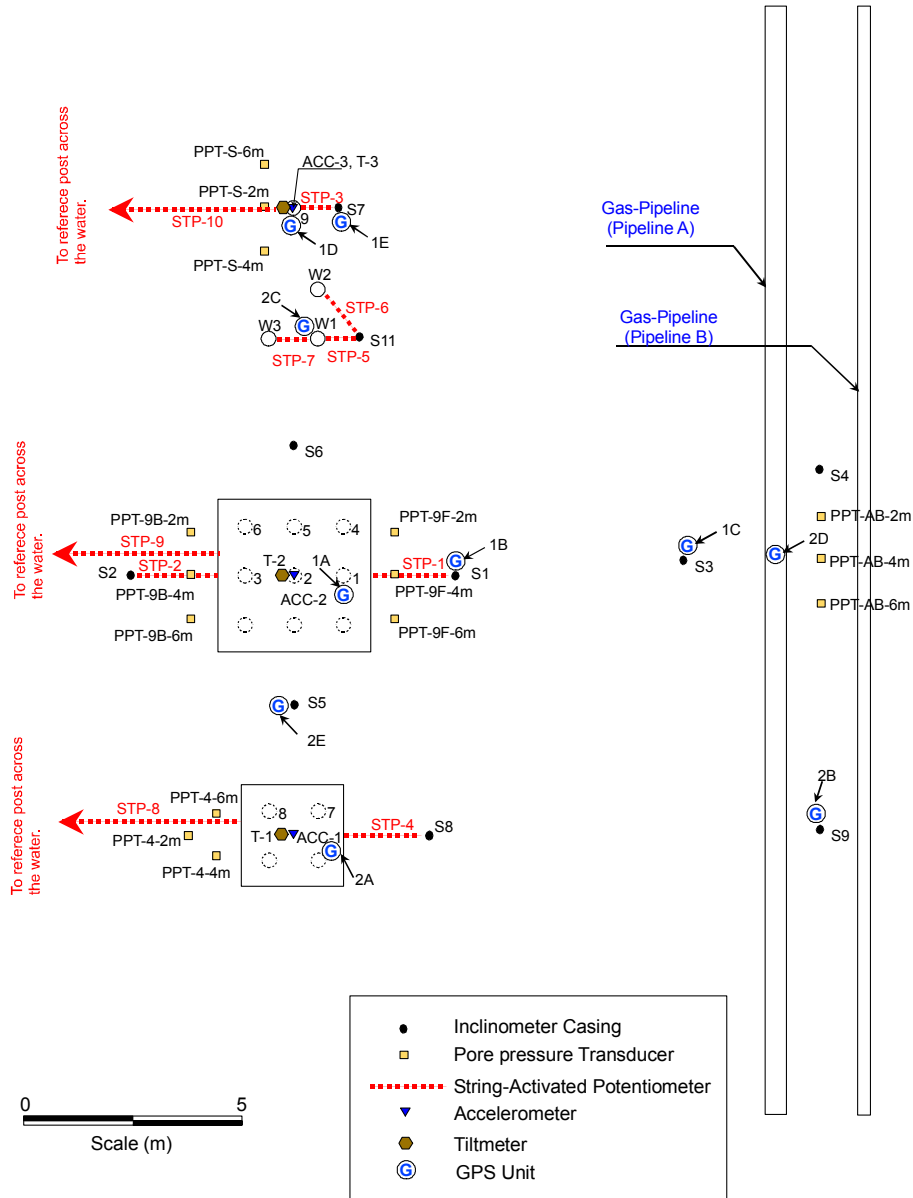


Fig. 5.5 Layout of instrumentation for second full-scale lateral spreading test

As shown in Figure 5.6, the explosives under the steep slope (S5 to S1) were detonated first. Approximately 15 second later, the primary blasting sequence was initiated at the rear of the embankment (No. 2) and continued sequentially toward the waterway.

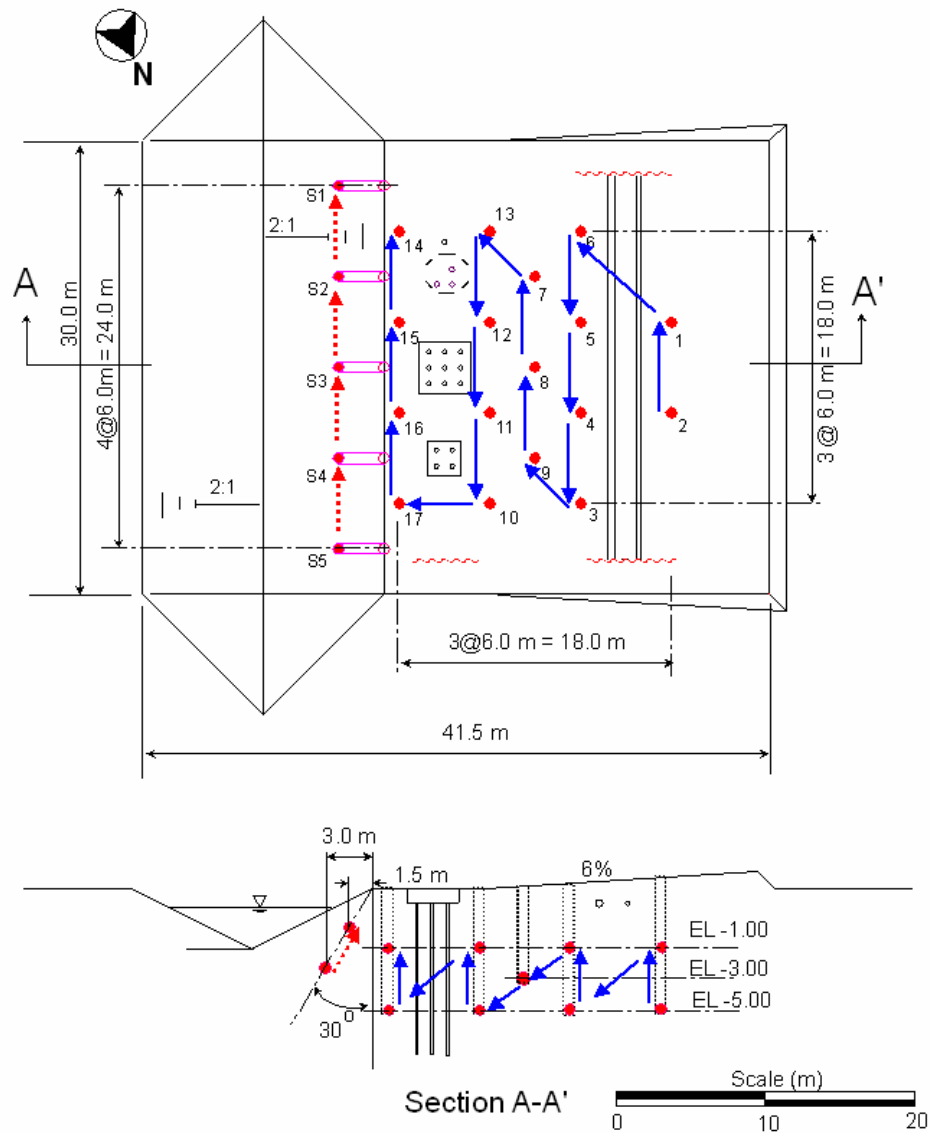


Fig. 5.6 Blasting sequence for second full-scale lateral spreading test

5.4 TEST RESULTS

5.4.1 Excess Pore Pressure

The excess pore-pressure ratio, R_u , time history for each location in the second test is given in Appendix H. A typical R_u time history is shown in Figure 5.7. This transducer was located upslope of the 9-pile group at 4 m depth. The excess pore-water pressures began to build up immediately after the initiation of blasting at the slope toe, between 0–3 seconds. Once the

primary blasting occurred, at 18 seconds, excess pore-water pressures continued to increase and reached the maximum at about 25 seconds.

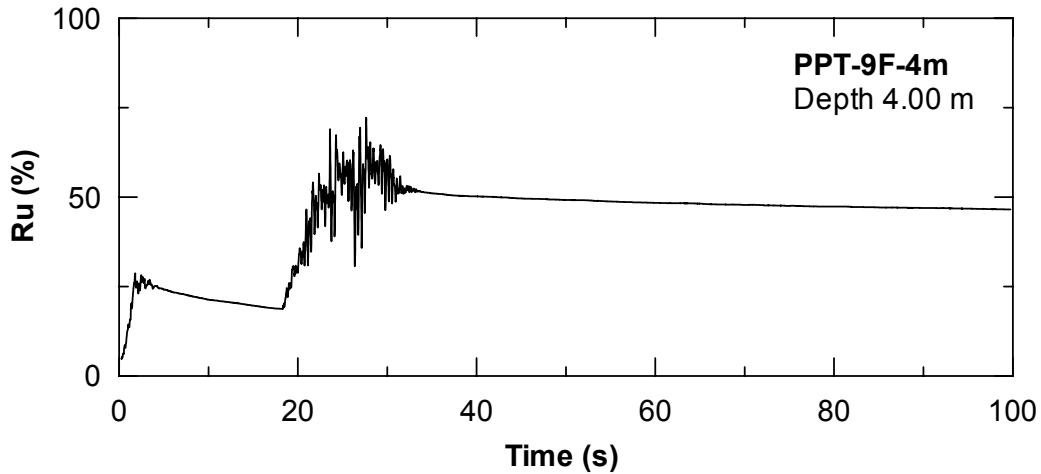


Fig. 5.7 Excess pore-pressure time history nearby 9-pile group

The R_u in the second test appeared to be much less than measured during the first test with values at the end of the blast ranging between 25%–60% and averaging 41%. The lower R_u measured in the second test may be because the soil conditions were less susceptible to liquefaction due to two possible reasons. First, the soil was densified as a result of the first test, which in turn decreased the potential of liquefaction. Based on survey data one day after the first test, soil settlement was 10–15 cm in the vicinity of the piles (Fig. 5.8), corresponding to the vertical strain of about 3–4%. This settlement occurred due to the dissipation of excess pore-water pressure in the loose sand layer. Second, the groundwater table in the second test was lower than that observed in the first test as mentioned previously. Associated with this lower water table, the effective overburden stress for the soil in the second test was higher than that in the first test. As such, with relatively the same blasting energy for both tests, the soil in the second test was more difficult to liquefy (i.e., required higher excess pore-water pressure build-up to liquefy the soil).

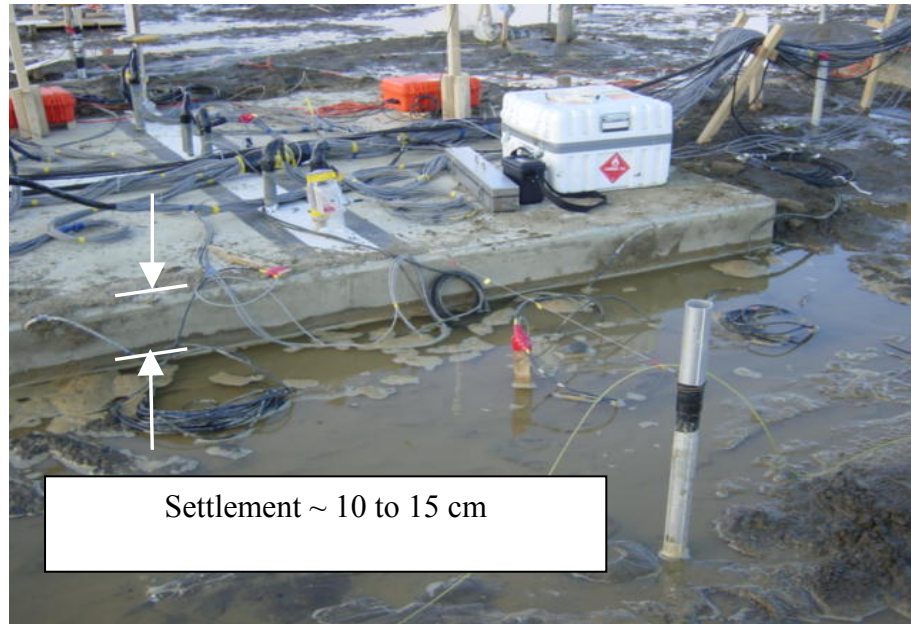


Fig. 5.8 Observed settlement near 9-pile group (one day after the first experiment)

5.4.2 Displacements of Soil and Test Lifelines

5.4.2.1 Surface Displacement

GPS units were used to monitor the movements of both the ground surface and test lifelines during lateral spreading. The measurements were conducted by a research team from Caltrans (Turner 2002). The results of each GPS unit are given in Appendix I.

Displacements in longitudinal, transverse, and vertical directions obtained at 1 minute and 20 hours after the blasting are summarized in Tables 5.1–5.2, respectively. Similar to the first full-scale test, no horizontal creep was observed over 20 hours after the blast. Most of the horizontal displacement associated with the lateral spreading took place within ten seconds after the blast.

Table 5.1 Summary of GPS data for second Japan blast test, approximately 1.3 minutes following blasting (data from Caltrans)

Location	Displacement (m)			Horizontal Displacement (m) (x-y plane)	Angle to Flow Direction (Degree)
	Longitudinal (x)	Transverse (y)	Vertical (z)		
1A	0.155	-0.022	0.009	0.157	8.06
1B	0.151	-0.017	0.066	0.151	6.34
1C	0.195	-0.048	0.015	0.201	13.81
1D	0.299	0.004	0.002	0.299	-0.70
1E	0.226	0.054	0.010	0.232	-13.37
2A	0.183	-0.012	0.009	0.184	3.83
2B	0.103	-0.039	0.028	0.110	20.98
2C	0.473	0.002	-0.019	0.473	-0.19
2D	0.170	-0.020	-0.107	0.171	6.71
2E	0.445	-0.018	-0.015	0.445	2.27

Table 5.2 Summary of GPS data for second Japan blast test, approximately 20 hours following blasting (data from Caltrans)

Location	Displacement (m)			Horizontal Displacement (m) (x-y plane)	Angle to Flow Direction (Degree)
	Longitudinal (x)	Transverse (y)	Vertical (z)		
1A	0.149	-0.023	-0.001	0.151	8.76
1B	0.149	-0.016	0.047	0.150	6.24
1C	0.193	-0.034	-0.009	0.196	9.99
1D	0.296	0.011	-0.015	0.296	-2.17
1E	0.224	0.055	-0.012	0.230	-13.79
2A	0.171	-0.021	0.007	0.172	6.99
2B	0.104	-0.045	0.044	0.114	23.36
2C	0.475	0.005	-0.024	0.475	-0.57
2D	0.169	-0.022	-0.144	0.170	7.37
2E	0.459	-0.008	-0.022	0.459	1.00

Figure 5.9 presents the horizontal displacement vectors of the second test obtained from GPS units and survey data. The horizontal soil movements on the upslope side that occurred in the second test were significantly lower than those in the first test with an average value of 15 cm. This is likely because the soil condition in the second test was less susceptible to liquefaction as mentioned earlier, and the duration of blasting was significantly shorter than in the first test. Similar to the first test, the magnitude of soil movement generally decreased with increasing distance from the waterway. The maximum soil movement was observed between both pile groups with a magnitude of 46 cm. Based on displacement time histories recorded by GPS unit 2E as presented in Figure 5.10, it was found that 10 cm of the 46 cm of soil movement contributed to failure of the slope immediately after the first set of the blast at the slope toe. The movements of the single pile, 4-pile group, and 9-pile group were slightly less than in the first test with magnitudes of 28 cm, 18 cm, and 16 cm, respectively. Both of the transverse pipelines moved together with the surrounding soil with the maximum movement approximately 15 cm at the center of the pipelines.

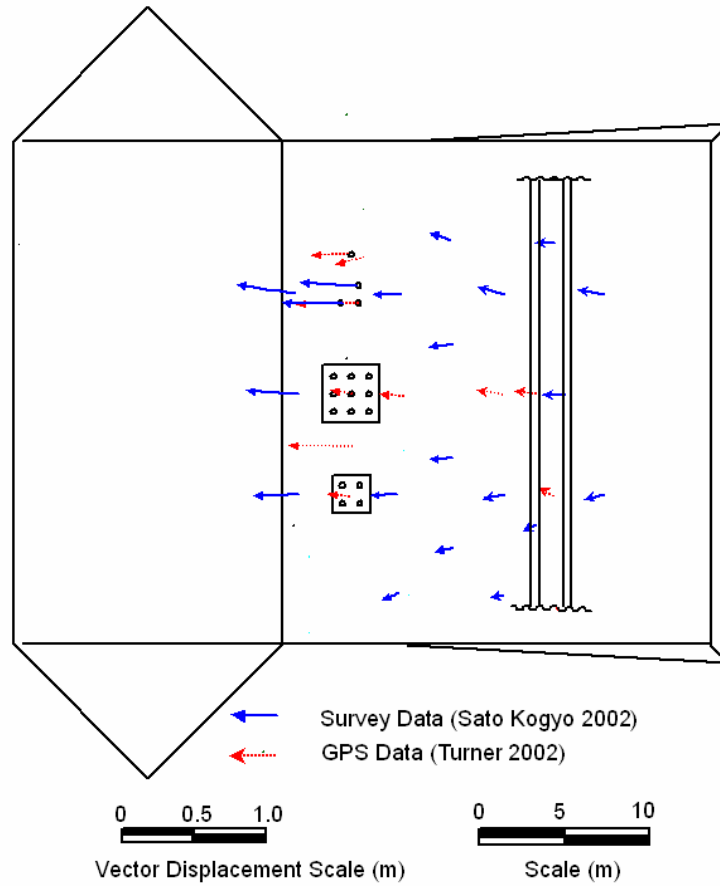


Fig. 5.9 Horizontal displacement vectors after second test

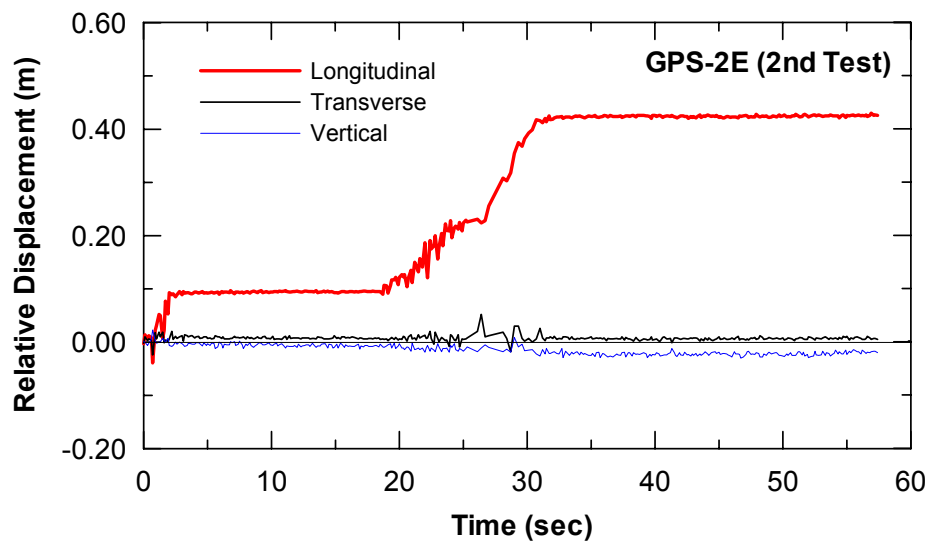


Fig. 5.10 Displacement time histories of GPS unit 2E

5.4.2.2 Soil Displacement Profile

Typical soil displacement profiles at the end of the second test are shown in Figure 5.11. The results show that the magnitude of soil displacements of the second test was approximately 50% of that measured in the first test. This may be because the soil in the second test was less susceptible to liquefaction as mentioned earlier. Appendix J summarizes the soil displacement profile of each location measured in the second test. A summary of lateral soil movements at the ground surface is provided in Table 5.3.

Table 5.3 Summary of displacement at ground surface from slope inclinometer data, second blast test

Location	Displacement in A-Axis (m)	Displacement In B-Axis (m)	Total Vector (m)	Remarks
S1	-	-	-	Casing damaged.
S2	0.351	-0.033	0.353	
S3	0.143	0.066	0.157	
S4	0.136	-0.046	0.143	
S5	0.392	-0.076	0.400	
S6	0.429	0.025	0.430	
S7	0.218	-0.057	0.225	
S8	0.119	-0.015	0.120	
S9	0.091	0.038	0.098	
S10	0.090	-0.012	0.091	
S11	0.212	-0.001	0.212	

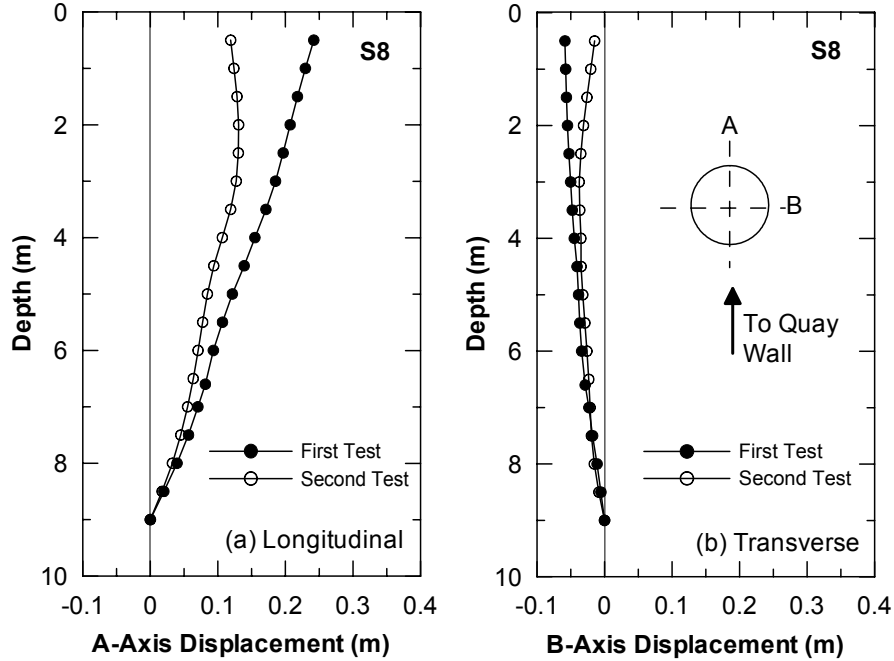


Fig. 5.11 Soil displacement profiles obtained from slope inclinometer (S8)

5.4.3 Pile and Pipeline Responses

All strain gages were re-zeroed prior to the second test. Additional strains measured in the second test were added to those measured in the first test to obtain the total strains, as well as the total bending moments in the second test. Strain time histories measured in the second test for individual piles and pipelines are given in Appendix K.

5.4.3.1 Single Pile

Strain profiles of the single pile measured in the second test are presented in Figure 5.12a. These strains were added to those measured in the first test to calculate the total moments along the pile in the second test. Moment distributions along the length of the single pile at the ends of the first and second tests are presented in Figure 5.12b. Similar to the first test, the moments of the first 4 m in the second test were negligible, and the maximum moment occurred in the dense soil layer at a depth of about 9 m. As expected, the moment in the second test was larger than in the first test because the pile experienced larger movement. The moment profiles indicate that the single pile yielded after the second test with the plastic hinge length of more than 1 m.

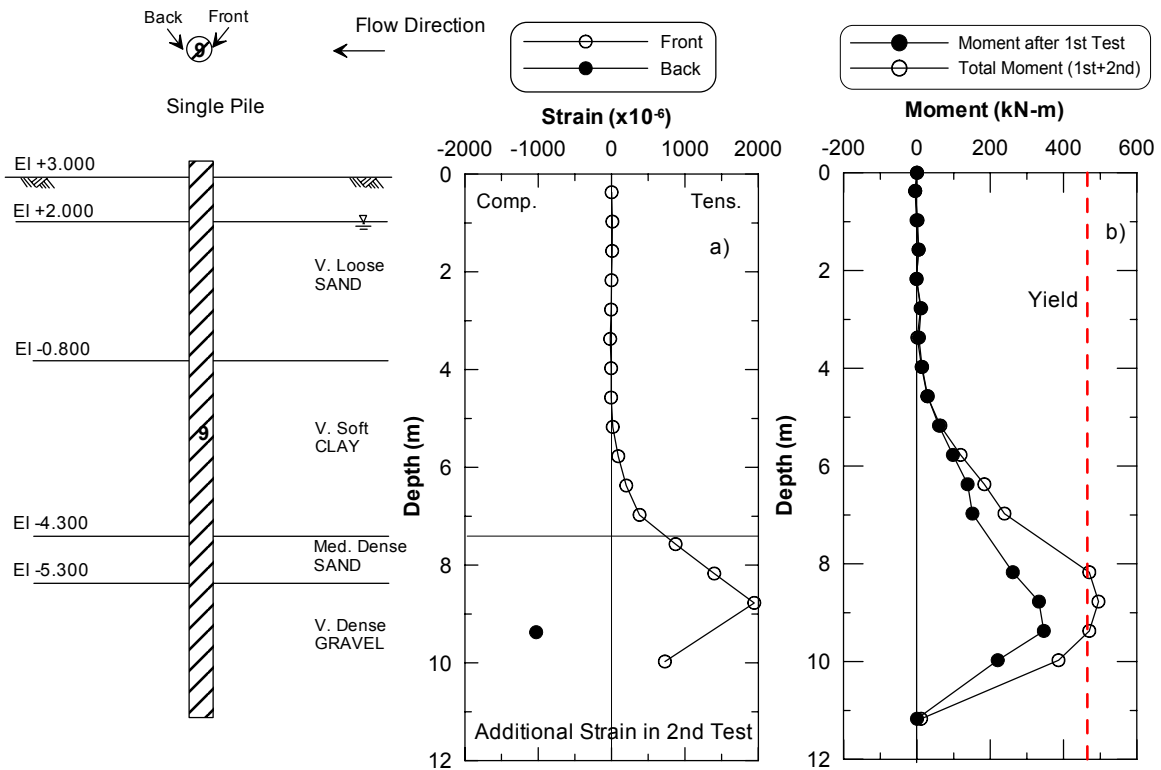


Fig. 5.12 Strain and moment profiles of single pile after second full-scale lateral spreading test

5.4.3.2 4-Pile Group

Strain time histories of instrumented piles in the 4-pile group are presented in Appendix K. Strain gages on the back side (downstream) of pile No. 8 were completely damaged due to the effect of blasting. Profiles of additional strain for piles No. 7 and No. 8 due to lateral spreading in the second test are presented in Figures 5.13a and 5.14a, respectively. These strains were added to those measured in the first test to calculate total moments along the pile in the second test. Moment distributions along the length of each pile at the end of the first and the second tests are presented in Figures 5.13b and 5.14b. As expected, the maximum positive moments in the second test were greater than those of the first test because the total movements of the pile groups increased. However, the negative moments at the pile heads in the second test were very similar to the first test. This might be due to the fact that the negative moments at the pile heads in the second test reached the ultimate moment capacity of the connection between the piles and the cap. Both piles in the groups remained elastic after the completion of the second test.

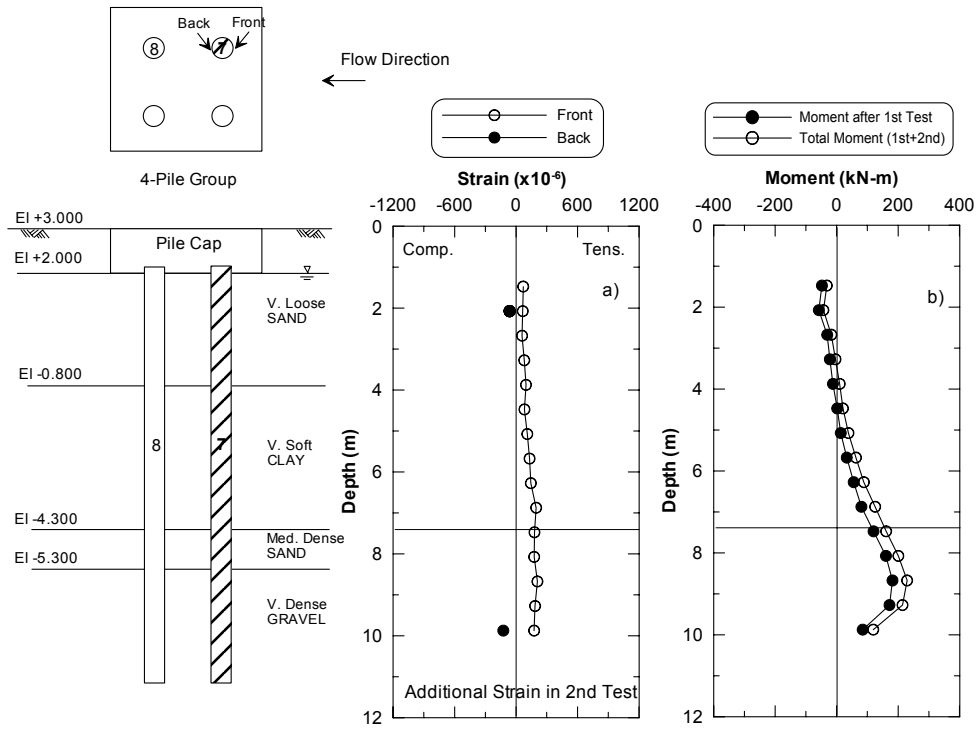


Fig. 5.13 Strain and moment profiles of pile No. 7 of 4-pile group after second full-scale lateral spreading test

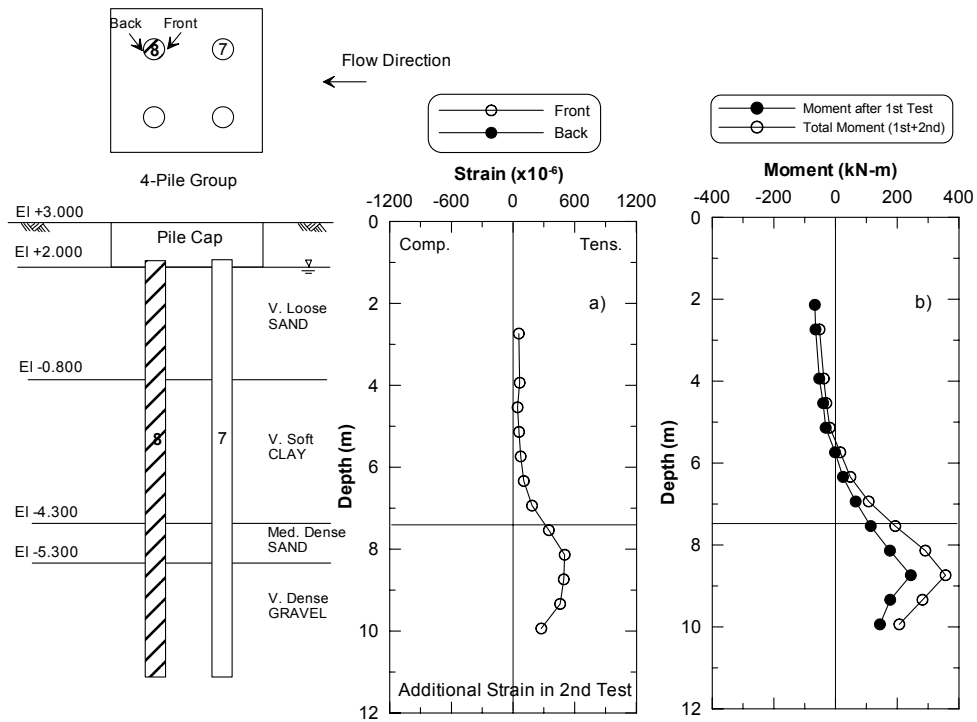


Fig. 5.14 Strain and moment profiles of pile No. 8 of 4-pile group after second full-scale lateral spreading test

5.4.3.3 9-Pile Group

Strain time histories of individual instrumented piles in the 9-pile group are presented in Appendix K. It should be noted that the time-history data for piles No. 4 and No. 5 were lost due to technical error in the data-acquisition system. Fortunately, the residual strains at the end of the second test could be restored. Strain profiles of each pile measured in the second tests are shown in Figures 5.15a–5.20a. The moment distributions of each pile are presented in Figures 5.15b–5.20b. The characteristics of bending moment profiles of the piles in the 9-pile group were similar to those of the 4-pile group. All piles remained elastic after the test. The moments of piles No. 2 and No. 4 were lower than the others due to the lower degree of fixity at pile tips, as described earlier.

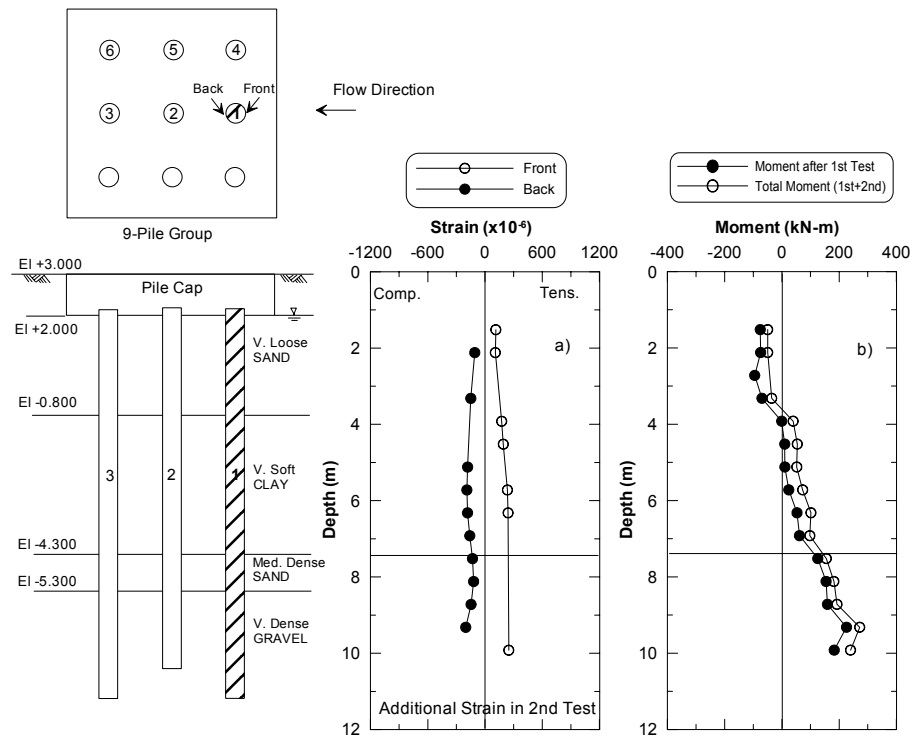


Fig. 5.15 Strain and moment profiles of pile No. 1 of 9-pile group after second full-scale lateral spreading test

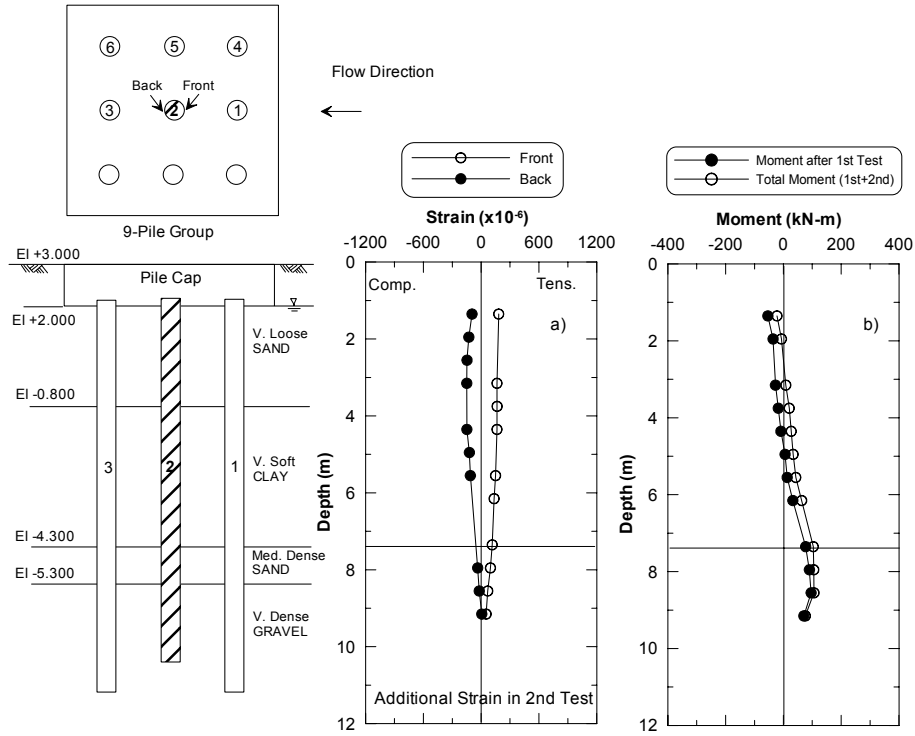


Fig. 5.16 Strain and moment profiles of pile No. 2 of 9-pile group after second full-scale lateral spreading test

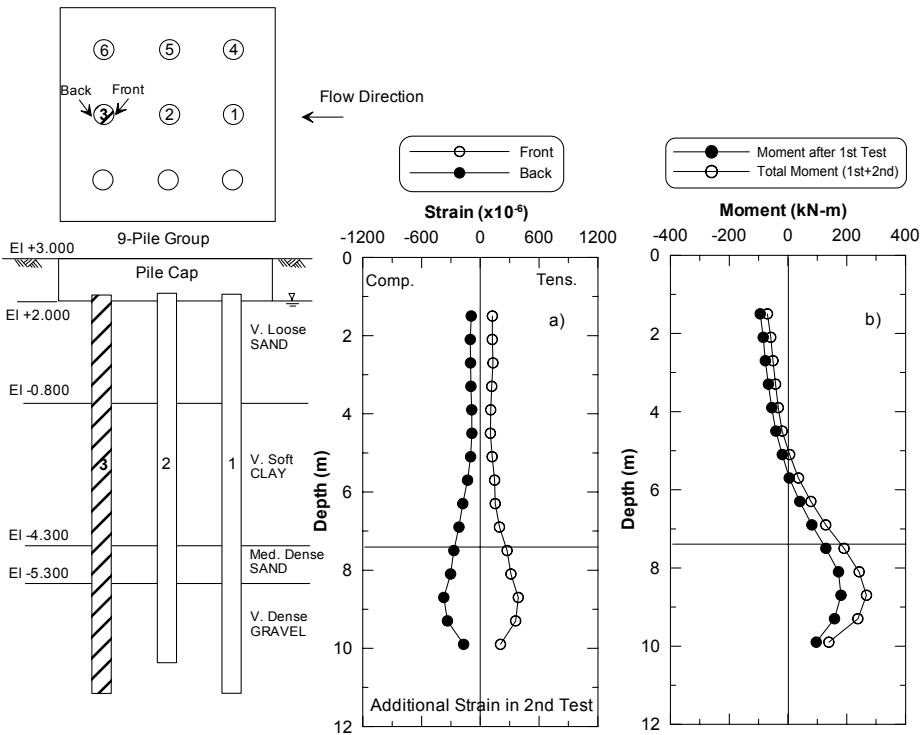


Fig. 5.17 Strain and moment profiles of pile No. 3 of 9-pile group after second full-scale lateral spreading test

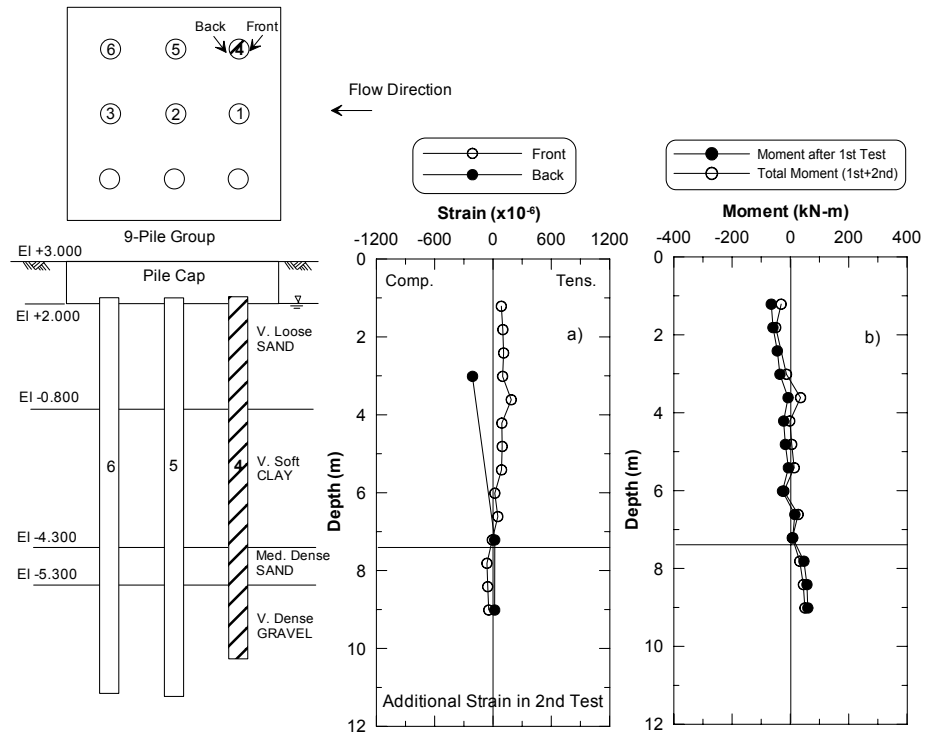


Fig. 5.18 Strain and moment profiles of pile No. 4 of 9-pile group after second full-scale lateral spreading test

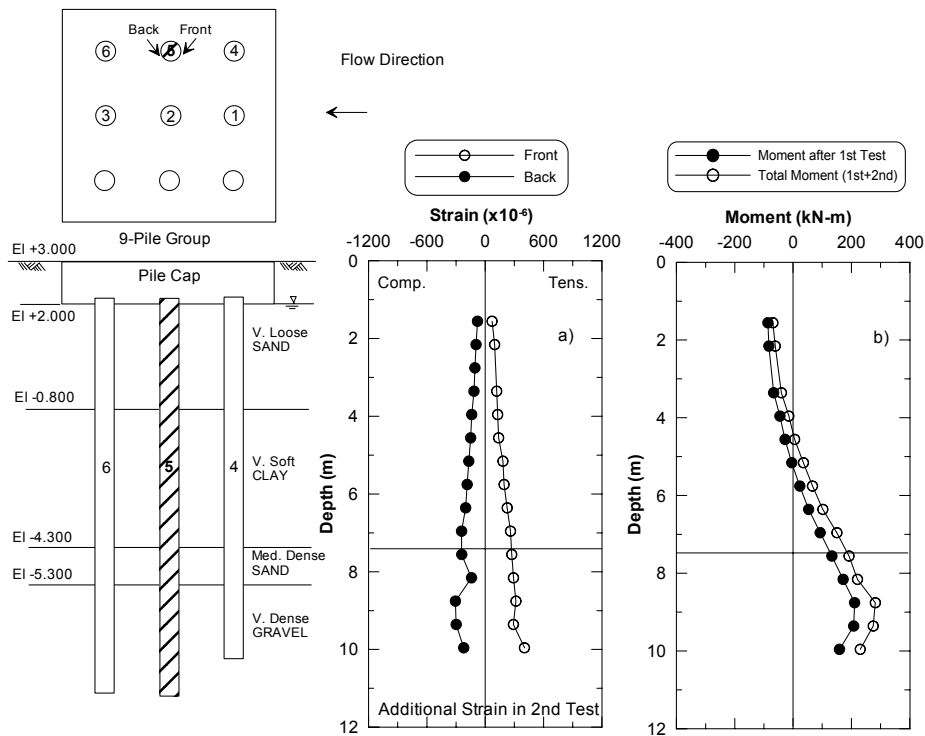


Fig. 5.19 Strain and moment profiles of pile No. 5 of 9-pile group after second full-scale lateral spreading test

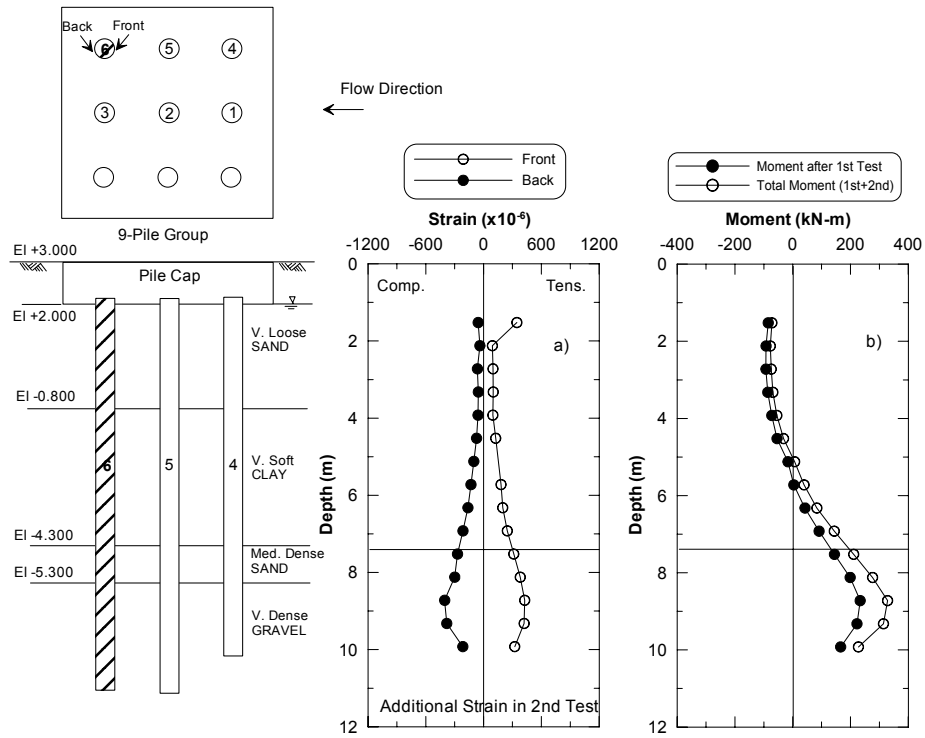


Fig. 5.20 Strain and moment profiles of pile No. 6 of 9-pile group after second full-scale lateral spreading test

5.4.3.4 Pipelines

Strain time histories along the transverse gas pipeline (pipeline A) and the electrical conduit (pipeline B) are presented in Appendix K. These were the additional strains measured in the second test only. Figures 5.21–5.22 present profiles of additional strain along pipelines A and B measured in the second test.

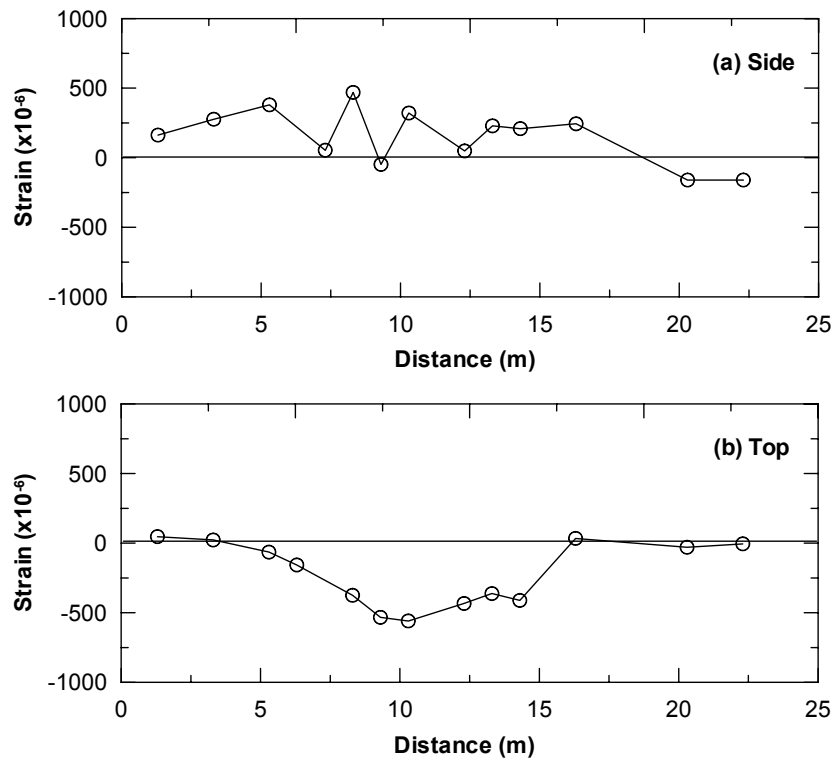
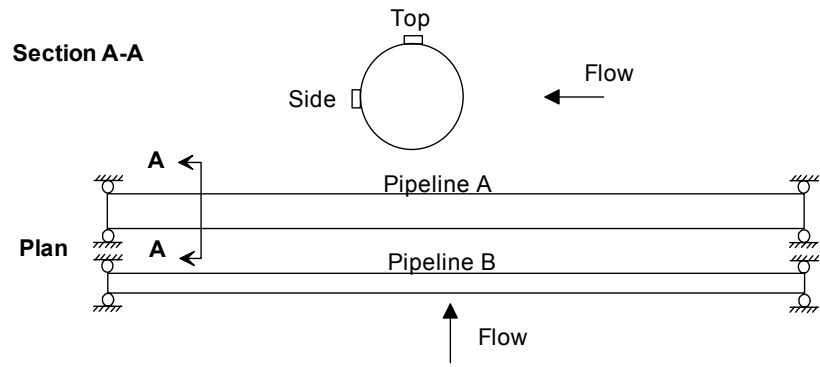


Fig. 5.21 Profiles of additional strain along pipeline A in second test: (a) side gages and (b) top gages

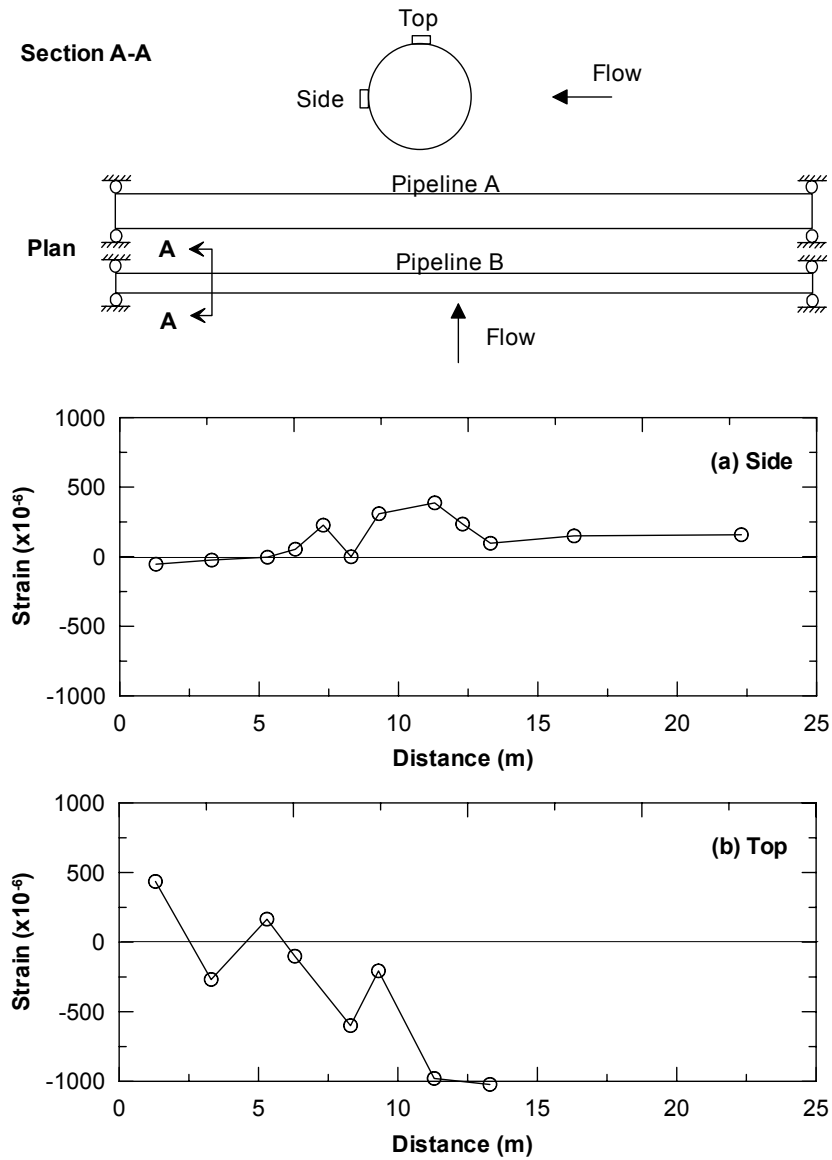


Fig. 5.22 Profiles of additional strain along pipeline B in second test: (a) side gages and (b) top gages

5.4.4 Results from Other Instrumentation

5.4.4.1 Accelerometers

The data from accelerometers attached on the top of foundations are presented in Figure 5.23. Similar to the first test, acceleration at the pile head decreased with increasing foundation stiffness. The acceleration of the single pile was the highest, while that of the 9-pile group was lowest.

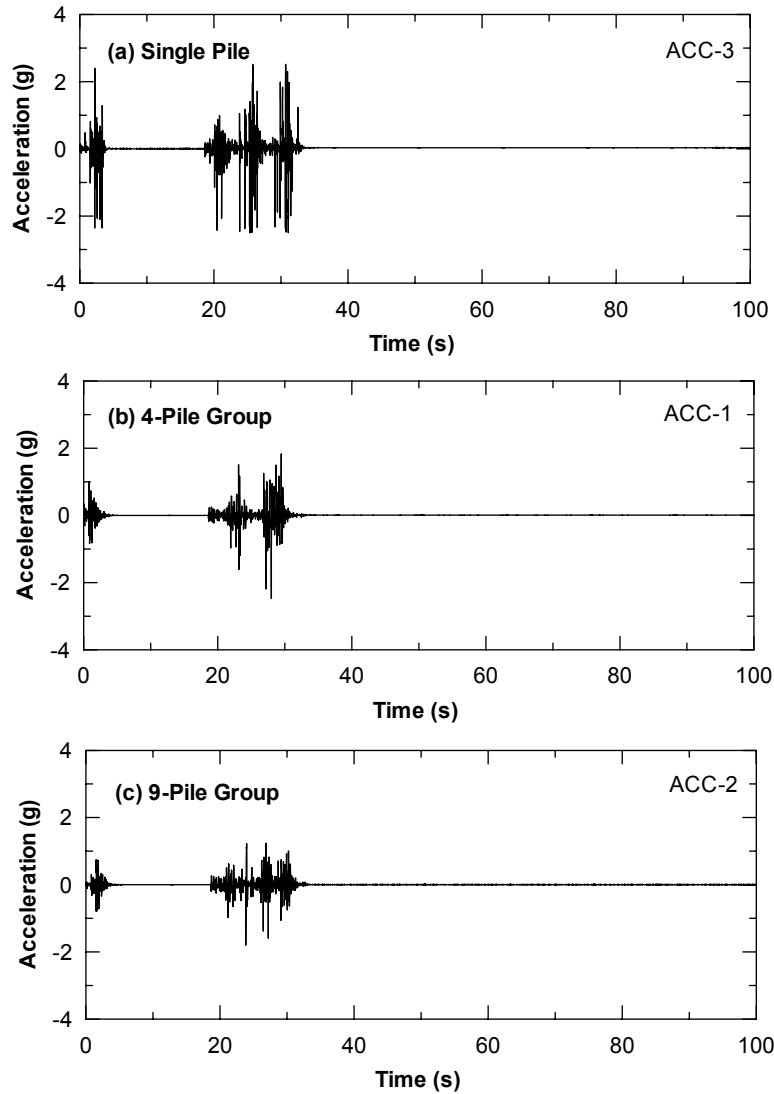


Fig. 5.23 Pile-head acceleration time histories in second test: (a) single pile, (b) 4-pile group, and (c) 9-pile group

5.4.4.2 Tiltmeters

Figure 5.24 shows that the pile-head rotation of the single pile (free-head condition) at the end of the test was approximately 1.5 degrees, while the rotation of the 9-pile group (fixed-head condition) was insignificant, about 0.1 degrees. These rotations were additional rotations measured in the second test only. The total rotations can be obtained by summing up the rotations measured in the second test with those measured in the first.

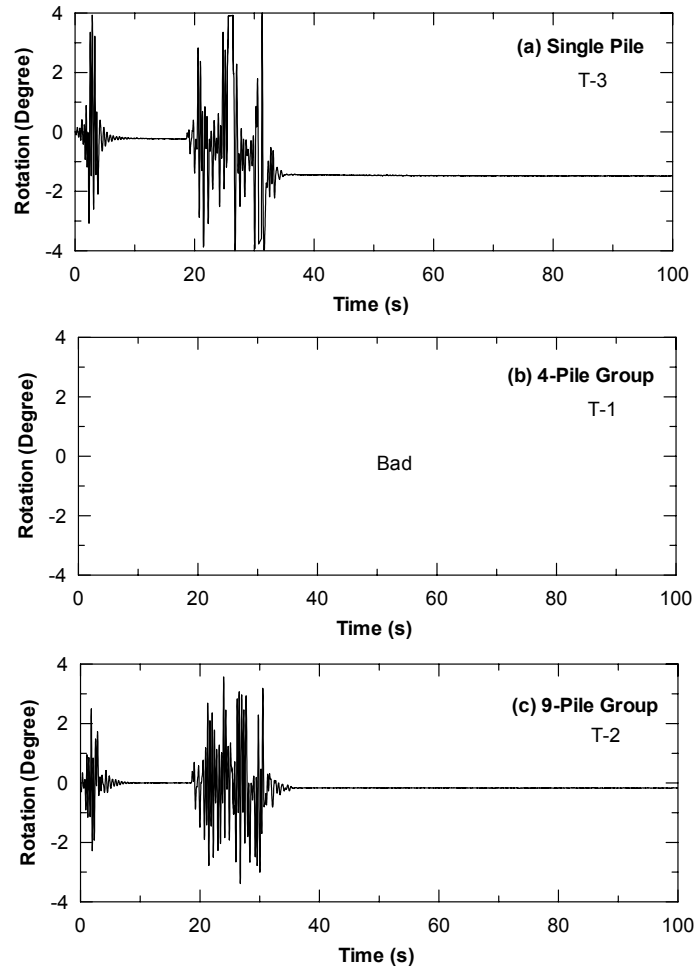


Fig. 5.24 Pile-head rotations for (a) single pile, (b) 4-pile group, and (c) 9-pile group

5.4.4.3 Linear Potentiometers

Relative displacements obtained from string activated linear potentiometers are presented in Figures 5.25–5.28. A summary of relative movements is given in Table 5.4. The movements of the 4-pile group (19 cm) and 9-pile group (17 cm) were almost the same, while the movement of the single pile was approximately 10 cm more than the pile groups. The soil in front of the pile caps moved approximately the same amount as the pile caps. The soil on the downstream behind the 9- pile group moved 20 cm more than the pile cap.

The displacement measurements from GPS units were verified against linear potentiometer measurements in several locations, as summarized in Table 5.5. Excellent agreement between measurements from GPS units and linear potentiometers were observed, with

the differences being less than 1.4 cm except at STP-3 where the GPS measurement was 3.8 cm lower than that measured by linear potentiometer.

Table 5.4 Summary of relative displacements after second full-scale lateral spreading test

Name	Location	Relative Movement (m)	Interpretation
STP-1	9-pile group and Inc. S1 (upstream)	0	The pile group and the soil had the same movement.
STP-2	9-pile group and Inc. S2 (downstream)	0.196	The soil moved 196 mm more than the pile group.
STP-3	Single pile and Inc. S7 (upstream)	0.038	The pile moved 38 mm more than the soil.
STP-4	4-pile group and Inc. S8 (upstream)	0.025	The soil moved 25 mm more than the pile group.
STP-5	Single pile (W1) and Inc. S11 (upstream)	0.132	The pile moved 132 mm more than the soil.
STP-6	Single pile (W2) and Inc. S11 (upstream)	0.085	The pile moved 85 mm more than the soil.
STP-7	Single pile (W1) and Single pile (W3)	0.018	Pile W3 moved 18 mm more than pile W1.
STP-8	4-pile group	-0.187	The 4-pile group moved 187 mm.
STP-9	9-Pile Group	-0.169	The 9-pile group moved 169 mm.
STP-10	Single Pile	-0.285	The single pile moved 285 mm.

Table 5.5 Verification of GPS measurements with data from potentiometers

GPS Location	Potentiometer Location	GPS Measurement (m)	Potentiometer Measurement (m)
1A	STP-9	0.157	0.169
1D	STP-10	0.299	0.285
2A	STP-8	0.184	0.187
GPS 1A -1B	STP-1	0.006	0.000
GPS 1E -1D	STP-3	0.073	0.038

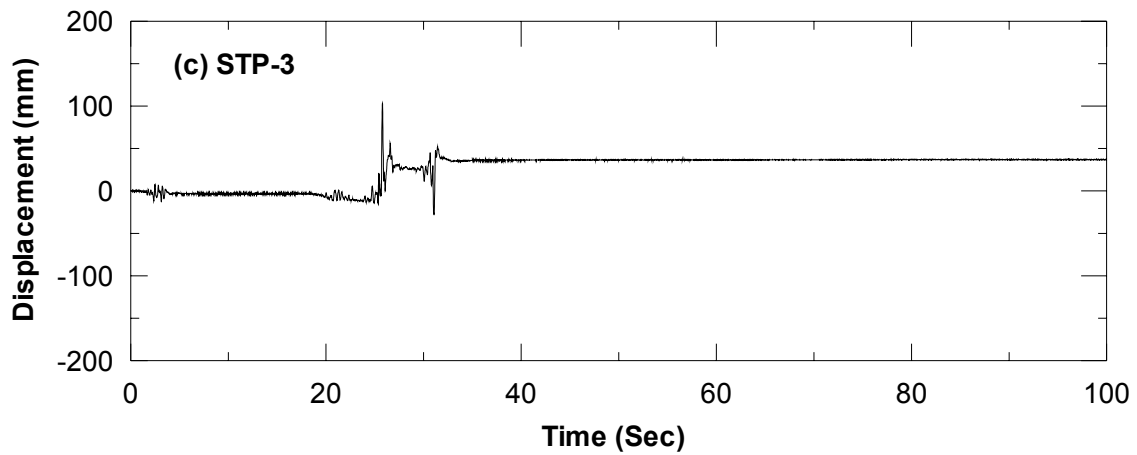
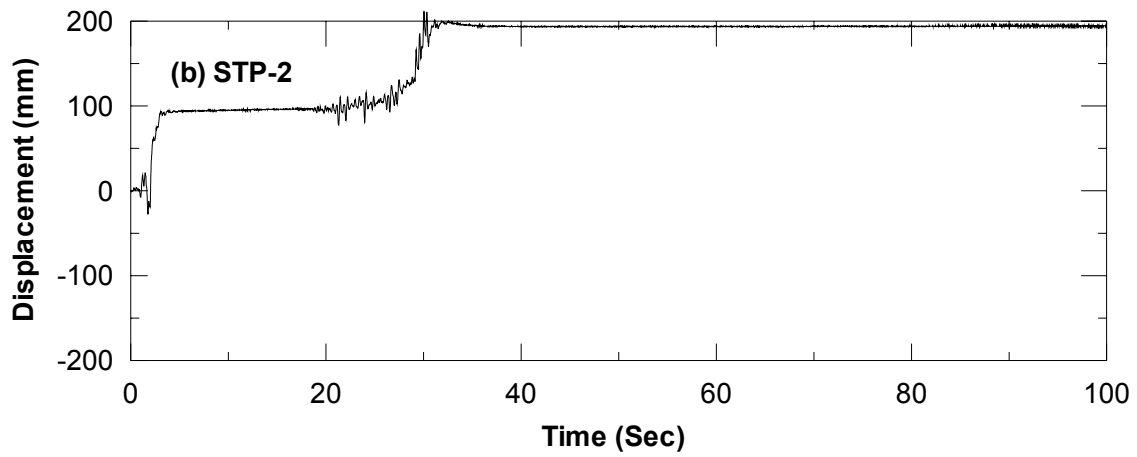
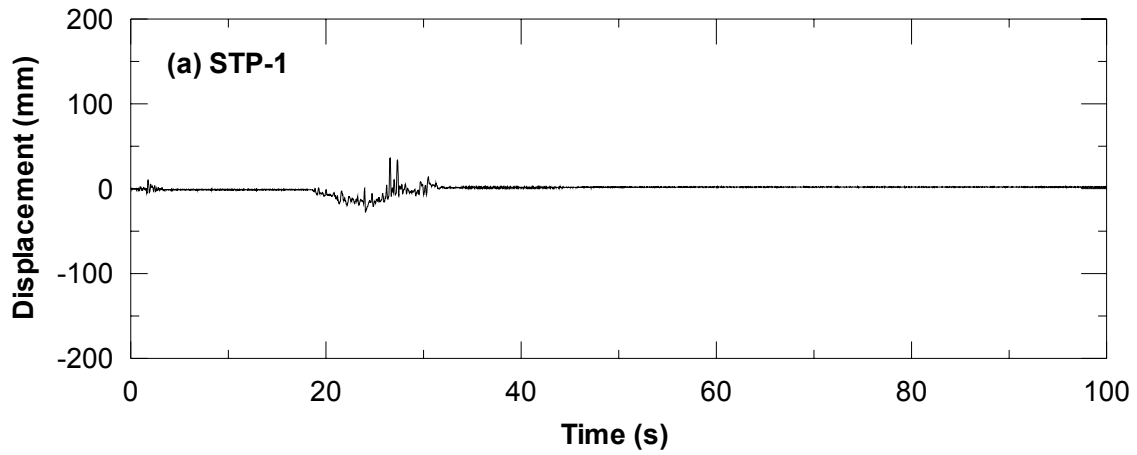


Fig. 5.25 Relative displacement between (a) S1 and 9-pile group, (b) S2 and 9-pile group, and (c) S7 and single-pile, second blast test

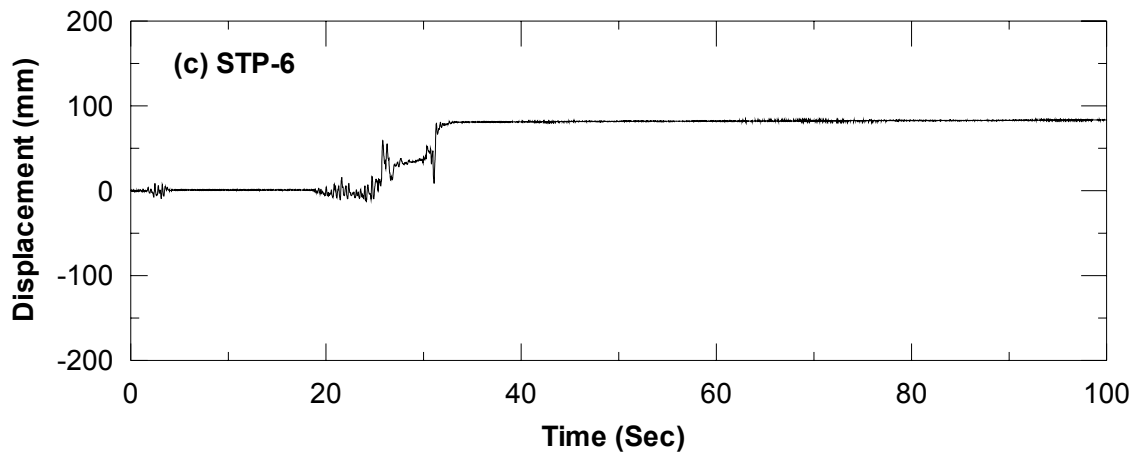
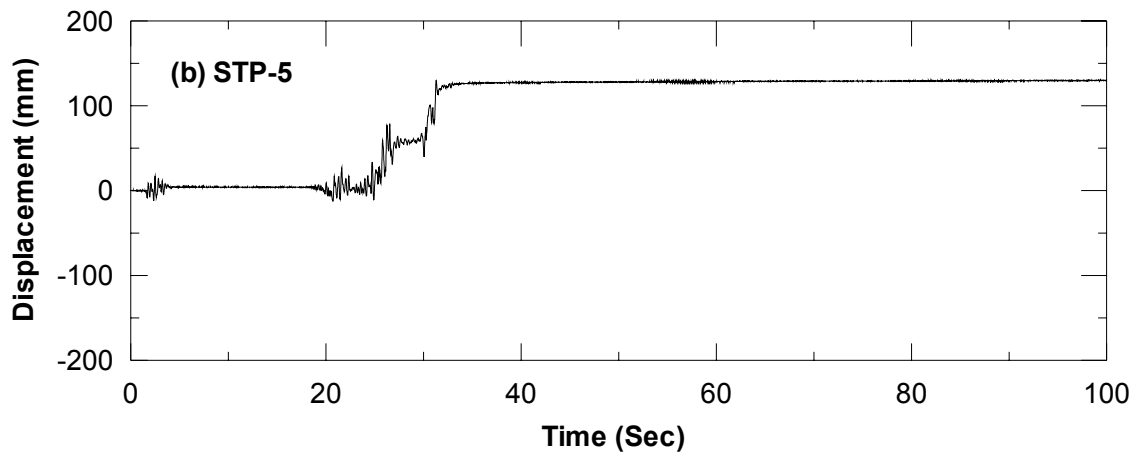
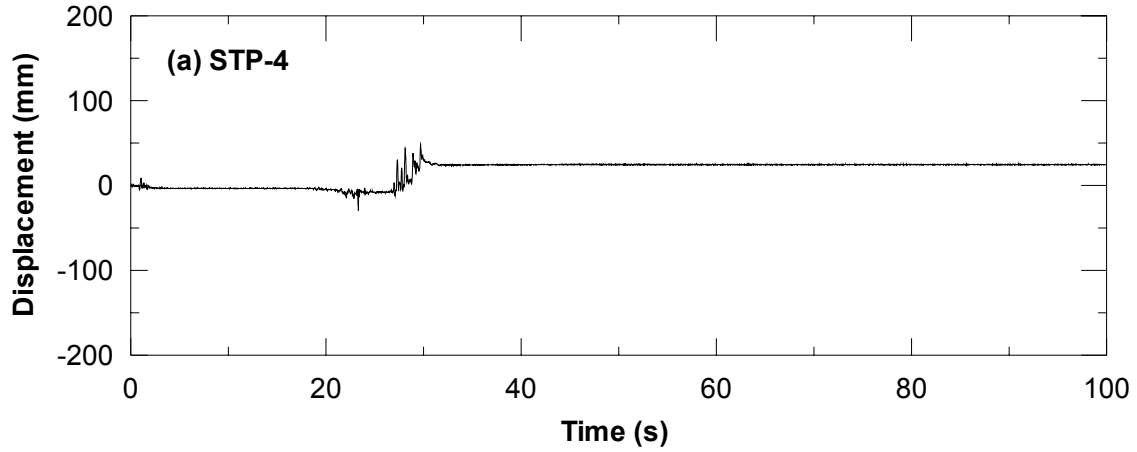


Fig. 5.26 Relative displacement between (a) S8 and 4-pile group, (b) S11 and W1 pile, and (c) S11 and W2 pile, second blast test

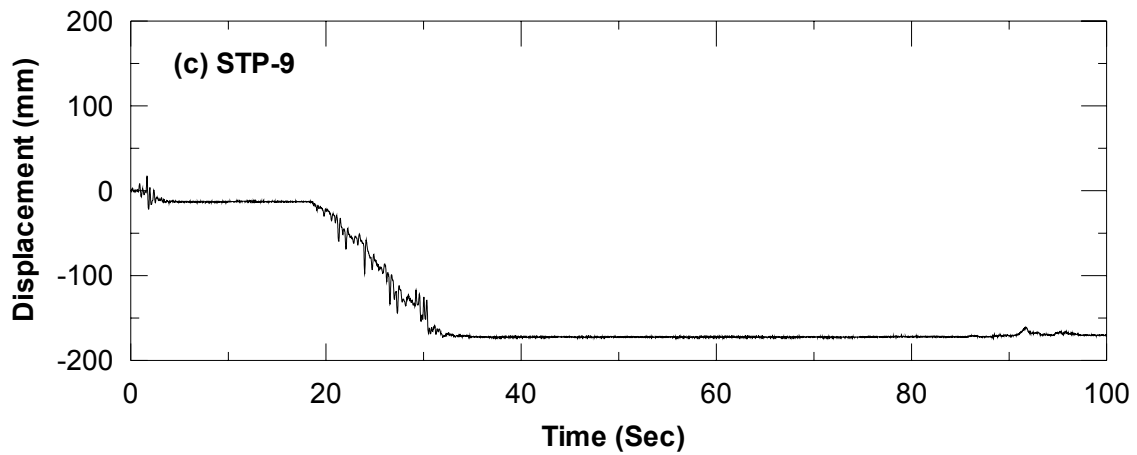
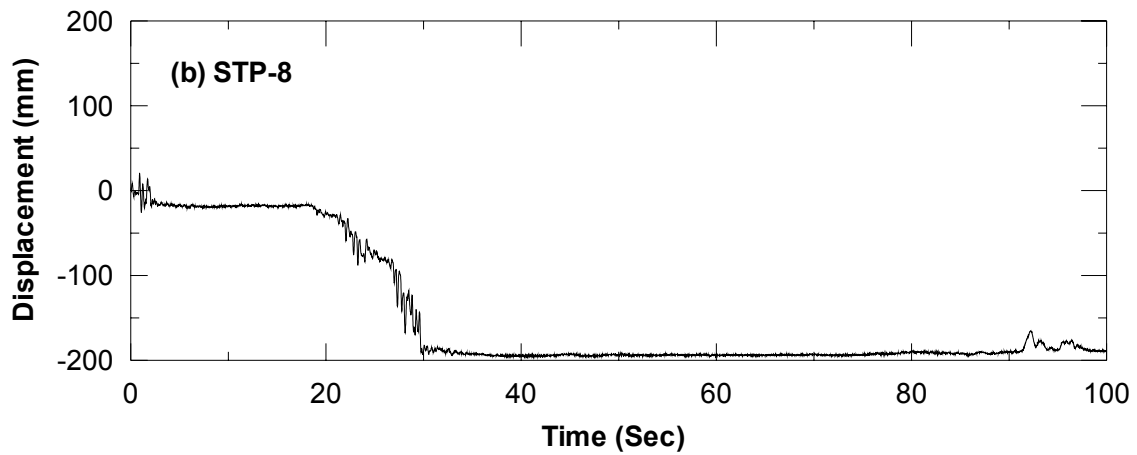
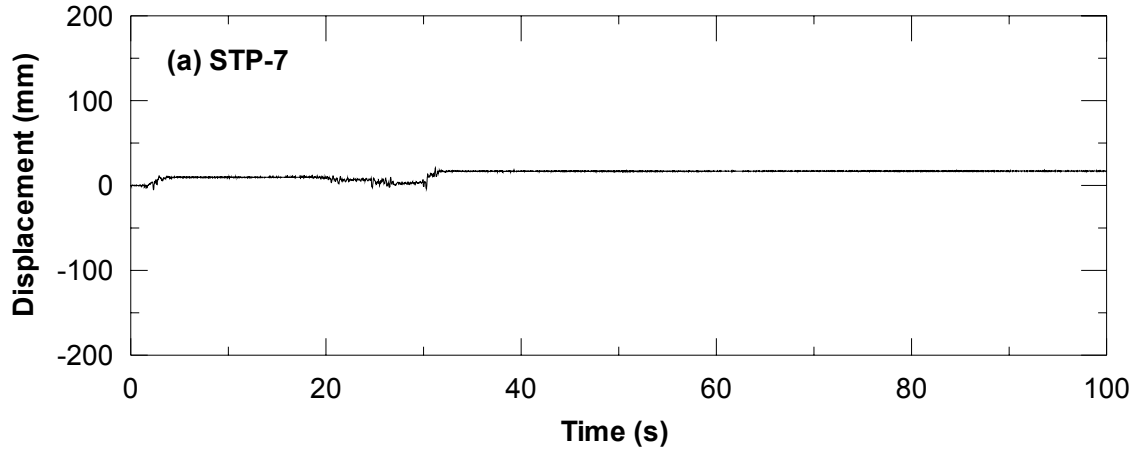


Fig. 5.27 Relative displacement between (a) pile W1 and pile W3, (b) 4-pile group and reference post, and (c) 9-pile group and reference post

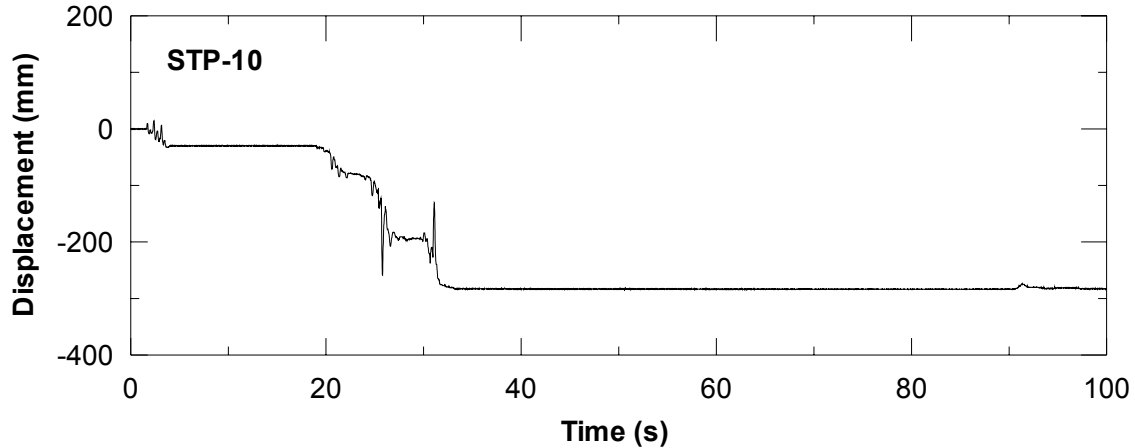


Fig. 5.28 Relative displacement between single pile and reference post

5.5 PILE-CAP CONDITION AFTER TEST

After completion of the tests, the soil surrounding the pile caps was excavated to investigate the structural performance as shown in Figures 5.29–5.30. Only a little concrete spalling surrounding the pile heads was observed, indicating that some rotations between the piles to the pile caps might occur, but could not be quantitatively identified. No pull-out of piles from the pile cap was observed on the connections of both pile groups though both pile groups experienced total movements of nearly 40 cm. However, if either a stronger or thicker layer of shallow soil overlying the liquefied soil layer exists, the amount of force exerted by the soil would become higher and possibly cause damage to the connections.



Fig. 5.29 Concrete spalling underneath pile cap of 4-pile group (pile N3)



Fig. 5.30 Concrete spalling underneath pile cap of 9-pile group (pile No. 8)

6 Analyses of Pile Responses

The first section of this chapter involves the use of strain gage data from both the first and second full-scale tests to back-calculate the pile responses, as well as evaluate loading conditions along the piles subjected to lateral spreading. The back-calculated pile responses are then compared to the measurements. The results from the analyses are presented and discussed. The second section focuses on the application of pushover analysis using the p - y method to predict the behavior of piles subjected to lateral spreading and then compares this with the results from the experiments. Both single piles and pile groups are considered in the analyses using the same set of baseline soil properties. The analysis approach and results are presented in this chapter. Finally, the design implications of piles subjected to lateral spreading are given.

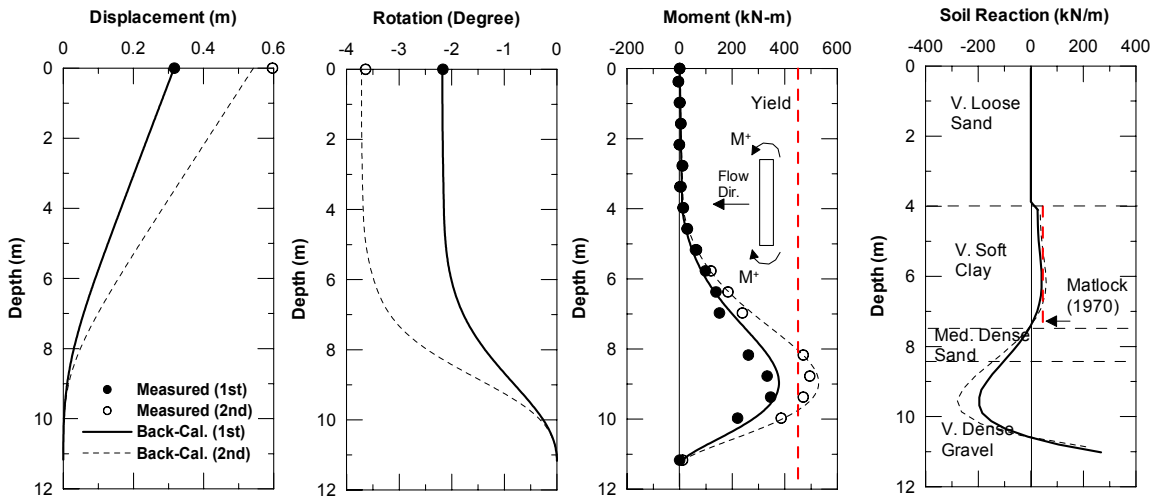
6.1 BACK-CALCULATION OF PILE RESPONSES

Strain gages attached to the test piles were used to calculate the curvatures along the length of the piles. The moments in the piles corresponding to maximum soil surface displacements were determined using moment-curvature relationships as shown in Fig. 4.6. All strain gages were re-zeroed before each test. Additional strains measured in the second test were added to those measured in the first test to obtain the total curvatures, as well as the total bending moments in the second test. The lateral soil reactions were then back-calculated by double differentiating the moment data. The pile rotations and pile displacements were obtained by single- and double-integrating the curvature data, respectively. Since the data had some amount of scatter, some curve fitting was necessary. In this analysis, polynomials of an appropriate order were used to fit the experimental moment curves.

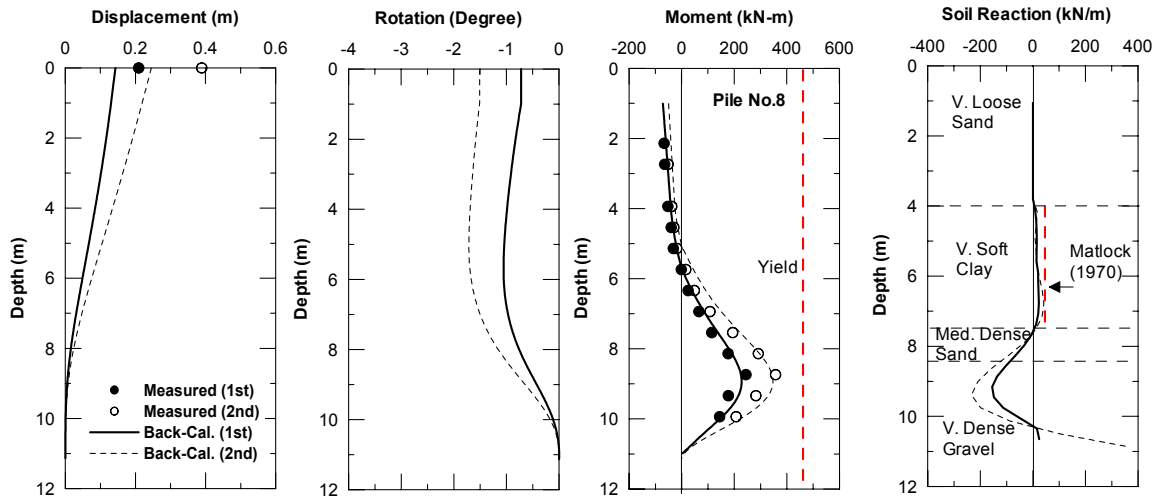
6.1.1 Single Pile

Moment distributions along the length of the single pile at the ends of the first and the second blast tests are presented in Figure 6.1. The solid and dotted lines in the moment plot represent curve fitting to the moment data for the first and second tests, respectively.

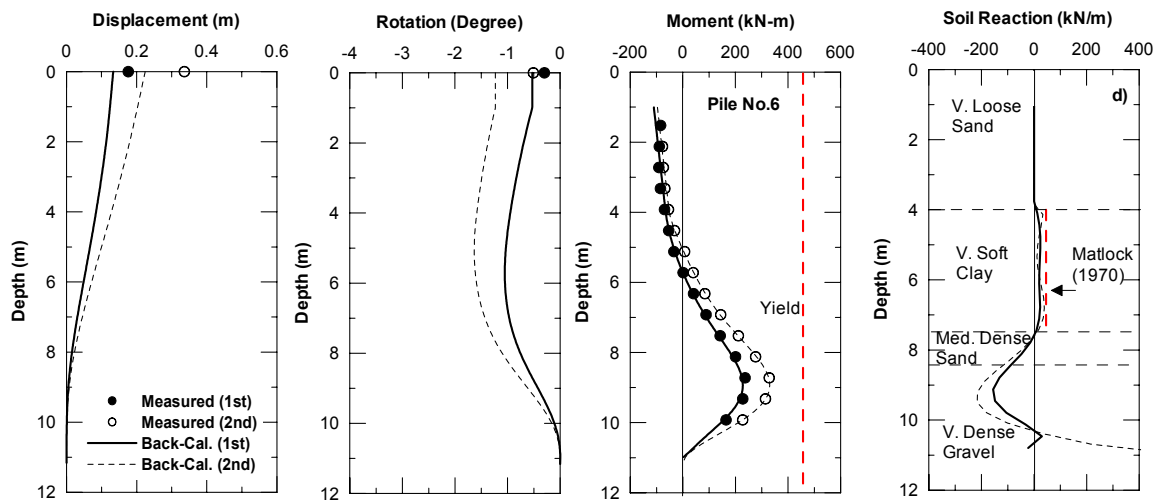
As mentioned earlier in the previous chapters, the moment was insignificant through the first 4 m of the very loose liquefied sand layer, indicating that the resultant force on the pile produced by the liquefied soil was negligible. This is also confirmed by the back-calculated soil reaction as shown in Figure 6.1. Below the liquefied soil layer, the moment increased with depth for the next 3.5 m, through a very soft clay layer. Though the R_u in this layer also reached 100%, the clay layer behaved differently from the liquefied sand. As indicated by the back-calculated soil reaction, the soft clay layer exerted a driving force to the pile (+ sign), while the dense gravel layer provided a resisting force (− sign). Although it was anticipated that the second sand layer would also be liquefied and provide zero resisting force to the pile as similar to the first sand layer, the back-calculated soil reaction indicated some soil resistance from this layer. This is likely because the thickness of this layer was so thin that very limited strain gage data were not able to capture this phenomenon. The back-calculated soil reactions in the clay layer in the second test were slightly higher than in the first test. However, they were comparable to the ultimate soil resistance estimated using Matlock's soft clay p - y curves (Matlock 1970), implying that the movements of the clay layer were nearly large enough to cause the soil to reach its ultimate pressure. The back-calculated pile-head rotations and pile-head displacements of the single pile were in good agreement with the measurements obtained from both blast tests.



a) Single Pile



b) 4-Pile Group



c) 9-Pile Group

Fig. 6.1 Back-calculated pile responses (a) single pile, (b) 4-pile group, and (c) 9-pile group

6.1.2 Pile Groups

The moment of each pile in the group was quite similar, as presented in Figure 6.2. However, the moments of piles No. 2 and No. 4 of the 9-pile group were smaller than the others because both piles were shorter in length and therefore had a smaller degree of fixity into the dense soil layer.

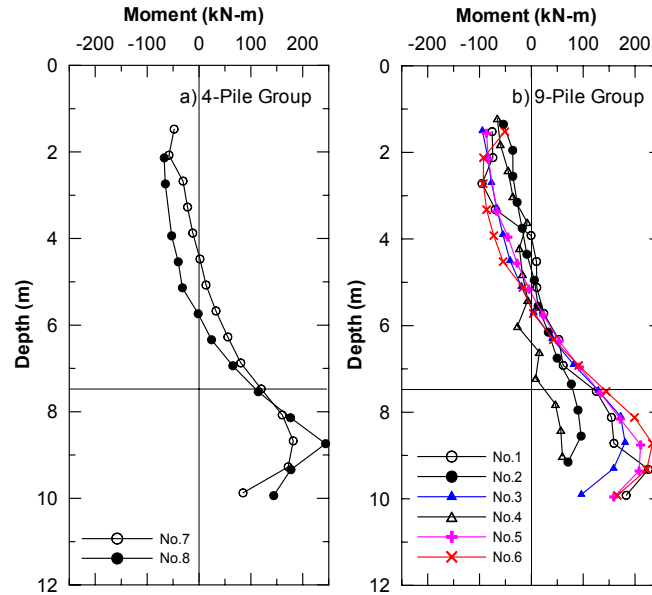


Fig. 6.2 Moment distribution of each pile from first full-scale test: (a) 4-pile group and (b) 9-pile group

Due to the similarity of the moment of each pile in the group, the moment profiles of pile No. 8 in the 4-pile group and pile No. 6 in the 9-pile group were used to back-calculate the pile responses as presented in Figures 6.1b and 6.1c. The shape of the moment profiles obtained from the first and second experiments agreed well with the expected behavior of a pile with a fixed-head condition, where a negative moment occurred at the pile head due to the effect of pile-head restraint.

As expected, the maximum positive moments in the second test were greater than that of the first test because the total movements of the pile groups increased. However, the negative moment at the pile heads in the second test was very similar to that of the first test. Based on a force equilibrium analysis, the ultimate moment capacity at the connection between a pile head and a pile cap, which considered only the tensile force from the steel v-shape anchor bars (see Fig. 4.10), was estimated as 90 kN-m. This estimated moment capacity was very close to the measured negative moments at the end of the first test. The negative moments at the pile heads in

the second test were therefore limited to this ultimate moment capacity. Increasing the pile-cap movement would only result in an increase of pile-head rotation underneath the pile cap. The slight decrease of the moment at the pile head in the second test may be due to the loss of concrete bonding to the steel pipe piles, which was neglected in the analysis.

The pile moment distribution for the first 4 m of soil, where the very loose liquefied sand layer existed, was approximately linear, resulting in zero soil reaction as confirmed by the back-calculated soil reaction in Figures 6.1b–c. This finding agrees well with the previous conclusion obtained from the single pile case. Similar to the single pile case, the clay layer provided a driving force to the pile, while the dense gravel layer exerted a resisting force. However, the back-calculated soil reactions in the clay layer were less than those obtained from the single pile case, likely due to a shadowing effect.

The back-calculated displacements of both pile groups were approximately 25% and 35% lower than the measured values for the first and second tests, respectively. This may be because some translation and/or rotation at the pile tips had occurred during the tests, while in the analyses, both were assumed to be zero. The amount of rotations at the pile tips required to match the measured displacements at the pile cap of the 9-pile group was small, about 0.2 and 0.5 degrees for the first and second tests, respectively. The back-calculated pile-head rotations of the 9-pile group were significantly higher than the measured ones, particularly in the second test. One possible reason is that for this type of pile cap, a complete fixity of the pile to the pile cap was not obtained. As a result, some rotation at the pile-head underneath the pile cap might occur resulting in a difference in rotations between the pile cap and the pile heads.

6.2 PUSH-OVER ANALYSIS USING *P-Y* METHOD

6.2.1 Concept of *p-y* Method

A pseudo-static pushover analysis using the *p-y* analysis method is extensively used in current design practice to analyze the response of a laterally loaded pile due to the simplicity of this method in modeling compared to the 2D or 3D finite element method based soil constitutive model. The application of this method in current design practice is mainly focused on the analysis of piles under lateral load moving against the stationary soil mass. However, in many cases, such as a pile subjected to lateral spreading, the soil mass itself will move toward and exert load on the pile, which will displace the pile a certain amount depending on the relative

stiffnesses between the pile and the soil. In this case, the soil loading must be considered by taking into account the relative movement between the soil and pile.

Figure 6.3 presents a basic concept of using the p - y analysis method to analyze the behavior of a pile subjected to the movement of the soil mass (Reese *et al.* 2000). If the soil mass is stationary (i.e., no kinematic loading), the p - y curve is symmetric about the p -axis (curve 1) and the governing equation for this case is

$$EI \frac{d^4 y_p}{dz^4} - p y_p = 0 \quad (6.1)$$

where EI is the pile stiffness, y_p is the pile displacement, and z is the depth.

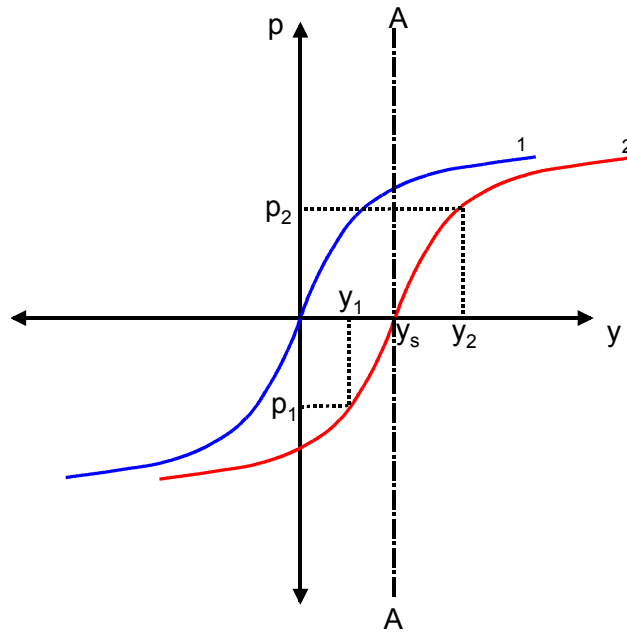


Fig. 6.3 Concept of p - y curves to account for movement of soil mass (after Reese *et al.* 2000)

However, if the soil mass moves, the soil resistance curve is offset according to the movement of the soil mass, y_s (curve 2). When the pile movement, y_p , is less than the soil mass movement, y_s , (i.e., $y_p = y_1$) the soil exerts a driving force, p_1 , on the pile. However, if the pile movement, y_p , is greater than the soil movement, y_s , (i.e., $y_p = y_2$), the soil in this case provides the resistance force, p_2 , to the pile. To predict the behavior of a pile subjected to lateral spreading, the free-field soil displacement, y_s , needs to be known first, and then imposed to the

boundary ends of the Winkler soil springs along depths as shown in Figure 6.4. The response of the pile can then be obtained by solving the following differential equation:

$$EI \frac{d^4 y_p}{dz^4} - p(y_p - y_s) = 0 \quad (6.2)$$

The above equation can be solved by either finite difference or finite element methods. This concept was incorporated into the LPILE Plus 4.0m computer code (Reese *et al.* 2000) using the finite difference technique to solve the above differential equation. A new feature of the LPILE Plus 4.0m computer program allows users to input the free-field soil movement to the soil springs. The program also facilitates users by automatically generated p - y curves based on soil types that are user specified. All the analyses in this report were conducted using this program.

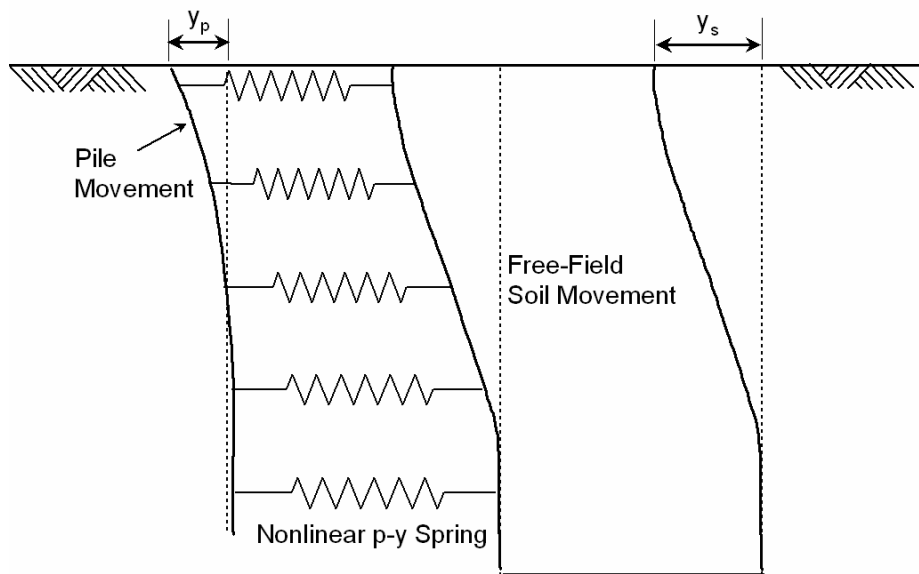


Fig. 6.4 p - y analysis model for single pile subjected to lateral spreading

6.2.2 Analyses of Single Piles

In the analysis of single piles subjected to lateral spreading, the free-field soil movement profiles as presented in Figure 6.5 were obtained from the measured soil displacement profile of a slope inclinometer between the pile groups (denoted as S5 in Fig. 4.18). Based on these data, simplified linear displacement profiles of the free-field soil movements were used for the boundary condition at the end of soil springs with the largest displacements at the ground surface

of 0.43 m for the first test and an additional 0.46 m from the second test, for a total of 0.89 m. The movement at the top of the very dense gravel layer was assumed to be zero. Soil springs at different depths were calculated based on standard p - y springs available in design practice. The p - y curves for sand were developed based on Reese *et al.*'s (1974) recommendations, while the p - y curves for clay were obtained based on Matlock's (1970) recommendations. Though one might anticipate a decrease in the shear strength of the clay layer due to the effect of blasting, the cone test results conducted one day after the first test showed no change of shear strength in this layer. The average undisturbed shear strength was therefore used in the analyses. Since the maximum response of the piles due to lateral spreading occurred at the end of the test, where the soil had already been liquefied, the p - y curves for liquefied soil were used for the saturated sand layers. The details of p - y curves for liquefied sand used in this study are described below.

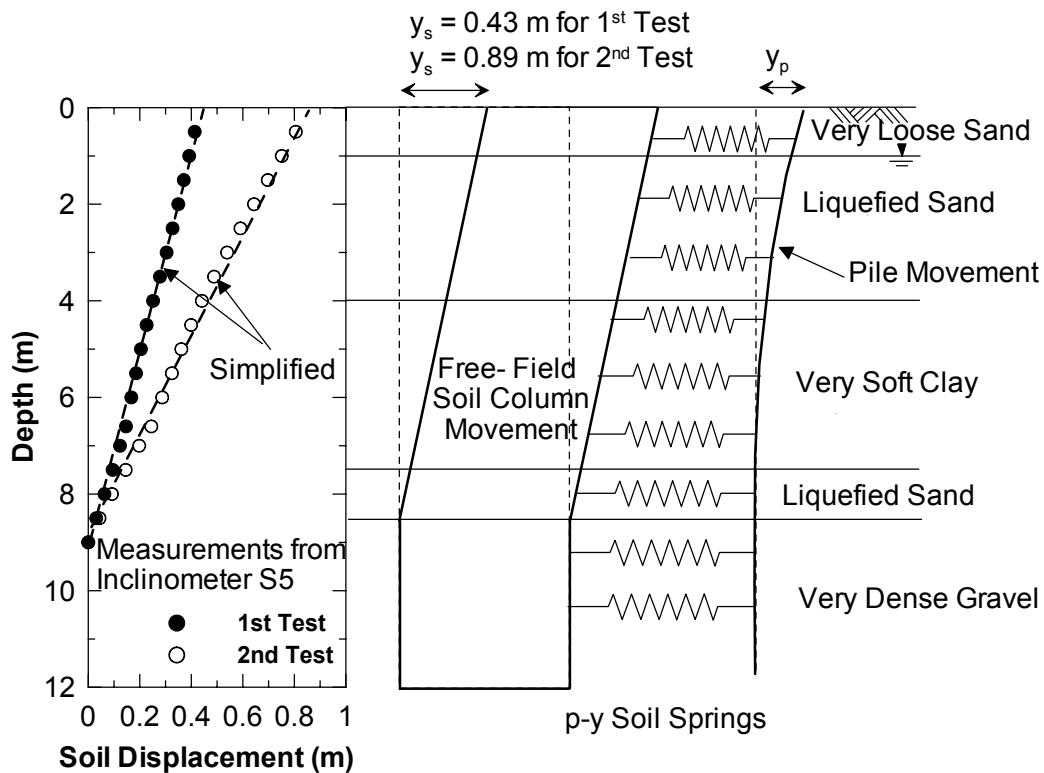


Fig. 6.5 p - y analysis model for single pile

Current research based on the results of full-scale lateral pile load tests in liquefied soil at Treasure Island in the San Francisco Bay suggested that the p - y curves of liquefied soil with soil relative density of 55% are concave due to soil dilation (Ashford and Rollins 2002). The characteristics of p - y curves for liquefied soil, however, depend on the soil relative density

(Wilson et al. 2000; Tokimatsu et al. 2001). Results from the centrifuge tests at the University of California at Davis (Wilson et al. 2000) indicated that for the soil relative density of 40%, the p - y curves are flat, inferring that the soil pressure of liquefied soil is negligible, while for the soil relative density of 55% the p - y curves showed the dilation behavior as that obtained from the full-scale lateral load test at Treasure Island (Ashford and Rollins 2002). The relative densities at the Japan test site were slightly over 30% for the first 4-m of the sand layer and about 45% for the second sand layer at depths between 7.5–8.5 m (see Fig. 2.3). As a result, the liquefied soil layer at the Tokachi site should not provide any loading or resistance to the pile. Therefore, zero soil spring stiffness was used for the liquefied soil layer (i.e., from depths 1–4 m and from 7.5–8.5 m). Table 6.1 summarizes the soil properties and parameters of the soil springs used in this study. Recommendations for passive pressure of liquefied sand using a p -multiplier of 0.1 to reduce ultimate pressure obtained from Reese et al.’s sand p - y curves (e.g., Liu and Dobry 1995; Wilson et al. 1999) were also used in this study for comparison.

Table 6.1 Summary of soil properties used in analyses of piles subjected to lateral spreading

Depth		Soil type	γ_t' (kN/m ³)	c (kN/m ²)	ϕ (deg.)	K (kN/m ³)	ϵ_{50}
From (m)	To (m)						
0.0	1.0	Very Loose Sand	7	-	29	5,400	-
1.0	4.0	Liquefied Sand	7	-	28	5,400	-
4.0	7.5	Very Soft Clay	7	15	-	-	0.02
7.5	8.5	Liquefied Sand	9	-	32	16,300	-
8.5	12.0	Very Dense Gravel	11	-	45	34,000	-

Note: g_t' = Effective soil unit weight
c = Soil cohesion
 ϕ = Soil friction angle
k = Subgrade reaction constant
 ϵ_{50} = Strain corresponding to one-half the maximum principal stress difference

Varying tip conditions for the single piles at the Tokachi site allowed for both flexible and rigid piles to be considered in the analyses. The single pile installed by the University of California, San Diego (UCSD) was embedded about 3 m into the dense gravel layer (see Fig. 4.29) to ensure that it would behave as a flexible pile. The piles installed by Waseda University (WU) were shorter in length and their pile tips were located just above the dense gravel layer. As a result, their behavior was similar to that of a rigid pile.

6.2.3 Analyses of Pile Groups

Two special considerations incorporated into the analysis of the pile groups were the effect of pile-head restraint at the pile cap and the effect of pile groups. The approach used to analyze the behavior of the pile groups subjected to lateral spreading in this study was adopted from the method proposed by Mokwa (1999). A summary of Mokwa's method is presented below.

The piles in a group were modeled as an equivalent single pile with four times the flexural stiffness of a single pile for the 4-pile group and nine times the flexural stiffness of a single pile for the 9-pile group. Figure 6.6 shows a sample of the numerical model used for analyzing the behavior of 4-pile group subjected lateral spreading. The p -multiplier approach was used to reduce the soil stiffnesses for each pile in the group to account for group effects. The reduced soil spring stiffnesses were then summed to develop the combined soil springs for the pile groups. The soil pressure acting on the pile cap was modeled using a soil spring that accounted for the width of the pile cap. In addition, the pile-head boundary condition of the group-equivalent pile was determined by estimating the rotational restraint provided by the pile cap using a rotational spring. Finally, the group-equivalent single pile, incorporating both the effects of pile-head restraint and of pile group behavior was analyzed by specifying the free-field soil profile at the boundary end of each soil spring. The input free-field soil movement profile was the same as that used in the single piles. Details of these steps are described following.

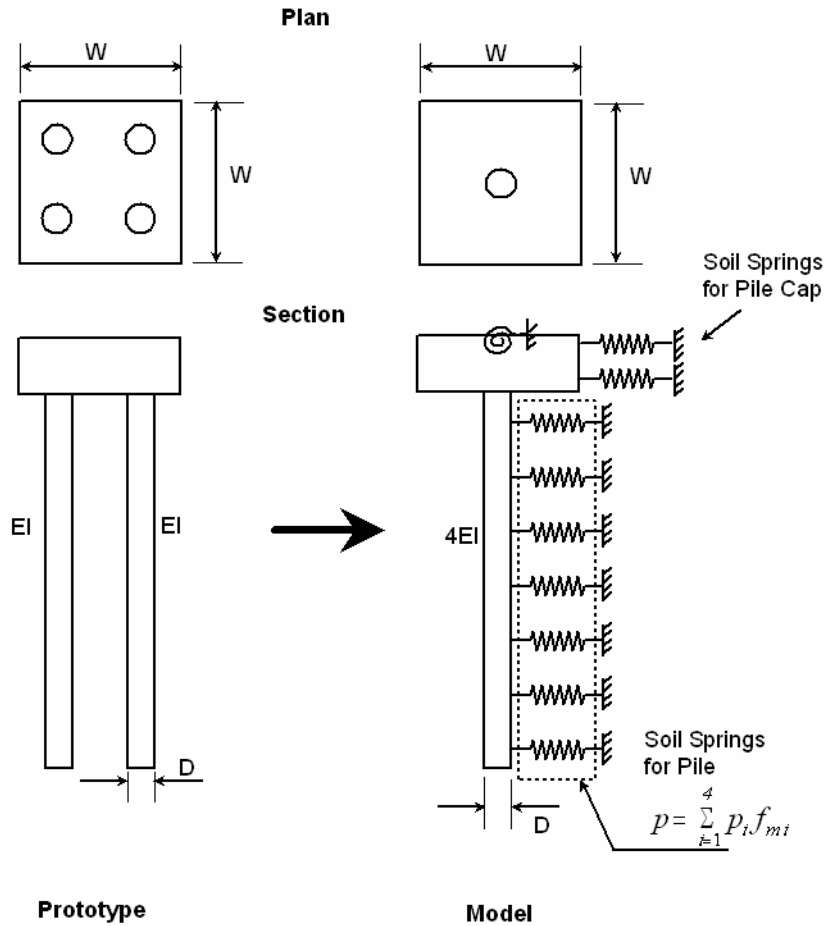


Fig. 6.6 p - y analysis model for pile group (after Mokwa 1999)

6.2.3.1 Pile Group Effect

The effect of the pile group was incorporated by using p -multiplier approach. The p -multipliers were obtained from results of previous research on 9-pile groups (i.e., Brown and Reese 1985; Morrison and Reese 1986; McVay et al. 1994; McVay et al. 1995; Rollins et al. 1998; Ashford and Rollins 2002) as shown in Figure 6.7. The p - y curves for a group-equivalent single pile were determined by summing the adjusted soil spring of each pile in the group as

$$p = \sum_{i=1}^N p_i f_{mi} \quad (6.3)$$

where p_i is the p -value for the single pile, f_{mi} is the p -multiplier determined from Figure 6.7, and N is the number of piles in the group.

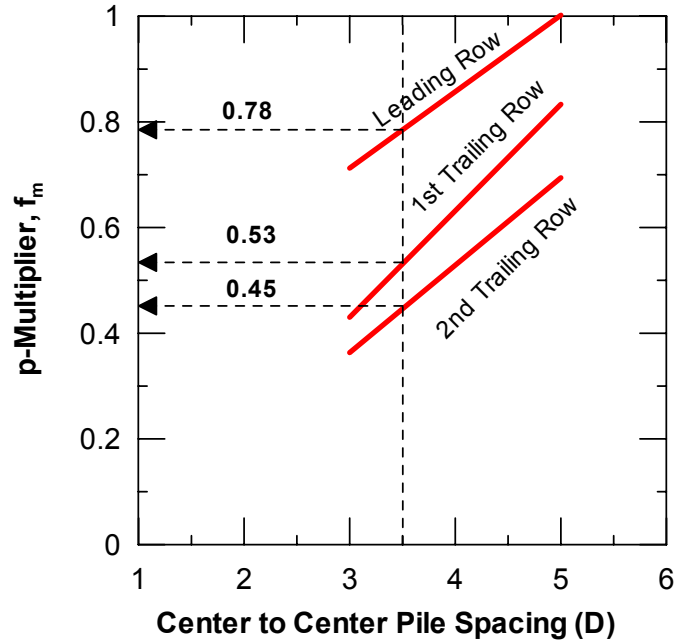


Fig. 6.7 Relationships between p -multiplier and pile spacing for each row in the group (after Mokwa 1999)

For the pile spacing of $3.5D$, the p -multipliers for the leading row, first trailing row, and second trailing row were 0.78, 0.53, and 0.45, respectively. Based on equation (6.3), the p -values for the equivalent pile representing the 4-pile group and the 9-pile group were 2.6 and 5.3 times the p -value of a single pile, respectively.

6.2.3.2 Resistance of Pile Cap

The soil pressure acting on the pile caps was modeled by using the sand p - y curves (Reese et al. 1974), considering the pile cap width as the pile diameter. Prior to conducting the test, the pile cap (1 m deep) was located in the very loose sand layer above the water table. It should be noted that based on site observations, the top 1 m of soil became nearly saturated at the end of the test due to the upward flow of water after the liquefaction occurred. The effective stress in this layer, therefore, decreased as compared to dry soil. To incorporate this effect into the analysis, the buoyant soil unit weight of saturated sand rather than the dry unit weight was implemented into the analysis to estimate the soil springs for the pile cap.

6.2.3.3 Rotational Soil Spring

Although a pile with a fixed-head condition is usually assumed in analysis of a pile group, in reality some rotation of the pile cap often occurs in the pile group, mainly caused by the vertical movement of the piles in the group, as presented in Figure 6.8 (Mokwa 1999; Mokwa and Duncan 2003).

The rotational stiffness, $k_{m\theta}$, of the pile group can be estimated as

$$k_{m\theta} = \frac{M}{\theta} \quad (6.4)$$

where M is the moment that resists rotation and θ is the rotation of the pile head.

Assuming that the relationship between M and θ is linear up to the ultimate restraining moment of the pile group, $k_{m\theta}$ can be determined if the ultimate moment, M_{ult} , and the ultimate pile-head rotation, q_{ult} , are known. The M_{ult} is a function of the resisting force of each pile and the moment arm, X_i , as

$$M_{ult} = \sum_{i=1}^N (Q_{si} + Q_E) X_i \quad (6.5)$$

where N is the number of piles in the group, Q_{si} is the ultimate skin resistance, Q_E is the ultimate end-bearing resistance, and X_i is the moment arm. Q_E is equal to zero for the upward pile.

The Q_{si} of the upward-moving pile can be directly estimated using the static pile theory such as the α -method or β -method. In this study the α -method was used for cohesive soils and the β -method was used for cohesionless soils. To determine M_{ult} , it is convenient to take the moment of the pile undergoing downward movement. The soil parameters used and the calculated skin resistance are summarized in Table 6.2. It was assumed that the uplift skin resistance was the same as the compression skin resistance. The estimated skin friction was then reduced by multiplying with the axial group efficiency to account for group effects in the vertical direction. This group efficiency factor of 0.70 was used for the case of 3.5D spacing (Das 1995).

Based on Mokwa's approach (Mokwa 1991), the ultimate angular rotation of the pile cap can be determined from the geometry as presented in Figure 6.8. For a case of a skin friction pile during the lateral loading, the front of the pile cap tends to move downward and the back upward. The amount of rotation can be determined from the geometry as

$$\theta = \tan^{-1}\left(\frac{2\Delta_{ult}}{S}\right) \quad (6.6)$$

where S is the pile spacing and Δ_{ult} is the relative displacement between the soil and the pile required to fully mobilize.

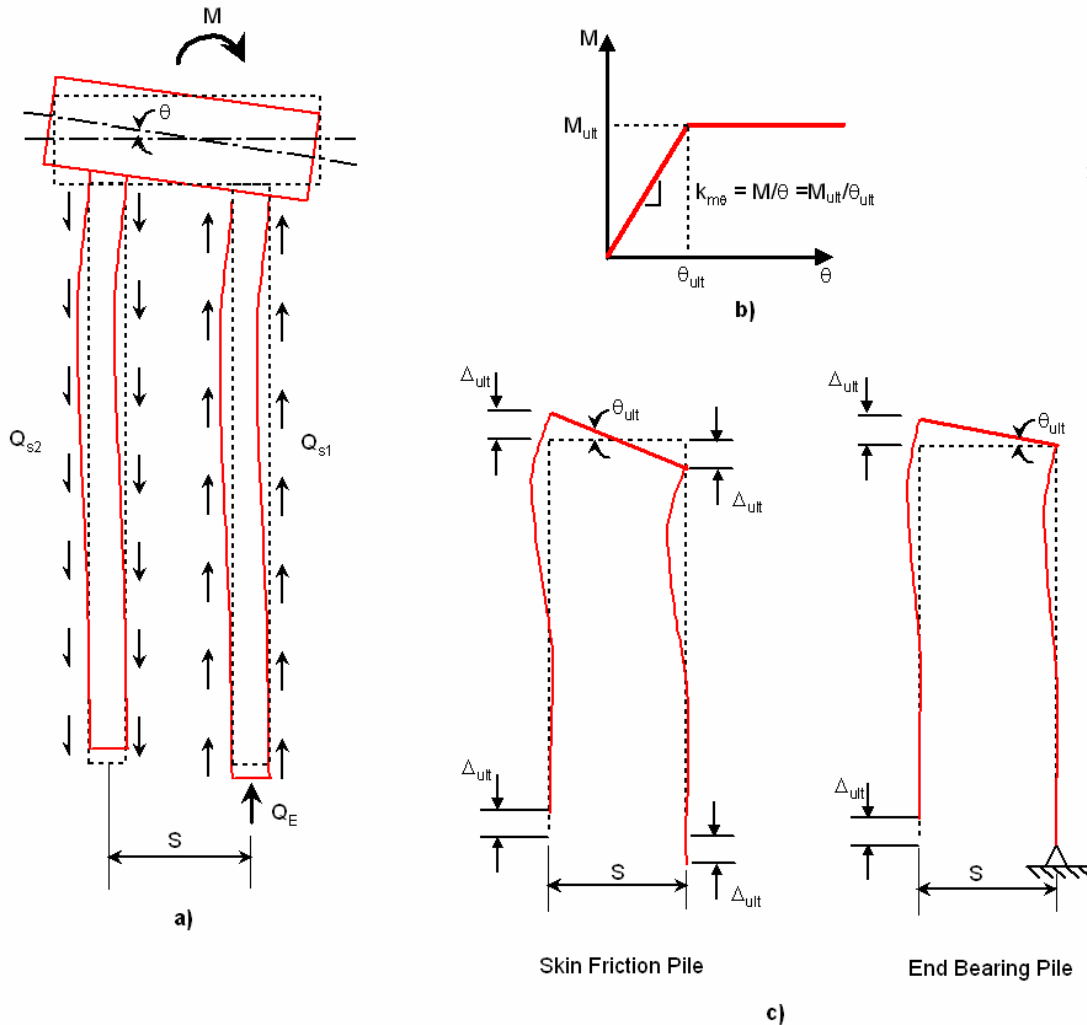


Fig. 6.8 Conceptual model for estimating pile group rotational restraint: (a) pile-cap rotational restraint model, (b) assumed linear relationship between m and θ , and (c) schematic diagrams for estimating ultimate pile-cap rotation (after Mokwa and Duncan 2003)

However, for a case of an end-bearing pile group which was applied for the Tokachi experiments, the front piles do not move, while the trailing piles move upward. Therefore, the angular rotation of the pile cap for this case can be determined from the geometry as

$$\theta = \tan^{-1}\left(\frac{\Delta_{ult}}{S}\right) \quad (6.7)$$

Das (1995) suggested that the maximum frictional resistance along the pile would be fully mobilized when the relative displacement between the soil and the pile is about 5 mm to 8 mm irrespective of pile size and length. For the purpose of calculating q_{ult} , the Δ_{ult} was assumed to be 8 mm for the piles in this study.

Based on the above equations, the rotational spring stiffnesses for the 4-pile group and the 9-pile group can be determined as 16,500 kN-m/rad and 74,600 kN-m/rad, respectively.

Table 6.2 Summary of soil parameters and estimated ultimate pile skin resistance

Depth		Soil type	c (kN/m ²)	ϕ (deg.)	α	K	δ	Q_s (kN)
From (m)	To (m)							
0	1.0	Very Loose Sand	-	29	-	-	-	-
1.0	4.0	Liquefied Sand	-	-	-	-	-	-
4.0	7.5	Very Soft Clay	15	-	1.0	-	-	52.5
7.5	8.5	Liquefied Sand	-	-	-	-	-	-
8.5	12.0	Very Dense Gravel	-	45	-	0.29	22.5	24.0

Note: $Q_s = \sum \alpha c A_s + \sum K \sigma_v' \tan \delta A_s$

where Q_s = Pile frictional resistance

α = Empirical adhesion factor

A_s = Pile surface area

K = Earth pressure coefficient = $1 - \sin \phi$

σ_v' = Effective vertical stress at the depth under consideration

δ = Soil-pile friction angle = 0.5ϕ

6.2.4 Results of Analyses

6.2.4.1 Single Piles

Figure 6.9 presents a comparison between computed and measured pile responses of the UCSD single pile (i.e., flexible pile). When using zero spring stiffness for liquefied soil, the predicted pile-head displacements (Fig. 6.9a), pile-head rotations (Fig. 6.9b), and moment profiles (Fig. 6.9c) were in good agreement with the pile responses measured from both tests. Using the p -multiplier approach for the liquefied soil layer overestimated the pile response. Because the behavior of liquefied soil at the test site could be well represented by using zero soil spring, only this method was used to analyze the behavior of rigid piles and pile groups in subsequent sections.

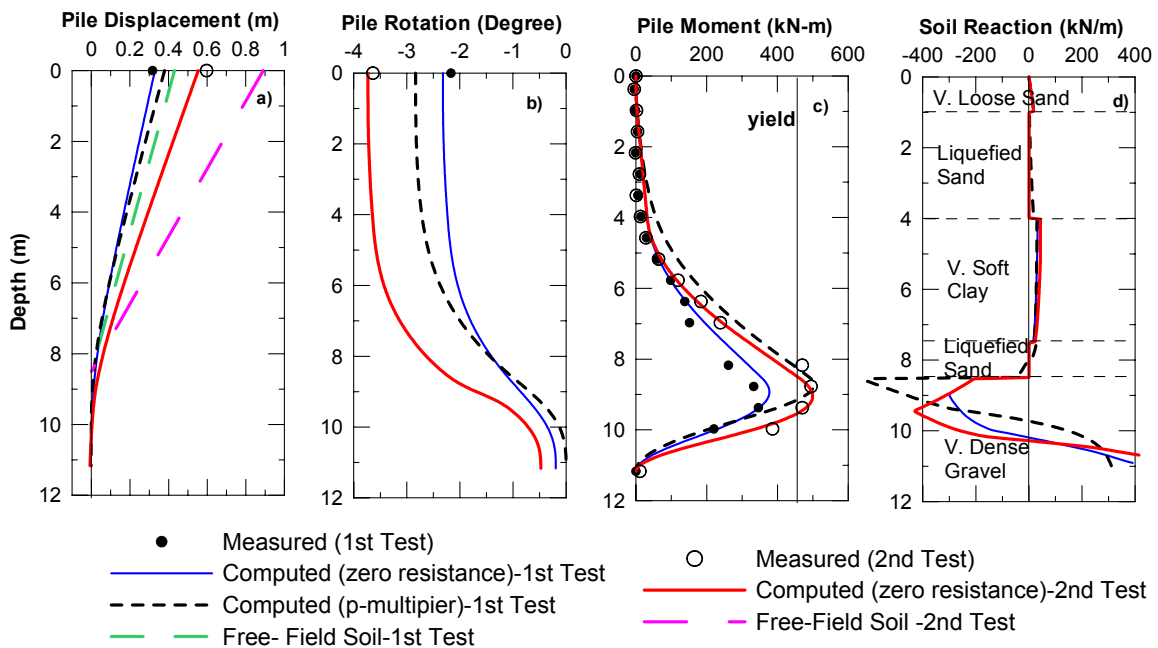


Fig. 6.9 Comparison between measured and computed pile responses for UCSD single pile (flexible pile) first and second tests

Figure 6.9a shows that for the first 8 m, the free-field movement of the soil mass was greater than the movement of the pile, which implies that the soil provided the driving force to the pile, as is also shown by the positive soil reaction in Figure 6.9d except for the liquefied layer where zero reaction was assumed. Negative soil resistance indicated that the soil mass moved

less than the pile, and therefore the soil provided the resistance force to the pile as mostly occurred in very dense gravel layer (Fig. 6.9d).

The lateral responses of the pile are dependent on the magnitude of free-field soil displacement, increasing the free-field soil displacement results in higher maximum moment and pile-head displacement. However, if the free-field soil movement is large enough to cause the lateral soil pressures to be fully mobilized, the response of the pile will be independent of the free-field soil movement. Analyses were conducted to determine the magnitude of surface displacement required to cause the soil to reach their ultimate values. The pile stiffness was first assumed to remain linear-elastic throughout the analyses. The analyses were done by gradually increasing the ground surface displacement, while the soil displacement profile was assumed to be linear. Figure 6.10a shows that once the ground surface displacements are larger than 1.4 m, the laterally spreading soils reach their ultimate values, resulting in no change on the pile responses. However, the analysis results indicate that the maximum moment in the pile is greater than the actual yield moment; therefore, the pile will yield before the soils reach the ultimate pressure, which was indeed observed from the pile moment data in the second test. Additional analyses were then conducted using the actual nonlinear pile properties as shown in Figure 4.6. Figure 6.10b shows the analysis results of a nonlinear pile which indicates that the pile yields when the soil surface displacement reaches 0.65 m. Since the pile yielded, increasing the ground displacement increases the pile-head displacement. The measured pile displacements and maximum moments from both tests were also plotted in Figure 6.10b, indicating that the prediction of pile response using the p - y analysis method did a good job on the single pile case.

Figure 6.11 presents the results of the analysis for the case of WU single piles (i.e., rigid piles). Good agreement was obtained between the computed and measured pile responses. For this case, the movements of the pile and the free-field soil were very similar, which indicates rigid pile behavior. The displacements and rotations of the rigid piles were greater than the flexible pile, since the bottom of the flexible pile was more restrained. Due to this restrained behavior, the flexible pile underwent more bending which showed up as a greater bending moment. The rigid piles moved as a whole and hence showed significantly less bending. The soil pressure exerted on the pile for the rigid pile case was very small compared to the case of flexible pile. Only small resisting forces in the dense gravel layer were observed.

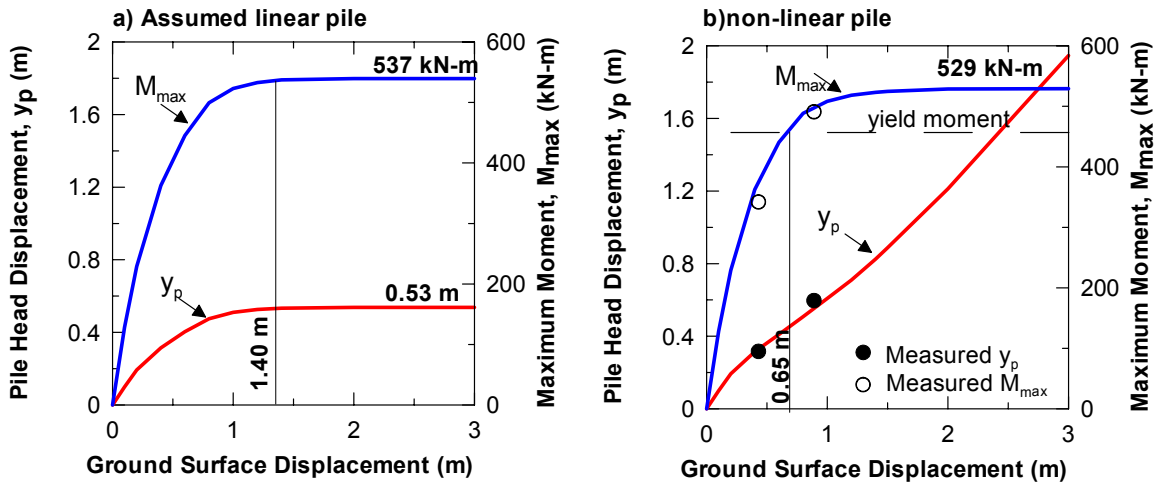


Fig. 6.10 Pile-head displacement and maximum moment vs. ground surface displacement for UCSD single pile: (a) assume linear pile and (b) nonlinear pile

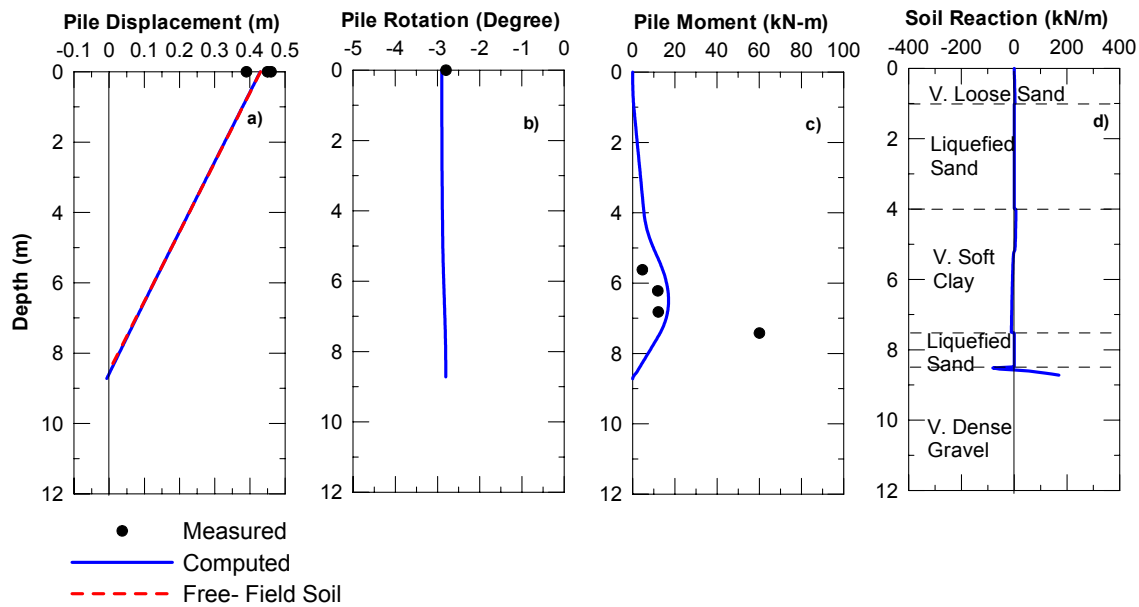


Fig. 6.11 Comparison between measured and computed pile responses for WU single piles (rigid piles) for first test

6.2.4.2 Pile Groups

Although the test results from the Tokachi experiments indicated that small rotations might occur at the tops of the piles due to the cracking of the concrete around the embedded piles and the elongation of the anchor bars, this effect was assumed to be small, especially for the first test (i.e.,

the maximum negative moment at the piles top was lower than the ultimate moment capacity at the connection). As a result, the rotations of the caps and the tops of the piles were assumed to be identical. However, for the second test, this assumption might not be valid and the effect of the difference in the rotations between the caps and the tops of the piles has to be taken into consideration. Due to the limitation of the LPILE plus 4.0m program in modeling this effect, the analyses were conducted only to predict the results from the first experiment.

Figure 6.12–6.13 present the results of the calculated and measured pile responses of the 4-pile group and the 9-pile group, respectively. The same set of baseline soil properties used in the case of single piles was also used for analyzing the behavior of pile groups with the same input free-field soil displacement profile. Three types of boundary conditions at the pile head were considered in this study for the purpose of comparison; these include the free-head condition, fixed-head condition, and the rotationally restrained pile-head boundary condition. Neither the free-head nor fixed-head condition provided a reasonable estimate of the measured pile behavior. The free-head case overestimated the maximum positive moment at depth, and gave zero moment at the pile head, while the fixed-head case underpredicted the maximum positive moment but overestimated the maximum negative moment. The deflections at the pile head obtained from the fixed-head case were smaller than those measured by 51% for the 4-pile group, and 49% for the 9-pile group. The free-head case overpredicted the pile-head deflection by 53% and 60% for the 4-pile group and the 9-pile group, respectively.

The analysis results obtained using the rotationally restrained pile-head boundary condition considerably improved the agreement between measured and computed responses for both the 4-pile group and the 9-pile group as shown in Figures 6.12 and 6.13, respectively. The computed pile moments were in a reasonable range of those moments measured from the test. The errors between the computed and measured pile group displacements were less than 3% for the 4-pile group and 13% for the 9-pile group. The pile-head rotation was somewhat overestimated on the 9-pile group as shown in Fig. 6.13b, likely due to the difference in the amount of rotation between the tops of the piles and the caps as discussed earlier. In summary, the p - y method by incorporating the rotational spring at the pile head can be used to predict the response of a pile group subjected to lateral spreading with reasonable accuracy if the free-field soil displacement is known. For design purposes, both free-head and fixed-head cases should be considered. By conducting the analyses on both cases, one can consider using the maximum

positive moment obtained from the free-head case and the maximum negative moment obtained from the fixed-head case for a conservative design.

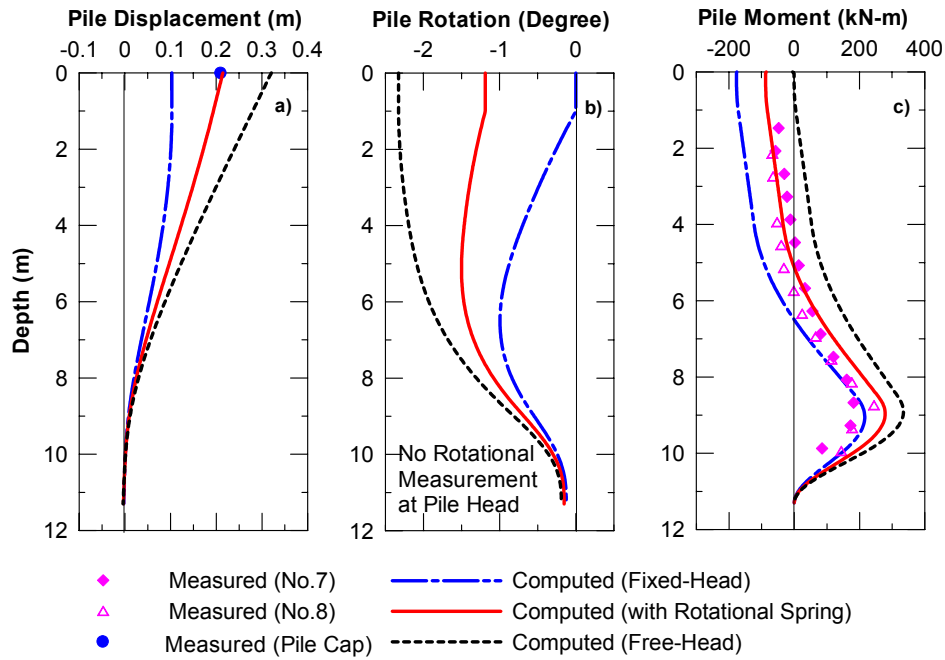


Fig. 6.12 Comparison between measured and computed pile responses for 4-pile group first test

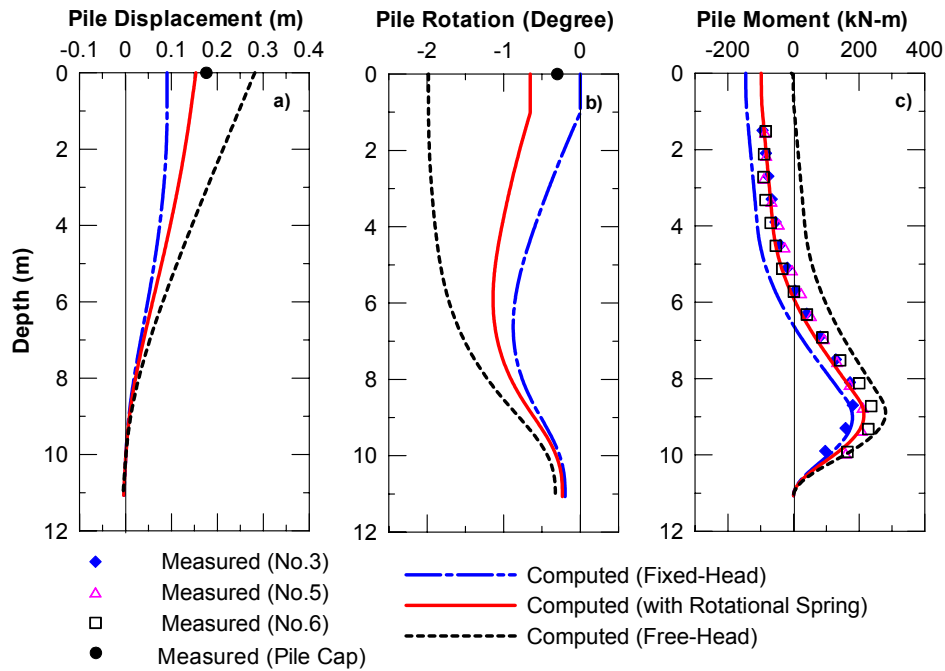


Fig. 6.13 Comparison between measured and computed pile responses for 9-pile group first test

In a similar manner to the single piles, analyses were carried out to determine the displacement necessary to develop the ultimate soil pressure on the pile groups.

Figure 6.14 shows that for both pile groups, once the ground surface movement is larger than 1.0 m, no significant changes of pile-head displacement, as well as maximum bending moments are anticipated. The maximum positive and negative moments are well below the yield moment of 450 kN-m.; as a result, the piles should not yield even when undergoing large lateral spreading. The largest movements of pile caps are limited at 0.26 m for the 4-pile group and 0.18 m for the 9-pile group. The negative moments are limited at 95 kN-m for the 4-pile group and 105 kN-m for the 9-pile group. It should be noted that these analyses were carried out based on the assumption that the ultimate moment capacity of the connection between the piles and the pile cap was so large such that the rotations of the pile heads and the cap were identical throughout the analyses. However, the analysis results indicate that after the ground surface displacement reaches about 0.5 m, the maximum negative moment becomes greater than the actual ultimate capacity of the connection (90 kN-m). This caused the yielding of the pile-cap connection, which in turn resulted in a decrease of the overall stiffnesses of the pile groups. Therefore, the movements and maximum positive moments of both pile groups measured in the second test were larger than the calculated limit values as shown in Figure 6.14.

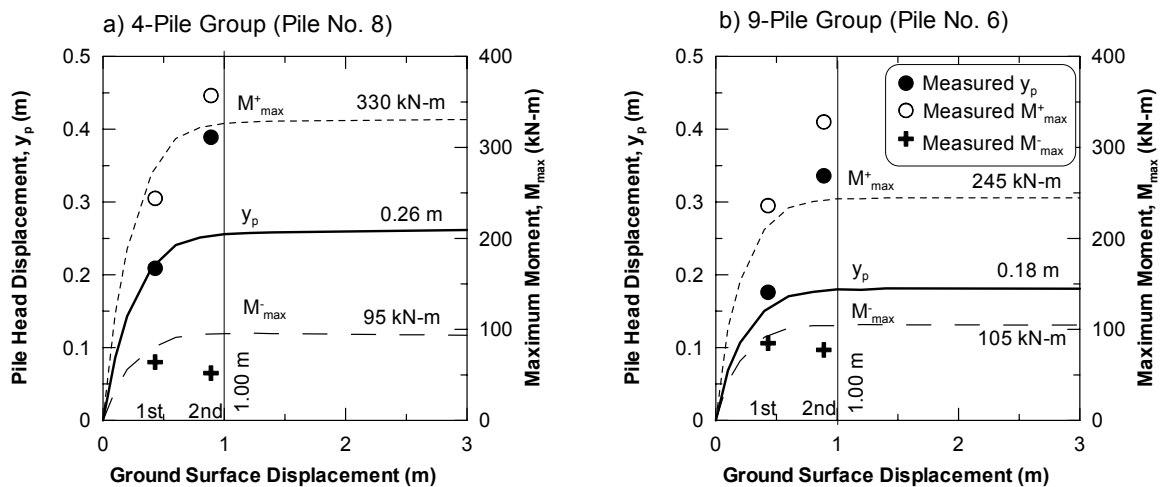


Fig. 6.14 Pile-head displacement and maximum moment vs. ground surface displacement: (a) 4- pile group and (b) 9-pile group

6.2.5 Design Implications

The input free-field soil displacement profiles used in this study were based on test measurements. However, in design situations, this free-field soil profile must be estimated. Empirical procedures may be used to estimate surface free-field soil displacement due to lateral spreading (e.g., Bardet et al. 2002; Youd et al. 2002). The soil movement profile for the laterally spreading soil can then be obtained based on a linear distribution as was done in this study, or another reasonable distribution such as a half-cosine curve (Finn and Thavaraj 2001). Pile response due to lateral spreading can then be estimated using the p - y analysis method described previously. The soil springs for liquefied sand may be neglected if the soil relative density is less than 40%, as was the case in this study. For higher soil relative density, there is no consensus among researchers on the appropriate method for developing p - y springs for liquefied soil. A p -multiplier may be used to reduce the p - y spring stiffness and ultimate soil pressure obtained from traditional methods. Multipliers between 0.1 and 0.35 have been recommended for liquefied sand (e.g., Liu and Dobry 1995; Wilson et al. 1999). However, the modified p - y curves should be used with caution, especially when the ground deformation is large. Back-calculated p - y curves of liquefied sand based on the results from full-scale testing (Ashford and Rollins 2002) or centrifuge testing (Wilson et al. 1999) show the dilation behavior at large soil displacement. The soil pressure at large displacement can be significantly higher than that obtained from the p -multiplier approach (Ashford and Rollins 2002), and this may lead to an unconservative design. More physical tests are still needed at the relative density of greater than 40% in order to further justify the use of appropriate soil springs for liquefied sand.

It should be noted that the method presented herein considers only kinematic loading from laterally spreading soils without accounting for inertial loading from the foundation or superstructure because this effect was assumed to be small in the full-scale tests. However, for seismic design, the peak response due to a combination of both inertial and kinematic loads during shaking may be higher than the response at the end of shaking due to kinematic loading from lateral spreading alone. In any case, analyses should be conducted to determine the critical design load case. In addition, because this method is a pseudo-static pushover analysis, it provides only an approximate solution to the dynamic problem of lateral spreading. For important structures, a more sophisticated analysis may be necessary for design purposes, such

as a dynamic time history analysis or 3D FEM analysis using an appropriate soil constitutive model.

7 Summary and Conclusions

Two full-scale lateral spreading experiments using controlled blasting were conducted in the port of Tokachi on Hokkaido Island, Japan, to assess the behavior of piles and pipelines subjected to lateral spreading. The soil was very loose and highly susceptible to liquefaction. The test piles included a single pile, a 4-pile group, and a 9-pile group. The pipelines included two transverse pipelines (i.e., gas pipeline and electrical conduit) and one longitudinal gas pipeline. The piles and pipelines were extensively instrumented with strain gages to measure the distribution of bending moment during lateral spreading which allowed the back-calculation of the loading condition and the assessment of damage and the performance of the piles. Other instrumentation, including pore-pressure transducers, GPS units, and inclinometers, was also installed to measure pore-pressure buildup and movements of the soils, piles, and pipelines during lateral spreading. Based on the results, the following conclusions can be made:

- Controlled blasting successfully liquefied the soil and induced lateral spreading with magnitudes of free-field soil displacements at the locations of the test piles of over 40 cm for both tests.
- Back-calculated soil reactions of both the single pile and the pile groups indicated that liquefied soil layer imparted insignificant force to the piles. The moment developed in the piles was caused by the mobile soft clay layer, which imparted driving forces to the piles, while the dense gravel layer provided resisting forces.
- Pile-head restraint in the pile group contributed resisting the moment induced by lateral spreading, which resulted in the smaller maximum positive moment, as well as smaller pile-head displacement when compared to the case of a single pile.
- The degree of fixity at pile tips had a major effect on the moments of individual piles in the group. The larger the degree of fixity, the higher the developed moment in the pile.

- The single pile yielded at the end of the second test. Both the 4-pile and 9-pile groups performed well during both tests. The piles in the group remained elastic. Little concrete spalling was observed at the pile to pile-cap connection at the end of the second test, indicating that some rotations between the piles to the pile caps might occur.

Based on the test results, a pushover analysis using the p - y method was assessed in order to study the potential in implementing this method in predicting the behavior of piles subjected to lateral spreading in design practice. Analyses were conducted by using a single set of baseline soil properties to compute the responses of both the single piles and pile groups. Responses of the single piles subjected to lateral spreading were determined by imposing the known free-field soil movement profile measured during the test to the boundary condition of Winkler springs along the piles. The soil springs used in this study were based upon standard p - y springs currently used in design practice. No soil resistance was used for the liquefied soil layer. For the case of pile groups, the piles in the groups were modeled as an equivalent single pile with four times the flexural stiffness of a single pile for the 4-pile group and nine times the flexural stiffness of a single pile for the 9-pile group. In addition, two special considerations were required to incorporate into the model, which included modeling of pile-head restraint using the rotational spring, and a decrease of soil spring stiffnesses to account for the group effect using the p -multiplier approach. Then, the analyses for the case of the pile groups can be conducted in a similar way as for the single pile case. Computed pile responses for each pile foundation were compared to the measured responses obtained from the full-scale test.

Reasonably good agreement for all types of pile foundations considered in this study was obtained between the computed and measured responses. The results provide justification for the use of the p - y analysis method in piles subjected to lateral spreading problems. However, the major limitation of p - y analysis method is that the analysis is pseudo-static and hence can provide only an approximate solution to the dynamic problem of lateral spreading. Moreover, the p - y method has limitations due to its empirical approach and inability to account for soil shear. Hence, a comparison with more sophisticated analysis, which considers the inertia of the piles and soil, and uses a proper constitutive relationship, is still needed in order to decisively assess the applicability of the p - y method. The full-scale and/or physical model tests such as centrifuge tests are also needed to further study the reliability of this method before implementing into design practice.

REFERENCES

- Abdoun, T. H. (1997). *Modeling of Seismically Induced Lateral Spreading of Multi-Layer Soil Deposit and Its Effect on Pile Foundations*, Ph. D. Thesis, Dept. of Civil Engineering, Rensselaer Polytechnic Institute, Troy, NY.
- Abdoun, T. H., Dobry, R., O'Rourke, T. D., and Chaudhuri, D.(1996). "Centrifuge modeling of seismically-induced lateral deformation during liquefaction and its effect on a pile foundation." *Proc. Sixth Japan-U.S. Workshop on Earthquake Resistant Design of Lifeline Facilities and Countermeasures against Soil Liquefaction*, Technical Report NCEER-96-0012, NCEER, SUNY-Buffalo, NY, pp. 525-539.
- Ashford, S. A., Rollins, K. M. (2002). *TILT: Treasure Island Liquefaction Test Final Report, Report No. SSRP-2001/17*, Department of Structural Engineering, UCSD.
- Ashford, S. A., Rollins, K. M., Bradford, S. C., Weaver, T. J., and Baez, J. I. (2000). "Liquefaction mitigation using stone columns around deep foundations: full-scale test results." *Soil Mechanics 2000, Transportation Research Record No. 1736*, TRB, Washington D.C., pp.110-118.
- Bardet, J-P., Tobita, T. Mace, N., and Hu, J. (2002). "Regional modeling of liquefaction-induced ground deformation." *Earthquake Spectra*, 18(1) 19-46.
- Bartlett, S. F., and Youd, T. L. (1995). "Empirical prediction of liquefaction-induced lateral spread." *Journal of Geotechnical Engineering*, ASCE, 121 (4), 316-329.
- Benuzka, L. (1990). *Loma Prieta Earthquake Reconnaissance report*, Report by EERI and NRC, Supplement to Vol.6 of Earthquake Spectra, 448 p.
- Bergdahl, U., Broms, B. B., and Muromachi, T. (1988). "Weight sounding test (WST): International reference test procedure." *Proc. of the First International Symposium on Penetration Testing*, Vol. 1, Orlando, pp. 77-90.
- Brown, D. A., and Reese, L. C. (1985). "Behavior of a large scale pile group subjected to cyclic lateral loading," *Report to the Minerals Management Services*, U.S. Dept. of Interior, Reston, VA. Dept. of Research, FHWA, Washington DC and U.S. Army Engineer Waterways Experiment Station , Vicksburg, Mississippi.
- Charlie, W. A., Rwebyogo, F. J., and Doehring, D. O. (1992). "Time-dependent cone penetration resistance due to blasting." *Journal of Geotechnical Engineering*, 118(8), 1200–1215.

- Das, B. M. (1995). *Principles of Foundation Engineering*, Third Edition, PWS Publishing Company, Boston, MA.
- Dobry, R. and Abdoun, T. H., (2001). “Recent studies on seismic centrifuge modeling on liquefaction and its effect on deep foundations.” State-of-the-Art Paper, *Proc. 4th Intl. Conf. on Recent Advances in Geotechnical Earthquake Engineering and Soil Dynamics and Symposium to Honor Prof. W.D.L. Finn* (S. Prakash, ed.), San Diego, CA, SOAP-3, Vol. 2., pp.1-30.
- Finn, W. D., and Thavaraj, T. (2001). “Deep foundations in liquefiable soils: case histories, centrifuge tests and methods of analysis.” *Fourth International Conference on Recent Advances in Geotechnical Earthquake Engineering and Soil Dynamics*, S. Prakash, ed., University of Missouri-Rolla, paper no. SOAP-1, 1-11.
- Gohl, W. B., J. A. Howie, and C. E. Rea. (2001). “Use of controlled detonation of explosives for liquefaction testing.” *Proceedings, 4th Int. Conf. on Recent Advances in Geotechnical Earthquake Geotechnical Engineering and Soil Dynamics and Symposium in Honor of Professor W. D. Liam Finn*, Edited by Prakash, S., San Diego, CA, March 26-31, paper No. 9.13, pp 1-9 (CD).
- Hamada, M. (1992). “Large ground deformations and their effects on lifelines: 1964 Niigata Earthquake.” *Ch.3 of Case Studies of Liquefaction and Lifeline Performance during Past Earthquakes*, Report No. NCEER-92-0001, Vol.1, (Hamada and O’Rourke, eds.) National Center for Earthquake Engineering Research, Buffalo, N.Y, pp. 3-1 to 3-123.
- Hamada, M., and O’Rourke, T., eds. (1992). *Case Studies of Liquefaction and Lifeline Performance during Past Earthquakes*, Report No. NCEER-92-0001, Vol.1, National Center for Earthquake Engineering Research, Buffalo, N.Y.
- Hamada, M. (2000). “Performance of foundations against liquefaction-induced permanent ground displacement.” *Proc. 12th World conference on Earthquake Engineering, Auckland, New Zealand*, Paper No. 1754.
- Japanese Geotechnical Society (1995): Method for Swedish weight sounding test (JIS A 1221-1995), *Ground survey method*, pp.213-220 (in Japanese)
- Kulhawy, F. H., and Mayne, P. W. (1990). “Manual on estimating soil properties for foundation design.” *Research Project 1493-6*, EL-6800, Electric Power Research Institute, Palo Alto, CA.

- Liu, L. and Dobry, R. (1995). "Effect of Liquefaction on Lateral Response of Piles by Centrifuge Model Tests," *NCEER Bulletin, January, pp.7-11*.
- Lunne, T., and Klevan, A. (1982). "Role of CPT in North Sea foundation engineering," *Norwegian Geotechnical Institute, Publication 139, 1-14*.
- Matlock, H. (1970). "Correlations for design of laterally loaded piles in soft clay." *Proc., 2nd Annual Offshore Technology Conf.*, Paper No. OTC 1204, Houston, Texas, 577-594.
- McVay, M., Bloomquist, D., Vanderlinde, D., and Clausen, J. (1994). "Centrifuge modeling of laterally loaded pile groups in sands." *ASTM Geotechnical Testing Journal*, 17, 129-137.
- McVay, M., Casper, R., and Shang, T. (1995). "Lateral response of three-row groups in loose to dense sands at 3D and 5D pile spacing," *Journal of Geotechnical Engineering, ASCE*, 121(5), 436-441.
- Meneses, J., Hamada, M., Kurita, M., and Elgamal, A. (2002). "Soil-pile interaction under liquefied sand flow in 1g shake table tests," *Proceedings International Conference on Advances and New Challenges in Earthquake Engineering Research*, Harbin and Hong Kong, China.
- Meyersohn, W.D. (1994). "Pile response to liquefaction induced lateral spread." Ph.D. thesis, Dept. of Civil and Environmental Engineering, Cornell University, Ithaca, N.Y.
- Mokwa, R. L. (1999). "Investigation of the resistance of pile caps to lateral spreading," Ph. D. Thesis, Dept. of Civil Engineering, Virginia Polytechnic Institute and State University, Blacksburg, Virginia.
- Mokwa, R. L. and Duncan, J. M. (2003). "Rotational restraint of pile caps during lateral loading." *Journal of Geotechnical and Geoenvironmental Engineering, ASCE*, 129(9), 829-837.
- Morrison, C., and Reese, L. C. (1986). "A lateral-load test of full-scale pile group in sand," *GR86-1, FHWA, Washington D.C.*
- Nagao, K., Maeda, S., Toshida, N., and Kiku, H. (2003). "In-situ full scale liquefaction test by controlled blasting." *Symposium on the Seismic Performance of Urban, Reclaimed and Port Areas—Dynamic Behaviors and Stabilities of Earth and Soil-Retaining Structures*, Tokyo, Japan.
- NAVFAC (1982). "Soil mechanics," *Design Manual 7.1, Manual No. NAVFAC DM-7.1*, Department of the Navy, Naval Facilities Engineering Command, Alexandria, VA.

- Narin van Court, W. and Mitchell, J. K. (1994). "Explosive compaction: Densification of loose, saturated, cohesionless soils by blasting." *Geotechnical Engineering Report No. UCB/GT/94-03*, Department of Civil Engineering, University of California, Berkeley, CA.
- O'Rourke, T. D. (1996). "Lessons learned for lifeline engineering from major urban earthquakes," *Proceedings, Eleventh World Conference on Earthquake Engineering, Elsevier Science Ltd.*, 18 p.
- Port and Airport Research Institute (PARI). (2002). (*Personal Communication*), Japan.
- Peck, R. B, Hanson, W. E., and Thornburn, T. H. (1974). *Foundation Engineering*, 2nd ed., John Wiley and Sons, New York.
- Port and Harbour Research Institute (PHRI). (1997). *Handbook on Liquefaction Remediation of Reclaimed Land*, A.A. Balkema, Rotterdam, Brookfield.
- Ramos, R., Abdoun, T. H., and Dobry, R. (2000). "Effect of lateral stiffness of superstructure on bending moments of pile foundation due to liquefaction-induced lateral spreading." *Proc. 12th World Conference on Earthquake Engineering, Auckland*, New Zealand, Paper No. 0902.
- Reese, L. C., Cox, W. R., and Koop, F. D. (1974). "Analysis of laterally loaded piles in sand," *Proc. 6th Offshore Technology Conference*, Paper 2080, Houston, Texas, 473-483.
- Reese, L.C., Wang, S. T., Isenhower, W. M., and Arrellaga, J. A. (2000). *Computer Program LPILE Plus Version 4.0 Technical Manual*, Ensoft, Inc., Austin, Texas.
- Rollins, K. M., Lane, J. D., Nicholson, P. G., and Rollins, R.E. (2004). "Liquefaction hazard assessment using controlled-blasting techniques." *Proc. 11th International Conference on Soil Dynamics & Earthquake Engineering and 3rd International Conference on Earthquake Geotechnical Engineering*, Berkeley, CA, Stallion Press, Volume 2, pp. 630-637.
- Rollins, K. P., Peterson, K. T., and Weaver, T. J. (1998). "Lateral load behavior of full-scale pile group in clay," *Journal of Geotechnical and Geoenvironmental Engineering*, ASCE, 124(6), 468-478.
- Sato Kogyo Co. (2002). (*Personal Communication*), Japan.
- Seed, R. B., and Harder, L.F. (1990). "SPT-based analysis of cyclic pore pressure generation on undrained residual strength," *Proceedings of the H. Bolton Seed Memorial Symposium*, University of California, Berkeley, May 10-11, pp. 351-376.
- Seed, H. B., and Idriss, I. M. (1971). "A simplified procedure for evaluating soil liquefaction potential," *JSMFD*, ASCE, 97(9), pp. 1249-1274.

- Takahashi, Y. (2002). "A result of the ground surface displacement measured by GPS and an investigation on the flowing characteristics of the liquefaction soil." (Internal workshop on Full-Scale Lateral Spreading Tests, Japan, June 24-25).
- Tokida, K., Iwasaki, H., Matsumoto, H., and Hamasa, T. (1993). "Liquefaction potential and drag force acting on piles in flowing soils." *Soil Dynamic and Earthquake Engineering, Computational Mechanics*, South Hampton, England, pp. 349-364.
- Tokimatsu, K., Suzuki, H., and Suzuki, Y. (2001). "Back-calculated p-y relation of liquefied soils from large shaking table tests." *Fourth International Conference on Recent Advances in Geotechnical Earthquake Engineering and Soil Dynamics*, S. Prakash, ed., University of Missouri-Rolla, paper 6.24.
- Turner, L. L., (2002). *Measurements of Lateral Spread Using a Real Time Kinematic Global Positioning System*, California Department of Transportation Division of New Technology & Research, 94 p.
- Wilson, D. W., Boulanger, R. W., and Kutter, B. L. (1999). "Lateral resistance of piles in liquefying soil." *OTRC'99 Conf. On Analysis, Design, Construction & Testing of Deep Foundations*, J. M. Rosset, ed., Geotechnical Special Publication No. 88, ASCE, pp. 165-179.
- Wilson, D. W., R.W. Boulanger, and M. L. Kutter (2000). "Observed seismic lateral resistance of liquefying sand," *Journal of Geotechnical and Geoenvironmental Engineering*, ASCE, 126(10), 898-906.
- Youd, T. L., Hansen, C. M., and Barlett, S. F. (2002). "Revised multi-linear regression equations for prediction of lateral spread displacement." *Journal of Geotechnical and Geoenvironmental Engineering*, ASCE, 128(12), 1007-1017.
- Youd, T. L., Rollins, K. M., Salazar, A. F., and Wallace, R. M. (1992). "Bridge damage caused by liquefaction during the 22 April 1991 Costa Rica earthquake." *Proc. Tenth World Conference on Earthquake Engineering*, Madrid, Spain, pp. 153-158.

Appendix A: Summary of Soil Properties and Boring Logs

Table A.1 Summary of soil properties for borehole No. 1 (after PARI 2002)

BH	Sample No.	Depth (m)		SPT N-Values	w_n (%)	G_s	Soil Composition (%)				C_u	C_c	LL	PL	PI	USCS	Soil Description	q_u (kN/m ²)
		From	To				Gravel	Sand	Silt	Clay								
Bor.1	1-1	0.65	0.95	0	86.0	2.60	0.0	26.9	63.3	9.8			61.4	30.8	30.6	MH	SILT with sand	13.4
	T1-1	0.70	1.50	-	99.7	2.65	0.0	0.0	74.8	25.2			77.2	36.0	41.2	MH	SILT	
	1-2	1.65	1.95	12	27.4	2.70	0.1	93.2	6.7							SP-SM	Poorly graded SAND with silt	
	1-3	2.65	2.95	10	35.9	2.65	0.1	91.3	8.6							SP-SM	Poorly graded SAND with silt	
	1-4	3.65	3.95	3	33.0	2.65	0.1	82.9	17.0							SM	Silty SAND	
	1-5	4.65	4.95	1	35.2	2.66	0.1	81.7	18.3							SM	Silty SAND	
	1-6	5.65	5.95	0	59.4	2.66	0.1	51.0	39.6	9.3						SM	Silty SAND	

Table A.2 Summary of soil properties for borehole No. 2

BH	Sample No.	Depth (m)		SPT N-Values	w_n (%)	G_s	Soil Composition (%)				C_u	C_c	LL	PL	PI	USCS	Soil Description	q_u (kN/m ²)
		From	To				Gravel	Sand	Silt	Clay								
Bor.2	2-1	0.65	0.95	0	48.4	2.65	0.0	71.9	24.5	3.6						SM	Silty SAND	23.9
	2-2	1.65	1.95	0	86.8	2.63	0.0	14.3	64.4	21.3			65.6	37.6	28.0	MH	SILT	
	2-3	2.65	2.95	1	34.1	2.66	0.0	89.7	10.3							SP-SM	Poorly graded SAND with silt	
	2-4	3.50	4.00	0	54.5	2.65	0.0	59.6	31.1	9.3						SM	Silty SAND	
	2-5	4.50	5.00	0	70.3	2.63	0.0	36.0	52.3	11.7			59.4	31.4	28.0	MH	Sandy SILT	
	T2-1	5.00	5.80	-	59.9	2.72	0.0	1.8	49.5	48.7			54.1	24.2	29.9	CH	Fat CLAY	
	2-6	5.50	6.00	0	66.6	2.67	0.0	3.6	80.6	15.8			72.8	41.2	31.6	MH	SILT	
2-7	6.65	6.95	12	80.8	2.65	0.0	30.4	67.5	12.1						SM	Silty SAND		

Table A.3 Summary of soil properties for borehole No. 3

BH	Sample No.	Depth (m)		SPT N-Values	w_n (%)	G_s	Soil Composition (%)				C_u	C_c	LL	PL	PI	USCS	Soil Description	q_u (kN/m ²)
		From	To				Gravel	Sand	Silt	Clay								
Bor.3	T3-2	5.90	6.70	-	81.5	2.66	0.0	0.0	52.1	47.9			73.5	29.6	43.9	CH	Fat CLAY	29.7

Note: w_n = Natural Water Content, G_s = Specific Gravity, C_u = Coefficient of Uniformity, C_c = Coefficient of Gradation, LL = Liquid Limit, PL = Plastic Limit, PI = Plastic Index, USCS = Unified Soil Classification System, q_u = Unconfined Compressive Strength

Table A.4 Summary of soil properties for borehole A-4 (after PARI 2002)

BH	Sample No.	Depth (m)		SPT N-Values	w _n (%)	G _s	Soil Composition (%)				C _u	C _c	LL	PL	PI	USCS	Soil Description
		From	To				Gravel	Sand	Silt	Clay							
A-4	P1	0.00	0.20	-	9.3	2.67	16.5	76.7	6.8	0.0	3.8	0.6	NP	NP	NP	SP-SM	Poorly graded SAND w/ silt and gravel
	P2-1	1.00	1.40	1	33.6	2.74	0.0	64.8	26.2	9.0	37.9	5.6	NP	NP	NP	SM	Silty SAND
	P2-2	1.00	1.40	-	63.4	2.74	0.0	21.0	66.8	12.2	-	-	45.0	22.7	22.3	CL	Lean CLAY w/ sand
	P3	2.00	2.35	3	21.5	2.72	0.0	85.6	12.3	2.1	4.0	2.2	NP	NP	NP	SM	Silty SAND
	P4	3.00	3.30	3	45.6	2.68	0.0	45.9	44.1	10.0	47.6	2.4	45.1	21.2	23.9	CL	Sandy CLAY
	P5	4.00	4.40	2	40.3	2.66	0.0	57.9	29.6	12.5	111.3	1.6	38.9	19.2	19.7	SC	Clayey SAND
	P6-1	5.00	5.35	2	54.2	2.73	0.0	8.7	64.3	27.0	-	-	48.7	22.7	26.0	CL	Lean CLAY
	P6-2	5.00	5.35	-	62.8	2.71	0.0	1.6	50.9	47.5	-	-	60.2	27.9	32.3	CH	Fat CLAY
	P7-1	6.00	6.30	28	53.4	2.69	0.0	14.2	65.8	20.0	-	-	51.4	22.0	29.4	CH	Fat CLAY
	P7-2	6.00	6.30	-	27.1	2.69	0.0	83.4	12.8	3.8	7.8	4.2	NP	NP	NP	SM	Silty SAND

Table A.5 Summary of soil properties for borehole A-5 (after PARI 2002)

BH	Sample No.	Depth (m)		SPT N-Values	w _n (%)	G _s	Soil Composition (%)				C _u	C _c	LL	PL	PI	USCS	Soil Description
		From	To				Gravel	Sand	Silt	Clay							
A-5	P1	0.00	0.20	-	16.9	2.67	40.9	57.5	1.6	0.0	42.1	0.1	NP	NP	NP	SW	Well-graded SAND w/ gravel
	P2	1.00	1.30	4	12.9	2.66	16.0	72.1	7.9	4.0	5.3	1.3	NP	NP	NP	SW-SM	Well-graded SAND w/ silt and gravel
	P3	2.00	2.40	1	23.3	2.69	3.7	86.8	6.7	2.8	2.1	1.2	NP	NP	NP	SW-SM	Well-graded SAND w/ silt
	P4	3.00	3.46	1	29.9	2.70	24.0	56.9	12.6	6.5	29.3	10.6	NP	NP	NP	SM	Silty SAND w/ gravel
	P5	4.00	4.45	0	70.6	2.65	0.0	12.3	70.7	17.0	-	-	52.0	24.9	27.1	CH	Fat CLAY
	P6	5.00	5.45	0	71.9	2.78	0.0	18.9	67.1	14.0	-	-	54.3	25.2	29.2	CH	Fat CLAY w/ sand
	P7	6.00	6.45	0	80.8	2.67	0.0	7.0	73.5	19.5	-	-	65.1	27.7	37.4	CH	Fat CLAY
	P8	7.00	7.35	1	61.5	2.66	0.0	8.6	69.4	22.0	-	-	47.8	22.6	25.2	CL	Lean CLAY
	P9	8.00	8.30	10	23.2	2.73	0.0	87.6	8.4	4.0	4.9	2.9	NP	NP	NP	SM	Silty SAND
	P10	9.00	9.30	41	24.4	2.73	16.5	67.8	10.9	4.8	30.2	7.1	NP	NP	NP	SM	Silty SAND w/ gravel
	P11	10.00	10.30	33	22.9	2.66	0.0	80.7	13.3	6.0	14.6	6.8	NP	NP	NP	SM	Silty SAND
	P12	11.00	11.30	44	19.2	2.74	3.3	77.6	12.1	7.0	37.3	12.1	NP	NP	NP	SM	Silty SAND

Note: w_n = Natural Water Content, G_s = Specific Gravity, C_u = Coefficient of Uniformity, C_c = Coefficient of Gradation, LL = Liquid Limit, PL = Plastic Limit, PI = Plastic Index, USCS = Unified Soil Classification System

Table A.6 Summary of Soil Properties for borehole B-1 (after PARI 2002)

BH	Sample No.	Depth (m)		SPT N-Values	w _n (%)	G _s	Soil Composition (%)				C _u	C _c	LL	PL	PI	USCS	Soil Description
		From	To				Gravel	Sand	Silt	Clay							
B-1	P1	0.00	0.20	-	30.6	2.70	8.4	73.0	10.6	8.0	43.2	18.3	NP	NP	NP	SM	Silty SAND
	P2	1.00	1.30	5	15.1	2.74	9.8	79.4	8.3	2.5	3.8	1.1	NP	NP	NP	SW-SM	Well-graded SAND w/ silt
	P3	2.00	2.30	3	26.8	2.73	1.2	81.8	12.5	4.5	9.5	4.6	NP	NP	NP	SM	Silty SAND
	P4	3.00	3.35	2	25.7	2.77	6.9	74.4	14.1	4.6	12.7	6.1	NP	NP	NP	SM	Silty SAND
	P5	4.00	4.40	1	56.0	2.66	0.0	29.0	57.9	13.1	-	-	46.6	24.6	22.0	CL	Lean CLAY w/ sand
	P6	5.00	5.45	1	71.3	2.68	0.0	21.8	65.0	13.2	-	-	57.5	23.9	33.6	CH	Fat CLAY w/ sand
	P7	6.00	6.45	1	65.4	2.68	3.9	21.9	64.0	10.2	34.9	4.1	57.5	23.3	34.3	CH	Fat CLAY w/ sand
	P8	7.00	7.30	12	29.6	2.70	3.7	74.0	15.3	7.0	24.7	11.1	NP	NP	NP	SM	Silty SAND

Table A.7 Summary of soil properties for borehole B-3 (after PARI 2002)

BH	Sample No.	Depth (m)		SPT N-Values	w_n (%)	G_s	Soil Composition (%)				C_u	C_c	LL	PL	PI	USCS	Soil Description
		From	To				Gravel	Sand	Silt	Clay							
B-3	P1	0.00	0.20	-	18.0	2.73	2.9	81.7	11.4	4.0	12.4	5.8	NP	NP	NP	SM	Silty SAND
	P2	1.00	1.30	5	25.5	2.70	4.1	77.9	13.0	5.0	10.2	4.9	NP	NP	NP	SM	Silty SAND
	P3	2.00	2.30	2	28.4	2.75	2.4	78.3	15.8	3.5	7.4	3.4	NP	NP	NP	SM	Silty SAND
	P4	3.00	3.45	1	28.6	2.71	0.0	77.2	18.8	4.0	13.0	6.3	NP	NP	NP	SM	Silty SAND
	P5	4.00	4.45	0	31.2	2.71	0.0	77.2	16.8	6.0	21.9	10.1	NP	NP	NP	SM	Silty SAND
	P6	5.00	5.45	1	49.8	2.71	0.0	44.8	38.2	17.0	-	-	39.6	19.4	20.1	CL	Sandy lean CLAY
	P7	6.00	6.30	2	76.5	2.70	0.0	3.6	78.4	18.0	-	-	66.5	29.9	36.6	CH	Fat CLAY
	P8	7.00	7.30	1	64.7	2.70	0.0	4.6	54.4	41.0	-	-	60.9	27.3	33.6	CH	Fat CLAY
	P9	8.00	8.30	21	25.4	2.72	0.0	82.4	13.4	4.2	9.2	4.7	NP	NP	NP	SM	Silty SAND

Note: w_n = Natural Water Content, G_s = Specific Gravity, C_u = Coefficient of Uniformity, C_c = Coefficient of Gradation, LL = Liquid Limit, PL = Plastic Limit, PI = Plastic Index, USCS = Unified Soil Classification System

Table A.8 Summary of soil properties for borehole B-4 (after PARI 2002)

BH	Sample No.	Depth (m)		SPT N-Values	w_n (%)	G_s	Soil Composition (%)				C_u	C_c	LL	PL	PI	USCS	Soil Description
		From	To				Gravel	Sand	Silt	Clay							
B-4	P1	0.00	0.20	-	20.0	2.69	8.0	74.1	13.9	4.0	13.4	5.5	NP	NP	NP	SM	Silty SAND
	P2	1.00	1.35	2	10.1	2.67	32.9	55.6	7.5	4.0	77.4	0.3	NP	NP	NP	SW-SM	Well-graded SAND w/ silt and gravel
	P3	2.00	2.30	2	49.7	2.70	0.0	46.7	45.3	8.0	29.5	1.5	NP	NP	NP	ML	Sandy SILT
	P4	3.00	3.45	1	43.3	2.70	17.6	51.9	20.0	10.5	109.3	16.7	NP	NP	NP	SM	Silty SAND w/ gravel
	P5	4.00	4.45	0	31.8	2.70	0.0	79.6	14.4	6.0	21.9	10.4	NP	NP	NP	SM	Silty SAND
	P6	5.00	5.30	1	53.8	2.69	0.0	41.8	40.2	18.0	-	-	46.7	22.1	24.6	CL	Sandy lean CLAY
	P7	6.00	6.30	1	54.9	2.70	0.0	31.9	52.1	16.0	-	-	46.0	21.5	24.5	CL	Sandy lean CLAY
	P8-1	7.00	7.20	1	69.0	2.72	0.0	1.2	50.8	48.0	-	-	66.0	30.0	36.1	CH	Fat CLAY
	P8-2	7.20	7.45	-	32.8	2.74	0.0	77.1	16.9	6.0	12.7	6.3	NP	NP	NP	SM	Silty SAND
P9	11.00	11.30	44	21.3	2.72	0.0	76.6	16.9	6.5	16.7	8.1	NP	NP	NP	SM	Silty SAND	

Table A.9 Summary of soil properties for borehole C-1 (after PARI 2002)

BH	Sample No.	Depth (m)		SPT N-Values	w_n (%)	G_s	Soil Composition (%)				C_u	C_c	LL	PL	PI	USCS	Soil Description
		From	To				Gravel	Sand	Silt	Clay							
C-1	P1	0.00	0.20	-	20.9	2.68	10.7	79.9	6.9	2.5	2.2	1.1	NP	NP	NP	SW-SM	Well-graded SAND w/ silt
	P2	1.00	1.30	8	20.9	2.68	16.0	71.5	8.5	4.0	6.6	2.2	NP	NP	NP	SM	Silty SAND w/ gravel
	P3	2.00	2.30	0	75.8	2.75	0.0	24.5	56.5	19.0	-	-	61.2	27.8	33.4	CH	Fat CLAY w/ sand
	P4	3.00	3.45	0	84.4	2.68	0.0	4.4	67.6	28.0	-	-	78.8	28.8	50.0	CH	Fat CLAY
	P5	4.00	4.45	0	78.5	2.67	0.0	7.6	62.4	30.0	-	-	66.3	26.5	39.9	CH	Fat CLAY
	P6	5.00	5.45	1	82.7	2.67	0.0	6.4	65.6	28.0	-	-	71.7	30.1	41.6	CH	Fat CLAY
	P7	6.00	6.45	0	83.9	2.72	0.0	11.9	58.1	30.0	-	-	68.2	26.2	42.0	CH	Fat CLAY
	P8	7.00	7.10	13	44.7	2.67	0.0	76.5	17.7	5.8	22.5	8.3	NP	NP	NP	SM	Silty SAND

Note: w_n = Natural Water Content, G_s = Specific Gravity, C_u = Coefficient of Uniformity, C_c = Coefficient of Gradation, LL = Liquid Limit, PL = Plastic Limit, PI = Plastic Index, USCS = Unified Soil Classification System

Table A.10 Summary of soil properties for borehole D-1 (after PARI 2002)

BH	Sample No.	Depth (m)		SPT N-Values	w_n (%)	G_s	Soil Composition (%)				C_u	C_c	LL	PL	PI	USCS	Soil Description
		From	To				Gravel	Sand	Silt	Clay							
D-1	P1	0.00	0.20	-	14.8	2.72	31.6	61.7	4.7	2.0	23.7	0.1	NP	NP	NP	SW-SM	Well-graded SAND w/ silt and gravel
	P2	1.00	1.30	3	15.3	2.69	9.3	78.7	7.5	4.5	19.6	0.7	NP	NP	NP	SM	Silty SAND
	P3-1	2.00	2.35	1	20.0	2.65	12.6	74.4	10.0	3.0	32.7	0.9	NP	NP	NP	SM	Silty SAND
	P3-2	2.00	2.35	-	69.9	2.64	0.0	8.4	75.6	16.0	-	-	NP	NP	NP	ML	SILT
	P4	3.00	3.45	1	27.9	2.68	0.0	76.1	16.9	7.0	41.0	18.7	NP	NP	NP	SM	Silty SAND
	P5	4.00	4.40	2	31.1	2.76	0.0	79.5	15.5	5.0	18.1	8.6	NP	NP	NP	SM	Silty SAND
	P6	5.00	5.40	2	24.2	2.68	19.6	64.4	11.0	5.0	16.9	6.8	NP	NP	NP	SM	Silty SAND w/ gravel
	P7	6.00	6.30	2	30.4	2.68	2.7	66.5	17.8	13.0	-	-	29.7	20.0	9.7	SC	Clayey SAND
P8	7.00	7.10	34	37.1	2.65	0.0	57.3	36.7	6.0	25.2	4.8	NP	NP	NP	SM	Silty SAND	

Note: w_n = Natural Water Content, G_s = Specific Gravity, C_u = Coefficient of Uniformity, C_c = Coefficient of Gradation, LL = Liquid Limit, PL = Plastic Limit, PI = Plastic Index, USCS = Unified Soil Classification System

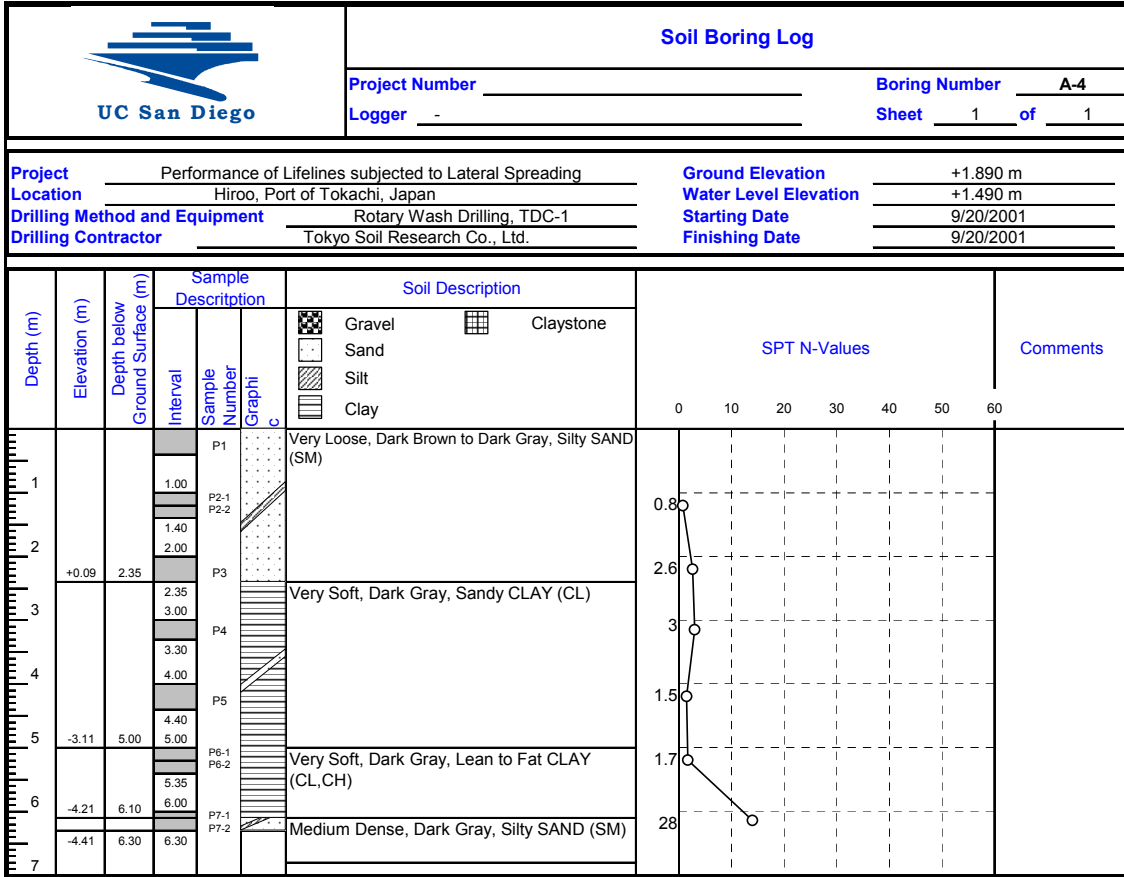


Fig. A.1 Boring log of borehole A-4 (after PARI 2002)

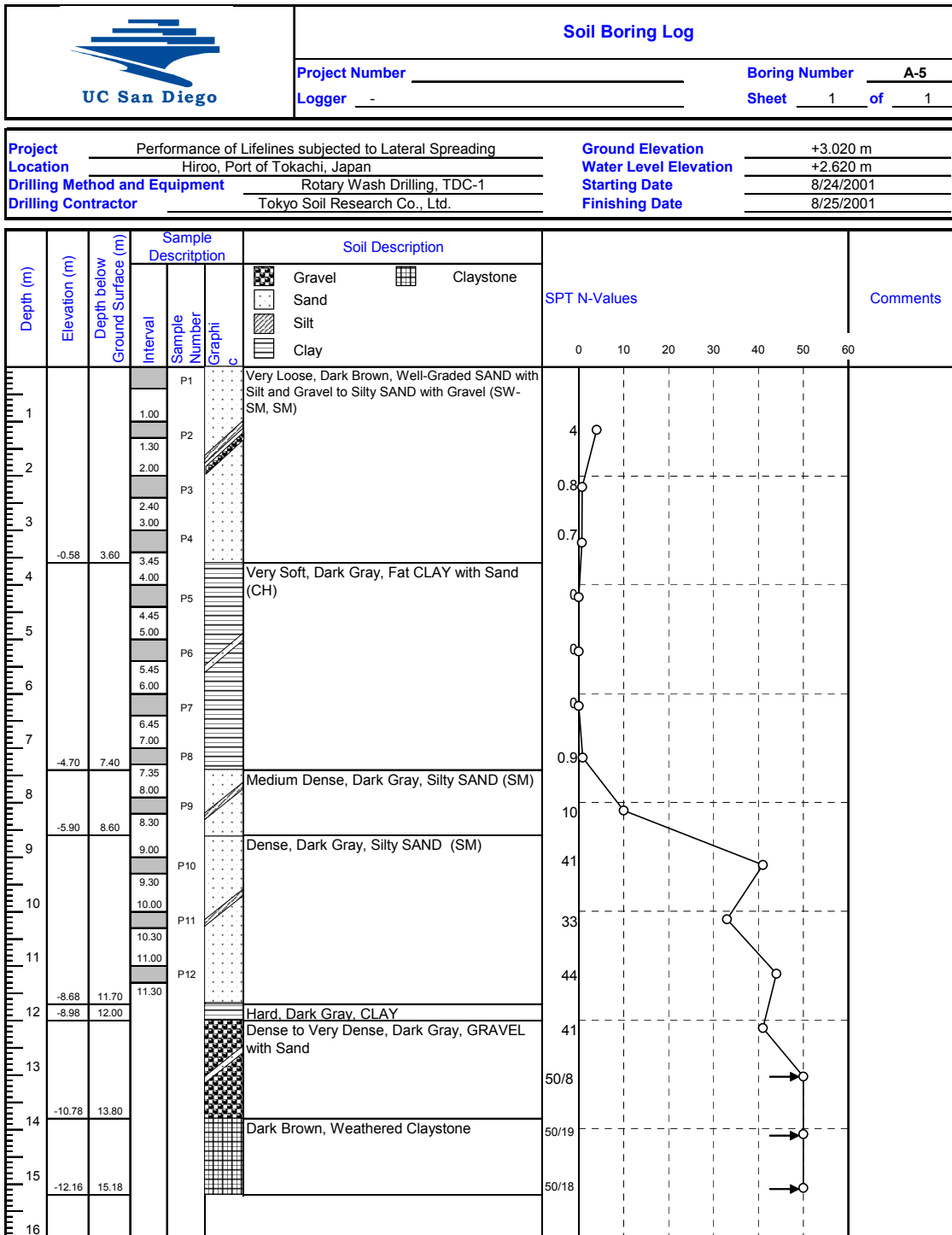


Fig. A.2 Boring log of borehole A-5 (after PARI 2002)

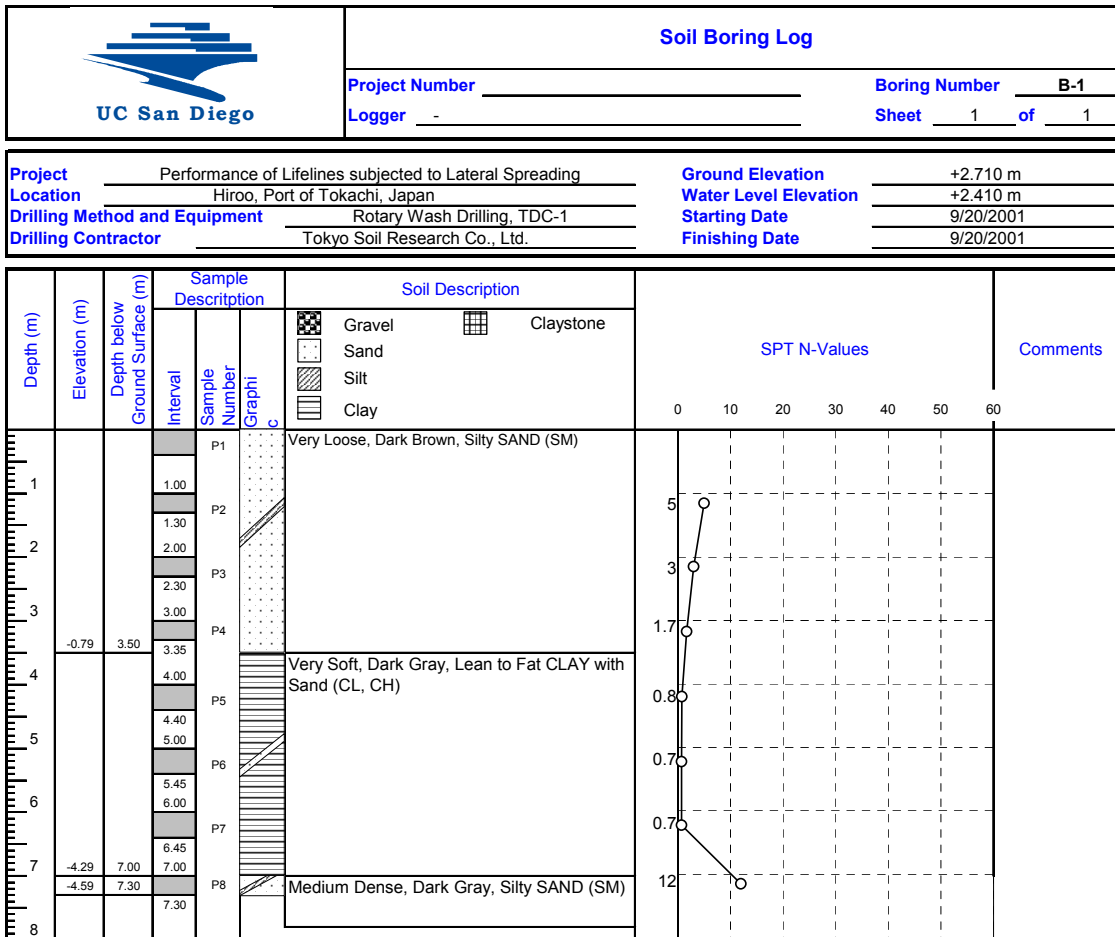


Fig. A.3 Boring log of borehole B-1 (after PARI 2002)

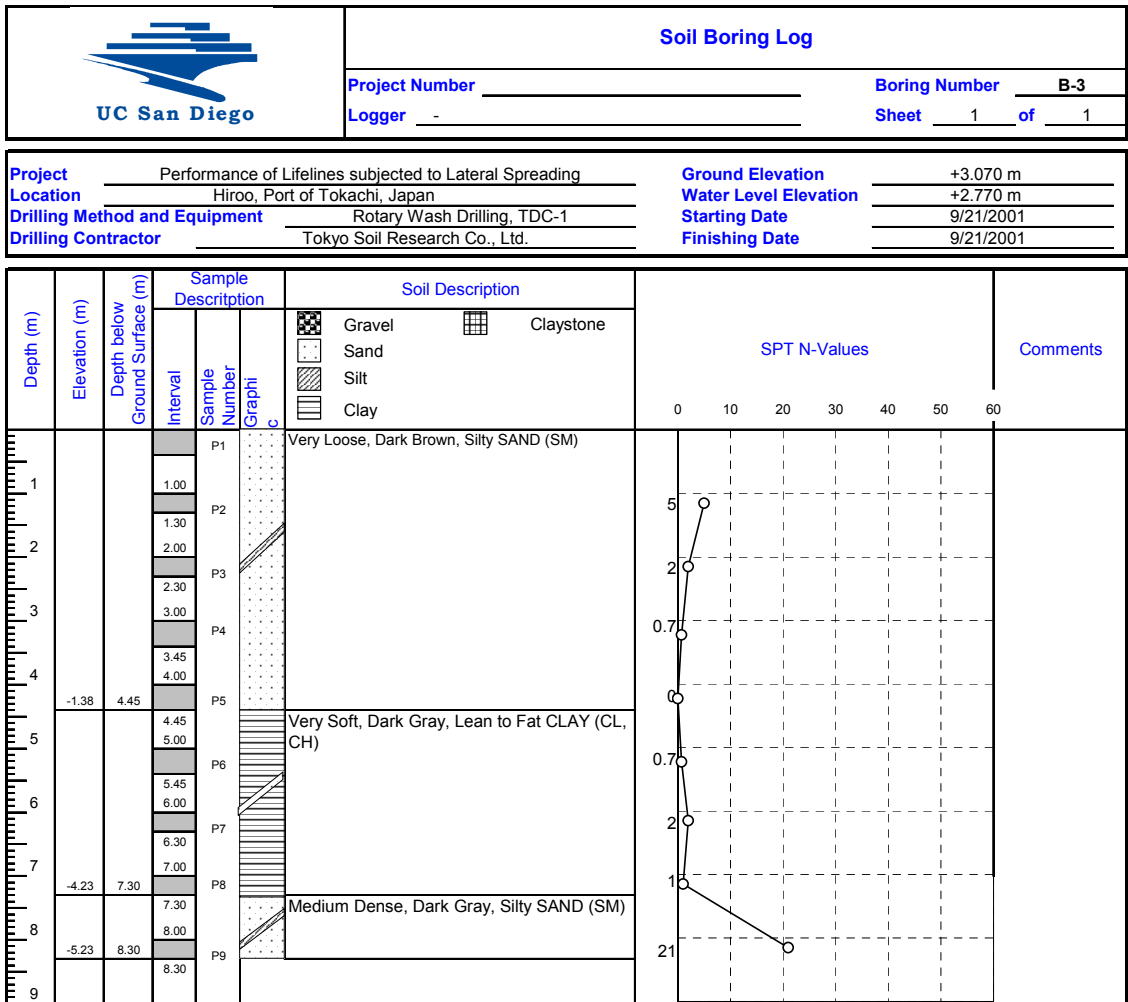


Fig. A.4 Boring log of borehole B-3 (after PARI 2002)

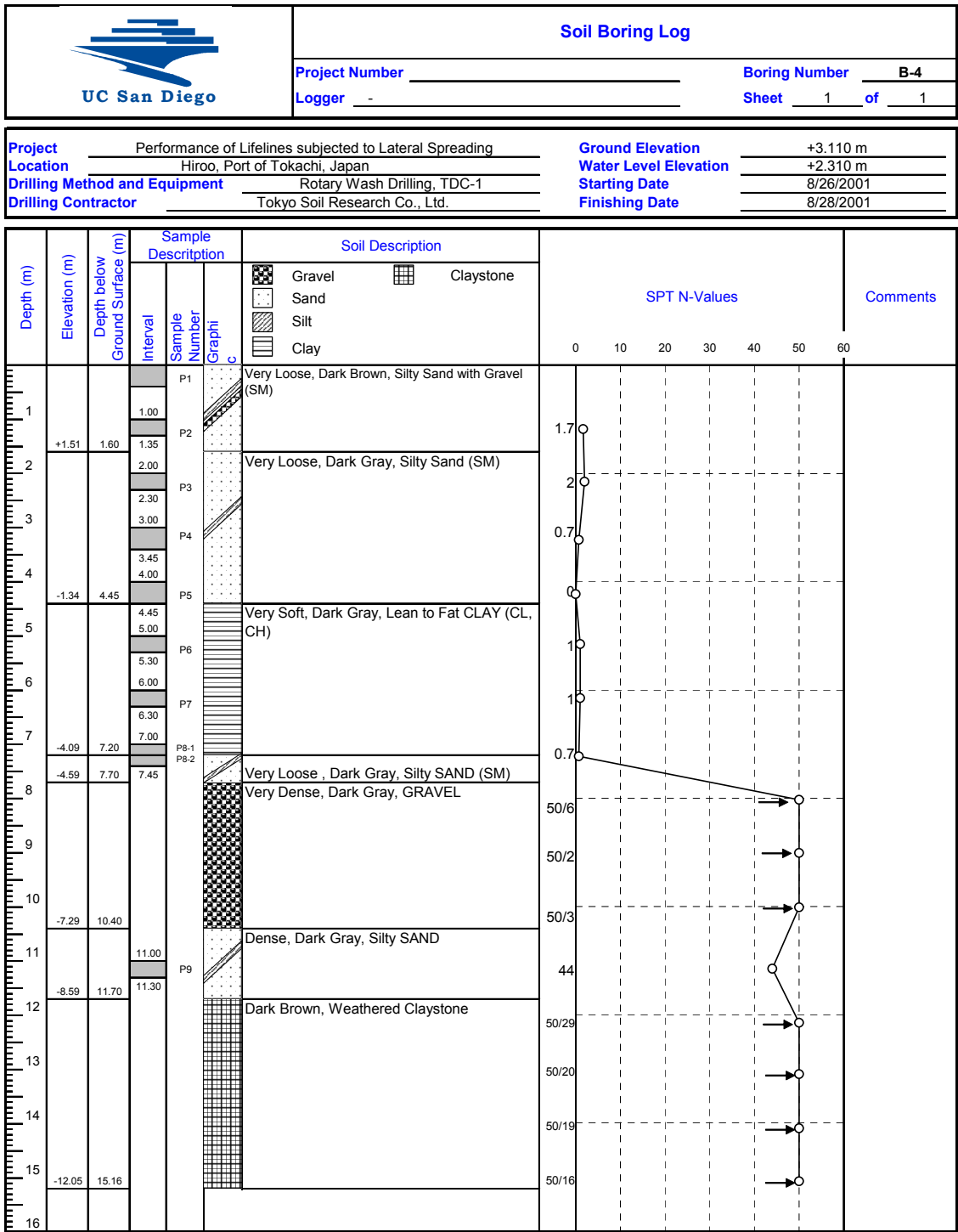


Fig. A.5 Boring log of borehole B-4 (after PARI 2002)

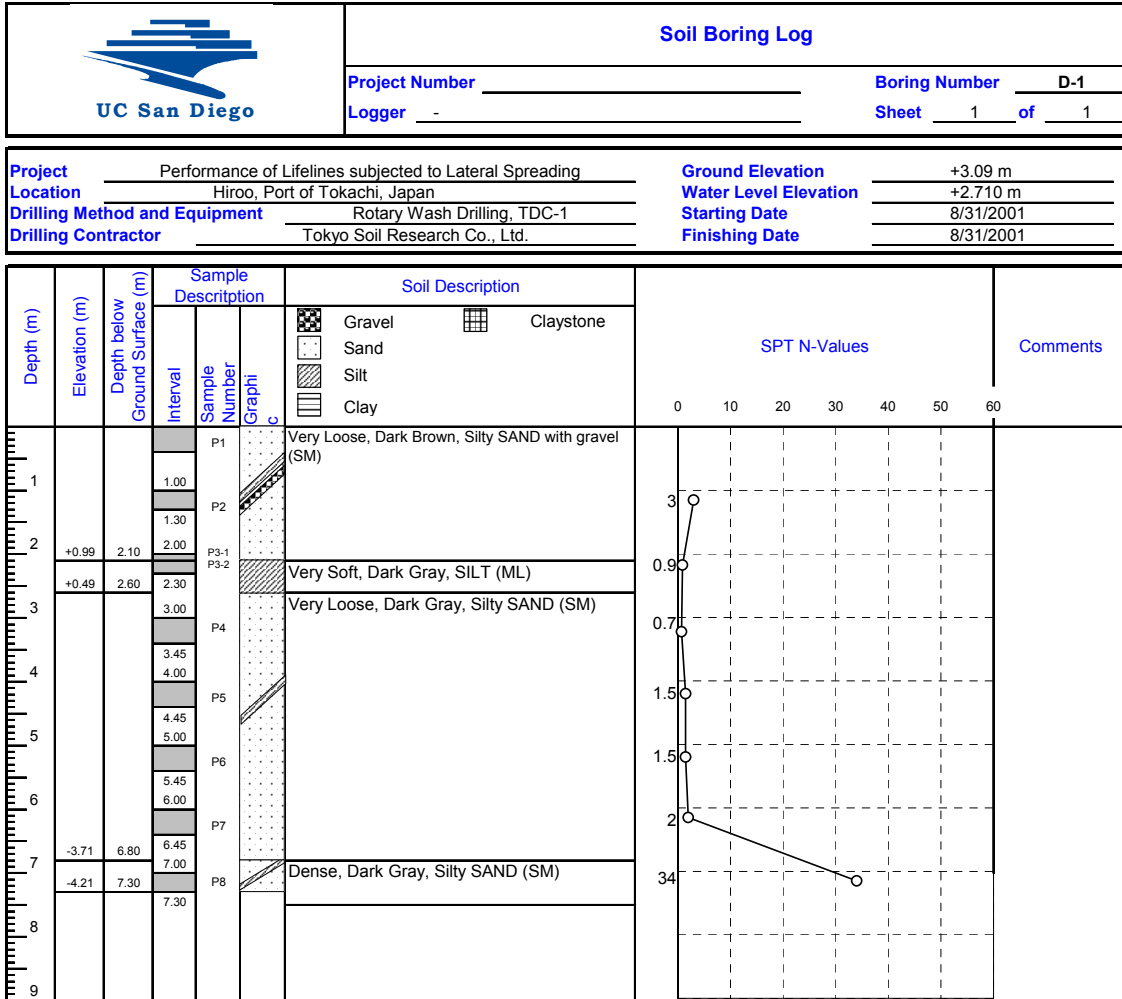


Fig. A.7 Boring log of borehole D-1 (after PARI 2002)

Appendix B: Swedish Weight Sounding Test Results

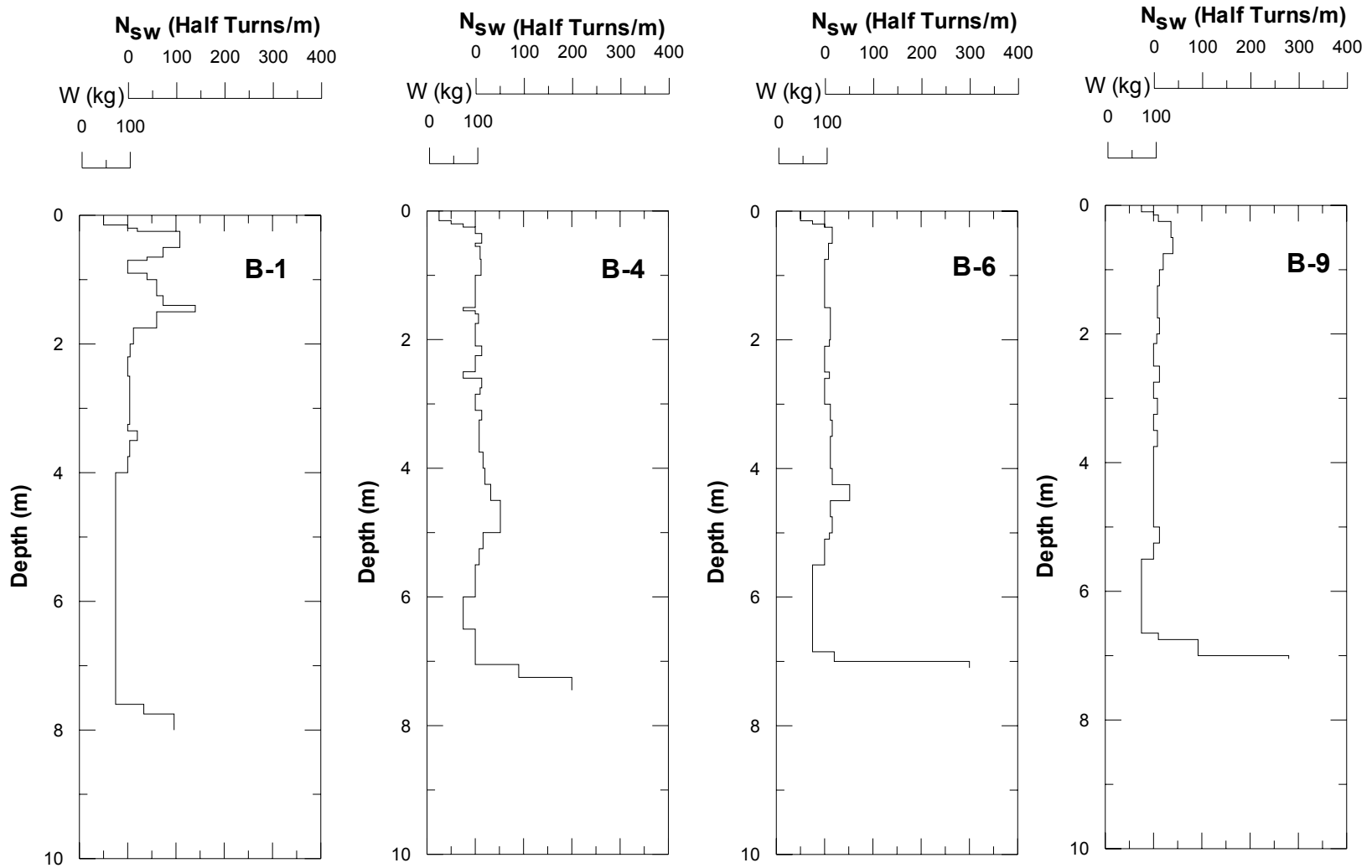


Fig. B.1 Results of Swedish weight sounding tests for B-1, B-4, B-6, and B-9 (after PARI 2002)

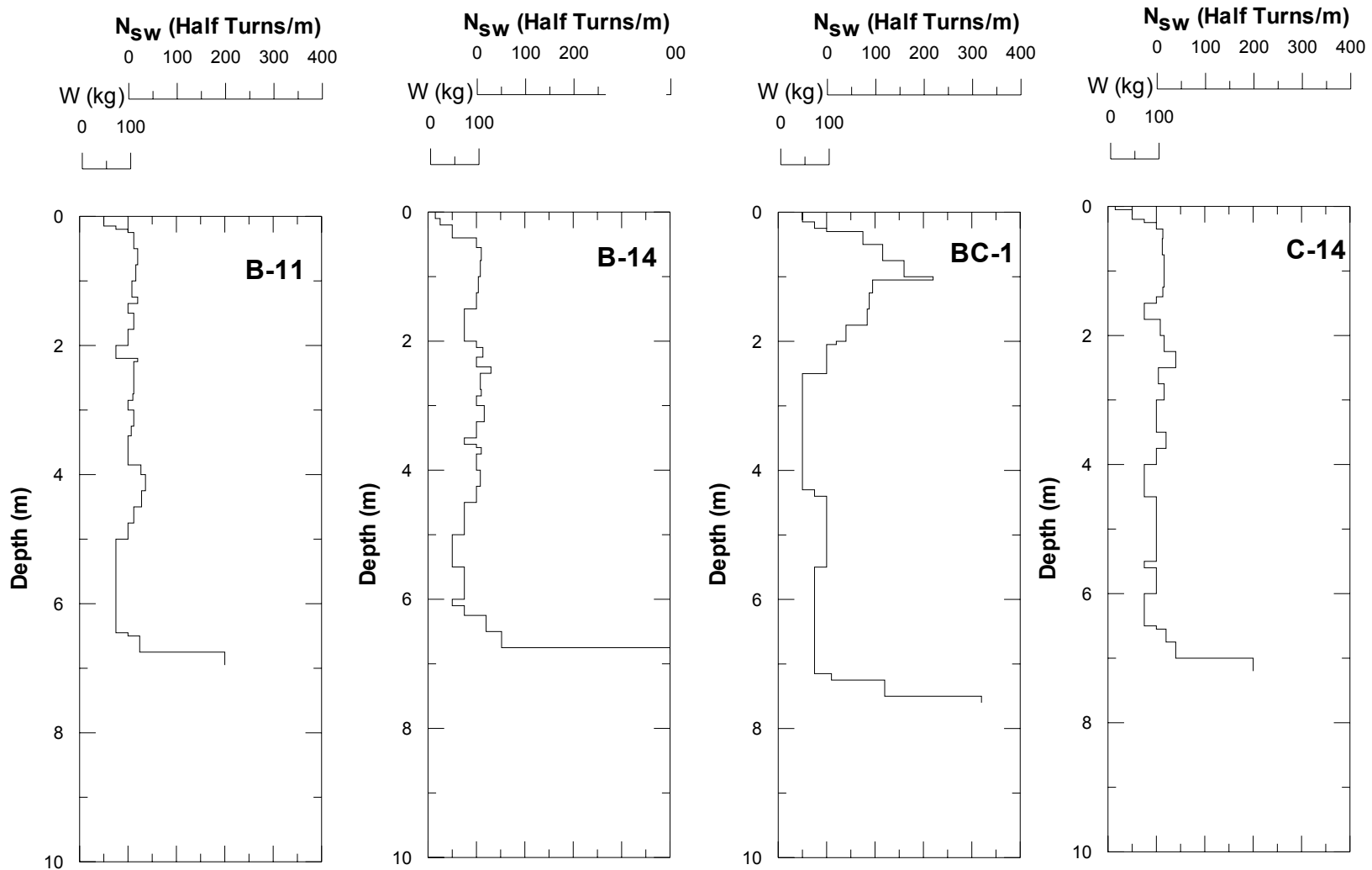


Fig. B.2 Results of Swedish weight sounding tests for B-11, B-14, BC-1, and C-14 (after PARI 2002)

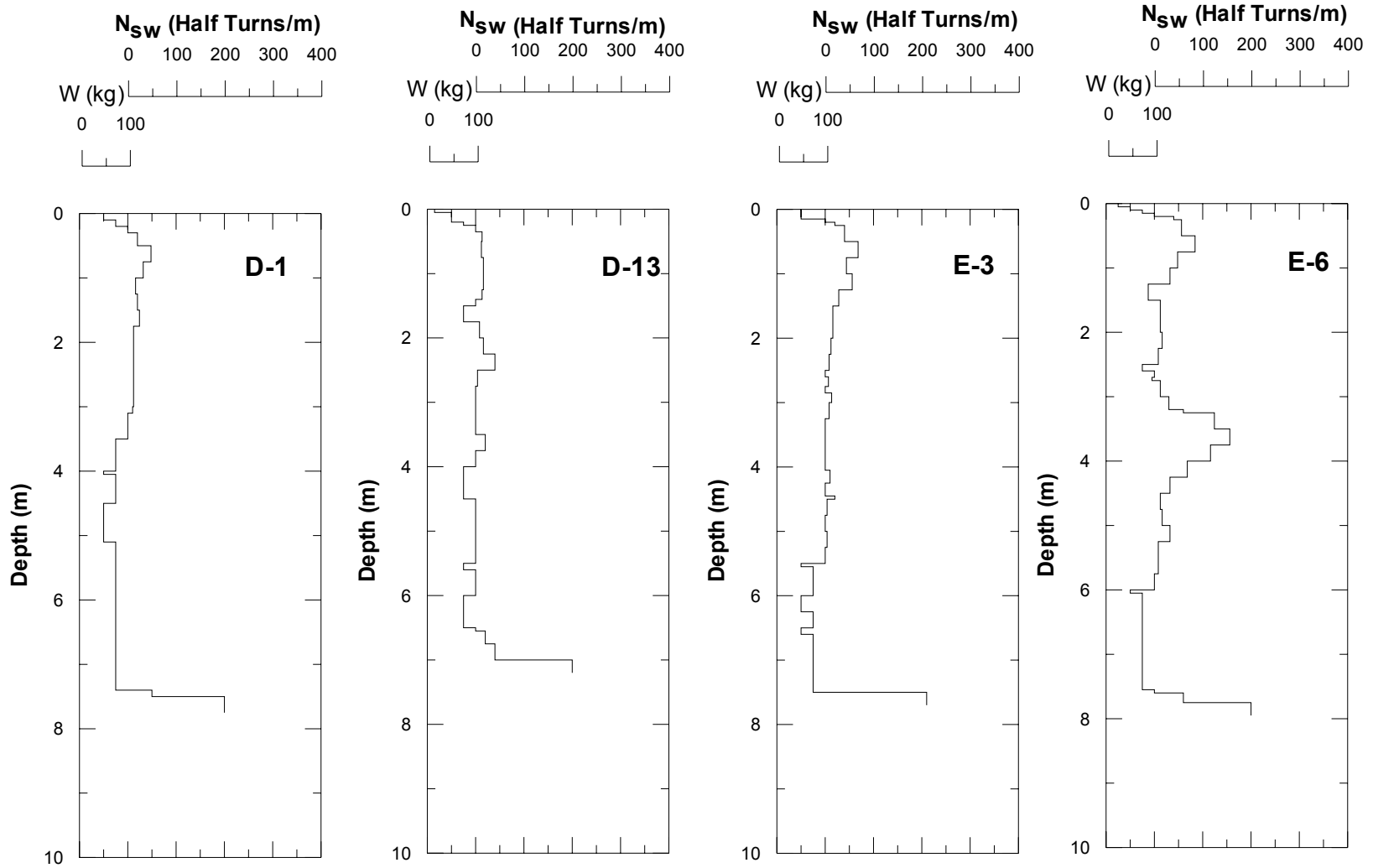


Fig. B.3 Results of Swedish weight sounding tests for D-1, D-13, E-3, and E-6 (after PARI 2002)

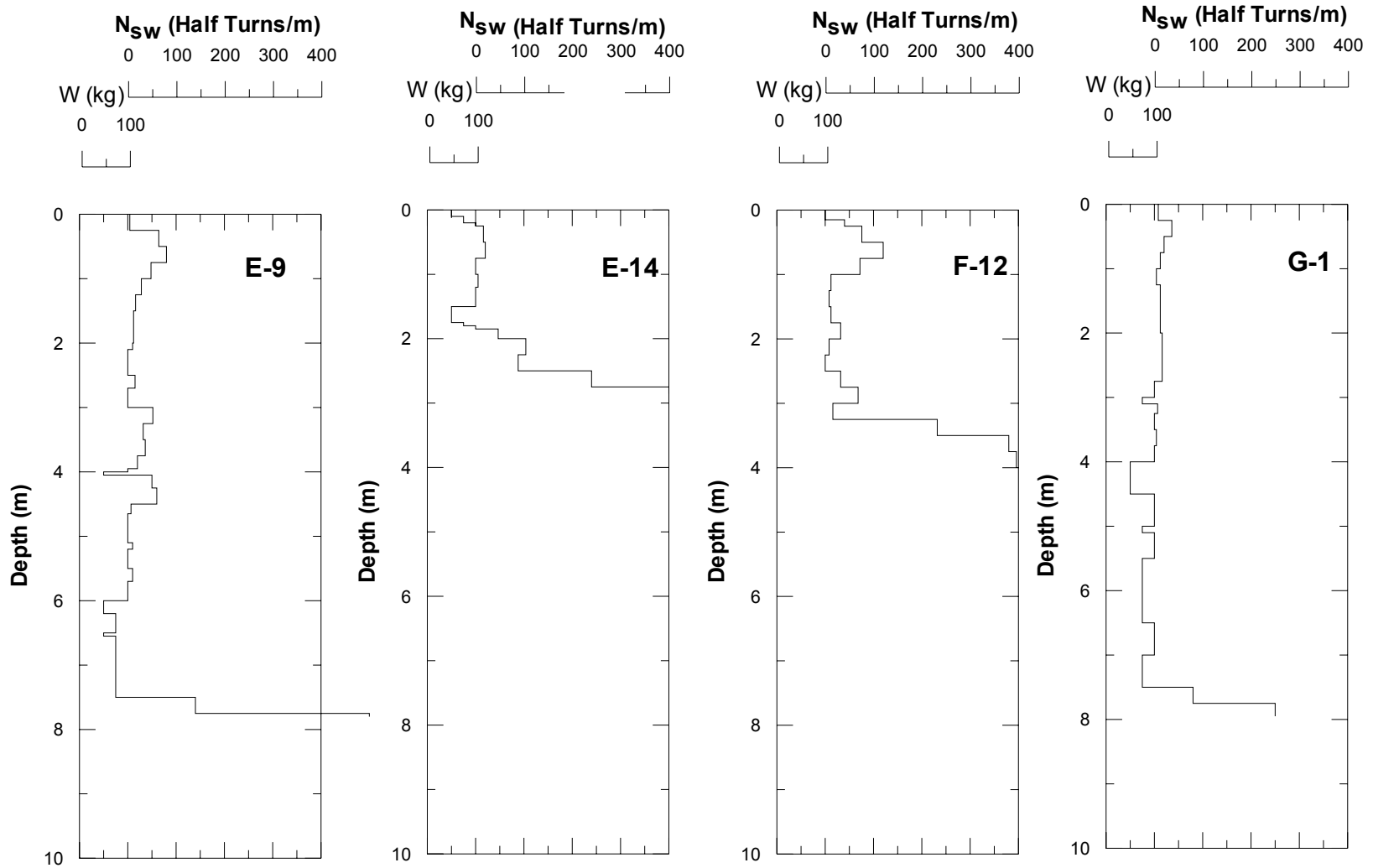


Fig. B.4 Results of Swedish weight sounding tests for E-9, E-14, F-12, and G-1 (after PARI 2002)

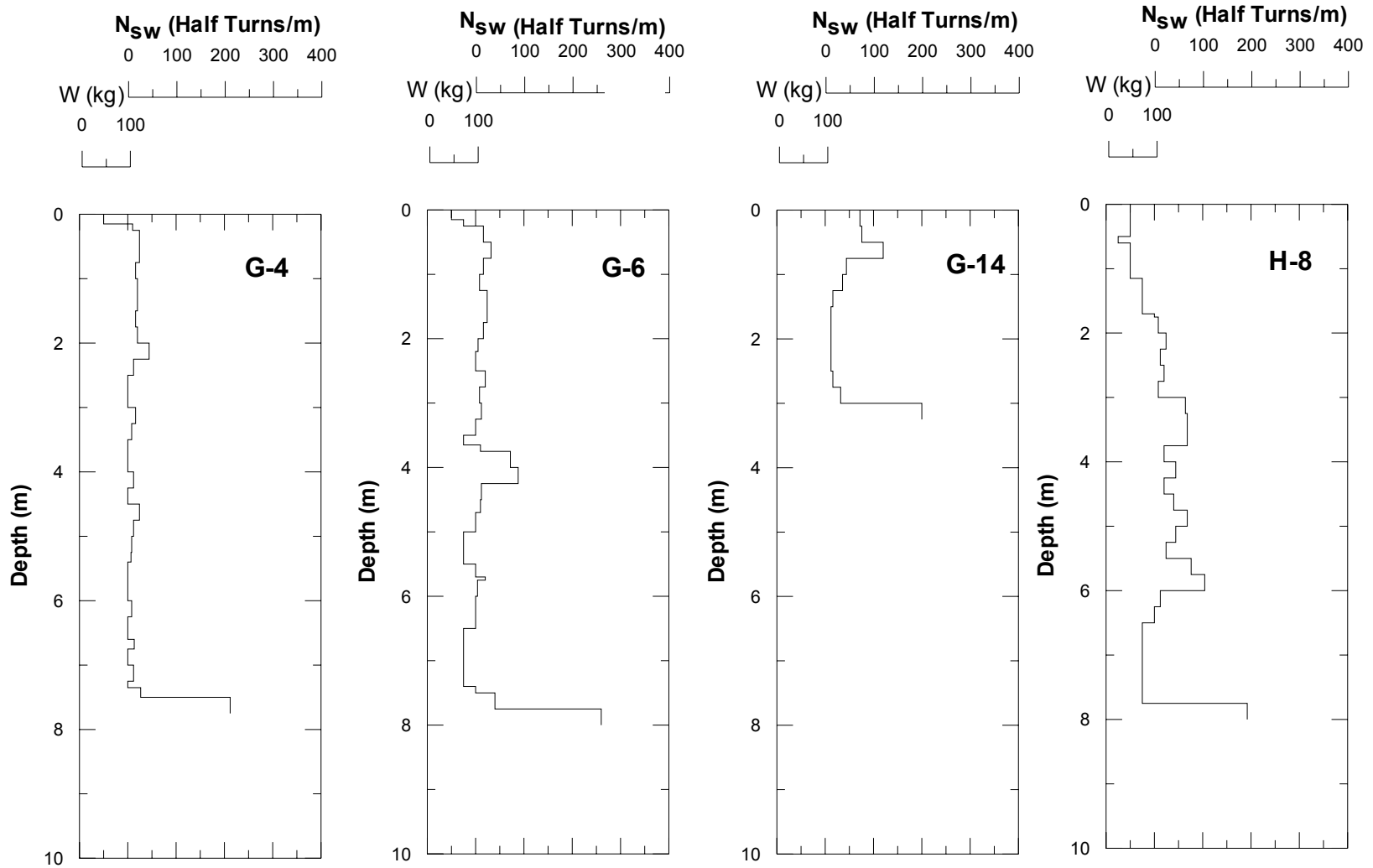


Fig. B.5 Results of Swedish weight sounding tests for G-4, G-6, G-14, and H-8 (after PARI 2002)

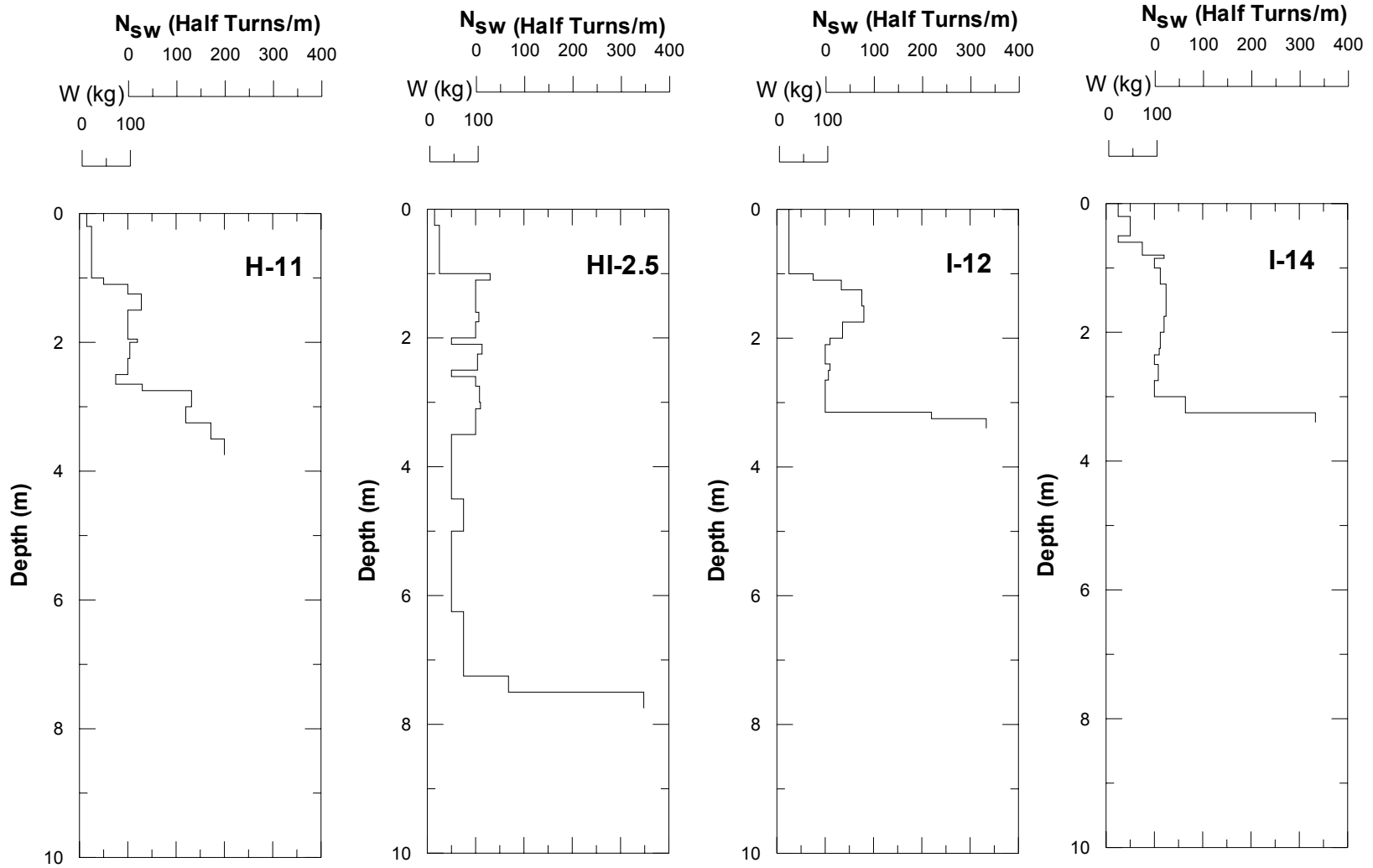


Fig. B.6 -Results of Swedish weight sounding tests for H-11, HI-2.5, I-12, and I-14 (after PARI 2002)

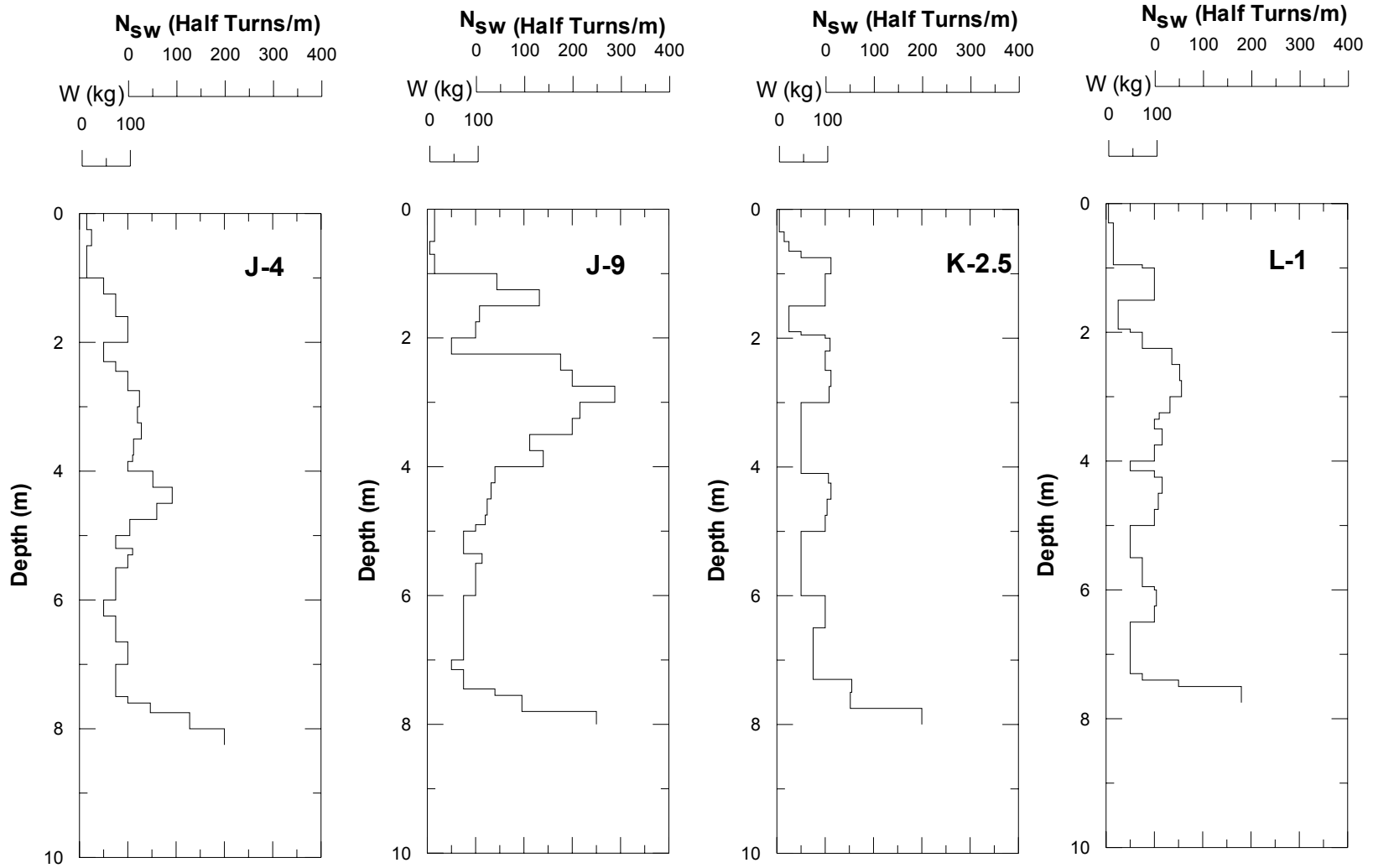


Fig. B.7 Results of Swedish weight sounding tests for J-4, J-9, K-2.5, and I-14 (after PARI 2002)

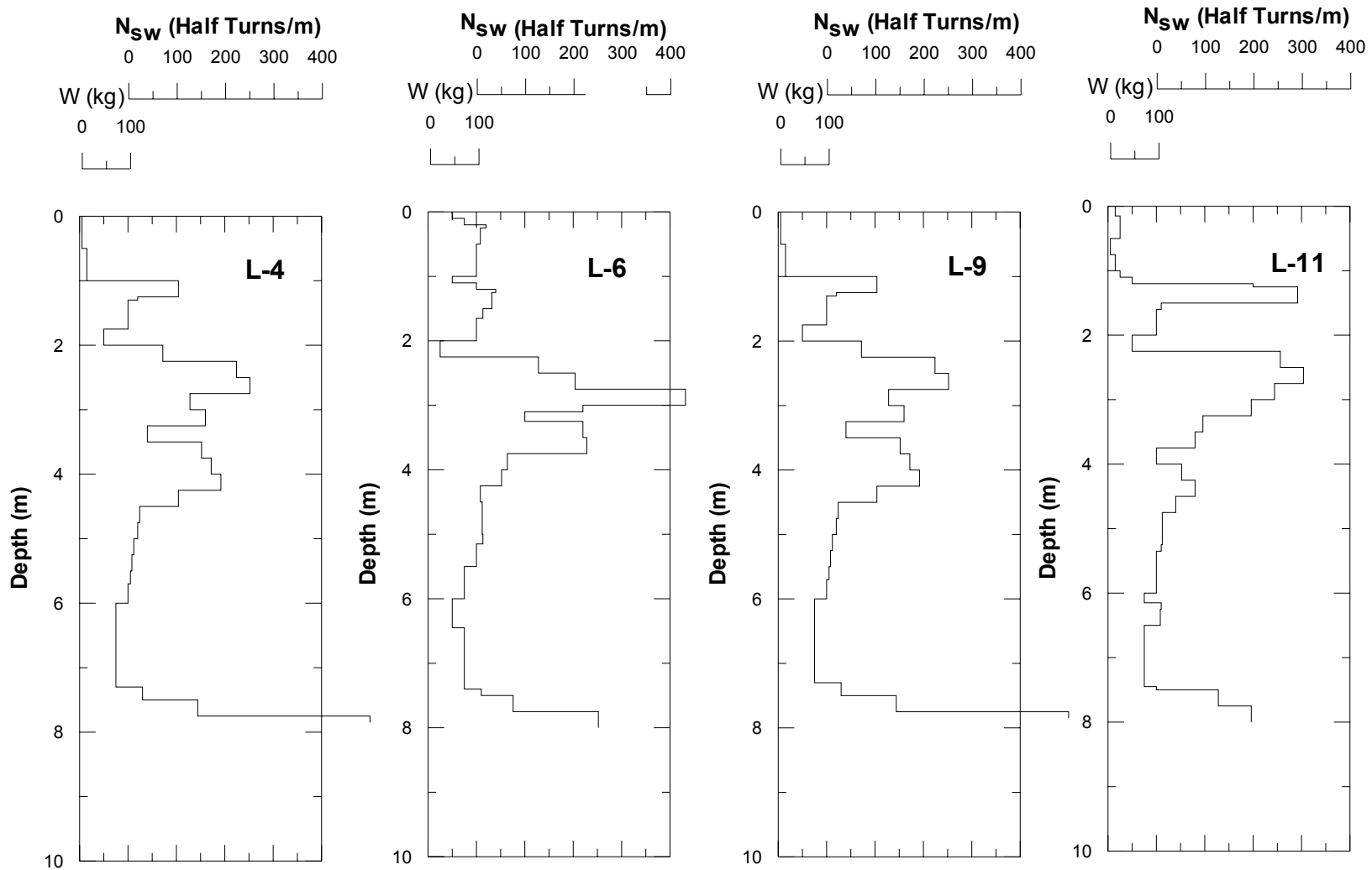


Fig. B.8 Results of Swedish weight sounding tests for L-4, L-6, L-9, and L-11 (after PARI 2002)

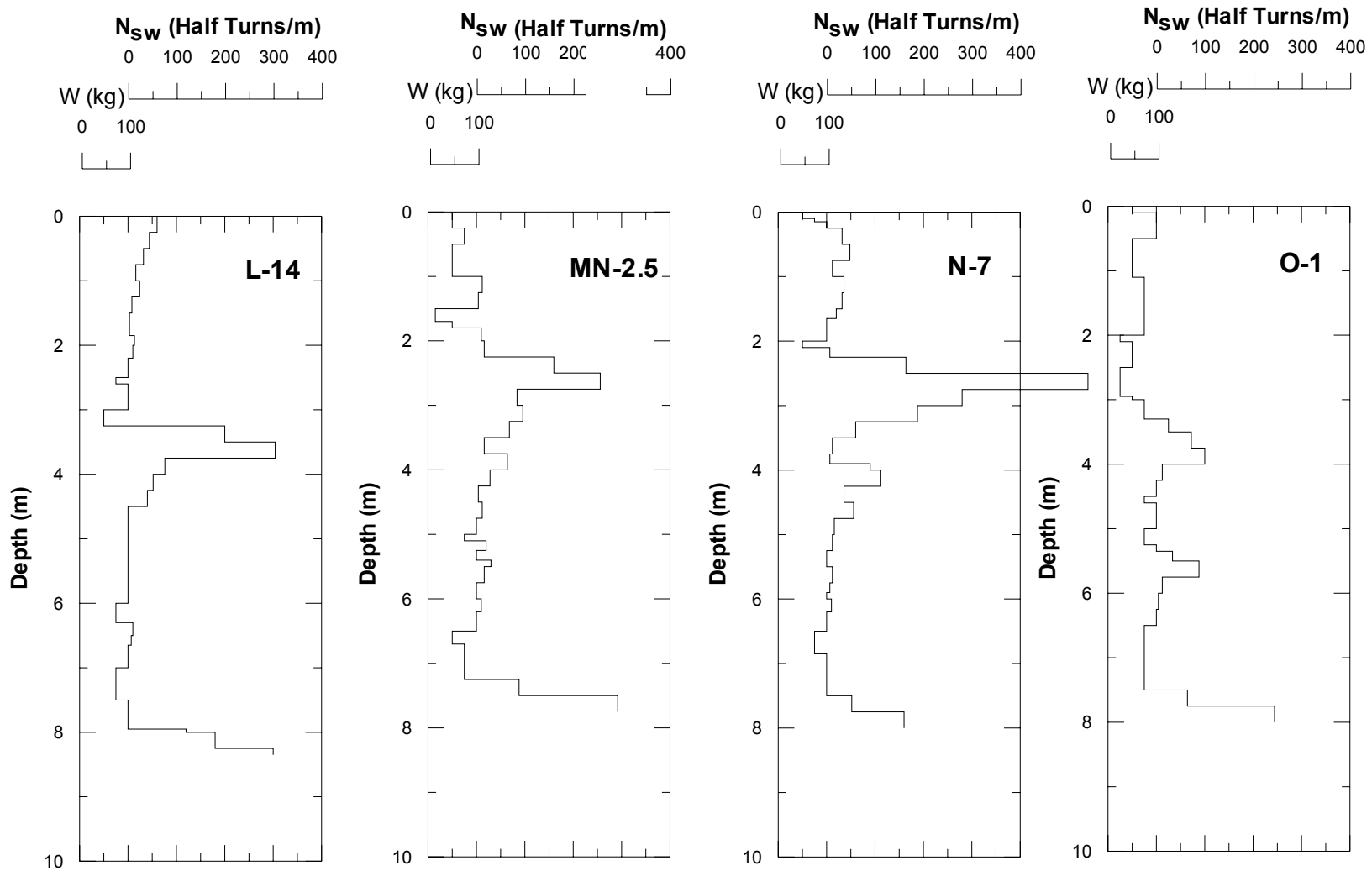


Fig. B.9 Results of Swedish weight sounding tests for L-14, MN-2.5, N-7, and O-1 (after PARI 2002)

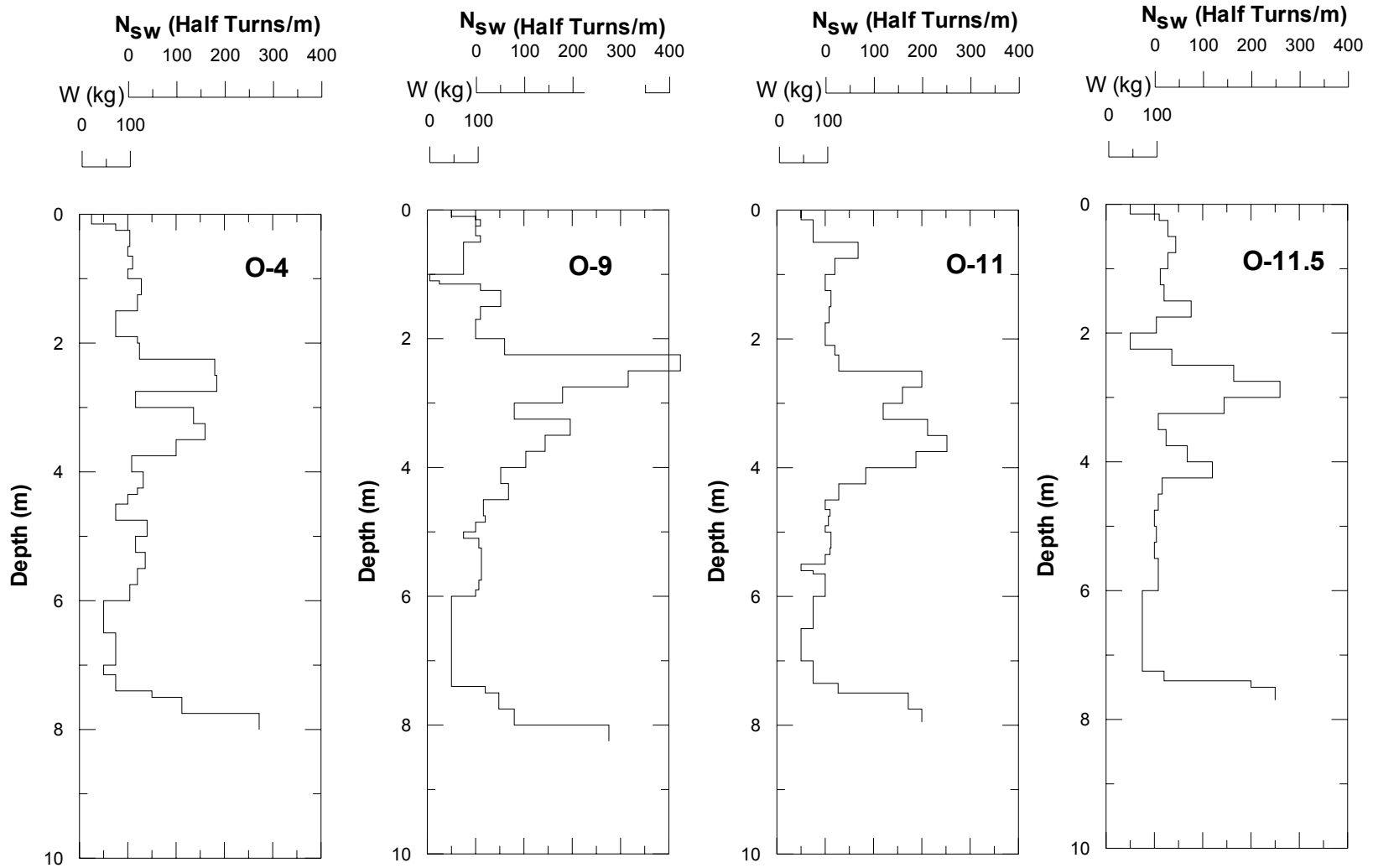


Fig. B.10 Results of Swedish weight sounding tests for O-4, O-9, O-11, and O-11.5 (after PARI 2002)

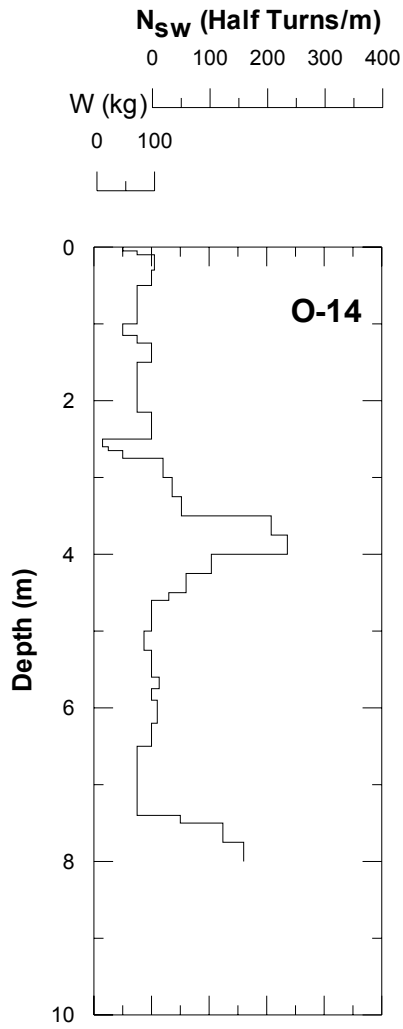


Fig. B.11 Results of Swedish weight sounding tests for O-14 (after PARI 2002)

Appendix C: Sieve Analysis Results

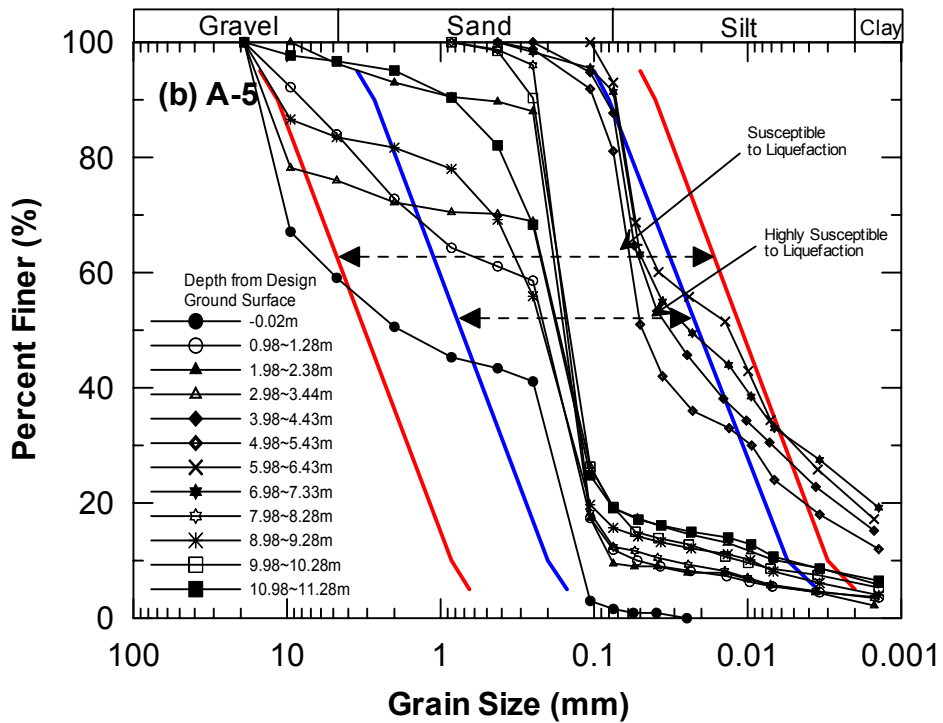
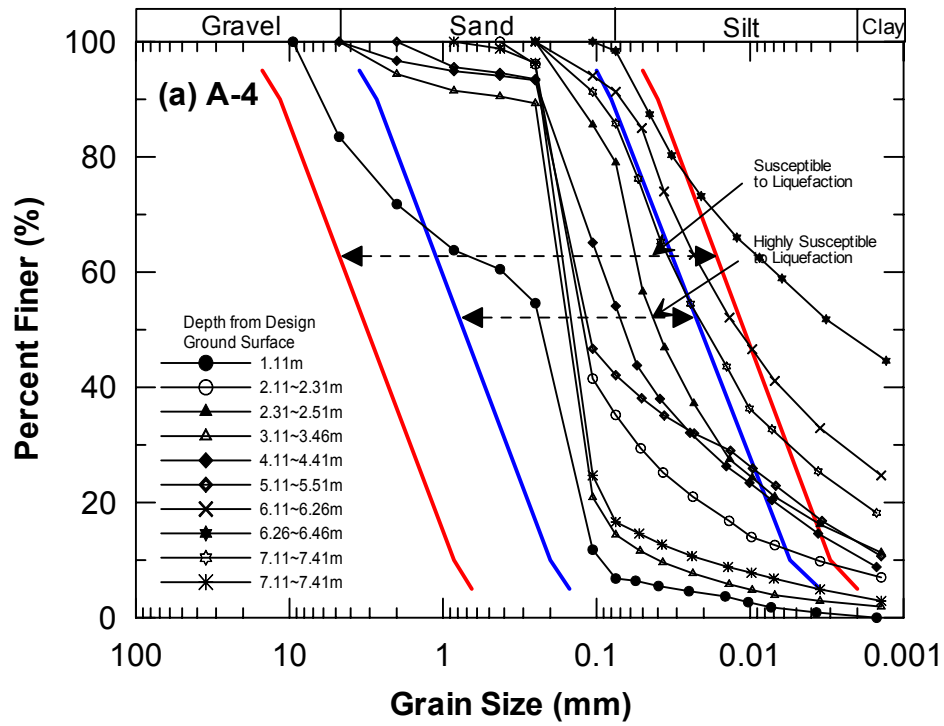


Fig. C.1 Grain-size distribution for boreholes (a) A-4 and (b) A-5 (after PARI 2002)

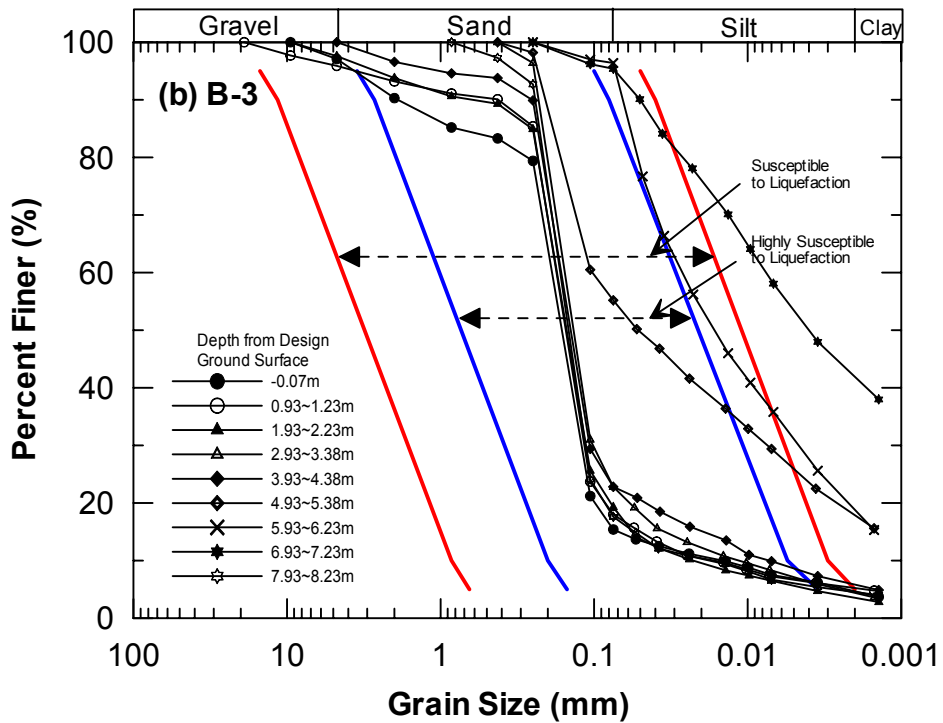
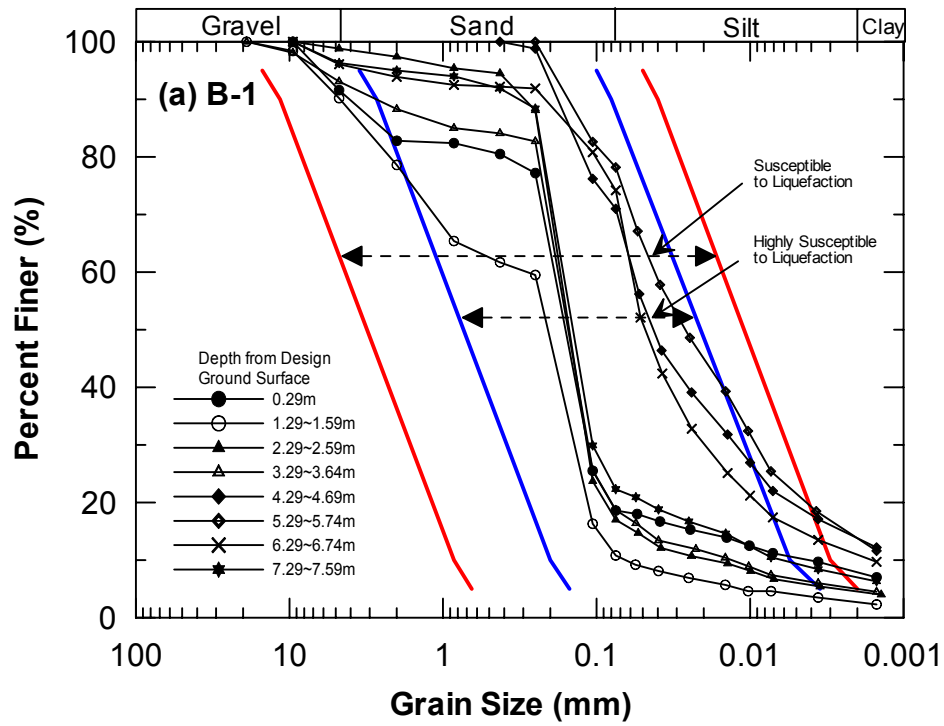


Fig. C.2 Grain-size distribution for boreholes (a) B-1 and (b) B-3 (after PARI 2002)

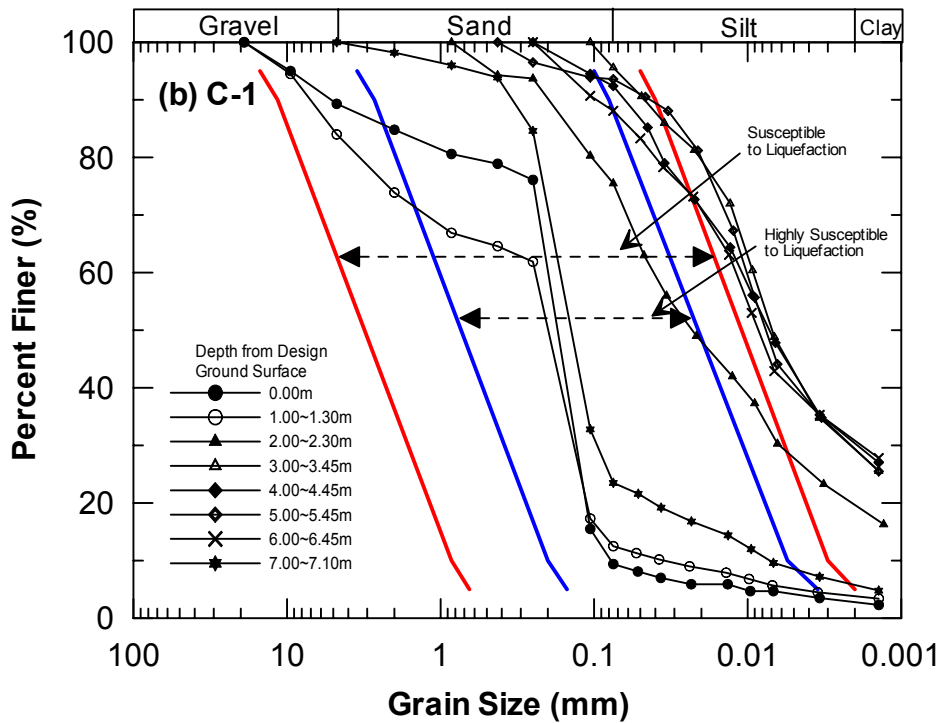
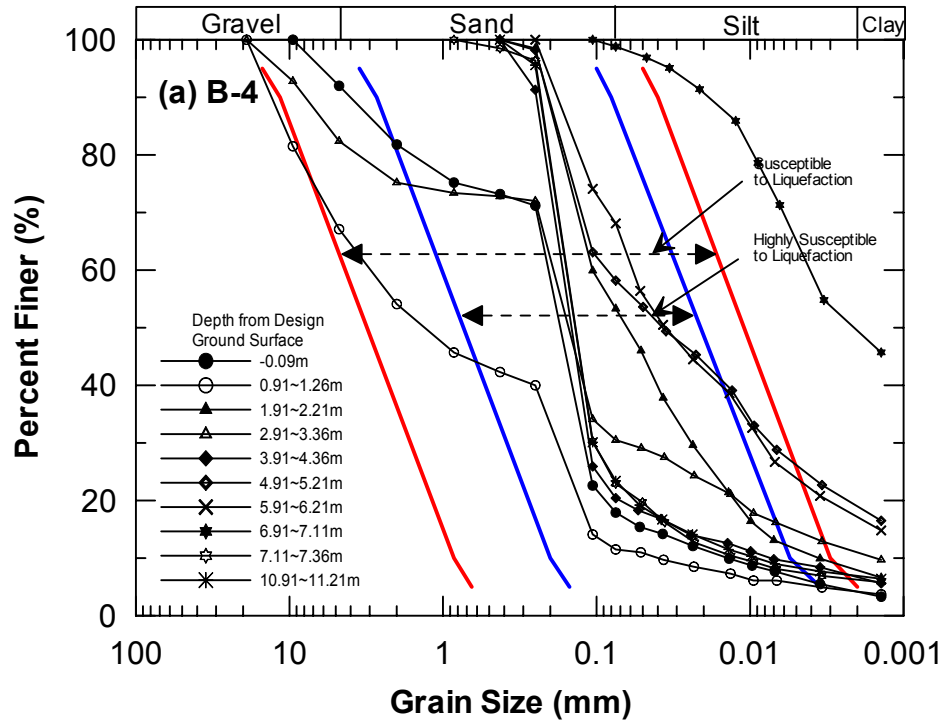


Fig. C.3 Grain-size distribution for boreholes (a) B-4 and (b) C-1 (after PARI 2002)

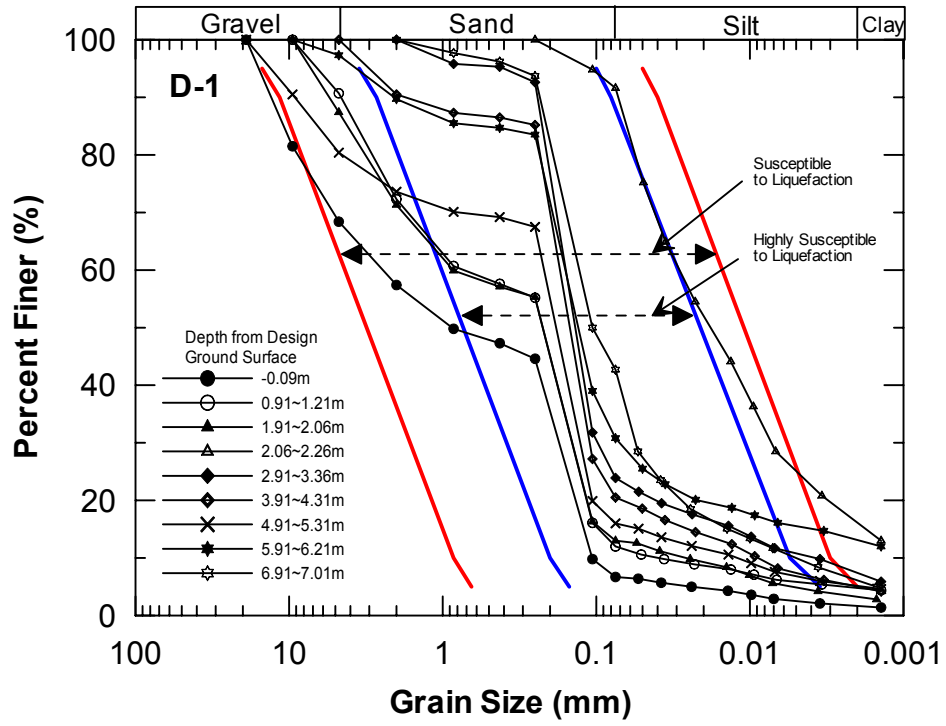


Fig. C.4 Grain-size distribution for borehole D-1 (after PARI 2002)

**Appendix D: Excess Pore-Water Pressure Data
(First Test)**

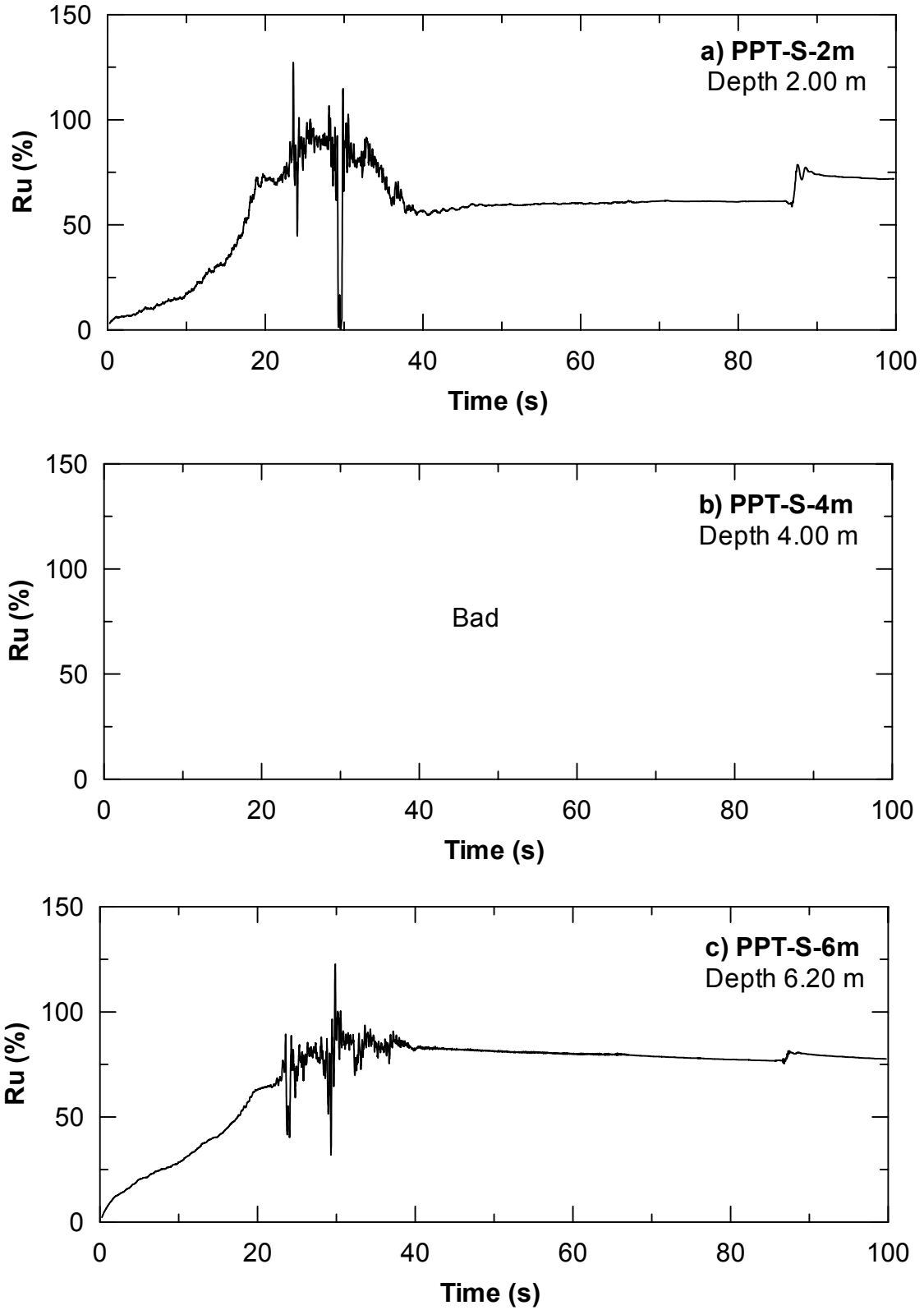


Fig. D.1 Excess pore-water pressure ratio time histories nearby single pile: (a) PPT-S-2m, (b) PPT-S-4m, and (c) PPT-S-6m

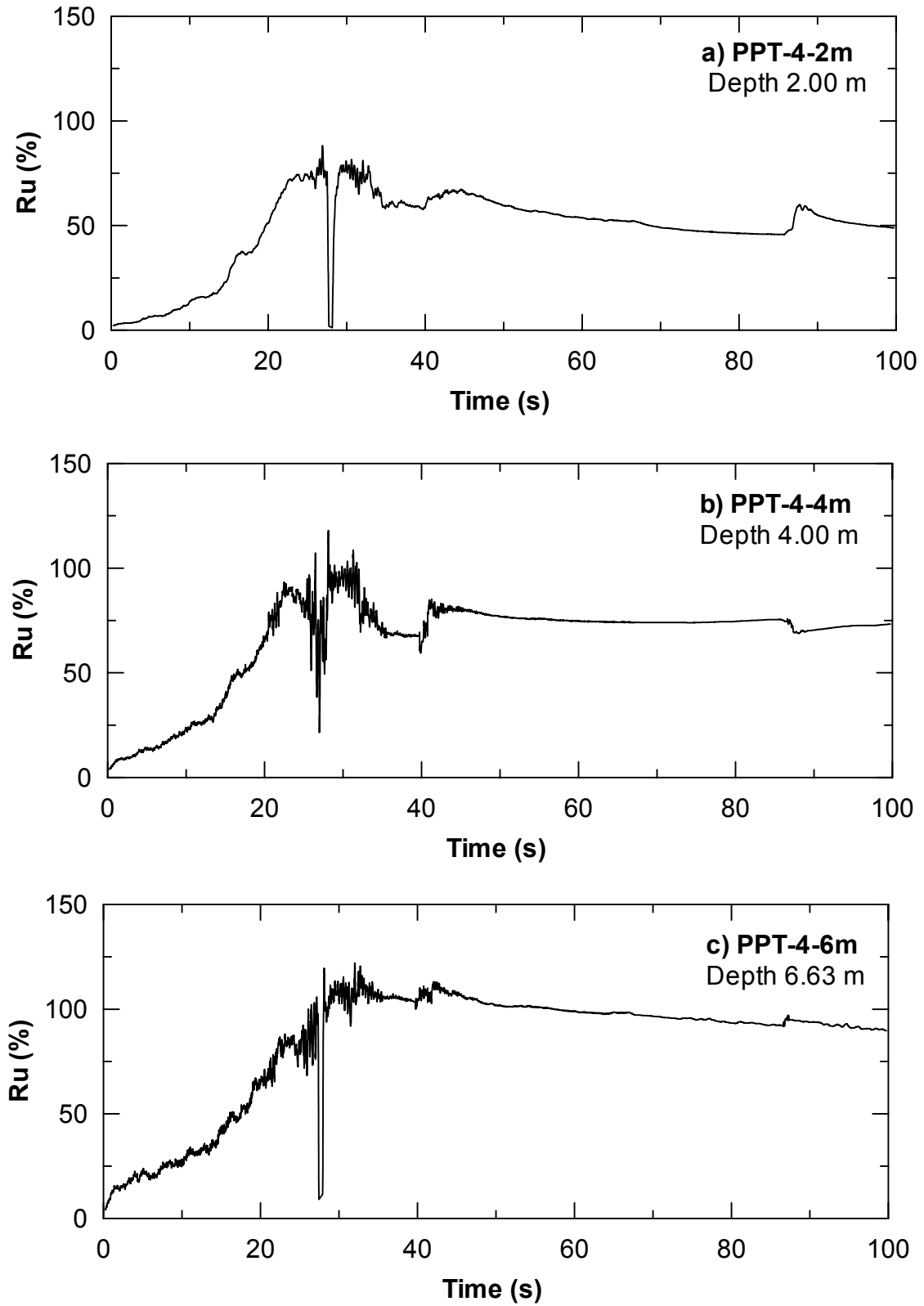
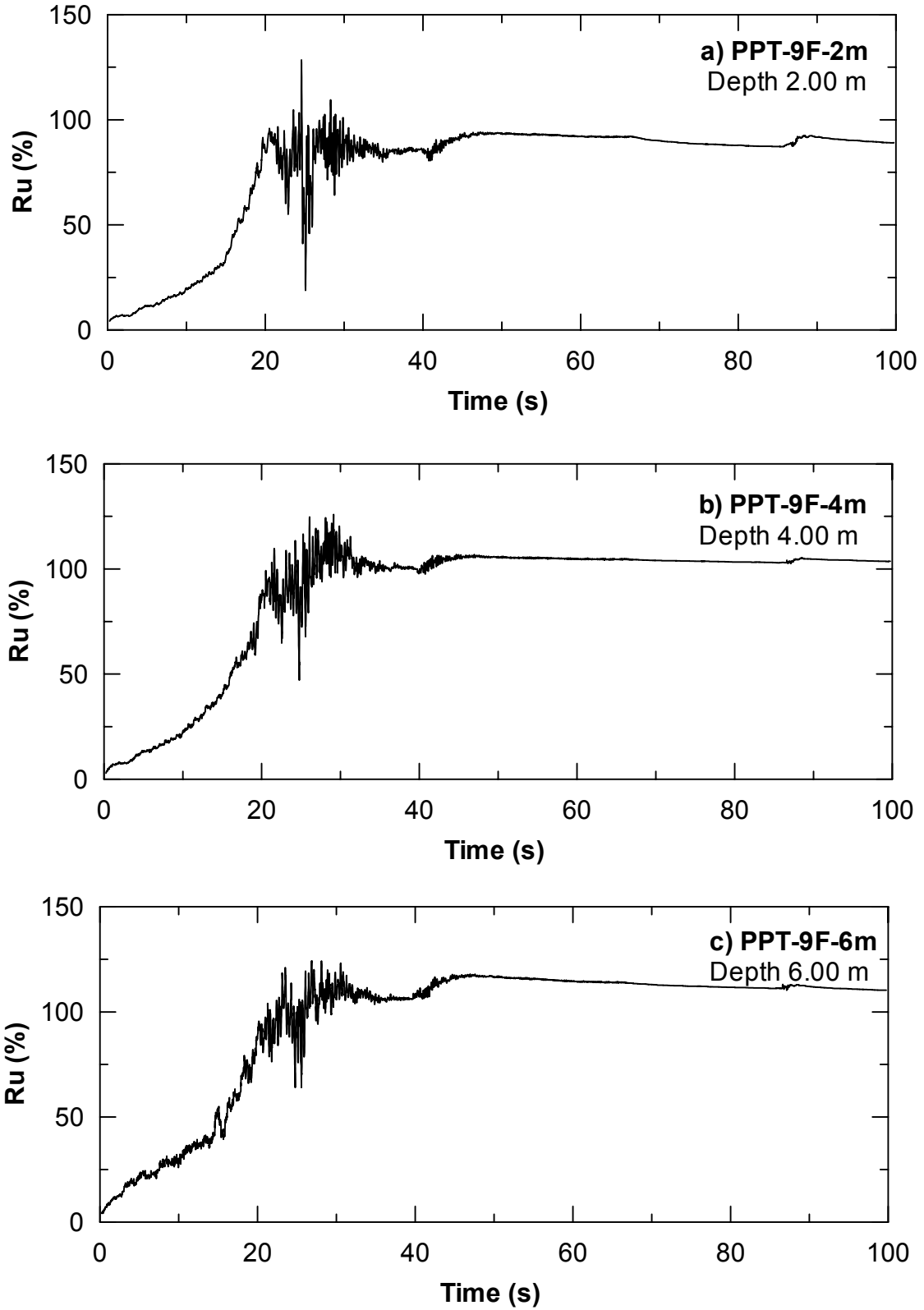


Fig. D.2 Excess pore-water pressure ratio time histories nearby 4-pile group: (a) PPT-4-2m, (b) PPT-4-4m, and (c) PPT-4-6m



**Fig. D.3 Excess pore-water pressure ratio time histories nearby 9-pile group (front side):
 (a) PPT-9F-2m, (b) PPT-9F-4m, and (c) PPT-9F-6m**

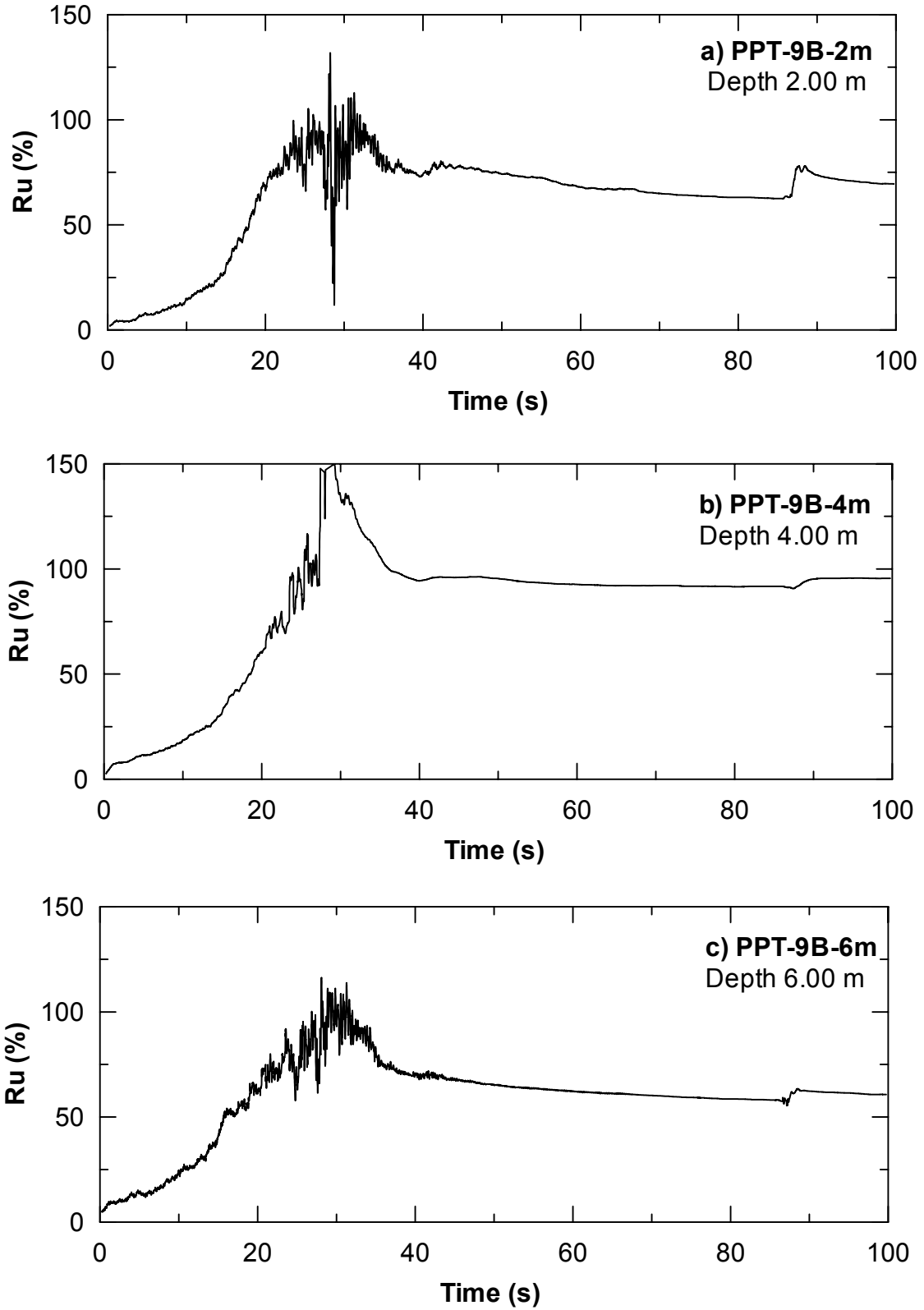
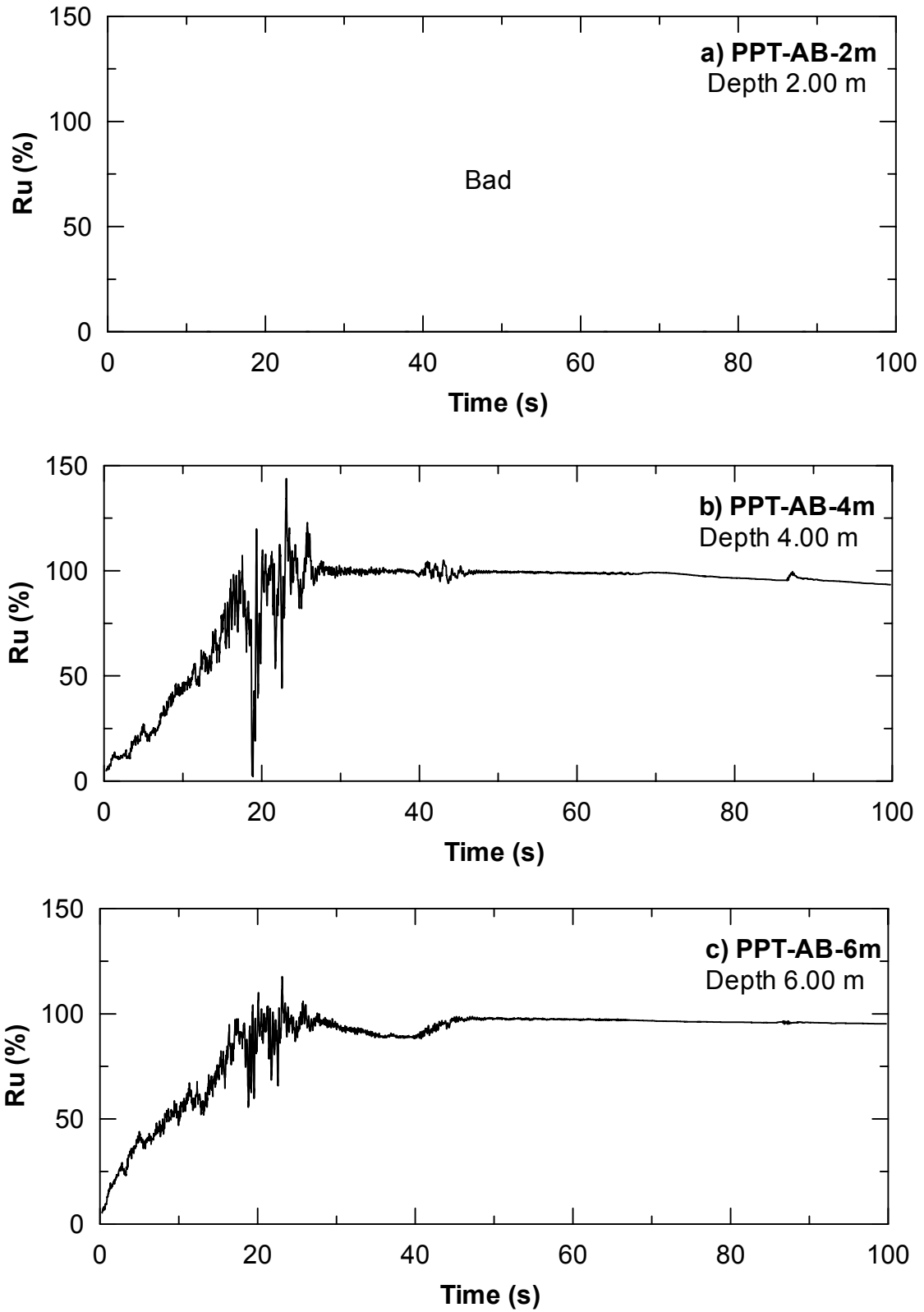


Fig. D.4 Excess pore-water pressure ratio time histories nearby 9-pile group (back side):

(a) PPT-9B-2m, (b) PPT-9B-4m, and; (c) PPT-9B-6m



**Fig. D.5 Excess pore-water pressure ratio time histories between pipelines A and B:
 (a) PPT-AB-2m, (b) PPT-AB-4m, and (c) PPT-AB-6m**

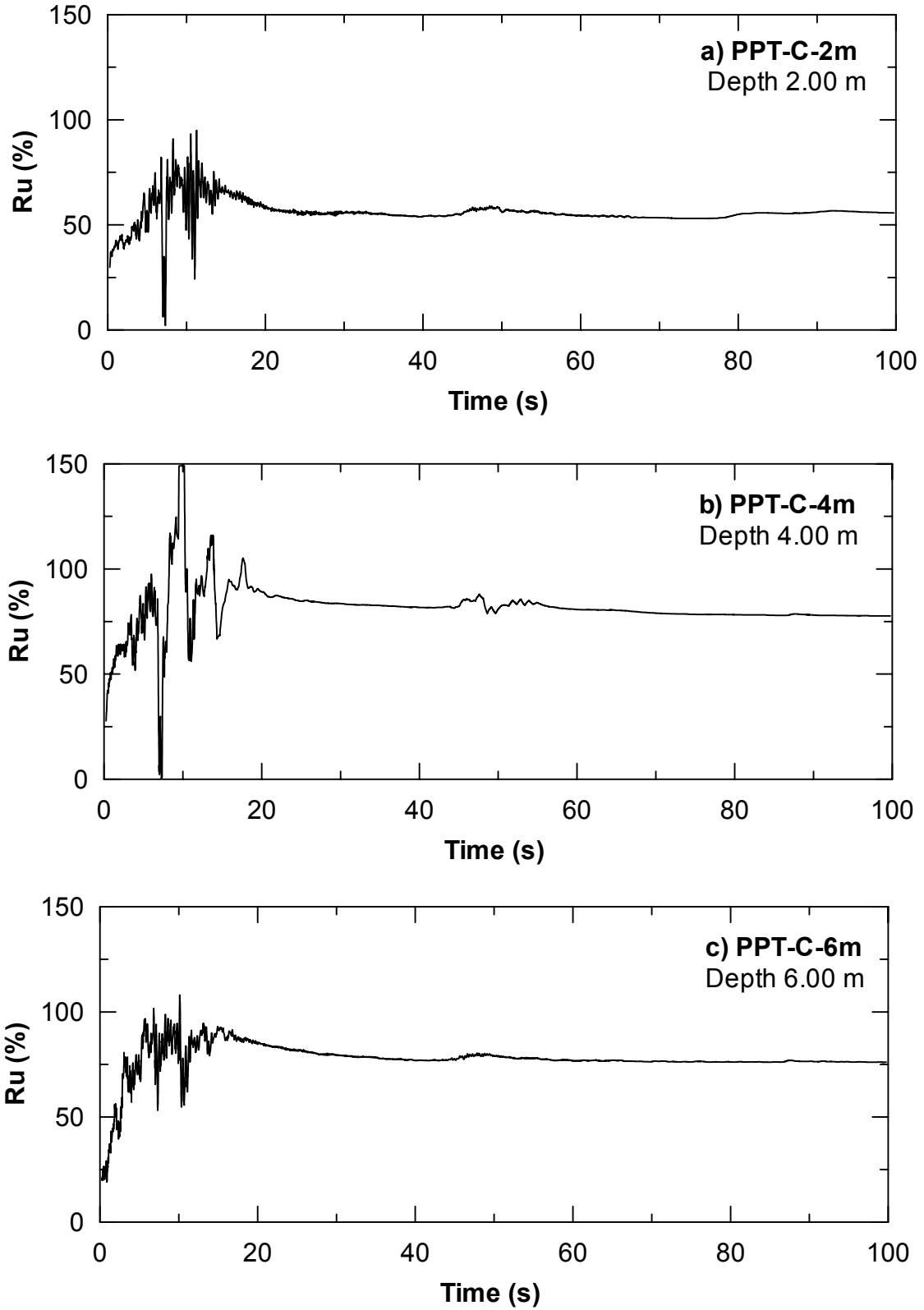


Fig. D.6 Excess pore-water pressure ratio time histories nearby pipeline C: (a) PPT-C-2m, (b) PPT-C-4m, and (c) PPT-C-6m

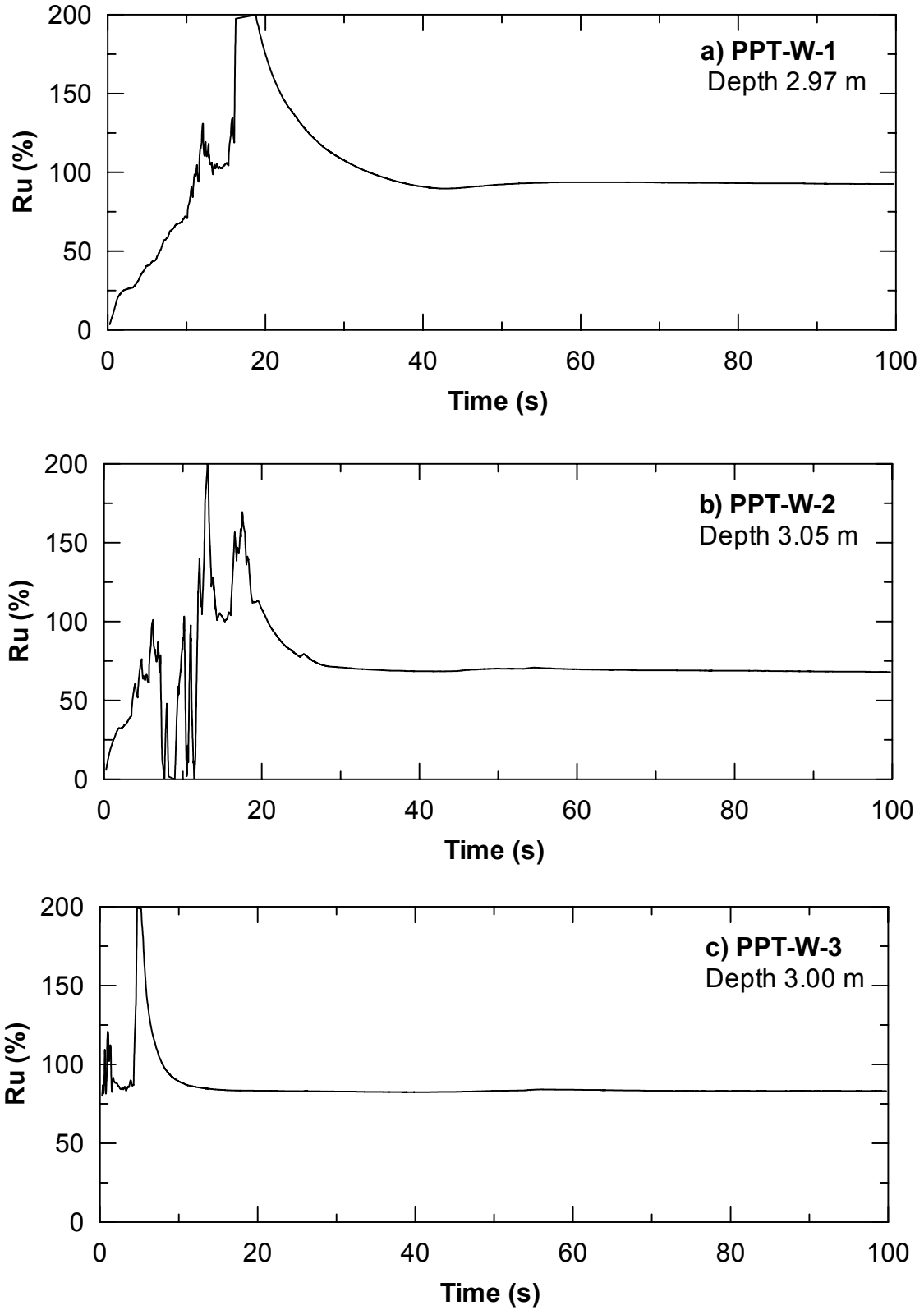


Fig. D.7 Excess pore-water pressure ratio time histories: (a) PPT-W-1, (b) PPT-W-2, and (c) PPT-W-3

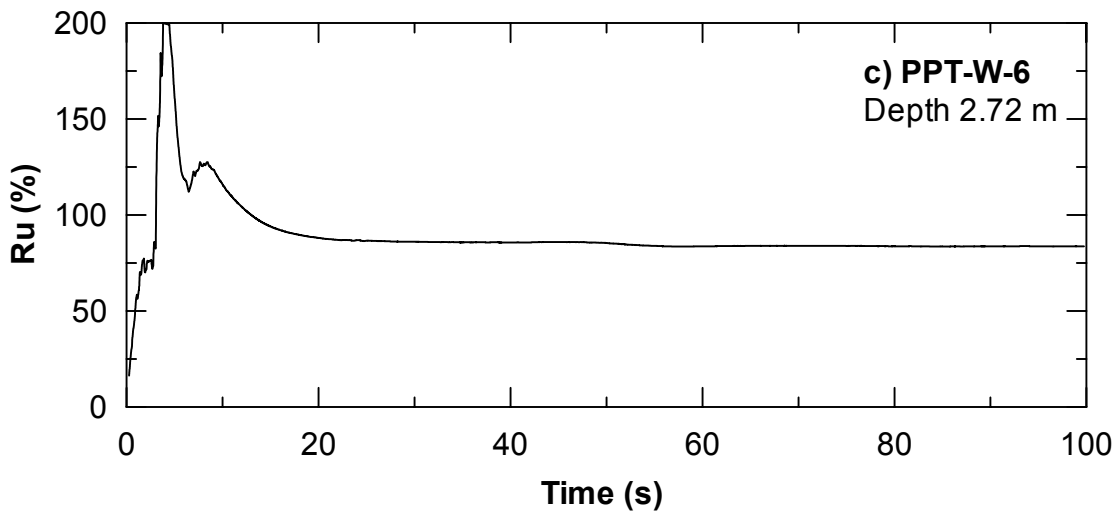
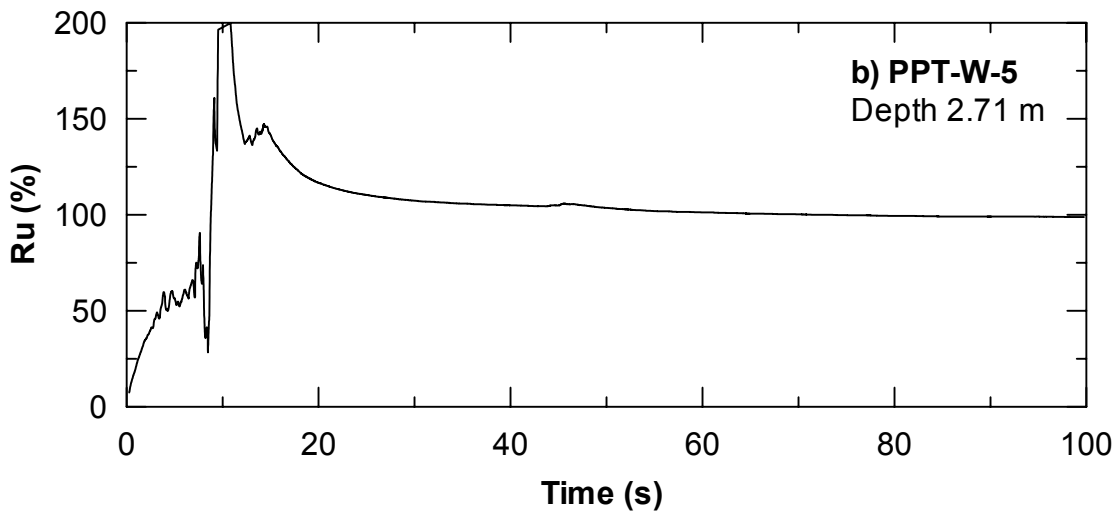
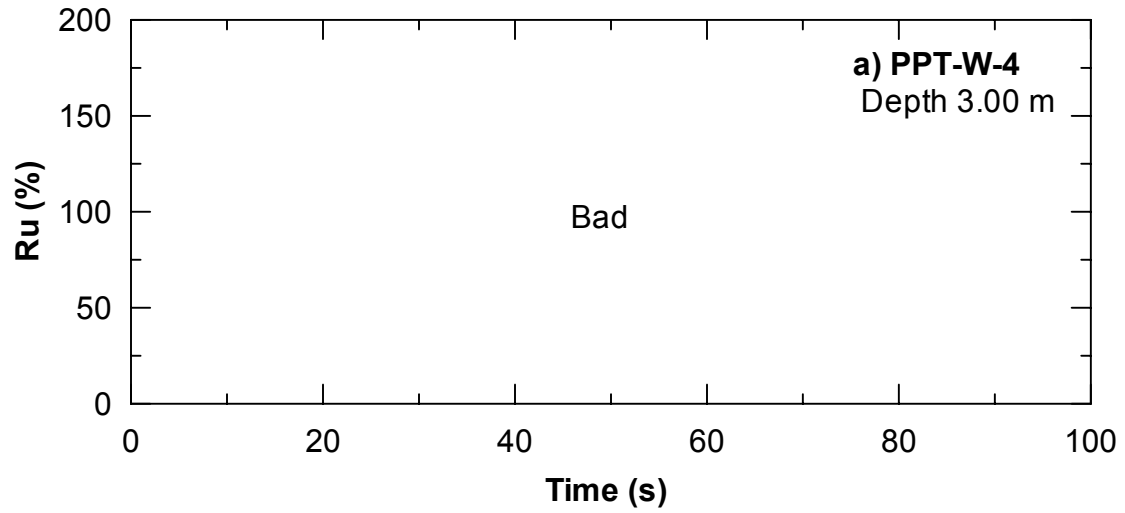
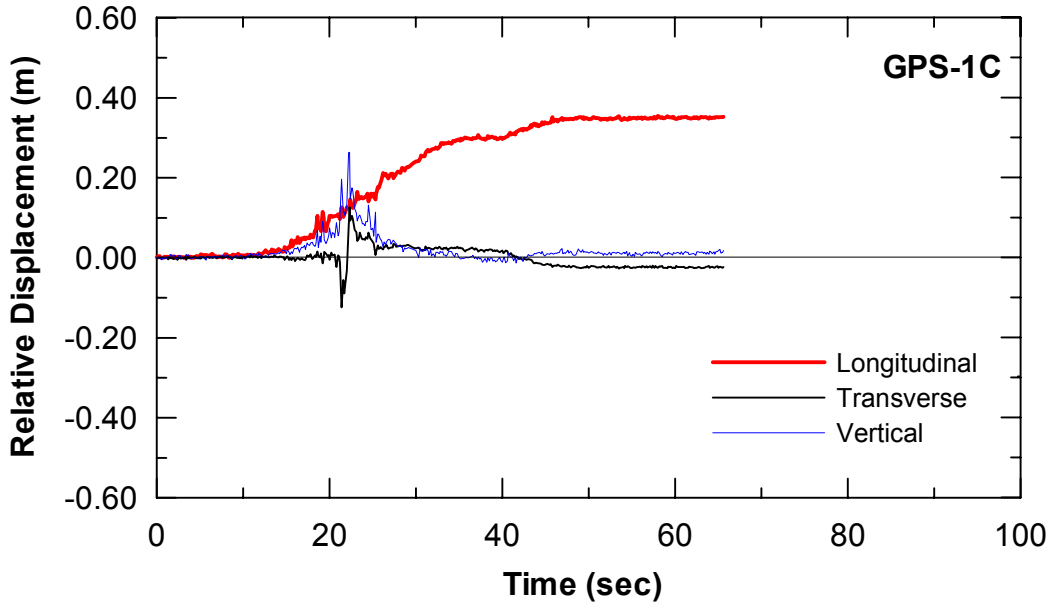
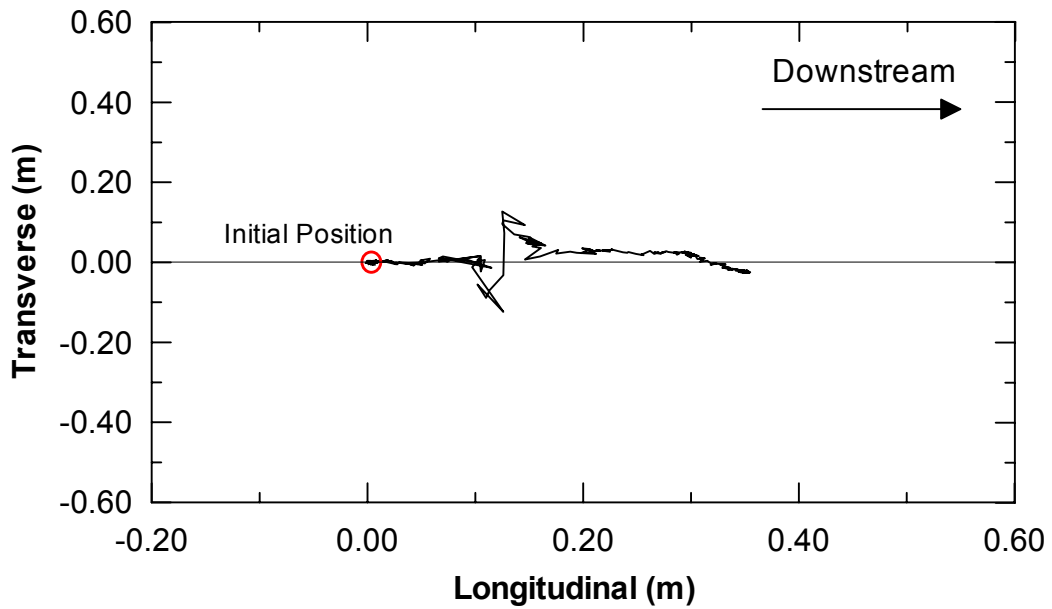


Fig. D.8 Excess pore-water pressure ratio time histories: (a) PPT-W-4, (b) PPT-W-5, and (c) PPT-W-6

Appendix E: GPS Data (First Test)

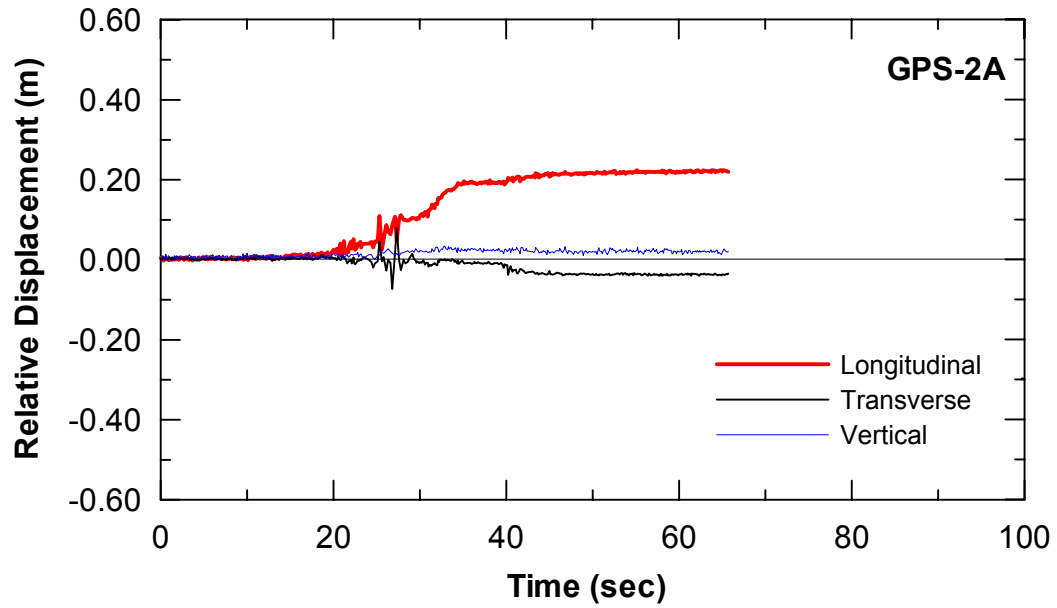


(a) Displacement Time-History

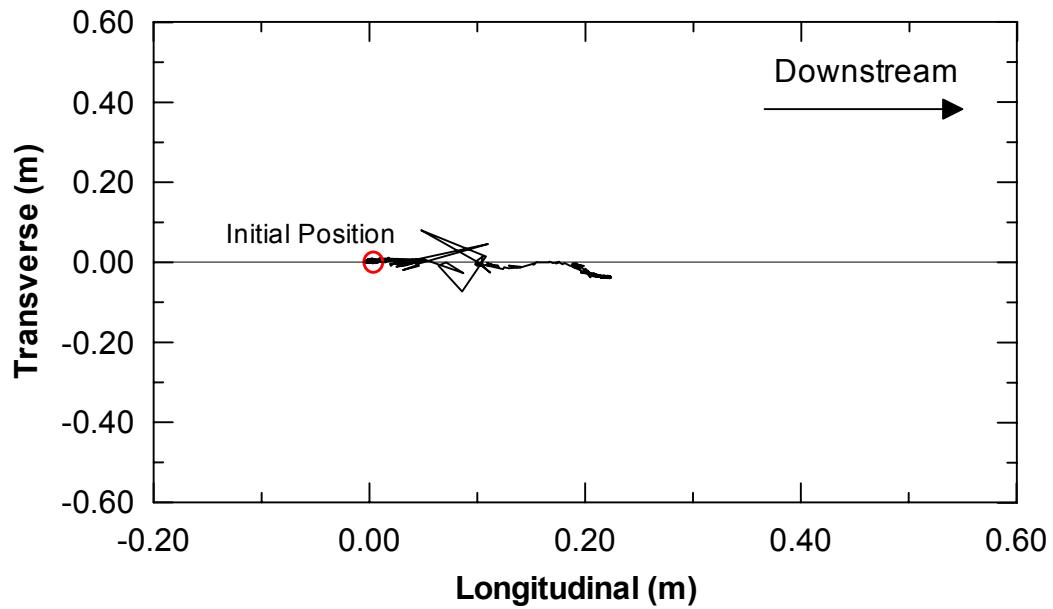


(b) Displacement Path

Fig. E.1 Global positioning system data of unit 1D (first test): (a) displacement time history and (b) displacement path (after Turner 2002)

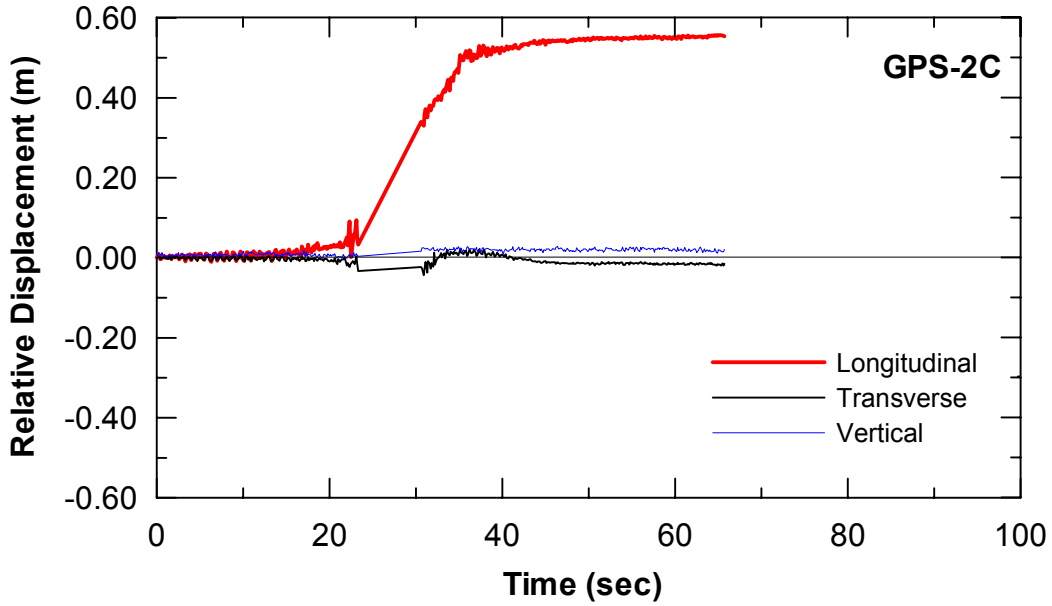


(a) Displacement Time-History

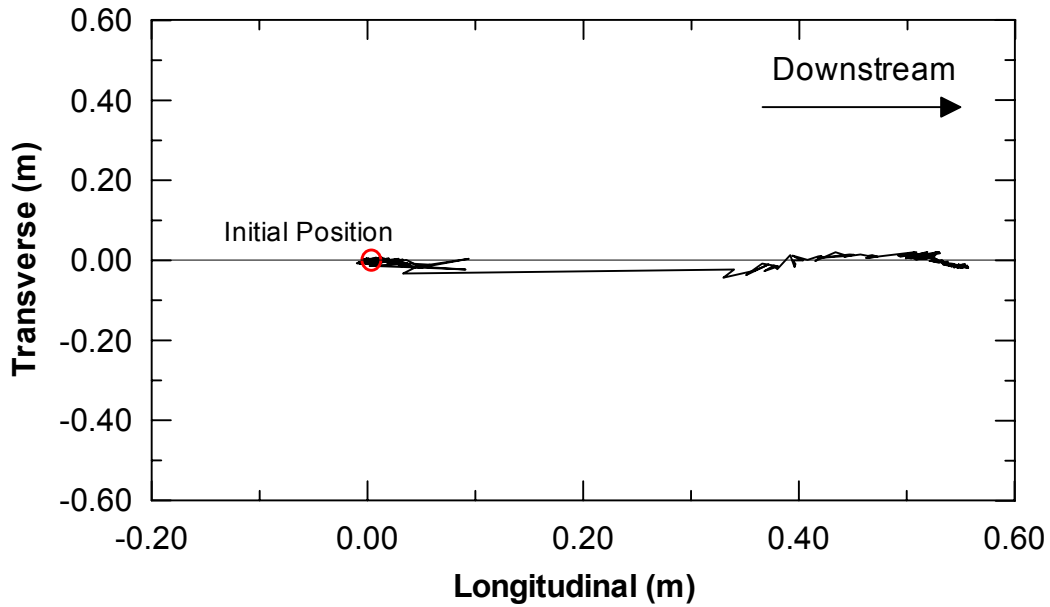


(b) Displacement Path

Fig. E.2 Global positioning system data of unit 2A (first test): (a) displacement time history, and (b) displacement path (after Turner 2002)

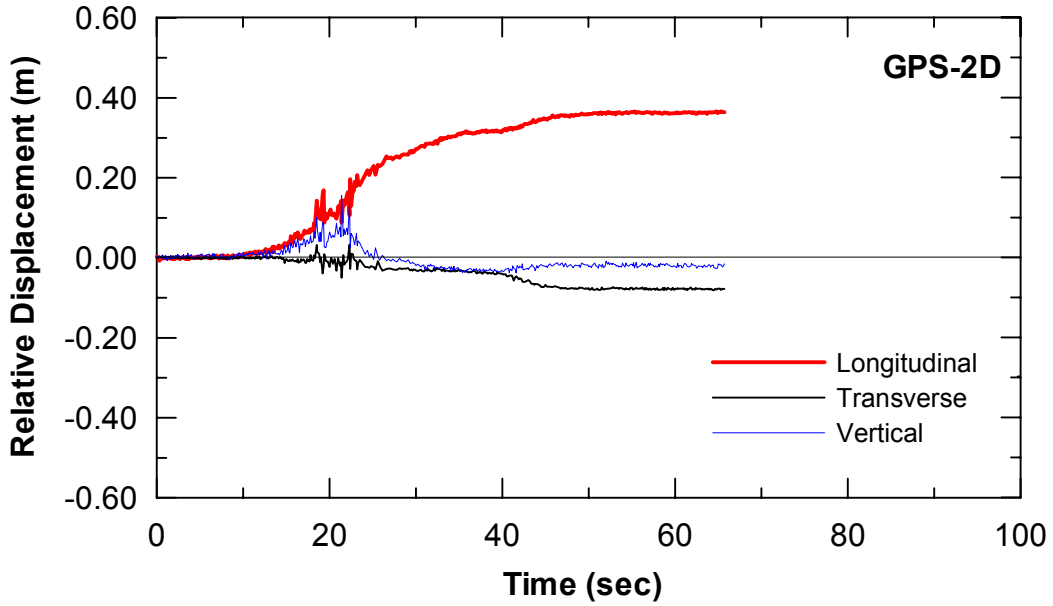


(a) Displacement Time-History

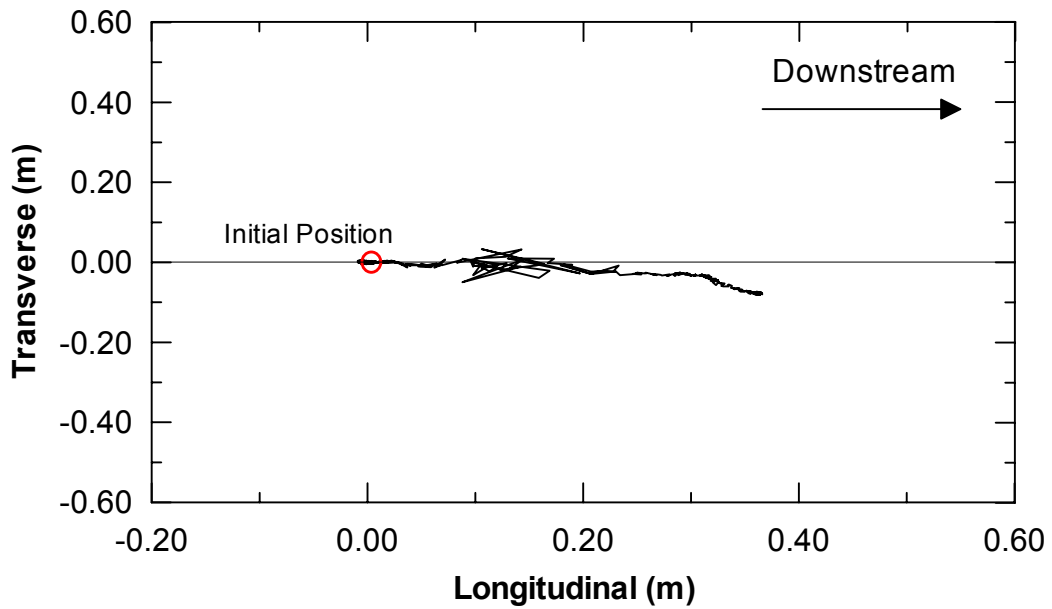


(b) Displacement Path

Fig. E.3 Global positioning system data of unit 2C (first test): (a) displacement time history, and (b) displacement path (after Turner 2002)

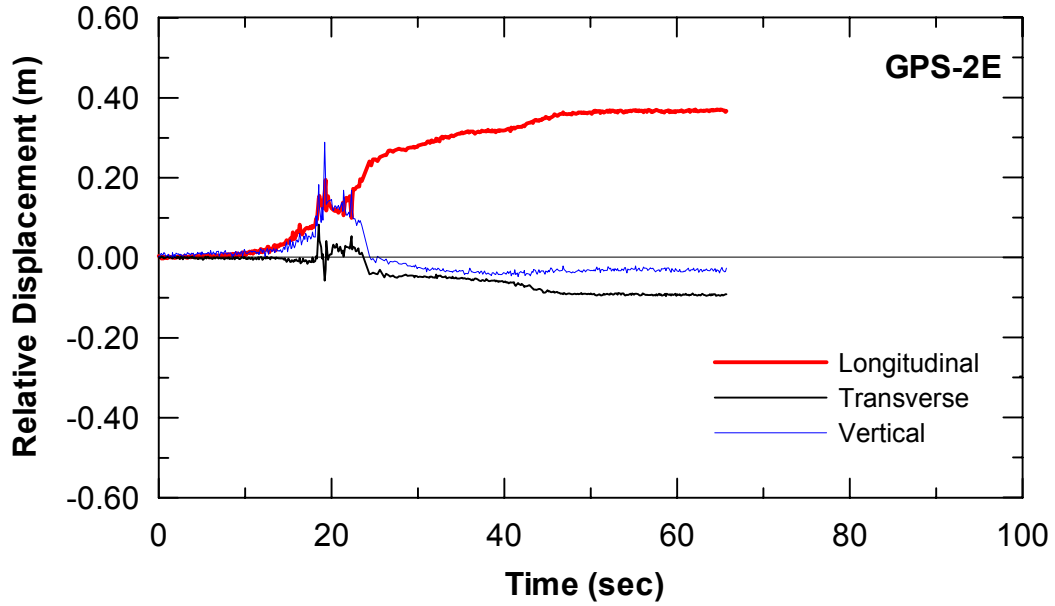


(a) Displacement Time-History

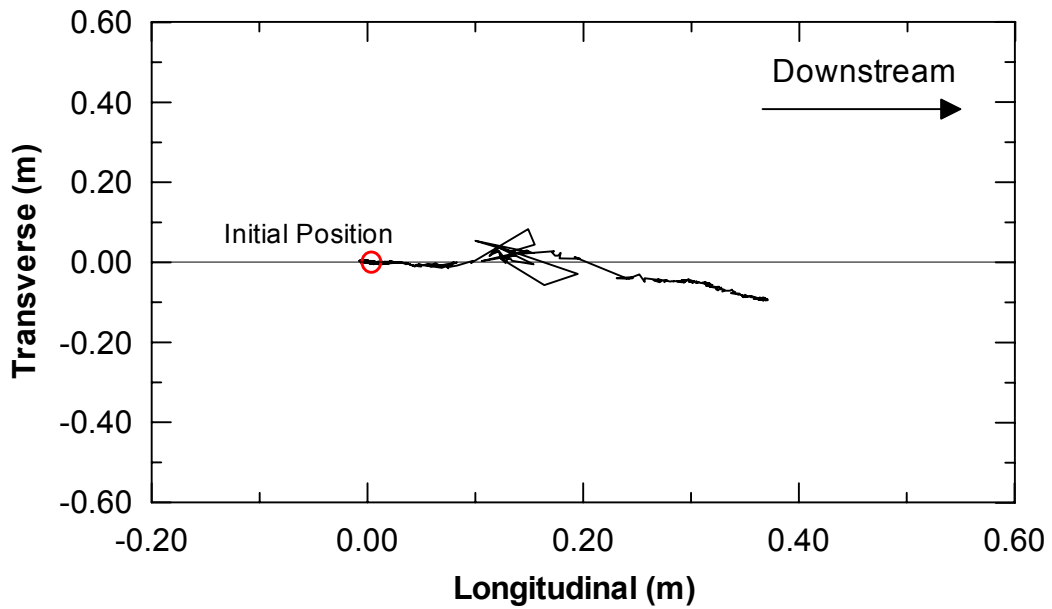


(b) Displacement Path

Fig. E.4 Global positioning system data of unit 2D (first test): (a) displacement time history, and (b) displacement path (after Turner 2002)

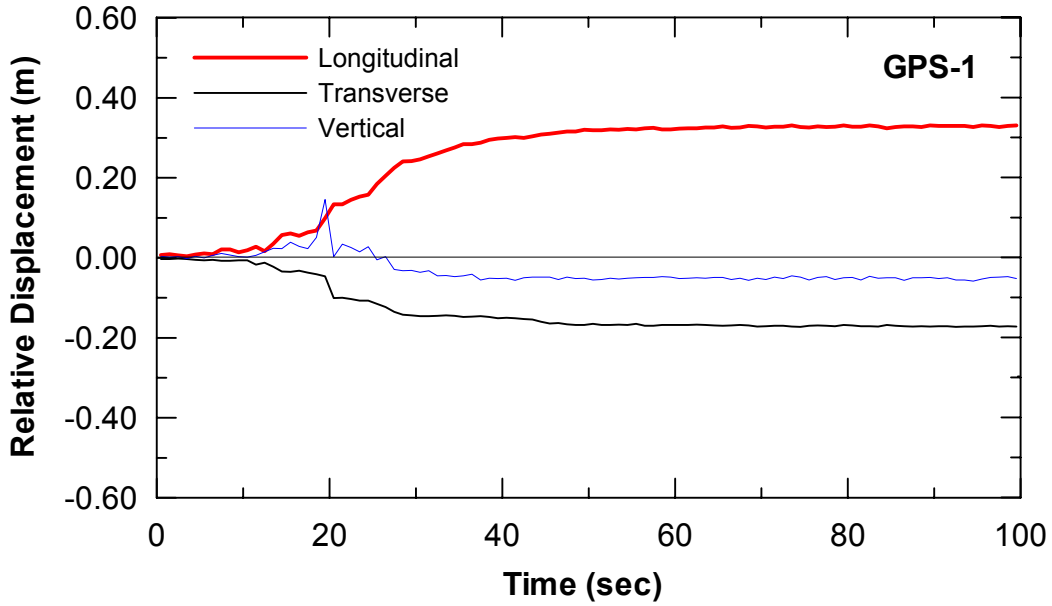


(a) Displacement Time-History

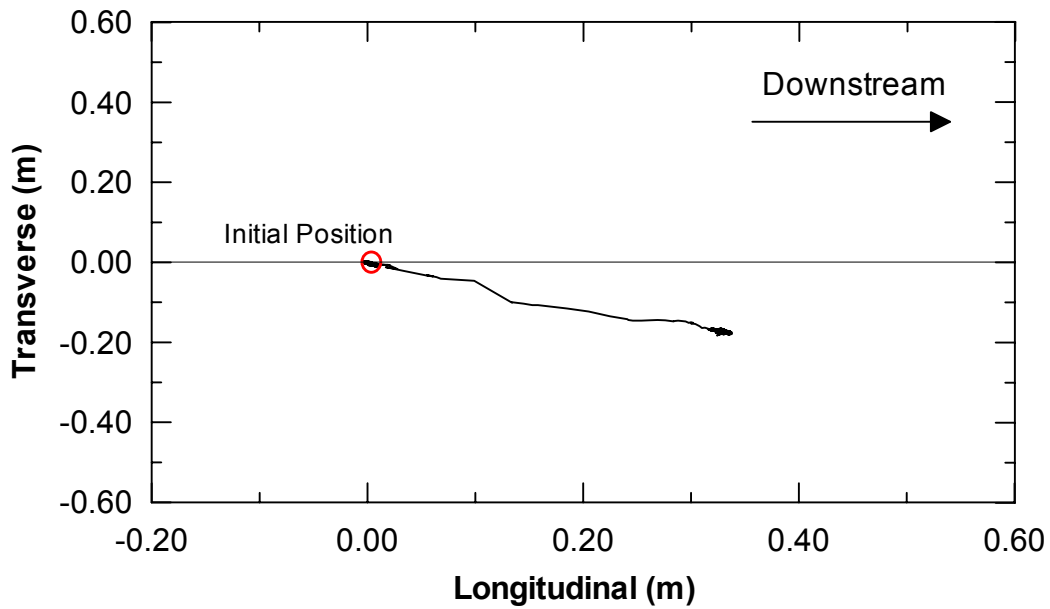


(b) Displacement Path

Fig. E.5 Global positioning system data of unit 2E (first test): (a) displacement time history and (b) displacement path (after Turner 2002)

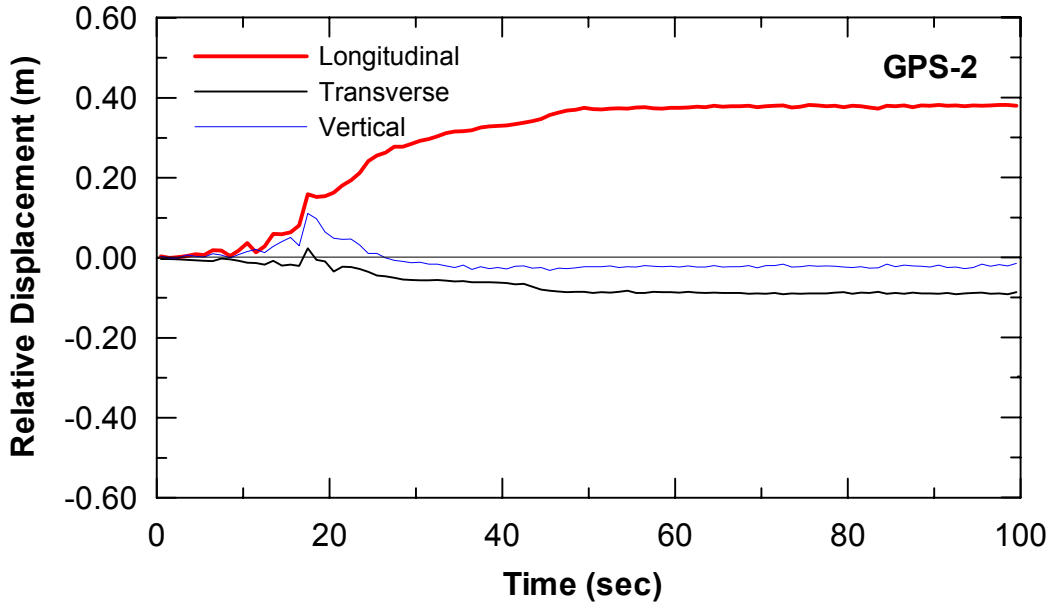


(a) Displacement Time-History

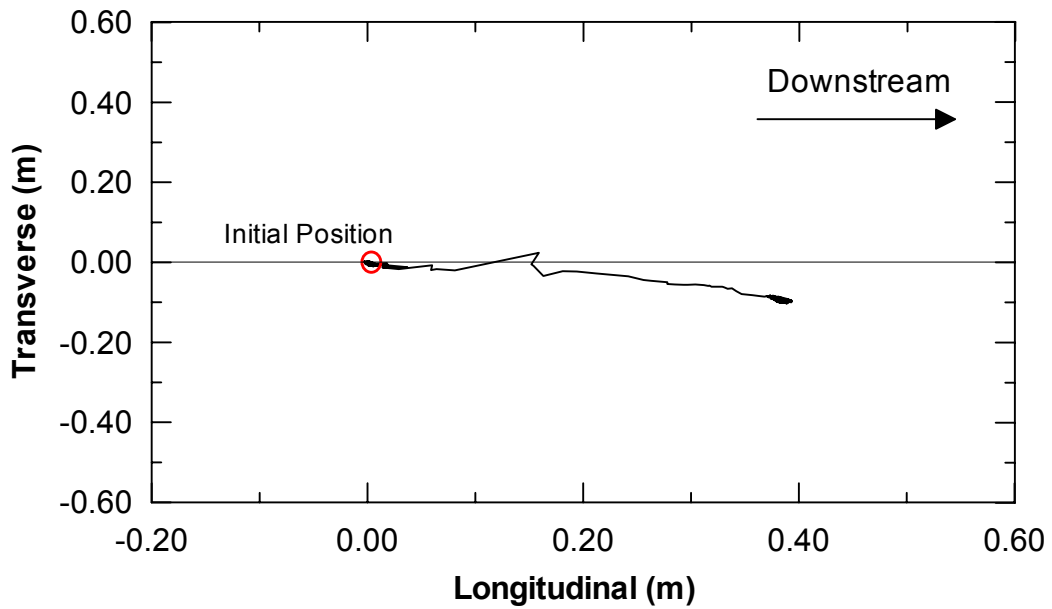


(b) Displacement Path

Fig. E.6 Global positioning system data of unit 1 (first test): (a) displacement time history and (b) displacement path (after Takahashi 2002)

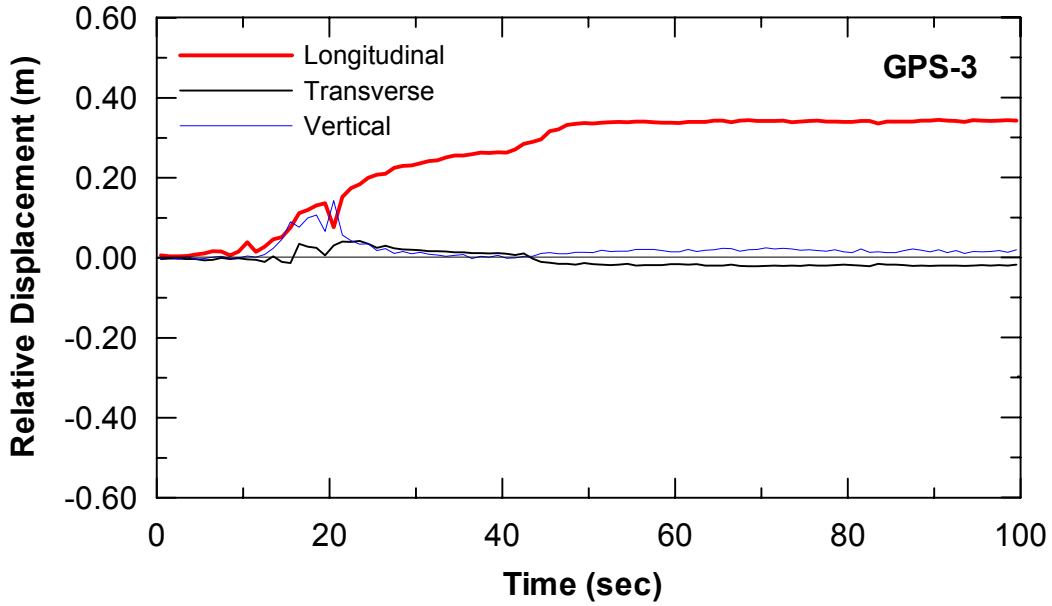


(a) Displacement Time-History

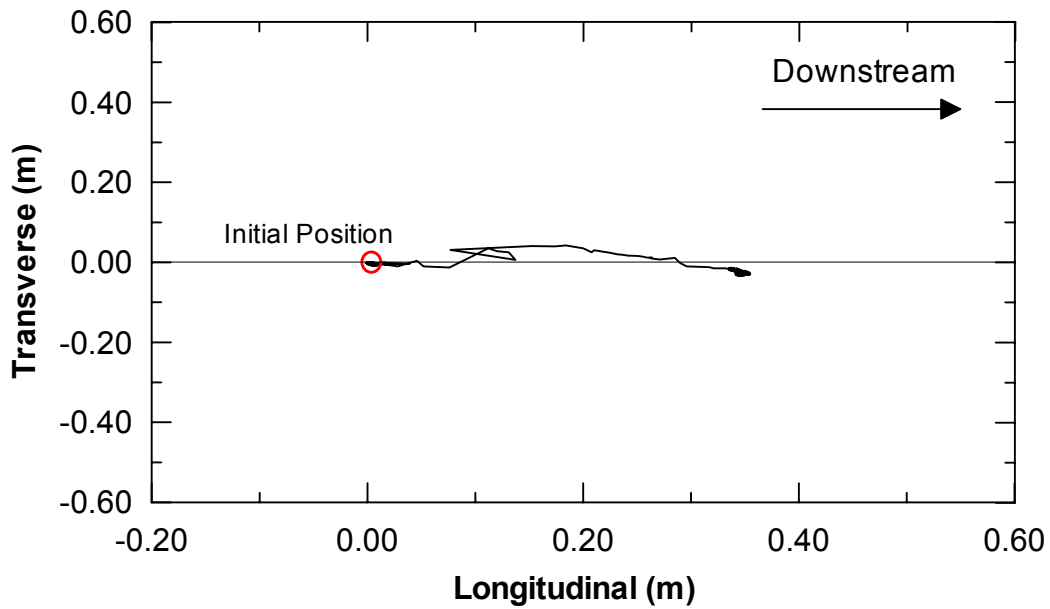


(b) Displacement Path

Fig. E.7 Global positioning system data of unit 2 (first test): (a) displacement time history and (b) displacement path (after Takahashi 2002)

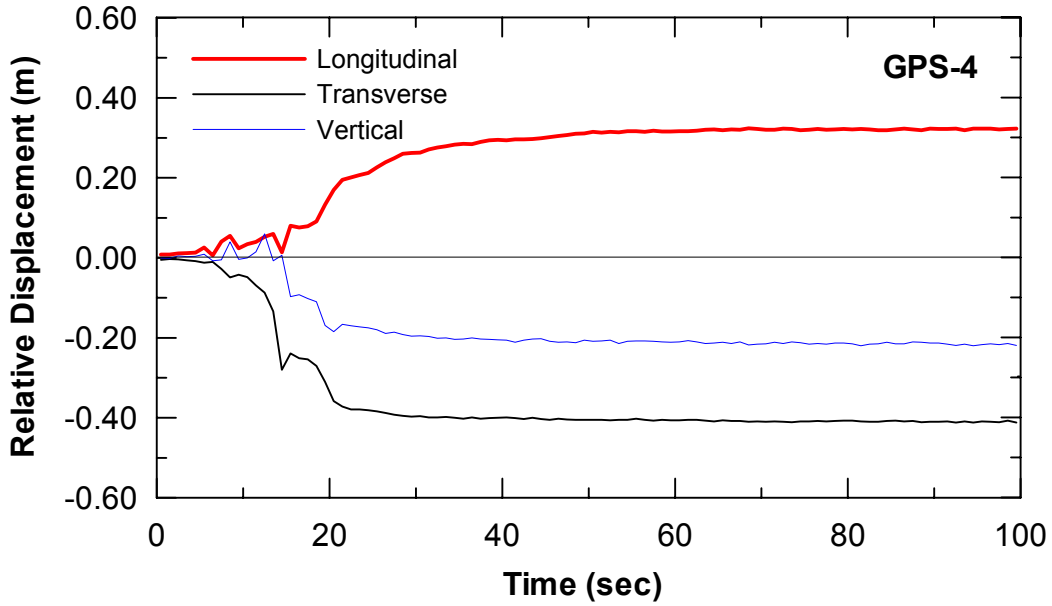


(a) Displacement Time-History

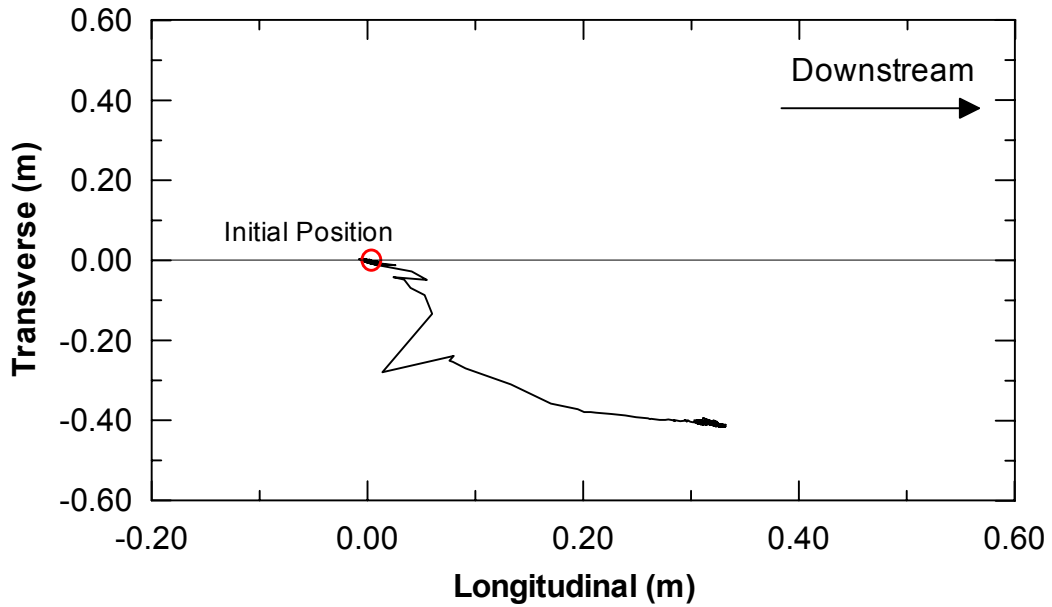


(b) Displacement Path

Fig. E.8 Global positioning system data of unit 3 (first test): (a) displacement time history and (b) displacement path (after Takahashi 2002)

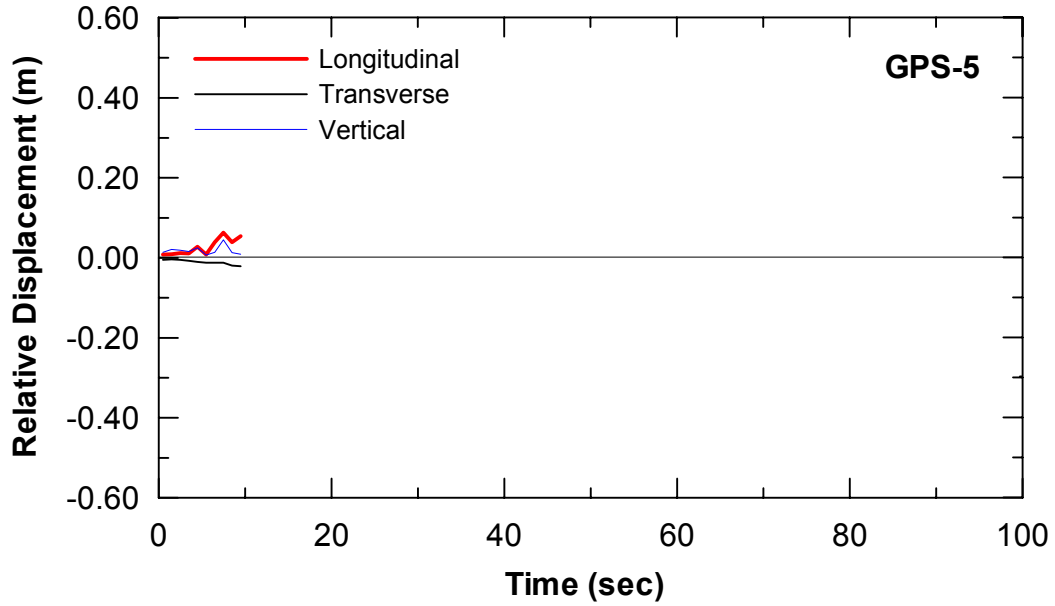


(a) Displacement Time-History

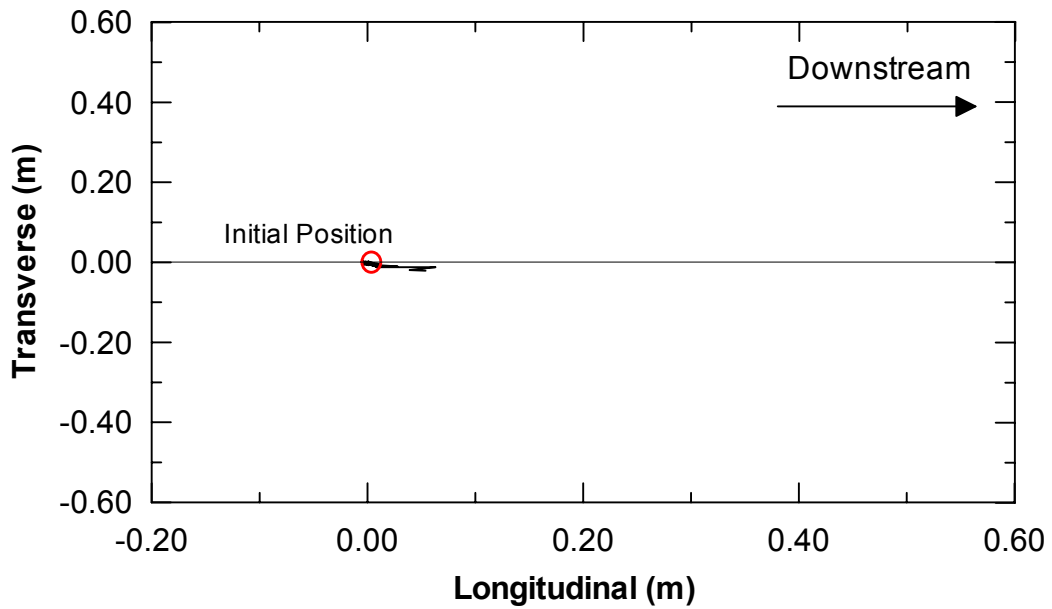


(b) Displacement Path

Fig. E.9 Global positioning system data of unit 4 (first test): (a) displacement time history and (b) displacement path (after Takahashi 2002)

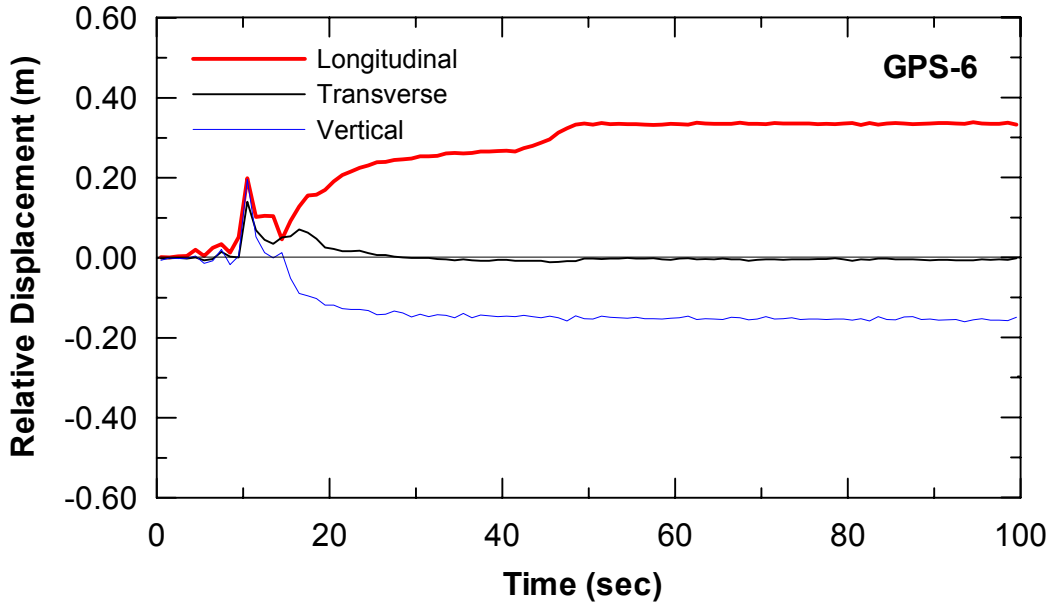


(a) Displacement Time-History

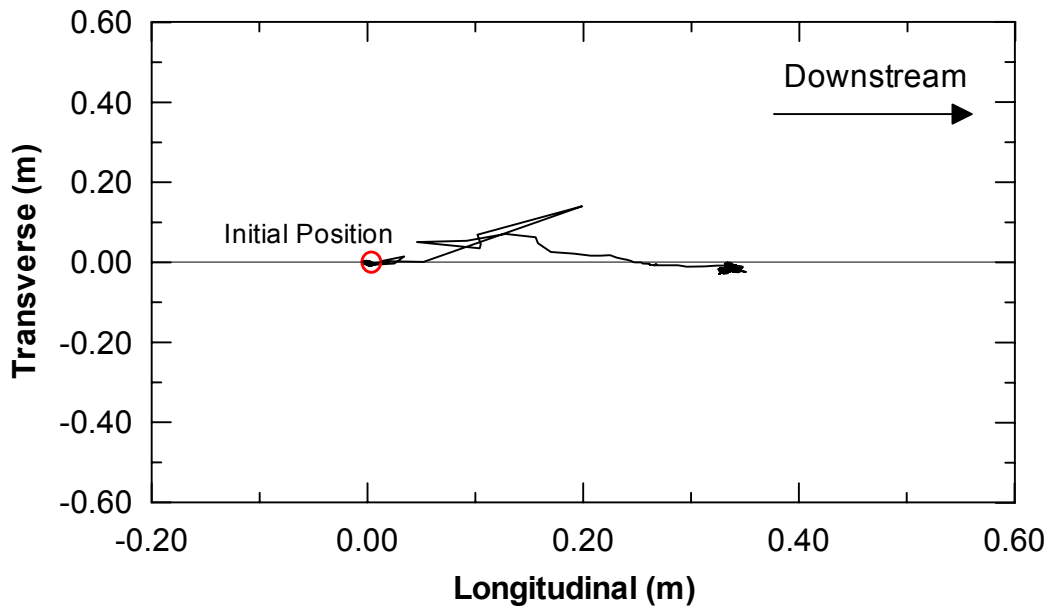


(b) Displacement Path

Fig. E.10 Global positioning system data of unit 5 (first test): (a) displacement time history, and (b) displacement path (after Takahashi 2002)

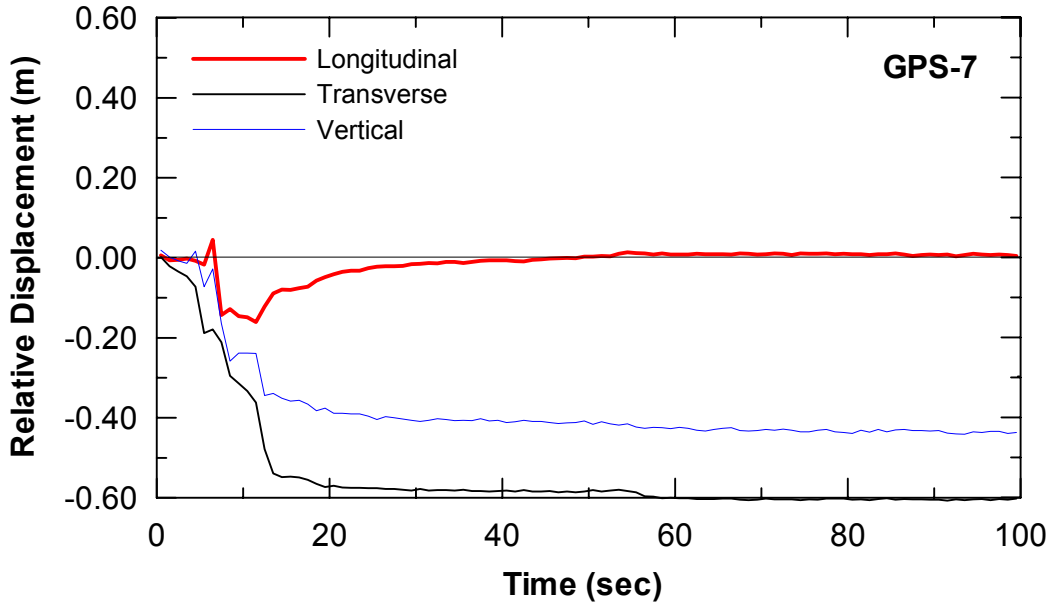


(a) Displacement Time-History

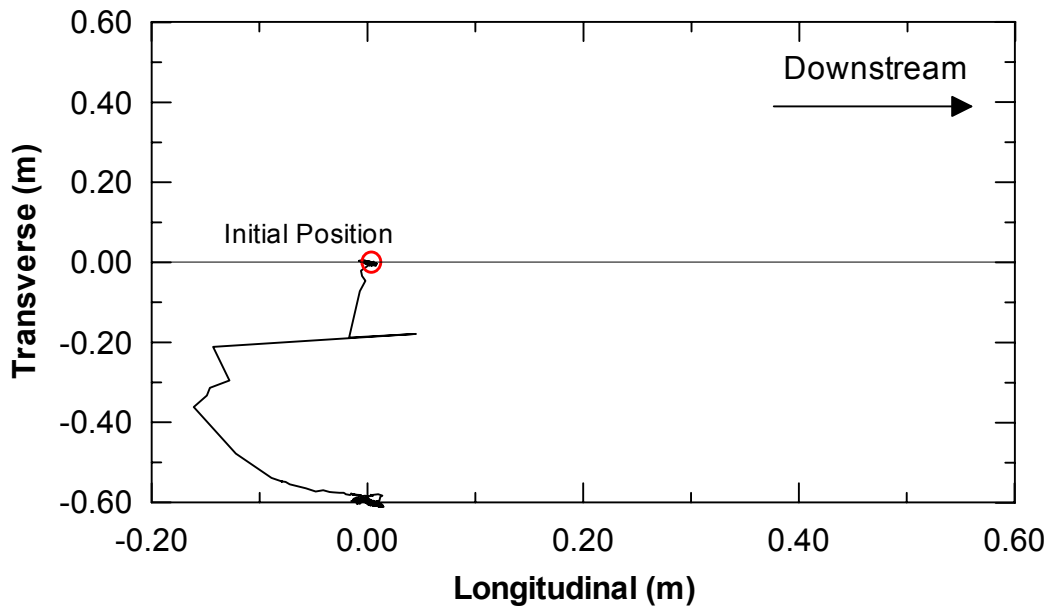


(b) Displacement Path

Fig. E.11 Global positioning system data of unit 6 (first test): (a) displacement time history and (b) displacement path (after Takahashi 2002)

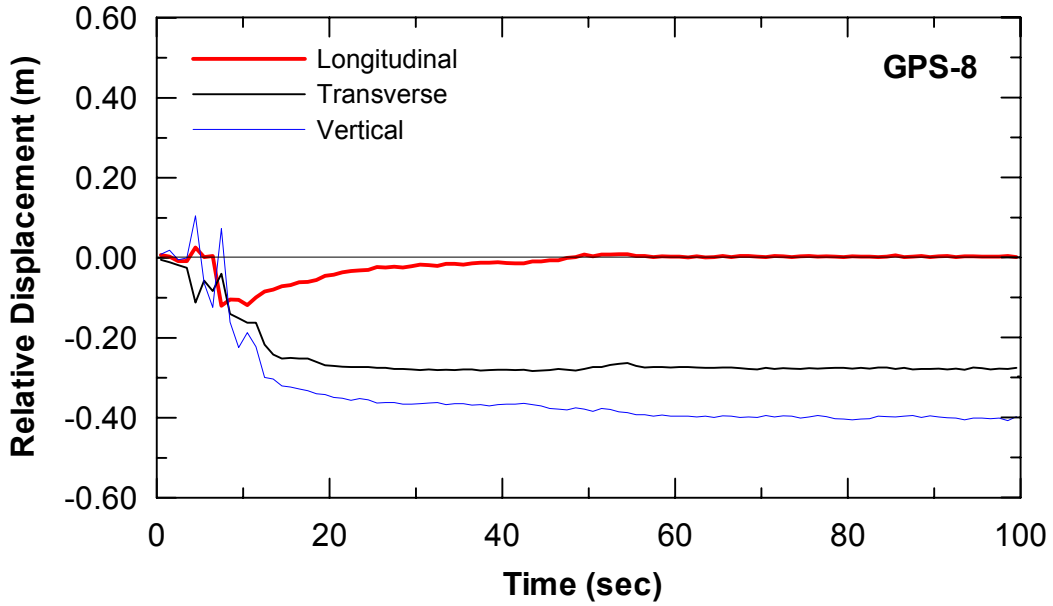


(a) Displacement Time-History

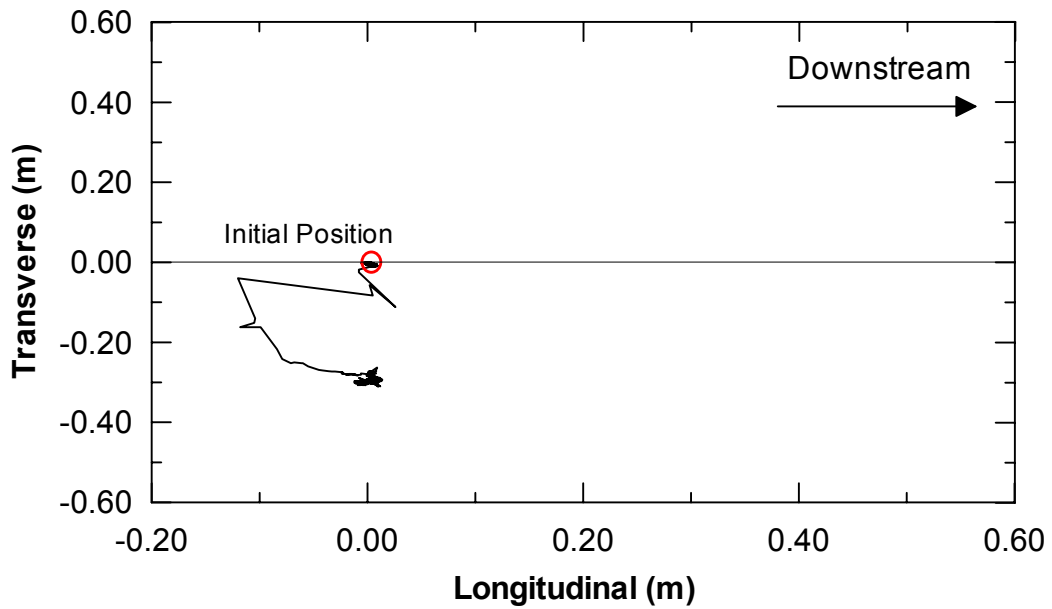


(b) Displacement Path

Fig. E.12 Global positioning system data of unit 7 (first test): (a) displacement time history and (b) displacement path (after Takahashi 2002)

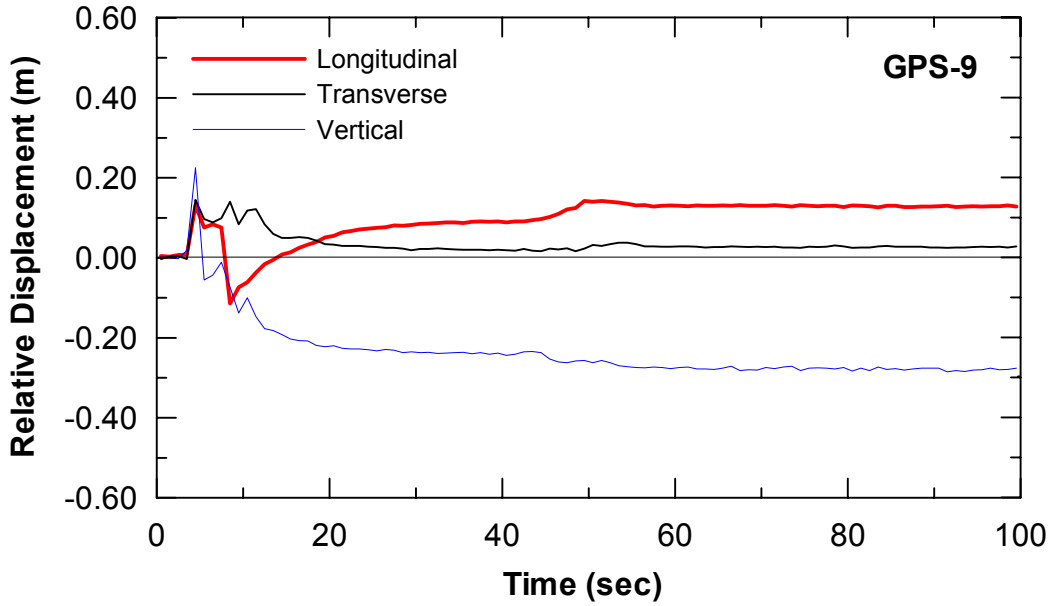


(a) Displacement Time-History

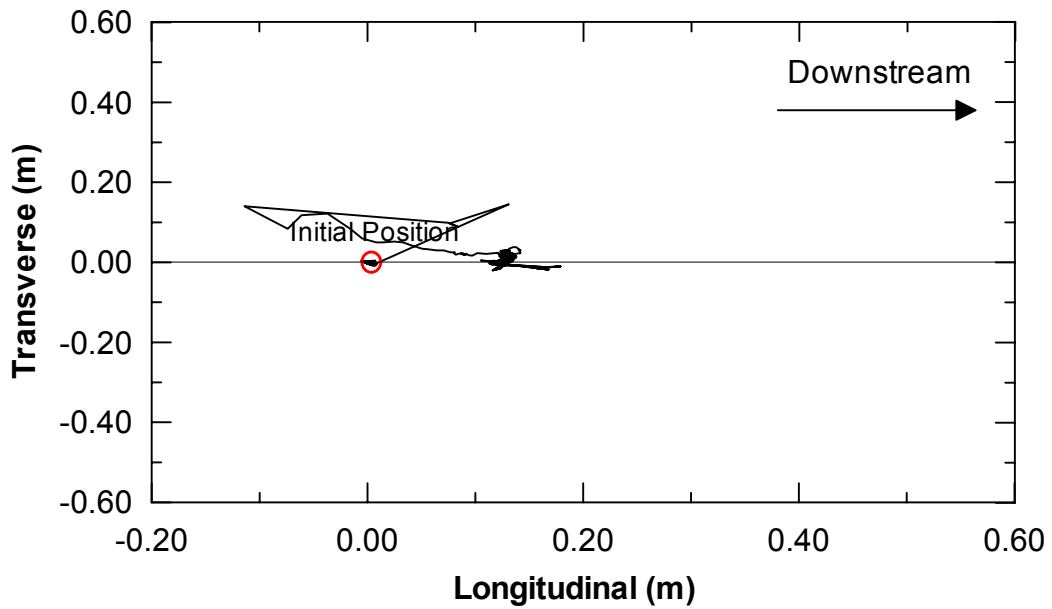


(b) Displacement Path

Fig. E.13 Global positioning system data of unit 8 (first test): (a) displacement time history and (b) displacement path (after Takahashi 2002)

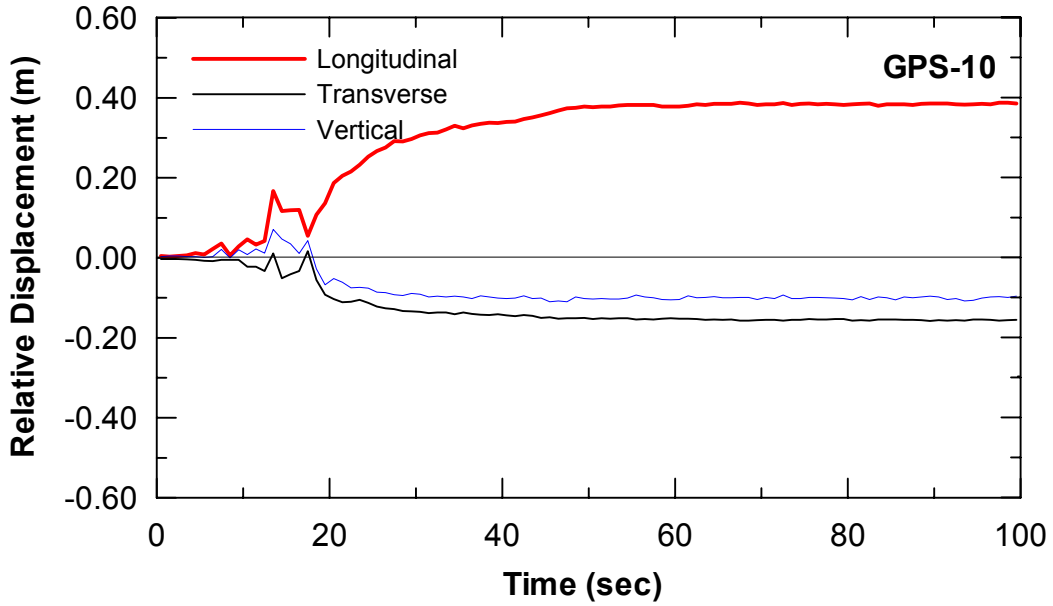


(a) Displacement Time-History

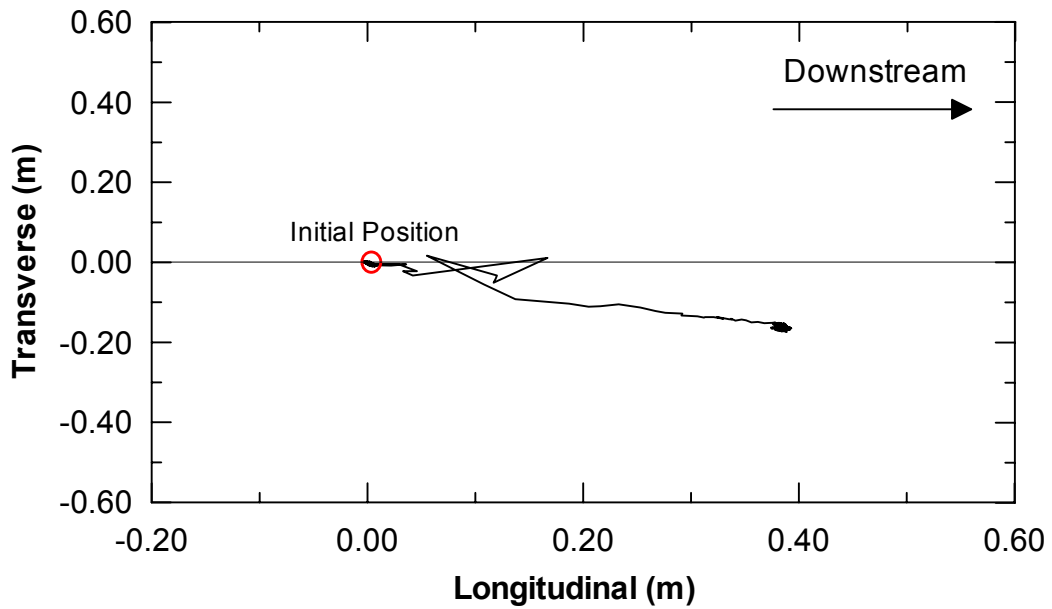


(b) Displacement Path

Fig. E.14 Global positioning system data of unit 9 (first test): (a) displacement time history and (b) displacement path (after Takahashi 2002)



(a) Displacement Time-History



(b) Displacement Path

Fig. E.15 Global positioning system data of unit 10 (first test): (a) displacement time history and (b) displacement path (after Takahashi 2002)

Appendix F: Inclinometer Data (First Test)

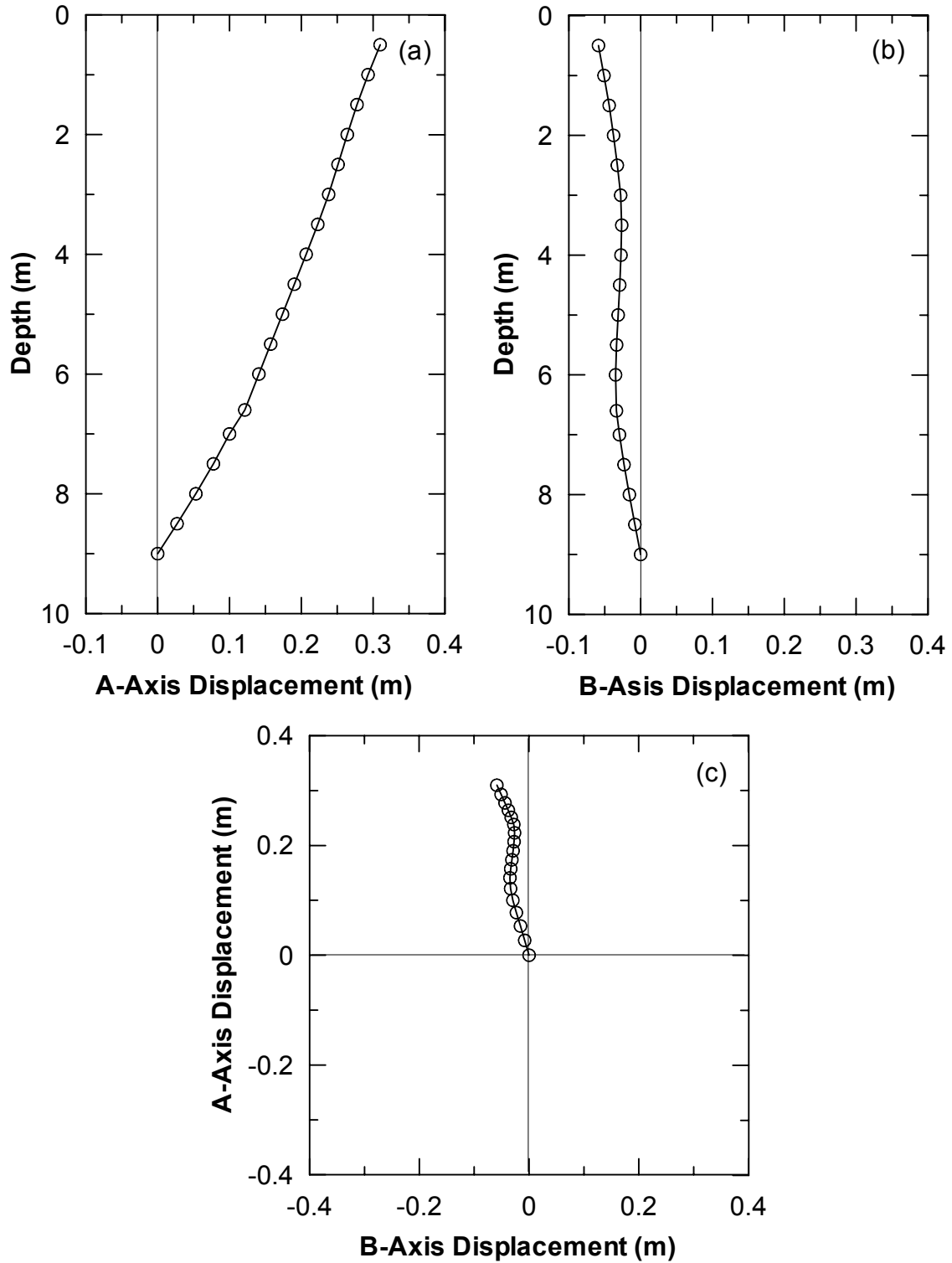


Fig. F.1 Soil displacement from inclinometer Casing S2 (a) section view A-direction, (b) section view B-direction, and (c) plan view

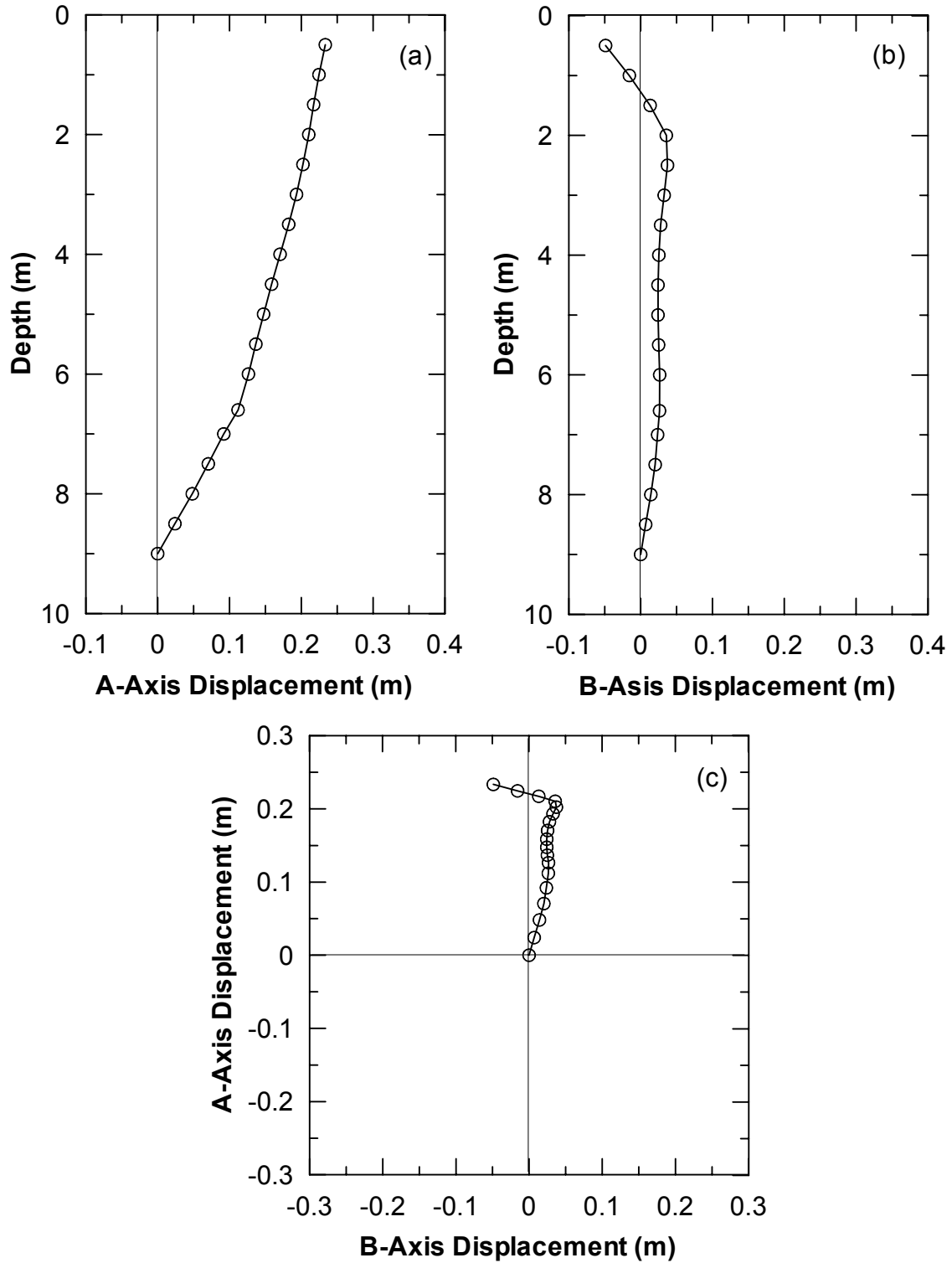


Fig. F.2 Soil displacement from inclinometer Casing S3 (a) section view A-direction, (b) section view B-direction, and (c) plan view

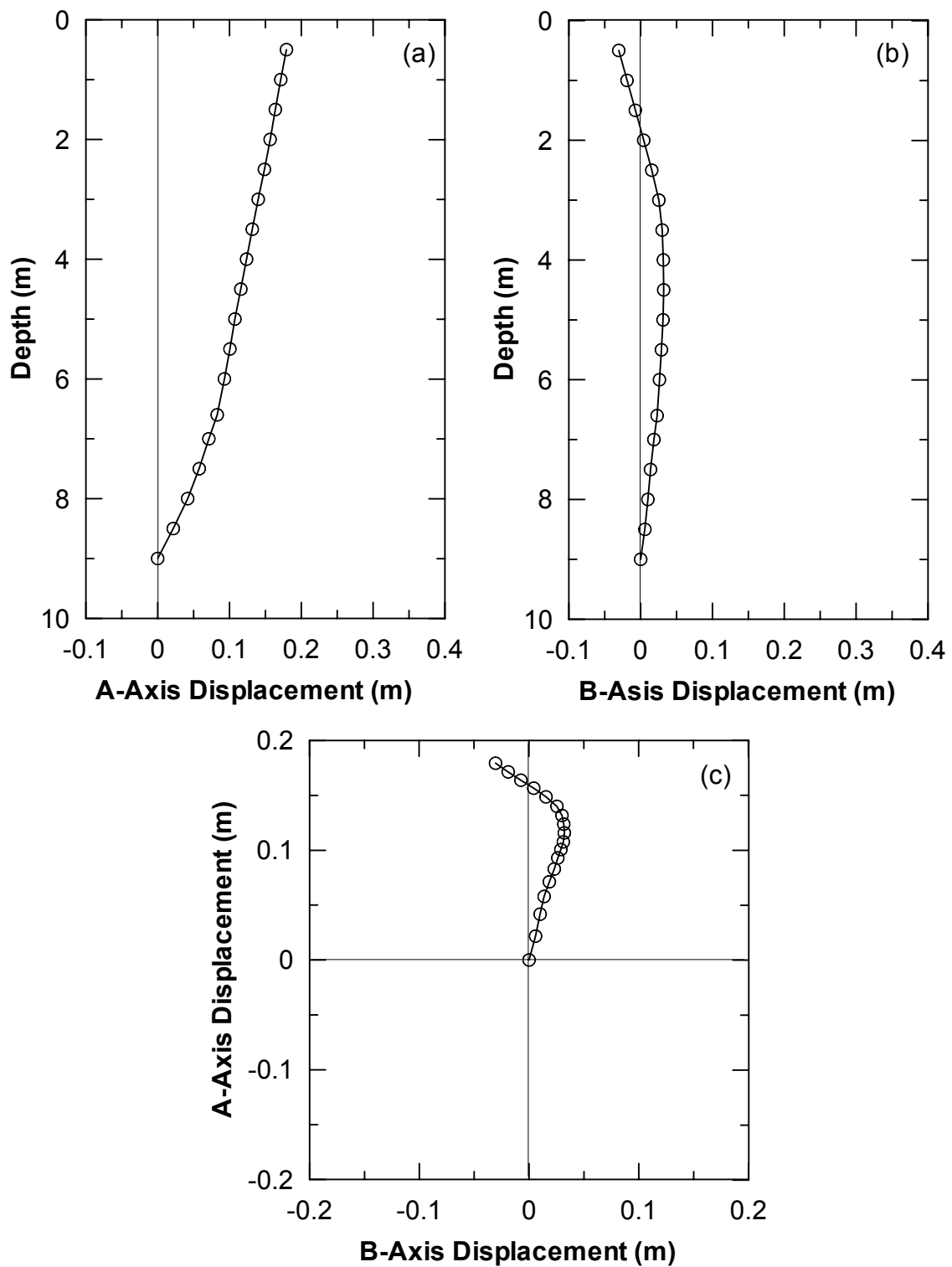


Fig. F.3 Soil displacement from inclinometer Casing S4 (a) section view A-direction, (b) section view B-direction, and (c) plan view

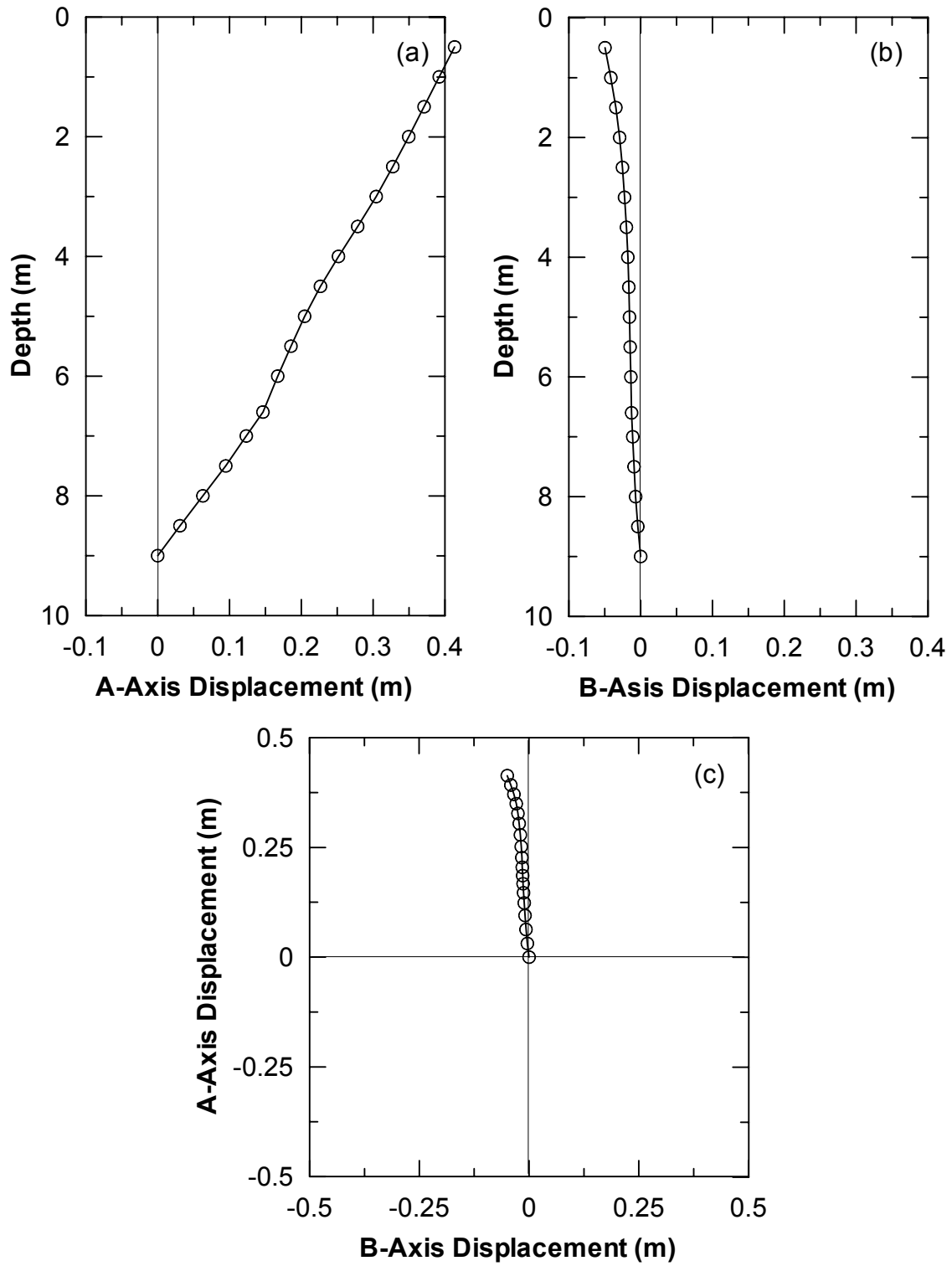


Fig. F.4 Soil displacement from inclinometer Casing S5 (a) section view A-direction, (b) section view B-direction, and (c) plan view

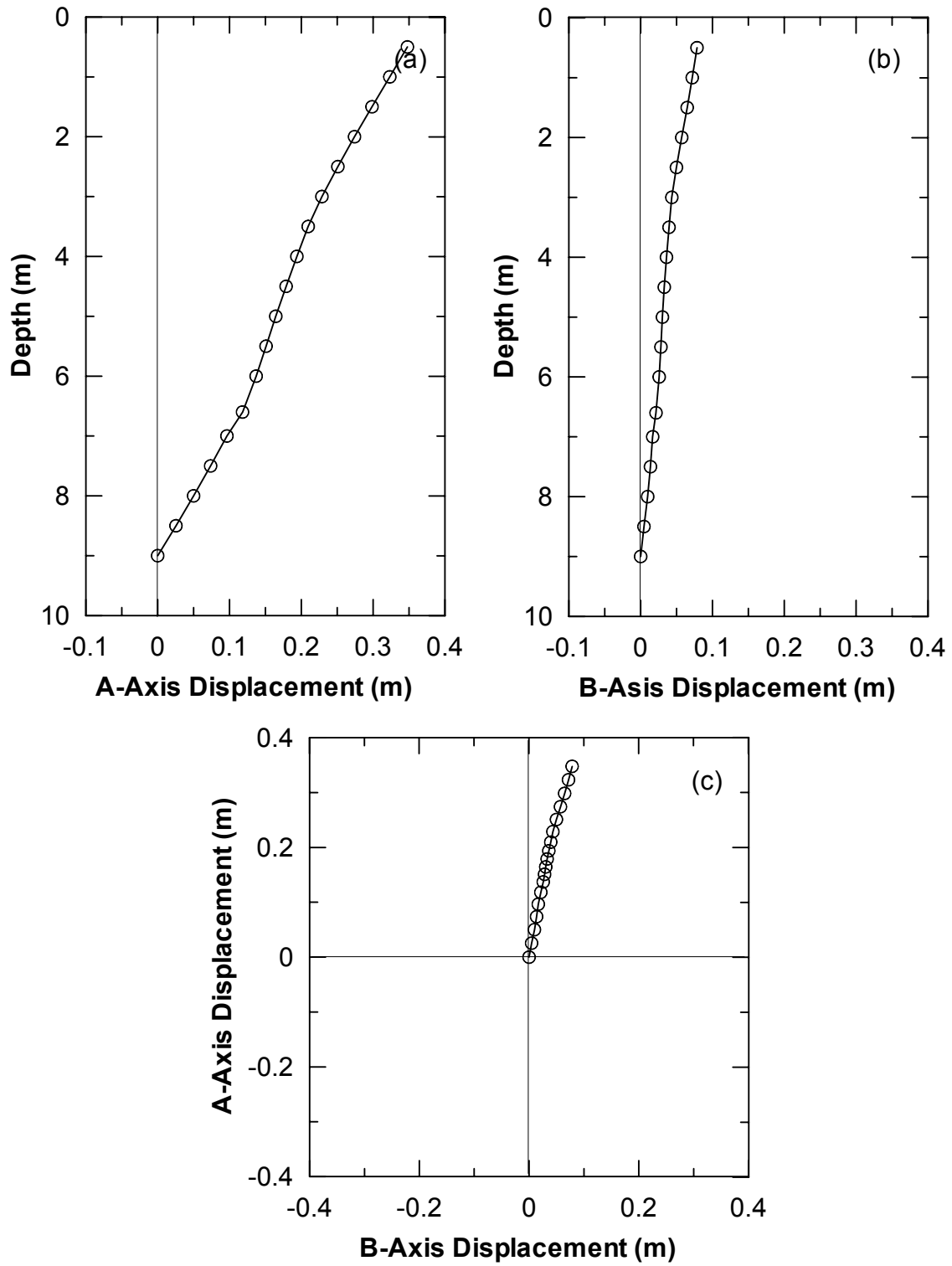


Fig. F.5 Soil displacement from inclinometer Casing S6 (a) section view A-direction, (b) section view B-direction, and (c) plan view

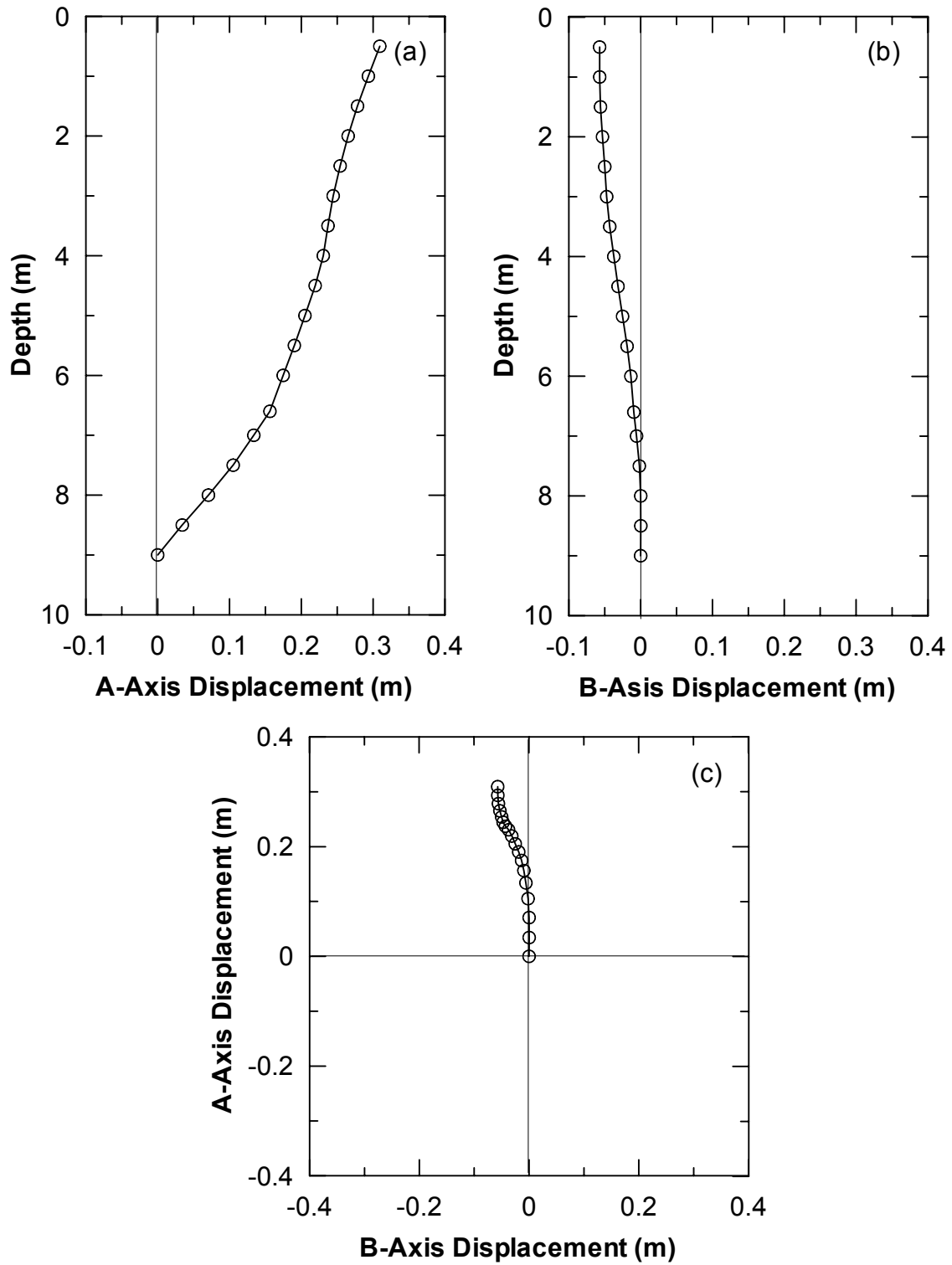


Fig. F.6 Soil displacement from inclinometer Casing S7 (a) section view A-direction, (b) section view B-direction, and (c) plan view

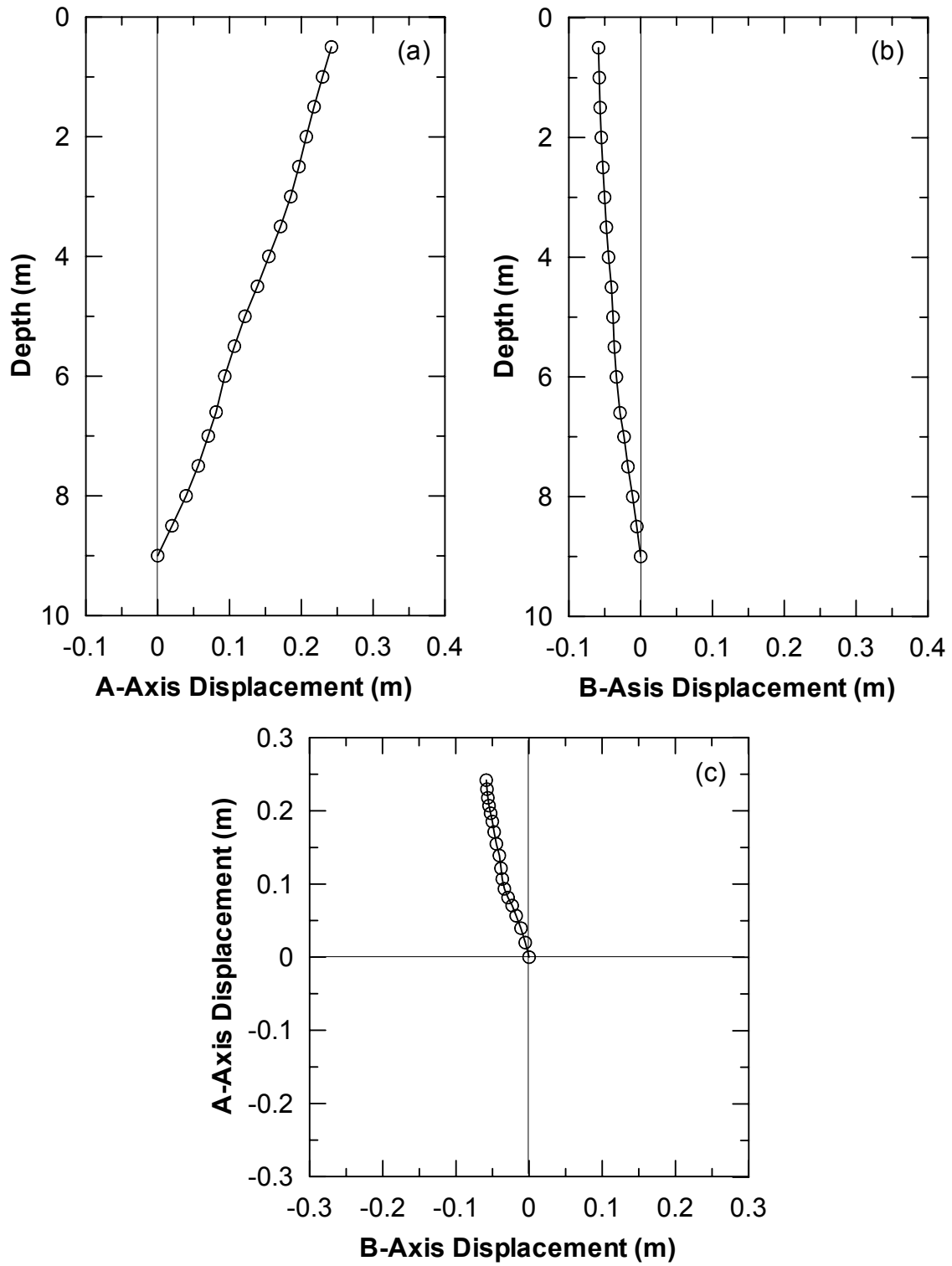


Fig. F.7 Soil displacement from inclinometer Casing S8 (a) section view A-direction, (b) section view B-direction, and (c) plan view

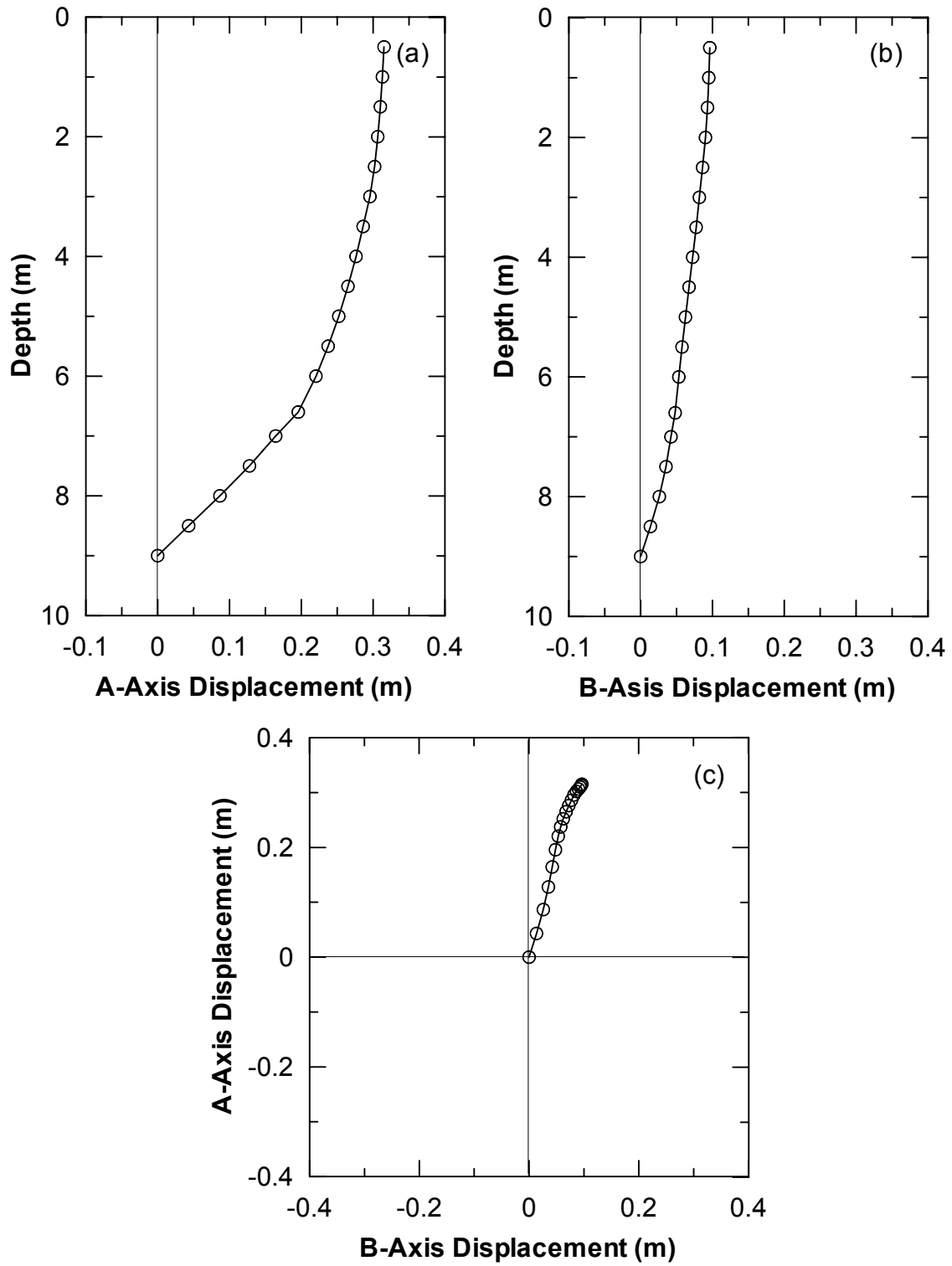


Fig. F.8 Soil displacement from inclinometer Casing S9 (a) section view A-direction, (b) section view B-direction, and (c) plan view

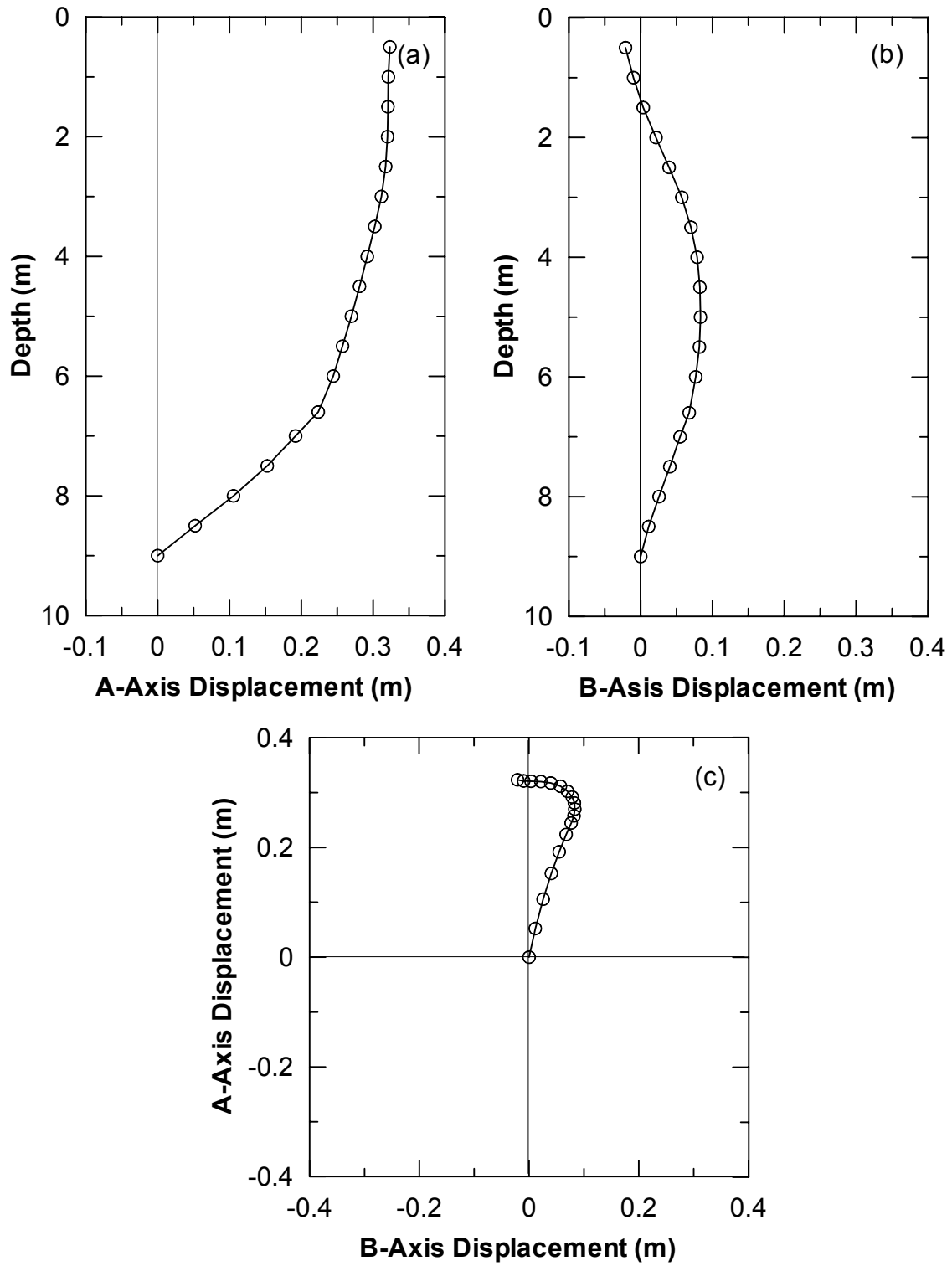


Fig. F.9 Soil displacement from inclinometer Casing S10 (a) section view A-direction, (b) section view B-direction, and (c) plan view

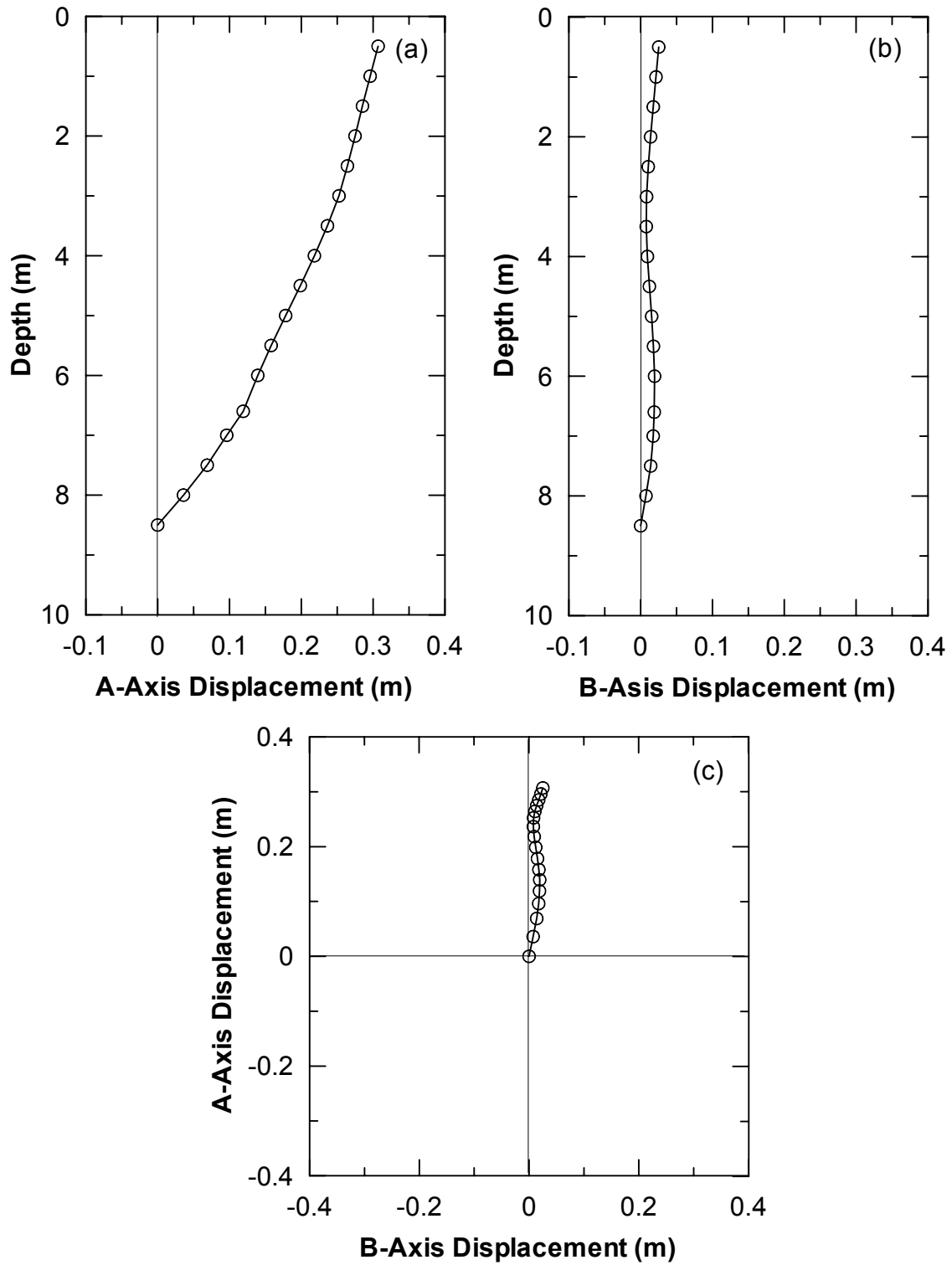


Fig. F.10 Soil displacement from inclinometer Casing S11 (a) section view A-direction, (b) section view B-direction, and (c) plan view

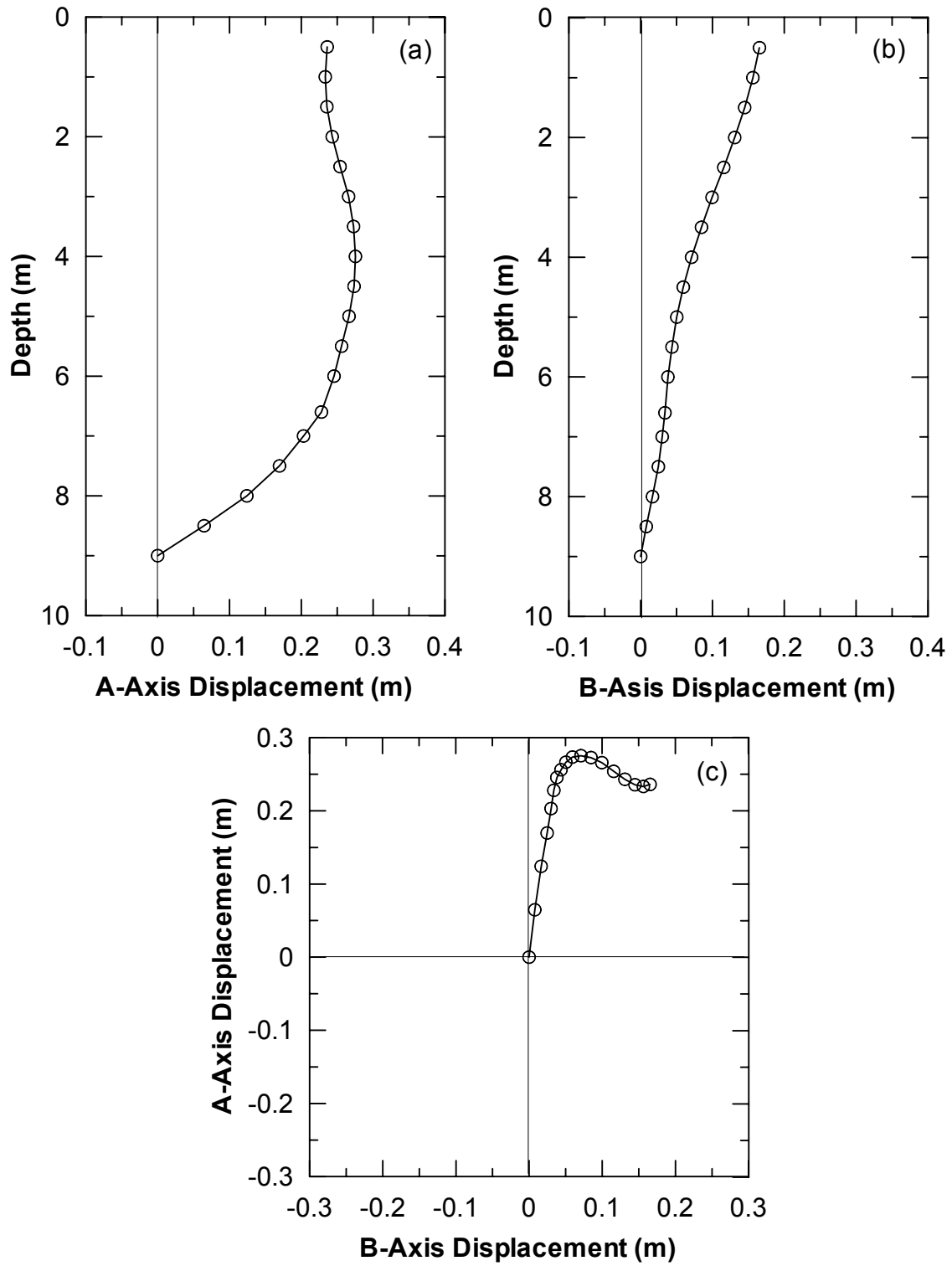


Fig. F.11 Soil displacement from inclinometer Casing S12 (a) section view a-direction, (b) section view b-direction, and (c) plan view

Appendix G: Strain Gage Data (First Test)

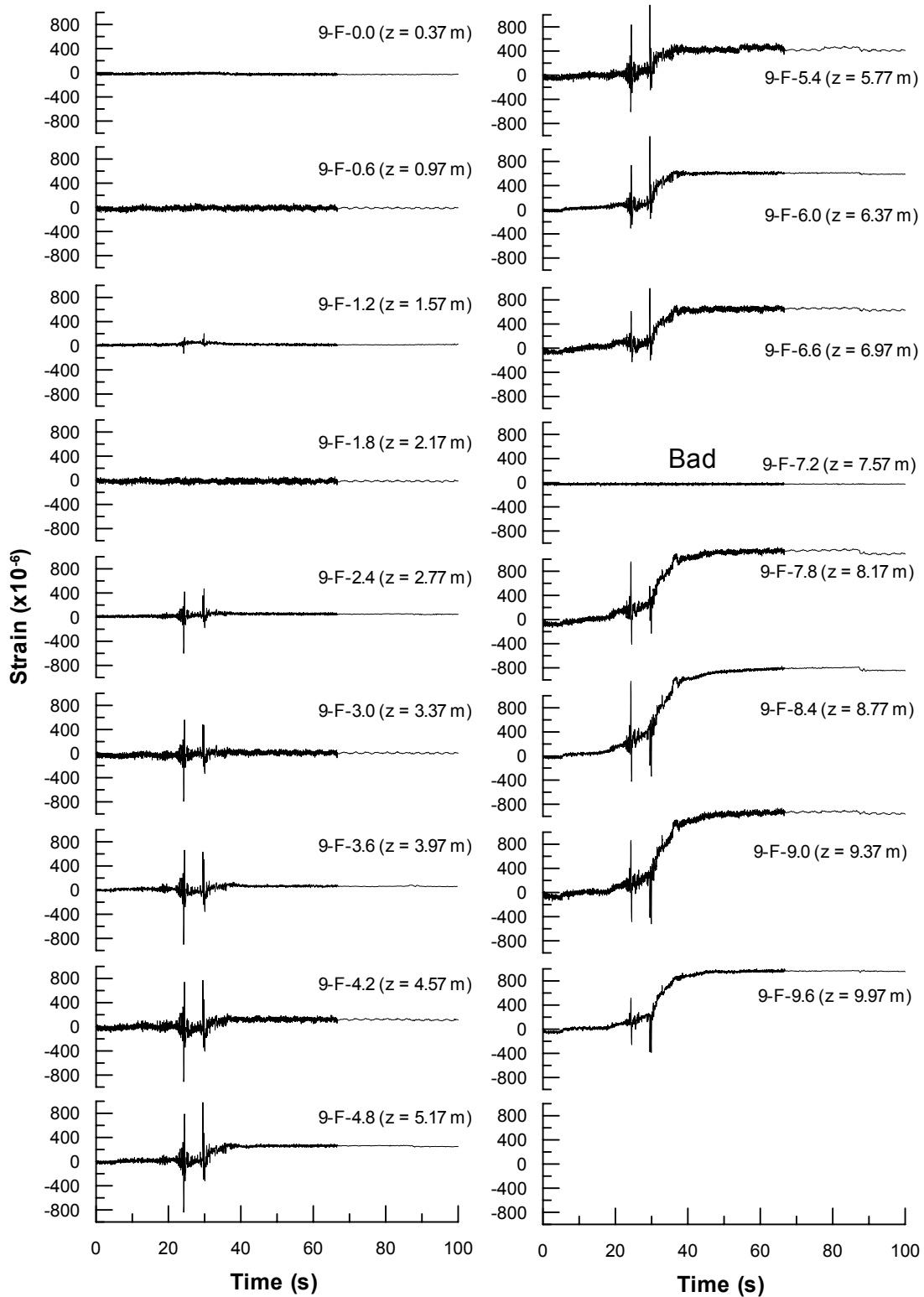


Fig. G.1 Time histories of strain along single pile (No. 9) at front side

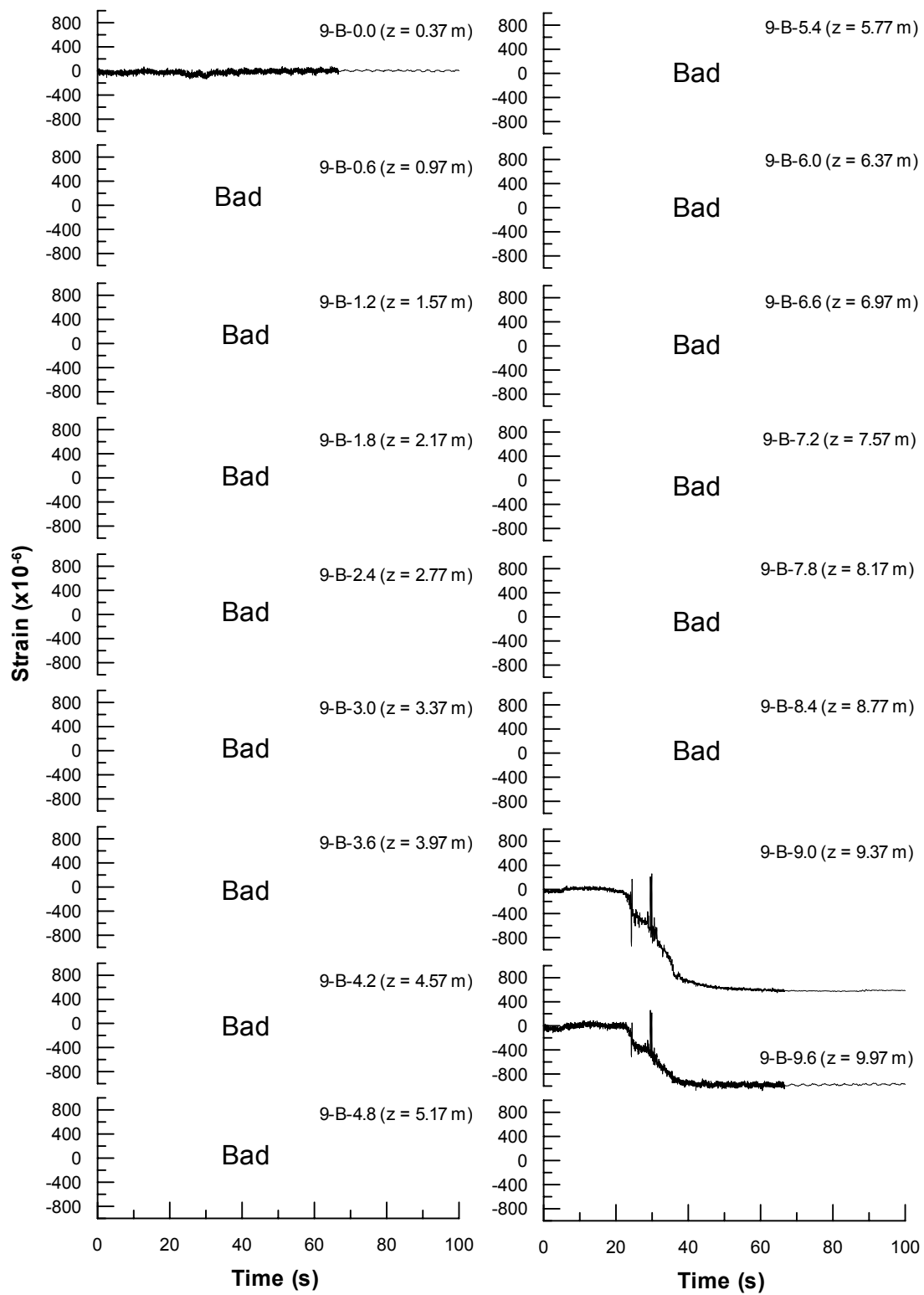


Fig. G.2 Time histories of strain along single pile (No. 9) at back side

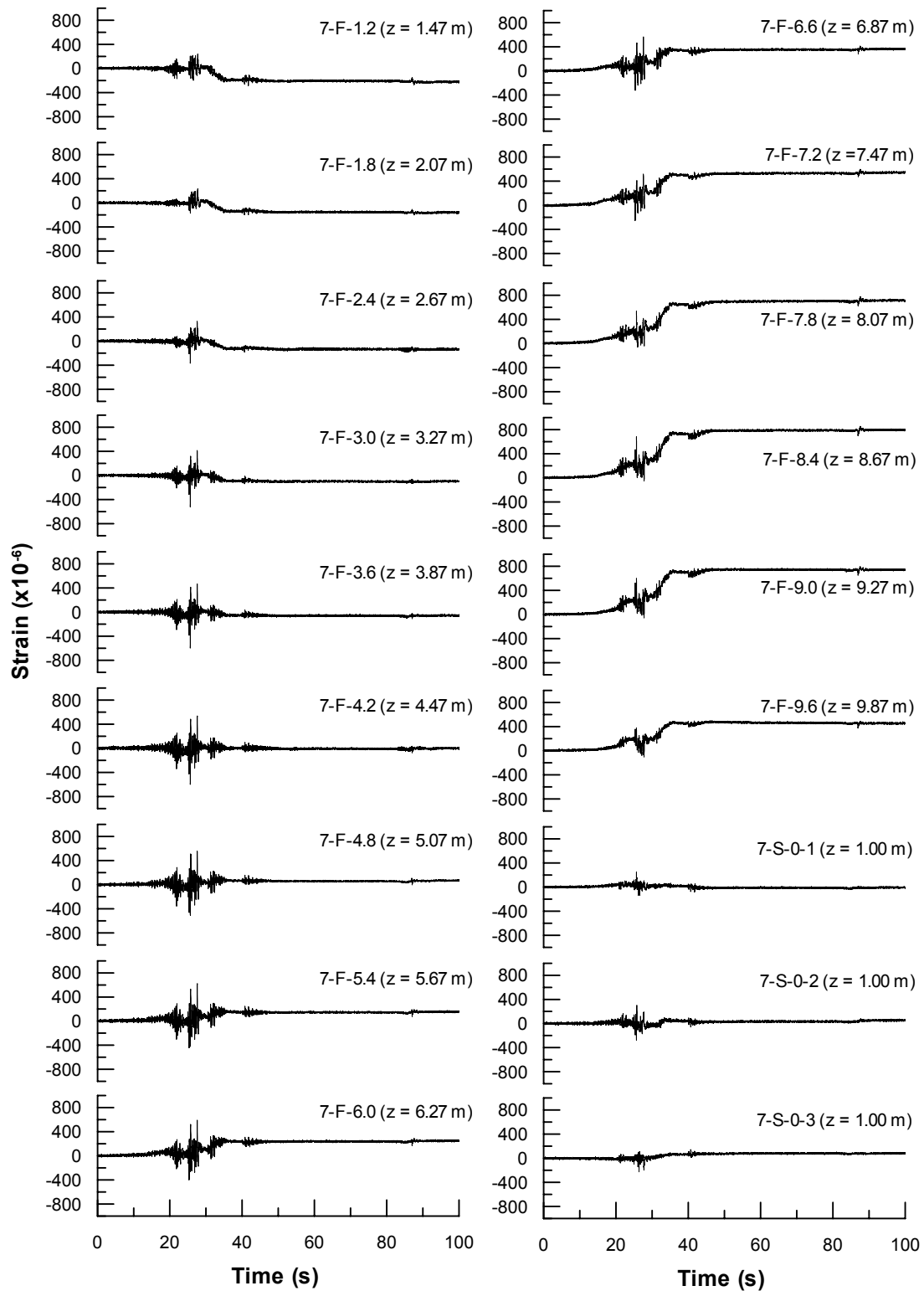


Fig. G.3 Time histories of strain along pile No. 7 of 4-pile group at front side

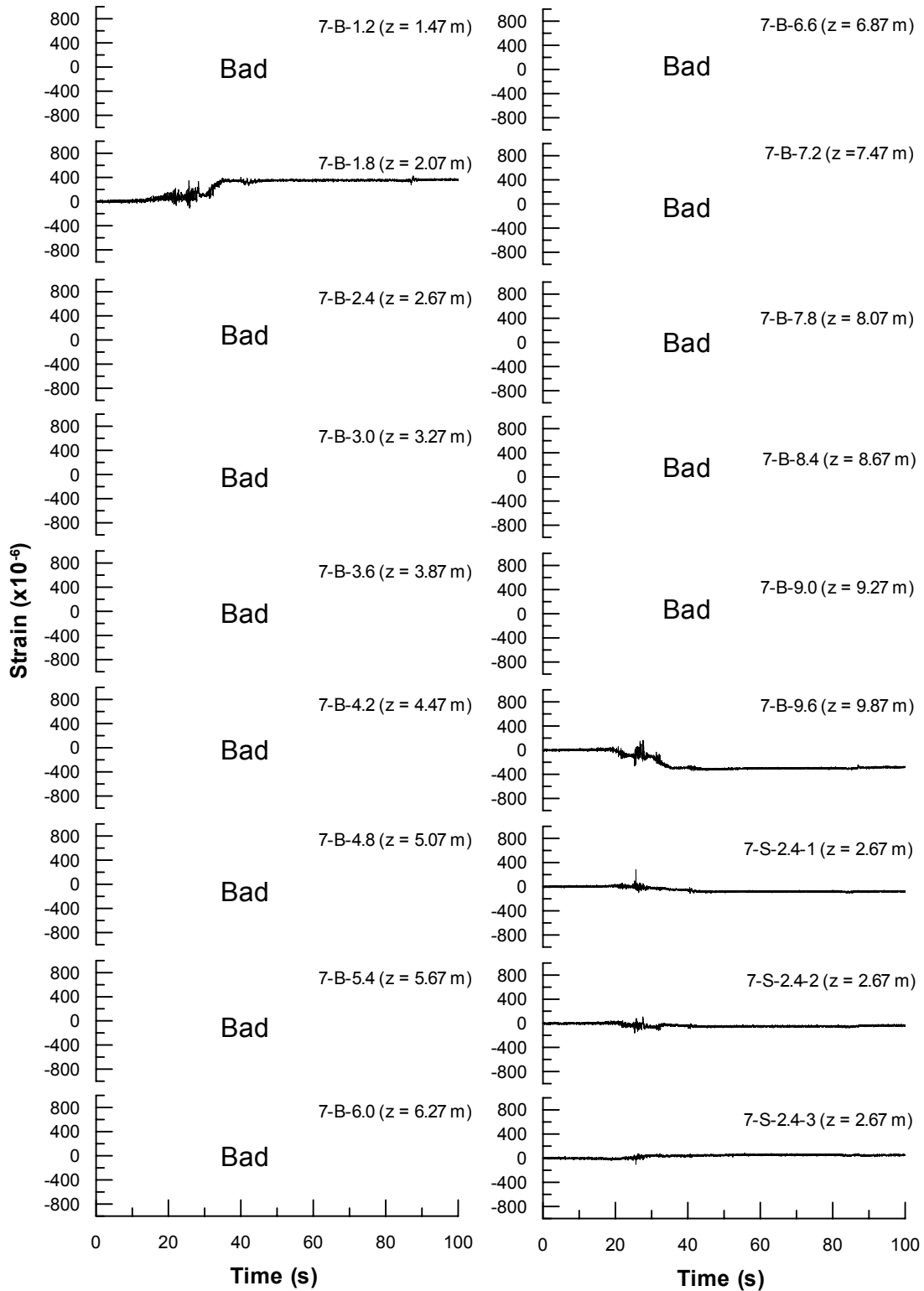


Fig. G.4 Time histories of strain along pile No. 7 of 4-pile group at back side

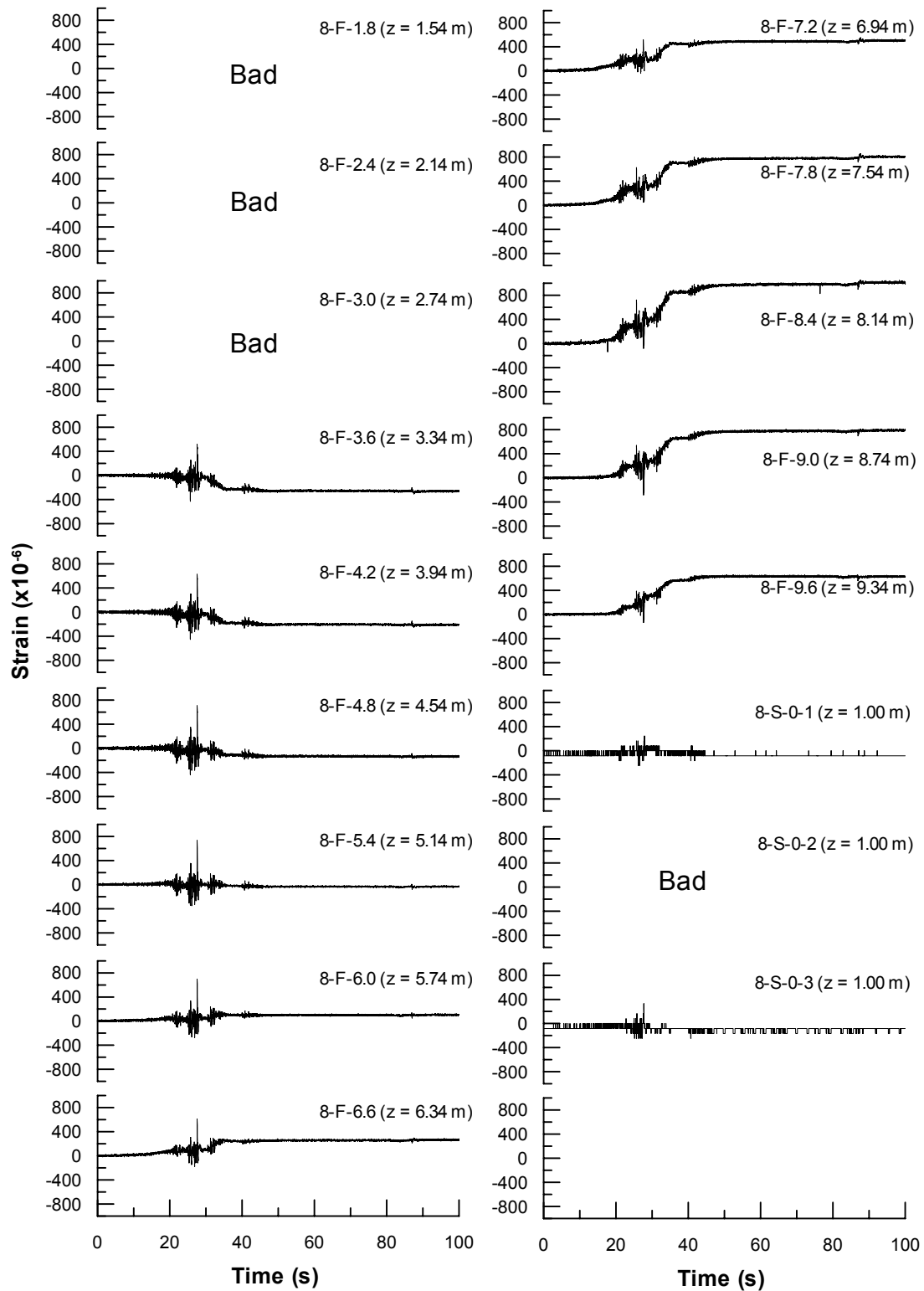


Fig. G.5 Time histories of strain along pile No. 8 of 4-pile group at front side

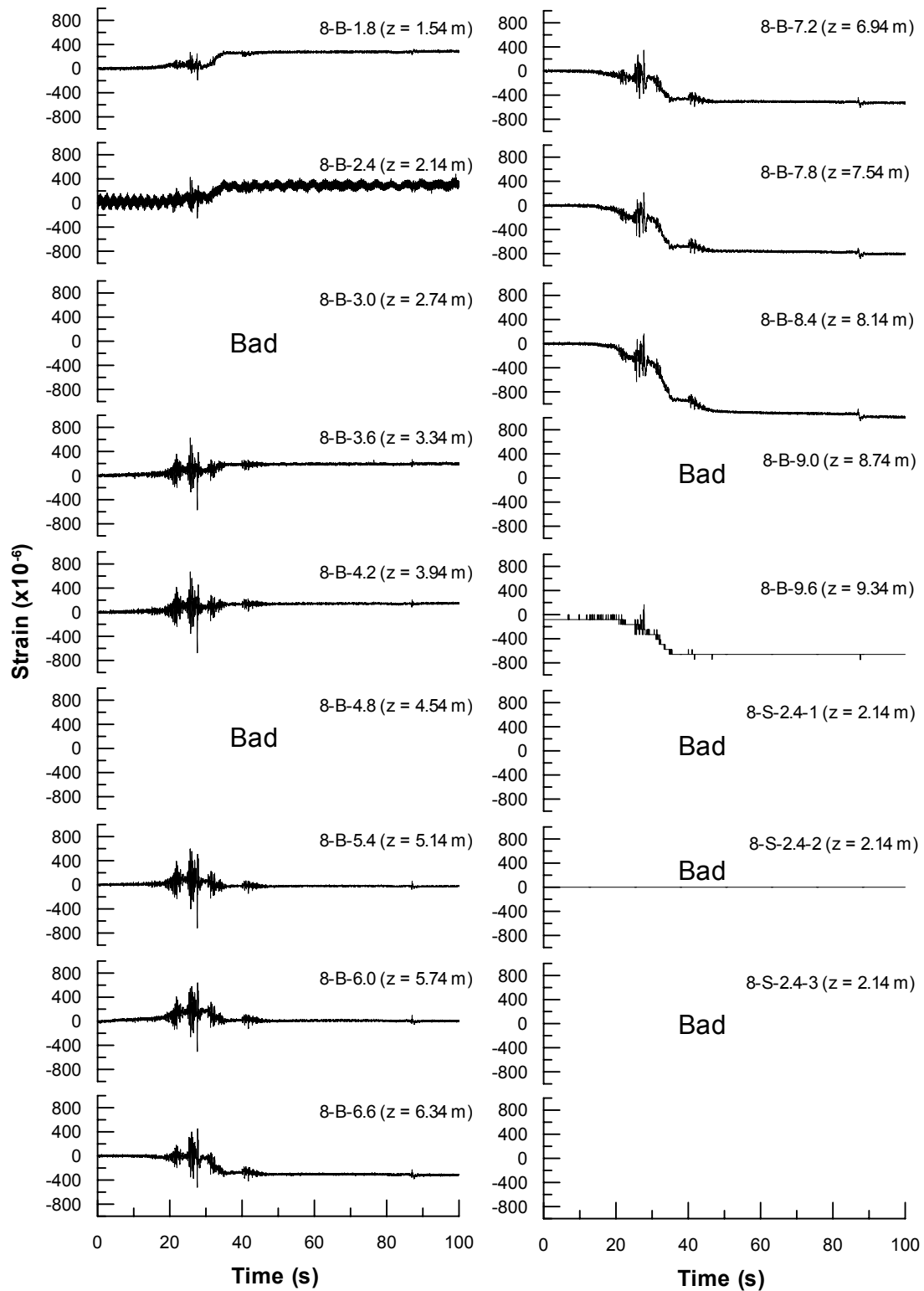


Fig. G.6 Time histories of strain along pile No. 8 of 4-pile group at back side

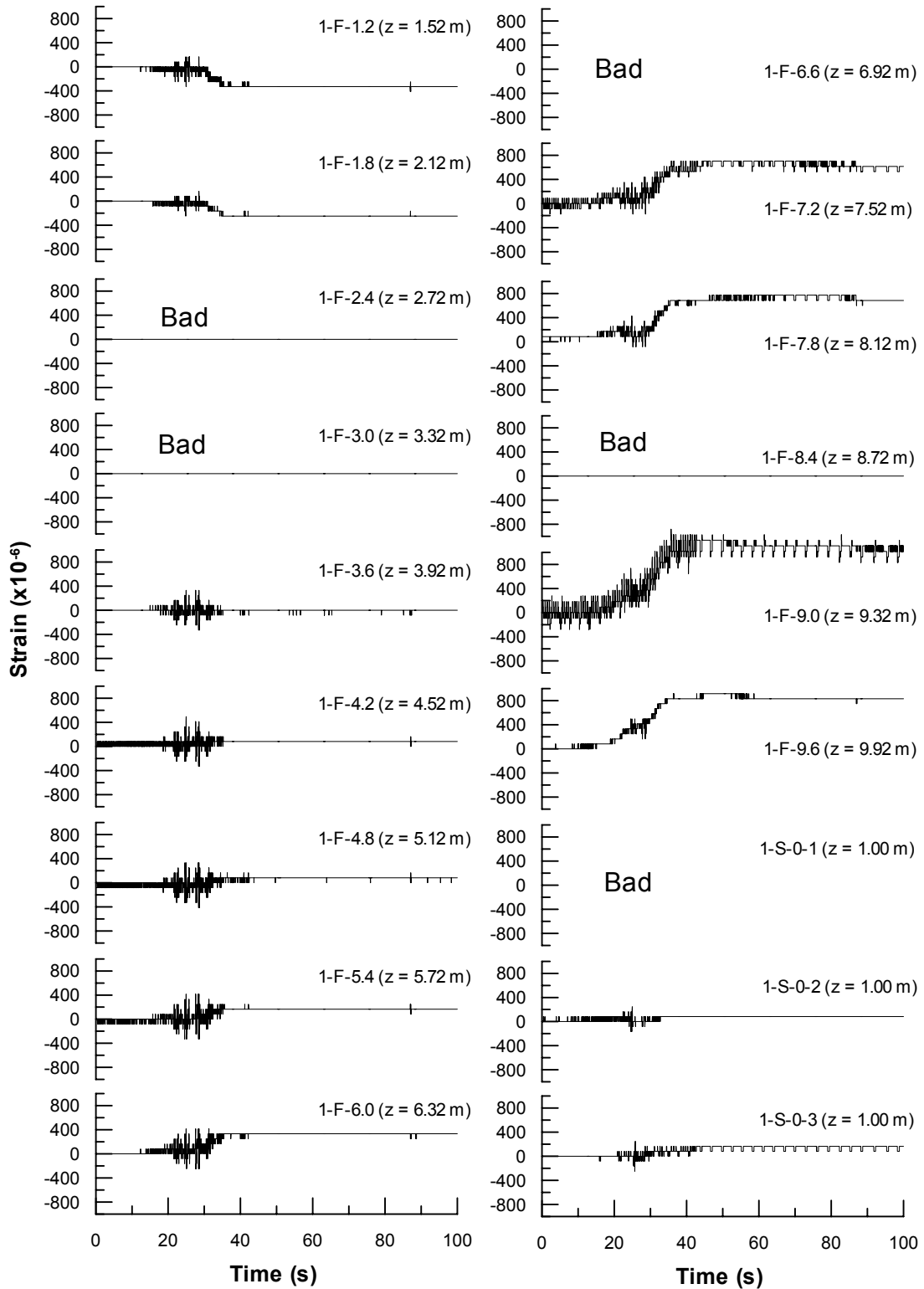


Fig. G.7 Time histories of strain along pile No. 1 of 9-Pile group at front side

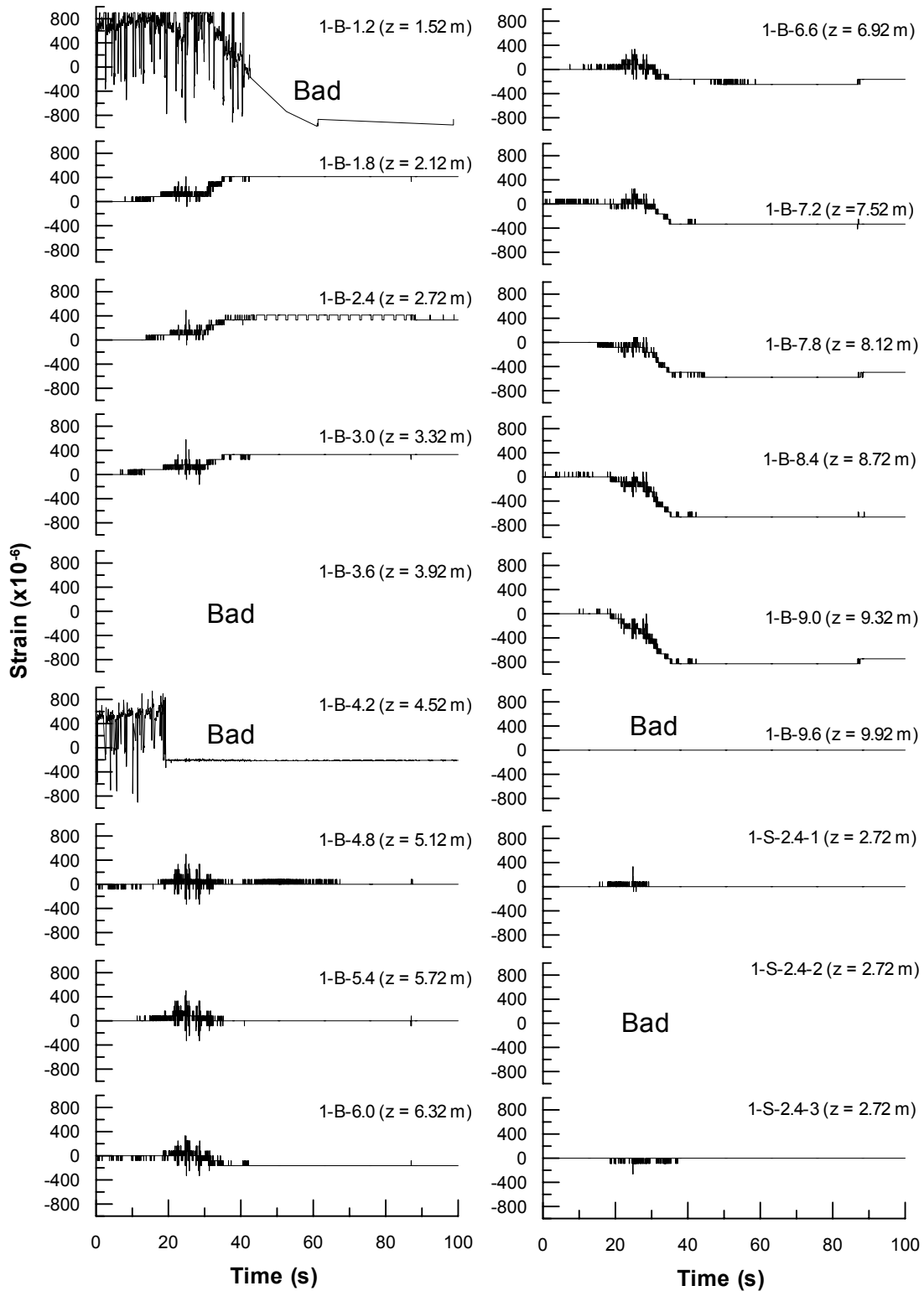


Fig. G.8 Time histories of strain along pile No. 1 of 9-pile group at back side

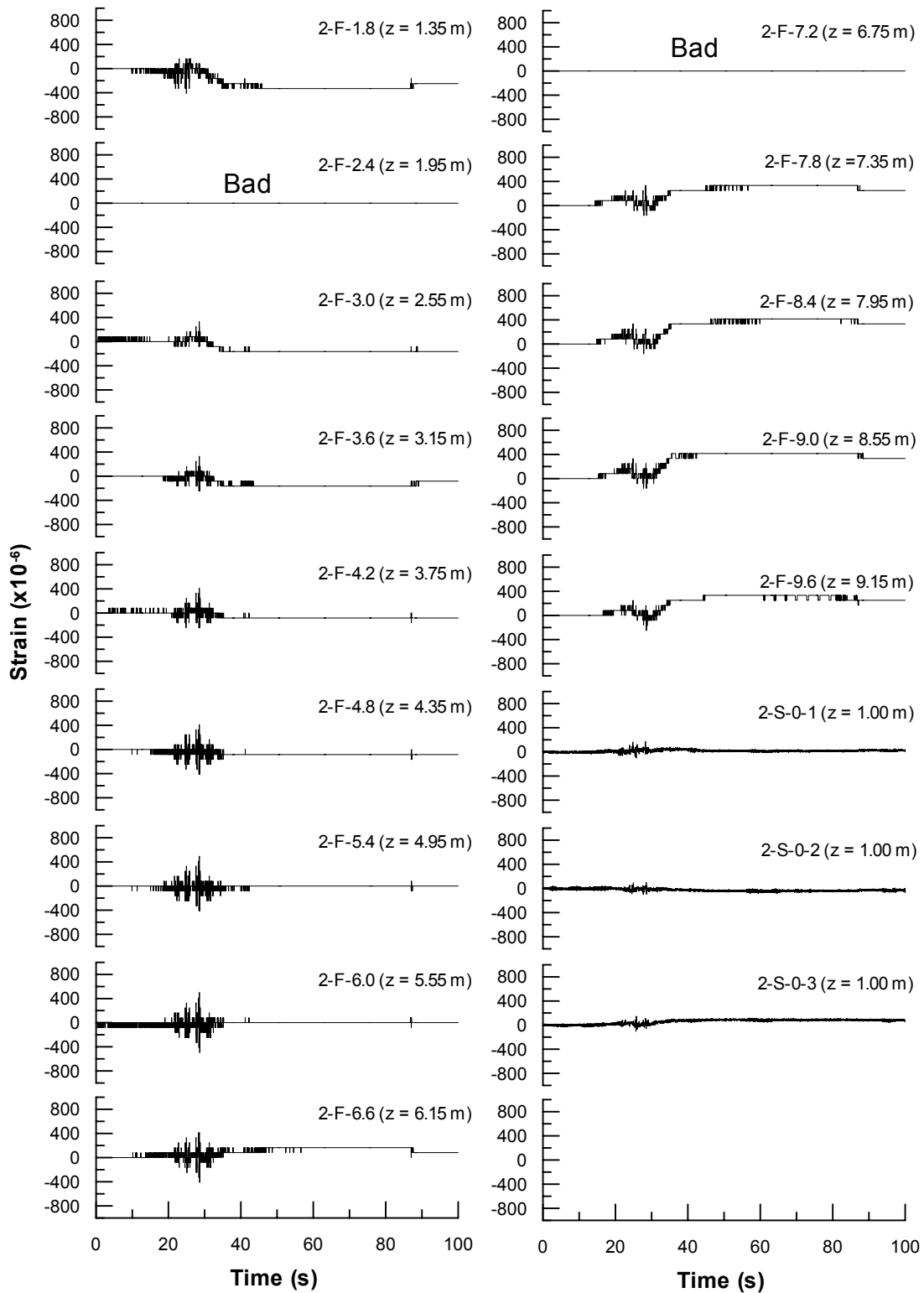


Fig. G.9 Time histories of strain along pile No. 2 of 9-pile group at front side

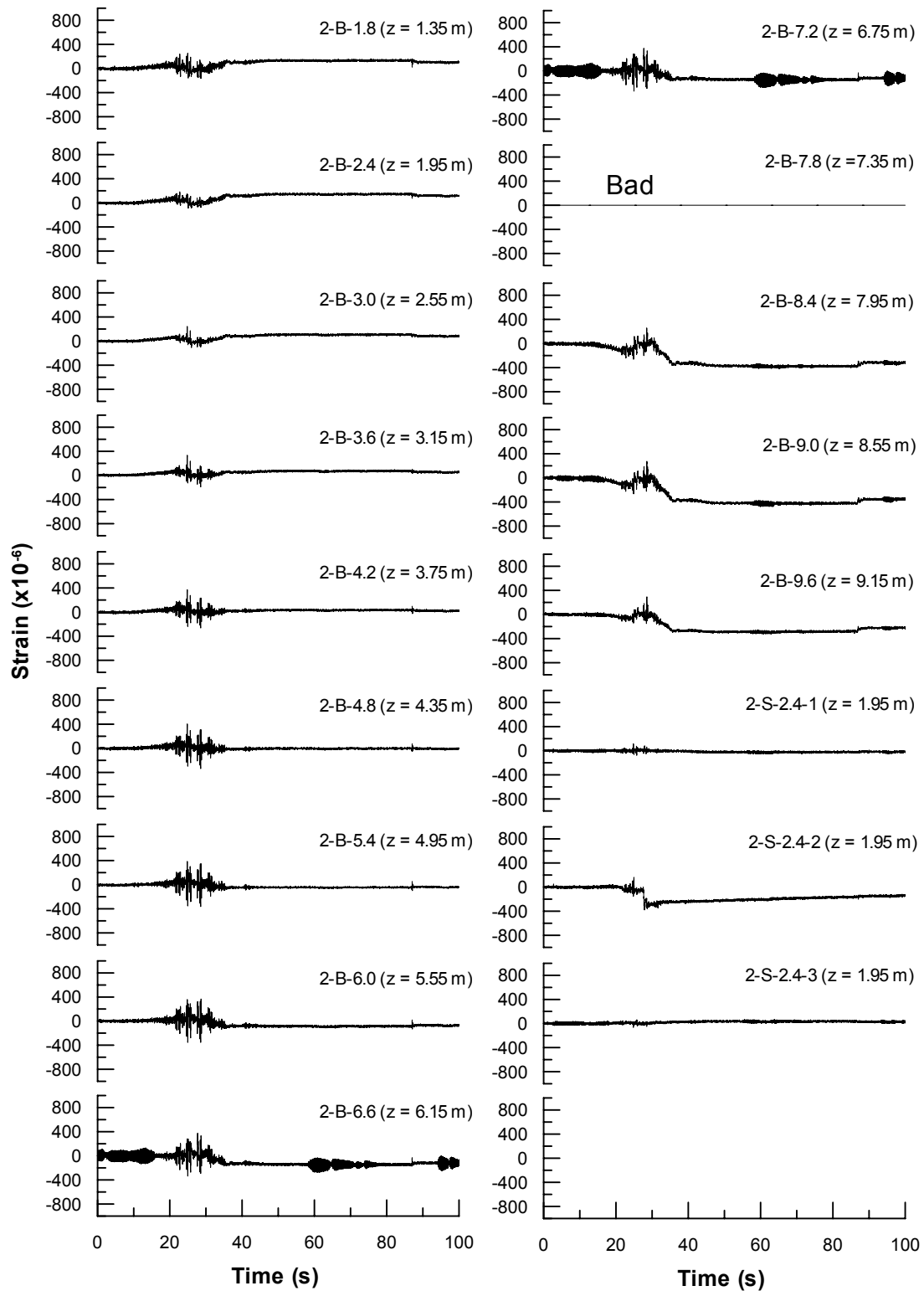


Fig. G.10 Time histories of strain along pile No. 2 of 9-pile group at back side

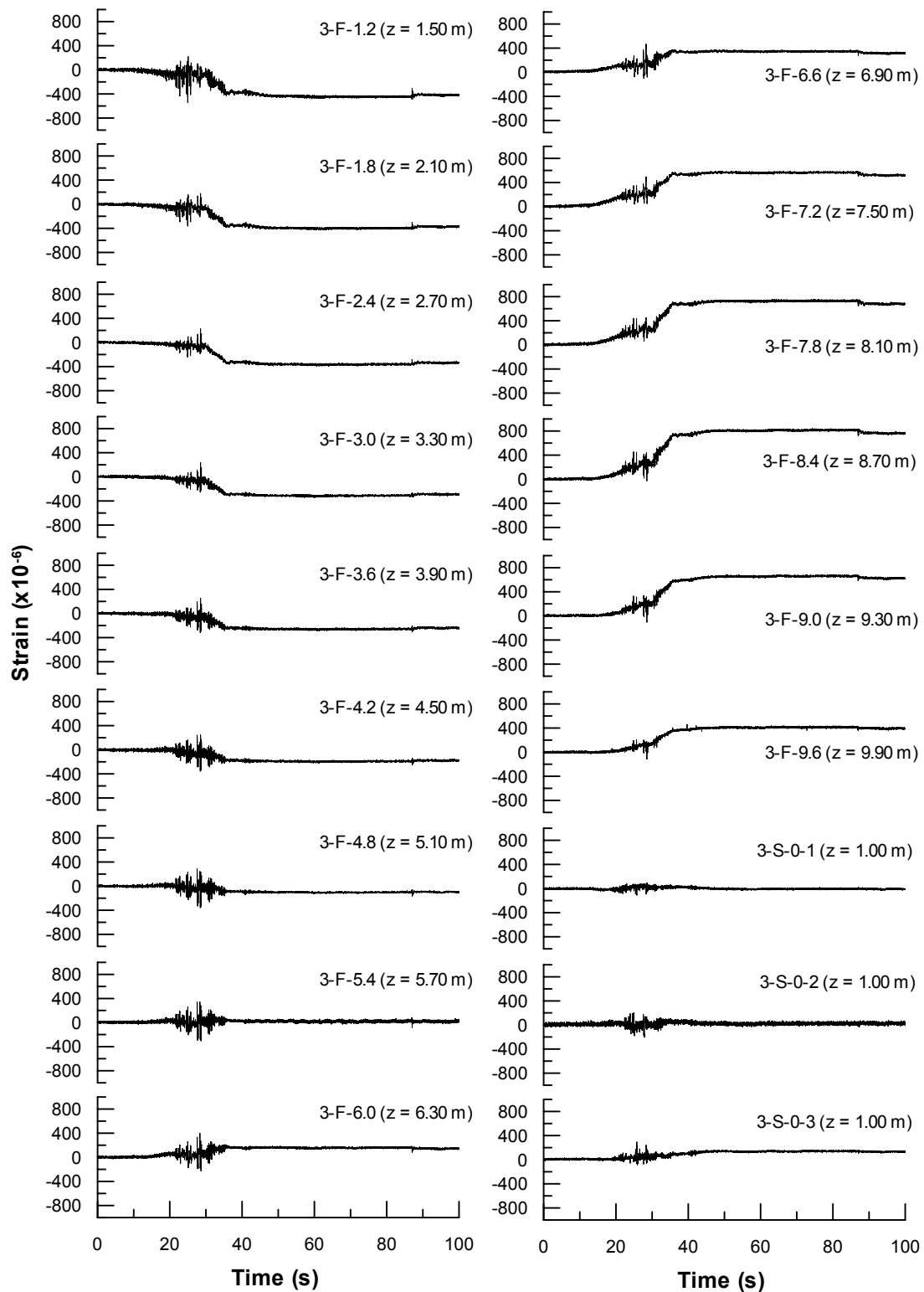


Fig. G.11 Time histories of strain along pile No. 3 of 9-pile group at front side

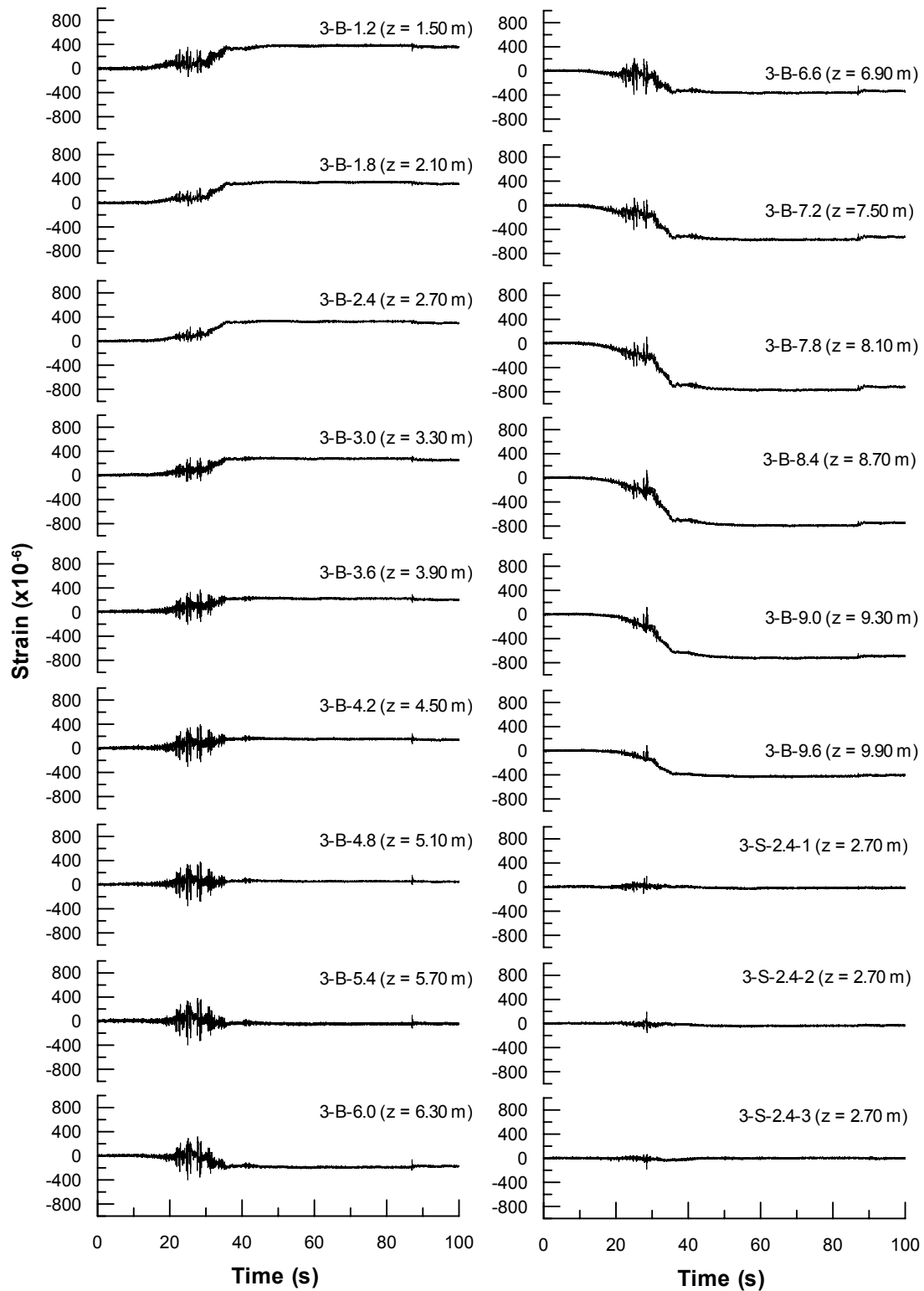


Fig. G.12 Time histories of strain along pile No. 3 of 9-pile group at back side

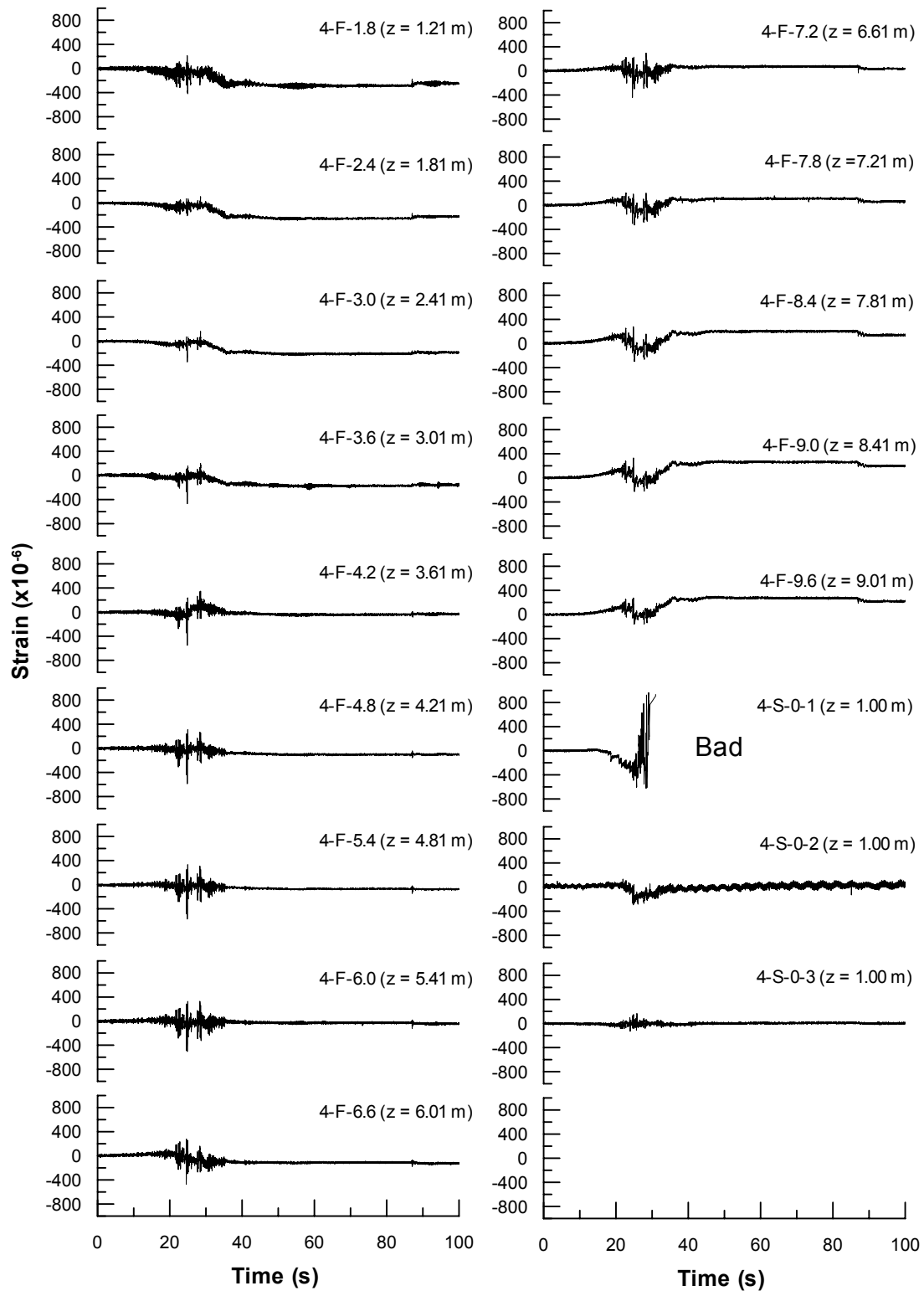


Fig. G.13 Time histories of strain along pile No. 4 of 9-pile group at front side

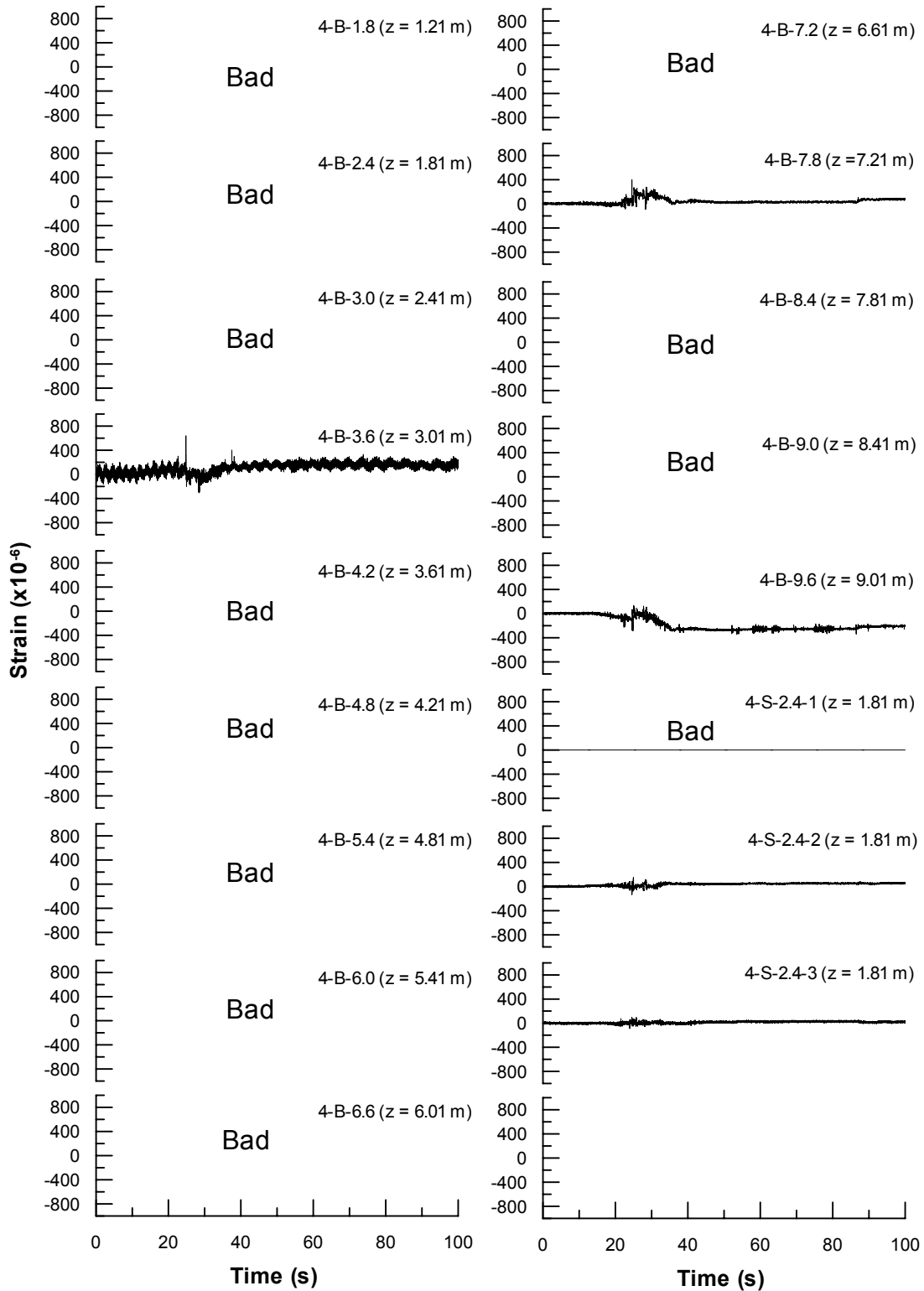


Fig. G.14 Time histories of strain along pile No. 4 of 9-pile group at back side

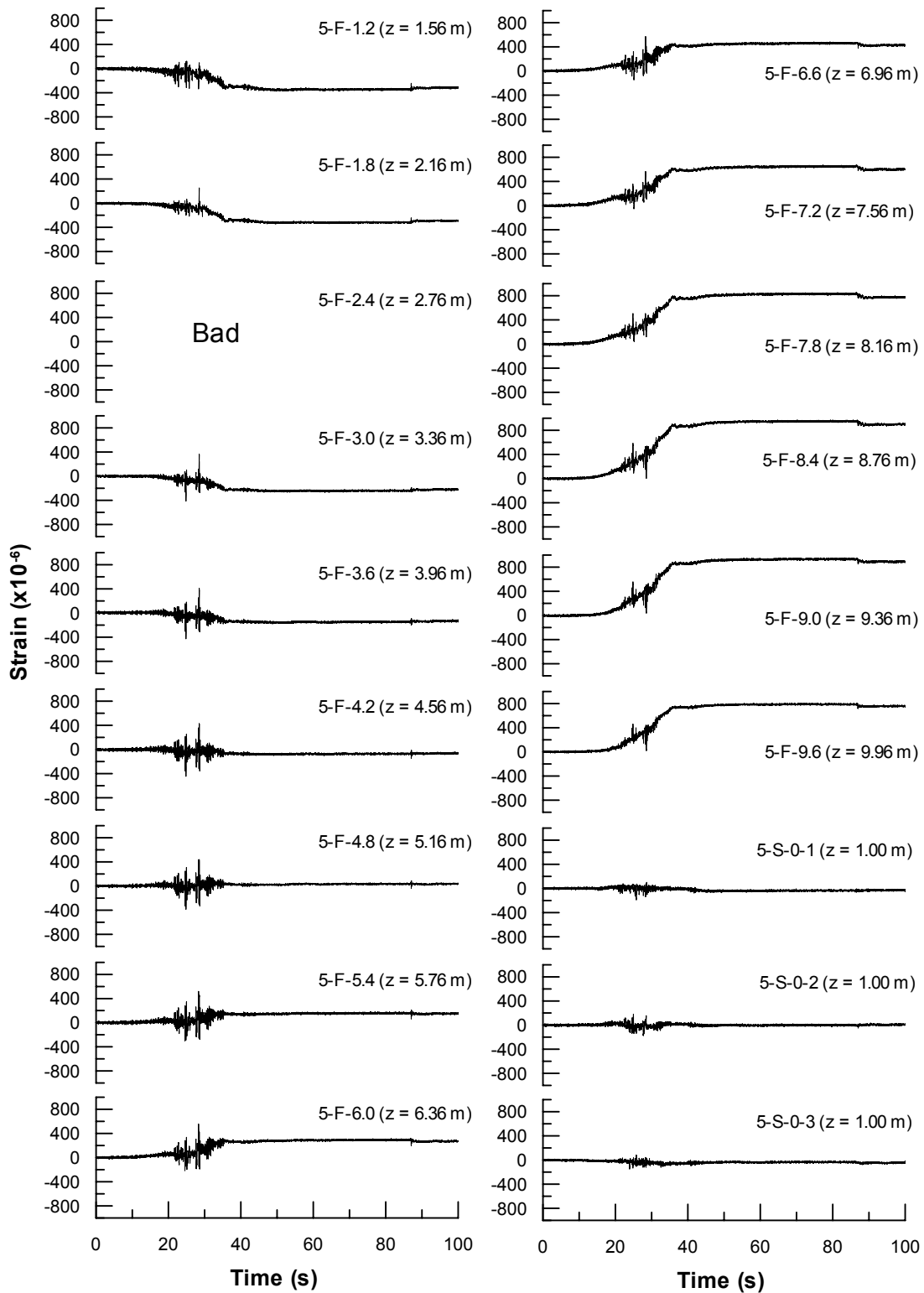


Fig. G.15 Time histories of strain along pile No. 5 of 9-pile group at front side

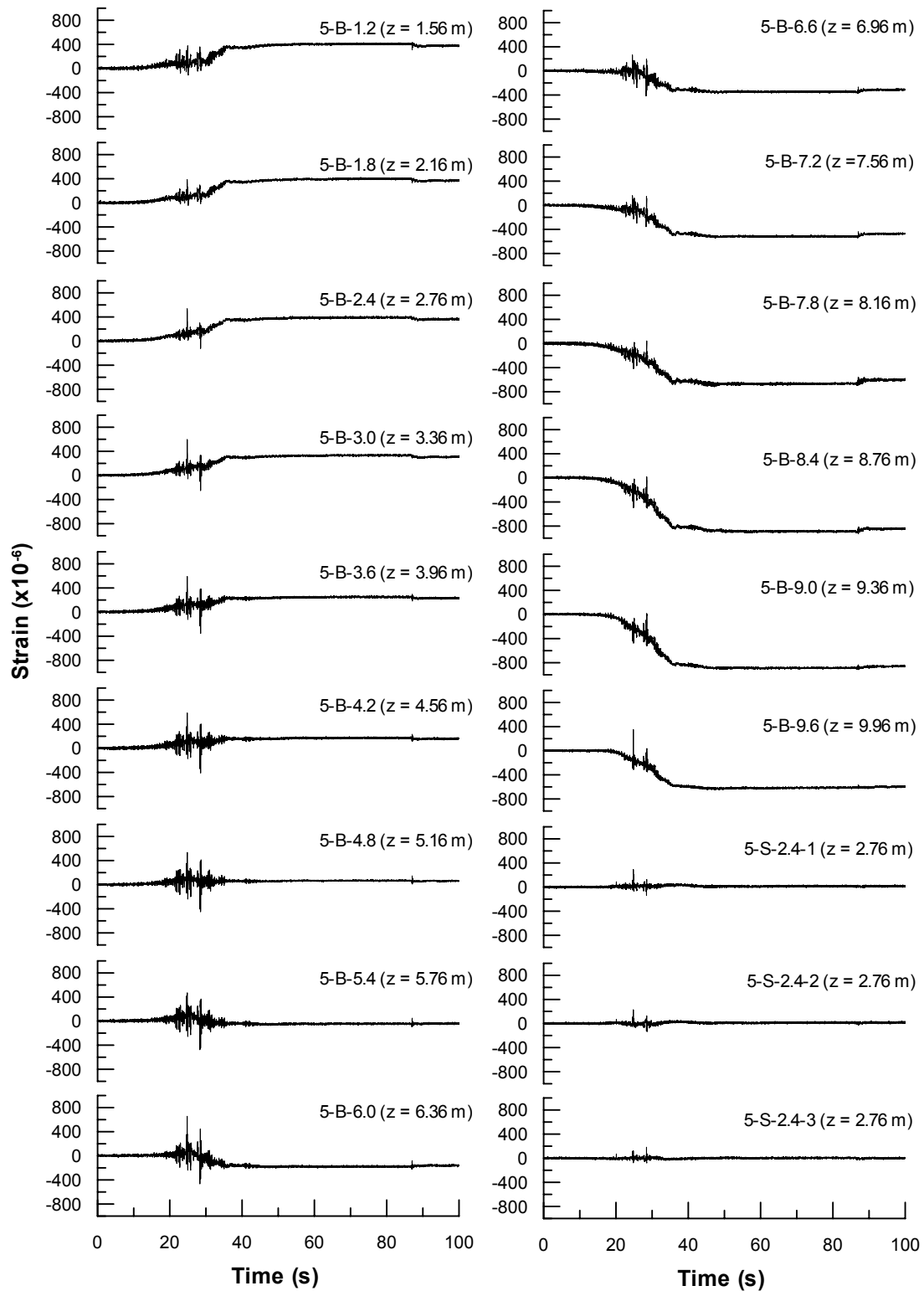


Fig. G.16 Time histories of strain along pile No. 5 of 9-pile group at back side

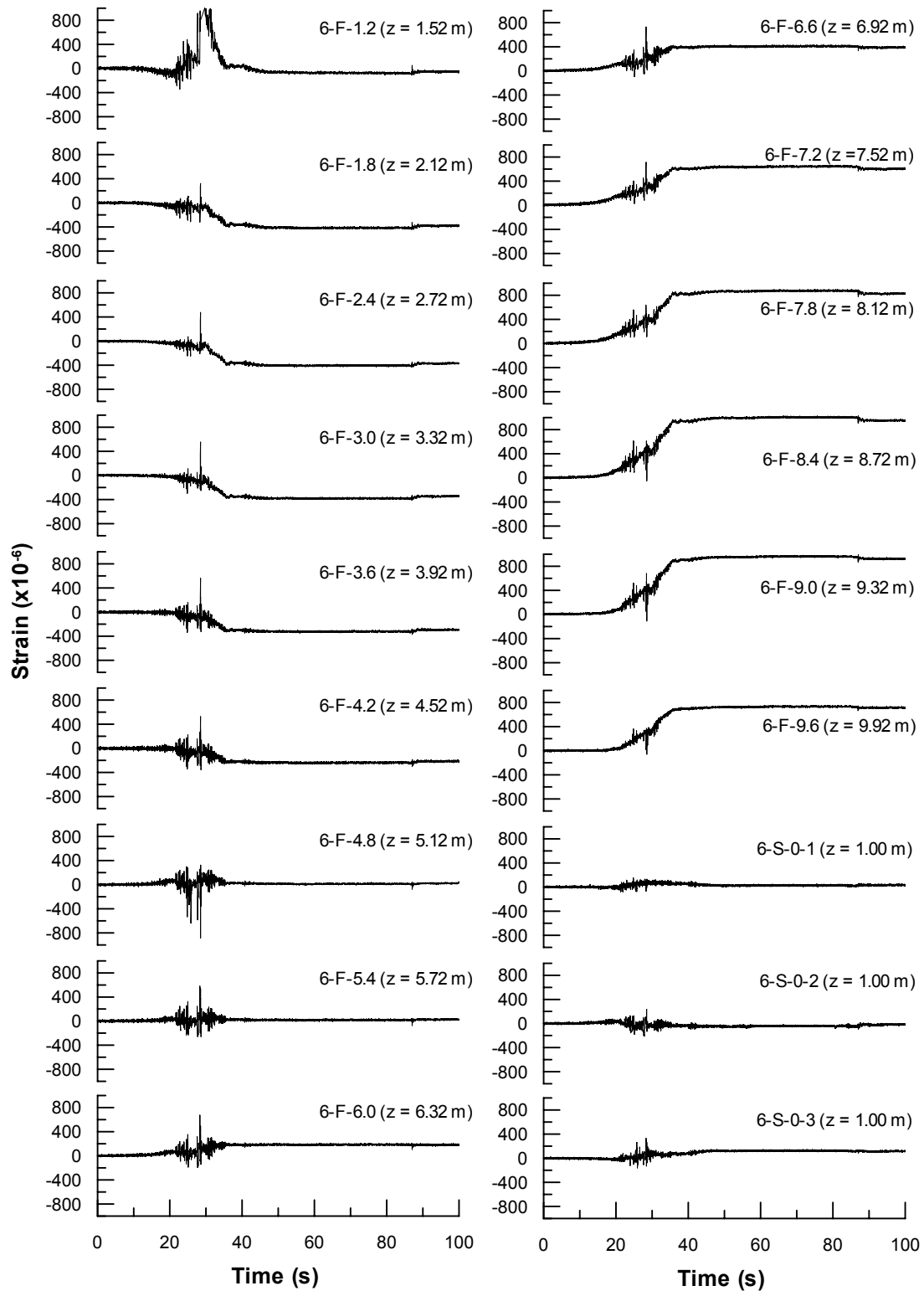


Fig. G.17 Time histories of strain along pile No. 6 of 9-pile group at front side

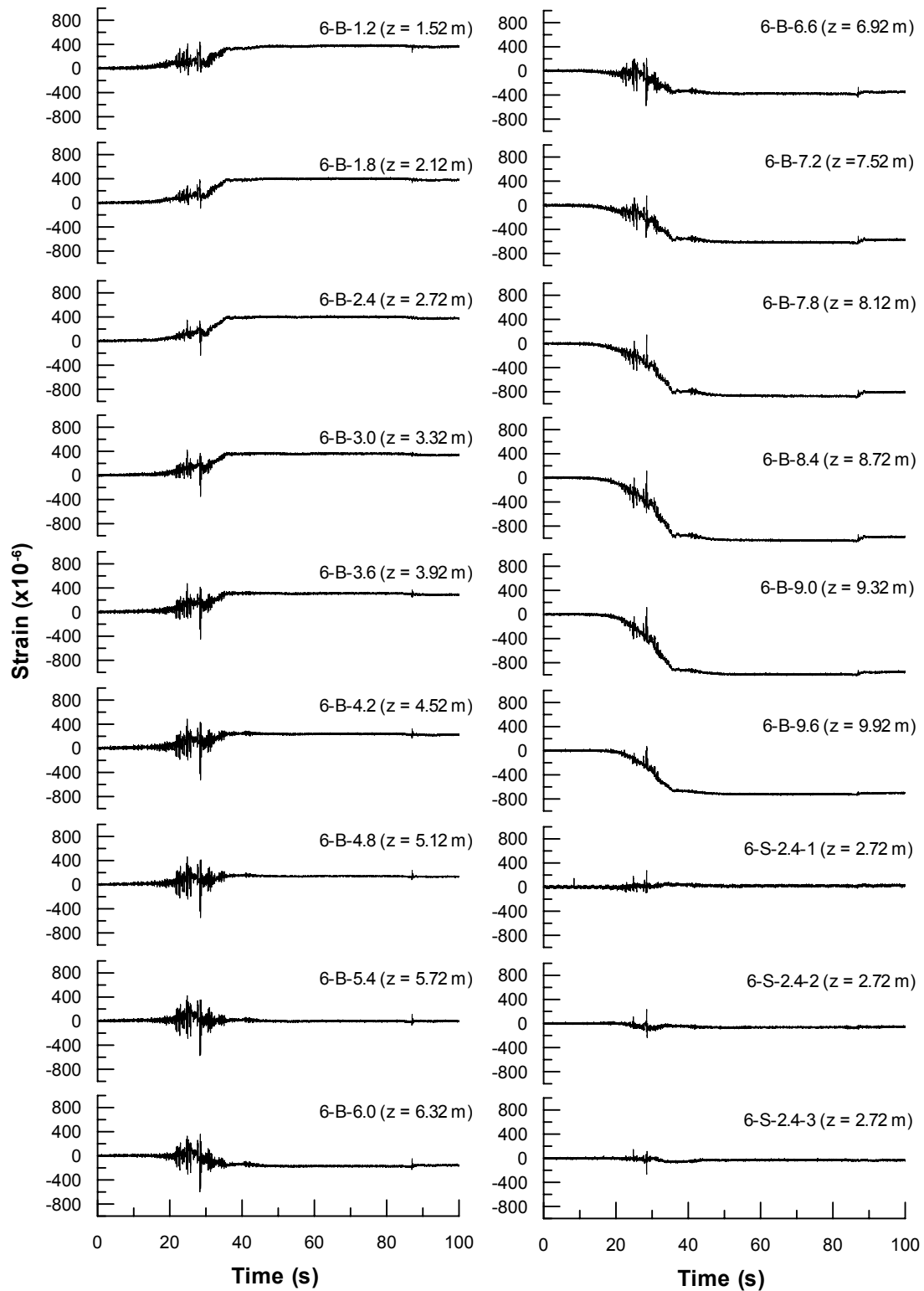


Fig. G.18 Time histories of strain along pile No. 6 of 9-pile group at back side

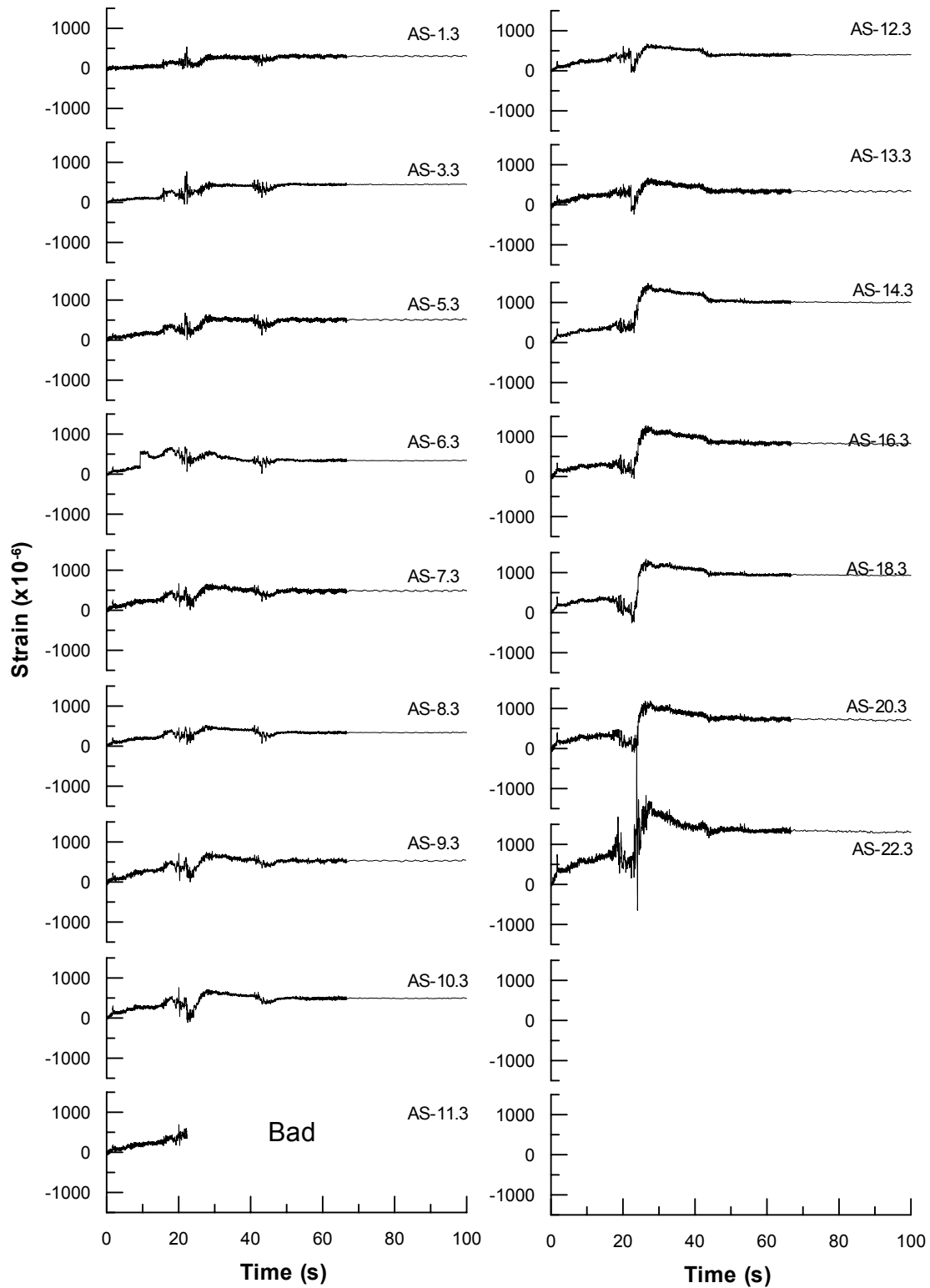


Fig. G.19 Time histories of strain along transverse pipeline A (side)

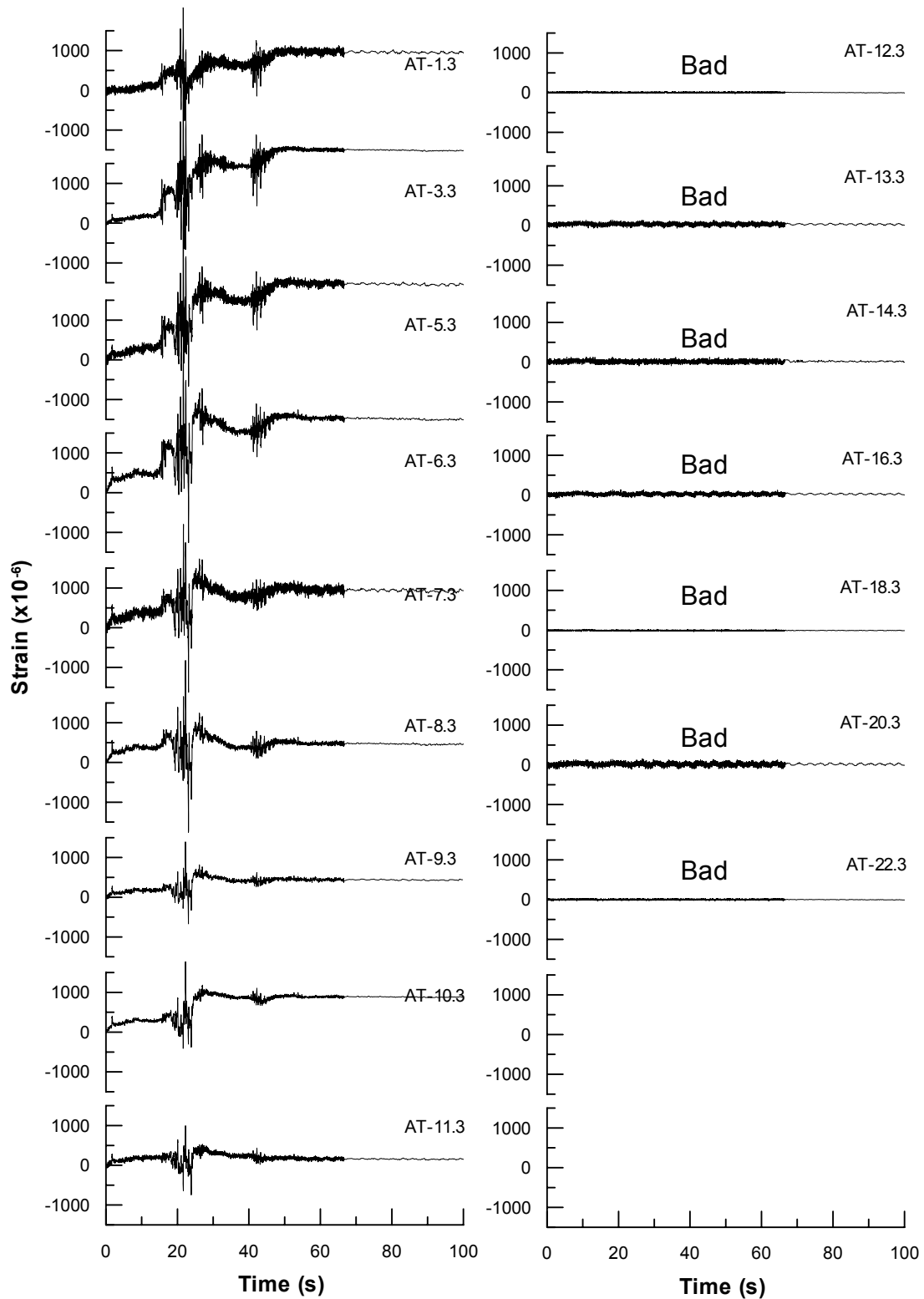


Fig. G.20 Time histories of strain along transverse pipeline A (top)

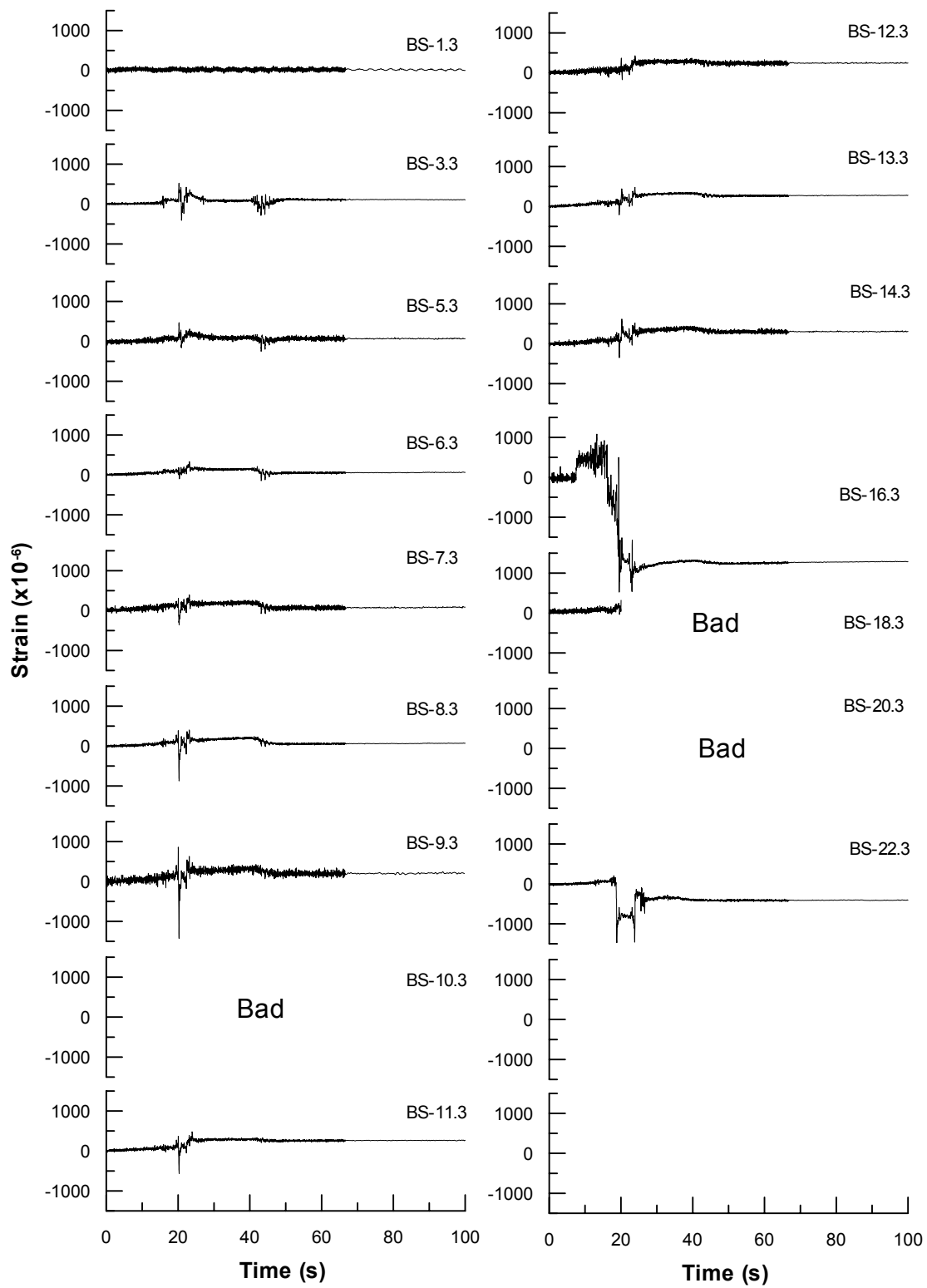


Fig. G.21 Time histories of strain along transverse pipeline B (side)

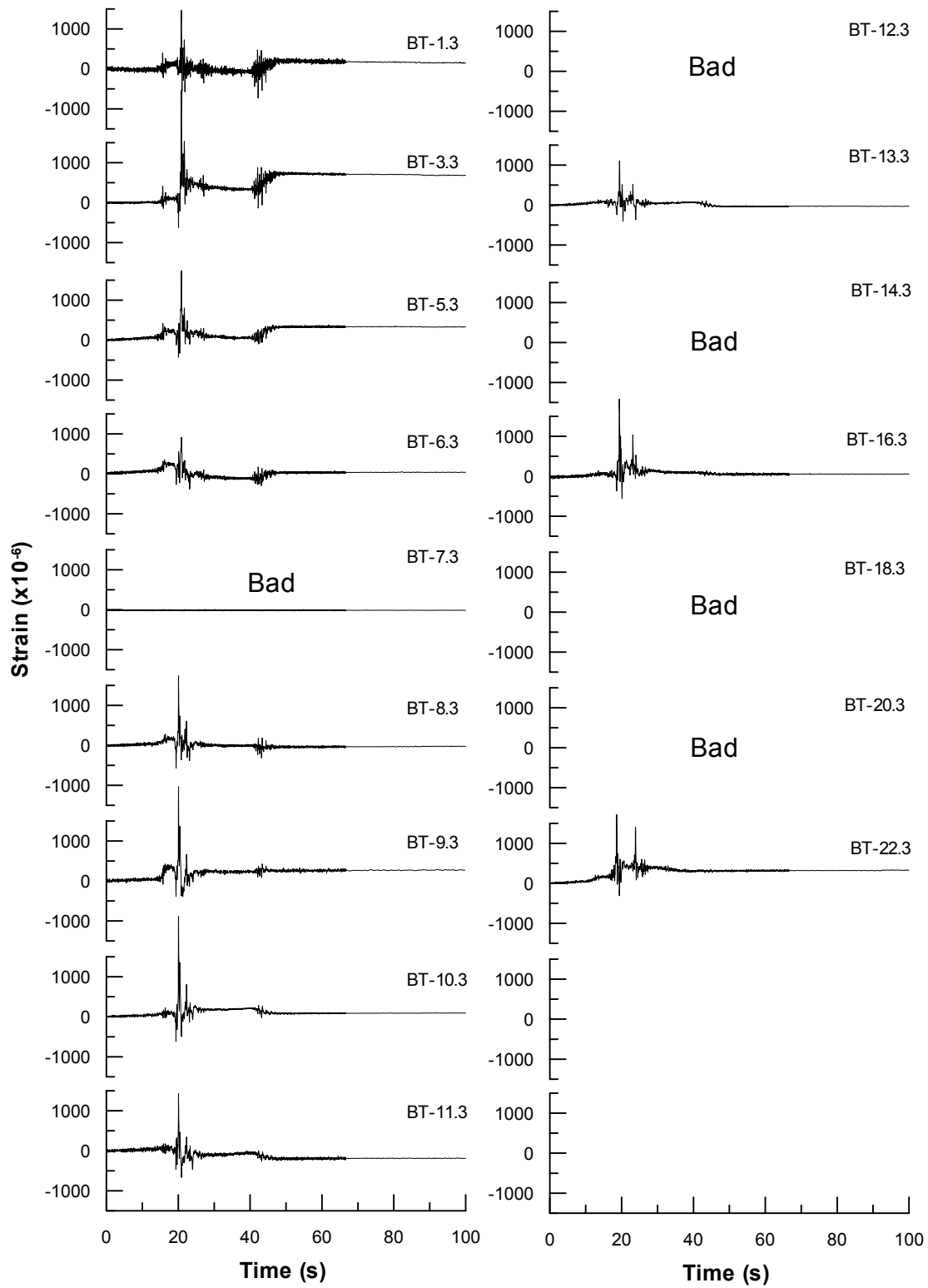


Fig. G.22 Time histories of strain along transverse pipeline B (top)

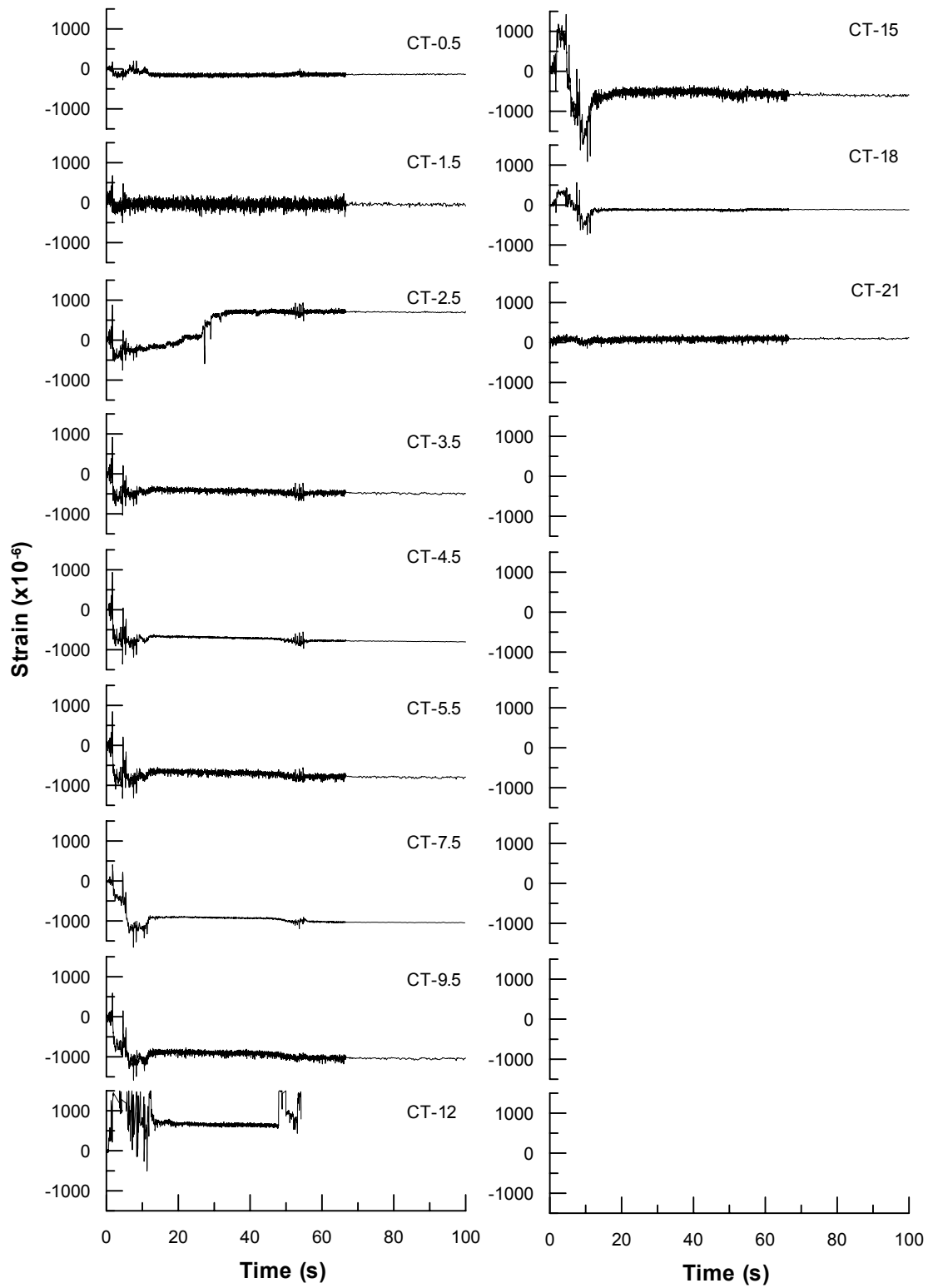


Fig. G.23 Time histories of strain along longitudinal pipeline C (top)

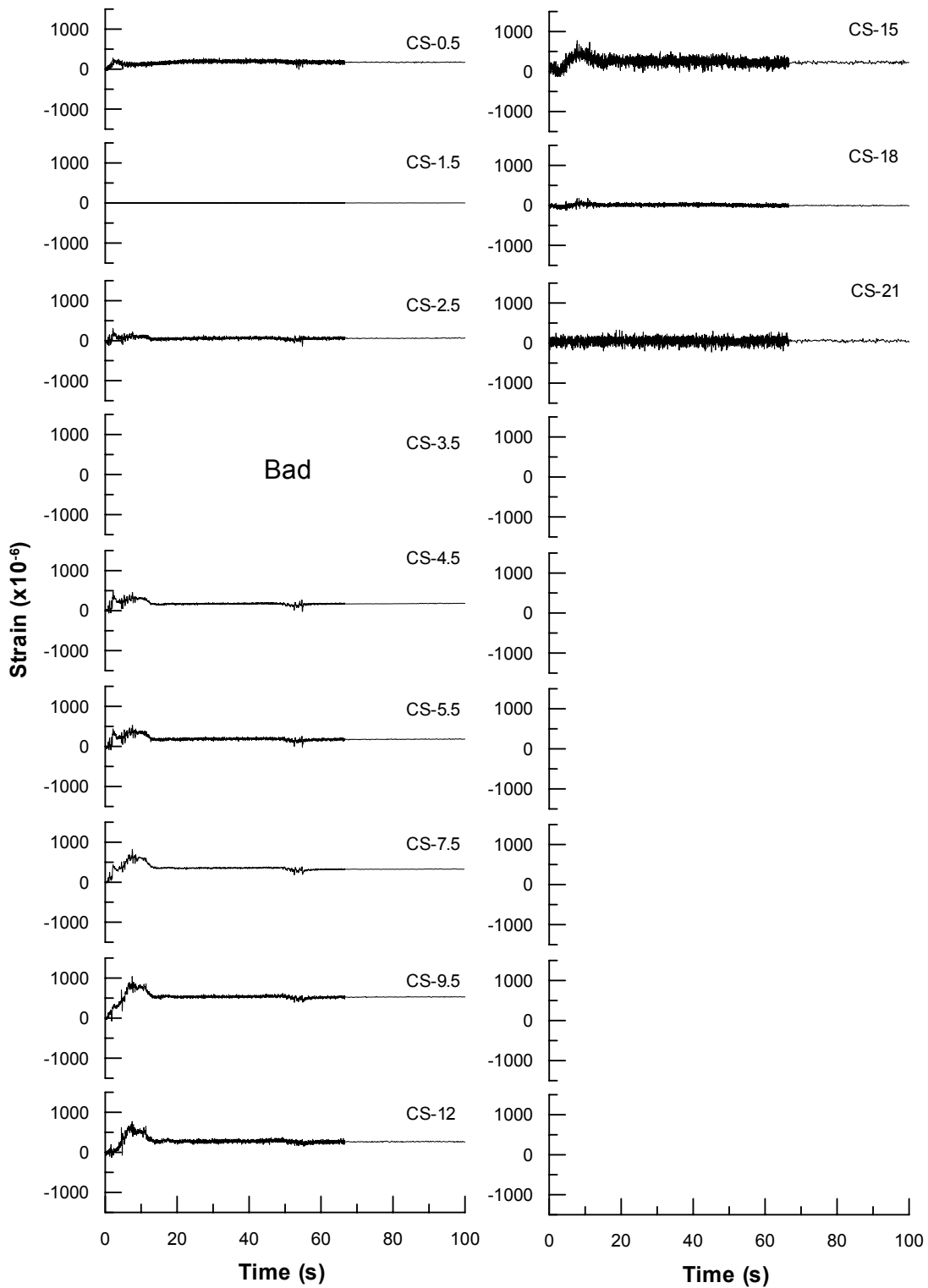


Fig. G.24 Time histories of strain along longitudinal pipeline C (Side)

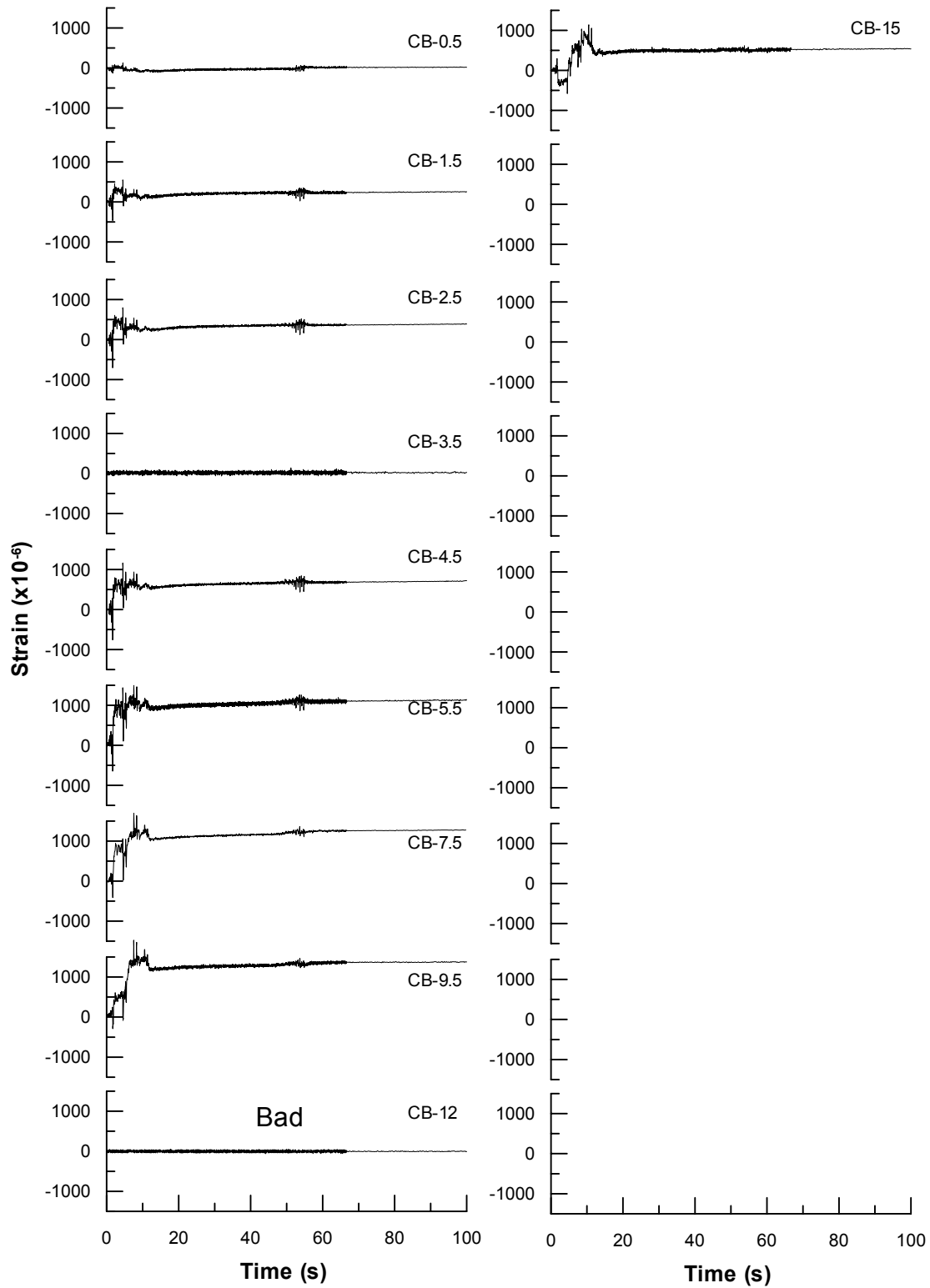
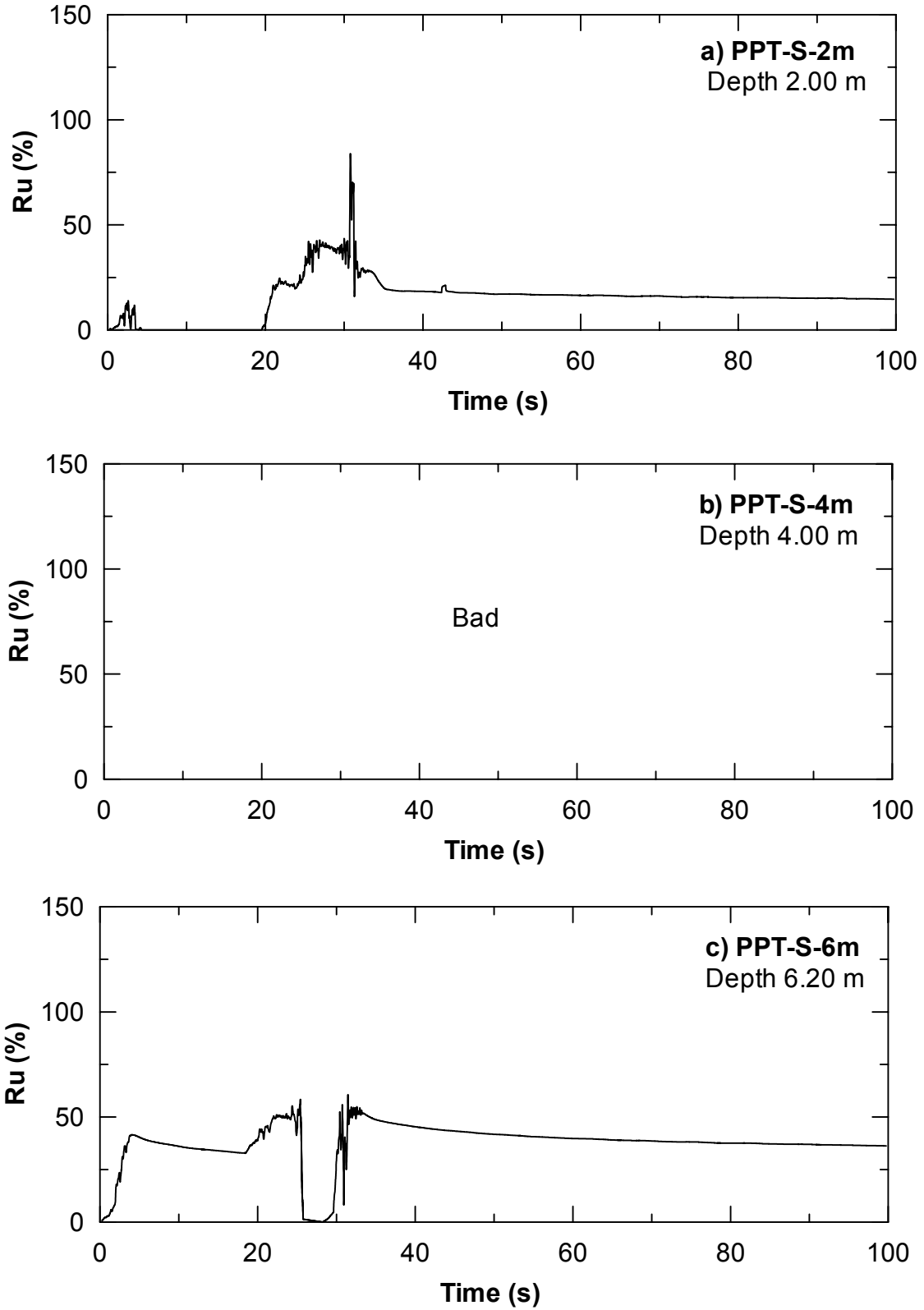


Fig. G.25 Time histories of strain along longitudinal pipeline C (bottom)

**Appendix H: Excess Pore-Water Pressure Data
(Second Test)**



**Fig. H.1 Excess pore-water pressure ratio time histories nearby single pile (second test):
 (a) PPT-S-2m, (b) PPT-S-4m, and (c) PPT-S-6m**

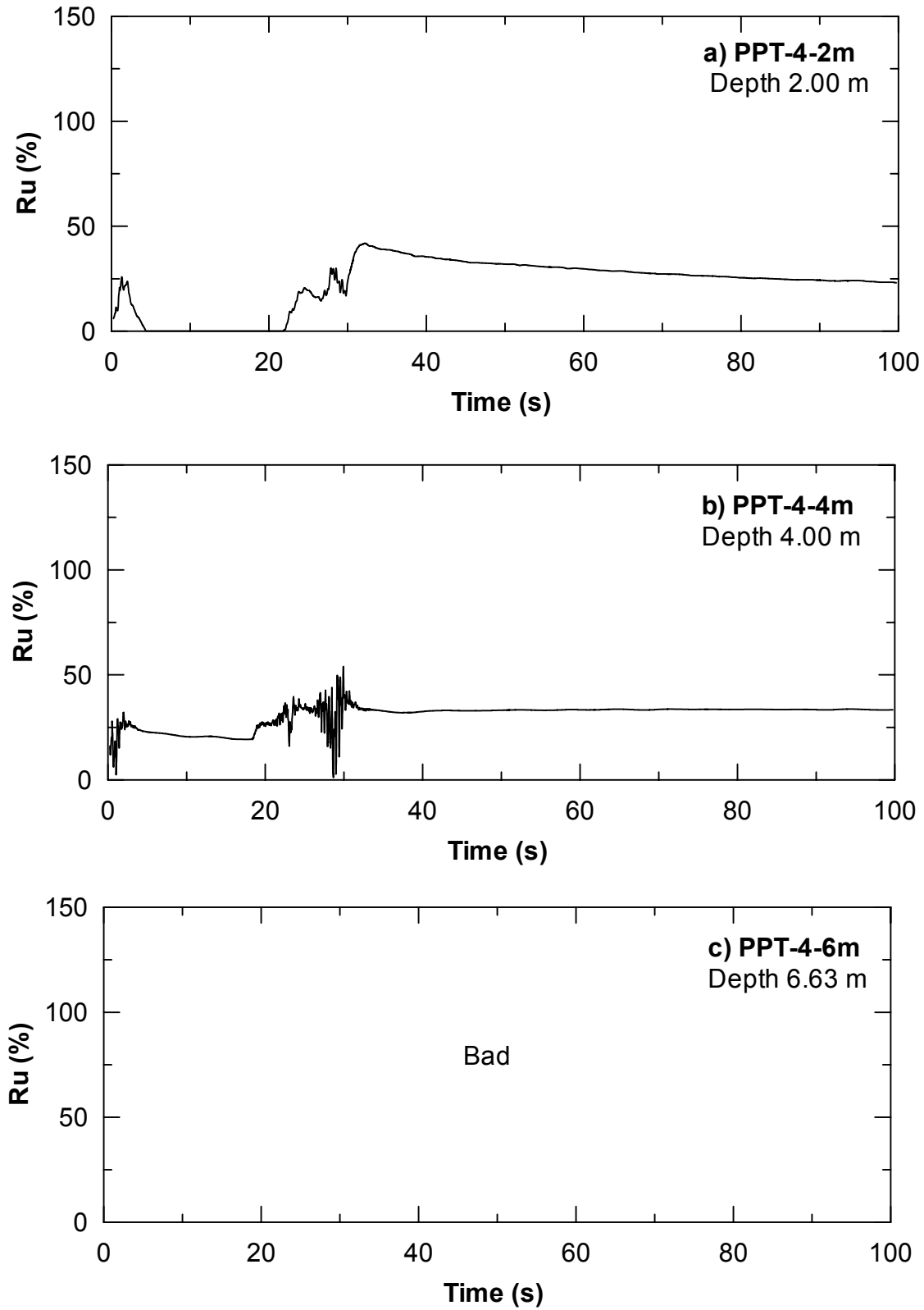


Fig. H.2 Excess pore-water pressure ratio time histories nearby 4-pile group (second test): (a) PPT-4-2m, (b) PPT-4-4m, and (c) PPT-4-6m

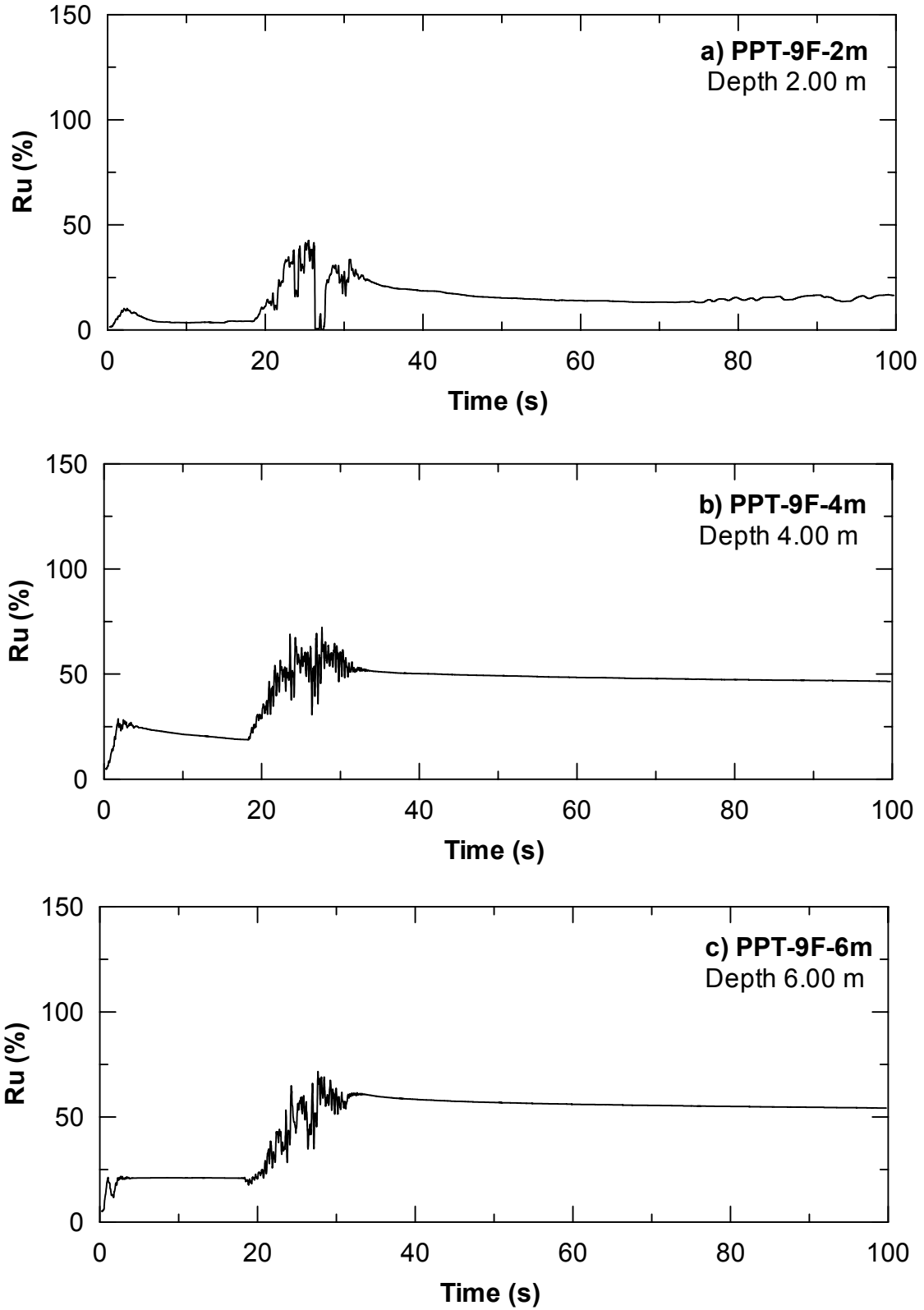


Fig. H.3 Excess pore-water pressure ratio time histories nearby 9-pile group, front side (second test), (a) PPT-9F-2m, (b) PPT-9F-4m, and (c) PPT-9F-6m

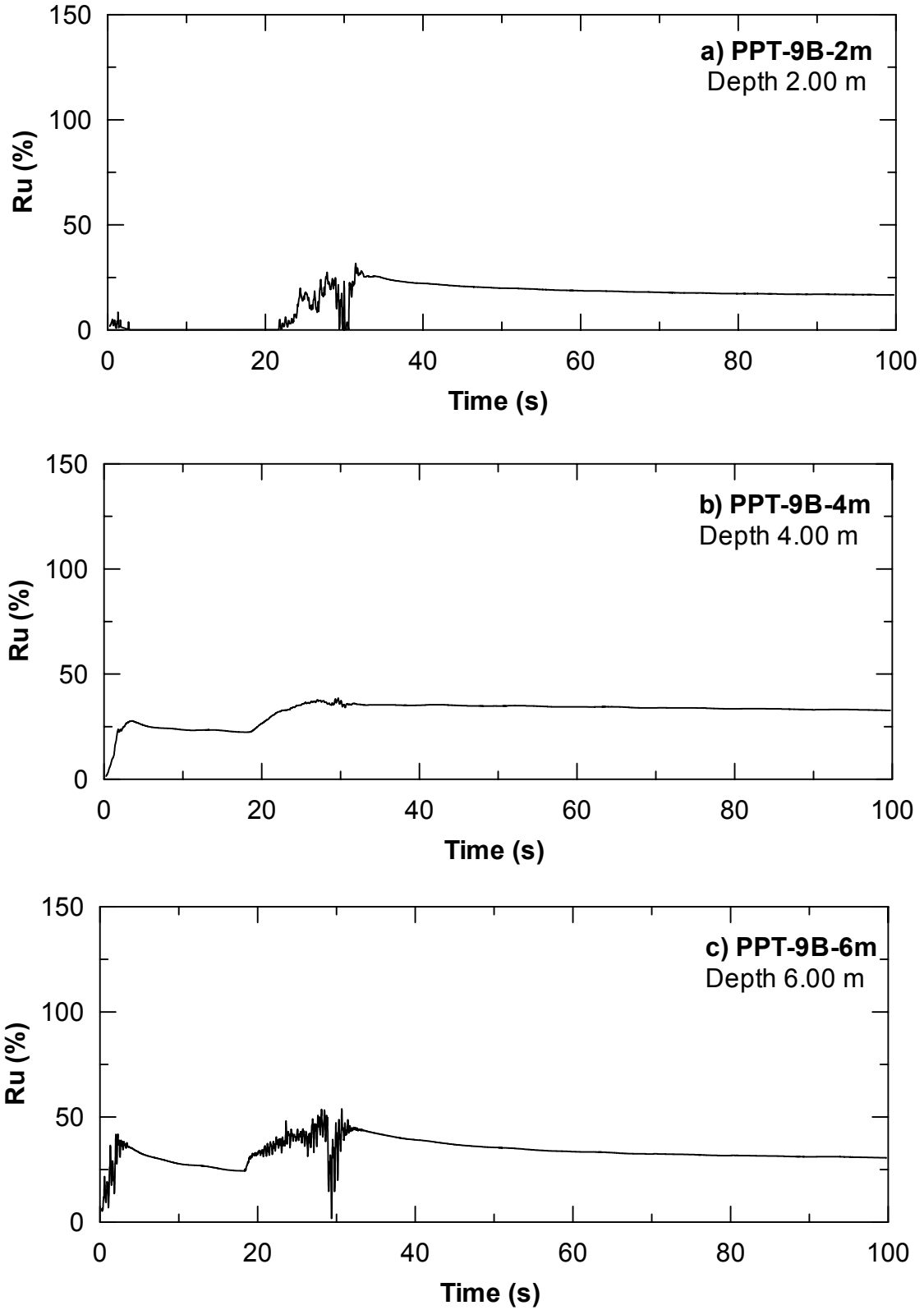


Fig. H.4 Excess pore-water pressure ratio time histories nearby 9-pile group, back side (second test): (a) PPT-9B-2m, (b) PPT-9B-4m, and (c) PPT-9B-6m

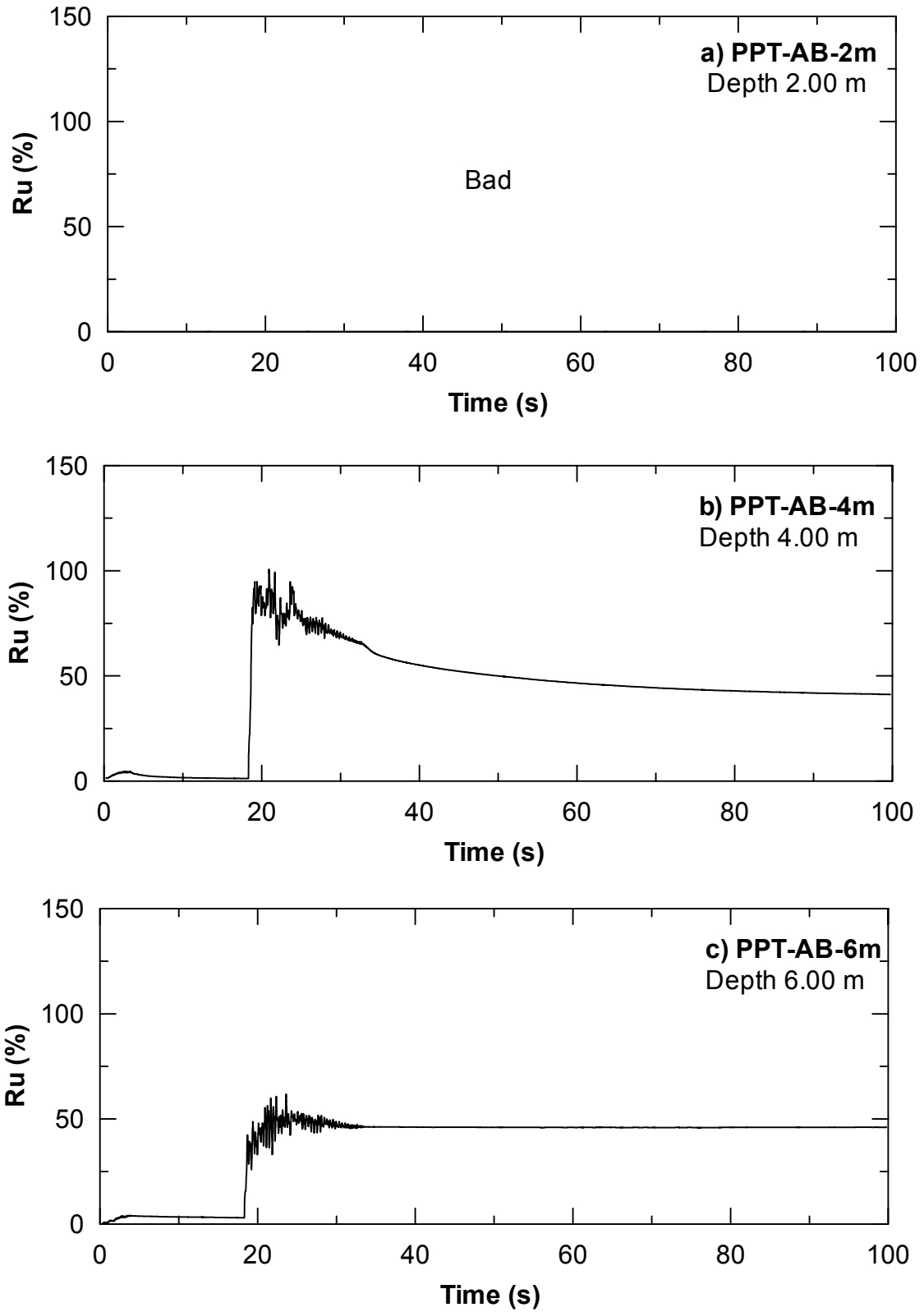
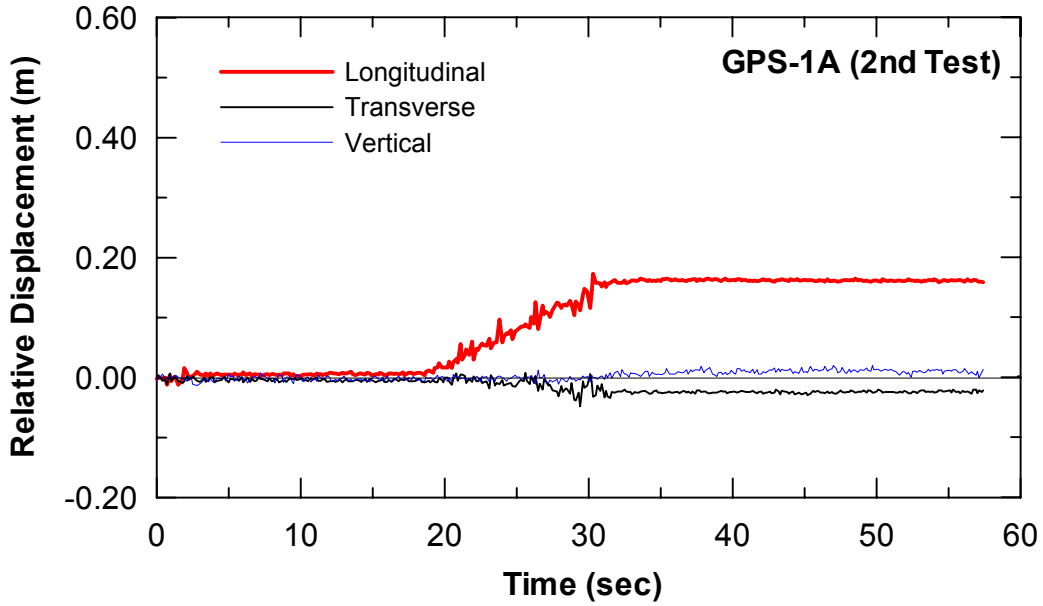
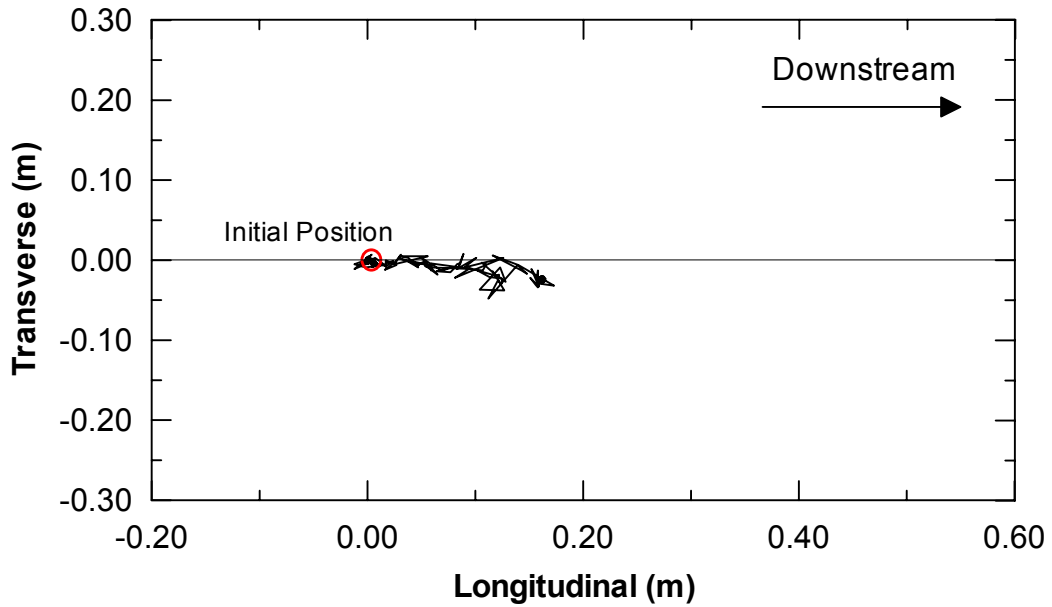


Fig. H.5 Excess pore-water pressure ratio time histories nearby transverse pipelines (second test): (a) PPT-AB-2m, (b) PPT-AB-4m, and (c) PPT-AB-6m

Appendix I: GPS Data (Second Test)

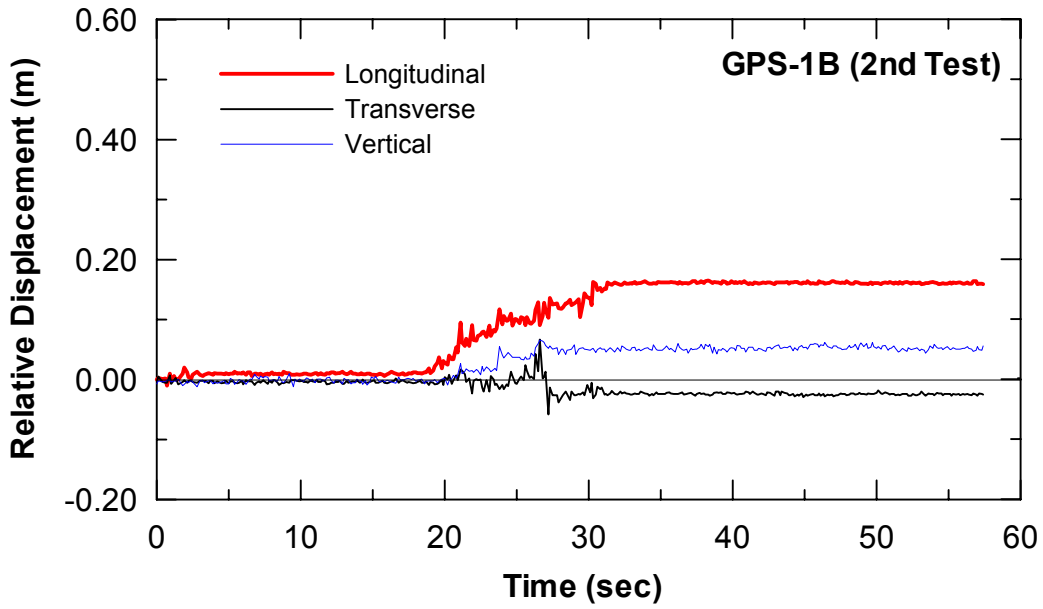


(a) Displacement Time-History

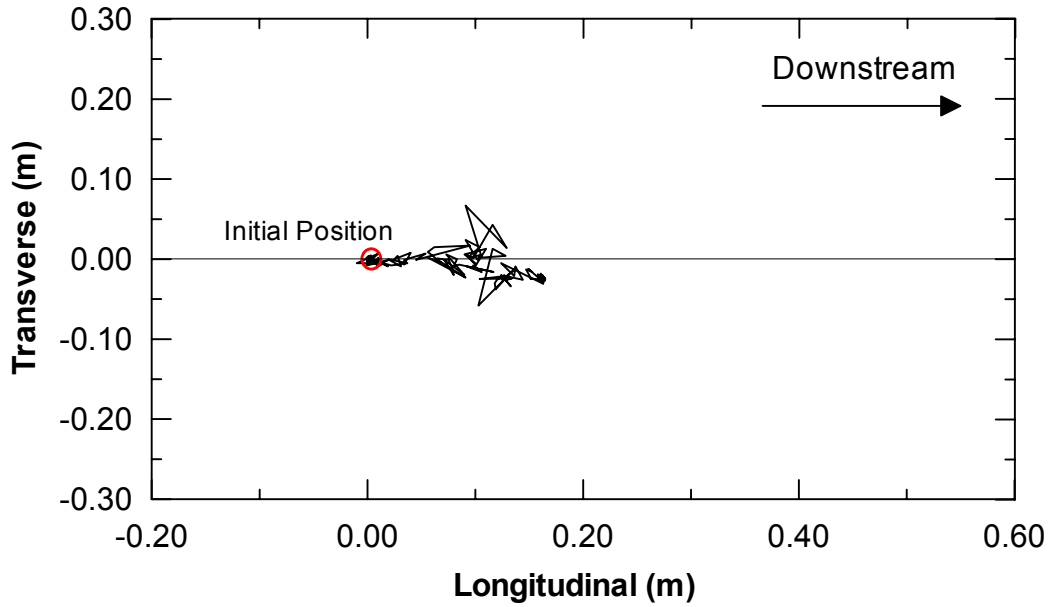


(b) Displacement Path

Fig. I.1 Global positioning system data of unit 1A (second test): (a) displacement time history and (b) displacement path (after Turner 2002)

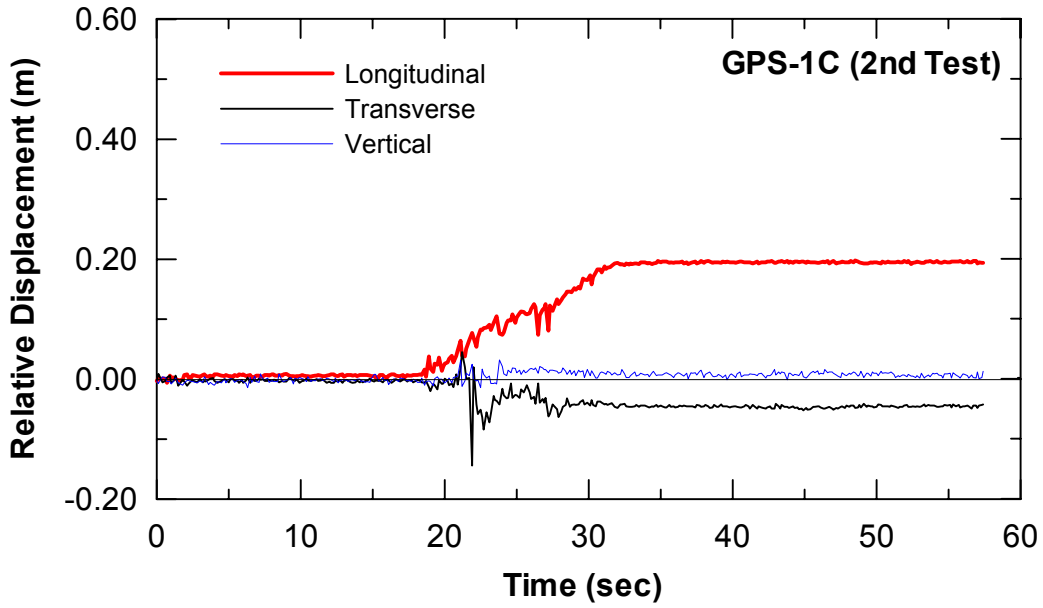


(a) Displacement Time-History

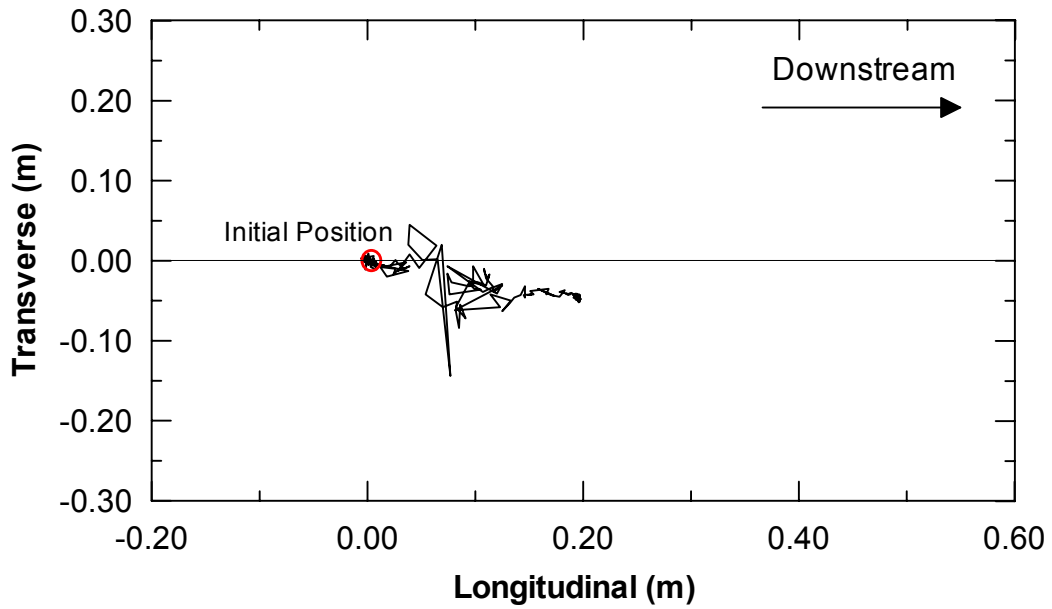


(b) Displacement Path

Fig. I.2 Global positioning system data of unit 1B (second test): (a) displacement time history and (b) displacement path (after Turner 2002)

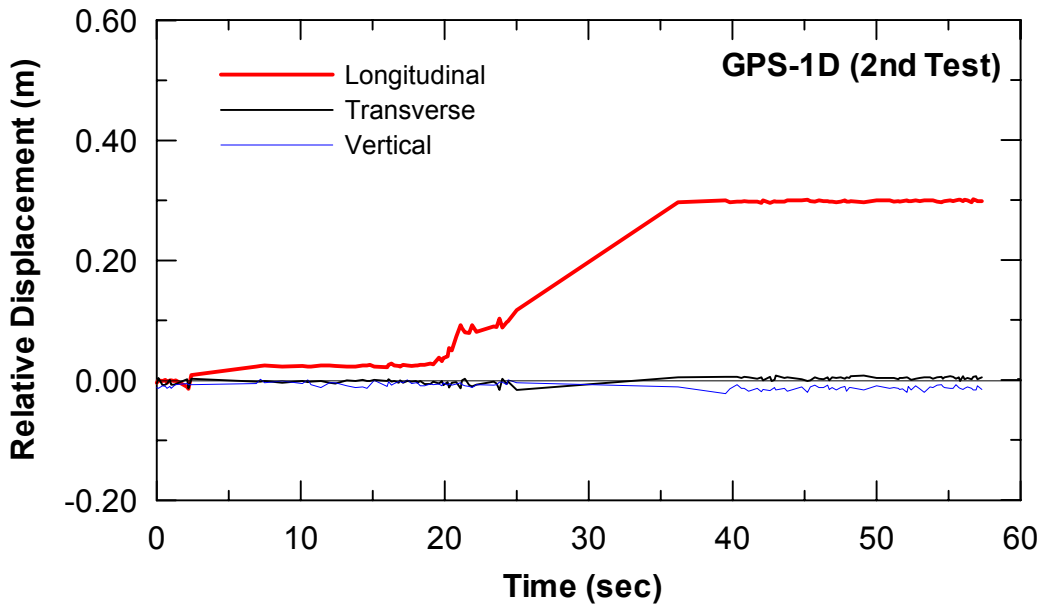


(a) Displacement Time-History

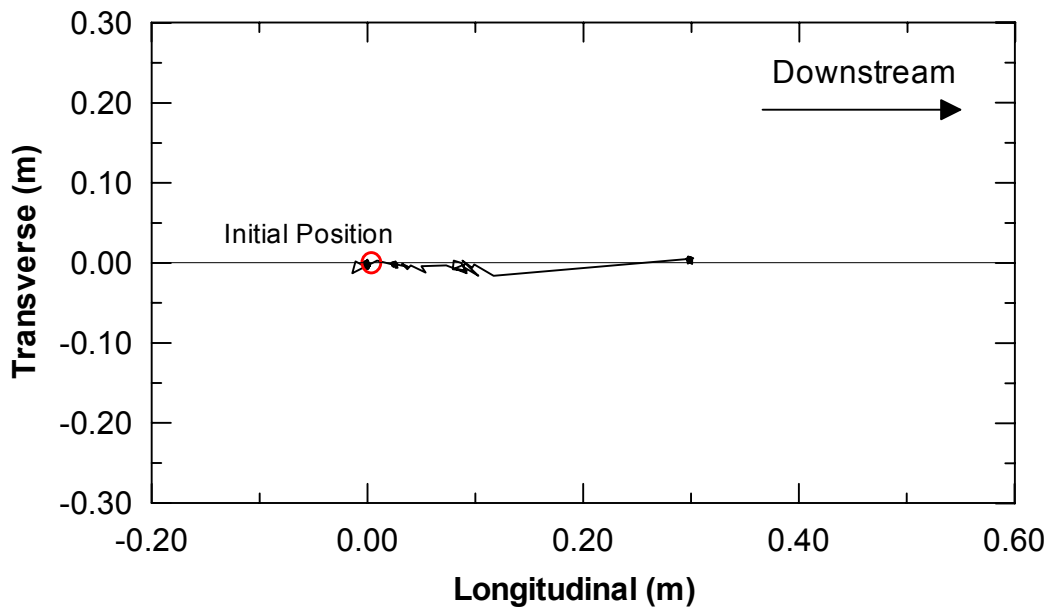


(b) Displacement Path

Fig. I.3 Global positioning system data of unit 1C (second test): (a) displacement time history and (b) displacement path (after Turner 2002)

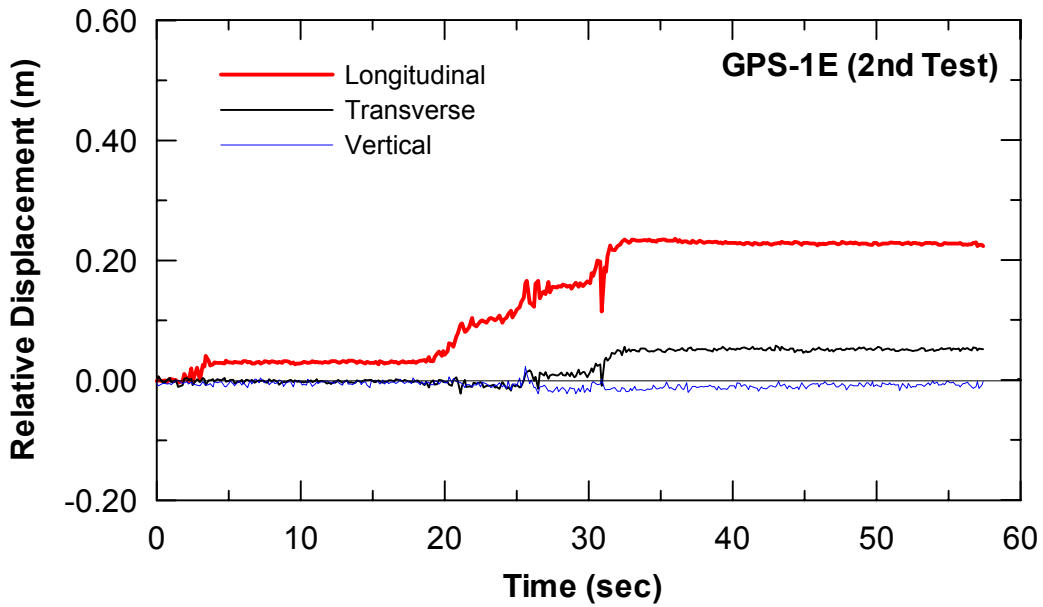


(a) Displacement Time-History

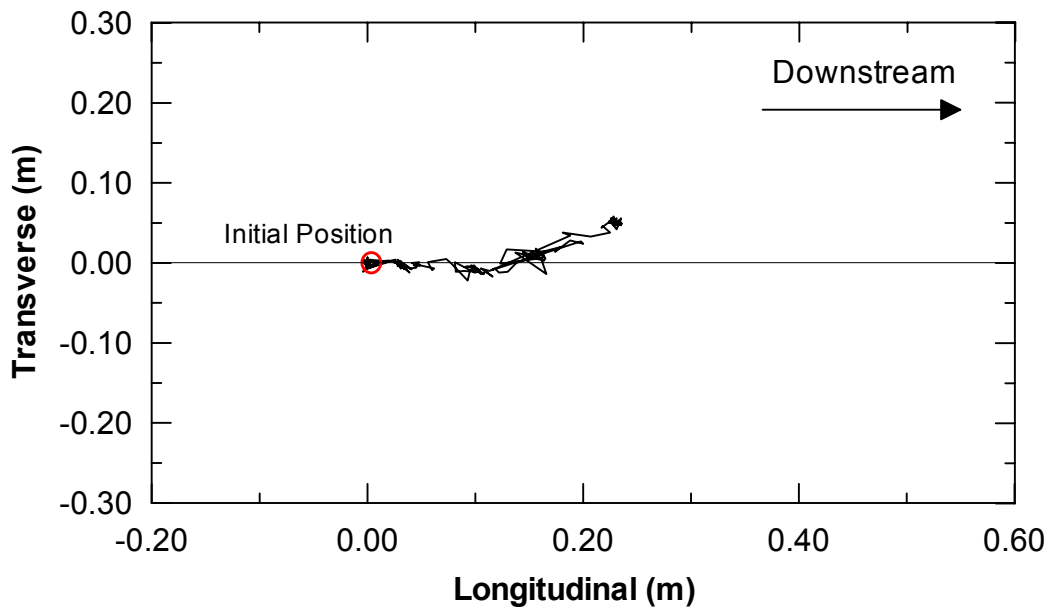


(b) Displacement Path

Fig. I.4 Global positioning system data of unit 1D (second test): (a) displacement time history and (b) displacement path (after Turner 2002)

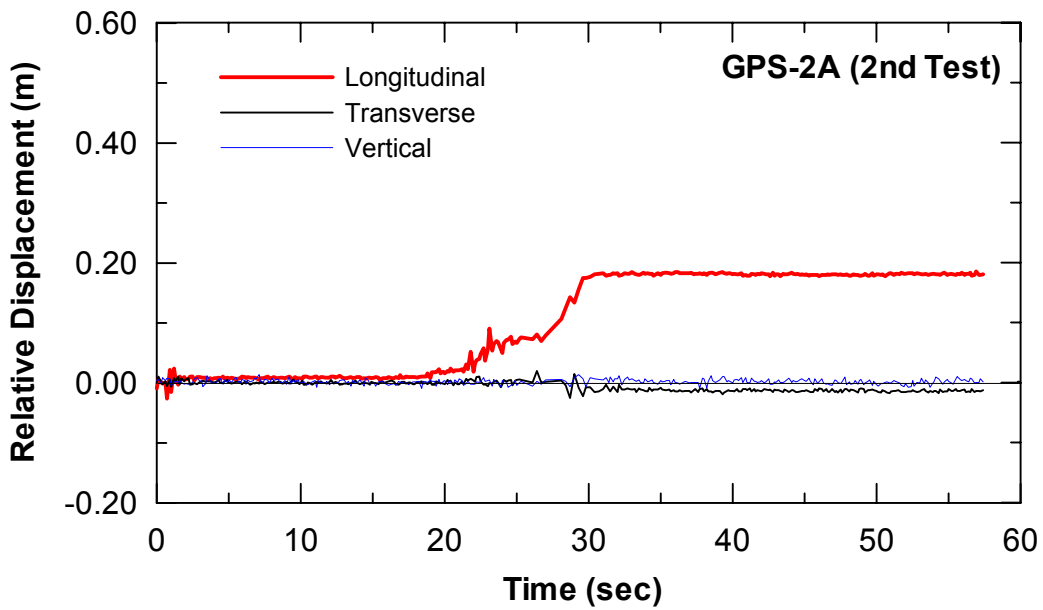


(a) Displacement Time-History

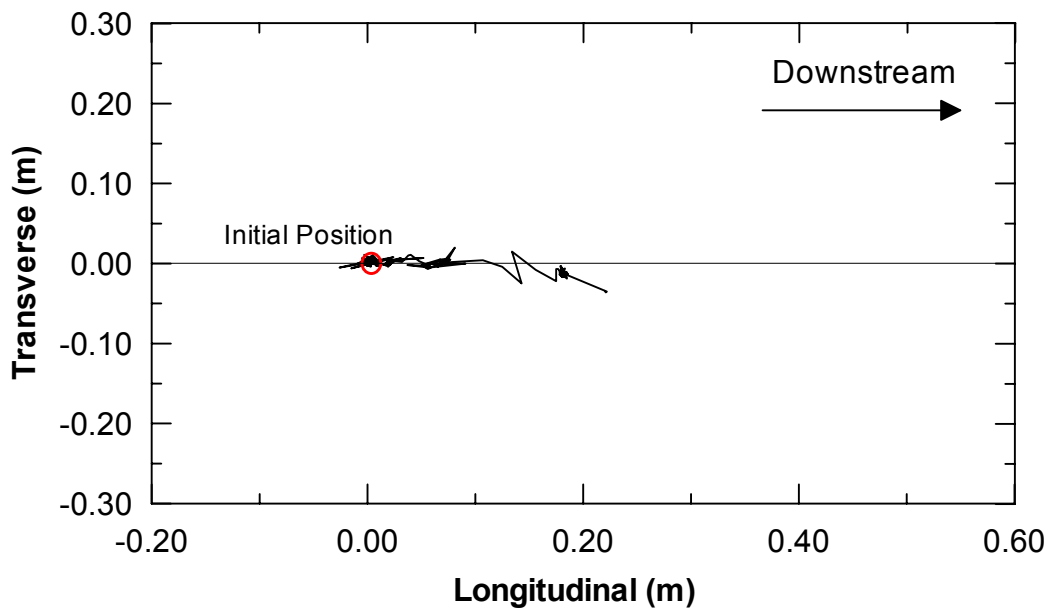


(b) Displacement Path

Fig. I.5 Global positioning system data of unit 1E (second test): (a) displacement time history and (b) displacement path (after Turner 2002)

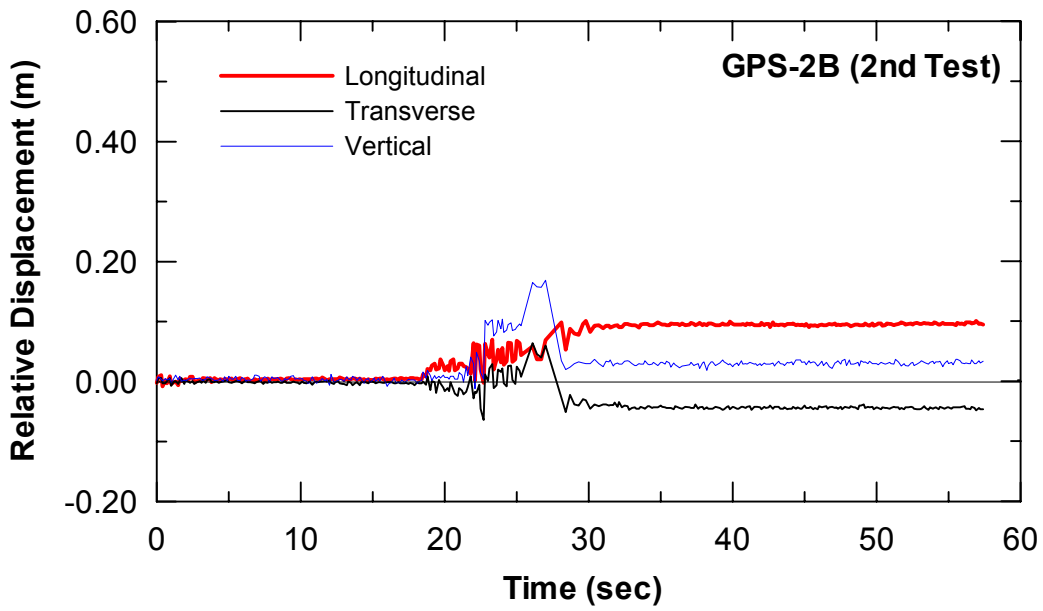


(a) Displacement Time-History

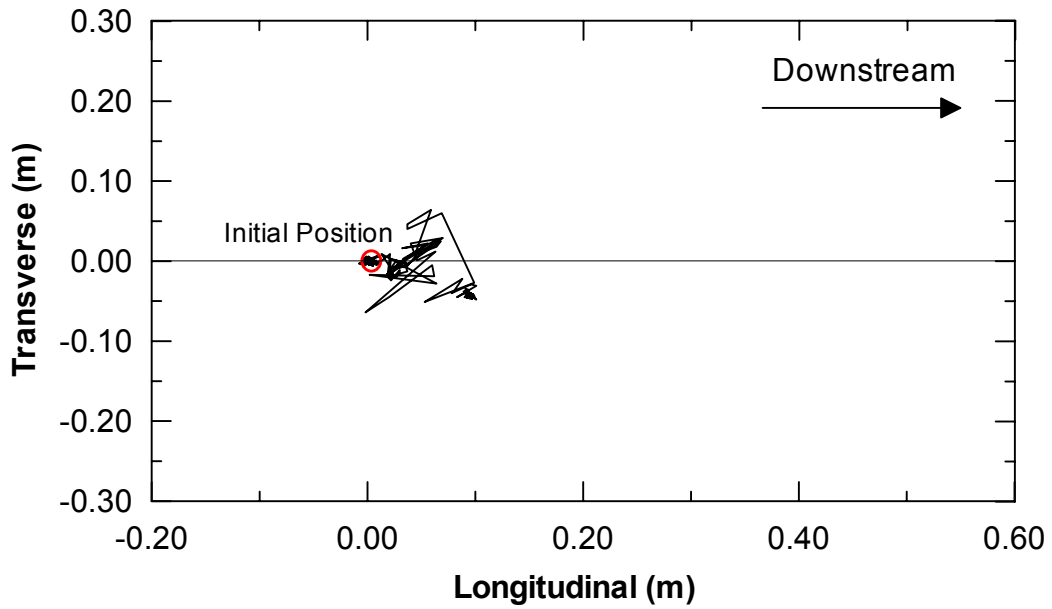


(b) Displacement Path

Fig. I.6 Global positioning system data of unit 2A (second test): (a) displacement time history and (b) displacement path (after Turner 2002)

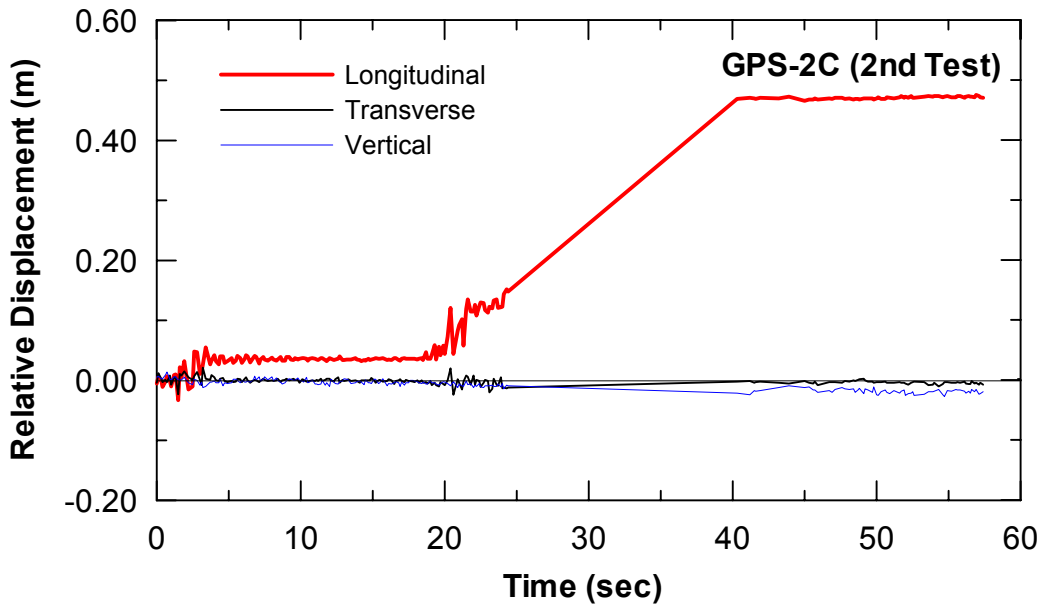


(a) Displacement Time-History

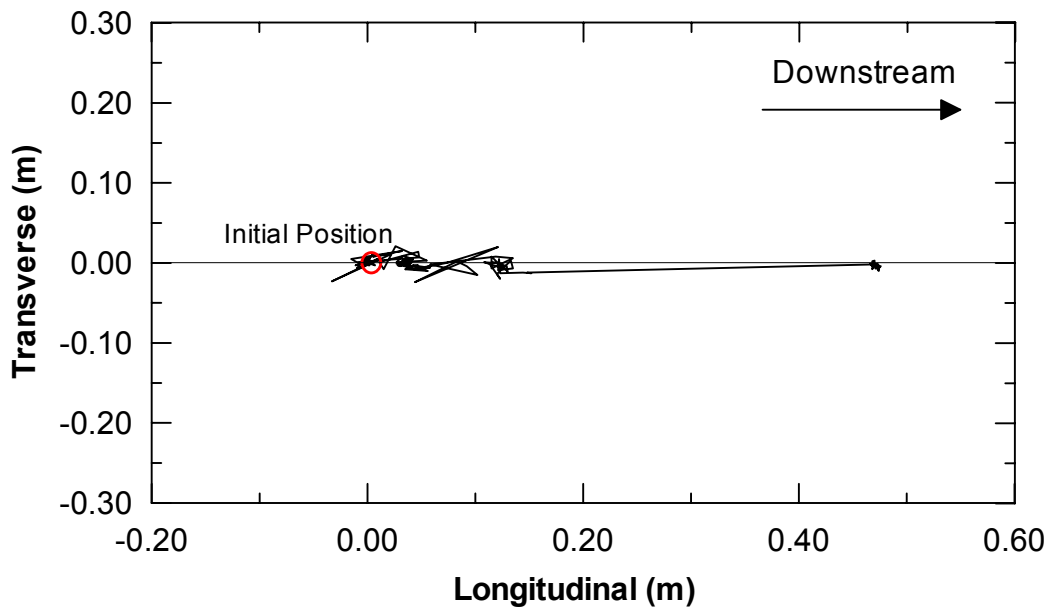


(b) Displacement Path

Fig. I.7 Global positioning system data of unit 2B (second test): (a) displacement time history and (b) displacement path (after Turner 2002)

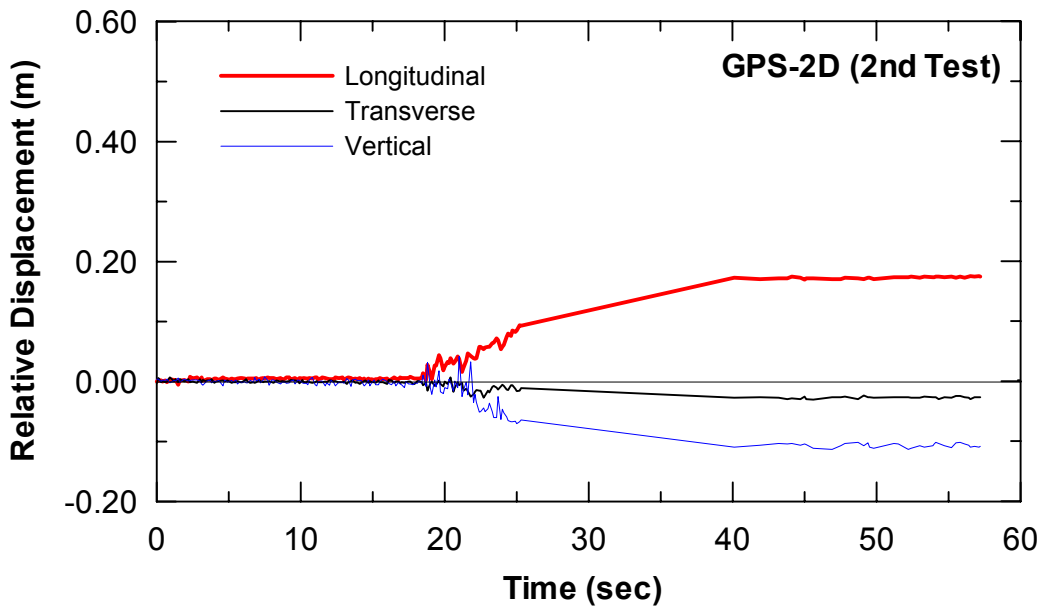


(a) Displacement Time-History

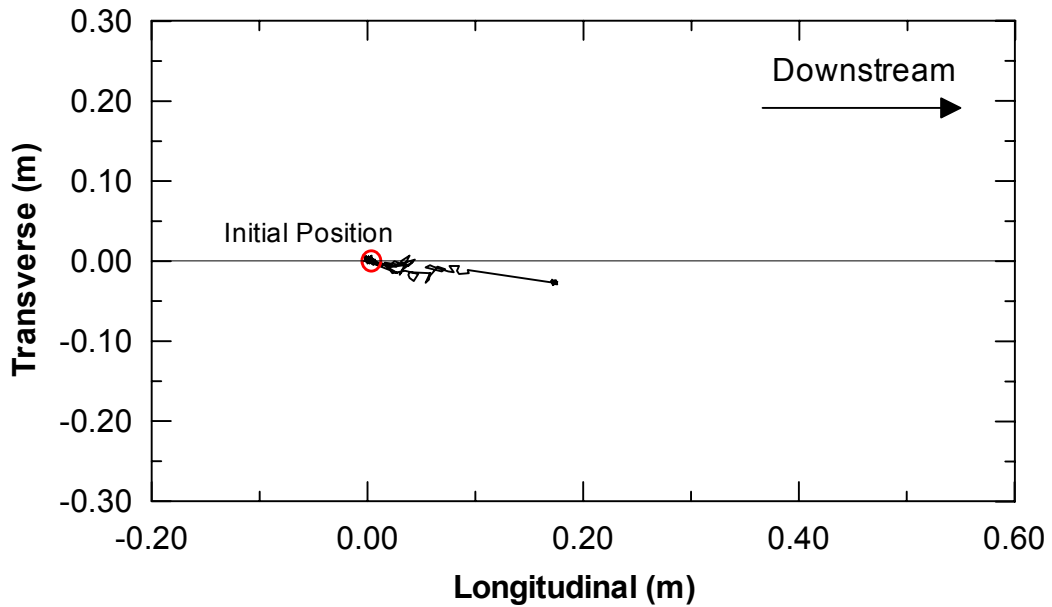


(b) Displacement Path

Fig. I.8 Global positioning system data of unit 2C (second test): (a) displacement time history and (b) displacement path (after Turner 2002)

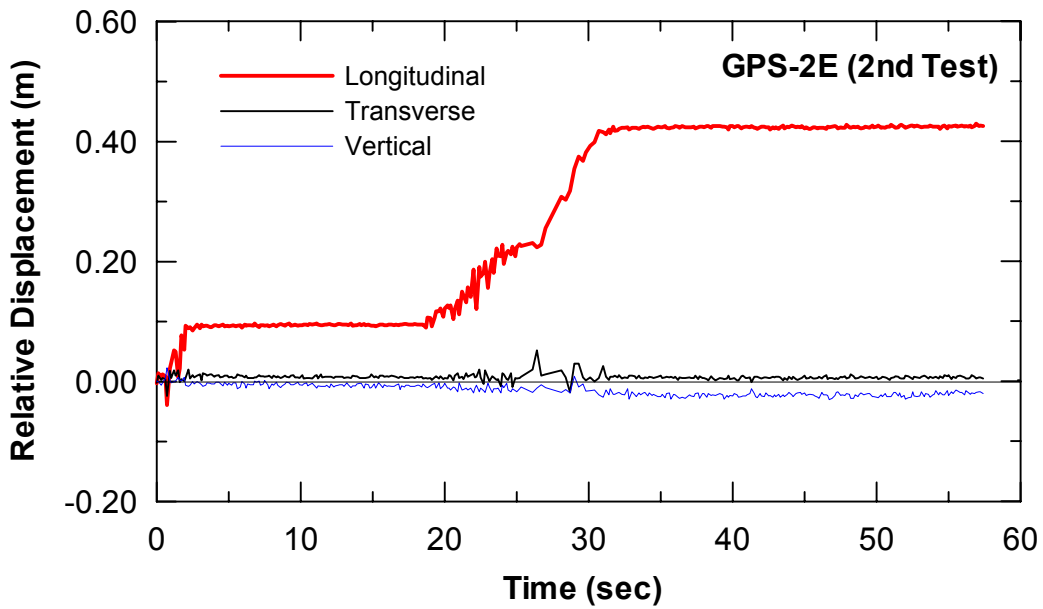


(a) Displacement Time-History

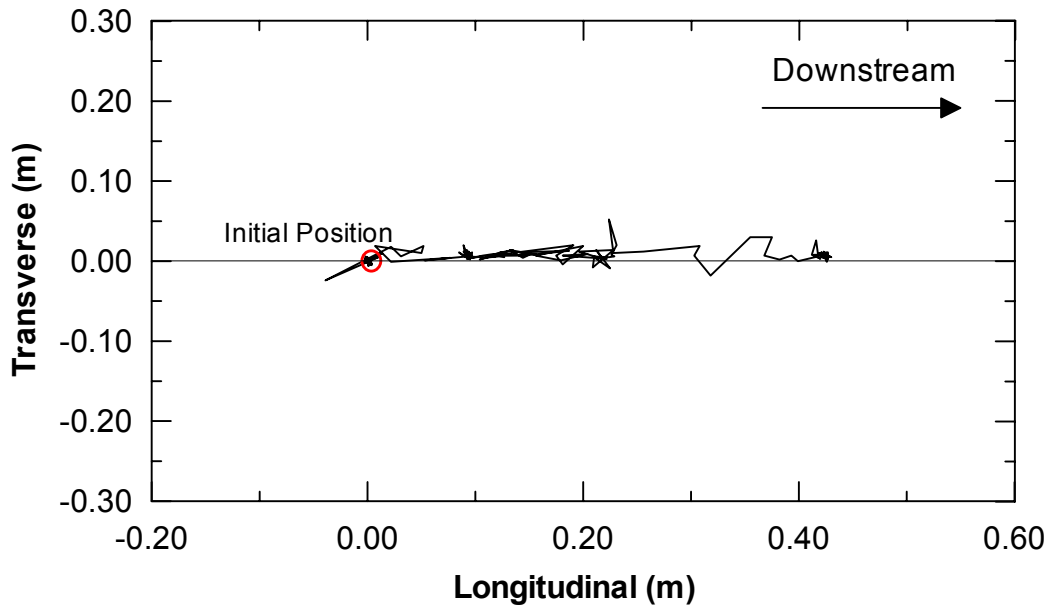


(b) Displacement Path

Fig. I.9 Global positioning system data of unit 2D (second test): (a) displacement time history and (b) displacement path (after Turner 2002)



(a) Displacement Time-History



(b) Displacement Path

Fig. I.10 Global positioning system data of unit 2E (second test): (a) displacement time history and (b) displacement path (after Turner 2002)

Appendix J: Inclinometer Data (Second Test)

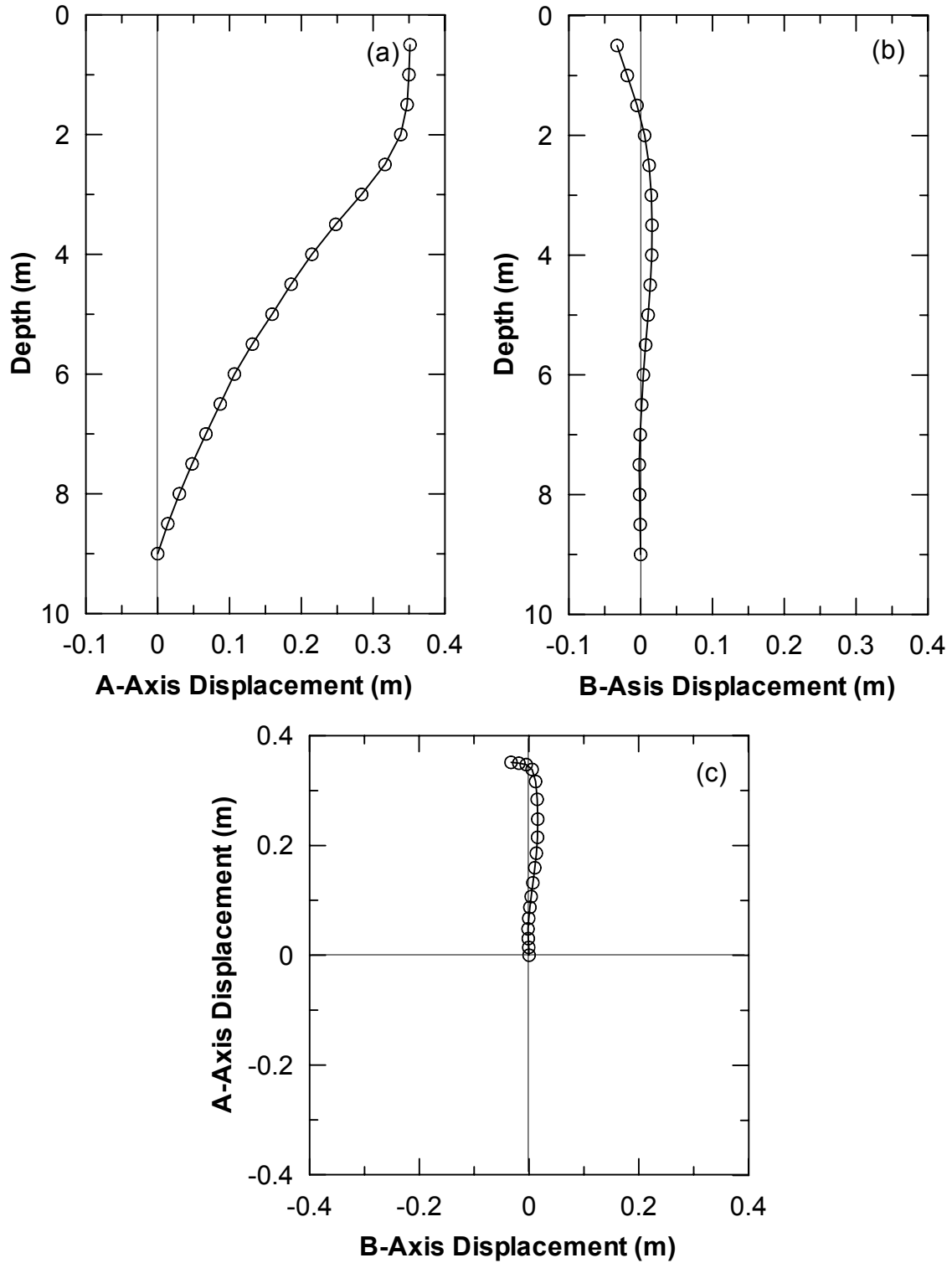


Fig. J.1 Soil displacement from inclinometer Casing S2 for second test: (a) section view A-direction, (b) section view B-direction, and (c) plan view

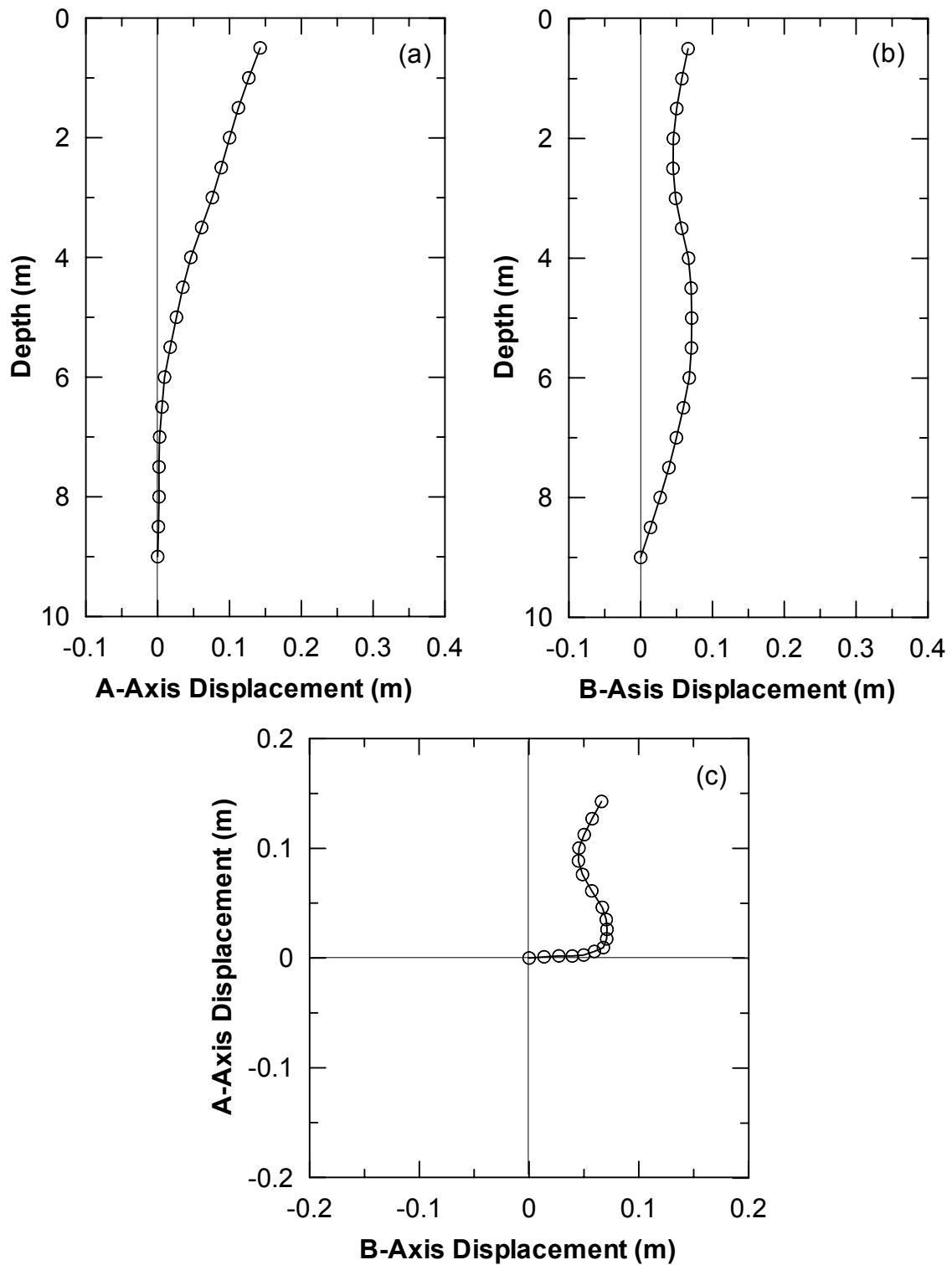


Fig. J.2 Soil displacement from inclinometer Casing S3 for second test: (a) section view A-direction, (b) section view B-direction, and (c) plan view

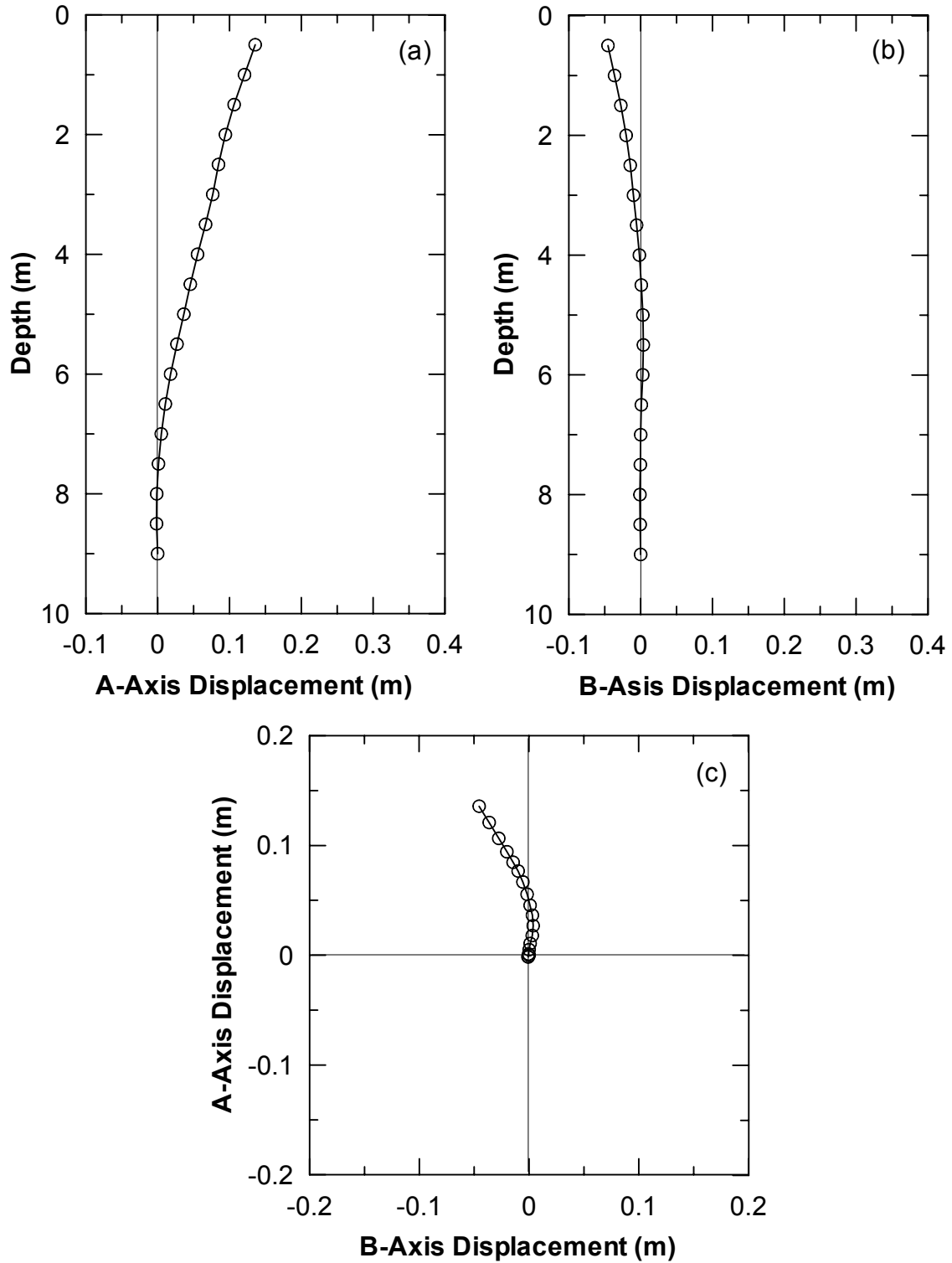


Fig. J.3 Soil displacement from inclinometer Casing S4 for second test: (a) section view A-direction, (b) section view B-direction, and (c) plan view

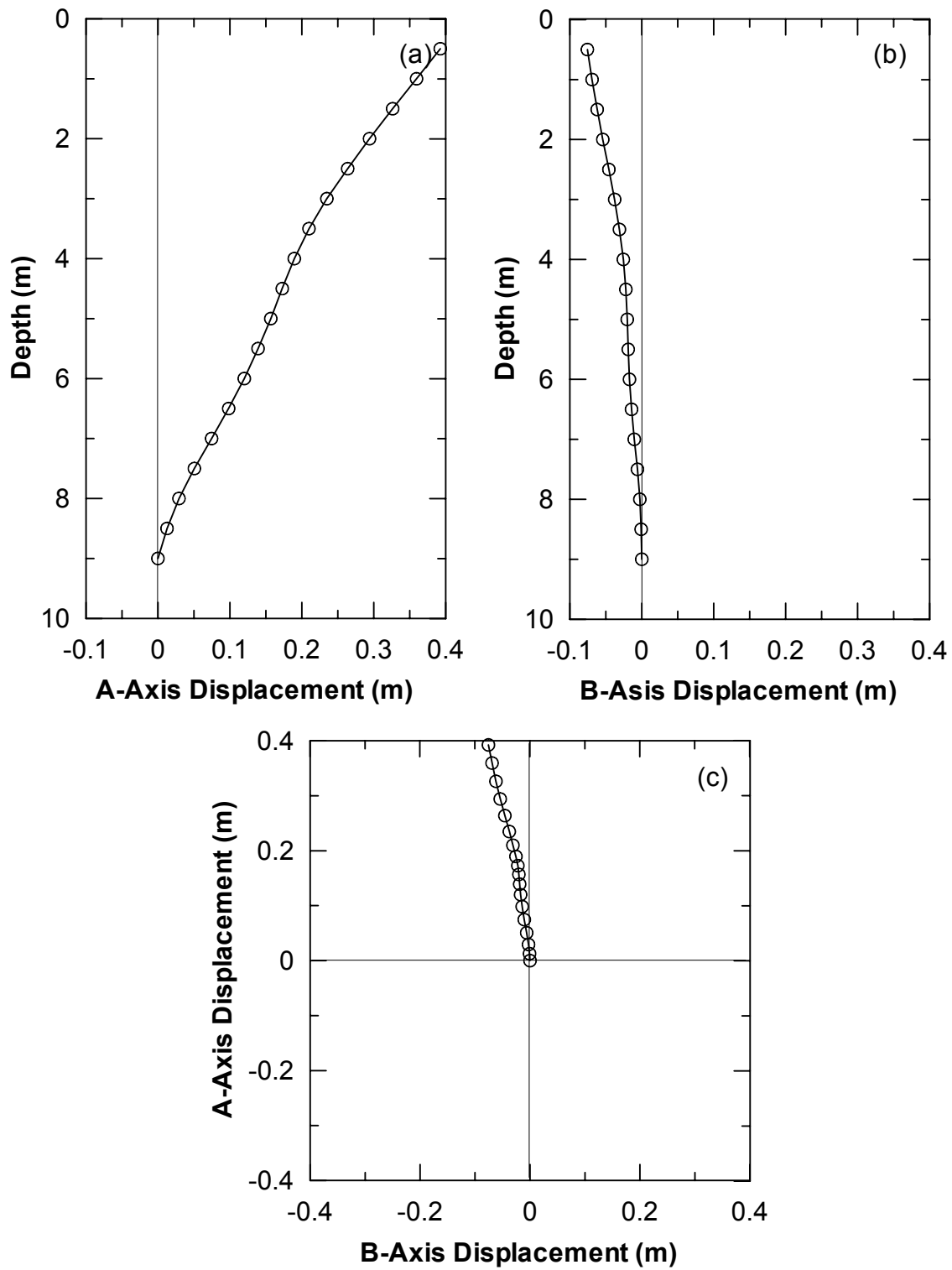


Fig. J.4 Soil displacement from inclinometer Casing S5 for second test: (a) section view A-direction, (b) section view B-direction, (c) plan view

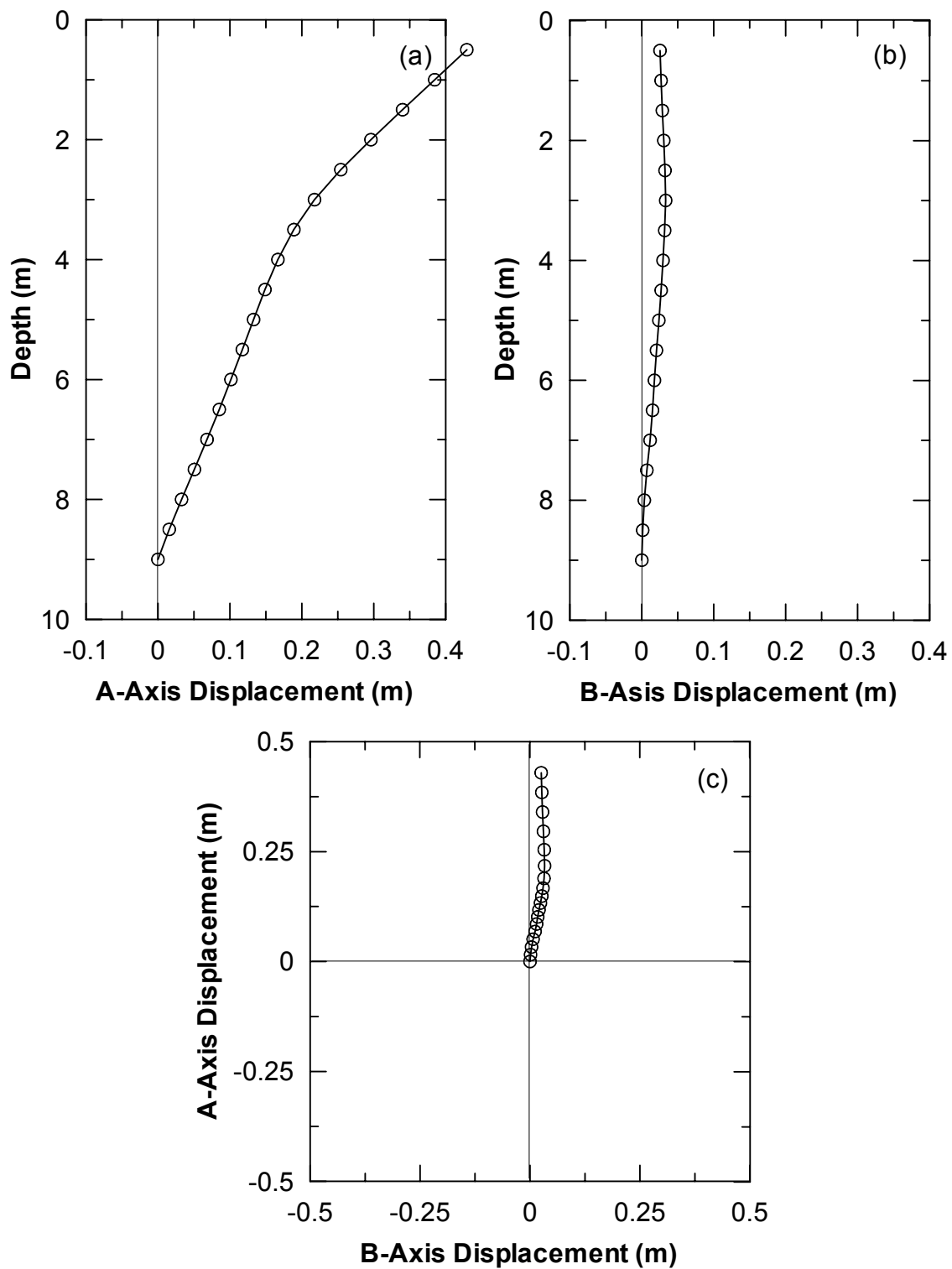


Fig. J.5 Soil displacement from inclinometer Casing S6 for second test: (a) section view A-direction, (b) section view B-direction, (c) plan view

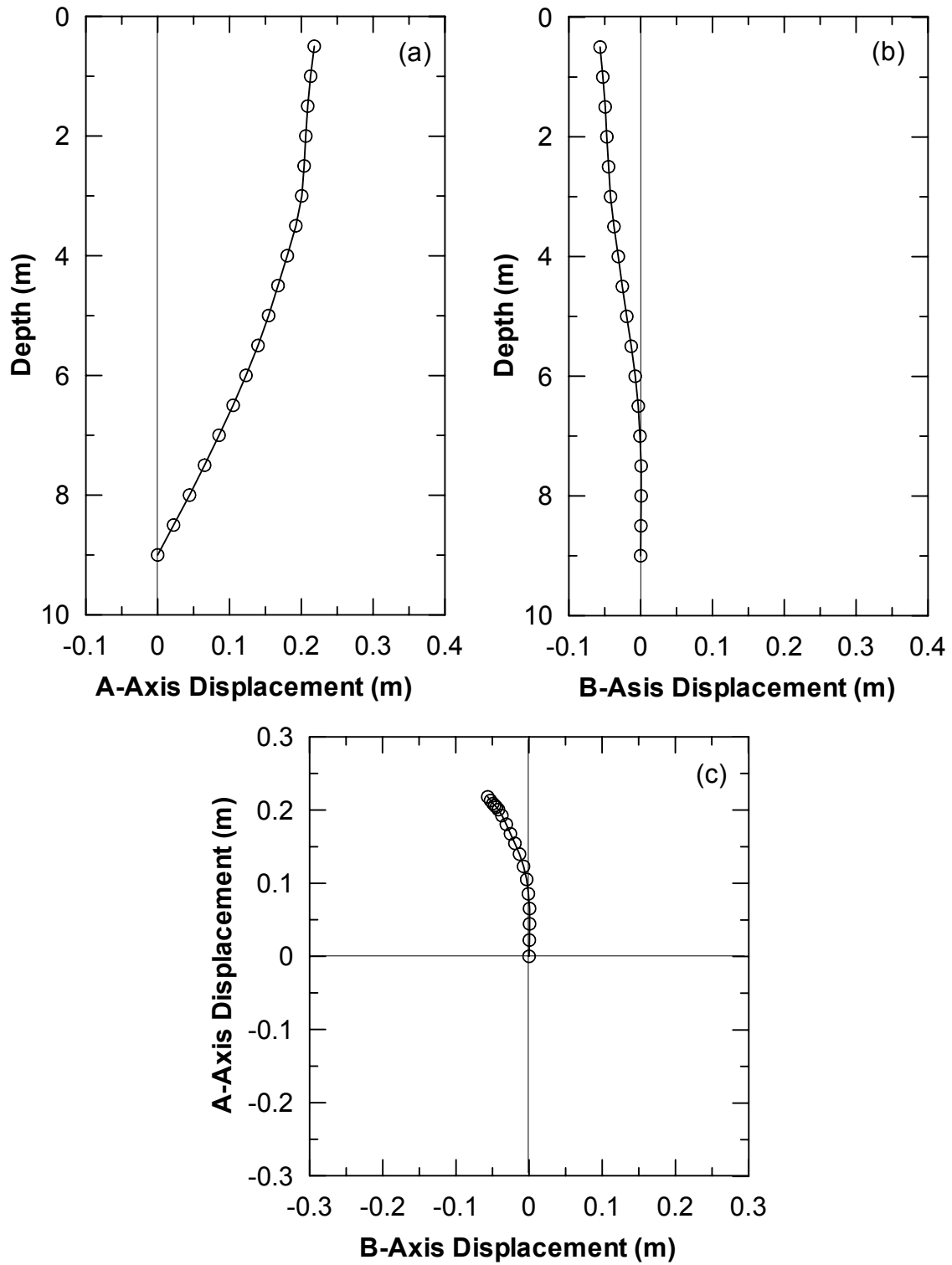


Fig. J.6 Soil displacement from inclinometer Casing S7 for second test: (a) section view A-direction, (b) section view B-direction, (c) plan view

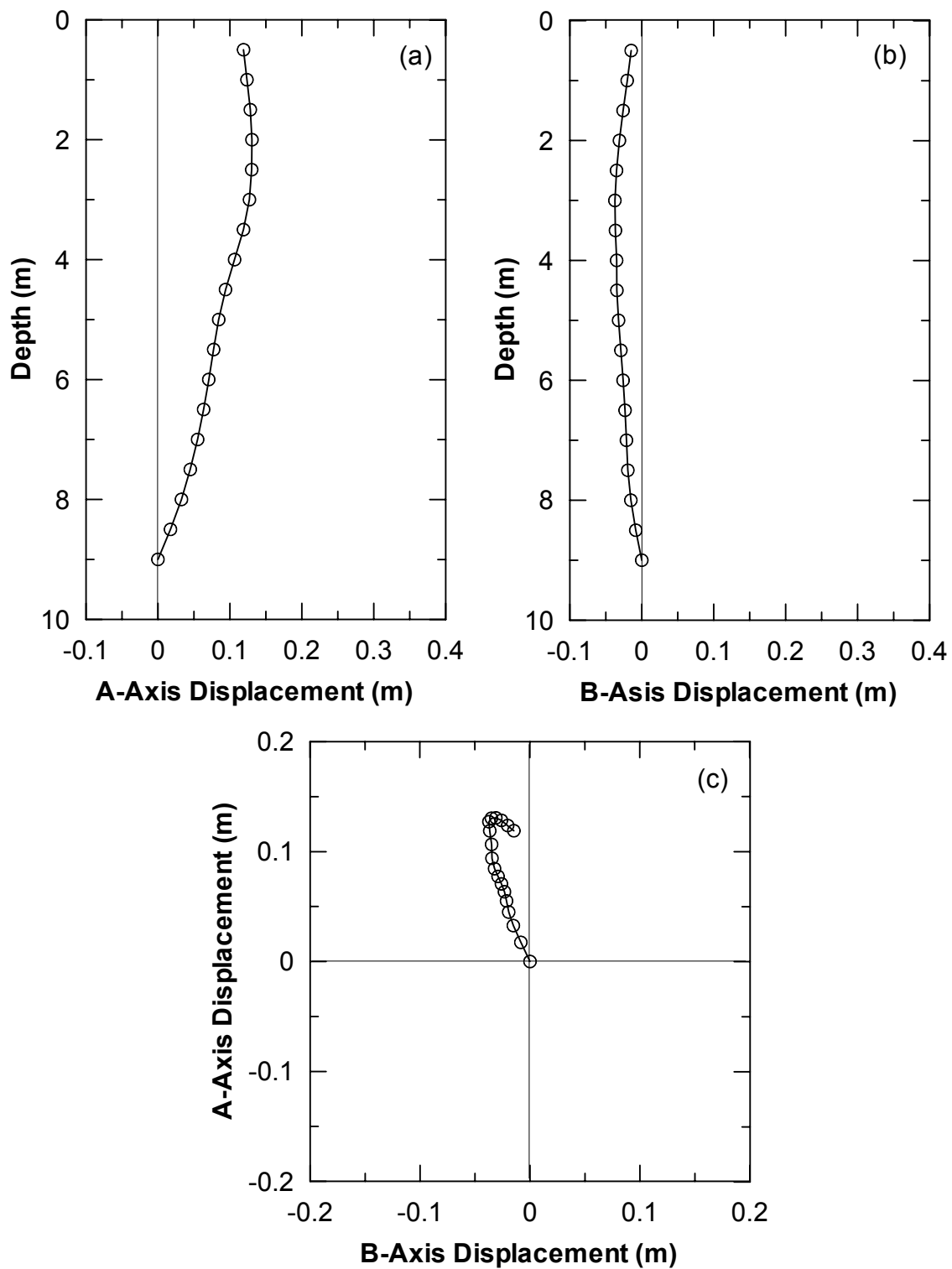


Fig. J.7 Soil displacement from inclinometer Casing S8 for second test: (a) section view A-direction, (b) section view B-direction, and (c) plan view

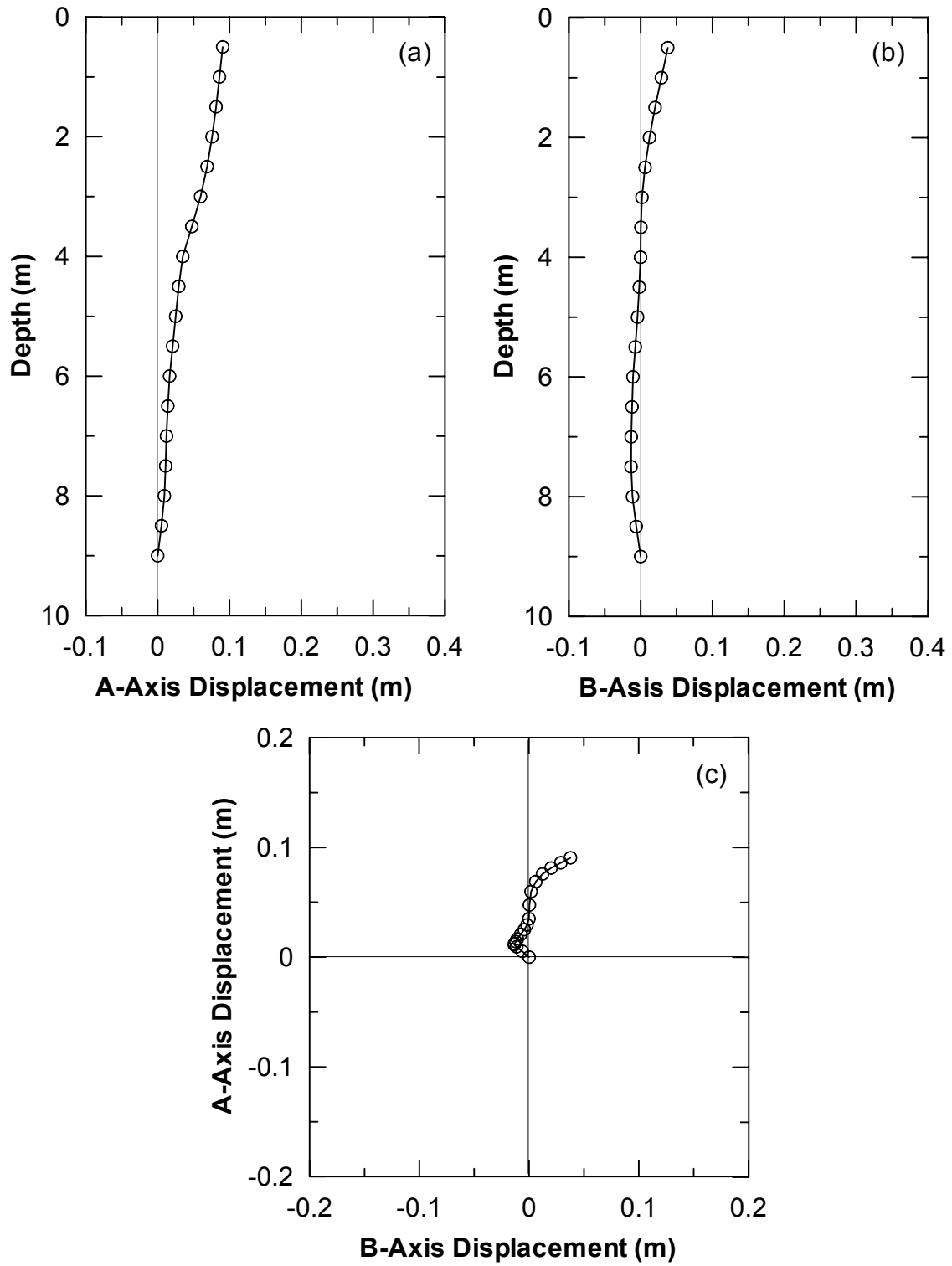


Fig. J.8 Soil displacement from inclinometer Casing S9 for second test: (a) section view A-direction, (b) section view B-direction, and (c) plan view

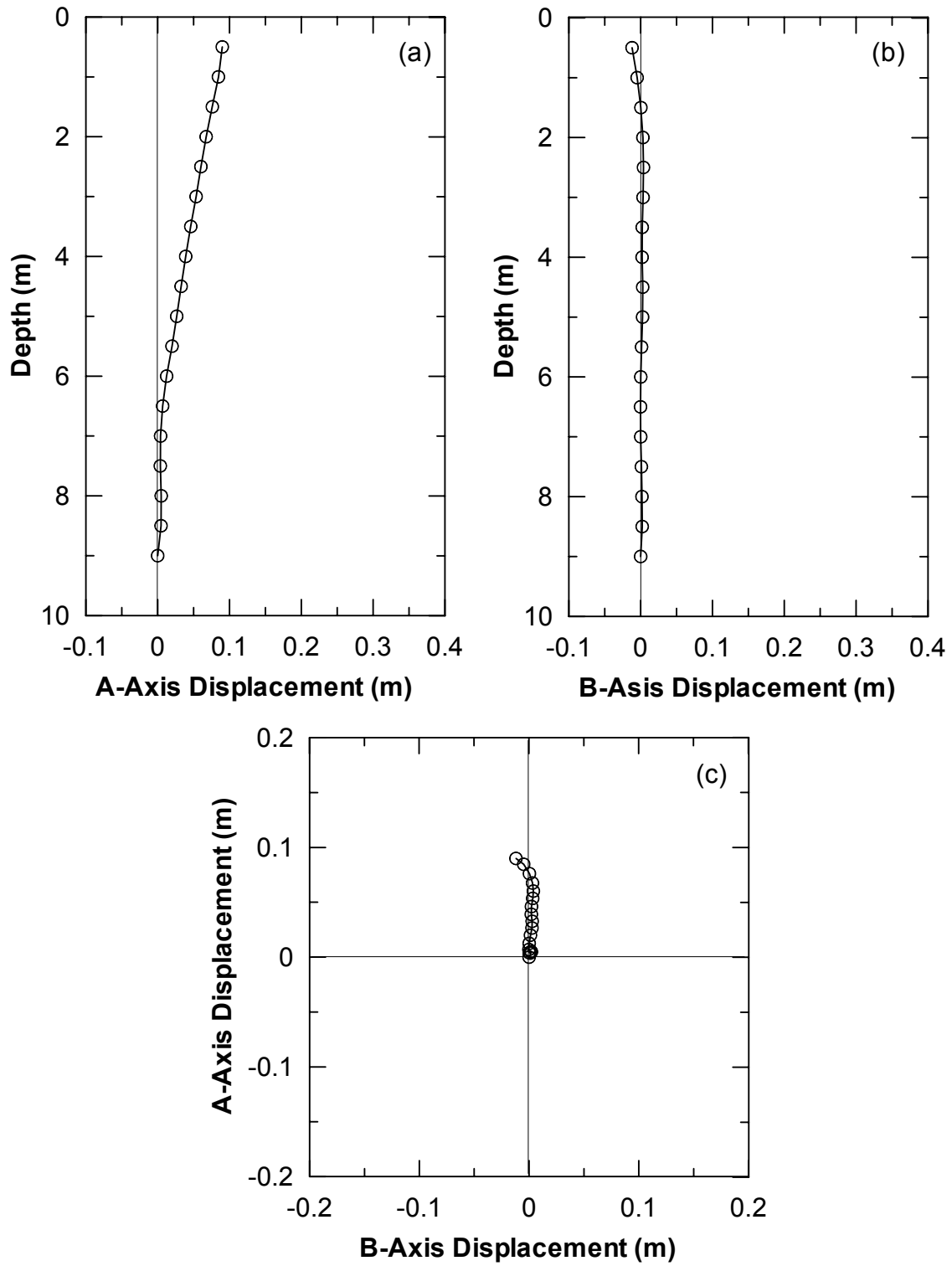


Fig. J.9 Soil displacement from inclinometer Casing S10 for second test: (a) section view A-direction, (b) section view B-direction, and (c) plan view

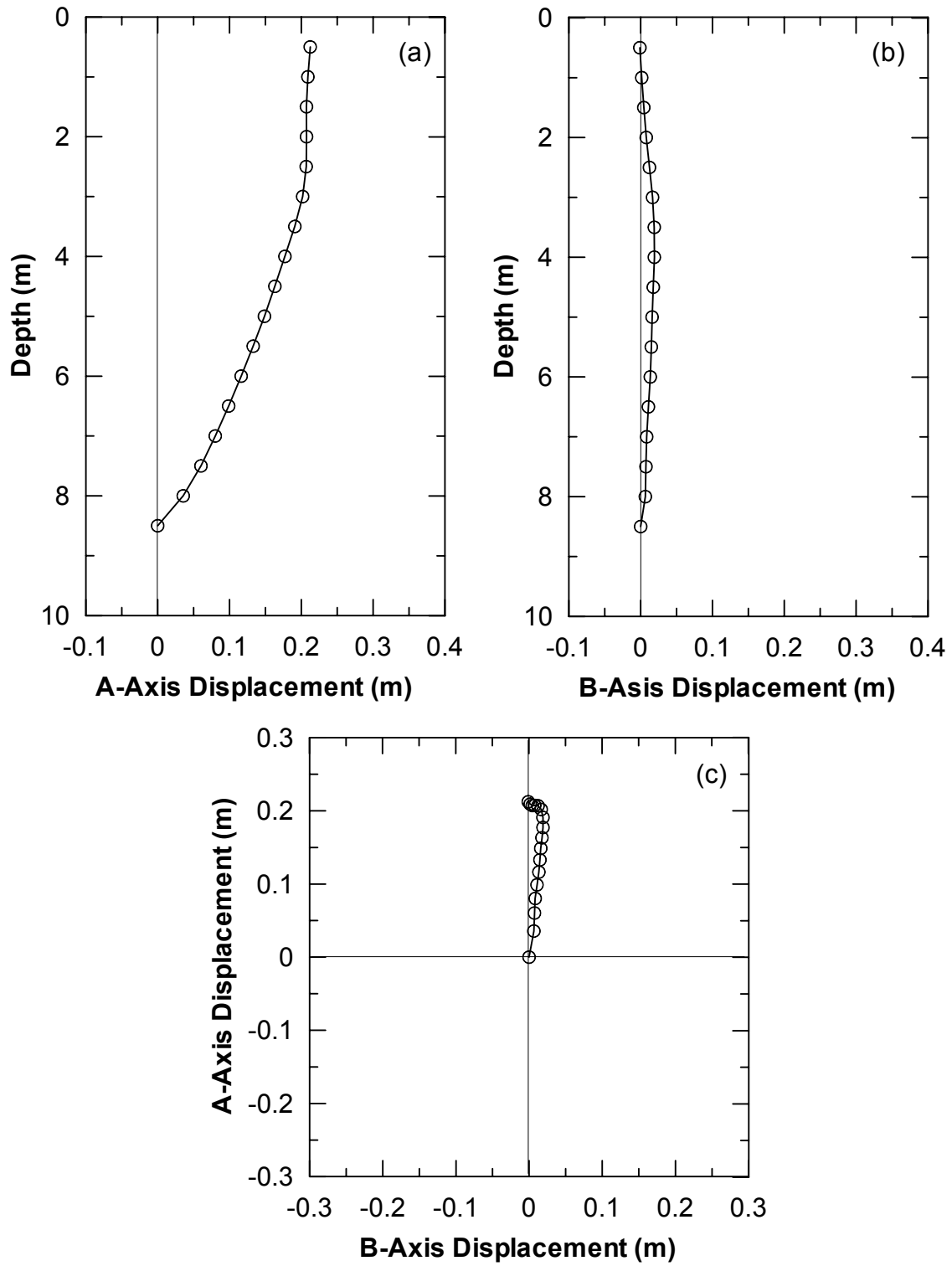


Fig. J.10 Soil displacement from inclinometer Casing S11 for second test: (a) section view A-direction, (b) section view B-direction, and (c) plan view

Appendix K: Strain Gage Data (Second Test)

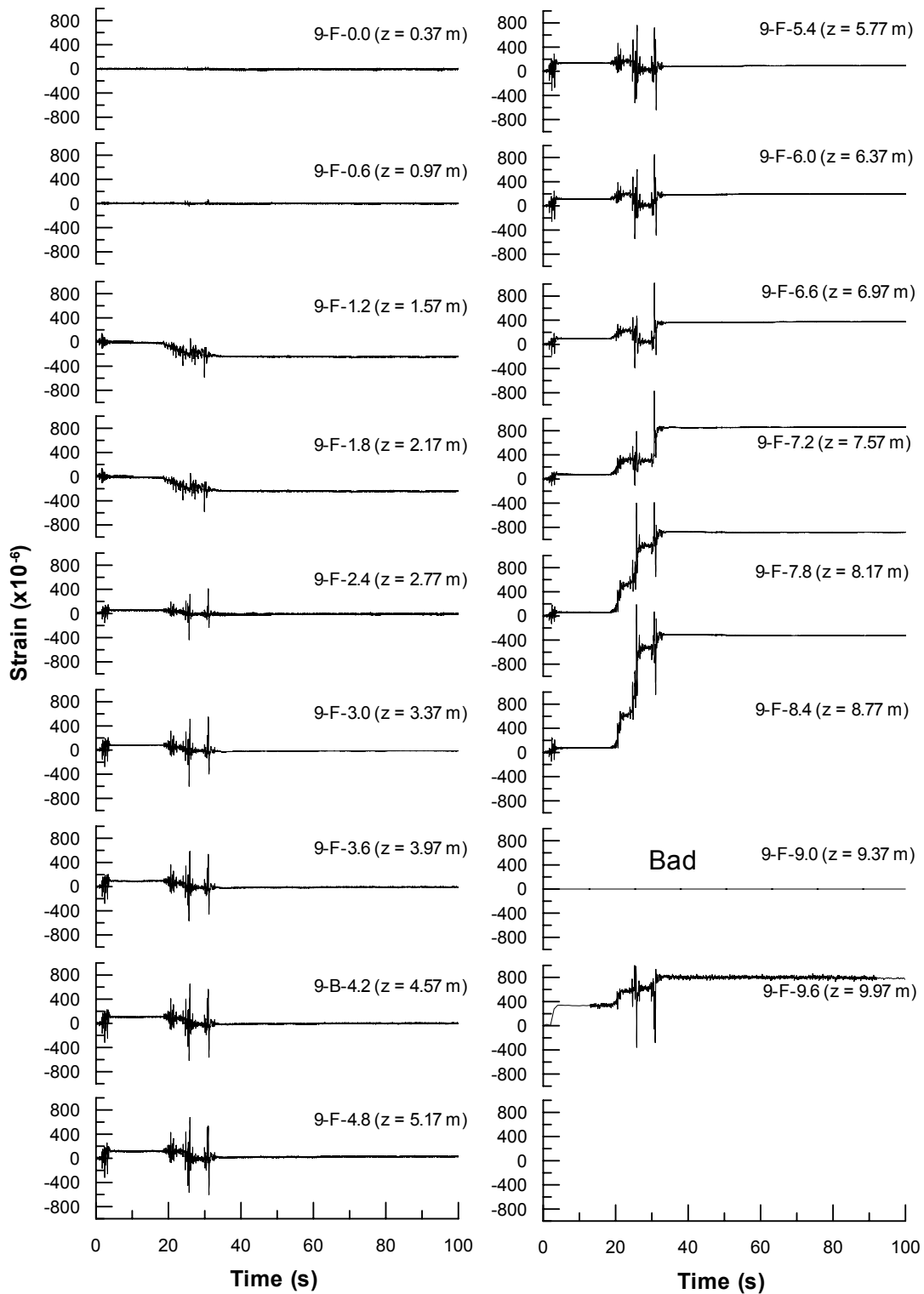


Fig. K.1 Time histories of strain along single pile (No. 9) at front side, second test

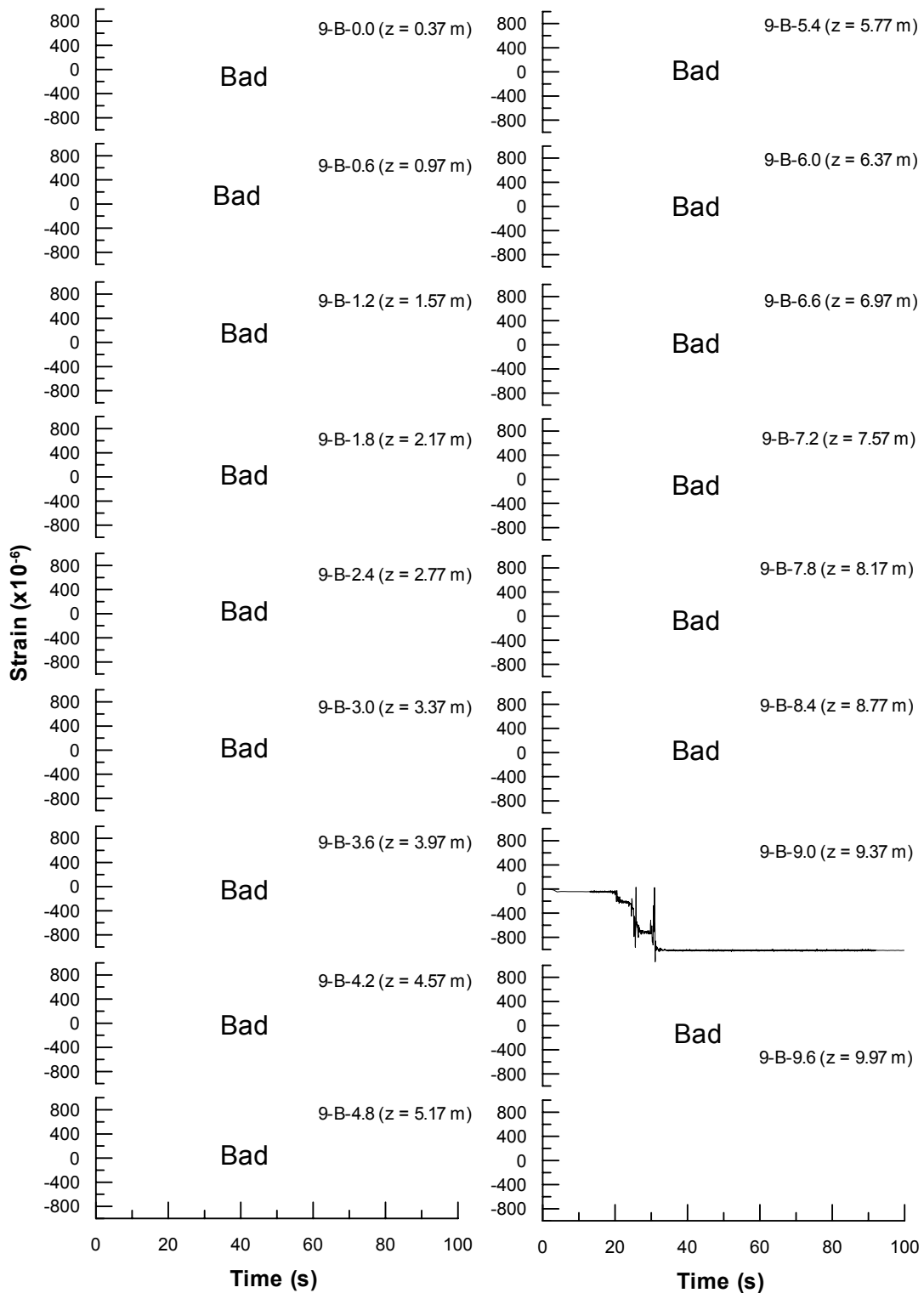


Fig. K.2 Time histories of strain along single pile (No. 9) at back side, second test

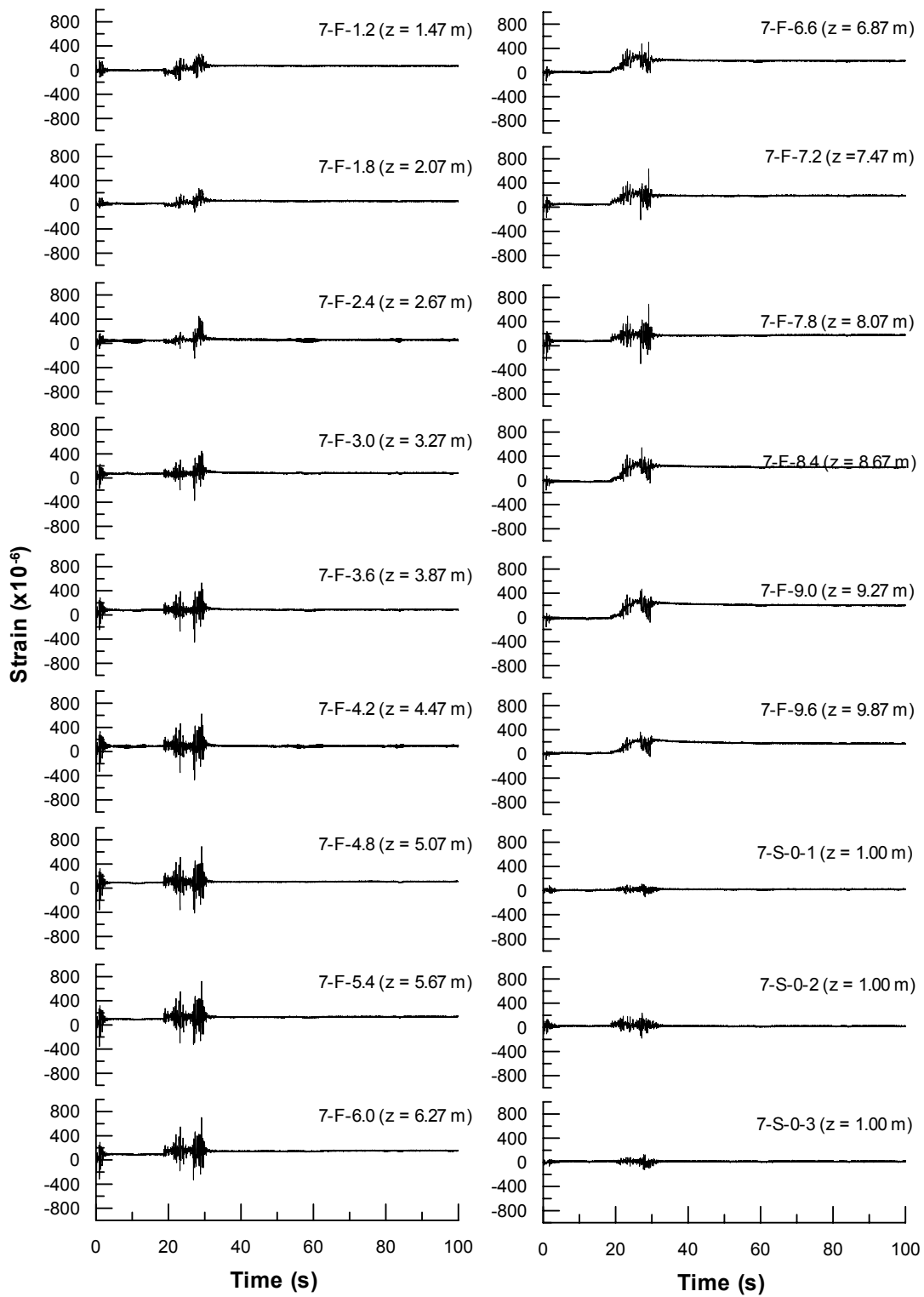


Fig. K.3 Time histories of strain along pile No. 7 of 4-pile group at front side, second test

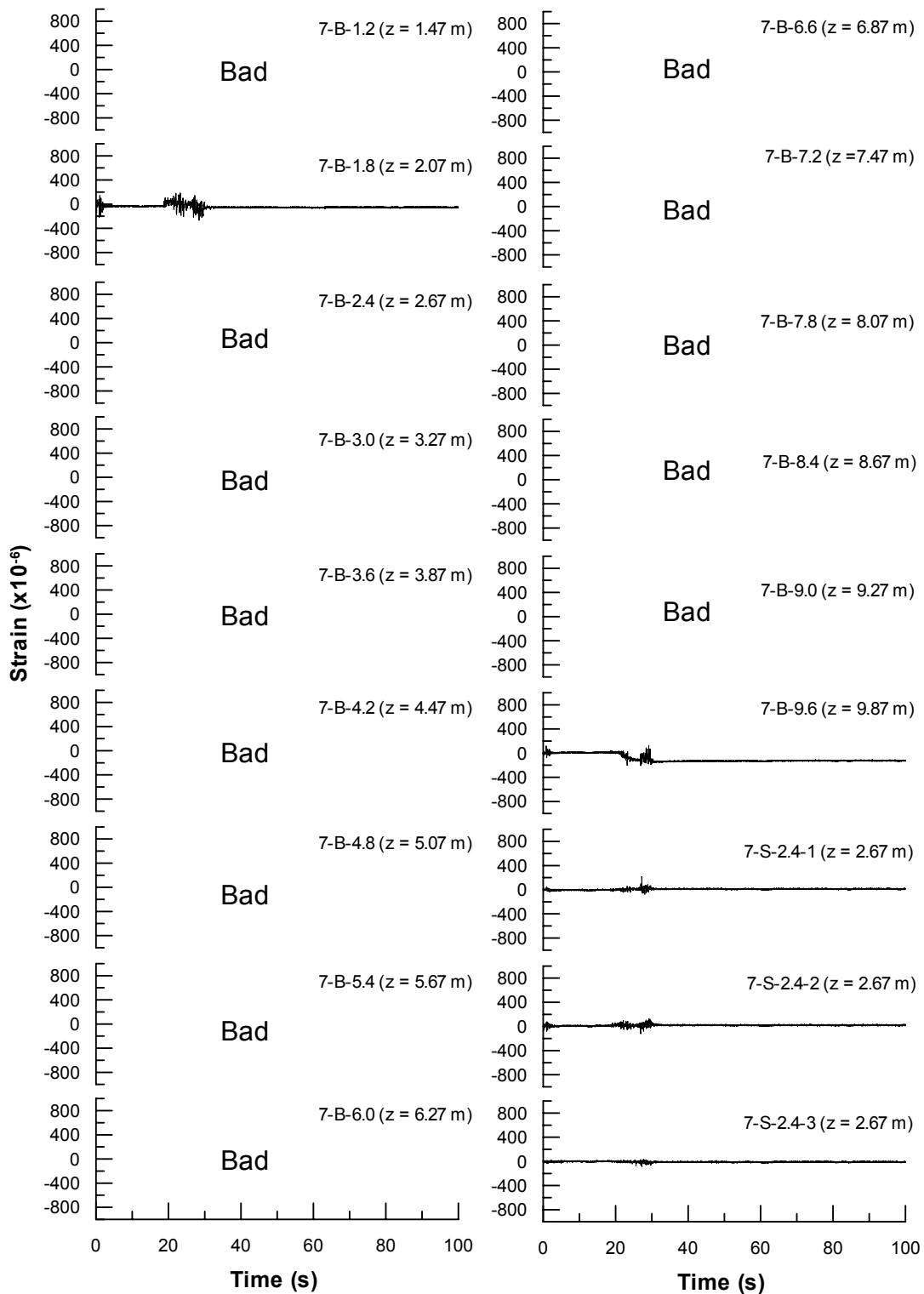


Fig. K.4 Time histories of strain along pile No. 7 of 4-pile group at back side, second test

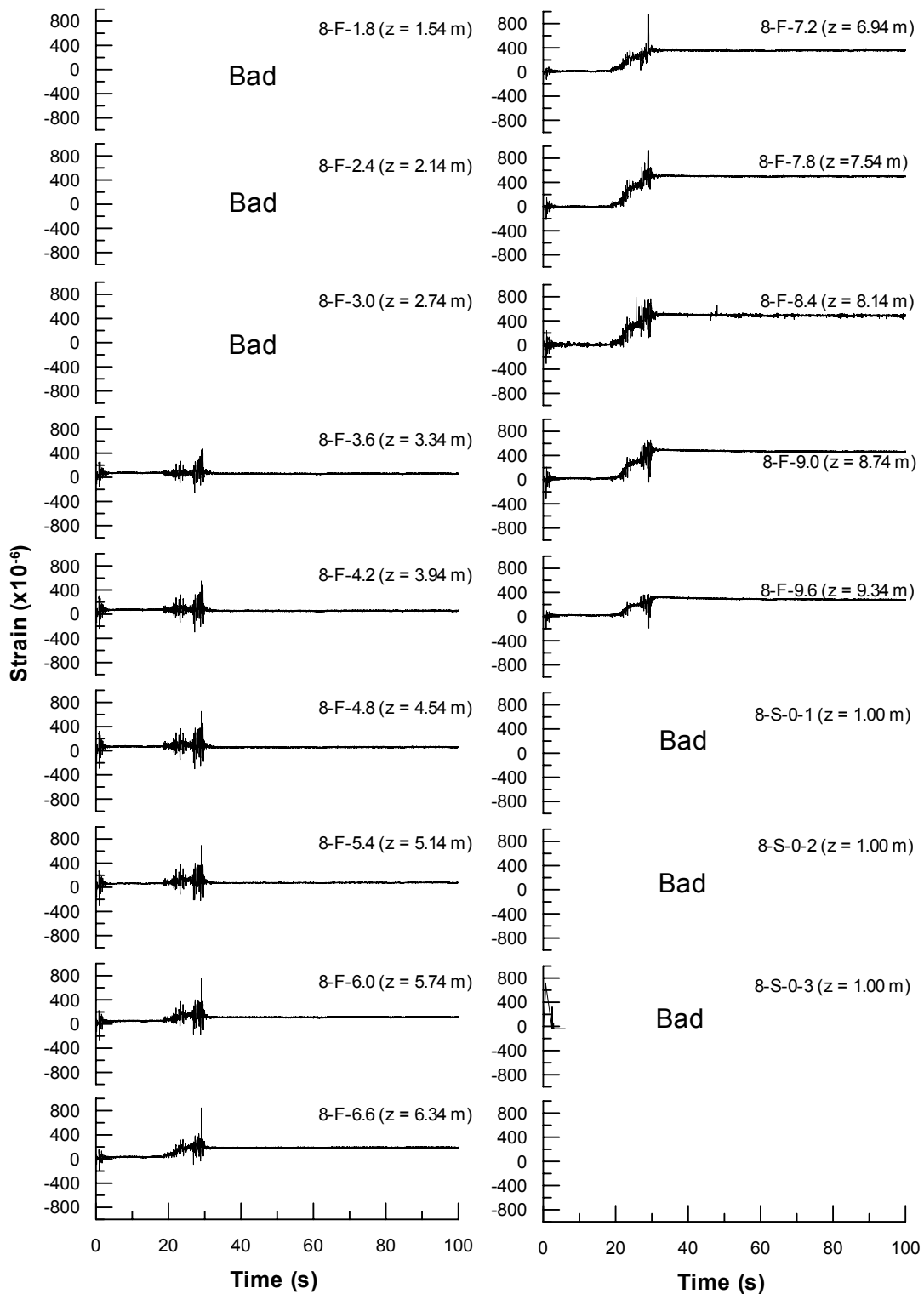


Fig. K.5 Time histories of strain along pile No. 8 of 4-pile group at front side, second test

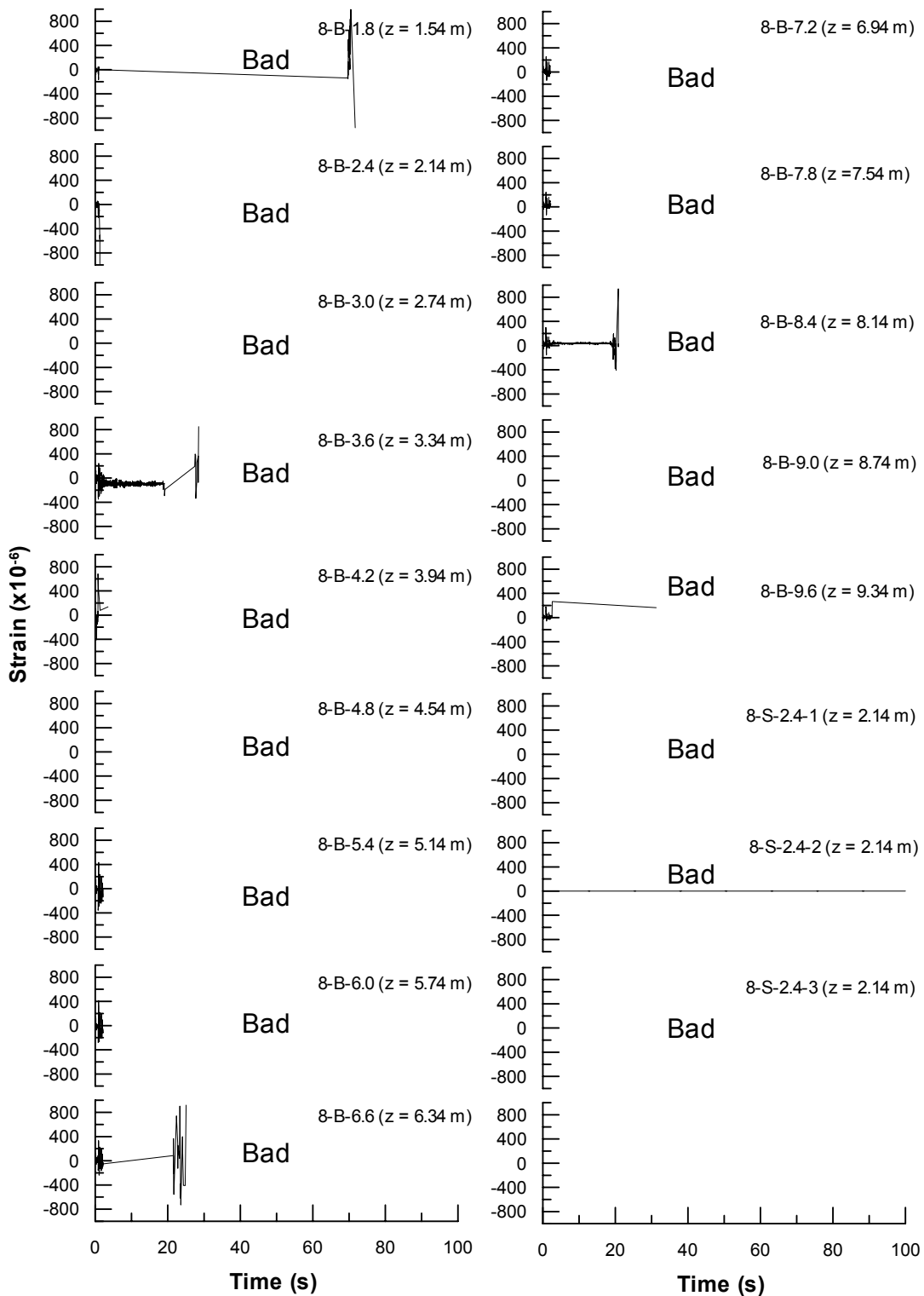


Fig. K.6 Time histories of strain along pile No. 8 of 4-pile group at back side, second test

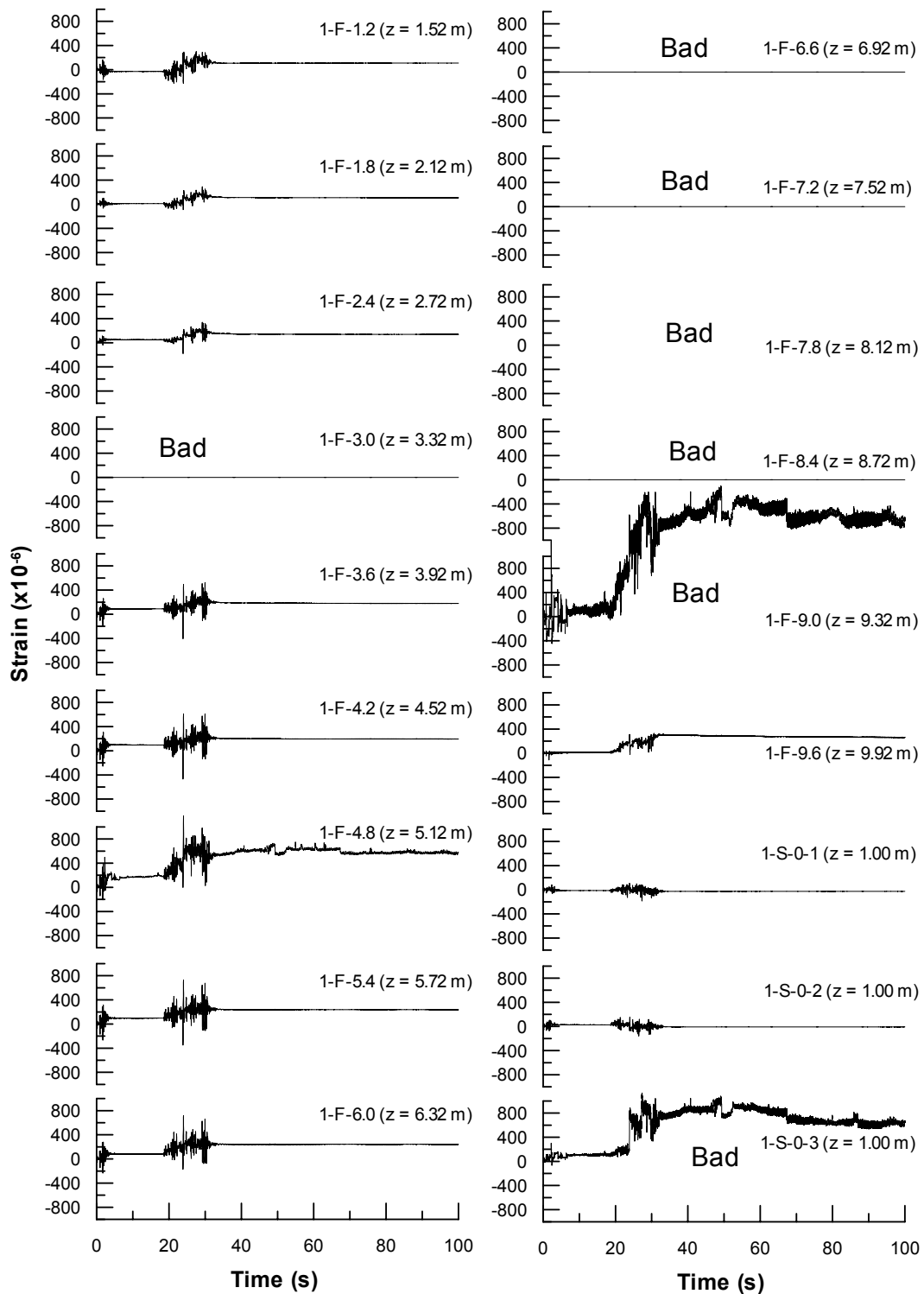


Fig. K.7 Time histories of strain along pile No. 1 of 9-pile group at front side, second test

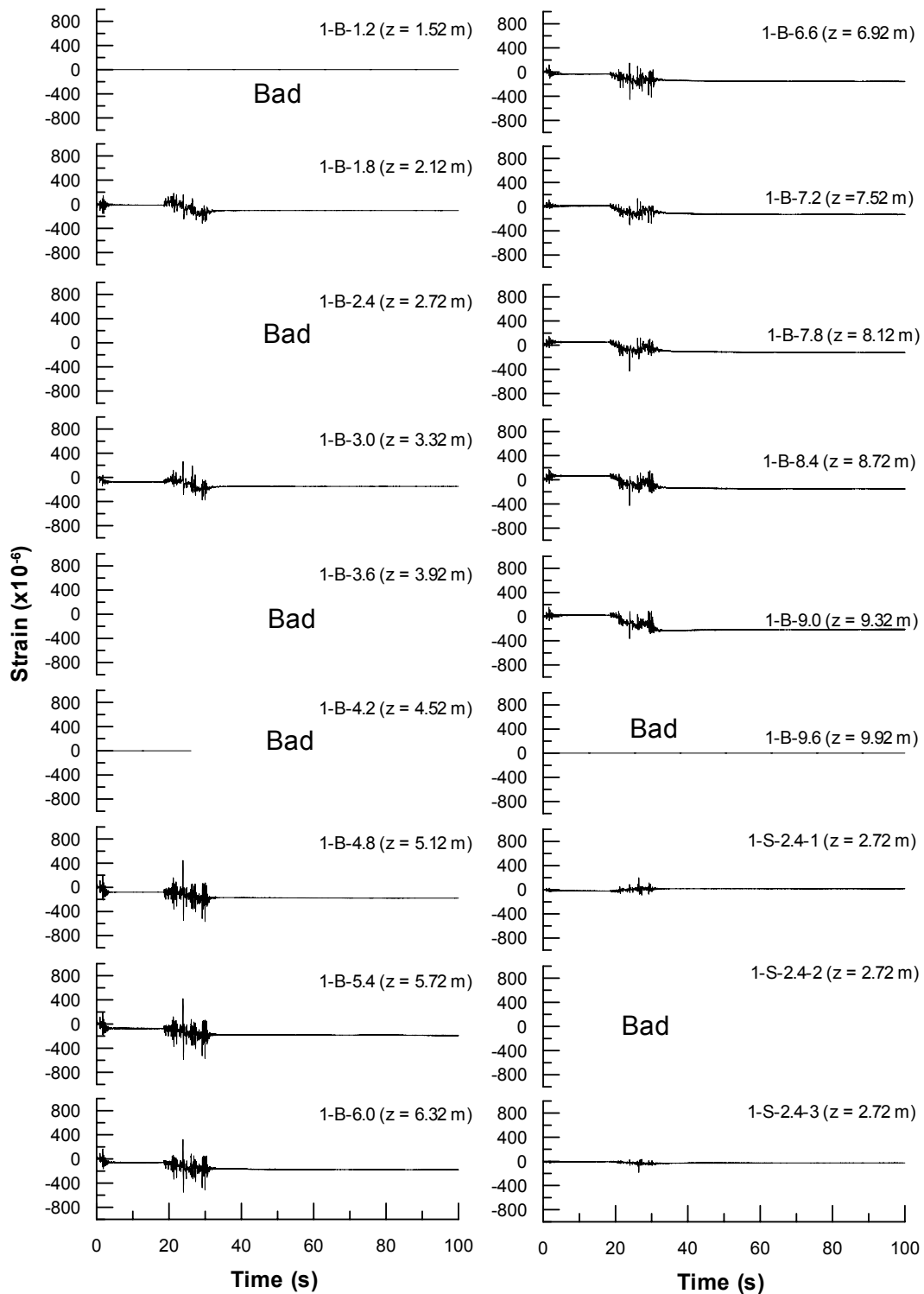


Fig. K.8 Time histories of strain along pile No. 1 of 9-pile group at back side, second test

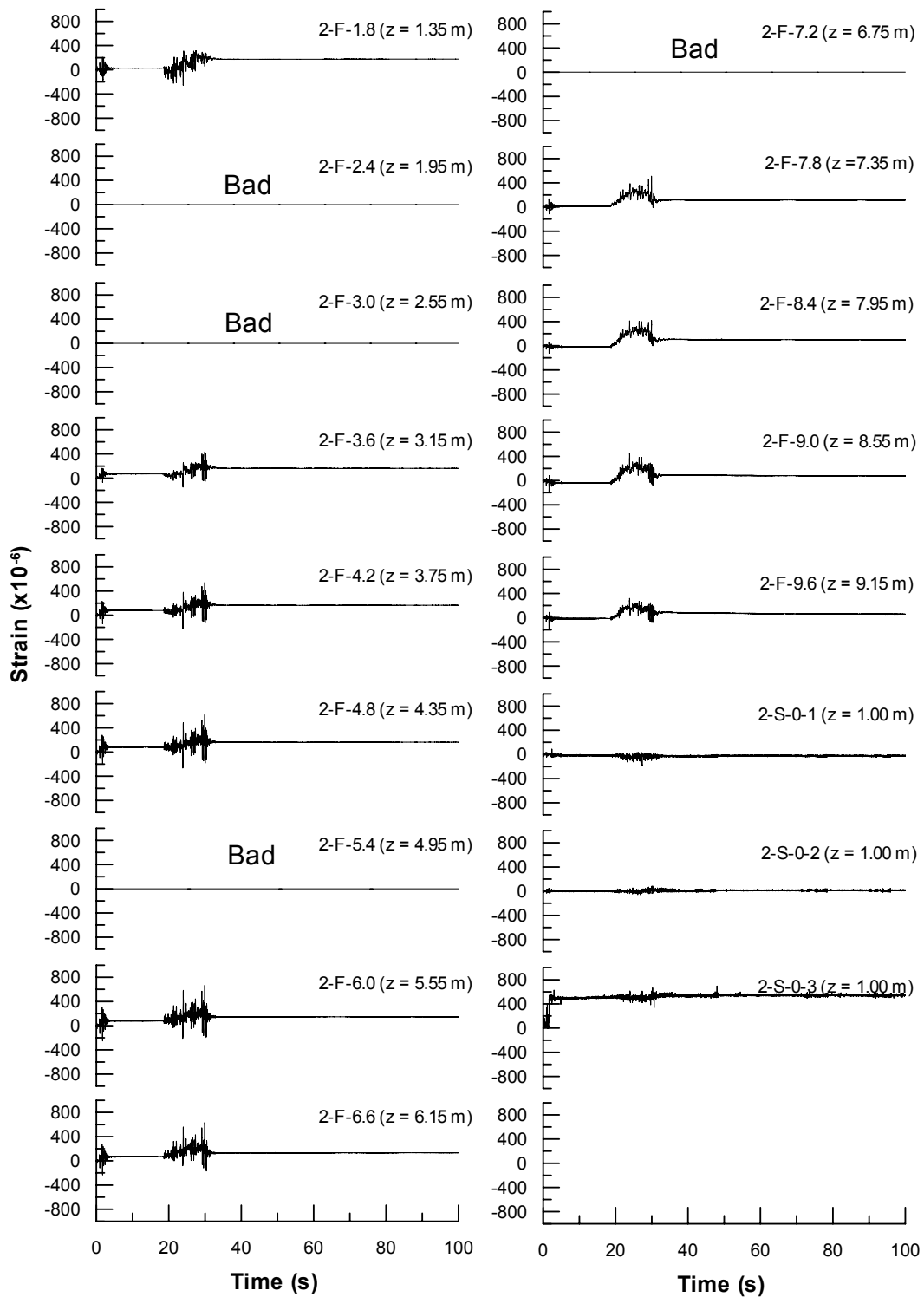


Fig. K.9 Time histories of strain along pile No. 2 of 9-pile group at front side, second test

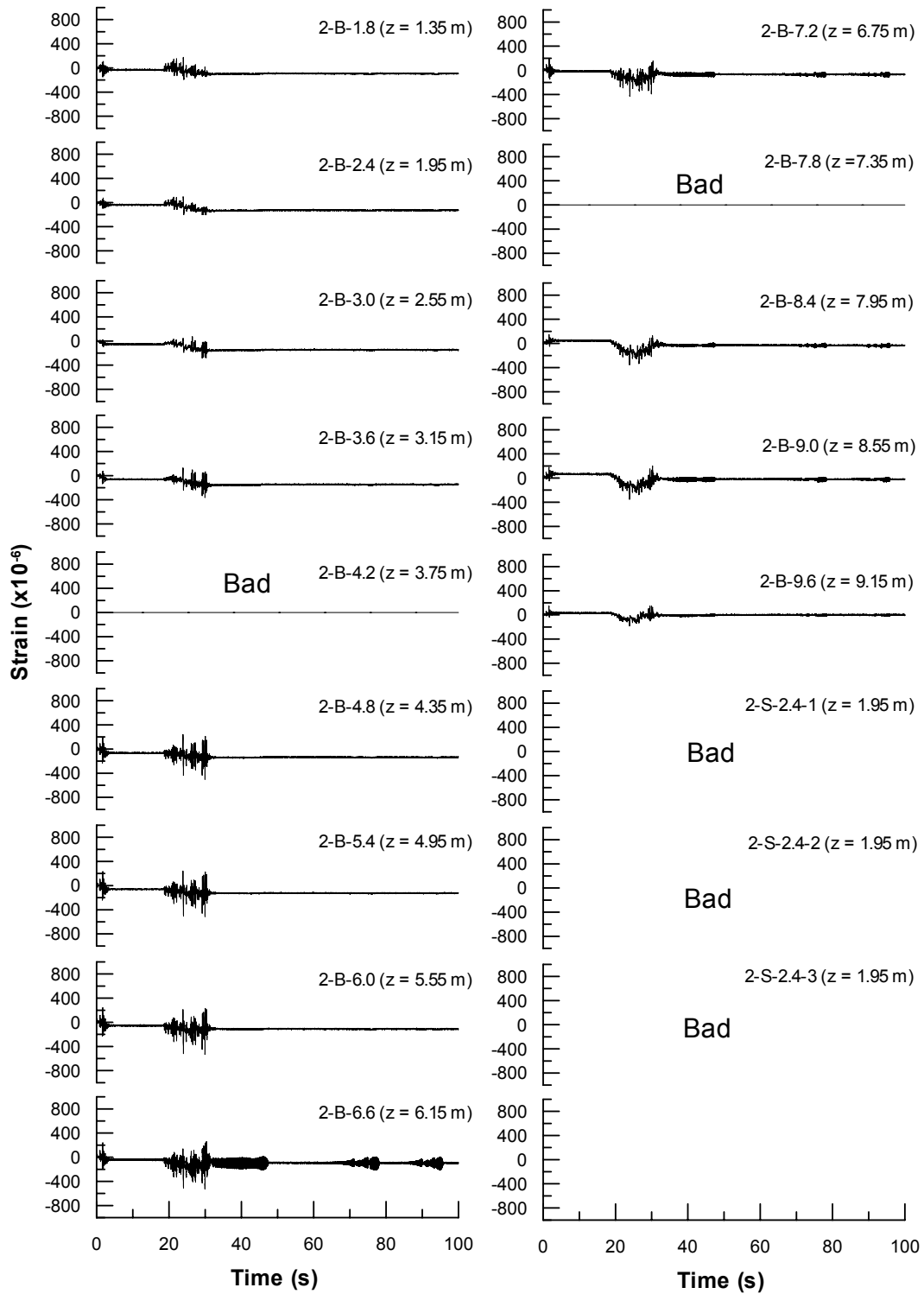


Fig. K.10 Time histories of strain along pile No. 2 of 9-pile group at back side, second test

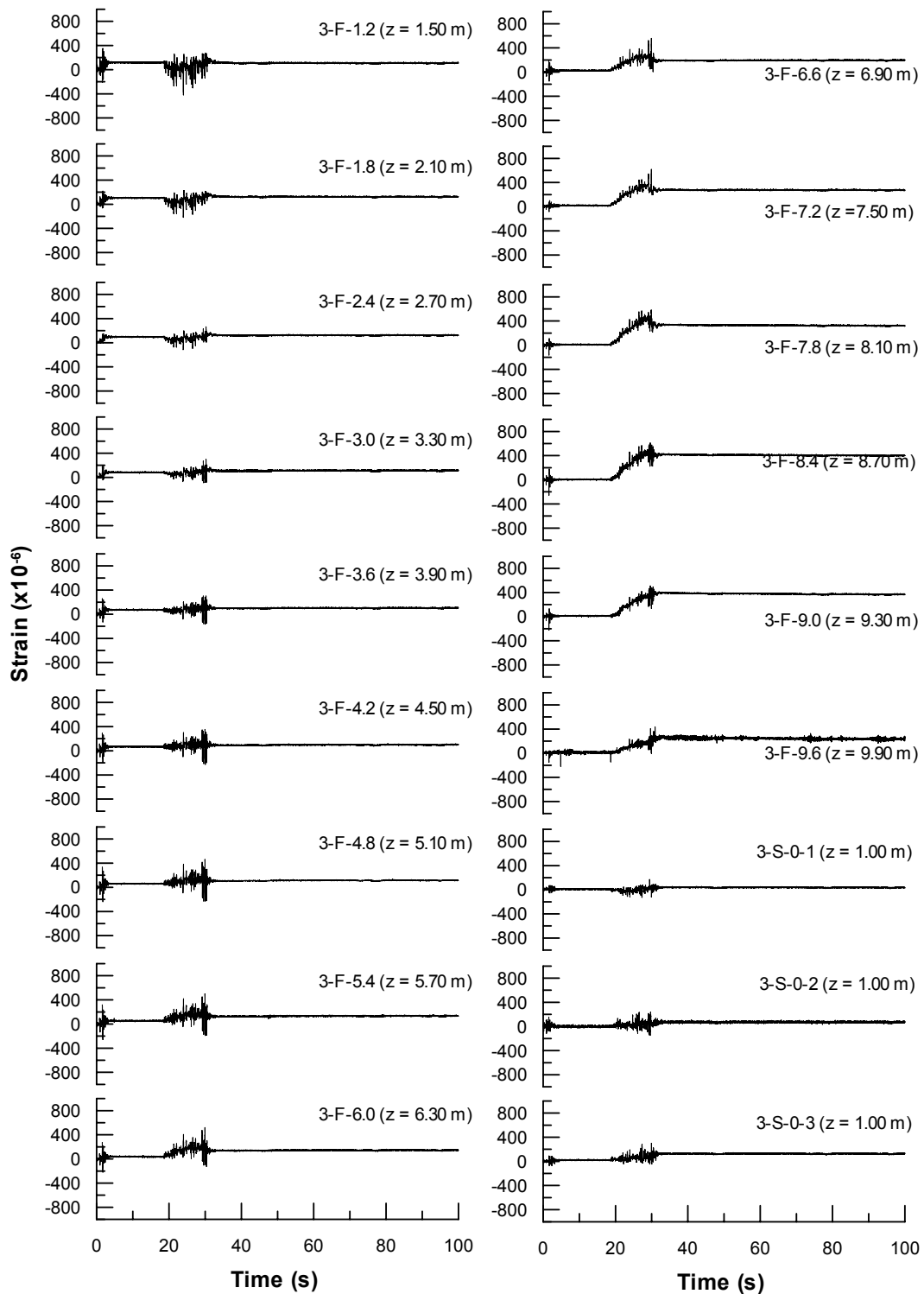


Fig. K.11 Time histories of strain along pile No. 3 of 9-pile group at front side, second test

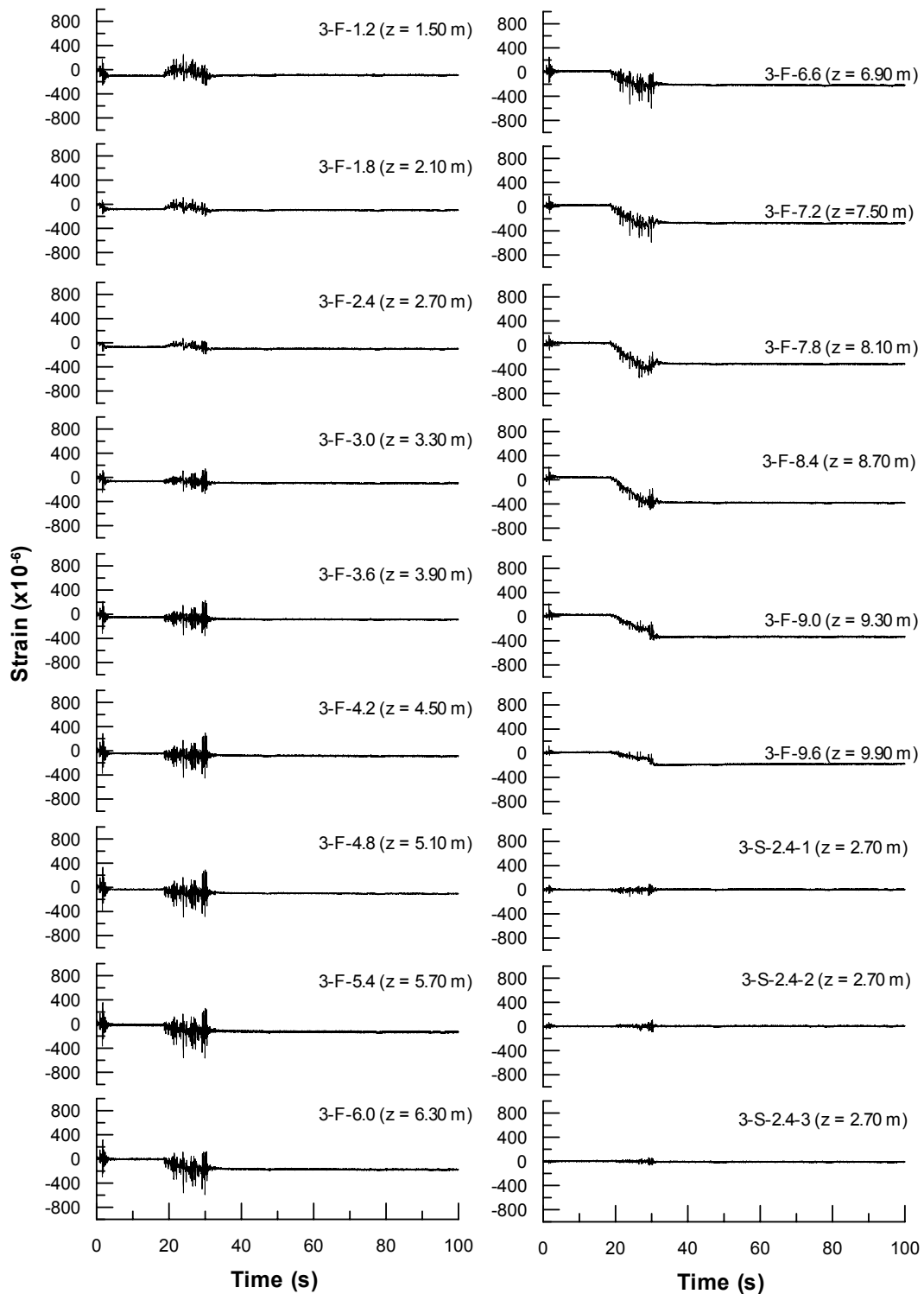


Fig. K.12 Time histories of strain along pile No. 3 of 9-pile group at back side, second test

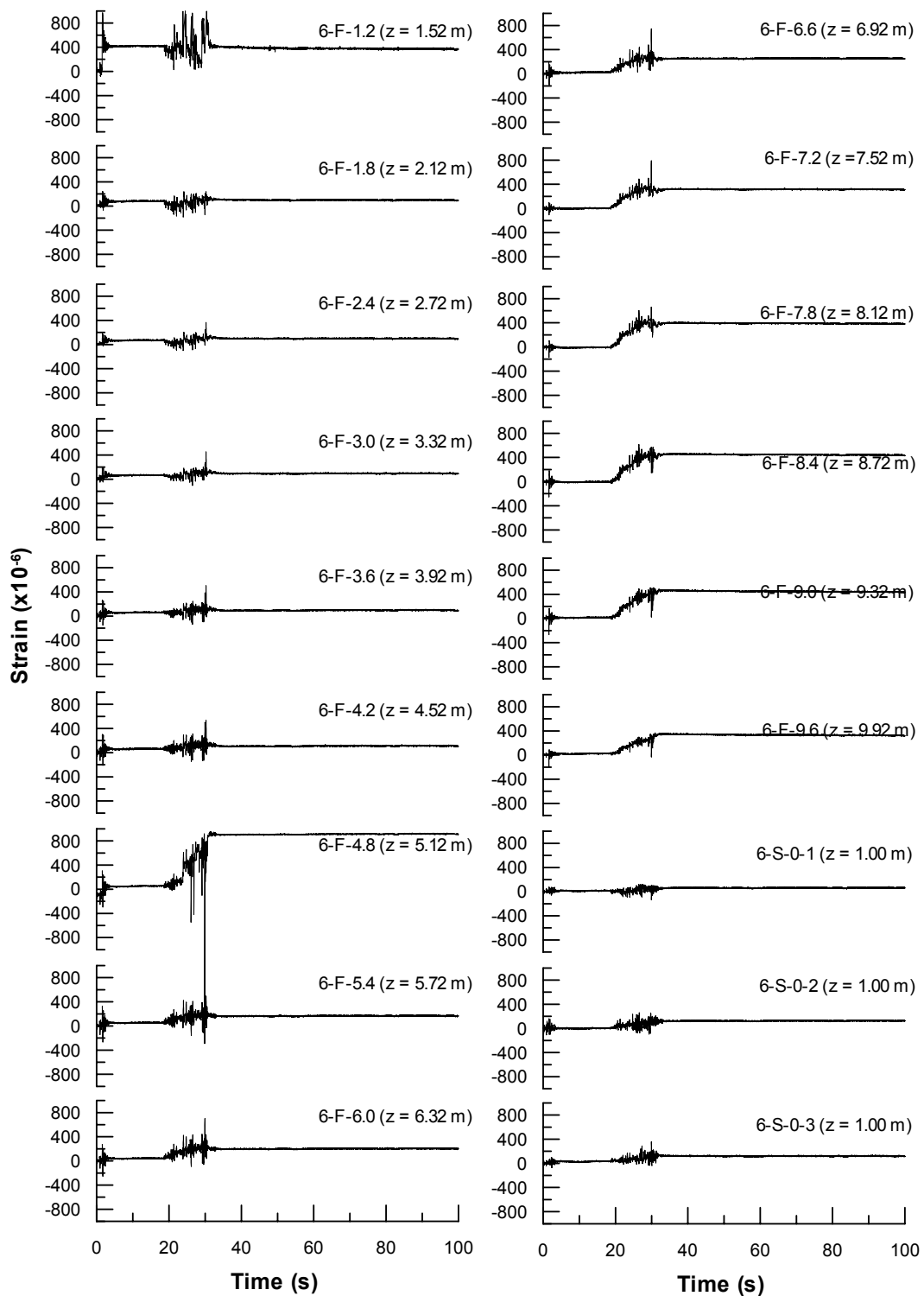


Fig. K.13 Time histories of strain along pile No. 6 of 9-pile group at front side, second test

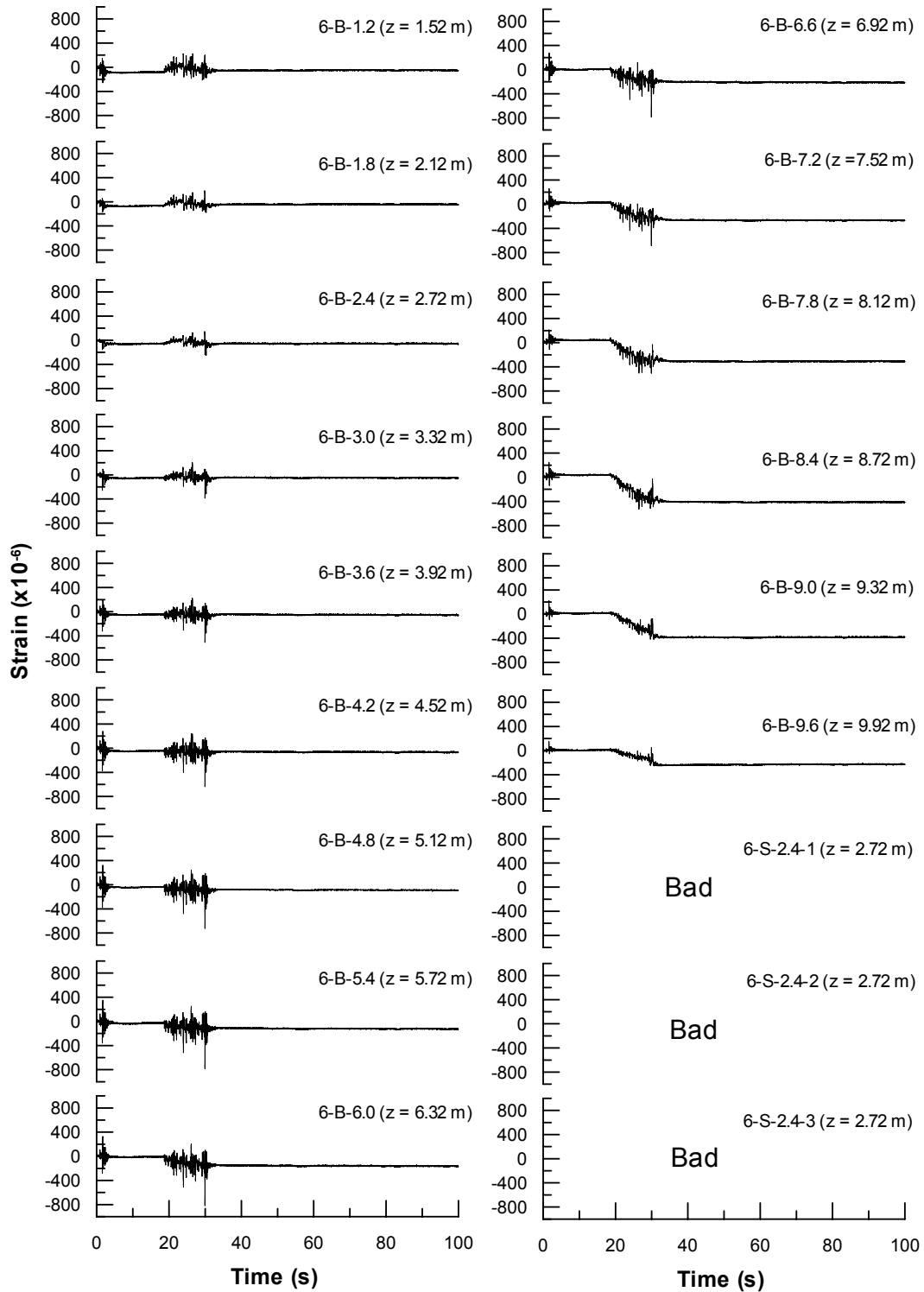


Fig. K.14 Time histories of strain along pile No. 6 of 9-pile group at back side, second test

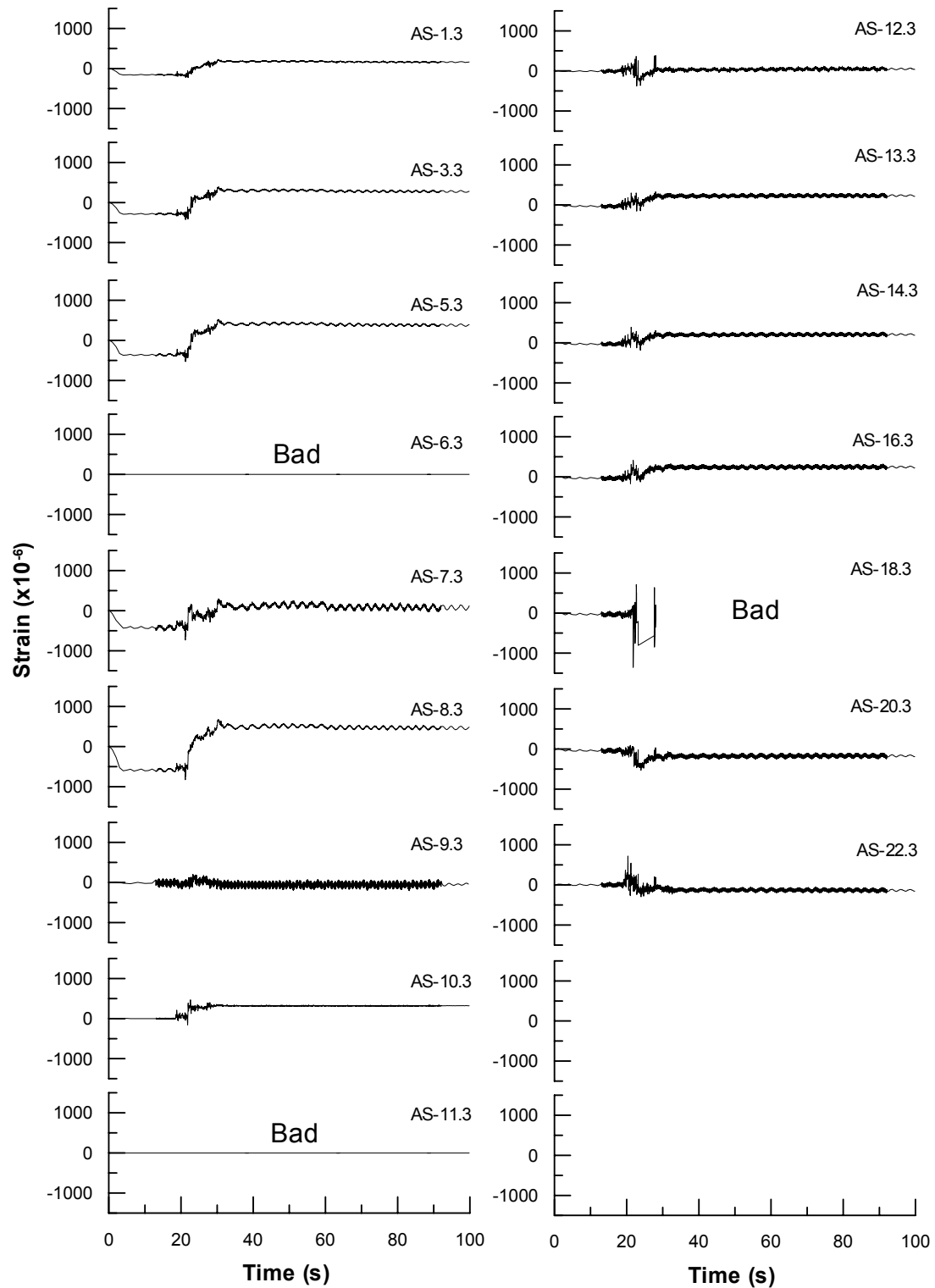


Fig. K.15 Time histories of strain along transverse pipeline A (side), second test

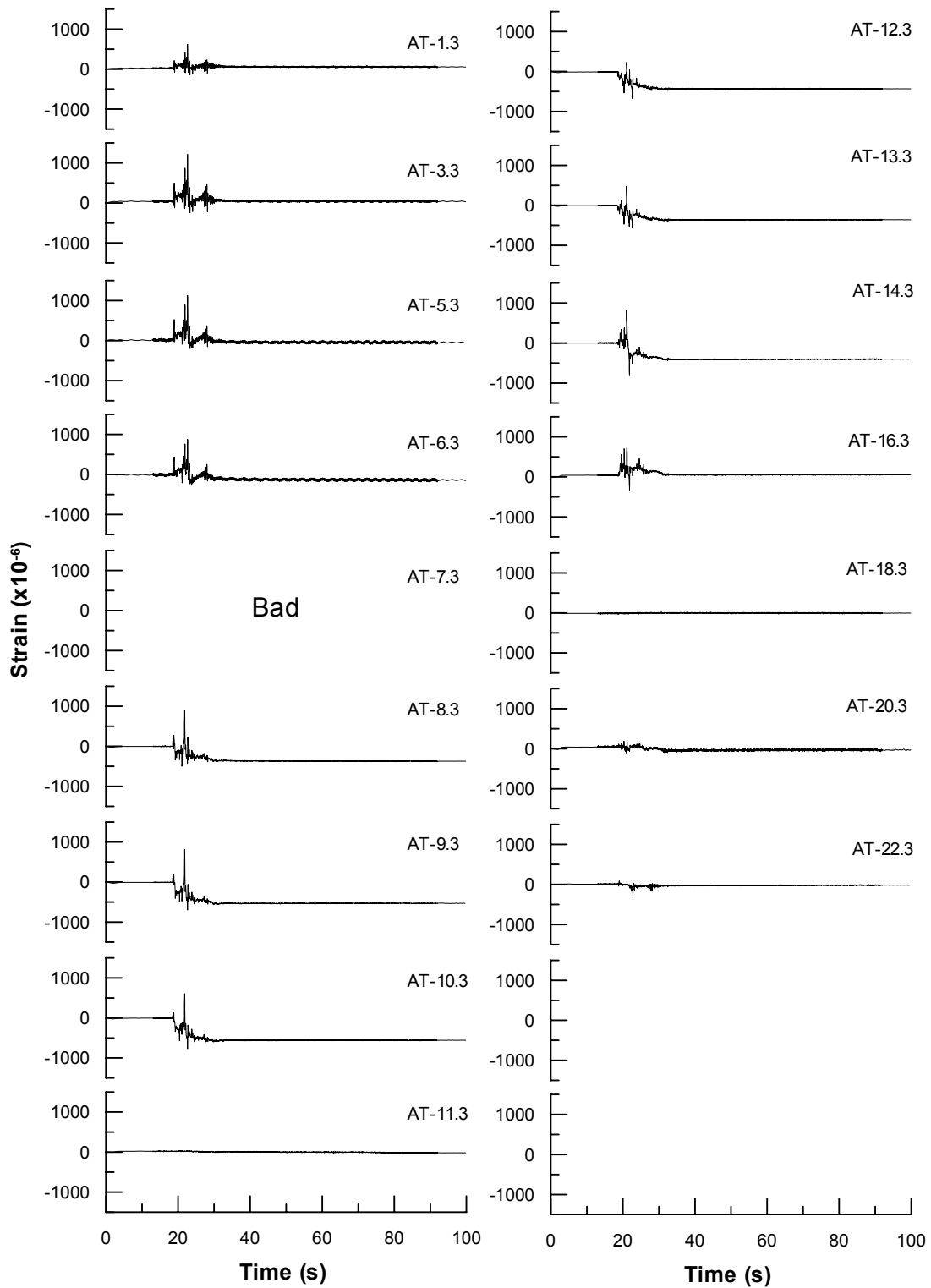


Fig. K.16 Time histories of strain along transverse pipeline A (top), second test

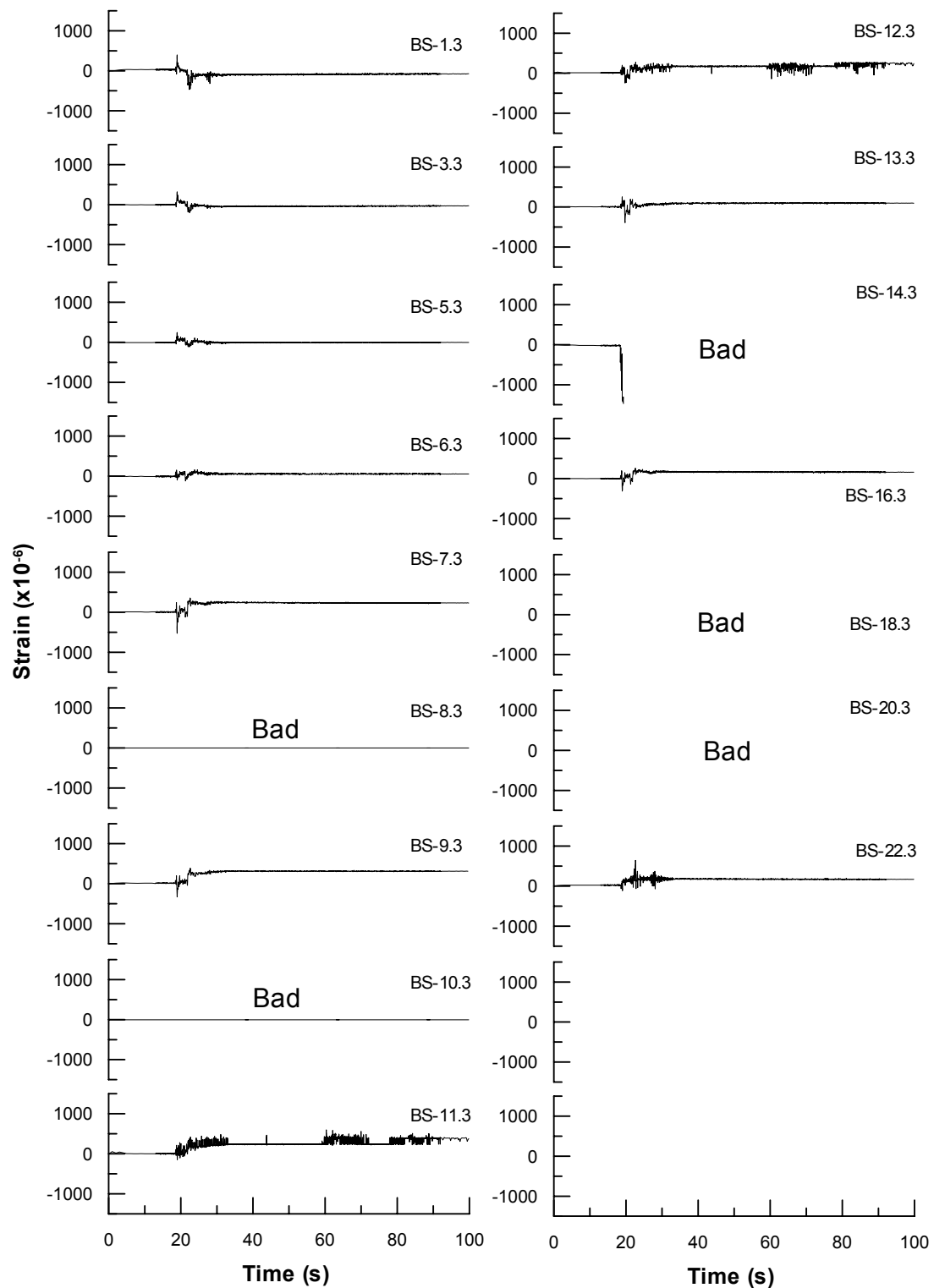


Fig. K.17 Time histories of strain along transverse pipeline B (side), second test

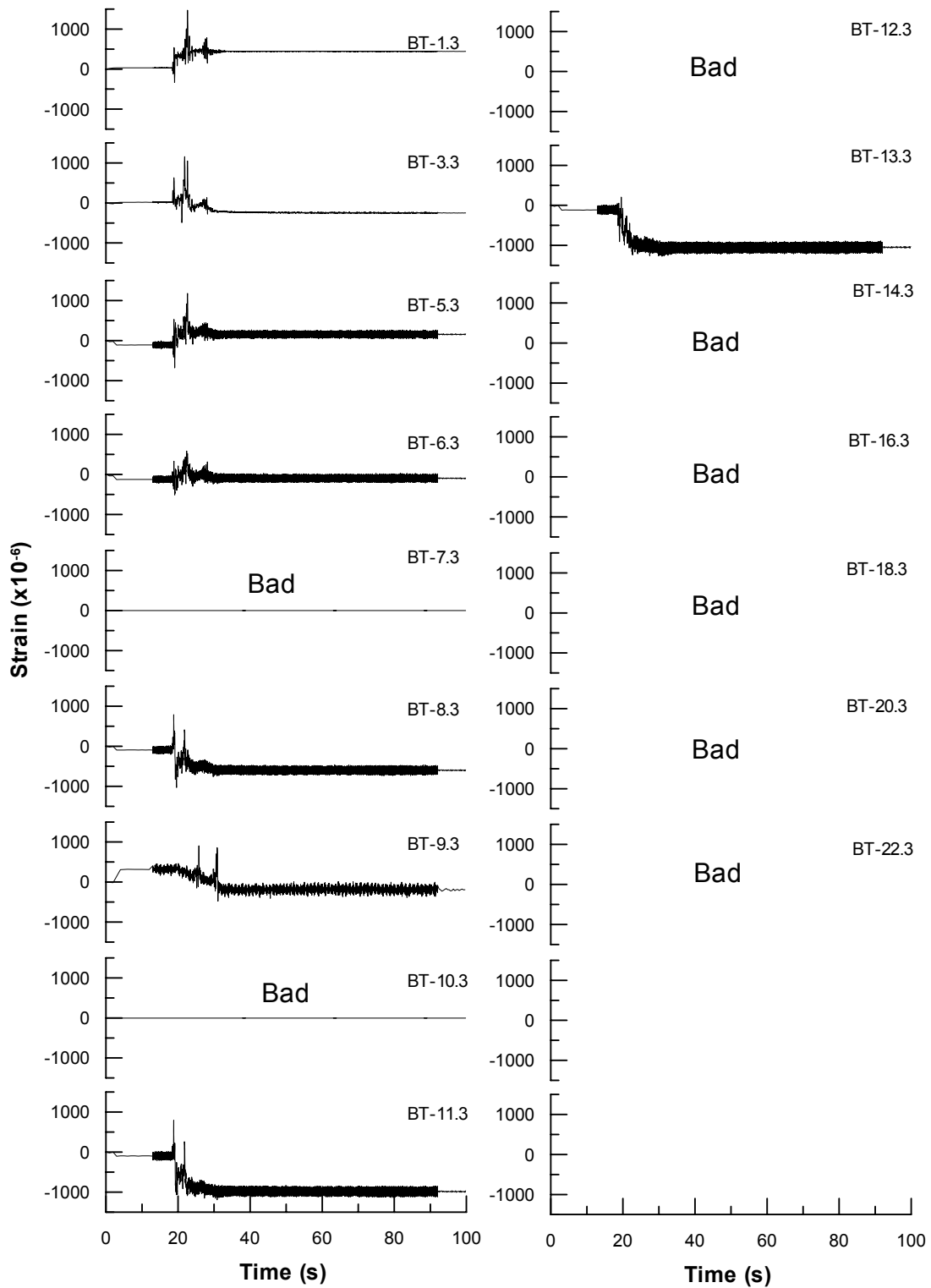


Fig. K.18 Time histories of strain along transverse pipeline B (top), second test

PEER REPORTS

PEER reports are available from the National Information Service for Earthquake Engineering (NISEE). To order PEER reports, please contact the Pacific Earthquake Engineering Research Center, 1301 South 46th Street, Richmond, California 94804-4698. Tel.: (510) 665-3405; Fax: (510) 665-3420.

- PEER 2006/04** *Probabilistic Seismic Evaluation of Reinforced Concrete Structural Components and Systems.* Tae Hyung Lee and Khalid M. Mosalam. August 2006.
- PEER 2006/03** *Performance of Lifelines Subjected to Lateral Spreading.* Scott A. Ashford and Teerawut Juirnarongrit. July 2006.
- PEER 2006/02** *Pacific Earthquake Engineering Research Center Highway Demonstration Project.* Anne Kiremidjian, James Moore, Yue Yue Fan, Nesrin Basoz, Ozgur Yazali, and Meredith Williams. April 2006.
- PEER 2006/01** *Bracing Berkeley. A Guide to Seismic Safety on the UC Berkeley Campus.* Mary C. Comerio, Stephen Tobriner, and Ariane Fehrenkamp. January 2006.
- PEER 2005/16** *Seismic Response and Reliability of Electrical Substation Equipment and Systems.* Junho Song, Armen Der Kiureghian, and Jerome L. Sackman. April 2006.
- PEER 2005/15** *CPT-Based Probabilistic Assessment of Seismic Soil Liquefaction Initiation.* R. E. S. Moss, R. B. Seed, R. E. Kayen, J. P. Stewart, and A. Der Kiureghian. April 2006.
- PEER 2005/14** *Workshop on Modeling of Nonlinear Cyclic Load-Deformation Behavior of Shallow Foundations.* Bruce L. Kutter, Geoffrey Martin, Tara Hutchinson, Chad Harden, Sivapalan Gajan, and Justin Phalen. March 2006.
- PEER 2005/13** *Stochastic Characterization and Decision Bases under Time-Dependent Aftershock Risk in Performance-Based Earthquake Engineering.* Gee Liek Yeo and C. Allin Cornell. July 2005.
- PEER 2005/12** *PEER Testbed Study on a Laboratory Building: Exercising Seismic Performance Assessment.* Mary C. Comerio, editor. November 2005.
- PEER 2005/11** *Van Nuys Hotel Building Testbed Report: Exercising Seismic Performance Assessment.* Helmut Krawinkler, editor. October 2005.
- PEER 2005/10** *First NEES/E-Defense Workshop on Collapse Simulation of Reinforced Concrete Building Structures.* September 2005.
- PEER 2005/09** *Test Applications of Advanced Seismic Assessment Guidelines.* Joe Maffei, Karl Telleen, Danya Mohr, William Holmes, and Yuki Nakayama. August 2006.
- PEER 2005/08** *Damage Accumulation in Lightly Confined Reinforced Concrete Bridge Columns.* R. Tyler Ranf, Jared M. Nelson, Zach Price, Marc O. Eberhard, and John F. Stanton. April 2006.
- PEER 2005/07** *Experimental and Analytical Studies on the Seismic Response of Freestanding and Anchored Laboratory Equipment.* Dimitrios Konstantinidis and Nicos Makris. January 2005.
- PEER 2005/06** *Global Collapse of Frame Structures under Seismic Excitations.* Luis F. Ibarra and Helmut Krawinkler. September 2005.
- PEER 2005/05** *Performance Characterization of Bench- and Shelf-Mounted Equipment.* Samit Ray Chaudhuri and Tara C. Hutchinson. May 2006.
- PEER 2005/04** *Numerical Modeling of the Nonlinear Cyclic Response of Shallow Foundations.* Chad Harden, Tara Hutchinson, Geoffrey R. Martin, and Bruce L. Kutter. August 2005.
- PEER 2005/03** *A Taxonomy of Building Components for Performance-Based Earthquake Engineering.* Keith A. Porter. September 2005.
- PEER 2005/02** *Fragility Basis for California Highway Overpass Bridge Seismic Decision Making.* Kevin R. Mackie and Bozidar Stojadinovic. June 2005.
- PEER 2005/01** *Empirical Characterization of Site Conditions on Strong Ground Motion.* Jonathan P. Stewart, Yoojoong Choi, and Robert W. Graves. June 2005.
- PEER 2004/09** *Electrical Substation Equipment Interaction: Experimental Rigid Conductor Studies.* Christopher Stearns and André Filiatrault. February 2005.

- PEER 2004/08** *Seismic Qualification and Fragility Testing of Line Break 550-kV Disconnect Switches.* Shakhzod M. Takhirov, Gregory L. Fenves, and Eric Fujisaki. January 2005.
- PEER 2004/07** *Ground Motions for Earthquake Simulator Qualification of Electrical Substation Equipment.* Shakhzod M. Takhirov, Gregory L. Fenves, Eric Fujisaki, and Don Clyde. January 2005.
- PEER 2004/06** *Performance-Based Regulation and Regulatory Regimes.* Peter J. May and Chris Koski. September 2004.
- PEER 2004/05** *Performance-Based Seismic Design Concepts and Implementation: Proceedings of an International Workshop.* Peter Fajfar and Helmut Krawinkler, editors. September 2004.
- PEER 2004/04** *Seismic Performance of an Instrumented Tilt-up Wall Building.* James C. Anderson and Vitelmo V. Bertero. July 2004.
- PEER 2004/03** *Evaluation and Application of Concrete Tilt-up Assessment Methodologies.* Timothy Graf and James O. Malley. October 2004.
- PEER 2004/02** *Analytical Investigations of New Methods for Reducing Residual Displacements of Reinforced Concrete Bridge Columns.* Junichi Sakai and Stephen A. Mahin. August 2004.
- PEER 2004/01** *Seismic Performance of Masonry Buildings and Design Implications.* Kerri Anne Taeko Tokoro, James C. Anderson, and Vitelmo V. Bertero. February 2004.
- PEER 2003/18** *Performance Models for Flexural Damage in Reinforced Concrete Columns.* Michael Berry and Marc Eberhard. August 2003.
- PEER 2003/17** *Predicting Earthquake Damage in Older Reinforced Concrete Beam-Column Joints.* Catherine Pagni and Laura Lowes. October 2004.
- PEER 2003/16** *Seismic Demands for Performance-Based Design of Bridges.* Kevin Mackie and Božidar Stojadinovic. August 2003.
- PEER 2003/15** *Seismic Demands for Nondeteriorating Frame Structures and Their Dependence on Ground Motions.* Ricardo Antonio Medina and Helmut Krawinkler. May 2004.
- PEER 2003/14** *Finite Element Reliability and Sensitivity Methods for Performance-Based Earthquake Engineering.* Terje Haukaas and Armen Der Kiureghian. April 2004.
- PEER 2003/13** *Effects of Connection Hysteretic Degradation on the Seismic Behavior of Steel Moment-Resisting Frames.* Janise E. Rodgers and Stephen A. Mahin. March 2004.
- PEER 2003/12** *Implementation Manual for the Seismic Protection of Laboratory Contents: Format and Case Studies.* William T. Holmes and Mary C. Comerio. October 2003.
- PEER 2003/11** *Fifth U.S.-Japan Workshop on Performance-Based Earthquake Engineering Methodology for Reinforced Concrete Building Structures.* February 2004.
- PEER 2003/10** *A Beam-Column Joint Model for Simulating the Earthquake Response of Reinforced Concrete Frames.* Laura N. Lowes, Nilanjan Mitra, and Arash Altoontash. February 2004.
- PEER 2003/09** *Sequencing Repairs after an Earthquake: An Economic Approach.* Marco Casari and Simon J. Wilkie. April 2004.
- PEER 2003/08** *A Technical Framework for Probability-Based Demand and Capacity Factor Design (DCFD) Seismic Formats.* Fatemeh Jalayer and C. Allin Cornell. November 2003.
- PEER 2003/07** *Uncertainty Specification and Propagation for Loss Estimation Using FOSM Methods.* Jack W. Baker and C. Allin Cornell. September 2003.
- PEER 2003/06** *Performance of Circular Reinforced Concrete Bridge Columns under Bidirectional Earthquake Loading.* Mahmoud M. Hachem, Stephen A. Mahin, and Jack P. Moehle. February 2003.
- PEER 2003/05** *Response Assessment for Building-Specific Loss Estimation.* Eduardo Miranda and Shahram Taghavi. September 2003.
- PEER 2003/04** *Experimental Assessment of Columns with Short Lap Splices Subjected to Cyclic Loads.* Murat Melek, John W. Wallace, and Joel Conte. April 2003.
- PEER 2003/03** *Probabilistic Response Assessment for Building-Specific Loss Estimation.* Eduardo Miranda and Hesameddin Aslani. September 2003.

- PEER 2003/02** *Software Framework for Collaborative Development of Nonlinear Dynamic Analysis Program.* Jun Peng and Kincho H. Law. September 2003.
- PEER 2003/01** *Shake Table Tests and Analytical Studies on the Gravity Load Collapse of Reinforced Concrete Frames.* Kenneth John Elwood and Jack P. Moehle. November 2003.
- PEER 2002/24** *Performance of Beam to Column Bridge Joints Subjected to a Large Velocity Pulse.* Natalie Gibson, André Filiatrault, and Scott A. Ashford. April 2002.
- PEER 2002/23** *Effects of Large Velocity Pulses on Reinforced Concrete Bridge Columns.* Greg L. Orozco and Scott A. Ashford. April 2002.
- PEER 2002/22** *Characterization of Large Velocity Pulses for Laboratory Testing.* Kenneth E. Cox and Scott A. Ashford. April 2002.
- PEER 2002/21** *Fourth U.S.-Japan Workshop on Performance-Based Earthquake Engineering Methodology for Reinforced Concrete Building Structures.* December 2002.
- PEER 2002/20** *Barriers to Adoption and Implementation of PBEE Innovations.* Peter J. May. August 2002.
- PEER 2002/19** *Economic-Engineered Integrated Models for Earthquakes: Socioeconomic Impacts.* Peter Gordon, James E. Moore II, and Harry W. Richardson. July 2002.
- PEER 2002/18** *Assessment of Reinforced Concrete Building Exterior Joints with Substandard Details.* Chris P. Pantelides, Jon Hansen, Justin Nadauld, and Lawrence D. Reaveley. May 2002.
- PEER 2002/17** *Structural Characterization and Seismic Response Analysis of a Highway Overcrossing Equipped with Elastomeric Bearings and Fluid Dampers: A Case Study.* Nicos Makris and Jian Zhang. November 2002.
- PEER 2002/16** *Estimation of Uncertainty in Geotechnical Properties for Performance-Based Earthquake Engineering.* Allen L. Jones, Steven L. Kramer, and Pedro Arduino. December 2002.
- PEER 2002/15** *Seismic Behavior of Bridge Columns Subjected to Various Loading Patterns.* Asadollah Esmaeily-Gh. and Yan Xiao. December 2002.
- PEER 2002/14** *Inelastic Seismic Response of Extended Pile Shaft Supported Bridge Structures.* T.C. Hutchinson, R.W. Boulanger, Y.H. Chai, and I.M. Idriss. December 2002.
- PEER 2002/13** *Probabilistic Models and Fragility Estimates for Bridge Components and Systems.* Paolo Gardoni, Armen Der Kiureghian, and Khalid M. Mosalam. June 2002.
- PEER 2002/12** *Effects of Fault Dip and Slip Rake on Near-Source Ground Motions: Why Chi-Chi Was a Relatively Mild M7.6 Earthquake.* Brad T. Aagaard, John F. Hall, and Thomas H. Heaton. December 2002.
- PEER 2002/11** *Analytical and Experimental Study of Fiber-Reinforced Strip Isolators.* James M. Kelly and Shakhzod M. Takhirov. September 2002.
- PEER 2002/10** *Centrifuge Modeling of Settlement and Lateral Spreading with Comparisons to Numerical Analyses.* Sivapalan Gajan and Bruce L. Kutter. January 2003.
- PEER 2002/09** *Documentation and Analysis of Field Case Histories of Seismic Compression during the 1994 Northridge, California, Earthquake.* Jonathan P. Stewart, Patrick M. Smith, Daniel H. Whang, and Jonathan D. Bray. October 2002.
- PEER 2002/08** *Component Testing, Stability Analysis and Characterization of Buckling-Restrained Unbonded Braces™.* Cameron Black, Nicos Makris, and Ian Aiken. September 2002.
- PEER 2002/07** *Seismic Performance of Pile-Wharf Connections.* Charles W. Roeder, Robert Graff, Jennifer Soderstrom, and Jun Han Yoo. December 2001.
- PEER 2002/06** *The Use of Benefit-Cost Analysis for Evaluation of Performance-Based Earthquake Engineering Decisions.* Richard O. Zerbe and Anthony Falit-Baiamonte. September 2001.
- PEER 2002/05** *Guidelines, Specifications, and Seismic Performance Characterization of Nonstructural Building Components and Equipment.* André Filiatrault, Constantin Christopoulos, and Christopher Stearns. September 2001.
- PEER 2002/04** *Consortium of Organizations for Strong-Motion Observation Systems and the Pacific Earthquake Engineering Research Center Lifelines Program: Invited Workshop on Archiving and Web Dissemination of Geotechnical Data, 4–5 October 2001.* September 2002.

- PEER 2002/03** *Investigation of Sensitivity of Building Loss Estimates to Major Uncertain Variables for the Van Nuys Testbed.* Keith A. Porter, James L. Beck, and Rustem V. Shaikhutdinov. August 2002.
- PEER 2002/02** *The Third U.S.-Japan Workshop on Performance-Based Earthquake Engineering Methodology for Reinforced Concrete Building Structures.* July 2002.
- PEER 2002/01** *Nonstructural Loss Estimation: The UC Berkeley Case Study.* Mary C. Comerio and John C. Stallmeyer. December 2001.
- PEER 2001/16** *Statistics of SDF-System Estimate of Roof Displacement for Pushover Analysis of Buildings.* Anil K. Chopra, Rakesh K. Goel, and Chatpan Chintanapakdee. December 2001.
- PEER 2001/15** *Damage to Bridges during the 2001 Nisqually Earthquake.* R. Tyler Ranf, Marc O. Eberhard, and Michael P. Berry. November 2001.
- PEER 2001/14** *Rocking Response of Equipment Anchored to a Base Foundation.* Nicos Makris and Cameron J. Black. September 2001.
- PEER 2001/13** *Modeling Soil Liquefaction Hazards for Performance-Based Earthquake Engineering.* Steven L. Kramer and Ahmed-W. Elgamal. February 2001.
- PEER 2001/12** *Development of Geotechnical Capabilities in OpenSees.* Boris Jeremi . September 2001.
- PEER 2001/11** *Analytical and Experimental Study of Fiber-Reinforced Elastomeric Isolators.* James M. Kelly and Shakhzod M. Takhirov. September 2001.
- PEER 2001/10** *Amplification Factors for Spectral Acceleration in Active Regions.* Jonathan P. Stewart, Andrew H. Liu, Yoojoong Choi, and Mehmet B. Baturay. December 2001.
- PEER 2001/09** *Ground Motion Evaluation Procedures for Performance-Based Design.* Jonathan P. Stewart, Shyh-Jeng Chiou, Jonathan D. Bray, Robert W. Graves, Paul G. Somerville, and Norman A. Abrahamson. September 2001.
- PEER 2001/08** *Experimental and Computational Evaluation of Reinforced Concrete Bridge Beam-Column Connections for Seismic Performance.* Clay J. Naito, Jack P. Moehle, and Khalid M. Mosalam. November 2001.
- PEER 2001/07** *The Rocking Spectrum and the Shortcomings of Design Guidelines.* Nicos Makris and Dimitrios Konstantinidis. August 2001.
- PEER 2001/06** *Development of an Electrical Substation Equipment Performance Database for Evaluation of Equipment Fragilities.* Thalia Agnanos. April 1999.
- PEER 2001/05** *Stiffness Analysis of Fiber-Reinforced Elastomeric Isolators.* Hsiang-Chuan Tsai and James M. Kelly. May 2001.
- PEER 2001/04** *Organizational and Societal Considerations for Performance-Based Earthquake Engineering.* Peter J. May. April 2001.
- PEER 2001/03** *A Modal Pushover Analysis Procedure to Estimate Seismic Demands for Buildings: Theory and Preliminary Evaluation.* Anil K. Chopra and Rakesh K. Goel. January 2001.
- PEER 2001/02** *Seismic Response Analysis of Highway Overcrossings Including Soil-Structure Interaction.* Jian Zhang and Nicos Makris. March 2001.
- PEER 2001/01** *Experimental Study of Large Seismic Steel Beam-to-Column Connections.* Egor P. Popov and Shakhzod M. Takhirov. November 2000.
- PEER 2000/10** *The Second U.S.-Japan Workshop on Performance-Based Earthquake Engineering Methodology for Reinforced Concrete Building Structures.* March 2000.
- PEER 2000/09** *Structural Engineering Reconnaissance of the August 17, 1999 Earthquake: Kocaeli (Izmit), Turkey.* Halil Sezen, Kenneth J. Elwood, Andrew S. Whittaker, Khalid Mosalam, John J. Wallace, and John F. Stanton. December 2000.
- PEER 2000/08** *Behavior of Reinforced Concrete Bridge Columns Having Varying Aspect Ratios and Varying Lengths of Confinement.* Anthony J. Calderone, Dawn E. Lehman, and Jack P. Moehle. January 2001.
- PEER 2000/07** *Cover-Plate and Flange-Plate Reinforced Steel Moment-Resisting Connections.* Taejin Kim, Andrew S. Whittaker, Amir S. Gilani, Vitelmo V. Bertero, and Shakhzod M. Takhirov. September 2000.
- PEER 2000/06** *Seismic Evaluation and Analysis of 230-kV Disconnect Switches.* Amir S. J. Gilani, Andrew S. Whittaker, Gregory L. Fenves, Chun-Hao Chen, Henry Ho, and Eric Fujisaki. July 2000.

- PEER 2000/05** *Performance-Based Evaluation of Exterior Reinforced Concrete Building Joints for Seismic Excitation.* Chandra Clyde, Chris P. Pantelides, and Lawrence D. Reaveley. July 2000.
- PEER 2000/04** *An Evaluation of Seismic Energy Demand: An Attenuation Approach.* Chung-Che Chou and Chia-Ming Uang. July 1999.
- PEER 2000/03** *Framing Earthquake Retrofitting Decisions: The Case of Hillside Homes in Los Angeles.* Detlof von Winterfeldt, Nels Roselund, and Alicia Kitsuse. March 2000.
- PEER 2000/02** *U.S.-Japan Workshop on the Effects of Near-Field Earthquake Shaking.* Andrew Whittaker, ed. July 2000.
- PEER 2000/01** *Further Studies on Seismic Interaction in Interconnected Electrical Substation Equipment.* Armen Der Kiureghian, Kee-Jeung Hong, and Jerome L. Sackman. November 1999.
- PEER 1999/14** *Seismic Evaluation and Retrofit of 230-kV Porcelain Transformer Bushings.* Amir S. Gilani, Andrew S. Whittaker, Gregory L. Fenves, and Eric Fujisaki. December 1999.
- PEER 1999/13** *Building Vulnerability Studies: Modeling and Evaluation of Tilt-up and Steel Reinforced Concrete Buildings.* John W. Wallace, Jonathan P. Stewart, and Andrew S. Whittaker, editors. December 1999.
- PEER 1999/12** *Rehabilitation of Nonductile RC Frame Building Using Encasement Plates and Energy-Dissipating Devices.* Mehrdad Sasani, Vitelmo V. Bertero, James C. Anderson. December 1999.
- PEER 1999/11** *Performance Evaluation Database for Concrete Bridge Components and Systems under Simulated Seismic Loads.* Yael D. Hose and Frieder Seible. November 1999.
- PEER 1999/10** *U.S.-Japan Workshop on Performance-Based Earthquake Engineering Methodology for Reinforced Concrete Building Structures.* December 1999.
- PEER 1999/09** *Performance Improvement of Long Period Building Structures Subjected to Severe Pulse-Type Ground Motions.* James C. Anderson, Vitelmo V. Bertero, and Raul Bertero. October 1999.
- PEER 1999/08** *Envelopes for Seismic Response Vectors.* Charles Menun and Armen Der Kiureghian. July 1999.
- PEER 1999/07** *Documentation of Strengths and Weaknesses of Current Computer Analysis Methods for Seismic Performance of Reinforced Concrete Members.* William F. Cofer. November 1999.
- PEER 1999/06** *Rocking Response and Overturning of Anchored Equipment under Seismic Excitations.* Nicos Makris and Jian Zhang. November 1999.
- PEER 1999/05** *Seismic Evaluation of 550 kV Porcelain Transformer Bushings.* Amir S. Gilani, Andrew S. Whittaker, Gregory L. Fenves, and Eric Fujisaki. October 1999.
- PEER 1999/04** *Adoption and Enforcement of Earthquake Risk-Reduction Measures.* Peter J. May, Raymond J. Burby, T. Jens Feeley, and Robert Wood.
- PEER 1999/03** *Task 3 Characterization of Site Response General Site Categories.* Adrian Rodriguez-Marek, Jonathan D. Bray, and Norman Abrahamson. February 1999.
- PEER 1999/02** *Capacity-Demand-Diagram Methods for Estimating Seismic Deformation of Inelastic Structures: SDF Systems.* Anil K. Chopra and Rakesh Goel. April 1999.
- PEER 1999/01** *Interaction in Interconnected Electrical Substation Equipment Subjected to Earthquake Ground Motions.* Armen Der Kiureghian, Jerome L. Sackman, and Kee-Jeung Hong. February 1999.
- PEER 1998/08** *Behavior and Failure Analysis of a Multiple-Frame Highway Bridge in the 1994 Northridge Earthquake.* Gregory L. Fenves and Michael Ellery. December 1998.
- PEER 1998/07** *Empirical Evaluation of Inertial Soil-Structure Interaction Effects.* Jonathan P. Stewart, Raymond B. Seed, and Gregory L. Fenves. November 1998.
- PEER 1998/06** *Effect of Damping Mechanisms on the Response of Seismic Isolated Structures.* Nicos Makris and Shih-Po Chang. November 1998.
- PEER 1998/05** *Rocking Response and Overturning of Equipment under Horizontal Pulse-Type Motions.* Nicos Makris and Yiannis Roussos. October 1998.
- PEER 1998/04** *Pacific Earthquake Engineering Research Invitational Workshop Proceedings, May 14–15, 1998: Defining the Links between Planning, Policy Analysis, Economics and Earthquake Engineering.* Mary Comerio and Peter Gordon. September 1998.

- PEER 1998/03** *Repair/Upgrade Procedures for Welded Beam to Column Connections.* James C. Anderson and Xiaojing Duan. May 1998.
- PEER 1998/02** *Seismic Evaluation of 196 kV Porcelain Transformer Bushings.* Amir S. Gilani, Juan W. Chavez, Gregory L. Fennes, and Andrew S. Whittaker. May 1998.
- PEER 1998/01** *Seismic Performance of Well-Confined Concrete Bridge Columns.* Dawn E. Lehman and Jack P. Moehle. December 2000.